19th INTERNATIONAL CONGRESS OF SPELEOLOGY

38º Congresso Brasileiro de Espeleologia

20-27 DE JULHO DE 2025 - BELO HORIZONTE - MINAS GERAIS – BRASIL

PROCEEDINGS

VOLUME II

Session 06: Karst Geomorphology

Session 07: Karst Hydrogeology and Speleogenesis

Union Internationale de Spéléologie
www.uis-speleo.org

Brazilian Speleological Society

CECAV
NATIONAL CENTER FOR CAVE RESEARCH AND CONSERVATION
ICMBio-MMA

ICMBio
INSTITUTO CHICO MENDES
MMA

Proceedings of the 19th International Congress of Speleology

38° Congresso Brasileiro de Espeleologia

VOLUME II / VII

Session 06: Karst Geomorphology

Session 07: Karst Hydrogeology and Speleogenesis

Proceeding of the 19th International Congress of Speleology

General coordination of the Congress
Allan CALUX

Coordination of Scientific Conference
Rodrigo Lopes FERREIRA & Allan CALUX

Editorial Board of the Scientific Conference
Allan CALUX, Javiera Elena de la Fuente CASTELLÓN, Amanda Jevaux SOUSA,
Nivaldo COLZATO & Jocy Brandão CRUZ

Union Internationale de Spéléologie
www.uis-speleo.org

sbe Brazilian Speleological Society

CECAV
NATIONAL CENTER FOR CAVE RESEARCH AND CONSERVATION
ICMBio-MMA

ICMBio
INSTITUTO CHICO MENDES
MMA

Cover design
Javiera de la FUENTE

Cover photos
Fulano, Ciclino, Beltrano

TECHNICAL-SCIENTIFIC COMMITTEE

General Coordinators: Dr. Rodrigo Lopes Ferreira and Dr. Allan Calux

Alex Hubbe
András Hegedus
André Strauss
Annette Summers
Bogdan P. Onac
Boris Watz
Bulat Mavlyudov
Carlos Grohmann
Christiane Donato
Daniel Menin
Daivisson Batista Santos
Diego Bento
Donald McFarlane
Elizandra Goldoni Gomig
Enrico Bernard
Friedrich Oedl
Giselle Utida
Gyula Hegedüs
Hernani Mota de Lima
Jan Urban
Jean Claude Thies
Jocy Cruz
Joel Rodet
John Brush
Jordana Ribeiro
José Antônio Ferrari
José G. Palacios Vargas
José-Maria Calaforra
Lívia Medeiros
Lucas Padoan de Sá Godinho
Luciana Alt
Marconi Souza Silva
Maria Alejandra Perez
Mário Dantas
Mario Parise
Nadja Zupan Hajna
Natalia Morata
Natalie Uomini
Nathalia Uasapud Henríquez
Paolo Forti
Patricia Kambesis
Paul Williams
Pedro Henrique Mendes Carvalho
Philipp Häuselmann
Rafaela Bastos Pietrobon
Rodrigo Severo
Simone Devus
Taraneh Khaleghi
Valdir Felipe Novello
Vitor Moura

PAPER EVALUATORS

Alessandra Vasconcelos
Alexandra Figueiredo
Aline Ghilardi
Allan Calux
Amos Frumkin
Anamaria Häuselmann
André Gomide
Andrzej Tyc
Ángel Fernández Cortés
Biswajeet Pradhan
Boaz Zissu
Bruno Lartiges
Cameron Wet
Carla Galeazzi
Carlo Germani
Carole Nehme
Carolina Scherer
Chris Groves
Christoph Spötl
Claudio Cruz
Dana Riechelmann
Dante Ernesto Salomo Suarez
Darryl Granger
David Labat
Débora Moreira de Oliveira Moura
Diego Bento
Dorothy Vesper
Douglas Zeppelini Filho
Edvard Dias Magalhães
Eliane Chim
Elver Luiz Maier
Elvis Pereira Barbosa
Fabrizio Nestola
Ferdinando Didonna
Ferenc Forray
Fernanda Quaglio
Fernando Gazquez
Fernando Laureano Verassani
Fernando Morais
Filip Duszynski
Francisco Giutierrez Santolalla
Francisco Sauro
Franck Bréhier
Franck Junod
Franco Urbani
Franziska Lechleitner
Gaspar González
George Veni
Gergely Balazs
Gheorghe Ponta
Giovanna Monticelli
Gisele Sessegolo
Grazielle Nascimento Silva
Gregory Middelton
Gustavo Soares de Araujo
Heleno dos Santos Macedo
Isabella Nicole Pisoni
Isabella Serena Liso
Ivanna Bustos
James Baldini
Janaina Carla dos Santos
Janaina Carla dos Santos
Jason Gulley
Jean-Philip Brugal
Jean-Pierre Bartholeyns
Jim Kennedy
Jiri Adamovic
Jo de Waele
Joan J. Fornos
João V. L. Cavalcante de Oliveira
Joel Despain
Joffer Fernandes
John Gunn
José Luis Bortolini Rosales
Juan B. Morales Malacara
Julia James
Kai Bosworth
Katherine Schmid
Kevin Bingham
Leandro Maciel
Lee Anne Bledsoe
Lee Florea
Lívia Medeiros
Liz Reed
Loeta Tyree
Luana Pereira Lima
Luca Antonio Dimuccio
Luciana Prado
Luis Mejía Ortiz
Luiz Afonso Vaz de Figueiredo
Luiz Eduardo Panisset Travassos
Manuela Correa Pereira
Marco Vattano
Marcus Paulo de Oliveira
Margarita Ojeda Carrasco
Maria Augusta Bacellar
Maria Conceição S. Meneses Lage
Maria Jacqueline Rodet
Mariana Barbosa Timo
Mario Parise
Martin Dixon
Mathias Vuille
Michael Gallay
Michael Ray Taylor
Michal Filippi
Michal Gradzinki
Michel Philips
Mick Sutton
Mirian Liza Alves Forancelli Pacheco
Mykah Carden
Mylene Berbert-Born
Natalie Uomini
Nicolás M. Stríkis
Oana Moldovan
Paulo Galvão
Paulo Rodrigo Simões
Pavel Bella
Philippe Audra
Philippe Brunet
Phillipe Fosse
Priscila Christina Borges Dias Randow
Rachel Bosch
Raoni Araújo
Ricardo Fraga
Rick Toomey
Roberto Bixio
Rubens Hardt
Rudolf Pavuza
Saul Hartman Riffel
Sebastian Breitenbach
Sílvia Alves Peixoto
Simone Bernadini
Sindiany Suelen Caduda dos Santos
Soledad Cuezva
Stefan Vasile
Stefano Fabbri
Stein-Erik Lauritzen
Stephan Kempe
Stephane Jaillet
Tamara Gonzalez Duran
Thaís Giovannini Pellegrini
Todrigo Antônio Castro Souza
Tudor Tamas
Val Hildreth-Werker
Victor Polyak
Willamy Saboia de Amorim
William Elliot
William Sallum Filho
Willians Lourenço Porto
Xianfeng Wang
Yakolén Tepebasi
Yuri Dublyansky
Yuri Popov
Yzila Liziane Farias Maia de Araújo

ORGANIZING COMMIITTE

Honorary president
José Ayrton Labegalini

Chairman
Allan Calux

Vice-Chairman
Jocy Brandão Cruz

Secretary General
Amanda Jevaux da S. de Sousa

Treasurer
Paulo Rosado Arenas

UIS Representative
Nivaldo Colzato

SBE Representative
Elizandra Goldoni Gomig

Scientific Coordinator
Rodrigo Lopes Ferreira & Allan Calux

Cataloging at Source

Sociedade Brasileira de Esopeleologia
19th Internacional Congress of Speleology: Belo Horizonte, Minas Gerais, Brazil July 20-27, 2025: proceedings. Volume 1 / edited by Allan Calux: SBE, 2025.
340xp. ; B&W.

1. Speleology. 2. Karstology. 3. Geomorphology. 4. Cave and karst science

CDU: 551.33

Printed in Brazil

SOCIEDADE BRASILEIRA DE ESPELEOLOGIA
Dr. Heitor Penteado, 1613 - Jardim Nossa Sra. Auxiliadora
Campinas, São Paulo, Brazil - ZipCode 13075-460

FOREWORD

The proceedings of the 19th International Congress of Speleology, held in Belo Horizonte (Brazil) from July 20 to 27, 2025, comprise seven volumes that gather over 400 scientific papers (extended abstracts) distributed across sixteen thematic sessions. These works were evaluated by an extensive group of reviewers, each guided by a Brazilian and a foreign coordinator, aiming to ensure their collective relevance, proper presentation, and compliance with the UIS Code of Ethics. The layout of the articles was prepared by the authors themselves and is their sole responsibility; however, the editorial team made an extra effort to maintain a minimum standard in their presentation.

These proceedings represent the work of more than a hundred individuals—scientists, technicians, and explorers who voluntarily dedicated thousands of hours to their production. To all of them, our heartfelt thanks. We hope you enjoy it and that the science compiled herein broadens the technical and academic horizons of karst and cave science.

VOLUME I.

VOLUME II.

VOLUME III.

VOLUME IV.

VOLUME V.

VOLUME VI.

VOLUME VII.

VOLUME II

Contents

Session 06: Karst Geomorphology

Session 07: Karst Hydrogeology and Speleogenesis

Session 06

KARST GEOMORPHOLOGY

Recharge landforms in a subjacent karst aquifer in Sete Lagoas, Minas Gerais, Brazil

Pedro Assunção (1,2,3), Rafael Magno (1), Camila Schuch (1), Lucas Padoan (1,4), Guilherme Ribas (2,5), Bruno Aguiar (2,6), Rodrigo de Paula (1) & Paulo Galvão (1)

(1) Universidade Federal de Minas Gerais, Programa de Pós-graduação em Geologia, Instituto de Geociências, Departamento de Geologia, CPMTC--IGC, Laboratório de Estudos Hidrogeológicos (LEHID), Belo Horizonte, Brasil, phassuncao@ufmg.br.

(2) Sociedade Excursionista e Espeleológica (SEE), Ouro Preto (MG), Brasil

(3) Espelogrupo Pains (EPA), Pains (MG), Brasil.

(4) Grupo da Geo de Espeleologia da USP (GGEO), São Paulo, (SP), Brasil

(5) MecRoc Engenharia Ltda., Belo Horizonte (MG), Brasil

(6) Gerência de Espeleologia da Vale S.A., Belo Horizonte (MG), Brasil

Abstract

Sinkholes and lakes are features of the karst landscape that can act as recharge points to the underground flow system. Among several types of sinkholes or dolines, caprock dolines are related to the interstratal karstification. In Sete Lagoas city, a well-developed urban area of the state of Minas Gerais, Brazil, there are several occurrences of this type of sinkhole, indicating that landscape subsidence in insoluble rocks could be associated to a karst aquifer development in an underlying soluble unit.. The objective of this work was to characterize sinkholes in metapelites that have never been studied diligently, in order to understand their genesis and the water dynamics associated to these karst features. Geomorphological/ and geostructural mapping and investigation, together with digital elevation models (DEMs) analysis from unmanned aerial vehicle (UAV) imagery were carried out to characterize the morphology of these features. An electrical resistivity tomography was carried out to represent the hydrodynamics in the subsurface. The results showed that there are 5 perennial and intermittent karst lakes, in addition to 8 caprock sinkholes in the study area . All the evidences support the hypothesis that both features are directly related to the metapelites and are conditioned by the underlying karstification. It became evident that these features are fundamental hydrodynamic structures, acting on the recharge of the aquifer system.

Résumé

Les dolines et les lacs sont des formes de relief du paysage karstique qui peuvent agir comme points de recharge pour le système souterrain. Il existe plusieurs types de dolines, dont certaines sont liées au karst intra-stratal, appelées dolines caprock. Dans la région karstique de Sete Lagoas, dans l'État de Minas Gerais, au Brésil, on observe la présence de ce type de doline, mais elles n'ont pas été étudiées de manière approfondie. L'objectif de ce travail était de caractériser les dolines dans les métapélites, afin de comprendre leur genèse et la dynamique de l'eau de ces formes karstiques reposant sur l'aquifère karstique. À cette fin, des cartes géomorphologiques et géostructurales ont été réalisées, et des modèles numériques de terrain (MNT) ont été générés à partir d'images de véhicules aériens sans pilote (UAV) pour caractériser la morphologie de ces formations. Une méthode de tomographie de résistivité électrique a également été utilisée pour comprendre l'hydrodynamique en sous-sol. Les résultats ont montré qu'il existe 5 lacs karstiques, certains pérennes et d'autres intermittents, en plus de 8 dolines classées comme caprock. Ces deux types de formations sont directement liées aux métapélites et conditionnées par le karst sous-jacent. Il est devenu évident que ces formations jouent un rôle fondamental dans le comportement hydrodynamique, contribuant à la recharge du système aquifère.

Resumo

Dolinas e lagoas são feições do relevo cárstico que podem atuar como pontos de recarga do sistema subterrâneo. Existem várias tipos de dolinas, algumas delas estão relacionadas ao carste subjacente, que são chamadas de dolinas de cobertura. Na região cárstica de Sete Lagoas, estado de Minas Gerais, Brasil, existe a ocorrência deste tipo de dolina, porém não foram estudadas profundamente. O objetivo deste trabalho foi caracterizar as dolinas em metapelitos, a fim de compreender a sua gênese e a dinâmica hídrica dessas feições cársticas sobrejacentes do aquífero cárstico. Para isso foram realizados o mapeamento geomorfológico/geoestrutural e modelo de elevação com drone para caracterizar a morfologia destas feições e método geofísico de eletrorresistividade para compreender a hidrodinâmica em subsuperfície. Os resultados mostraram que existem 5 lagoas cársticas algumas perenes e outras intermitentes, além de 8 dolinas classificadas do tipo encoberta por rocha. Ambas as feições estão diretamente relacionadas com os metapelitos e condicionadas pelo carste subjacente. Ficou claro que essas feições são parte fundamental do comportamento hidrodinâmico, atuando na recarga do sistema aquífero.

1. Introduction

Karst terrains occupy approximately 15% of the Earth's continental surface and they can be defined as a specific type of landscape, where a complex network of caves and subterranean conduits develop and are formed by the dissolution process of highly soluble rocks such as limestones, marls, or evaporites. These terrains commonly feature intrinsic landforms such as lapiés, stone towers, dolines and sinkholes, sinking streams, canyons, and blind valleys (FORD & WILLIAMS, 2007; GOLDSCHEIDER et al., 2020). In Brazil, about 3% of the country's territory is covered by karst terrains, which predominantly develop in limestones and dolomites deposited during the the Neoproterozoic and the Cambrian (AULER & FARRANT, 1996).

Water plays a fundamental role in the formation of these systems, as it is transmitted and stored through the network of caves and underground conduits, giving rise to karst aquifers. Regarding the origin of water, two types of recharge in karst aquifers can be highlighted: autogenic and allogenic. When recharge originates within the karst system itself, it is considered autogenic, while allogenic recharge originates from non-karstic regions. In terms of infiltration type, water can infiltrate either concentrically at recharge points (sinkholes and dolines) or diffusely through soils, epikarst, fractures, or the rock matrix (FORD & WILLIAMS, 2007; GOLDSCHEIDER & DREW, 2007; PALMER, 2007).

Karst landforms result from hydrological and geochemical processes involved in the development of the karst system, occurring at various scales. These features can be classified as input, output, or residual forms. Karst input features are those that allow the recharge of surface and/or meteoric water into the aquifer system (FORD & WILLIAMS, 2007; TRAVASSOS, 2019).

Dolines or sinkholes are karst recharge landforms and commonly appear as enclosed circular or oval depressions, wider than they are deep. Based on their genesis, dolines can be classified into various types. A noteworthy type is the caprock doline, where subsidence occurs in the overlying insoluble caprock, and can be considered a subtype of collapse doline. This type of doline is related to the underlying soluble rock, indicating the karstification processes in the lower rock layers (FORD & WILLIAMS, 2007; KRANJC, 2013; TRAVASSOS, 2019; FERREIRA & UAGODA, 2019).

Dolines related to interstratal karst are less frequent than other types of dolines. Interstratal karst refers to the dissolution occurring in more soluble rocks that are overlain by less soluble rocks, and it is subdivided into subjacent, entrenched, or deep-seated karst (KLIMCHOUCK & FORD, 2000).

In Brazil, this specific type of doline is still poorly identified and described (FERREIRA & UAGODA, 2020). In the Paraná Basin, a set of dolines in sandstones of the Furnas Formation (PR) and Aquidauana Formation (MS) were formed due to the presence of subjacent karst (SALLUN FILHO & KARMANN, 2007). Similarly, some dolines in sandstones of the Urucuia Group in the São Desidério region (BA) have been associated with subjacent karst in limestones of the São Desidério Formation (GODINHO & PEREIRA, 2013). A cave formed in metapelites in the city of Lagoa da Prata (MG) has its entrance within a collapse doline, and its genesis is related to subjacent karstification in carbonate rocks of the Sete Lagoas Formation (Bambuí Group) (ZENHA & MACIEL, 2003). The karst of the Peruaçu Cave National Park has also been interpreted as intrastratal karst and evolution into a fluviokarst (PEREIRA et al., 2006).

Several techniques are commonly used to characterize dolines, including electrical resistivity, a terrestrial geophysical method that allows indirect identification of karstified zones and delineation of the vadose and phreatic zones (ZHANG et al., 2024). Combined with geophysical methods, geological-structural mapping can be used to identify faults and folds that may influence karstification and, consequently, doline formation (ELGATTOUSSI et al., 2023; ŞENER et al., 2023; MAIA et al., 2024). Geomorphological mapping based on high-resolution topography obtained via drones (UAVs) can facilitate the identification and morphological characterization of dolines (FERREIRA et al., 2023). The use of Light Detection and Ranging (LIDAR) has become increasingly common for doline mapping, as it enables better delineation of their morphology, especially in heavily vegetated areas. In regions where aerial laser scanning is available, it can be a powerful tool; however, when such data is unavailable, UAV-based laser scanning for more localized characterizations can be an innovative alternative (TELBISZ et al., 2024; MAIA et al., 2024; KIM & HONG, 2024).

In Sete Lagoas (MG), various types of dolines and karst lakes occur, mainly where carbonate rocks of the Sete Lagoas Formation are exposed. However, there are also records of dolines occurring in metapelitic rocks of the Serra de Santa Helena Formation (Fig. 1). Although these dolines have been documented in metapelites, which are low-solubility rocks, their genesis, morphology, and hydrodynamic behavior remain uncertain (PESSOA, 1996; GALVÃO et al., 2017; MAGNABOSCO et al., 2020; ALVES et al., 2021; SCHUCH et al., 2023; MAGNO, 2024).

Thus, the objective of this study was to characterize dolines in metapelites through geomorphological/geo-structural mapping, drone-based topography, and electrical resistivity, to understand the genesis and hydrodynamic behavior of these karst features overlying the karst aquifer in northern Sete Lagoas, Minas Gerais, Brazil.

2. Materials and methods

2.1. Pre-existing Data

To characterize the local geology, geological maps (TULLER ET AL., 2010), produced by the Brazilian Geological Service (SGB) at a scale of 1:100,000, were used. For elevation data, the ALOS PALSAR satellite's digital elevation model (DEM) with a spatial resolution of 12.5 m was employed. Subsurface geological information was obtained from borehole data, including location and lithological profiles, acquired through two governmental open access platforms: SIAGAS (SGB) and SIAM (SEMAD-MG), as well as additional data provided by Ambev S.A. company and the Sete Lagoas Water and Sewerage Service (SAAE). Information on groundwater flow was based on previous studies conducted in the area (GALVÃO et al., 2017; ALVES et al., 2021; SCHUCH et al., 2023; MAGNO, 2024).

2.2. Geomorphological and Geostructural Mapping

The study area's landforms were initially analyzed through satellite image interpretation, enabling the identification of the most prominent karst features. Areas of major interest were visited in the field to characterize the karst recharge landforms, and to collect geographic coordinates, morphological attributes, and hydrogeological data. A total of 13 karst landforms were surveyed, including 8 dolines and 5 karst lakes. Dimensional estimates (axes and area) were conducted using geoprocessing tools in QGIS 3.16, while volume estimates were based on the forms and calculations proposed by Telbisz et al. (2024). Geological-structural mapping was conducted to detail the local geology, based on previous mapping efforts. A total of 45 field sites were surveyed where structural measurements of bedding, foliation, fractures, and faults were collected.

2.3. UAV-based Elevation Model

To obtain a high-resolution digital elevation model and detailed geomorphological mapping of karst landforms, topographic surveys and high-resolution aerial photographs were acquired using an unmanned aerial vehicle (UAV) (drone), specifically a DJI AIR 2S model equipped with an onboard optical sensor (1" CMOS, 20 megapixels, nominal focal length of 24 mm, f/2.8-11). The flight was conducted at an altitude of 130 meters with a 70% image overlap. The Agisoft Metashape software was used for photogrammetric processing and digital elevation model (DEM) generation.

2.4. Geophysics: electrical resistivity tomography

The geophysical survey involved acquiring electrical resistivity data (geoelectric profiles) using the electrical resistivity tomography (ERT) technique. The survey lines were positioned in areas of interest near karst features to investigate subsurface hydrological conditions and infiltration structures.

Five geoelectric profiles (L6, L7, L8, L9, L10) were executed, with lengths ranging from 320 to 500 meters and an electrode spacing of 20 meters. The chosen electrode array for the ERT survey was the Dipole--Dipole configuration, due to its high lateral resolution at multiple depth levels. The resistivity meter used was the X6xtal 500 model, manufactured by Auto Energia, featuring a 32-channel multipoint system with an actual power output (RMS) of 450 Watts and a peak power output (PMPO) of 698 Watts. An additional five geoelectric profiles (L1, L2, L3 L4 e L5) were previously conducted by Alves et al. (2021) at Lagoa Grande, during a period of reduced water levels, allowing electrical resistivity surveys of dolines on the lake bed (Fig. 1).

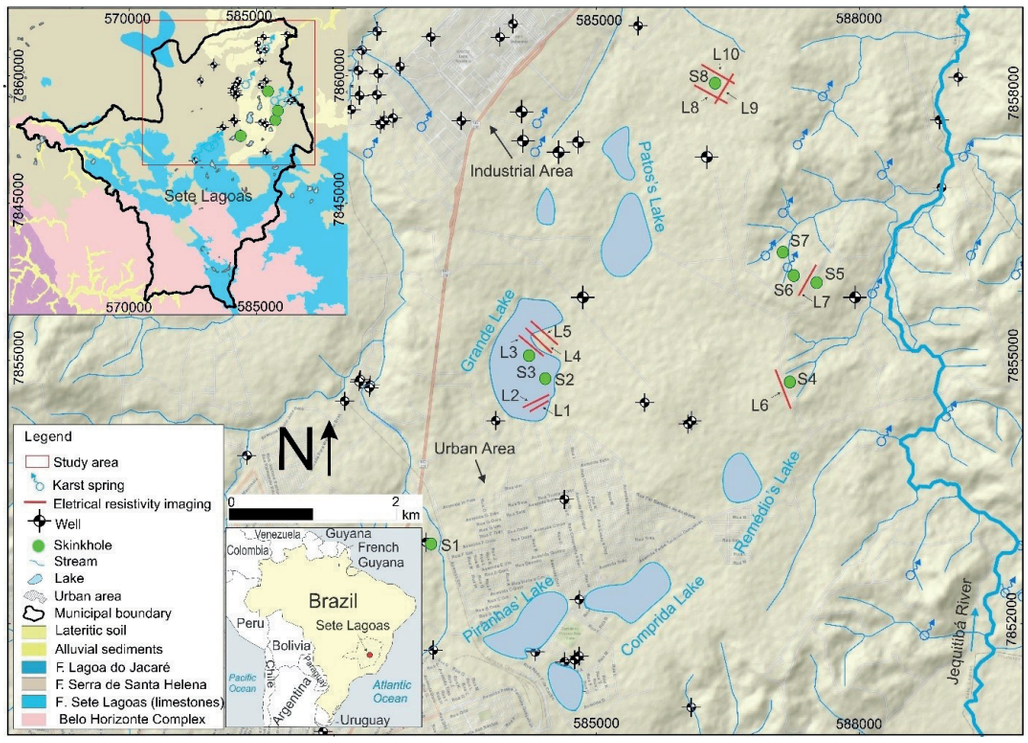

Figure 1: *Location of the study area in the northern region of the municipality of Sete Lagoas, state of Minas Gerais, Brazil, highlighting the karst features and the lines (L1 a L10) of the geoelectric profiles.*

3. Results

3.1. Morphology of Karst Landforms

The analyzed karst recharge landforms were categorized into two groups based on their hydrological conditions. Five of them are karst lakes, named: Lagoa Grande, Lagoa dos Patos, Lagoa das Piranhas, Lagoa do Remédio, and Lagoa Comprida. The lakes Grande, Piranhas, and Comprida are perennial, experiencing only a reduction in water level during the dry season. In contrast, Remédio and Patos lakes are intermittent, drying out completely during the dry season. Lagoa Grande is the largest among them and is connected to the underlying karst aquifer through sinkholes S3 and S2, as confirmed by Alves et al. (2021). The estimated depth of the lakes ranged from 5 to 10 m, with an average of 6 m. Their area varied from 156,305 m^2 to 794,872 m^2, with an average of 319,165 m^2, while the estimated volume ranged from 390,762 m^3 to 3,974,360 m^3, with an average of 1,222,929 m^3.

The other eight features were classified as caprock dolines (sinkholes) (S1, S2, S3, S4, S5, S6, S7, and S8), which do not contain water. Regarding their morphology, they were classified as bowl-shaped dolines, except for doline S4, which was formed by collapse. All of them occur in metapelites of the Serra de Santa Helena Formation, as confirmed by the presence of weathered metapelite outcrops in doline S4. The estimated depth of the dolines ranged from 2 to 25 m, with an average of 8 m. Their area varied from 287 m^2 to 8,416 m^2, with an average of 3,684 m^2, while the estimated volume ranged from 287 m^3 to 130,075 m^3, with an average of 25,825 m^3.

3.2. Geophysics and Geology

The 10 geoelectric profiles (Fig. 2) surveyed near the karst landforms indicated the presence of an upper zone with low resistivity and a lower zone with higher resistivity, with the contact between them (dashed line) at an approximate depth of 30 m. The upper zone was interpreted as the weathered metapelite/soil with groundwater storage (perched aquifer), while the lower zone corresponds to the metapelite bedrock (Serra de Santa Helena Formation). Some profiles (L2, L3, L7, and L8) revealed subvertical structures with intermediate resistivity, which may indicate water infiltration zones via brittle structures (faults or fractures). The geoelectric profiles reached a maximum depth of 75 m.

Therefore, none of the profiles penetrated the limestone of the Sete Lagoas Formation, which lies at depths greater than 100 m, as confirmed by geological profiles of tubular wells near some dolines. Profiles L1, L2, L3, L4, and L5 were interpreted by Alves et al. (2021), confirming hydraulic connection features between Lagoa Grande and the underlying karst aquifer. Profiles L6, L7, L8, and L9 were analyzed in this study and by Magno (2024), indicating the presence of structures that control recharge flow from caprock dolines to the underlying karst aquifer. The dolines are aligned with structural lineaments identified in the field, which were interpreted as normal faults.

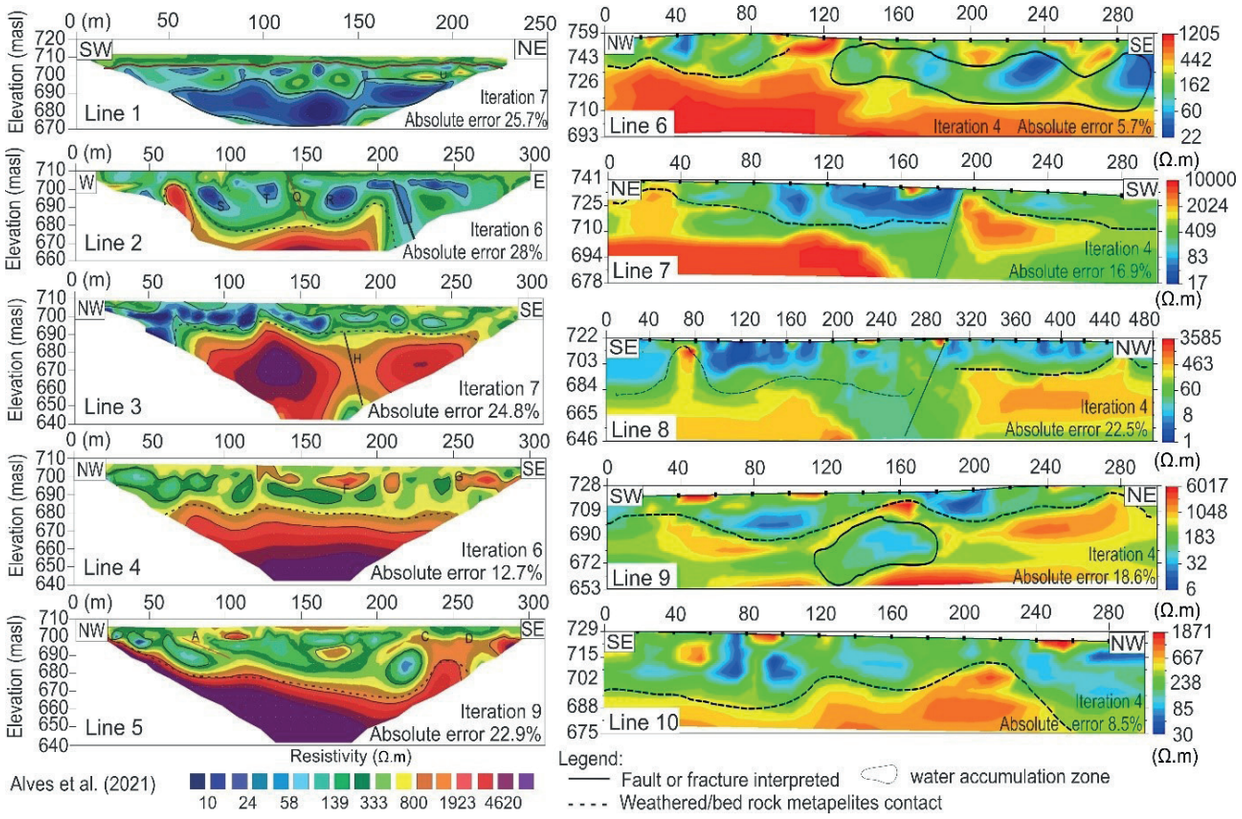

Figure 2: *Geoelectric profiles surveyed near the karst features, with hydrogeological interpretations of the electrical resistivity values of geological media.*

4. Discussion

The karst landforms (lakes and dolines) can be considered as punctual autogenic recharge features to the underlying karst aquifer, as they allow the infiltration of meteoric water or water from the perched aquifer into the zones of weathered metapelite rock and soil. The chemical characteristic of this recharge water is acidic, allowing the dissolution in the contact with the underlying limestone, and consequently enhancing the karstification process. The alignment of these dolines suggests that they were formed by infiltration along deep geological structures, likely normal faults, as evidenced by some of the geoelectric profiles. Additionally, in this area, the depth of the limestone of the Sete Lagoas Formation is shallower (100 m) when compared to other regions of the Bambuí Group basin (MAGNO, 2024), indicating that depth may be a favorable condition to the development of sinkholes in the less soluble cover unit, in a similar way as interpreted by Gao et al. (2005) in Minnesota (USA).

The lakes are of great hydrogeological importance, especially the perennial lakes, as they serve as permanent recharge areas throughout the year. The dolines were interpreted as caprock type (FORD & WILLIAMS, 2007), since their genesis is conditioned by the karstification of the underlying limestone (Sete Lagoas Formation), and further collapse of the metapelitic caprock (Serra de Santa Helena Formation). The proposed hydrogeological conceptual model considers these features as part of the hydrodynamic behavior, contributing to the recharge of the karst aquifer system (Fig. 3).

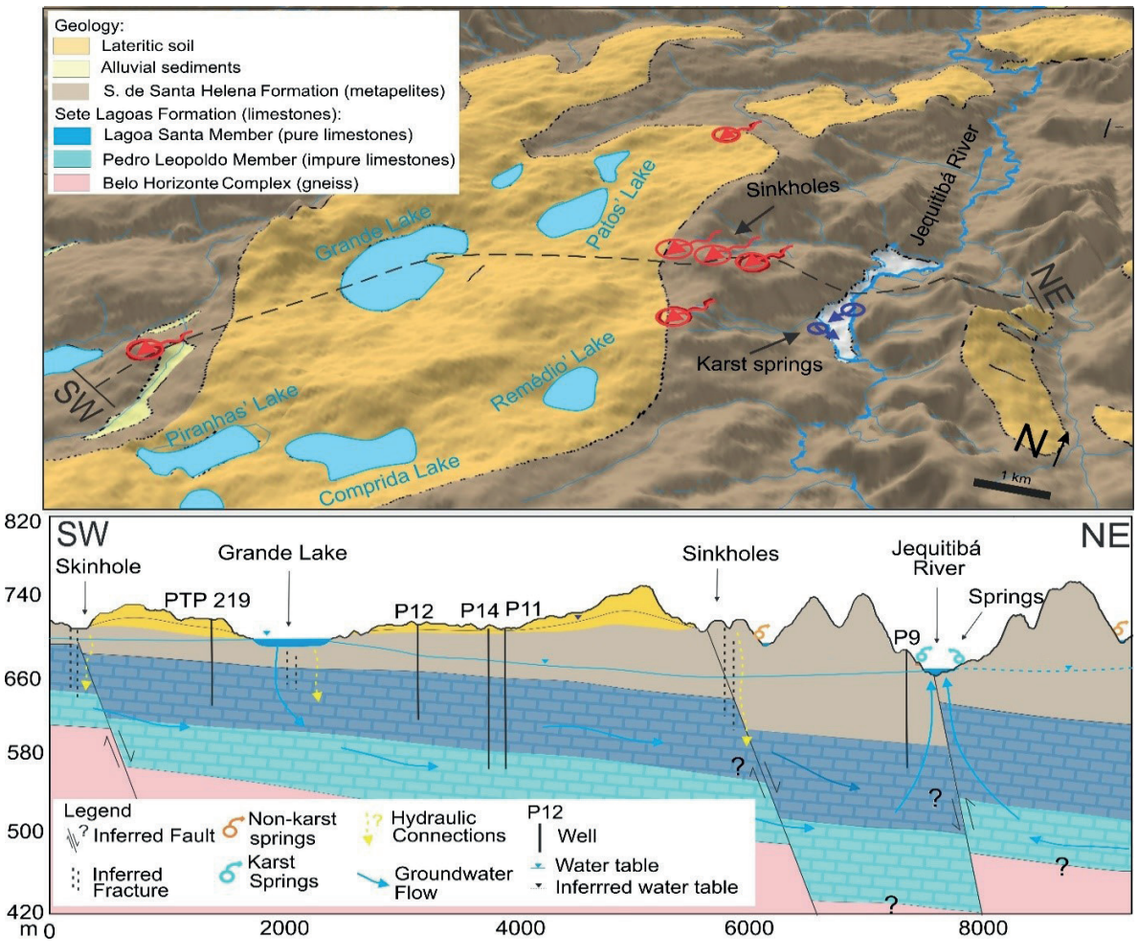

Figure 3: *Hydrogeological conceptual model and the role of karst landforms (lakes and dolines) in the recharge and hydraulic connection of the underlying karst aquifer.*

5. Conclusion

The geomorphological mapping, combined with geological-structural mapping and the electrical resistivity geophysical investigation, allowed for an understanding of how the recharge karst landforms (lakes and dolines) present in the area are important for maintaining the hydrodynamics of the underlying karst aquifer. The challenge in characterizing this type of doline is that the karstification that conditions its formation occurs at depth, requiring subsurface information. In this sense, geophysics helped to identify geological structures and their hydrological behavior. Field mapping, along with the high-resolution digital elevation model obtained by UAV, assisted in the morphological characterization of the dolines. However, there were limitations in estimating the volume of the dolines, as these models do not allow access to the interior of the dolines, which are occupied by vegetation. Therefore, the use of LIDAR is recommended in future studies to accurately map the morphology of the dolines.

Acknowledgments

This research was funded by the Fruta project, a partnership between IGAM, AMBEV S/A - Sete Lagoas Branch, and LEHID-UFMG (process 3228524; Ordinance No. 1305673/2021). The authors also thank the Postgraduate Program in Geology at UFMG and the Coordination for the Improvement of Higher Education Personnel (CAPES).

References

ALVES, M.; GALVÃO, P.; ARANHA, P. (2021). Karst hydrogeological controls and anthropic effects in an urban lake. Journal of Hydrology, 593: 1-16.

AULER, A., FARRANT, A.R. (1996). A brief introduction to karst and caves in Brazil. Proceedings of the University of Bristol Spelaeological Society, 20(3), 187-200.

GAO, Y., Alexander Jr., E. C., Barnes, R. J., 2005, Karst database implementation in Minnesota: analysis of sinkhole distribution: Environmental Geology, v. 47, p. 1083-1098.

KRANJC, A. (2013). Classification of closed depressions in carbonate karst. Treatise on geomorphology, 104-111.

ELGATTOUSSI, S., MELKI, F., GABTNI, H., & BOOTH REA, G. (2023). Structural control on a Ypresian karstic aquifer revealed by an integrated geophysical and geological approach: the Mateur imbricated thrust zone (northern Tunisia). Quarterly Journal of Engineering Geology and Hydrogeology, 56(4), qjegh2023-049.

FERREIRA, C. F., & UAGODA, R. E. S. (2019). Tipologias do carste e classificações de dolinas: uma revisão. Caminhos de Geografia, 20(70), 519-537.

FERREIRA, C. F., & UAGODA, R. E. S. (2020). Um panorama sobre mapeamentos de dolinas no Brasil, feições elementares do carste. Revista Brasileira de Geografia Física, 13(1), 302-321.

FERREIRA, C. F., HUSSAIN, Y., UAGODA, R., SILVA, T. C., & CICERELLI, R. E. (2023). UAV-based doline mapping in Brazilian karst: A cave heritage protection reconnaissance. Open Geosciences, 15(1), 20220535.

FORD D., WILLIAMS P. (2007). Karst geomorphology and hydrology, Ed. Unwin Hyman Ltd. London, 601 p.

Goldscheider, N.; Drew, D. (2007). Methods in Karst Hydrogeology. Taylor & Francis. International Contributrionsto Hydrogeology, p 201-222.

GOLDSCHEIDER, N., CHEN, Z., AULER, A. S., BAKALOWICZ, M., BRODA, S., DREW, D., ... Y VENI, G. (2020). Global distribution of carbonate rocks and karst water resources. Hydrogeology Journal, 28(5), p. 1661-1677.

GALVÃO, P.; HALIHAN, T.; HIRATA, R.; TERADA, R. (2017) Recharge sources and hydrochemical evolution of an urban karst aquifer, Sete Lagoas, MG, Brazil. Environmental Earth Sciences, v. 76, p. 159.

GODINHO, L. P., & DE ARAÚJO PEREIRA, R. G. F. (2013). Caracterização geomorfológica preliminar do sistema cárstico do rio João Rodrigues, São Desidério–BA.

KLIMCHOUK, A., & FORD, D. C. (2000). Types of karst and evolution of hydrogeologic setting. In: Speleogenesis. Evolution of karst aquifers. National Speleological Society, Huntsville, p. 45-53.

KIM, J., & HONG, I. (2024). Evaluation of the Usability of UAV LiDAR for Analysis of Karst (Doline) Terrain Morphology. Sensors, 24(21), 7062.

MAIA, R. P., AULER, A. S., BEZERRA, F. H., BORGES, S. V., LA BRUNA, V., PUJONI, D., ... & VIDAL, A. C. (2024). Fluid flow zones along fracture corridors inferred from collapse dolines in carbonates of the Irecê Basin, Brazil. Earth Surface Processes and Landforms, 49(13), 4506-4522.

MAGNABOSCO, R., GALVÃO, P., DE CARVALHO, A.M., (2020). An approach to map karst groundwater potentiality in an urban area, Sete Lagoas,

Brazil. Hydrol. Sci. J. Doi 10.1080/02626667.2020.1802031.

MAGNO, R. O. (2024). Fatores hidrogeológicos, espeleológicos e estruturais no desenvolvimento de zonas preferenciais de carstificação, nordeste do município de Sete Lagoas, MG. Dissertação de mestrado. Belo Horizonte.

PALMER, A.N. (2007). Cave Geology, 454. Dayton, OH: Cave Books.

PESSOA, P. (1996) Hydrogeological characterization of the region of Sete Lagoas - MG: Potentials and Risks. Master Thesis. Department of Geosciences, University of São Paulo. São Paulo.

PEREIRA, R. G. F. A., KARMANN, I., & FERREIRA, T. D. (2006). Geomorfologia e hidrogeologia cárstica do Parque Nacional Cavernas do Peruaçu. Anais. Geociências e as sociedades do futuro, 123.

TELBISZ, T., MARI, L., & SZÉKELY, B. (2024). LiDAR-based morphometry of Dolines in Aggtelek Karst (Hungary) and Slovak Karst (Slovakia). Remote Sens.p 16: 737.

TRAVASSOS, L. E. P. (2019). Princípios de carstologia e geomorfologia cárstica. Brasília: ICMBio. 242 p.

TULLER, M. P., RIBEIRO, J. H., SIGNORELLI, N., FÉBOLI, W. L. 2010. Projeto Sete Lagoas - Abaeté: estado de Minas Gerais. Belo Horizonte: CPRM. Escala 1:100.000. Programa Geologia do Brasil - PGB.

SALLUN FILHO, W., & KARMANN, I. (2007). Dolinas em arenitos da Bacia do Paraná: evidências de carste subjacente em Jardim (MS) e Ponta Grossa (PR). Revista Brasileira de Geociências, 37(3), 551-564.

ŞENER, M. F., ŞIMŞEK, M., UTLU, M., ÖZTÜRK, M. Z., & SÖZBILIR, H. (2023). Morphotectonic development of surface karst in Western Taurus (Türkiye). Carbonates and Evaporites, 38(4), 78.

ZENHA, E., & MACIEL, L. (2003). Toca do Lobo–uma surpreendente cavidade em metapelito. In Congresso Brasileiro de Espeleologia (Vol. 27, pp. 200-206).

ZHANG, J., SIRIEIX, C., GENTY, D., SALMON, F., VERDET, C., MATEO, S., ... & LARCANCHÉ, M. (2024). Imaging hydrological dynamics in karst unsaturated zones by time-lapse electrical resistivity tomography. Science of The Total Environment, 907, 168.

The Role of Tectonics in Cave Forming and Water Migration: an example from the Amatérská Cave (Czech Republic)

Vít Baldík (1), Jiří Rez (1), Roman Novotný (1)

(1) Czech Geological Survey, Leitnerova 22, Brno, Czech Republic. vit.baldik@geology.cz

Abstract

Amatérská cave system provided a wide spectrum of structural data which enabled us to draw certain conclusions about the role of tectonics in speleogenesis. Directions of the main cave systems are controlled by structures of the biggest scale – thrust faults and other big scale faults, whereas smaller faults and fractures control the cave corridor's directions locally. The size of cave corridors/domes is in direct correlation with fracture densities – denser fractures tend to cause bigger cave volumes. Preliminary modelling of fracture distribution using data from the cave and surrounding areas proved that the fracture network can be modelled with a high degree of confidence. Such models can be used for hydrodynamic modelling or in cave exploration.

1. Introduction

The role of tectonics in underground water migration and cave speleogenesis in carbonate karst terrains is crucial. Limestones have very small primary porosity and even smaller effective porosity. Underground water migration in these rocks is controlled by the so-called secondary porosity formed by fractures and other brittle structures. These structures' orientation and density (number of fractures per meter) control the direction of underground water migration and, consequently, the direction of cave corridors. Structures of all scales control karstification and underground water migration: main thrust faults control the main cave corridor trends in the whole karst scale, faults and cleavage control the directions of cave corridors in the cave system scale and joints and other fracture types control the cave corridors directions in the scale of individual cave parts/corridors (e.g. Rez, Baldík, 2023).

Amatérská cave system is the most extensive cave system in the Czech Republic (fig. 1). It is in the northern part of the Moravian Karst (the most significant karst area in the Czech Republic). Moravian Karst is mainly built of limestones of the Macocha Formation (ca. 1000 m thick sequence), which is the shallowest facies of the Moravo-Silesian Palaeozoic Unit (Middle Devonian to Mississippian). Macocha Formation is formed from several types of limestones, which are deposited in four distinct depositional cycles (Hladil 1986). Limestones of the Macocha formation lie over Palaeozoic basal clastics, which lie over Pre-Cambrian granitoids of the Brno Massif. Limestones of the Macocha Formation are overlain by several tens on meters (several hundred in the southern part of the Moraviam Karst) of limestones of the Líšeň Formation. This carbonate sequence is thrust over by Variscan flysch stack (Rozstání and Myslejovice Formations; Rez, Melichar, Kalvoda, 2011).

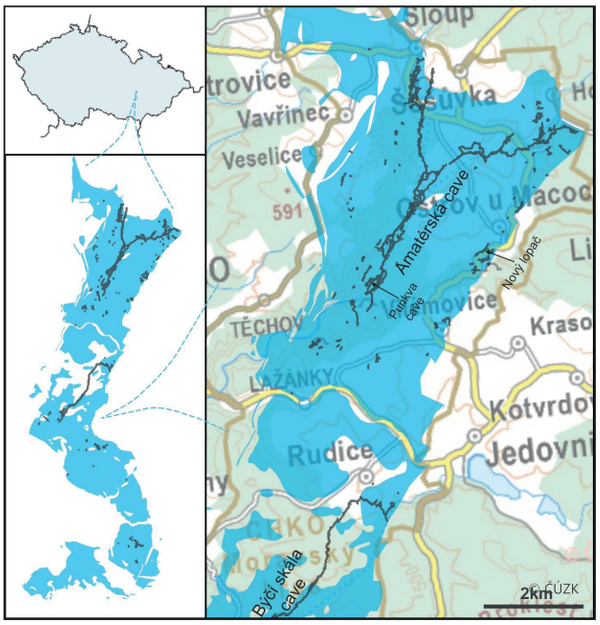

Figure 1: *Location of the cave systems in the Moravian Karst mentioned in the text. Blue polygons indicate the extent of limestones.*

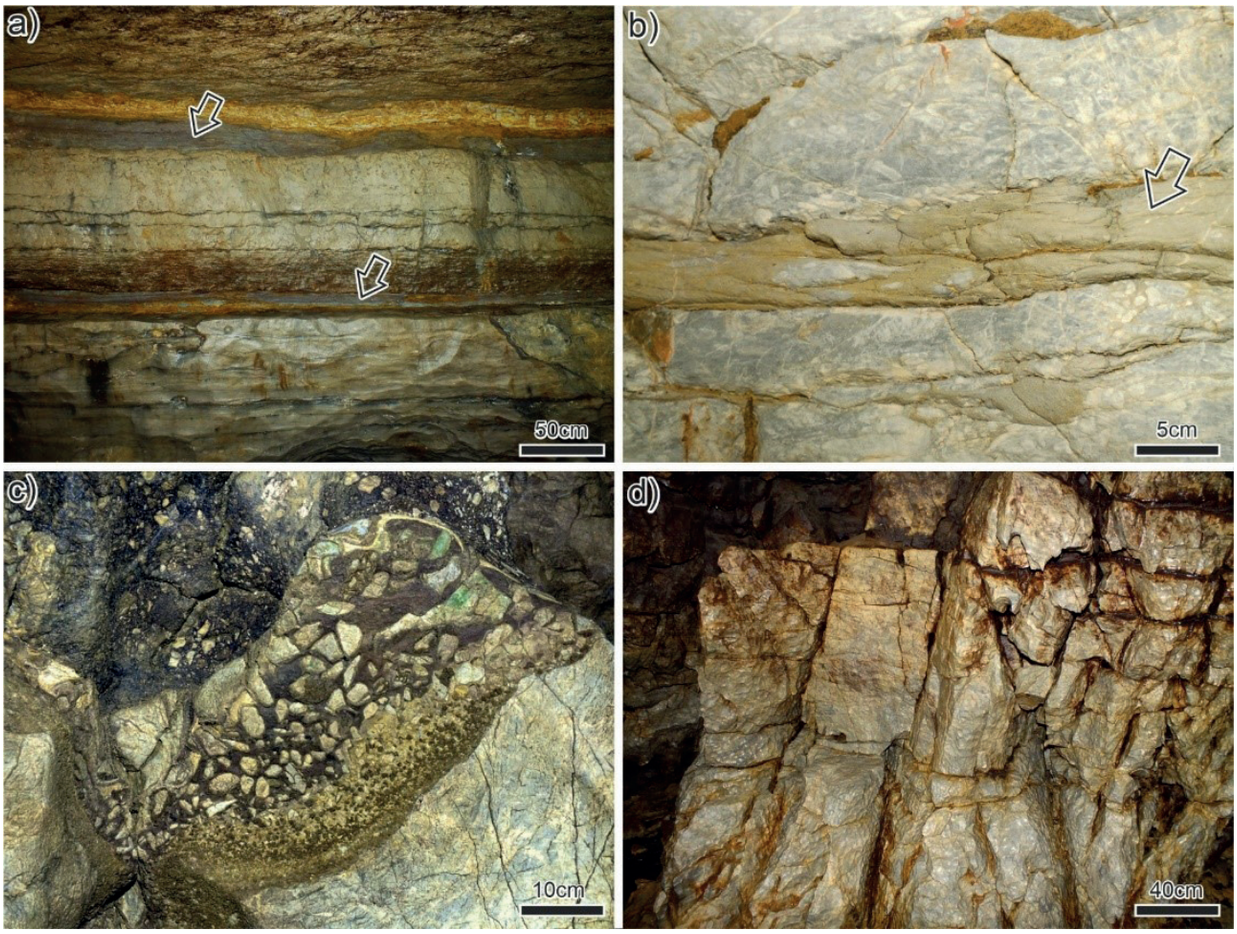

Figure 2: *Brittle structures in the Moravian Karst: a) thrust faults with pressure solution in the Býčí skála cave; b) thrust fault with pressure solution in the Nový Lopač cave; c) cataclastic/brecciated core of a fault in Punkva cave; d) fractures in Amatérská cave system.*

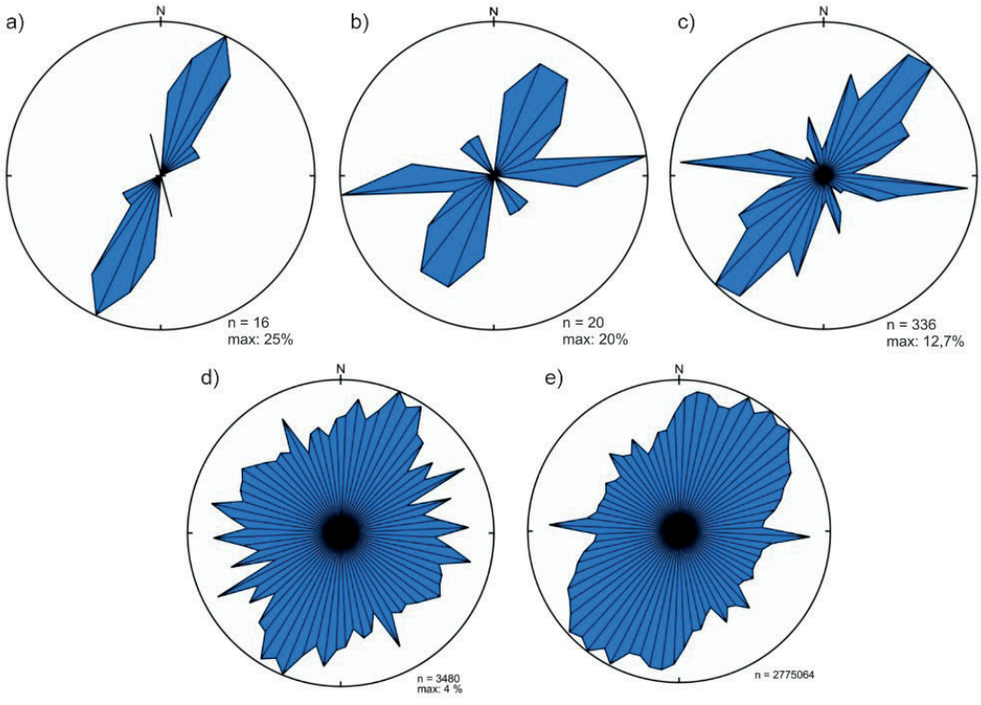

Figure 3: *Rose plots of main brittle structure types from the Amatérská cave: a) thrust faults; b) faults; c) cleavage; d) fractures; e) rose plot of cave corridors.*

2. Methods

Systems of fractures were studied in the Amatérská cave (New and Old Amatérská cave systems) in 28 places scattered throughout the whole cave system as uniformly as possible. A dataset of 30 fractures (50 in some areas) was acquired at each station, and minimum and maximum block size was determined (i.e. the minimal mean fracture spacing of the most dominant fracture system and maximal mean fracture spacing of the least dominant fracture system). The fracturing intensity was expressed as the RQD index (Deere & Miller, 1967; see equation in Figure 4). RQD = 100 have rocks without fractures, and RQD = 0 has the most highly fractured rocks (all blocks are smaller than 10 cm).

A preliminary fracture model was created using Schlumberger Petrel software. Main fracture systems were identified using a contoured equal-area plot – 25 in total plus random fractures making "noise" in the dataset. The number of fractures in each system was upscaled into the model grid (50 x 50 m). Each fracture system was then distributed into the whole grid using a Gaussian sequential simulation using variograms for each fracture system. Resulting fracture densities were then added together to obtain realistic fracture densities for each grid cell.

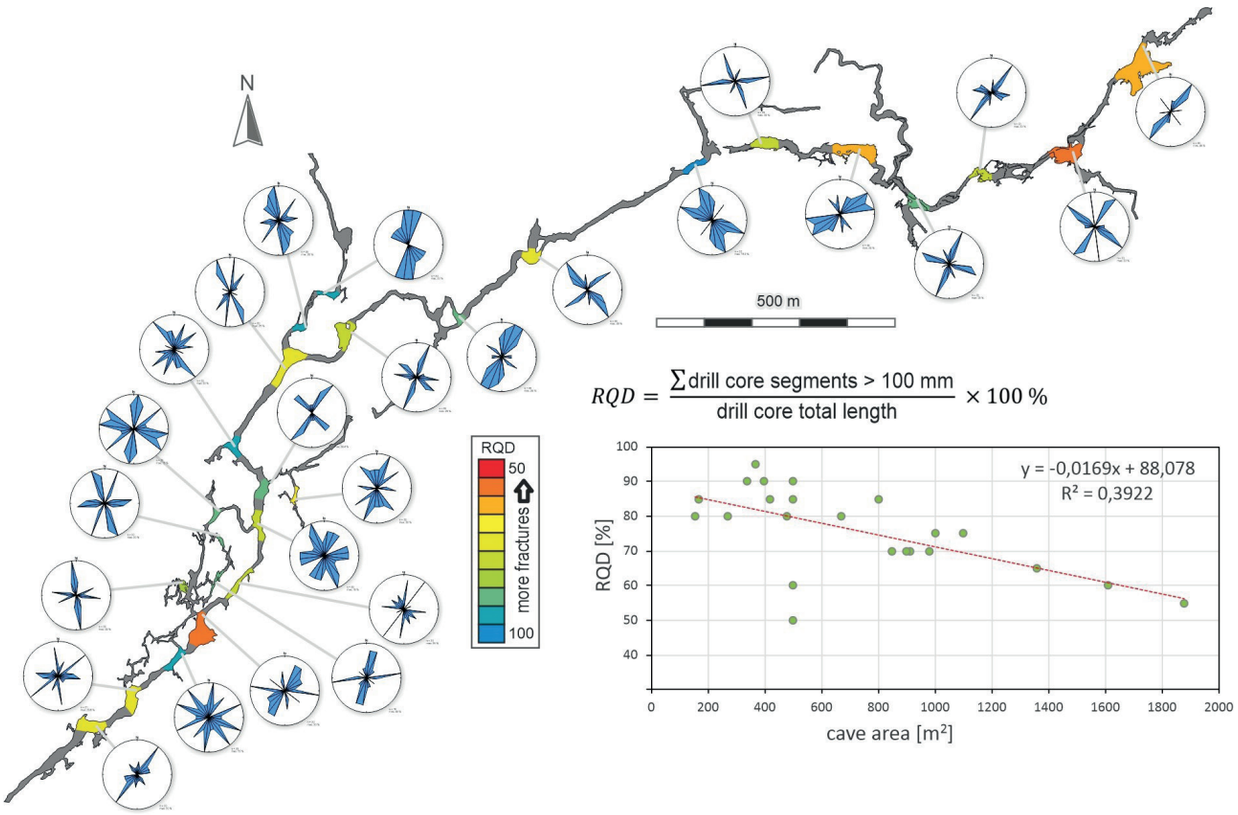

Figure 4: *Map of the Amatérská cave system with fracture analysis results – rose plots and RQD in each station. xy plot shows the relationship between RQD and the cave corridor/dome area.*

3. Results

Brittle tectonic structures are the most important for developing the Amatérská cave system. Several significant phases can be distinguished in the Moravian Karst (e.g. Rez et al., 2011; Rez et al., 2023). The oldest and most important is the Variscan thrust/fold structure, which is dominated by younger NNE-SSW oriented Variscan thrust faults (fig. 3a). These thrusts are up to several meters thick shear zones connected with pressure solution. These highly strained zones resemble sandstones or siltstones (fig. 2a, b), which confuse most explorers. These thrust faults caused the primary folding of the area and produced axial cleavage (fig. 3c). Other cleavage systems relate to younger fault systems (see figs. 3c and 3b). One can detect three main systems of faults: NNE-SSW, W-E and NW-SE (fig. 3b). more fault systems and their possible relationships are discussed in detail in Rez et al. (2023).

These major structures are complemented by fracture systems, which copy the orientation and localisation of their "parent" structures (fig. 3d).

4. Discussion

We can demonstrate, based on the Amatérská cave case study, that not only the directions of cave corridors are controlled by the orientation of fractures, but that the intensity of fracturing control the volume of cave corridors/domes (fig. 4). Smaller corridors have usually higher values of RQD (are less fractured), bigger corridors and domes have smaller values of RQD (are much more fractured). Limestones of the northern part of the Moravian Karst and non-calcareous rocks of the Culmian facies (wackes and conglomerates) are dominated by sub-vertical fractures, which can be divided into four main systems. All of these systems are associated with the main tectonic features of the area: NNE-SSW fractures corres-

pond with the main thrust faults, and NE-SW, W-E and NW-SE fractures are associated with young fault systems.

The preliminary fracture model in Figure 5 clearly shows the relationships between cave corridors and fracture densities. This not only confirms our findings that the main structures controlling the general directions of cave corridors are the thrust faults (all lines of red squares follow thrust faults), but it also helps us detect possible continuations of cave systems and direct future exploration.

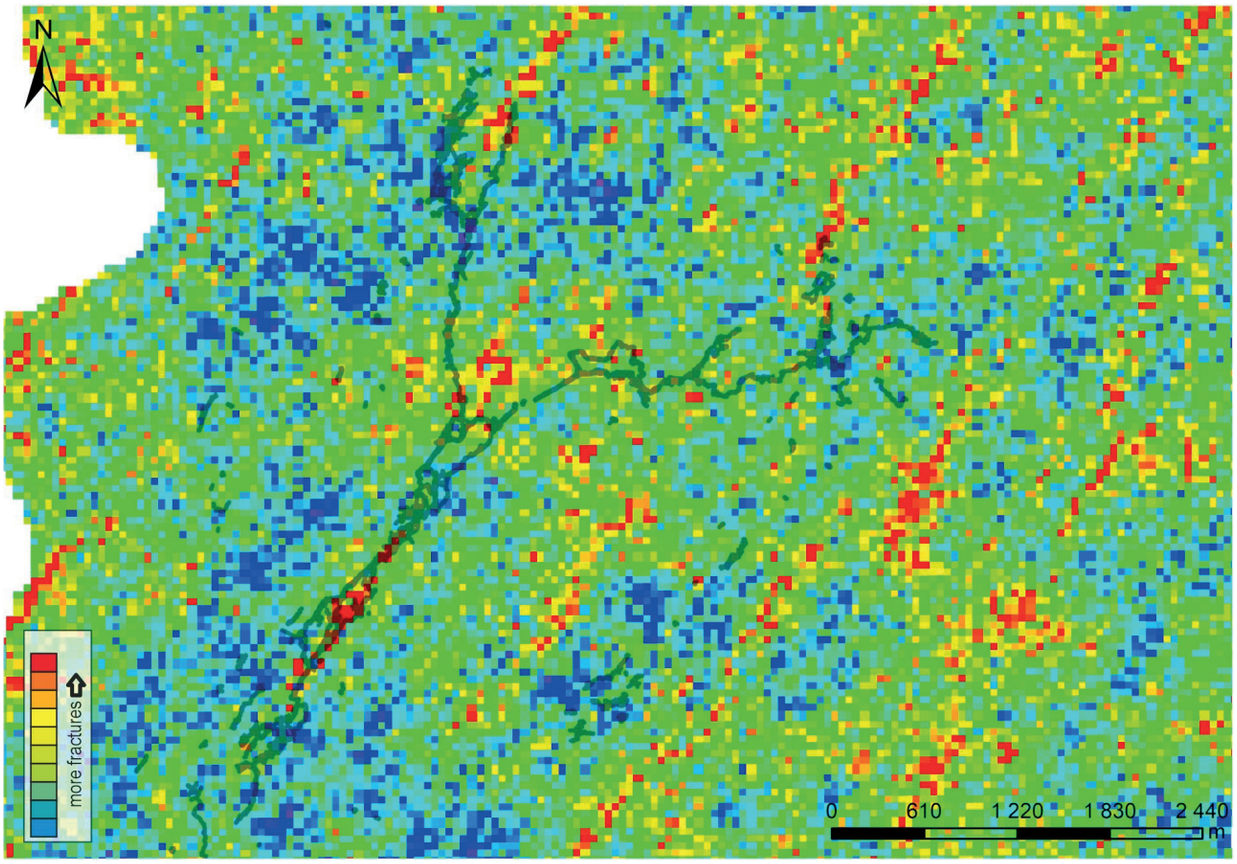

Figure 5: *Fracture model of the northern part of the Moravian Karst and adjacent areas. The floor plan of the Amatérská cave system is in grey.*

5. Conclusions

Results of several years of fieldwork (both on the surface and subsurface – in karstic caves) can be summarised in a few points: 1) brittle deformation structures control both underground water migration and karstification; 2) directions of the main cave systems are controlled by most significant structures – thrust faults and other big faults; 3) more minor faults and fractures control the cave corridor's directions locally; 4) the size of cave corridors/domes is in direct correlation with fracture densities; 5) from hydrogeological end environmental point of view, non-calcareous rocks of the infiltration area are as important as the karstified limestones, and we have to focus on their protection and also on increasing the environmental awareness of population.

Acknowledgments

Financial support through the Rock Environment and Natural Resource RENS project (SS02030023) is gratefully acknowledged.

References

Deere, D.U., Miller, D.W. (1967) The Rock Quality Designation (RQD) Index in Practice, Classification Systems for Engineering Purposes. ASTM STP, American Society for Testing and Materials, Philadelphia, PA, 91-101

HLADIL, J. (1983) Cyklická sedimentace v devonských karbonátech macošského souvrství. Zemní plyn a nafta 28, 1-15.

REZ, J., MELICHAR, R., KALVODA, J. (2011) Polyphase deformation of the Variscan accretionary wedge: an example from the southern part of the Moravian Karst (Bohemian Massif, Czech Republic). In: Kinematic Evolution and Structural Styles of Fold-and-Thrust Belts (edited by Poblet, J. & Lisle, R. J.). Geological Society Special publications 349. Geological Society, London, 223–235.

REZ, J., BALDÍK, V. (2023): Tektonika a krasovění: příčina a následek. In: Audy Marek: Speleofórum. Praha: Česká speleologická společnost.

REZ, J., KERNSTOCKOVÁ, M., BALDÍK, V. (2023) Stress analysis from the southern part of Moravian Karst (Czech Republic). Geologica Carpathica 74(3), 233-244.

Application of Drones for Geomorphological Characterization, Detection and Control of Environmental Liabilities in the Centripetal Polygonal Basin of Vargem da Lapa

Alberto Barioni (1), Augusto Sarreiro Auler (2), Juliana Mantovani (3) & Antonio Carlos Colangelo (4))

(1) Faculdade de Filosofia, Letras e Ciências Humanas, Universidade de São Paulo, São Paulo, Brazil e Meandros Espeleo Clube (alberto.barioni@alumni.usp.br), corresponding author

(2) Instituto do Carste, Belo Horizonte, Brazil / Carste Ciência Ambiental, Belo Horizonte, Brazil (aaluer@gmail.com)

(3)Faculdade de Filosofia, Letras e Ciências Humanas, Universidade de São Paulo, São Paulo, Brazil (jucmantovani@gmail.com)

(4) Faculdade de Filosofia, Letras e Ciências Humanas, Universidade de São Paulo, São Paulo, Brazil (accolang@usp.br)

Resumo

A popularização de RPA (Remotely Piloted Aircraft), mais comumente conhecidos como drones, vem fazendo destes, instrumentos praticamente obrigatórios no exercício das atividades de prospecção espeleológica e caracterização de feições do relevo cárstico. Todavia a oferta de dispositivos, ainda que financeiramente não tão acessíveis, nem mesmo a nível empresarial, faz com que os equipamentos utilizados sejam os modelos mais básicos, sem grandes recursos operacionais, muitas vezes limitando a tarefa à tomada de imagens para o apoio da logística de atividades de campo, ou para registro fotográfico de alto apelo estético, mas sem fins analíticos. Este trabalho, que teve como palco de estudos a Bacia Poligonal da Vargem da Lapa, no município de Lagoa Santa, Minas Gerais, Brasil, vem sugerir algumas normatizações que façam com que aplicações simples do dispositivo, possam ser empregadas de maneiras distintas, sem que seja necessário o empenho de grandes recursos técnicos e financeiros, permitindo alcançar elementos não visíveis em softwares de visualização do terreno, especialmente, aqueles resultantes das atividades antrópicas.

Abstract

The popularization of RPA (Remotely Piloted Aircraft), known as drones, has made these instruments almost indispensable in the practice of speleological prospect and characterization of karst landforms. However, the accessibility of such devices, seldomly affordable even at the corporate level, often results in the use of the most basic models, with limited operational capabilities. This frequently restricts their use to tasks such as capturing images to support fieldwork logistics or producing visually appealing graphic outputs. This research used the Poligonal Basin of Vargem da Lapa in the municipality of Lagoa Santa, Minas Gerais, Brazil, as a case study to propose standards that allow simple applications of the device to be employed in different ways without the need for significant technical and financial resources. This approach aims to uncover elements that are not visible in terrain visualization software, especially those resulting from human activities.

1. Introdução

A Bacia Poligonal da Vargem da Lapa, se posiciona como um recorte dentro de um importante cenário das Ciências da Terra brasileira, o Carste de Lagoa Santa na região central de Minas Gerais (Fig. 1), onde ainda no século XIX, o naturalista dinamarquês Peter Willian Lund teve seu interesse despertado pelas características do meio físico da região. O Carste se apresenta como um dos principais palcos de pesquisas arqueológicas, paleontológicas, espeleológicas e carstológicas do Brasil. (BARIONI, 2018)

A presença humana no Carste de Lagoa Santa, remonta há aproximadamente 12.000 anos sempre tendo uma relação estreita com o impacto antrópico sobre o ambiente cárstico. Muito comum neste período, era a alteração das entradas das cavernas, seja por meio do vistoso acervo rupestre deixado em seus paredões calcários ou pela surpreendente acumulação de vários metros de sedimento de origem antrópica (PILÓ, 1998).

Como uma das maiores dificuldades da tentativa da mensuração do impacto humano frente a qualquer sistema natural, é a dificuldade na distinção das mudanças naturais, daquelas que são resultados da intervenção antropogênica, tende a se tornar ainda mais imprecisa a constatação de impactos acionados pelo homem, em uma escala de tempo que contemplaria praticamente todo período Holocênico.

O âmago desta tarefa é desenvolver um estudo sobre a onde haja a capacidade de observar a discreta inter-relação dos elementos geomorfológicos e pedológicos desta peculiar paisagem na Bacia Poligonal da Vargem da Lapa, e identificar quais as forçantes antrópicas que possam estar influenciando a suscetibilidade do relevo à uma eventual alteração no equilíbrio dinâmico de dado ambiente, tendo como ferramenta de trabalho, a aplicação de RPA (Remotely Piloted Aircraft), como meio de captação de processos ativos no ambiente.

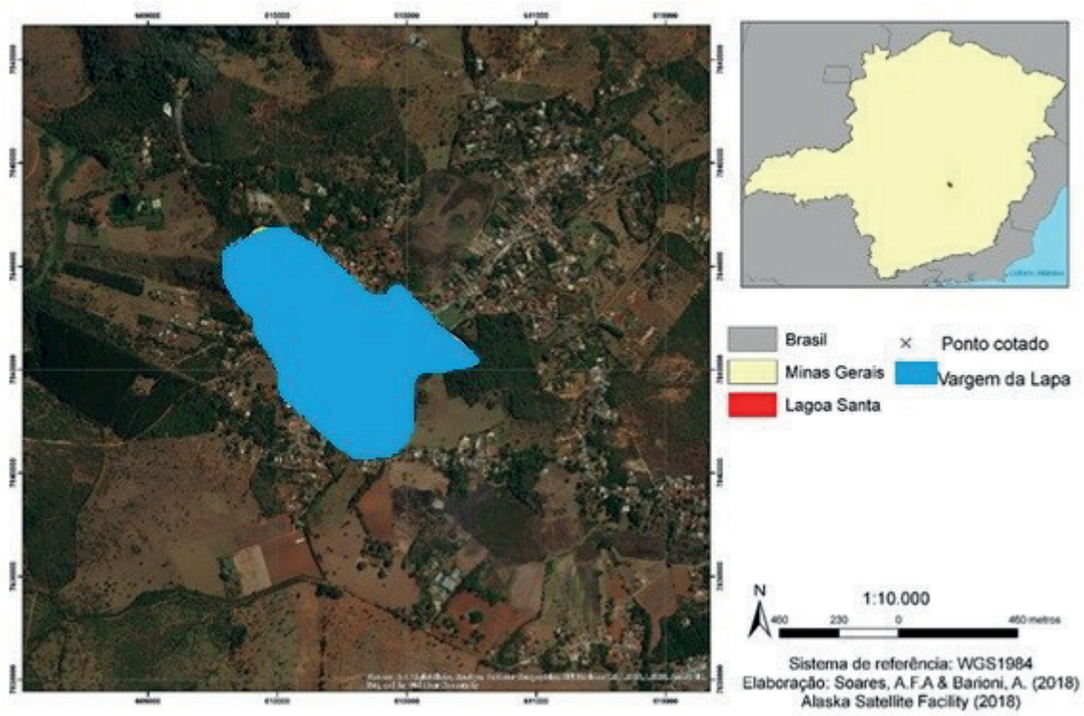

Figura 1: *Em azul, a totalidade da Bacia Poligonal Centrípeta da Vargem da Lapa no contexto local.*

2. Materiais e Métodos

A solução encontrada para a melhor avaliação da escala mais modesta, foi a utilização de um Drone para a obtenção das ortofotos da área da pesquisa em uma nova metodologia chamada RPA (CUNHA et al., 2016). O equipamento da marca DJI, modelo Phanton 3, dispõe de câmera com sensor fixo Sony Exmor de 1/3 polegadas e resolução de 12,4 MP instalada a um gimbal - dispositivo de giroscópio para estabilizar a câmera. Abertura da lente foi de f/3,61. O ISO utilizado nas fotos foi de 100, enquanto a velocidade do obturador foi de 1/100 de segundo, suficiente para estabilizar qualquer movimento brusco na imagem. O RPA conta com baterias de 4.480 mAh possibilitando autonomia média de 25 minutos.

Somado a isso, o aparelho conta com posicionamento via Global Navigation Satellite System (GNSS), sistema este, que opera simultaneamente com a estrutura satelital estadunidense, (Navstar GPS) russa (GLONNAS) e europeia, (Galileo) permitindo o georreferenciamento de excelente precisão de todas as imagens obtidas.

A administração do voo do RPA foi feita de maneira autômata pelo software para smartphone Drone Deploy, específico para o trabalho com RPA. Neste software, cabe ao usuário apenas gerar um polígono de onde o RPA deverá realizar as imagens, a que altura elas deverão ser tomadas e o percentual de sobreposição em latitude e longitude das tais. Feito isso, o próprio software estipula a quantidade de imagens e o tempo de voo para a obtenção das mesmas, além de controlar o trajeto do aparelho durante tal atividade.

Foram realizados dois grupos de voos para a obtenção das fotos ortogonais ao solo em duas alturas distintas, sendo uma a 200 metros de altitude do ponto de partida do aparelho buscando a cobertura total da bacia poligonal enquanto o segundo, foi realizado a uma altura de 75 metros, visando captar ainda mais detalhes das posições inferiores da bacia.

Para as imagens a 200 metros foram feitos dois voos apenas por precaução em relação à autonomia das baterias. Na ocasião o aplicativo obteve 469 fotografias com sobreposição longitudinal de 60% e transversal de 40%. Já para o único voo a 75 metros de altura, foram realizadas 189 fotos com a mesma taxa de sobreposição entre elas.

O processamento das imagens foi realizado em software Agisoft Metashape para a geração de modelos tridimensionais de prédios, objetos e estatuas que mais recentemente foi adaptado para o processamento de imagens oriundas de RPA´s.

Inicialmente são reconhecidas as coordenadas dos centroides de cada imagem, em seguida com o auxílio de um algoritmo de busca baseado no SIFT, (Scale Invariant Feature Transform) são reconhecidos os pontos homólogos entre as imagens. Este processo é capaz de tratar diversas imagens em um tempo diminuto, obviamente variável de acordo com a capacidade de processamento da máquina utilizada.

Uma vez os pontos fotogramétricos identificados, é criada uma nuvem de pontos esparsa e em seguida com base na posição de cada câmera, é gerada a nuvem de pontos densa, onde se torna possível obter dados de profundidade, completando a nuvem esparsa.

Na última etapa os pontos da nuvem densa são conectados com o auxílio de algoritmos de triangulação, de modo a construir uma malha de diversos triângulos e assim gerar o Modelo Digital do Terreno (MDT).

3. Resultados

O produto gráfico fornecido pelo RPA se mostrou uma importante ferramenta para a interpretação de fenômenos e ações morfológicas que possam estar sucedendo na área. O tamanho de pixel extremamente diminuto, serviu para uma melhor compreensão da paisagem da bacia. Para o voo a 75 metros de altura, o pixel apresentou tamanho de 13,3 cm (Fig. 2), ao passo que uma imagem do satélite World View 3, que atualmente

oferece a melhor resolução dentre os sistemas de aquisição de imagens disponíveis por satélite, entrega um pixel de 31 cm, além de ser muito mais onerosa. Já em softwares livres como Google Earth, raramente o pixel apresenta menos de 1 metro de dimensão (Fig. 3). Soma-se a isso baixo erro posicional dos três eixos da aeronave, os quais totalizados foram de 3,52m, que poderia ser ainda menor caso na área sobrevoada, houvessem pontos de controle de sistemas de GNSS de precisão.

Outro artifício conveniente que o RPA fornece, é a possibilidade de sobrepor o produto da interpolação das imagens no software Google Earth, favorecendo a melhor compreensão do ambiente e de fatos geomorfológicos.

Figura 2: *Imagem do maciço rochoso feita com RPA.Escala equivale a 20 metros*

No entanto este sistema se mostra limitado para a geração de Modelos Digitais de Terreno, visto que é apenas um sistema de captação de imagens e não de rastreamento da superfície, por meio de bandas espectrais. O processo de digitalização do relevo se mostrou vagaroso ainda que prático, uma vez que o sistema de digitalização, não reconhece autonomamente elementos não referentes ao relevo, como vegetação, construções ou mesmo uma simples superfície de uma lagoa, classificando-os como parte das vertentes. Dessa maneira, o produto tende a não apresentar plena concordância a morfologia do terreno, salvo se o usuário despender enorme quantidade de tempo para corrigir os erros.

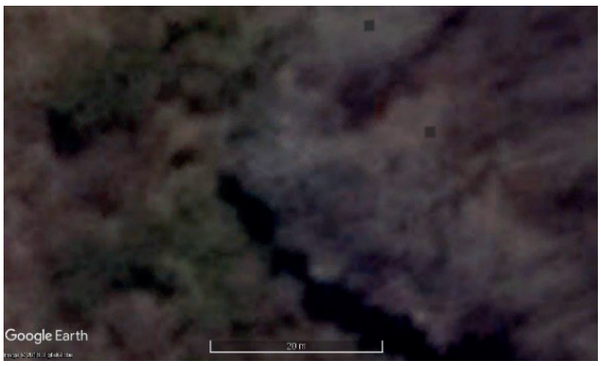

Figura 3: *Imagem disponível no Google Earth para o mesmo maciço. Escala equivale a 20 metros*

4. Discussão

Mesmo com RPA´s básicos, é possível extrair informações que não são visíveis em softwares de visualização de terreno tradicionais. Algumas técnicas que viabilizam a obtenção dessas informações incluem: a) Análise de Sombra e Iluminação. Utilizar diferentes ângulos de iluminação (voos em horários distintos) para realçar feições do relevo, como pequenas depressões ou elevações. b) Índices de Vegetação. Aplicar índices de vegetação (ex.: NDVI) para identificar áreas com vegetação densa (TAGLIARINI, 2020), que podem estar associadas a zonas de infiltração ou feições cársticas ocultas. c) Filtragem e Realce de Imagens: usar técnicas de processamento de imagens para realçar contrastes e identificar padrões no terreno que podem indicar feições cársticas ou áreas de interesse espeleológico.

Para a Exemplo de Aplicação na Bacia Poligonal da Vargem da Lapa, os RPA´s podem ser utilizados para: 1) Mapeamento de dolinas e sumidouros que caracterizam a região; 2) Monitoramento na evolução de processos erosivos e o impacto das atividades humanas (RODRIGUES, 2019); 3) Documentação das entradas de cavernas e outras feições espeleológicas; 4) Geração de modelos 3D que auxiliem no entendimento da dinâmica hidrológica da bacia.

5. Conclusão

É sabido que após seis anos desde a aplicação destas metodologias, as tecnologias disponíveis aos sistemas RPA, sofreram significativos incrementos além de expressiva redução nos custos de obtenção de aparelhos dotados de mais recursos como Lidar, câmeras multiespectrais e térmicas, além de softwares com maior poder de processamento de recursos capazes de subtrair cobertura vegetal, por exemplo.

No entanto a utilização desta metodologia, ainda que em suas aplicações mais básicas, também podem ser de grande valia em atividades que exijam mais dinamismo, bem como respostas mais imediatas ao usuário, como é o caso de frentes de prospecção por caminhamento em campo empenhadas por grupos de espeleologia, empresas do ramo das ciências ambientais ou mesmo o poder público em atos de fiscalização ou monitoramento.

Soma-se a isso, que neste estudo, a utilização do RPA trouxe o desenlace de sua aplicação como um recurso que possa ser adotado com frequência regular e constante, viabilizando o monitoramento de possíveis deflagrações de processos erosivos, sejam estes naturais, ou de fomento consequente às atividades antrópicas. Desta maneira, em aspecto mais célere, seria possível a viabilização de respostas mitigadoras, ou mesmo neutralizar novos passivos ambientais, em um ambiente cárstico tão impactado pela presença humana na área.

No que se refere ao monitoramento, RPA´s podem ser vistos como um recurso muito conveniente, uma vez que tal metodologia permite a fácil replicação de voos de controle, sendo uma tarefa simples, a repetição dos voos - apenas sua programação acerca da área, sobreposição e altura – situações que não são tão viáveis com a presença in loco do observador, seja por inviabilidade de acesso, dimensionamento ideal do passivo, ou mesmo dificuldade de controle da replicação da metodologia de captação de imagens.

Agradecimentos

Este trabalho seria inviável sem o apoio da empresa Carste Ciência e Meio Ambiente, proprietária do RPA, que gentilmente forneceu o equipamento para este estudo. Também somos extremamente gratos ao Parque Estadual do Sumidouro pela oferta do alojamento do Parque

e aos moradores da região José Hein da fazenda Kauaia, Letícia Rodrigues e s. João Bárbara Filho, os quais sempre foram muito solidários para/com as pesquisas no Carste de Lagoa Santa. Por fim destacamos os agradecimentos aos amigos Rodrigo Elias de Oliveira e André Strauss e Fernando Laureano Verassani.

Refêrencias

BARIONI A. Caracterização das formações superficiais do Carste de Lagoa Santa: um estudo de caso da Bacia Poligonal da Vargem da Lapa (Município de Lagoa Santa, Minas Gerais) – São Paulo, 2018. Dissertação de Mestrado 131 p.

CUNHA, A, A. (org). 2016. Controle de qualidade de posicionamento de ortofoto gerada pelo RPA (Remotely Piloted AircraftI) Phantom 3 com receptor GNSS embarcado. 12º Congresso de Cadastro Técnico Multifinalitário e Gestão Territorial.PILÓ, L. B. Morfologia cárstica e materiais constituintes: dinâmica e evolução da depressão poligonal Macacos--Baú – Carste de Lagoa Santa, MG. Tese de Doutorado. Departamento de Geografia da Faculdade de Filosofia, Letras e Ciências Humanas, Universidade de São Paulo. São Paulo, 1998.

Rodrigues, J, L. Mapeamento e avaliação de impacto ambiental utilizando aeronave remotamente pilotada no Parque Nacional Serra de Itabaiana. – São Cristóvão, SE, 2019. Dissertação de Mestrado 52 p.

TAGLIARINI, Felipe de Souza Nogueira. Imagens de drone e Índice de Vegetação por Diferença Normalizada (NDVI) para classificação segmentada em Áreas de Preservação Permanente (APP). - Botucatu, 2020. Tese de Doutorado 148 p.

Cave Sedimentology: History and Recent Advances

Rachel Bosch (1) & Dylan Ward (2)

(1) U.S. West Environmental Remediation, AECOM Technical Services, Inc., Cincinnati, Ohio, USA, rachel.bosch@aecom.com (corresponding author)
(2) Department of Geosciences, University of Cincinnati, Cincinnati, Ohio, USA, dylan.ward@uc.edu

Abstract

Clastic sediments in caves can provide insights into geomorphic, paleoclimatic, and contaminant transport processes that occur in cave and karst systems. A facies-based classification system for cave sediments, developed through international literature review and field observations in the Eastern United States, facilitates communication and consistency in cave sedimentology research. This classification system has been adopted globally, and here we present two applications demonstrating its utility. In the first application, analysis of a major debris-flow deposit in Mammoth Cave using facies classifications, combined with geomorphic, geophysical, and terrestrial lidar techniques, revealed evidence of two distinct flow events. In the second application, we integrated the classification system with geochronology and numerical modeling to examine base level history and phreatic conduit growth in the Central Kentucky Karst region. The resulting model idealizes interactions among base level stability, conduit development, and cuesta-bench sinkhole plains, providing a plausible mechanism to explain cosmogenic dating and field observations. This work demonstrates how systematic classification of clastic sediment deposits advances our understanding of both sedimentation processes and karst landscape evolution.

Resumen

Les sédiments clastiques dans les grottes peuvent fournir des indices sur les processus géomorphologiques, paléoclimatiques et de transport des contaminants qui se produisent dans les systèmes karstiques. Un système de classification basé sur les faciès, développé à partir d'une revue de la littérature internationale et d'observations de terrain dans l'Est des États-Unis, facilite la communication et la cohérence dans la recherche sédimentologique des grottes. Ce système, adopté mondialement, est illustré ici par deux applications. Dans la première, l'analyse d'un important dépôt d'écoulement de débris dans la grotte de Mammoth, utilisant les classifications des faciès et des techniques géomorphologiques, géophysiques et lidar terrestre, a révélé deux événements d'écoulement distincts. Dans la seconde, nous avons intégré le système avec la géochronologie et la modélisation numérique pour examiner l'histoire du niveau de base et la croissance des conduits phréatiques dans la région karstique du Kentucky central. Le modèle résultant idéalise les interactions entre la stabilité du niveau de base, le développement des conduits et les plaines de dolines, fournissant un mécanisme plausible pour expliquer la datation cosmogénique et les observations de terrain.

Resumo

Sedimentos clásticos em cavernas podem fornecer informações sobre processos geomorfológicos, paleoclimáticos e de transporte de contaminantes que ocorrem em sistemas cársticos. Um sistema de classificação baseado em fácies, desenvolvido através de revisão da literatura internacional e observações de campo no leste dos Estados Unidos, facilita a comunicação e a consistência na pesquisa sedimentológica de cavernas. Este sistema, adotado globalmente, é demonstrado aqui através de duas aplicações. Na primeira, a análise de um depósito de fluxo de detritos na Caverna Mammoth, utilizando classificações de fácies e técnicas geomorfológicas, geofísicas e lidar terrestre, revelou dois eventos distintos de fluxo. Na segunda, integramos o sistema com geocronologia e modelagem numérica para examinar a história do nível de base e o crescimento de condutos freáticos na região cárstica do centro de Kentucky. O modelo resultante quantifica interações entre estabilidade do nível de base, desenvolvimento de condutos e planícies de dolinas, fornecendo um mecanismo plausível para explicar a datação cosmogênica e observações de campo. Este trabalho demonstra como a classificação sistemática de depósitos de sedimentos clásticos avança nossa compreensão dos processos de sedimentação e da evolução da paisagem cárstica.

1. Introduction

1.1. Classification of Clastic Sediments in Karst Conduits and Characterization of an In-Cave Debris Flow Deposit

A boulder pile in Mammoth Cave, Kentucky, USA was first documented by John Wilcox of the Cave Research Foundation in 1971, who marked it as "sandstone breakdown" on the cave map. Palmer et al. (2019) examined the pile, later named Mt. Ararat, and observed large sandstone blocks beneath a solution-weathered limestone ceiling, leading to their hypothesis that the deposit resulted from a major flood event. Subsequent investigation by Bosch et al. (2019) confirmed both the sandstone presence and identified an unsorted, chaotic sediment deposit. The researchers applied the classification system of Bosch & White (2004; 2018) to characterize the formation, identifying it as a diamicton cave deposit - specifically, from a debris flow comprising matrix-supported material ranging from clay to boulder size, lacking bedding or sorting. Comparison with Pierson's (1986) studies of terrestrial and submarine debris flows, which document upstream fine material and downstream coarse material distributions, supported this

interpretation. The sediment distribution and morphology at Mt. Ararat in Mammoth Cave align with these established debris flow patterns.

These debris flow characteristics highlight a fundamental aspect of karstic drainage basins: their subsurface conduit systems can transmit insoluble materials ranging from colloids and clays to boulders, as demonstrated by the Mt. Ararat deposit. Clastic sediments originate from surface streams, land surface materials, and bedrock dissolution residues. These sediments, mixed within the conduit system, lose their source characteristics and are deposited in caves or discharged from karst springs. There are also multiple mechanisms for transport of clastic sediments. Cave deposits provide a useful representation of the types of materials being transported through the aquifer, so it was necessary to develop a means for classifying these deposits.

Given the importance of clastic sediments in contaminant transport, the facies concept of clastic sediments in caves was refined emphasizing their relevance to the storage and transport of certain classes of contaminants, integrating the nomenclature of cave sediment facies with traditional sedimentation terminology, as well as calculating the hydrologic conditions that would have likely been required to produce the observed sediment deposits (BOSCH & WHITE, 2018).

Previous studies (WHITE, 2007; HERMAN et al., 2012) discussed sediment sources, deposits, and transport mechanisms. The facies concept, initially proposed by WHITE & WHITE (1997) and expanded by BOSCH & WHITE (2004), has been useful in describing clastic sediments in various cave systems (e.g., CHESS et al., 2010; FARRANT & SMART, 2011; LABORDA-LÓPEZ et al., 2024; MARTÍNPEREA et al., 2023; PALMER, 2011; PARÉS et al., 2018; VAN HENGSTUM et al., 2011 ; XIE et al., 2013). The system classifies cave sediment deposits into five facies by grain size, sorting, and sedimentary structures: backswamp, channel, diamicton, slackwater, and thalweg (Fig. 1).

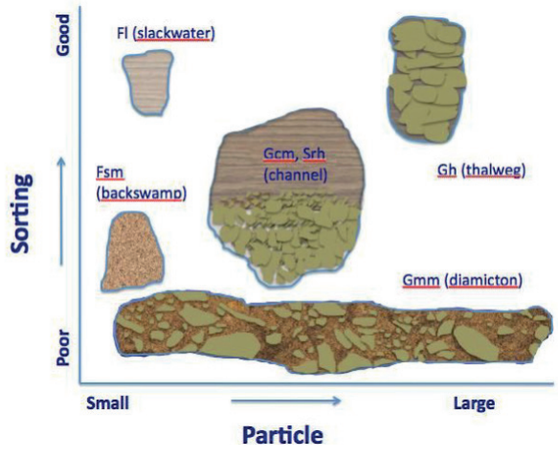

Figure 1: *Qualitative sketch showing the division of cave sediments into facies based on grain size and sorting, including MIALL's (1996) facies codes.*

Debris flow deposits in caves worldwide often provide stratigraphy for anthropological or archaeological studies. Examples include El Sidrón Cave, Spain (SANTAMARÍA et al., 2010), Scladina Cave, Belgium (ABRAMS et al., 2014), and the Great Cave of Niah, Borneo (GILBERTSON et al., 2005). Geological studies, such as those by GILLIESON (1986) and CHESS et al. (2010), describe similar deposits. In a study of a modern event, VAN GUNDY & WHITE (2009) detailed a volume of material that they estimated at 1800 m3 (from before and after measurements of the sediment source area) that was transported completely into, through, and out of Mystic Cave in West Virginia, USA, during the "1985 Potomac Valley flood." The observed sediments that were discovered wedged into crevices in the cave after the storm contained a broad "range of particle sizes with a significant fraction of cobble-sized colluvium." When they divided mean-known discharges during the storm event by the cross-sectional area of smaller conduits in Mystic Cave, they arrived at an estimated water velocity of 5–9 m/s required to move that volume of water through some portions of the cave.

Figure 2: *Head of Mt. Ararat as seen from Big Avenue, standing to the northeast of the deposit. Photo used with permission of the photographer, A. N. PALMER.*

Mt. Ararat is located at the junction of Big Avenue and Noah's Way in the Joppa member of the Ste. Genevieve limestone in Mammoth Cave, Mammoth Cave National Park, Kentucky, USA (Fig. 2). The deposit is about 12–15 m wide with a maximum relief of 7 m and a 75 m long tail that extends into Noah's Way. The grains in this deposit consist of a buff-colored fine- to medium-grained quartz sandstone consistent with descriptions of the Big Clifty sandstone member of the Mississippian Golconda formation, which is stratigraphically about 60 m above the Joppa limestone The smooth ceiling above the deposit indicates the rocks are allochthonous.

Four discrete levels are observed consistently throughout the over four-hundred miles of mapped passage in the Mammoth Cave System and have been labeled A through D by PALMER (1989) with A at about 200 m above mean sea level (amsl), B at 177–186 m amsl, C at 166–167 m amsl, and D at 151–158 m amsl. The passages associated with the Mt. Ararat deposit correlate in elevation with other level C passages. Cosmogenic radionuclide burial dating using 26Al and 10Be to detail the sequence of events resulting in these cave levels (GRANGER et al., 2001) suggests the passage was last active as a cave stream flow route at base level around 1.21 Ma. Sedimentological analyses, terrestrial lidar, and geophysical data were used to deduce the sequence of events leading to the deposition of Mt. Ararat (BOSCH et al, 2021).

1.2. Extension of Sinkhole Plain Development Geochronology

At Mammoth Cave, cave passages that drain to the Green River are connected hydrologically along dipping bedding planes to the cuesta bench of the Dripping Springs Escarpment, which is retreating down dip toward the river. This escarpment is capped by chemically resistant and relatively impermeable sandstone (Fig. 3). The cuesta bench (i.e., the Sinkhole Plain) hosts only dissected, deranged fluvial catchments that each drain to one of thousands of sinkholes connected through karst conduits under the cuesta escarpment to the Green River. Topographic metrics indicate ongoing adjustment of fluvial networks related to incision through folded strata of differing resistance to physical and chemical erosion, and the Ohio River base level is known to be unstable on glacial-interglacial timescales. Multi-level caves often result from periods of base level stability, allowing larger passages to develop near the water table, or from changes in rock solubility as the base level river incises through layered stratigraphy.

Deciphering landscape response to climate-driven or fault-driven incision episodes is challenging in karst areas with dipping and folded rock layers. This study explores the implications of differing erosion rates of cuesta benches, depending on whether they are connected to base level by karst conduits or fluvial channels. Additionally, the concept of alternation between karstic and fluvially dominated landscapes is considered relative to periods of baselevel stability versus incision, or possible dependence upon rock type, structural geology, and landscape preconditioning. The Green River gorge's greater relief adjacent to Mammoth Cave suggests possible drainage capture or fault activity, contributing to greater cuesta dissection. Burial cosmogenic dating, exposure cosmogenic dating, and numerical modeling support this conceptual model and lend insight into landscape evolution of karst landscapes.

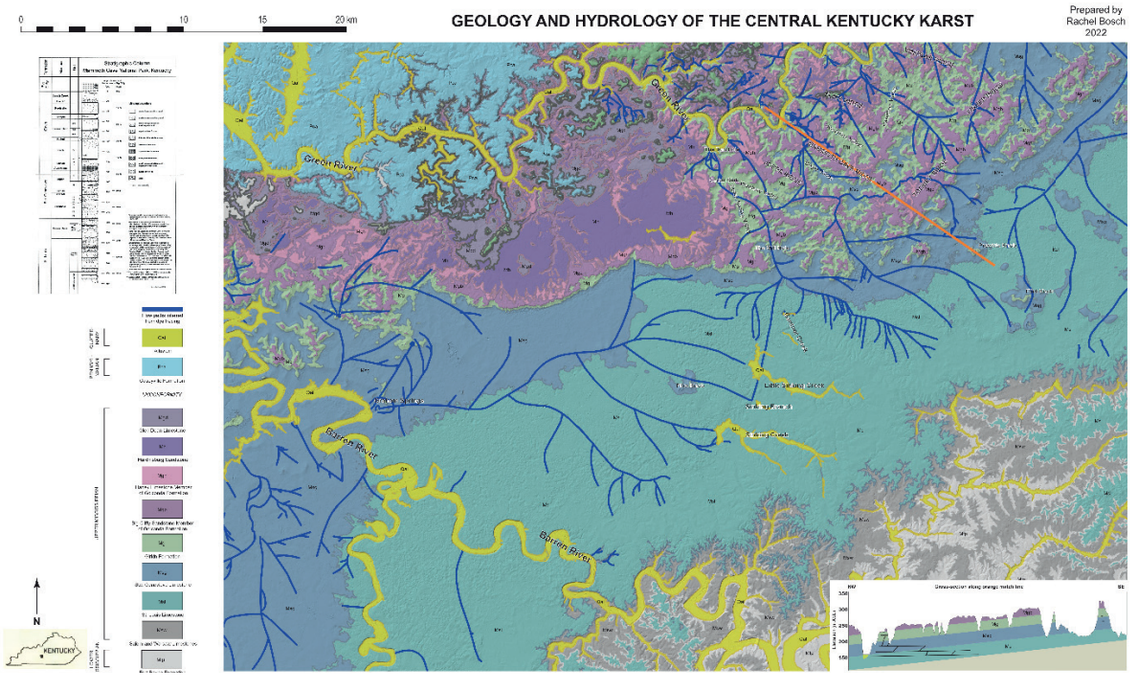

Figure 3: *Hydrogeologic map of the Central Kentucky Karst.*

2. Materials and methods

2.1. Classification of Clastic Sediments in Karst Conduits

The facies classification system for sediment deposits in caves was developed upon extensive field documentation. Caves included in this survey included Rock Spring (Pennsylvania, USA), Tytoona Cave (Pennsylvania, USA), Mystic Cave (West Virginia, USA), Hindman Cave (Pennsylvania, USA), and Columbian Avenue and the Logsdon/Hawkins River area in Mammoth Cave. Flow calculations to support the facies model were performed following the balance of torques method as presented by ALLEN (2012).

2.2. Characterization of an In-Cave Debris Flow Deposit

Methods used in the characterization of the debris-flow deposit, Mt. Ararat, included field observations both in the cave and on the overlying landscape, terrestrial lidar, laboratory and digital sedimentology, electrical resistivity, and digital morphological analyses. A RIEGL VZ-400i was used by surveyors from KCI Technologies to perform four three-dimensional terrestrial lidar scans in the cave. The resulting point clouds were merged to create a high-resolution stereolithography file of the surface of Mt. Ararat. Grain size distribution within Mt. Ararat was determined by dry sieving with a mechanical shaker of three samples from within the deposit combined with grid-square counting using a photograph of an exposed cross section of the deposit. Morphological analysis involved importing the lidar point cloud into CloudCompare to build a digital elevation model (DEM). This DEM was then analyzed in QGIS to extract a longitudinal profile and seven cross-sectional profiles.

2.3. Extension of Sinkhole Plain Development Geochronology

Sediment samples from a deposit inferred to represent channel facies were collected from Crystal Onyx Cave, a knob cave approximately 36 m above the Sinkhole Plain surface in Cave City, Kentucky, USA, and from bank deposits and modern streambed deposits in Little Sinking Creek, Smiths Grove, Kentucky, USA. These samples were submitted to the Purdue Rare Isotope Measurement Laboratory (PRIME Lab), Purdue University, Indiana, USA, for analysis of the cosmogenic nuclides 26Al and 10Be. A numerical model developed in Matlab by Ward (WARD & BOSCH, 2024) tracks the dip projection of base level to the surface, the position of the cuesta escarpment, and the expected length of conduit development during stable base level periods across a series of incision and stability periods. As the base level river lowers in the model, the fluvially connected cuesta bench lowers at the same rate, and the cuesta escarpment retreats toward the river. If the base level remains stable long enough, growing karst conduits break through, creating efficient subsurface drainage of the bench. At this point, the model's erosion rate on the bench decreases as surface streams become disconnected from each other and from the base level. Given a sufficiently long period of incision, it is assumed that the fluvial network recaptures the karst plateau through knickpoint propagation, and erosion rates on the bench catch up with base level lowering.

3. Results

3.1. Characterization of an In-Cave Debris Flow Deposit

During surface field investigation above the passage that contains Mt. Ararat, a sinkhole was found at about 140 m south-southwest from a metal bore hole that penetrates into the passage; it was dry at that time and is indicative of the closest modern place for water to enter that area of the cave. An entrance point for debris deposition over one million years ago may have looked somewhat like this but at 2–7 m higher in elevation. Results from sediment grain-size analysis revealed a maximum grain size of 100 cm and a D50 for the entire grain-size distribution of about 20 cm. Results from electrical resistivity to determine the depth of the subsurface portion of the deposit indicated three subsurface material layers: human-built trail material from 0 m to 0.25 m below ground surface (bgs), sand and boulders (interpreted as debris flow deposit) from 0.25 m to 0.75 m bgs, and vuggy/fractured limestone from 0.75 m to over 4.5 m bgs. Morphological analysis of the lidar data indicated two main peaks along the ridge of Mt. Ararat: one 7 m tall at the downstream end and the other at 4 m tall, 35 m upstream from the taller peak. The DEM and profiles of Mt. Ararat are included in Figure 4.

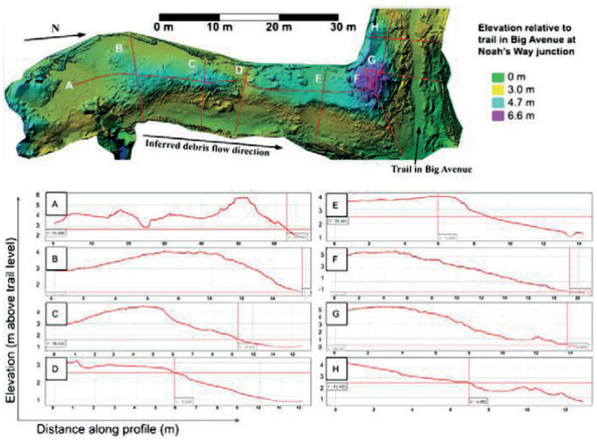

Figure 4: *DEM of Mt. Ararat with longitudinal profile (A) and cross-sectional profiles (B-H).*

3.2. Extension of Sinkhole Plain Development Geochronology

WHITE (2009) and KAUFMAN & BRAUN (2201 suggest similar efficiencies of fluvial and karst denudation in the same drainage basin over long timescales, but base level changes and other disequilibrium processes may introduce lags in the response of different parts of the landscape. Recent cosmogenic data for the Central Kentucky Karst suggest a reduced lowering rate for the Sinkhole Plain relative to the incision of the Green River. Results of 26Al/10Be paired cosmogenic dating of cave-buried sediments from Crystal Onyx Cave reported a burial age of about 5.1 million years (My). This is consistent with the chronology for Mammoth Cave established by GRANGER et al. (2001). From this, we calculate a lowering rate for the Sinkhole Plain at 36 m / 5.1 My, equal to 7 m/My. Results of 10Be cosmogenic erosion rate for stream sediments from Little Sinking Creek indicate a basin-average erosion rate of about 4.4 – 4.6 m/My, which is consistent with an approximate 7 m/My longer-term denudation of the Sinkhole Plain.

The numerical model results for cuesta distance from the river, cave conduit length, and depth of erosion for the base level river and the cuesta bench vary depending on the input interval of incision and stasis periods:

- Regular intervals of incision and stasis produce constant conduit growth in each interval;
- Random intervals with a similar distribution of stasis and incision periods result in similar behavior to regular intervals, but with relatively quicker karst capture of the bench; and
- Random intervals with stasis periods that are longer than incision periods result in a similar capture time but with different relative erosional dynamics. This conditions best simulates a pattern of discrete conduits which more realistically reflect field conditions observed in the Central Kentucky Karst.

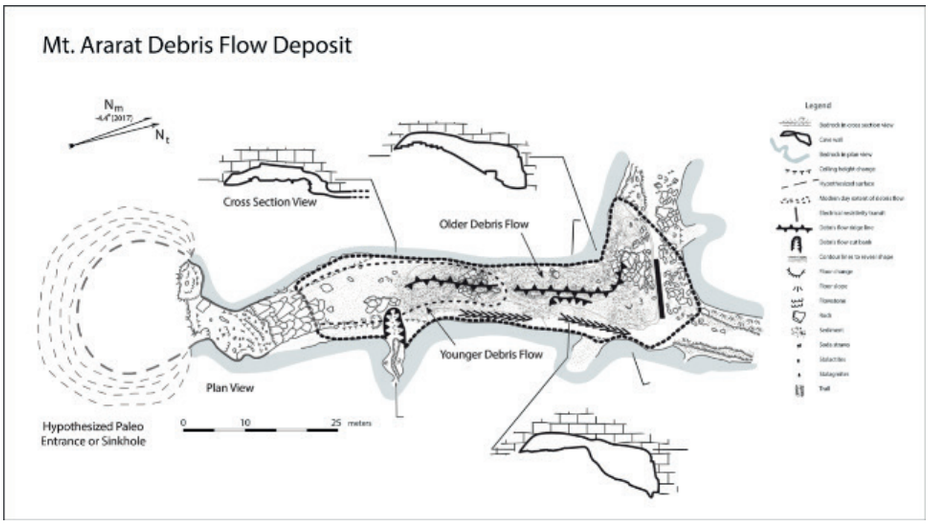

Figure 5: *Geomorphological map of Mt. Ararat.*

4. Discussion

4.1. Characterization of an In-Cave Debris Flow Deposit

Development of the facies concept of cave sediment classification has enabled many recent advances in karst geomorphology. Regarding the characterization of an in-cave debris flow depot, the evidence supports the hypothesis of sandstone-floored-pond collapse(s) or valley-wall landslide(s) that initiated two debris flow surges into a now-obscured sinkhole entrance in the paleo Doyle Valley floor releasing a total more than 3800 m3 of material into the cave system. The sediment was deposited taking the form of Mt. Ararat with most of the material coming to rest at the junction of Noah's Way and Big Avenue, and a secondary volume of material coming to rest on top of the tail of the first debris flow. Material was partially eroded from the eastern side via a north-flowing stream either after or between the two deposition events, and later down a steep side passage (Fig. 5).

4.2. Extension of Sinkhole Plain Development Geochronology

Concerning the extension of Sinkhole Plain development geochronology, the cosmogenic burial date for Crystal Onyx Cave plotted with the GRANGER et al. data (2001) yields an estimated 25 m/My long-term average Green River incision rate (Fig 6). This is significantly more rapid than the long-term estimated Sinkhole Plain denudation rate of 7 m/My or the more recent basin-average erosion rate of ~ 4.5 m/My. These differing rates are consistent with the results of an idealized numerical model which assumes that at the time of karst capture of the cuesta bench, the erosion rate of the Sinkhole Plain would have slowed dramatically with respect to the Green River (Fig. 7).

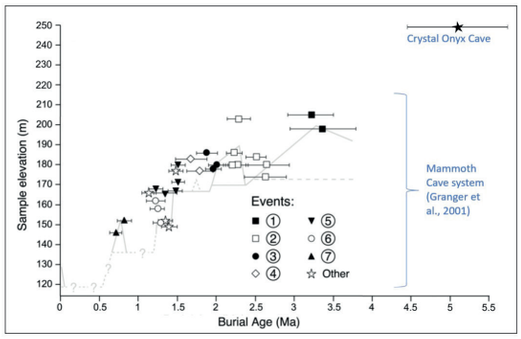

***Figure 6**: Crystal Onyx Cave burial data (WARD & BOSCH, 2024) plotted with Mammoth Cave system data from GRANGER et al. (2001).*

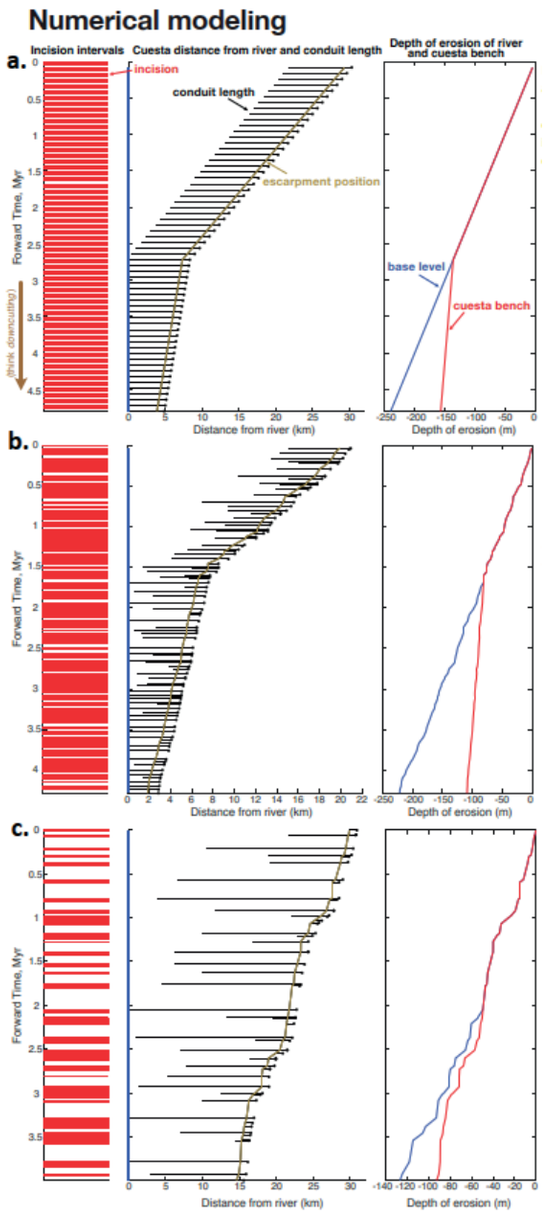

***Figure 7**: Numerical modeling results: a) regular intervals of incision, b) random intervals, stasis ~= incision, c) random intervals, stasis > incision.*

5. Conclusion

This research advances understanding of both clastic sediment dynamics and karst landscape evolution through two complementary applications. The facies classification system enabled detailed characterization of the Mt. Ararat debris flow deposit while also supporting enhanced geochronological analysis of the Mammoth Cave area. Beyond these specific cases, the classification system provides a framework for studying contaminant transport and geomorphic processes in karst systems worldwide. This systematic approach to analyzing cave sediments strengthens our ability to interpret the complex interactions between surface and subsurface processes in karst landscapes.

References

ABRAMS, G., BELLO, S.M., DI MODICA, K., PIRSON, S., BONJEAN, D. (2014). When Neanderthals used cave bear (Ursus spelaeus) remains: Bone retouchers from Unit 5 of Scladina Cave (Belgium): Quaternary International, v. 326, p. 274–287.

ALLEN, J. R. (2012). Principles of physical sedimentology. Springer Science & Business Media.

BOSCH, R., WARD, D., BIRD, A., STURMER, D., OLSON, R. (2021). A DEBRIS FLOW DEPOSIT IN MAMMOTH CAVE: FIELD CHARACTERIZATION. Journal of Cave and Karst Studies, 151.

BOSCH, R. F., WHITE, W. B. (2004). Lithofacies and transport of clastic sediments in karstic aquifers. In Studies of cave sediments: Physical and chemical records of paleoclimate (pp. 1-22). Boston, MA: Springer US.

BOSCH, R. F., WHITE, W. B. (2018). Lithofacies and transport for clastic sediments in karst conduits. In Karst Groundwater Contamination and Public Health: Beyond Case Studies (pp. 277-281). Springer International Publishing.

CHESS, D.L., C.A. CHESS, I.D. SASOWSKY, V.A. SCHMIDT, W.B. WHITE. (2010). Clastic sediments in the Butler Cave-Sinking Creek System, Virginia, USA. Acta carsologica 39: 11-26.

FARRANT, A. R., SMART, P. L. (2011). Role of sediment in speleogenesis; sedimentation and paragenesis. Geomorphology, 134(1-2), 79-93.

GILBERTSON, D., BIRD, M., HUNT, C., MCLAREN, S., BANDA, R.M., PYATT, B., ROSE, J. STEPHENS, M., (2005). Past human activity and geomorphological change in a guano-rich tropical cave mouth: Initial Interpretations of the Late Quaternary Succession in the Great Cave of Niah, Sarawak: Asian Perspectives, p. 16–41.

GILLIESON, D. (1986). Cave sedimentation in the New Guinea Highlands: Earth Surface Processes and Landforms, v.11, no. 5, p. 533–543.

GRANGER, D.E., FABEL, D., PALMER, A.N. (2001). Pliocene- Pleistocene incision of the Green River, Kentucky, determined from radioactive decay of Cosmogenic 26Al and 10Be in Mammoth Cave sediments: Geological Society of America Bulletin, v. 113, no. 7, p. 825–836.

HERMAN, E.K., TORAN, L., WHITE, W.B. (2012). Clastic sediment transport and storage in fluviokarst aquifers: an essential component of karst hydrogeology. Carbonates and Evaporites 27: 211-241.

KAUFMANN, G., BRAUN, J. (2001). Modelling karst denudation on a synthetic landscape: Terra Nova, v. 13, p. 313–320.

LABORDA-LÓPEZ, C., MARTÍN-PEREA, D.M., DEL CASTILLO, E., LINARES, M.A.A., IANNICELLI, C., PAL, S., ARROYO, X., AGUSTÍ, J., PIÑERO, P. (2024). Sedimentological evolution of the Quibas site: High-resolution glacial/interglacial dynamics in a terrestrial pre-Jaramillo to post-Jaramillo sequence from southern Iberian Peninsula. Quaternary International, 692, 28-44.

MARTÍN-PEREA, D. M., MAÍLLO-FERNÁNDEZ, J. M., MARÍN, J., ARROYO, X., & ASIAÍN, R. (2023). A step back to move forward: a geological re-evaluation of the El Castillo Cave Middle Palaeolithic lithostratigraphic units (Cantabria, northern Iberia). Journal of Quaternary Science, 38(2), 221-234.

MIALL, A.D. (1996). The geology of fluvial deposits. 582. Berlin: Springer Verlag.

PALMER, A.N. (1989). Geomorphic history of the Mammoth Cave System, in Karst Hydrology: Springer, p. 317–337.

PALMER, A. N. (2011). Distinction between epigenic and hypogenic maze caves. Geomorphology, 134(1-2), 9-22.

PALMER, A.N., OLSON, R., PALMER, M.V., (2019). Evidence for extreme floods in New Discovery and related passages in Mammoth Cave: Cave Research Foundation Newsletter, v. 47, no. 2, p. 3–6.

PARÉS, J.M., ÁLVAREZ, C., SIER, M., MORENO, D., DUVAL, M., WOODHEAD, J.D., ORTEGA, A.I., CAMPAÑA, I., ROSELL, J., DE CASTRO, J.B., CARBONELL, E. (2018). Chronology of the cave interior sediments at Gran Dolina archaeological site, Atapuerca (Spain). Quaternary Science Reviews, 186, 1-16.

PIERSON, T. C., (1986), Flow behavior of channelized debris flows, Mount St. Helens, Washington: in Hillslope Processes, Abrahams A.D. (ed.). Allen and Unwin: Boston; p. 269–296.

SANTAMARÍA, D., FORTEA, J., DE LA RASILLA, M., MARTINEZ, L., MARTINEZ, E., CAÑAVERAS, J.C., SÁNCHEZ-MORAL, S., (2010). The Technological and typological behaviour of a Neanderthal group from El Sidrón Cave (Asturias, Spain): Oxford Journal of Archaeology, v. 29, no. 2, p. 119–148.

VAN GUNDY, J.J., WHITE, W.B. (2009). Sediment flushing in Mystic Cave, West Virginia, USA, in response to the 1985 Potomac Valley Flood: International Journal of Speleology, v. 38, no. 2, p. 103–109.

VAN HENGSTUM, P. J., SCOTT, D. B., GRÖCKE, D. R., & CHARETTE, M. A. (2011). Sea level controls sedimentation and environments in coastal caves and sinkholes. Marine Geology, 286(1-4), 35-50.

WARD, D.J., BOSCH, R.F. (2024). An (over-) simplified model of sinkhole plain development near multistory cave systems in dipping rocks.

WHITE, W.B., WHITE, E.L. 1997. Storm pulses, thresholds, and fluid mechanics in the transport of clastic sediments in limestone aquifers. La Chaux de Fonds, Switzerland: Proceedings of the 12th International Congress of Speleology 2: 191-194.

WHITE, W.B. (2007). Cave sediments and paleoclimate. Journal of Cave and Karst Studies. 69: 76-93.

WHITE, W.B. (2009). The evolution of Appalachian fluviokarst: Journal of Cave and Karst Studies, p. 159–167.

WILCOX, J., (1971). New Discovery, Mammoth Cave, Mammoth Cave National Park, Kentucky: Cave Research Foundation, 1 sheet.

XIE, S., EVERSHED, R.P., HUANG, X., ZHU, Z., PANCOST, R.D., MEYERS, P.A., GONG, L., HU, C., HUANG, J., ZHANG, S., GU, Y. (2013). Concordant monsoon-driven postglacial hydrological changes in peat and stalagmite records and their impacts on prehistoric cultures in central China. Geology, 41(8), 827-83.

First evidence of ghost-rock in Botswana: their potential for ancient hominins research

Laurent Bruxelles (1), Oaitse Ledimo (2), Gregory Dandurand (1, 3) & Bastien Chadelle (1)

(1) TRACES, CNRS, University of Toulouse Jean Jaurès, 5 allées Antonio Machado, 31058 Toulouse, France. Laurent.bruxelles@cns.fr (corresponding author)

(2) Botswana National Museum, 161 Queens road, Gaborone, France

(3) INRAP, Rue de la République, 86000 Poitiers, France

Abstract

The geomorphological study of the fossiliferous area of the "Cradle of Humankind" in South Africa showed that the karst caves in which hominins (Australopithecus, Paranthropus and Homo) were discovered, resulted from emptying alterite residue of ghost-rock. For the first time, similar type of karstification was identified in Botswana, in on-going studies on caves paleontology and archaeology. Beyond considering it as another type of karstification, it appears that karst caves formed by ghost-rock process are favorable for trapping and preserving ancient hominin fossils, enabling us to focus our research in similar geological context of other countries located in Southern Africa.

Résumé

L'étude géomorphologique de l'aire fossilifère du « Berceau de l'Humanité » en Afrique du Sud a montré que les cavités karstiques dans lesquelles les hominines (Australopithecus, Paranthropus et Homo) ont été découvert découlent de la vidange de fantômes de roche. Pour la première fois, le même type de karstification vient d'être identifié au Botswana, dans des cavités que nous étudions et qui livrent leurs premiers fossiles. Plus que les autres types de karstification, il apparaît les cavités formées par fantômisation sont favorables au piégeage et à la conservation de fossiles anciens, ce qui permet d'orienter nos recherches dans les autres pays d'Afrique australe.

Resumen

El estudio geomorfológico de la zona fosilífera de la «Cuna de la Humanidad» en Sudáfrica ha demostrado que las cavidades kársticas en las que se descubrieron los homínidos (Australopithecus, Paranthropus y Homo) eran el resultado del vaciado de fantasmas de roca. Por primera vez, se acaba de identificar el mismo tipo de karstificación en Botsuana, en cavidades que estamos estudiando y que están dando sus primeros fósiles. Más que otros tipos de karstificación, parece que las cavidades formadas por fantasmas de rocas son favorables para atrapar y conservar fósiles antiguos, lo que significa que podemos orientar nuestras investigaciones hacia otros países del sur de África.

1. Introduction

For nearly twenty years now, the detailed study of the karst of the Cradle of Humankind (South Africa) led us to question the origin of the caves. A better knowledge of their genesis and evolution help us to understand the functioning of these caves as traps during several millions of years. Such geomorphological research can also provide some evidences for the exploration of new hominin sites at the scale of a larger region, such as Southern Africa. Therefore, the detailed exploration of the Sterkfontein cave as well as fifty surrounding caves allowed us to identify some of the most demonstrative examples of ghost-rock karst, known to date. In the framework of the "Hominins in Botswana: karst research project" we are leading, caves in the North Western part of Botswana are explored and studied, in collaboration with the team of the Botswana National Museum. This research brings additional evidences about the origin of these caves. Alike the cave of the Cradle of Humankind in South Africa (Bruxelles, 2017), the studied cave sites can be attributed to ghost-rock karstification.

2. Material and methods

The search for ancient hominin fossils, covering the period between 4 and 1 million years ago, in the Ngamiland region NW of Botswana, led us to prospect several groups of low karstic hills: i) the Aha Hills, ii) the Gcwihaba Hills and iii) the Koanaka Hills. Such sites form a series of marble and dolomite patches in the Kalahari landscape

Although located on karstic hills, the studied caves do not all have similar features. We distinguish two types of caves: i) vertical shafts in the Aha Hills (Whaxhu North and South caves) and ii) horizontal maze cave in both Gcwihaba and Koanaka hills.

In these last two hills, some of the caves (e.g. Gcwihaba, !Wadoum, Bones and Blue caves) have natural entrances whereas others (e.g. Deviners, Mongongo, Gecko, Dimapo caves) are only accessible through boreholes, mined specifically to reach voids detected by gravimetry (Ellis, 2000). The core of Gcwihaba and Koanaka hills revealed a dense network of interconnected underground galleries and chambers, developed at ~30-40 m depth (Fig. 2). The water base level is nearly 100 meters below

the surface but no cave reaches this base level at the moment. In order to precise the origin and evolution of the studied caves, much focus was given to organization of the cave conduits, the morphology, the detrital fillings as well as the cave morphological and infill link with the landscape.

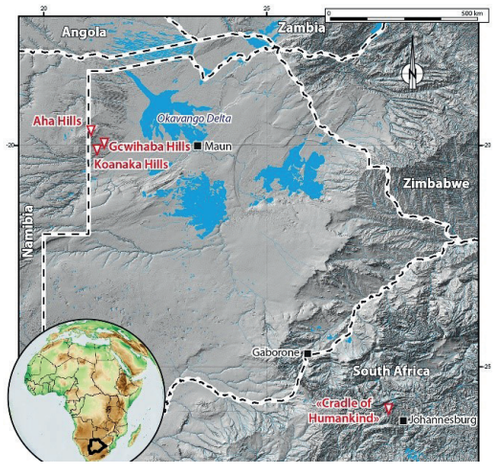

Figure 1: *Location of the studied areas: Cradle of Humankind in South Africa, Gcwihaba, Koanaka and Aha hills in Botswana (Bastien Chadelle).*

3. Results

Regarding the organization of karst networks, the studied caves are genuine three-dimensional mazes of galleries, spanning several kilometers of conduits (Fig. 2). No clear hydrological structuration is discernible. Field observation indicate that every fracture was exploited by dissolution. Therefore, it is not possible to determine a direction of the underground flow, an organization or a hierarchy of hydrogeological circulations.

Regarding the shape of the walls, two types of morphology can be distinguished: i) caves that are naturally open are marked by a strong biocorrosion phenomena due to the presence of large colonies of bats (Dandurand, 2019). The walls have been extensively corroded and show softened shapes, hollowed out with conches and niches. The cave ceilings are covered with biogenic cupolas; ii) In artificially opened caves, the walls and ceilings are highly irregular with a very rough surface. The soluble parts of the bedding have been dissolved, while the less soluble strata, often reinforced by fine silica partitions, are exposed in relief. The walls and ceiling are bristling with needles and silica sheets. It is noticeable that no classic (phreatic, epiphreatic, paragenetic or even hypogenic) forms of karstification is present.

We identified three types of infill within these networks:

I. In the areas deep in the caves, far from the surface and unaffected by biocorrosion, a black and sometimes grey to reddish sandy formation (Fig. 3A), composed of iron, manganese, and fragments of silica and needles (Fig. B & C). Subsidence reveals that this infill can exceed 10 m thick (Fig. 3D). Except in collapsed zones or areas where calcite flowstones precipitated, such formation cover the entire floor of the galleries (Fig. 3 A & B). This black sandy formation also covers all horizontal surfaces, morphologies and even the bottom of small lateral galleries, regardless of their size (Fig. 3B & C).

II. In areas close to the surface, the presence of orange quartz sand infill is dominant, contrast with the previous formations. Such sediment is aeolian sand (Kalahari sand), indicating an outer connection between the gallery and the hillside slope. This intrusive sand indicates the intersection of the underground gallery by the hillside, which has been regularly dusted for several thousands of years.

III. In areas, where the cave has been intersected by the topographical surface for a long time, a breccia infill from 1 to 10 m thick, can be observed. These are composed of clasts, gravel, and sand embedded in a silty matrix and cemented by calcite. The presence of bones, as found in Gcwihaba or Bones Caves, clearly shows the connection to the surface, sometimes for several million years, as is the case in the Cradle of Humankind in South Africa (Granger et al., 2015 & 2022).

As these entrances were accidentally cut by the surface, they have no functional link with the present-day landscape, which shows not a single karst feature.

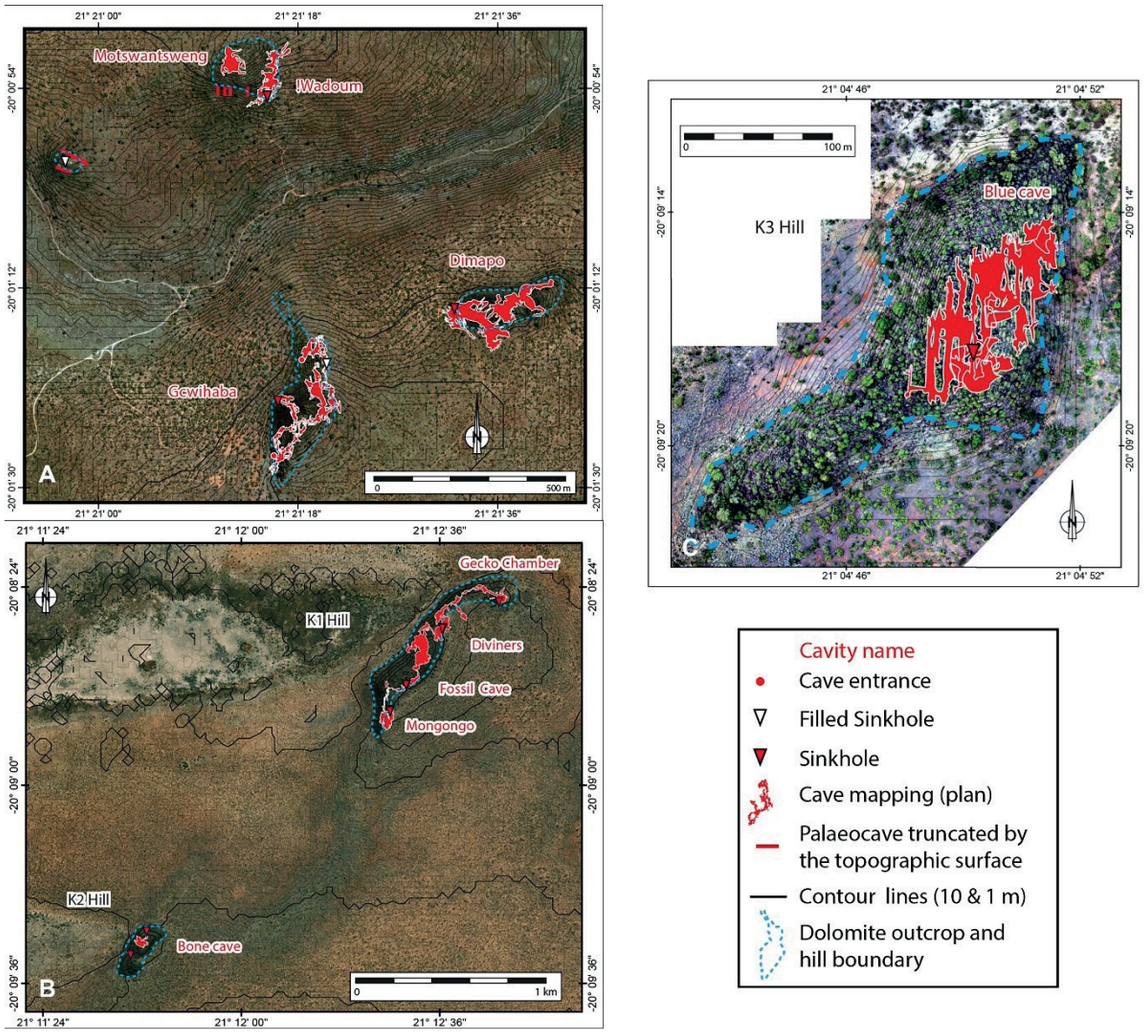

Figure 2: *Report of the main cave under Gcwihaba (A), Koanaka 1 & 2 (B) and Koanaka 3 (C) Hills. One can notice the huge density of galleries under these small dolomitic outcrops (Bastien Chadelle).*

4. Discussion

All these observational characteristics are comparable to the cave sites studied in the Cradle of Humankind. The genesis of latter site was attributed to ghost rock processes (Dubois et al., 2014; Bruxelles et al., 2017). Such processes result in maze caves with no network organization, no water flow features, and no connection with the landscape.

The most demonstrative element in our fieldwork observation and laboratory analysis is the presence of a high amount of black to reddish soft infill at the bottom-end of the studied caves. Made solely of iron and manganese, this dark accumulation contains a significant number of spines or thin sheets of silica, that were originally embedded in the dolomite bedrock. In this infill, no sedimentary structuring is noticeable that would indicate infill deposition by water or grain sorting. Such detrital cave formation was first described as “Wad” (Buttrick, 1986) in the Sterkfontein caves (Martini, 2003), and later identified as ghost rock in the same cave (Bruxelles et al., 2017). These black accumulations correspond to the previous descriptions and can be considered as the collapse of the initial ghost rock that occupied the entire cave site. Since the alterite was highly porous (up to 70%), the collapse of the porosity alone is sufficient to create a void between its top and the cave roof (Fig. 3). Such material can be later washed out by water, which explains why it is so rare to observe such quantities of ghost rock remnants in other geological contexts.

The dolomitic marbles of the Precambrian (800-600 Ma) consist of over 6,000 m of limestone and dolomitic strata (e.g. Damara formation), interspersed with limestone beds. Tectonic folding caused by the Pan-African orogenesis, between 800-900 Ma and 460 Ma, affected the carbonate beds and resulted in a dense network of fractures and faults. They allowed for very slow groundwater circulation, which in turn favored the chemical alteration of the bedrock.

In the dolomites, the particular ghost-rock speleogenesis occurred in two stages, instead of following a classical process (Quinif, 1999):

1- Frist stage: over millions of years, slow water circulation facilitated the weathering of the dolomite along open cracks, faults, and joints. However, the flow was not powerful enough to remove the residual alterite composed of insoluble iron, manganese and silica initially present in the bedrock. This led to the formation of a very porous alterite, organized as a 3D maze, mirroring the original tectonic and lithological pattern. When the water base-level dropped, associated with the evolution of the Okavango fluvial Delta, the alterite gradually emerged from the aquifer. Due to its high porosity (up to 70% void space according to Dubois et al., 2014), the alterite collapsed on itself. Such genesis explains the presence of black deposit on every horizontal surface as well as on the cave ground floor (Fig. 3).

It is the first time we observe such an abundant and well-preserved amount of ghost-rock in caves, as if nothing had changed since it collapsed in on itself. This is also due to the fact that no water flow occured in such arid area to wash away this soft and fragile alterite. However, in some places, the collapsed alterite has been flushed out and sinkholes of more than 10 m deep can be seen, such as in the Grand Canyon of Deviners Cave (Fig. 3D). Such setting allowed us to estimate the thickness of this dark to reddish infill and evaluate how much dolomite was affected by this process.

2-Second stage: when the cave is intersected by the topographical surface, the walls are reshaped by water dripping, condensation corrosion, and most of the ghost-rock disappears. In caves where bats live, the effect is even more pronounced, as the walls retreat significantly due to biocorrosion. However, in some places, such as in Gcwihaba Cave, remnants of in situ ghost-rock are still visible, providing evidence that this process was also at the origin of the cave's formation.

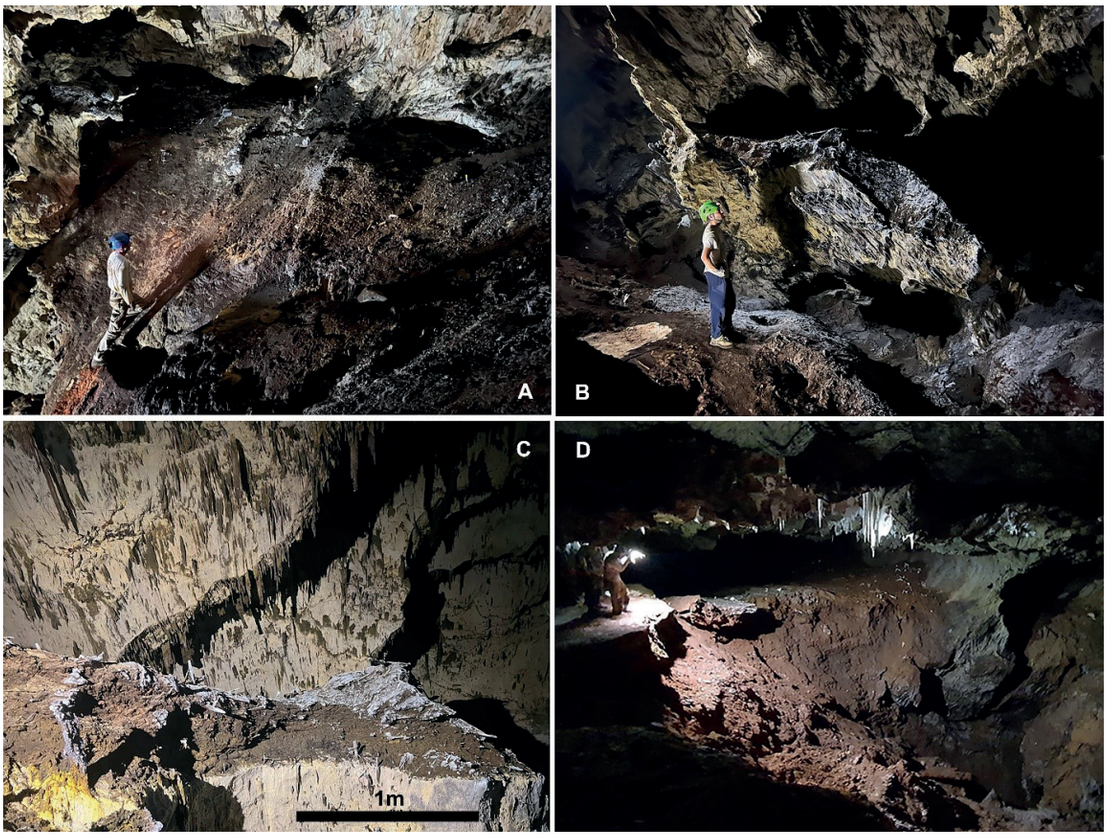

Figure 3: *Ghost rocks remnants and specific features. A: Collapsed ghost rock filling the bottom of Dimapo cave (Laurent Bruxelles). B: Collapsed ghost rock on the soil and the shelves of Dimapo cave, below silica spines and sheets (Laurent Bruxelles). C: Another example of remnant of collapsed ghost-rock on a horizontal surface (Laurent Bruxelles). D: De-clogging of ghost rock in Deviners cave (Grand Canyon) showing its thickness (Carole Bruxelles).*

5. Conclusion:

In these particular caves, we identified some of the most spectacular examples of ghost-rock speleogenesis. This geological phenomenon was previously unknown in Botswana. For the very first time, following the example of studies previously conducted in South-Africa, we were able to demonstrate the role of ghost-rock in the genesis of caves in Botswana.

Beyond its contribution to speleogenesis, the study of these caves revealed the significance of ghost-rock processes for the trapping and preservation of fossils of several million years old. In South-Africa, the density of voids due to dense maze cave network and their successive alterite erosional removal when the regional water base-level dropped, explains the presence of a large number of sites covering more than 4 million years of fossil records. Moreover, the absence of hydrogeological circulations limits the reworking or draining of infills under the surface openings and permits a good preservation of the fossil bearing deposits. These types of karsts represent a prime target for the research we are conducting in Southern Africa, and their discovery in Botswana is a very encouraging sign for our studies. This model can now be extended to other karsts in the region, and other ghost-rocks are now identified in Namibia, Zimbabwe, and Zambia. Such findings open up new research perspectives for more targeted fossil site exploration that could help documenting the history of our origins in Africa.

6. Ackowledgements:

We would like to thank the CNRS for its financial support in the framework of the Joint Research Program Homini'karst and the MITI for Bastien Chadelle PhD fundings. We also extend our thanks to the teams at the Botswana National Museum who are participating in this research, as well as to the French Embassy in Botswana for its support.

Bibliography:

BRUXELLES L. (2017) Des fantômes et des hommes. Le rôle de la fantômisation dans la formation des karsts à australopithèques d'Afrique du Sud. Karstologia n°69, p.1-8.

BUTTRICK D.B. (1986) «Wad» and Ferroan soil developed in the dolomitic area south of Pretoria, Master of Science in the Faculty of Science, University of Pretoria, 158 p.

DANDURAND G., DURANTHON F., JARRY M. et STRATFORD D., BRUXELLES L. (2019) Biogenic corrosion of bats in Drotsky's Cave, Gcwihaba Hills, NW Botswana. – Geomorphology, 327, p. 284-296.

DUBOIS C., QUINIF Y, BAELE J.-M., BARRIQUAND L., BINI A, BRUXELLES L., DANDURAND G., HAVRON C., KAUFMANN O., LANS B., MAIRE R., MARIN J., RODET J., ROWBERRY M., TOGNINI P. et VERGARI A. (2014) The process of ghost-rock karstification and its role in the formation of caves. Earth-Science Reviews, n° 131, 02/2014, p. 116-148.

ELLIS R. J. (2000) Gcwihaba caves park management plan 2020. Cave development, conservation and management. A further contribution to the development and management of the caves of the Gcwihaba and Koanaka Hills. SpeleoPro (Pty) Ltd. 83 p.

GRANGER D., GIBBON R., CLARKE R., KUMAN K., BRUXELLES L. et CAFFE M. (2015) Cosmogenic burial ages for Australopithecus StW 573 and the Oldowan Infill at Sterkfontein, Nature, n°522, p. 85-88, DOI: 10.1038/nature14268.

GRANGER D. E., STRATFORD D., BRUXELLES L., GIBBON R. J., CLARKE R., J. & KUMAN K. (2022) Cosmogenic nuclide dating of Australopithecus at Sterkfontein, South Africa. – PNAS, vol. 119, n°27.

MARTINI J.E.J., WIPPLINGER P.E., MOEN H.F.G. and KEYSER A., (2003) Contribution to the speleology of Sterkfontein Cave, Gauteng Province, South Africa. International Journal of Speleology, n° 32 (1/4), 2003, p. 43-69.

QUINIF Y. (1999) Fantômisation, cryptoaltération et altération sur roche nue, le tryptique de la karstification. Actes du colloque européen Karst-99, p. 159-164.

Unroofed caves in the Vena del Gesso romagnola area (N-Italy): distribution and age

Veronica Chiarini (1), Federico Guerra (2), Giovanni Sangiorgi (3), Luca Pisani (4), Jo De Waele*

(1) Department of Geosciences, University of Padua, Via G. Gradenigo 6, 35131 Padova, Italy, veronica.chiarini3@gmail.com
(2) BiGeA, University of Bologna, Italy, federico.guerra6@studio.unibo.it
(3) BiGeA, University of Bologna, Italy, giovanni.sangiorgi4@studio.unibo.it
(4) Centro di Documentazione Speleologica "F. Anelli", Bologna, Italy, biblioteca.speleologia@unibo.it
(5) BiGeA, University of Bologna, Italy, jo.dewaele@unibo.it (corresponding author)

Abstract

The Vena del Gesso romagnola area is composed of Messinian gypsum outcrops running in a W-NW/E-SE direction over a length of 20 km along the northern margin of the Apennines, ca. 30 km SE of Bologna (N-Italy). This ridge, sticking out of the clayey and marly landscape, hosts around 300 karst caves explored and surveyed for a total development of over 48 km. Field work carried out in the framework of the EvolGyps Project, funded by the Federazione Speleologica Regionale dell'Emilia-Romagna (FSRER) and aiming at understanding landscape evolution and the intimate connection between cave systems and fluvial networks, attested the presence of many calcite speleothems scattered in the woods, especially in some areas of the northern slopes of the gypsum outcrop. These flowstones are what is left of ancient gypsum caves, now completely eroded. Detailed fieldwork allowed to map these cave remnants, through the identification of speleothem distribution, morphological evidences (e.g, traces of cave galleries), and outcrops of cave sediments. Dating of the oldest flowstones of the surveyed area delivered ages between 312 ± 5.6 and 399 ± 15 ka, showing some of these unroofed caves to have formed during the cold stages of MIS 10 and 12.

1. Introduction: what is speleology?

The Emilia-Romagna region, in northern Italy, is known for the presence of important evaporite karst areas hosted in both Triassic (Upper Secchia Valley) and Messinian gypsum outcrops. These areas, studied from a geological, geomorphological, naturalistic, archaeological and historical standpoint since the 16th century, have been recognised as UNESCO World Heritage Site in September 2023 (Evaporitic Karst and Caves of Northern Apennines, EKCNA, site 1692), and are the world's only evaporite karst area on this list.

One of the main gypsum outcrops of EKCNA serial site is the Vena del Gesso romagnola, a Regional Park located about 12 km SW of the cities of Imola and Faenza (Fig. 1). This elongated gypsum ridge forms a hogback, extending for over 20 km in a W-NW/E-SE direction and with an average width of about 1 km, with the gypsum beds dipping toward the NE (the Po Plain). This karst area hosts around 300 natural caves with a total explored and surveyed length of more than 48 km.

During field surveys carried out in the framework of the EvolGyps Project, sponsored by the regional cave federation (FSRER), many calcite speleothems were found on the forest floors in some specific areas, often at the higher altitudes of the northern slopes (CHIARINI et al., 2024). These speleothems (mainly flowstones) have survived erosion and dissolution, whereas the original gypsum caves that hosted them have almost completely disappeared.

These flowstone fragments, some being close to 400 ka old, are often concentrated in single spots (as showing the intersection of vertical cave fragments, i.e. shafts), or are distributed linearly, probably along ancient sub-horizontal cave passages. The aim of this study is to map and characterise these unroofed caves, and put them in the framework of the known cave systems and the karst evolution over the past 600 kyrs. As a first step, only the central portion of the gypsum outcrop (Cà Monti area) between the Senio and Sintria rivers has been investigated.

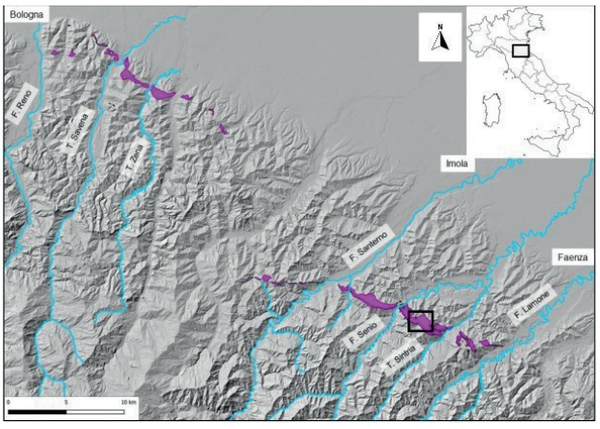

Figure 1: *The main gypsum outcrops (in violet) and the study area (black box).*

2. Materials and methods

The first speleothems collected and dated were those taken in the period 2014-2016, during a study on the evolution of Re Tiberio Cave, a multi-level cave system that clearly recorded a climate-driven river incision and aggradation of the nearby Senio River (COLUMBU et al.,

2015). Further investigations during those years allowed to find several old speleothems in the summit areas near Mt. Mauro and brought COLUMBU et al. (2017) to build a model explaining the evolution of gypsum caves in the Vena del Gesso area in relation to late Quaternary climate oscillations.

Further field surveys were carried out during the EvolGyps Project, in the 2021-2023 period. Although the aim of EvolGyps was to reconstruct both cave and landscape evolution using cave levels, river terraces, and their chronological determination, flowstone fragments scattered at the surface were also collected and dated.

The uranium-thorium (U-Th) dating of speleothems was carried out at the School of Earth Sciences at University of Melbourne in the years 2014-2016, and at the National Taiwan University, in the Research Center for Future Earth for the samples taken between 2021 and 2023. Subsamples (ca. 100 mg) to be used for analysis were obtained using a Dremel drill with a 1 mm-diameter drillbit. Each sample was dissolved in ultrapure HNO3, and then subjected to cyclic washing through ion exchange resin columns to physically-chemically separate uranium (U) and thorium (Th) from the carbonate matrix. This U-Th compound was then analysed, after mixing with a standard with a known composition of 229Th/233U/236U and drying for 12 hours on a plate at 80 °C. Compounds were analysed using a multi-collector inductively coupled plasma mass spectrometer (MC-ICP-MS). Analytical errors were 2s of the mean. [238U] = [235U] x 137.818 (±0.65‰) (HIESS et al., 2012). Decay constants used were 9.1705 × 10-6 yr-1 for 230Th, 2.8221 x 10-6 yr-1 for 234U (CHENG et al., 2013), and 1.55125 x 10-10 yr-1 for 238U (JAFFEY et al., 1971). Age corrections, were calculated using an estimated atomic 230Th/232Th ratio of 4 (± 2) x 10-6. Those are the values for a material at secular equilibrium, with the crustal 232Th/238U value of 3.8. The errors are arbitrarily assumed to be 50%.

The final results are reported as age ± error, both expressed in ka (= thousands of years before 1950). Dating of speleothems was mainly focused on the bottom (oldest part) of the speleothems.

Additional field surveys were carried out from the end of 2024 with the aim of identifying ancient traces of cave passages. These could be recognised by the presence of remnants of cave walls and antigravitative (paragenetic) ceiling channels, cave sediments or fragments of carbonate speleothems. These last were scattered along an elongated trace (i.e. the old cave passage) or found in patches (i.e. vertical cave shafts cut by surface erosion). Field observations have been supported and integrated by the analysis of a 2 m resolution DTM produced by LiDAR data provided by the Emilia-Romagna Region and compared with existing cave georeferenced maps.

All georeferenced data were analysed using the QGIS 3.22.4 software, and interpreted coupling the U/Th dates and the descriptions of data and outcrop morphologies.

3. Results and discussion

Over 50 locations with carbonate speleothems were found in the gypsum area between the Senio and Sintria rivers (Fig. 2). Most of these samples were pieces of old layered flowstones, some were thick curtains or parts of stalactites and columns. These speleothems were often used by local people to build dry walls, pave roads, or were even included into the walls of houses (Fig. 3). Carbonate flowstones were indeed the most resistant building material in this area, where rocks are almost exclusively composed of macrocrystalline (selenitic) gypsum.

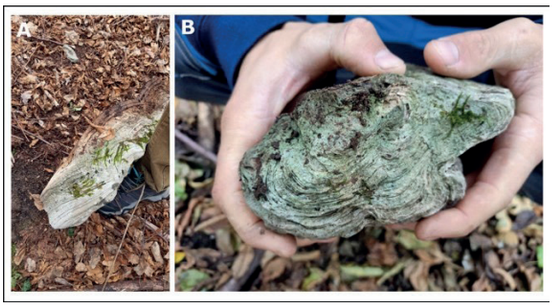

Figure 2: *Speleothems found on the forest floor in the area around Ca'Monti (Photos by Elisa Ponti (A) and Giovanni Sangiorgi (B)).*

Figure 3: *Speleothem fragments used for building the walls of a house at Ca' Monti (Photo by Veronica Chiarini).*

Aligned occurrences of carbonate speleothems can thus be explained by ancient road pavements, but some are away from any ancient tracks and are clearly naturally aligned.

In many cases the distribution of these speleothems is accompanied by rocky (gypsum) side walls, sometimes still hosting remnants of antigravitative (paragenetic) ceiling channels, or notches (Fig. 4). These morphologies are typical of gypsum caves in this area (DE WAELE et al., 2018; SEVIL-AGUARELES et al., 2025), and in a few cases they have survived erosion and dissolution.

With respect to unroofed caves in limestones (e.g., ZUPAN HAJNA et al., 2024), cave wall morphologies and cave sediments are much less preserved due to their fragility and the high solubility of gypsum.

Figure 4: *Large block with remnants of an antigravitative ceiling channel. Note also the gypsum wall in the back of the picture. This remnant of channel also displayed pieces of speleothems on its floor (area around Ca'Monti, photo by Giovanni Sangiorgi).*

Almost 30 speleothems were dated using the U/Th technique. Although some of these delivered younger ages, many were older than 300 ka (Fig. 5). Several of the old unroofed caves, according to the model that places the main speleogenetic phases during cold periods (COLUMBU

et al., 2015), appear to have formed during the cold stages of MIS 10 and 12, with speleothem ages mainly falling in the warmer phases of MIS 9 and 11, respectively.

Only CAMT5 has an age centered on the MIS10 glacial peak, thus appearing to have formed during a colder period.

Sample ID	Weight g	^{238}U $10^{-9}g/g$ [a]		$[^{230}Th/^{238}U]$ activity[c]		$^{230}Th/^{232}Th$ atomic ($\times 10^{-6}$)		Age (kyr BP) relative to 1950 AD	
BA 2.1*	0.050	804	± 60	0.9569	± 0.0045	3429		378.00	+29/-20
CAMT2	0,052	490,25	± 0,58	0,963	± 0,014	92,7	± 1,7	370	± 51
CAMT5	0,0505	608,48	± 0,64	0,9546	± 0,0029	88,9	± 3,6	350,7	± 9,9
CAMT7	0,0507	1501,08	± 1.4	0,9452	± 0,0025	3961	± 15	312,0	± 5,6
DM3-1	0,0494	769,24	± 0,74	0,9914	± 0,0032	1743,6	± 7,0	399	± 15

Figure 5: *U/Th analyses of some older speleothems.*

From the analysis of the map showing the traces of unroofed caves and the areas of major occurrence of loose speleothems together with the presently known cave systems (Fig. 6), it is evident that the old caves follow the same directions of the explored ones. This is an expected result, since gypsum caves normally follow the major discontinuities (fractures and bedding planes), in the past as today. This setting also suggests that the drainage pattern was not characterized by remarkable modifications during the time period in which both the old, now "unroofed", caves and the existing karst systems formed. The area where the highest concentration of speleothems was observed is characterized by the presence of relict karst systems characterised by entrances which often correspond to truncated shafts, and which present a relatively short planimetric development, thus suggesting a plausible old age for these cavities. The only exception is represented by the Bentini Abyss, which is one of the most important karst systems of the Messinian gypsum outcrop. The latter, however, develops at the western limit of the studied area, and is characterized by a subterranean drainage direction towards NW and SE (Fig. 6), while the topography of the unroofed caves surveyed in the same area suggests an opposite drainage direction. Thus, further investigations are needed.

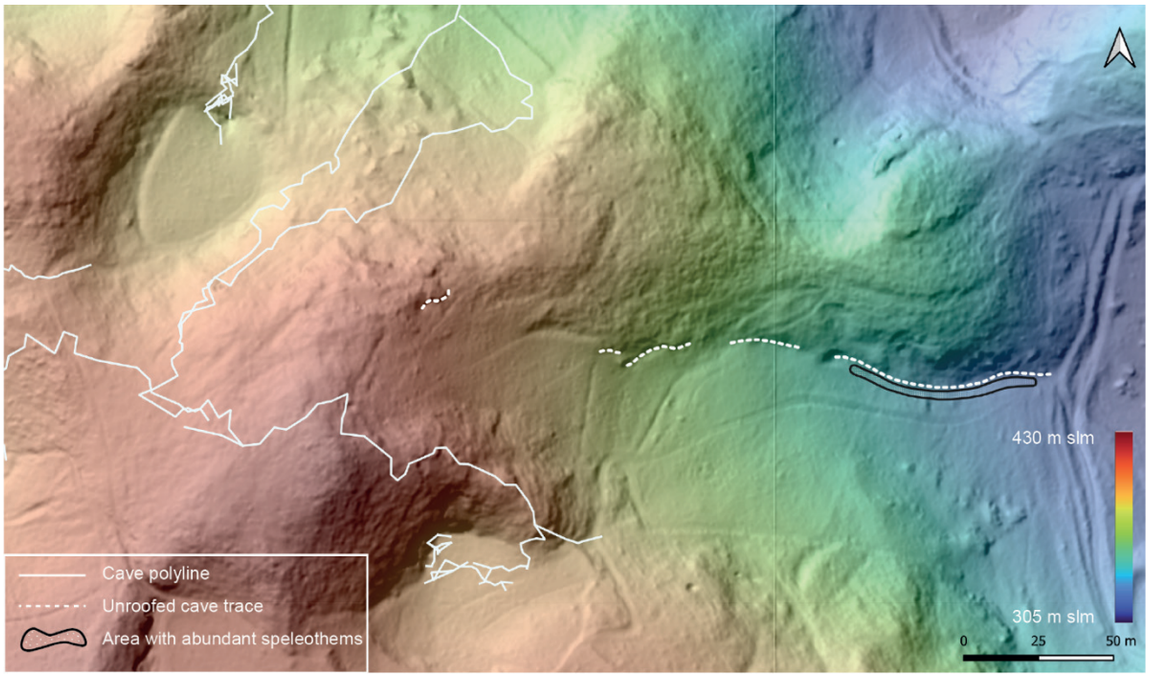

Figure 6: *Example of map showing the unroofed cave traces on a LiDAR image (2 m resolution, courtesy Emilia Romagna Region), areas of speleothem occurrence at the surface, and the underlying mapped galleries of the Bentini Abyss.*

4. Conclusions

Several fragments of speleothems have been found in the woods of the central portion of the Vena del Gesso romagnola area, between the Senio and Sintria rivers.

U/Th dating showed many of them to be older than 300 ka. A detailed geomorphological survey allowed to map the areas where these speleothems are more abundant together with some morphologies which are typical of subterranean gypsum environments (e.g., notches and antigravitative channels), thus enabling the identification of ancient cave portions, older than 300 ka, now destroyed by erosion.

The comparison between these ancient caves with the existing ones showed similarities in the direction of development of the cave galleries, confirming the structural setting as an important forcing factor for the development of gypsum caves.

In addition, it points out a relative stability of the drainage pattern during the formation of both the unroofed caves and the existing ones. If this is true for the less developed caves, further investigations are required for what concerns the relation of the ancient karst systems with the most developed active ones, such as the Bentini Abyss

Acknowledgements

Many thanks to the Regional Park of the Vena del Gesso romagnola for granting permission to enter the protected areas and sample the speleothems. U/Th dating was carried at the School of Earth Sciences at University of Melbourne, under the supervision of Dr. John Hellstrom, Prof. Russel Drysdale, and Dr. Petra Bajo, and at the National Taiwan University, in the Research Center for Future Earth, under the supervision of Prof. Chuan-Chou Shen and Dr. Chun Yuan Huang.

References

CHENG H., EDWARDS R.L., SHEN C.C., POLYAK V.J., ASMEROM Y., WOODHEAD J., HELLSTROM J., WANG Y., KONG X., SPÖTL C., WANG X., CALVIN A.E., 2013 Improvements in 230Th dating, 230Th and 234U half-life values, and U/Th isotopic measurements by multi-collector inductively coupled plasma mass spectrometry. Earth and Planetary Science Letters 372:82-91.

CHIARINI V., PISANI L., COLUMBU A., DE WAELE J. (2024) EvolGyps: landscape evolution in the Messinian gypsum areas of Emilia-Romagna. Memoria dell'Istituto Italiano di Speleologia II(46b):1-181.

COLUMBU A., DE WAELE J., FORTI P., MONTAGNA P., PICOTTI V., PONS-BRANCHU E., HELLSTROM J., BAJO P., DRYSDALE, R., 2015 Gypsum caves as indicators of climate-driven river incision and aggradation in a rapidly uplifting region. Geology 43(6):539-542.

COLUMBU A., CHIARINI V., DE WAELE J., DRYSDALE R., WOODHEAD J., HELLSTROM J., FORTI P., 2017 Late quaternary speleogenesis and landscape evolution in the northern Apennine evaporite areas. Earth Surface Processes and Landforms 42(10):1447-1459.

De WAELE J., FABBRI S., SANTAGATA T., CHIARINI V., COLUMBU A., PISANI L., 2018 Geomorphological and speleogenetical observations using terrestrial laser scanning and 3D photogrammetry in a gypsum cave (Emilia Romagna, N. Italy). Geomorphology 319:47-61.

JAFFEY A.H., FLYNN K.F., GLENDENIN L.E., BENTLEY W.C., ESSLING A.M., 1971. Precision measurement of half-lives and specific activities of 235U and 238U. Physical Review C 4(5):1889-1906.

HIESS J., CONDON D.J., MCLEAN N., NOBLE S.R., 2012 238U/235U systematics in terrestrial uranium-bearing minerals. Science 335(6076):1610- 1614.

SEVIL-AGUARELES J., PISANI L., CHIARINI V., SANTAGATA T., DE WAELE J., 2025 Gypsum cave notches and their palaeoenvironmental significance: A combined morphometric study using terrestrial laser scanning, traditional cave mapping, and geomorphological observations. Geomorphology 471:109576.

ZUPAN HAJNA N., PRUNER P., BOSAK P., MIHEVC A., 2024 Temporal insights into karst system evolution: A case study of the unroofed cave above Škocjanske Jame, NW Dinarides. Geomorphology 461:109282.

Speleogenesis and Cave Geomorphology in the Klamath Mountains, California and Oregon, Usa

Joel Despain (1), Niles Lathrop (2)

(1) Cave Research Foundation, Klamath Mountains Project, 27171 Highway 299 East, Bella Vista, CA 96008, USA, joeldespaincaves@protonmail.ch (corresponding author)

(2) Cave Research Foundation, Klamath Mountains Project, 27171 Highway 299 East, Bella Vista, CA 96008, USA, nlwlathrop@gmail.com

Abstract

The Klamath Mountains geomorphic province of northwestern California and southwestern Oregon, USA, occupies 30,0002 hectares of rugged mountains inland from the Pacific. Rocks in the Klamath Mountains are sedimentary, metamorphic, intrusive and ultramafic, being largely accreted terranes on an active continental margin. Carbonates include limestone and marbles of Devonian, Permian, Triassic and Jurassic ages. These are often highly fractured and intruded by Jurassic diorite and quartz. Stripe karst dominates and outcrops are often narrow bands that form cliffs, massifs and bare, alpine karst at elevation. Structural control on active and paleo conduits is highly varied and includes lithological contacts, bedding on both dip and strike, joints and minor faults. Klamath carbonates make up a small percentage of the landscape (< 5%) leading to wide-spread sinking stream, allogenic recharge, except in the Marble Mountains where autogenic recharge is also important. Both active and abandoned conduits are common as are numerous karst springs. Some caves are located hundreds of meters above active base level indicating a great age for these systems. There are approximately 300 caves, and extensive karst development is seen in the McCloud Limestone of Shasta County, California, near Oregon Caves National Monument in Josephine County, Oregon and in the Marble Mountains of Siskiyou County, California. The highest concentration of caves is in the Marble Mountains with 50 km of cave passages, including the former deepest cave in the US, Bigfoot-Meatgrinder (-370 m). The McCloud Limestone contains hypogenic caves derived from sulfuric acid dissolution, which has led to an unusual mineral assemblage in cave sediments.

1. Introduction

Caves and karst development are uncommon on the western margin of North America where volcanic, plutonic and non-carbonate marine rocks dominate. One exception is the Klamath Mountains of northwestern California and southwestern Oregon occupying 30,0002 hectares of rugged mountains inland from the Pacific Ocean. Rocks in the Klamath Mountains are sedimentary, metamorphic, intrusive and ultramafic, being largely accreted terrains on an active continental margin. Carbonates include limestone and marbles of Devonian, Permian, Triassic and Jurassic ages. While caves and karst are found throughout the region, even here these carbonates are uncommon and make-up less than 5% of the landscape. (Fig. 1) IRWIN (1994)

The Klamaths are composed of multiple steep ranges rising to 2800 m in the Trinity and Alps mountains. The area has high annual rain and snowfall during the winter months with more than 200 centimeters falling in the northwestern part of the region in some winters. Summers are hot and dry with frequent forest fires. There are many perennial rivers and streams making the region an important source of water for California. The Klamaths are sparsely populated with only a few small communities and a limited network of roads making field work challenging and time consuming.

Native Americans first made use of the caves across many millennia and human remains and artifacts are common. The cultural use by Native American nations continues today in many caves of the region. The Klamath Mountains are also known for their high biological diversity exemplified by conifer, amphibian and cave-adapted species, which include millipedes, spiders, isopods and many more. SLEETER & CALZIA (2012)

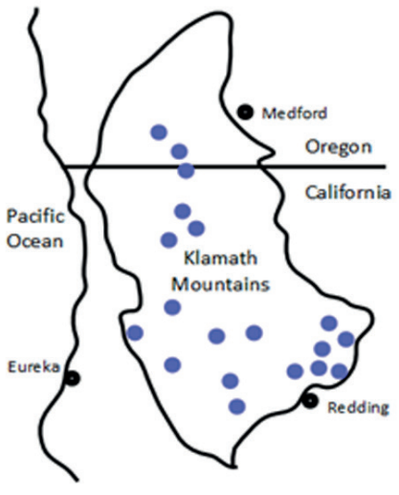

Figure 1: *Location of the Klamath Mountains with the approximate location of karst areas in blue.*

Geologic research in the Klamath Mountains has been sporadic with most work focused on the tectonic history of the many terranes, Jurassic emplacement of intrusive rocks and the marine depositional setting for the rocks of the region. The carbonates are little studied with the exception of the McCloud Limestone of Shasta County, which is important for

Wolfcampian (early Permian) indicator fossils. WILSON (1970) Caves in the McCloud were also studied in the early 1900s for the Pleistocene remains of extinct animals, greatly expanding the understanding of fauna in the western United States at that time. MERRIAM (1906)

All told, there are approximately 300 caves known in the region. The longest is more than 25 kilometers in length (Bigfoot Cave in the Marble Mountains) and more than 20 are longer than a kilometer. The best-known caves are two tour caves, Oregon Caves National Monument near Cave Junction, Oregon and Lake Shasta Caverns near Redding, California. JOHNSON (1990), DESPAIN (2022).

2. Materials and methods

This paper is synthesis of pertinent literature from multiple authors and caving projects dating back decades and from field observations and cave documentation projects in the region over the last dozen years.

Cave mapping and exploration work began with the Shasta Area Grotto (caving club) and the Klamath Mountains Conservation Task Force both internal organizations of the US National Speleological Society (NSS) in the 1970s. More recent work has been completed by the Klamath Mountains Project of the Cave Research Foundation.

Mapping work has used standard methods including analog instruments in the past and more recently digital tools for charting the caves and documenting their features and contents.

One very important book on the caves was the Guidebook to the 1990 NSS Convention, which was held in Yreka, California, a small town in the region, edited by Victoria Johnson (1990). The guidebook included maps of many caves of the region. Also important in more recent times is the 2022 report of the Klamath Mountains Cave Research Foundation Project by Joel Despain (2022) which also includes many maps and articles on the geology of specific caves.

3. Results

Four primary terranes have been identified by Irwin (1994) and other authors: 1) the Jurassic western terrane, 2) a second western terrane of Paleozoic and Triassic rocks, 3) a much smaller central metamorphosed terrane that is Devonian and 4) an eastern terrane that is early Paleozoic to Jurassic in age. Besides the accreted marine rocks, also prevalent are abundant plutonic rocks of Jurassic age that form large outcrops as well as dikes in the accreted rocks.

Karst-bearing carbonates are found primarily in the second western terrane and the eastern terrane and are nearly absent from the other two. Carbonates in the western terrane have largely been metamorphosed to marble while in the eastern terrane they remain limestones that are often fossiliferous. Most outcrops are small, being only a few square kilometers in size or even smaller. Stripe karst dominates and outcrops are often narrow bands that form cliffs and massifs and bare, alpine karst at elevation. However, larger bodies are found in the Marble Mountains of Siskiyou County and in the Permian McCloud and Triassic Hosselkaus limestones of Shasta County. Many of the outcrops are not individually mapped but rather are shown as components of mélange units containing a wide variety of marine rocks. IRWIN (1994)

The limestones vary in composition with dolomitic and argillaceous rocks as well as purer, calcite-rich limestones. Chert is common in some of the carbonates. Some units formed as banks while others are reef deposits. Bedding is retained in most units but is obscured in smaller more metamorphosed outcrops.

The origins and characteristics of many of the carbonate units have not been studied. Best researched is the McCloud Limestone. WATKINS (1993) wrote of its deposition: “It formed as isolated platforms about 30 km long that developed on volcanic highs as bank deposits and ramps of mixed volcaniclastic and carbonate sediments. Bank growth resulted in slope deposits of argillaceous spiculitic wackestone, limestone conglomerates, and limestone turbidites. Lateral growth of platforms occurred by progradation of slope deposits, and platform-top deposits consisting mainly of packstone and wackestone of subtidal origin. Rapid subsidence of platforms resulted in sediment accumulation rates of up to 30 cm/1000 year.”

Porosity, that allows the development of karst in the limestone, is highly varied and wide-spread. Cave passages often exhibit strong structural control along these areas of porosity. Many of the carbonate outcrops are heavily fractured with prominent joints and cracks. Very small to minor faults are common and bedding planes exist in most units. Lithological contacts are also common on the margins of the small carbonate outcrops and where dikes (usually diorite) intrude the karstic rocks. Cave passages in the Klamath Mountains have developed along all of these types of porosity.

Karst recharge is dominantly allogenic with streams rising on adjacent non-carbonate lithologies and entering caves as sinking streams. Sinks and dolines are uncommon except in the Marble Mountains where autogenic recharge is important. Both active and abandoned conduits are wide-spread and numerous karst springs are found across the region. Most water flow occurs and occurred in the vadose zone with few fluvial cave passages formed phreatically. Some caves such as Apogee in the Marble Mountains and October (Fig. 2) in the McCloud Limestone are located hundreds of meters above active base level, indicating a great age for these systems. The steep terrain of the region has created ample gradients supporting subterranean waterflow through the limestone and marble bedrock.

In most cases, caves in the Klamath Mountains have formed in small groups in a respective block of limestone. Frequently there will be one larger cave and smaller satellite caves nearby. The groups are often widely spaced across the landscape with kilometers between karstified outcrops of limestone or marble. These groups of caves range in elevation from as low as 200 meters to as high as 2000 meters. Thus, temperatures in the caves range from 16 to 0 degrees C with permanent ice occurring in the highest caves.

Caves across the greater region are highly varied. Some are linear and joint controlled while others contain complex mazes. Some are a single level, while others are multi-leveled. Many have active streams but others are dry and abandoned. Paul Gibson Cave is more than two kilometers long and formed as an anastomotic maze on a single level with an active stream and resurgence. The cave has large sediment deposits and very few speleothems. Scorpion Cave is a canyon complex 1.5 kilometers long formed on at least five levels and is dry and abandoned with many speleothems and very little sediment. There is little surface karst development such as dolines or sinks near these caves and most have formed in small bodies of limestone.

Oregon Caves is a nearly five kilometers long and formed as a complex maze on multiple levels with many side passages and multiple streams. This tour cave is a national monument managed by the National Park Service with copious sedimentation and rich displays of speleothems in some locations and none in others.

The greatest concentration of cave passages and development is in the Marble Mountains Wilderness Area on the Klamath National Forest in Siskiyou County, California. Here in a 20-kilometer square area, more than 50 kilometers of cave passages have been discovered and mapped since the 1970s. This includes the longest cave in the region and the former deepest cave in the US, Bigfoot with 25 kilometers of passageways and a depth of 370 m. Nearby are another ten caves more than a kilometer

in length. EHR, et al (1990) Bigfoot is also the longest alpine cave in the US and the Marble Mountains is the most concentrated area of cave development in California.

These caves have multiple levels, many vertical pits and many side passages adding to the complexity and length of the cave systems. The Marbles are described by cavers as being like a sandwich cookie with the cream filling being the marble and the cookies being the bounding dark schist that occurs above and below the carbonate and the caves. Many caves here descend steeply from the surface to the lithological contact with the schist and then have developed sub-horizontally along this contact. Speleothems vary with many areas containing none, but some locations being rich in beautiful displays of secondary deposits. KNUTSON (1990).

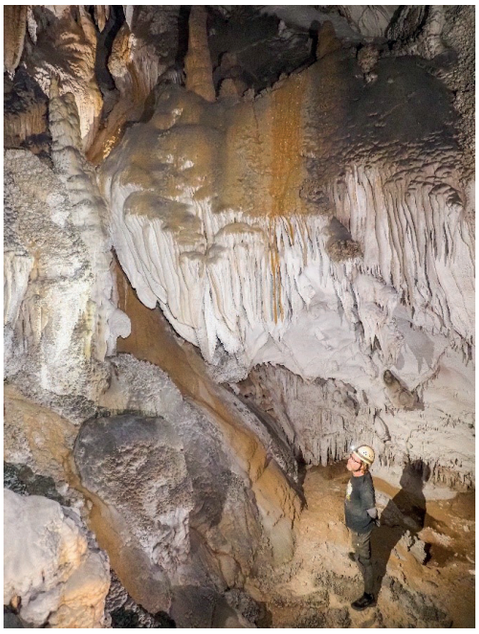

Figure 2: *A room in October Cave in the Permian McCloud limestone of the eastern Klamath accreted terrane. This cave was discovered four years ago and is still being explored. Photo by Heather Veerkamp*

In the eastern Klamath terrane, the Hosslekaus limestone contains many small caves and pits, but no larger systems have been found so far. Low Gap has the greatest concentration of caves in this area. This limestone is very remote, and there is still a great deal of potential for more cave discoveries.

The McCloud Limestone (Fig. 3) contains nearly 100 caves in total. Many of these are fluvial including deep pits at Packrat and Ringtail caves, small stream caves near the McCloud River and abandoned caves in the walls of steep, narrow canyons. These caves have heavy sediment loads and vadose features such as narrow canyons and paragenetic development. The McCloud is broken up by faulting and diorite dikes, limiting the size of the limestone outcrops and therefore the size of the caves. DESPAIN (2022)

Hypogene recharge coupled with sulfuric acid chemistry and elevated water temperatures have created some of the caves in the McCloud Limestone. These caves are inactive, extend vertically, formed phreatically and have hypogene morphology including cupolas, phreatic domes, wall notches from acidic pools and sudden passage terminations. Primary sediments in these caves include unusual clay minerals. A sample from January Cave contained smectite/montmorillonite, illite, and disordered kaolinite. Another sample from Ancient Palace adjacent to a diorite dike contained pitted and corroded quartz, opal-A, manganese-oxide and hydroxides, iron oxides and hydroxides, and minor authigenic calcite and alunite and trace allogenic fayalite. Fayalite is a high temperature olivine-group mineral that occurs in predominately ultramafic, volcanic and plutonic rocks or in metamorphosed iron-rich sediments and impure carbonates. XRD and SEM-EDX results suggests the material is an authigenic corrosion residue of both the altered diorite and limestone bedrock. The allogenic fayalite is assumed to be residuum from the diorite or limestone. LATHROP (2024) Ancient Palace also contains the largest cave room in California at 140 by 50 meters. The origins of the hypogene development are unknown but may be volcanogenic or associated with sulfate-rich ores found within the limestone. Apparent hypogene caves of the McCloud Limestone include January, Ancient Palace, Lake Shasta Caverns, Sa-Wel, Potter Creek, Deanna Lynn and Jacob David. DESPAIN (2022)

Figure 3: *A fall view of the McCloud limestone with the McCloud River arm of the Lake Shasta reservoir far below. The McCloud contains both epigene and hypogene caves. This view illustrates the steep landscape found in the Klamath Mountains. Photo by Heather Veerkamp*

4. Discussion

Decades of cave research and exploration in the Klamath Mountains have revealed an extensive and significant set of karst systems scattered about these remote mountains. Perhaps the most important aspect of this work is the discovery of a great variety of caves found here. There are carbonate caves of many sizes and types: Deep caves, shallow caves, simple caves and complex systems, active and abandoned caves, cold caves and warm caves all are prevalent in the region.

Most unusual are the hypogene caves of the McCloud Limestone adding to the complexity and diversity of karst systems in the region. The diversity of the caves has supported the evolution of many endemic cave-adapted species that are also quite diverse. And important to the region are the many karst springs that provide abundant cold water, critical for people and anadromous fish. But not all of the secrets of the karst have been revealed. Cavers continue to find and explore caves in the Klamaths, adding to the body of knowledge of these caves.

5. Conclusion

The caves of the Klamath Mountains are not the largest or deepest in the US or even in the western part of the country. But they are an important part of the karst of the nation due to the paucity of caves along the Pacific coast and the diversity of the caves of the region. These many caves are well worth the ceaseless efforts of cavers and researchers to find, document and understand the caves and karst of the region. The study of these caves will last far into the future providing more exciting discoveries for cavers and scientists seeking to understand these beautiful and intriguing caves.

Acknowledgments

The authors wish to thank the many cavers from the Shasta Area Grotto and the Klamath Mountains Conservation Task Force of the National Speleological Society and the Klamath Mountains Project of the Cave Research Foundation for their decades of work in the caves of the Klamath Mountains. Cavers have discovered a hidden world in these remote mountains and helped to bring it to light and to the world.

References

DESPAIN, J.D., ed. (2022) 2019 to 2021 Report of the Klamath Mountains Project, Cave Research Foundation.

EHR, B., HOYLE, D., LANKFORD, K., RICHARDSON, B., RICHARDSON, M., REAMS, C., Limestone Caves of the Marble Mountains Wilderness. 1990 NSS Convention Guidebook. JOHNSON, V., ed.

HACKER, B.R, DONATO, M.M., BARNES, C.G., MCWILLIAMS, M.O, ERNST, W.G (1995) Timescales of orogeny: Jurassic construction of the Klamath Mountains, Tectonics 14(3): 677–703. doi: 10.1029/94tc02454.

IRWIN, W.P. (1994) Geologic Map of the Klamath Mountains, California and Oregon. https://doi.org/10.3133/i2148

JOHNSON, V. (1990) Guidebook to the 1990 Convention of the National Speleological Society.

KNUTSON, S. (1990) Cave Management and Research: The Marble Valley Project 1974 to 1990. 1990 NSS Convention Guidebook. JOHNSON, V., ed.

LATHROP, N. (2024) Polygenetic Cave Sedimentation and Speleogeneis in the McCloud Limestone of Northern California, MS Thesis, Western Kentucky University.

MERRIAM, J.C. (1906) Recent Cave Exploration in California, American Anthropologist, New Series, 8 (2) 221-228.

SLEETER, Benjamin M., CALZIA, James P. (2012) Klamath Mountains Ecoregion, Status and Trends of Land Change in the Western United States—1973 to 2000, ed SLEETER, Benjamin M., WILSON, Tamara S., ACEVEDO, William, US. Geological Survey Professional Paper 1794–A

WATKINS, R. (1993) Permian Carbonate Platform Development in an Island-Arc Setting, Eastern Klamath Terrane, California, the Journal of Geology 101 (5): https://doi.org/10.1086/648257

WILSON, E.C. (1970) Conocardium langenheimi sp. n. (Mollusca: Bivalvia) in the lower Permian Series of the McCloud Limestone in northern California, Los Angeles County Museum, Contributions in Science (184)

Prospecção de cavernas a partir da detecção semiautomatica de depressões obtidas com Modelo Digital de Elevação (Mde), na região da APA Nascentes do Rio Vermelho - GO

Cristiano Fernandes Ferreira (1) & José Carlos Ribeiro Reino (2)

(1)Cecav/ICMBio, Parque Nacional de Brasília, Rodovia BR 450, km 8,5, via Epia, Brasília, Brasil, cristiano.ferreira@icmbio.gov.br
(2) Cecav/ICMBio, Parque Nacional de Brasília, Rodovia BR 450, km 8,5, via Epia, Brasília, Brasil, jose.reino@icmbio.gov.br

Resumo

O artigo aborda a prospecção de cavernas na região da Área de Proteção Ambiental Nascentes do Rio Vermelho (APANRV), em Goiás, utilizando a detecção semiautomática de depressões a partir de Modelos Digitais de Elevação (MDE). A principal dificuldade enfrentada na região é a falta de informações sobre a localização de cavernas, especialmente em áreas remotas com acesso limitado e dados oficiais escassos. O estudo se concentra na província cárstica de Mambaí, onde predominam rochas carbonáticas e um ambiente de carste coberto, com a presença de cerrado e matas galerias, que dificulta a identificação visual de feições como dolinas e cavernas. A metodologia envolve o uso de MDEs para gerar uma base de dados com depressões (polígonos), as quais são validadas em campo. Com base nos dados do satélite ALOS-PALSAR, foram selecionados alvos prioritários para inspeção in loco, resultando em 332 cavernas identificadas, sendo que cerca de 70% das cavernas estavam associadas a depressões previamente detectadas pelo sensoriamento remoto. A validação em campo também identificou novas depressões e cavernas fora dos polígonos prioritários. Os resultados indicam que a utilização de MDEs, embora eficaz, apresenta limitações, especialmente devido à escala dos dados e à dificuldade de representar adequadamente áreas com vegetação densa. A pesquisa conclui que o uso de MDEs pode ser uma ferramenta valiosa para a prospecção de cavernas em áreas de carste coberto, proporcionando uma alta taxa de sucesso (até 70%) na identificação de cavernas, e destacando a importância de combinar técnicas de sensoriamento remoto com validações em campo para aprimorar o mapeamento espeleológico e contribuir para a conservação dos recursos naturais da região.

Abstract

The article discusses the prospecting of caves in the Nascentes do Rio Vermelho Environmental Protection Area (APANRV) in Goiás, using the semi-automatic detection of depressions from Digital Elevation Models (DEMs). The main difficulty faced in the region is the lack of information about the location of caves, especially in remote areas with limited access and scarce official data. The study focuses on the karst province of Mambaí, where carbonate rocks and a covered karst environment predominate, with the presence of cerrado and gallery forests, which hinders the visual identification of features such as sinkholes and caves. The methodology involves the use of DEMs to generate a database with depressions (polygons), which are validated in the field. Based on data from the ALOS-PALSAR satellite, priority targets for on-site inspection were selected, resulting in 332 identified caves, with about 70% of the caves associated with depressions previously detected by remote sensing. Field validation also identified new depressions and caves outside the priority polygons. The results indicate that the use of DEMs, although effective, has limitations, especially due to the scale of the data and the difficulty of adequately representing areas with dense vegetation. The research concludes that the use of DEMs can be a valuable tool for cave prospecting in covered karst areas, providing a high success rate (up to 70%) in cave identification, and highlighting the importance of combining remote sensing techniques with field validations to improve speleological mapping and contribute to the conservation of the region's natural resources.

1. Introdução

Um dos maiores desafios para a prospecção de cavernas reside na falta de informações sobre a sua localização em campo, especialmente em áreas remotas, com bases de informações oficiais deficitárias, mapas em escalas inadequadas e exíguos relatos da população local sobre existência de cavidades em áreas de difícil acesso. Essa é exatamente a condição da província cárstica de Mambaí, nordeste do estado de Goiás, onde se insere a Área de Proteção Ambiental Nascentes do Rio Vermelho (APANRV), uma unidade de conservação da natureza, gerida pelo ICMBio e criada dentre outros motivos para conservar os recursos hídricos e as inúmeras cavernas presentes na região (Fig. 1). A área, com 1.776km^2, é caracterizada pela ocorrência de rochas carbonáticas do Grupo Bambuí, formação Lagoa do Jacaré, que estão em processo de exumação com a remoção de sedimentos detríticos atribuídos à retração da escarpa arenítica da Serra Geral (Grupo Urucuia). Essa região possui um clima do tipo tropical com estações secas e chuvosas bem definidas (CALDEIRA et al., 2021) e que apresenta uma vegetação típica do cerrado, ou seja,

savanas esparsas nas áreas planálticas e de vertentes com a inserção de matas galerias junto às drenagens. Essa geografia permitiu o desenvolvimento de um carste coberto em processo de exumação, em função de um reajuste dos níveis de base regionais com o aprofundamento da calha do Rio Vermelho e a formação de um canyon de mais de 80m de altura nesta drenagem. Essa e outras importantes calhas de escoamento funcionam como pontos principais de descarga dos sistemas cársticos adjacentes, apresentando surgências, ressurgências e janelas cársticas (CALDEIRA et al., 2021). Nos planaltos circundantes ocorrem campos de dolinas e outros tipos de depressões de difícil identificação visual em função da presença da vegetação nativa ou grandes dimensões (Fig. 2).

O estudo e mapeamento de dolinas é uma área das ciências do carste já há muitos anos desenvolvida (FERREIRA & UAGODA, 2020) e cujos propósito e técnicas atendem variados segmentos. Trabalhos pioneiros em geomorfologia cárstica se destacam desde o final do século passado, enfatizando principalmente aspectos morfométricos, distribuição e gênese (WILLIAMS, 1972; DAY, 1976; BONDESAN et al., 1992; KARMANN, 1994). Tais trabalhos se utilizaram principalmente de bases cartográficas antigas, com a interpretação de cartas topográficas, fotos aéreas e outros recursos para identificar dolinas. Mais recentemente outros trabalhos se utilizaram de Modelos Digitais de Elevação (MDE) para a identificação de dolinas por métodos automatizados (CARVALHO JÚNIOR et al., 2014; MIHEVC & MIHEVC, 2021; UTLU & ÖZTÜRK, 2023; TELBISZ et al., 2024). O mapeamento de dolinas atualmente visa sobretudo criar bases de dados para análises em geomorfologia (LONČAR & GRCIĆ, 2022), gerenciamento de áreas de risco (Salles et al., 2018), uso e ocupação (GUTIÉRREZ et al., 2014), conservação dos recursos hídricos e análises de vulnerabilidade do carste (MORENO-GÓMEZ et al., 2019). Entretanto, poucos trabalhos se debruçaram sobre o potencial da detecção de dolinas servir também para prospecção de cavernas (FERREIRA et al., 2022) dada a sua intrínseca relação de gênese e desenvolvimento.

No Brasil as cavernas são protegidas pela legislação (BRASIL, 2008) e o seu mapeamento é fundamental para o ordenamento territorial e licenciamento de atividades potencialmente lesivas ao meio ambiente, especialmente em áreas cársticas (AULER, 2016). Para a área de estudo poucas cavernas foram mapeadas e cadastradas na base oficial do governo federal (BRASIL, 2022) se considerada toda a sua real potencialidade. Essa condição é altamente indesejável visto o avanço de atividades potencialmente lesivas aos sistemas espeleológicos locais, como a mineração, agronegócio ou obras de infraestrutura (rodovias e ferrovias). O objetivo deste trabalho, portanto, é apresentar os resultados referentes à identificação de cavernas a partir do mapeamento semiautomático de depressões realizados previamente (FERREIRA et al., 2022) e até então não devidamente checado in loco. As atividades de campo serviram para confirmar a presença de dolinas, cavernas e caracterizar outros aspectos do quadro natural, criando assim uma base mais apropriada para o planejamento da unidade de conservação e tomada de decisão por parte dos gestores.

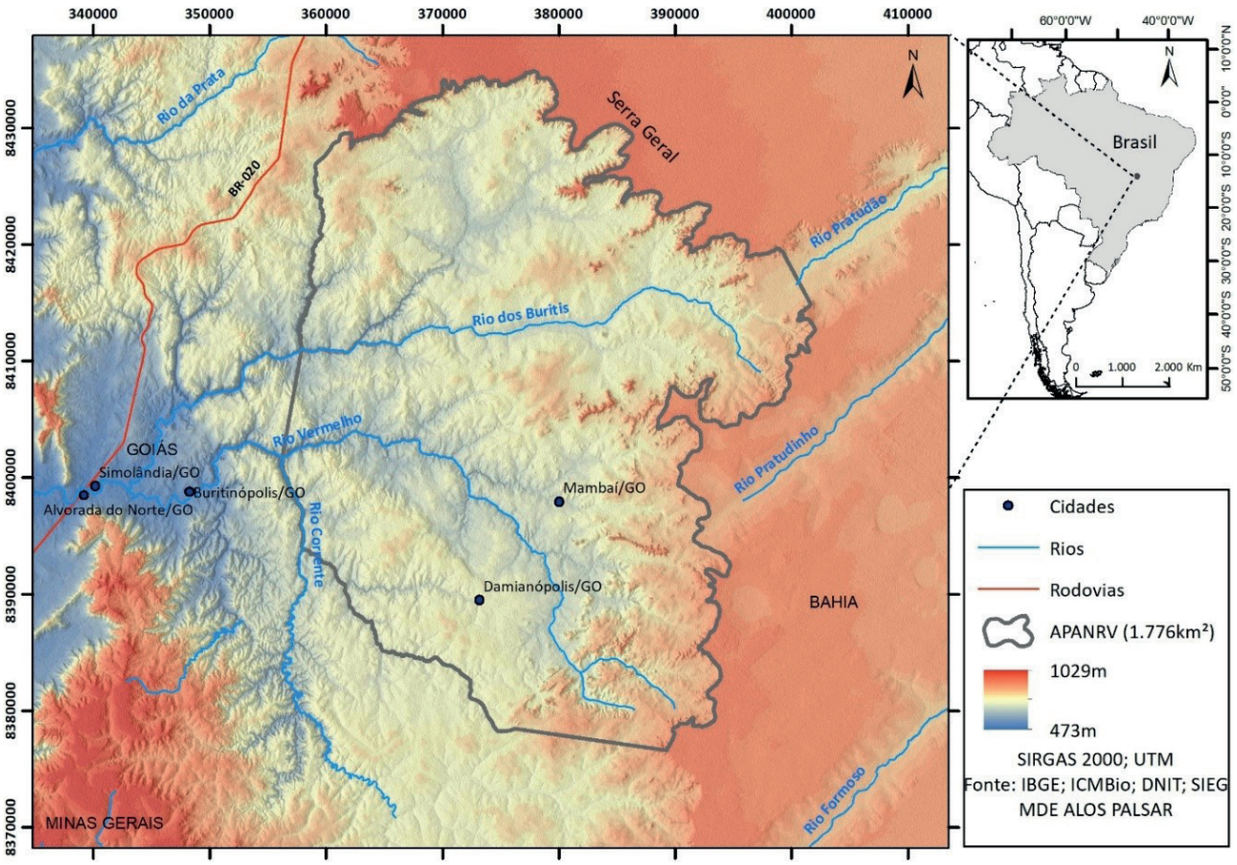

Figura 1: *Localização da área.*

Figura 2: *Exemplo de dolinas encontradas na região. No lado esquerdo uma dolina colmatada com vegetação rasteira sem entrada de caverna. Ao centro um ponto de recarga sob mata com caverna. Na direita uma dolina de sufusão com acesso a uma caverna.*

2. Materiais e Métodos

O uso de Modelos Digitais de Elevação para a detecção de depressões e dolinas em áreas cársticas está amplamente documentado na literatura (CARVALHO JÚNIOR et al., 2014; CAHALAN & MILEWSKI, 2018; FERREIRA & UAGODA, 2020) e consiste basicamente numa operação aritmética de soma e subtração. Ferramentas de restituição hidrológicas em rasters no geoprocessamento preenchem eventuais depressões, supostamente por serem defeitos do modelo (Hydrology>Fill). A subtração do modelo preenchido pelo modelo original gera uma base de depressões, que em uma área cárstica pode significar feições autênticas de ligação com o meio subterrâneo (FERREIRA e UAGODA, 2020). Polígonos são criados a partir desse processo e geralmente são inspecionados com o auxílio de imagens de satélites para um primeiro nível de validação. Entretanto, nem todos os trabalhos realizados neste tipo de abordagem avançam para uma etapa subsequente de validação, ou seja, a verificação em campo (WU et al., 2016; CAHALAN & MILEWSKI, 2018).

Neste trabalho optou-se por utilizar uma base de polígonos referentes a possíveis depressões já existente (FERREIRA et al., 2022) advindas de dados do satélite ALOS-PALSAR (Advanced Land Observing Satellite Phased Arrayed type L-Band SAR) com 12,5m de resolução espacial. Desta feita, a área de estudo restringiu-se ao da APANRV (1776km^2), de abrangência inferior ao trabalho original, mas ainda assim bastante extensa para o pleno recobrimento em campo. De um universo de milhares de polígonos gerados de forma automática, selecionou-se, na primeira etapa de validação por imagens de satélite (Google Earth e Imagery), um quantitativo inferior e exequível de alvos prioritários espalhados pela área para checagem in loco (Fig. 3). Os caminhamentos em campo buscaram também agregar outros polígonos, não considerados como prioritários, sempre que próximos do trajeto estabelecido para alcançar os alvos prioritários. Uma vez atingidos os alvos (pontos centroides) percorreu-se também os arredores, mesmo fora dos polígonos, buscando feições eventualmente ocultas pelas matas ou próximas das bordas, não atingidas pela delimitação automática que possui algumas limitações (linha de extravasamento e não bacia hidrológica, p.ex.).

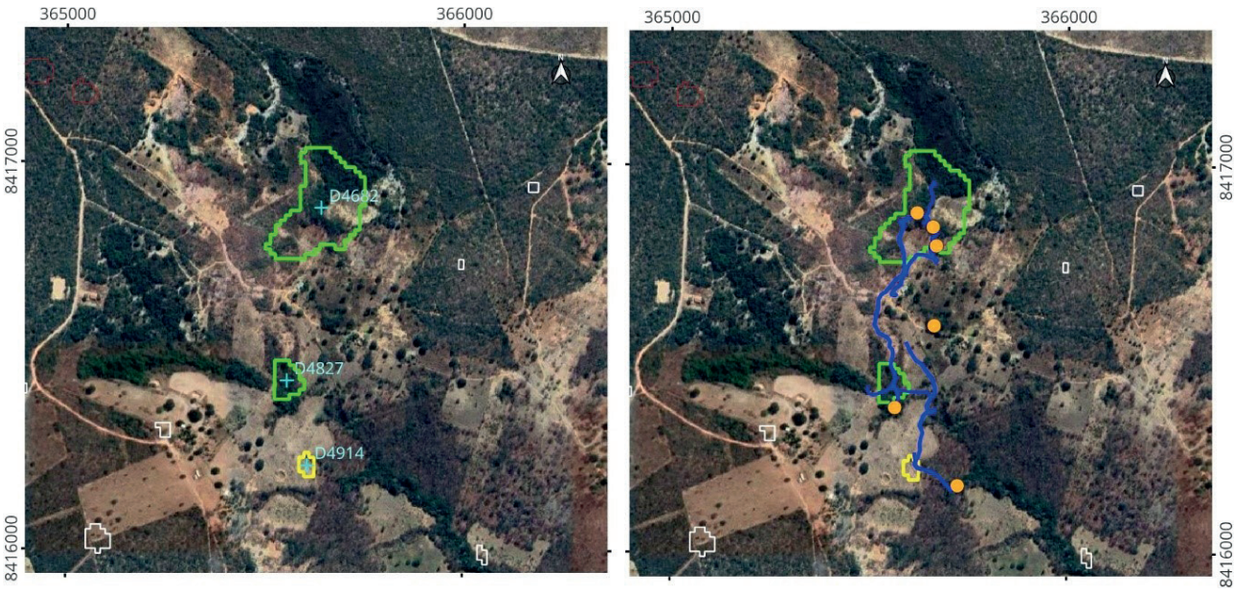

Figura 3: *Exemplos de alvos prioritários estabelecidos e ranqueados em níveis de maior possibilidade de acerto. Em verde depressões consideradas de maior potencial que as marcadas em amarelo, além das bancas consideradas não prioritárias. A delimitação dos polígonos se deu de forma automática, até no nível de "extravasamento" teórico da depressão. Na direita as linhas de caminhamento (azul) e as cavernas identificadas (laranja). Fonte: Imagens Google Earth.*

No ensejo das atividades de campo buscou-se não apenas validar as depressões do sensoriamento remoto (ainda em progresso) como mapear todo tipo de feição de importância do carste, seja dentro, nas proximidades ou nos trajetos dos alvos estabelecidos. Desta forma estabeleceu-se duas bases distintas, ou seja, uma do sensoriamento remoto prévio, constituída por polígonos de maior abrangência, com graus maiores e menores de possiblidade de serem depressões autênticas e outra, efetivamente de campo e numa escala de detalhe que se constitui de pontos referentes a dolinas, cavernas, sumidouros e surgências. Todas as feições foram fotografadas e sucintamente caracterizadas, com a descrição do uso e ocupação do local (matas, pasto, cerrado etc.), ocorrência de corpos hídricos (no caso das cavernas ou dolinas) e observações referentes ao potencial das cavernas para maior desenvolvimento, presença de algum risco (abelhas, abismos etc.) ou danos (lixo, p.ex.). A atividade de campo foi facilitada pelo uso de geoaplicativos em celulares (Avenza, p.ex.) o que permitiu carregar as bases de dados (imagens, polígonos, alvos e percursos) e traçar as melhores estratégias para alcançar os pontos planejados. Deve-se ressaltar que nesta etapa as cavernas não foram topografadas, ou seja, foram apenas coletados os pontos de entrada, que certamente serão em maior número que o de cavernas propriamente dito. Outras atividades deste projeto ocorrem de forma paralela ou serão retomadas adiante, como a topografia de detalhe das cavernas com maior potencial.

3. Resultados

Devido à dispersão dos alvos e grande abrangência territorial da área de estudo, foram percorridos cerca de 260km em trilhas de caminhamento em inúmeras expedições. Praticamente todos os alvos foram atingidos, excetuando-se aqueles em áreas de grande dificuldade ou restrição de acesso (7), em geral associados ou próximos às escarpas da Serra Geral. Por outro lado, houve um acréscimo substancial de novos polígonos inspecionados (90), mesmo não considerados prioritários num primeiro momento (235), muitos inclusive contendo depressões autênticas (dolinas) e cavernas (Fig. 4).

Polígonos	Qtde	%
Alvos prioritários	235	73,89%
Alvos checados	228	71,69%
Outros polígonos checados	90	28,30%
Polígonos totais checados	318	

Figura 4: *Quantidades totais de polígonos identificados por sensoriamento remoto checados em campo.*

No total foram identificadas 332 cavernas na área conforme a metodologia de trabalho proposta (Fig. 5). Cerca de 27% das cavernas foram identificadas justamente no interior de depressões cársticas previamente selecionadas como prioritárias (MDE), confirmando-as, portanto, como verdadeiras. Entretanto, se for ampliado um buffer de 50m ao redor dos objetos alvo criados em laboratório, essa percentagem amplia-se até cerca de 70%. Baseado em experiencia de campo, considera-se este limite discricionário como razoável para alcançar as feições que a metodologia de preenchimento até o nível de extravasamento em MDE's pode não ter abarcado, conforme relatado por FERREIRA & UAGODA (2020). As cavernas localizadas além deste limite de 50m e que compõem a amostra final representam, portanto, os possíveis erros de omissão, alcançando a métrica aproximada de 30%.

Cavernas	Qtde	%
Dentro dos polígonos	89	26,81%
50m dos polígnos	230	69,28%
Omissão (>50m polígonos)	102	30,72%
Total	332	100%

Figura 5: *Potencial do uso de depressões identificadas por sensoriamento remoto para prospecção de cavernas.*

É importante deixar claro que os objetos gerados automaticamente como depressões e estabelecidos como alvos de validação possuem em geral dimensões mais abrangentes que dolinas pontuais dispersas num campo ou planalto, muito em função da escala da base utilizada (ALOS-PALSAR, 12,5m). Os objetos advindos da análise dos MDE, grosso modo, funcionam como depressões compostas que podem conter inúmeras dolinas ou eventualmente apenas um ponto mais profundo (menos comum). Estes dados acerca da relação entre as dolinas identificadas em campo e sua contraparte identificadas em gabinete e de escala mais abrangente, ainda estão sendo tabulados. Mas é possível afirmar que para a área de estudo, cerca de metade das dolinas identificadas em campo (50%) apresentam entradas de cavernas em seu interior, normalmente no ponto mais profundo.

Quanto ao uso e ocupação das áreas onde estão as cavernas e suas dolinas (Fig. 6), identificou-se o predomínio de ocorrências em áreas de matas (78,5%). Praticamente todas as demais feições foram encontradas em áreas de pastagens (21%) e pouquíssimas em áreas degradadas ou regiões de veredas (< 1%). Nenhuma dolina contendo caverna foi identificada em área de cerrado preservado nas modalidades de campo aberto (e não mata galeria). Outro dado observado é que praticamente a metade das cavernas encontradas (154) possuem água em seu interior (cursos ou corpos d'água). Por fim, também foi observada baixa correlação das cavernas identificadas em campo com a base do CANIE para a área. Mesmo usando o buffer arbitrário de 50m a partir das 332 cavernas conferidas apenas 69 registros do CANIE foram convergentes. Mesmo que haja uma diminuição forte do número de entradas para de fato o número de cavernas cadastradas, não é de se esperar uma proporção de quase cinco para um nesta relação.

Uso do solo	Qtde	%
Mata	259	78,48%
Pasto	68	20,61%
Área Degradada	3	0,91%
Vereda	2	0,61%
Cerrado	0	0,00%

Figura 6: *Uso do solo prioritário nas cavernas mapeadas.*

4. Discussão

Considera-se que a proposta inicial de validação dos objetos prioritários foi exitosa e resultou numa taxa de positivos em relação a ocorrência de cavernas bastante significativa, especialmente se considerada a estratégia de caminhamento nas cercanias dos objetos e não apenas até seu ponto centroide (buffer de 50m). Foram 332 entradas de cavernas localizadas, sendo que quase 70% atreladas intimamente

às depressões identificadas previamente por sensoriamento remoto. Obviamente que esses resultados são especialmente importantes para uma área caracterizada por pouca ou nenhuma representatividade de morros testemunhos ou muralhas aflorantes (feições positivas) se comparado por exemplo, ao carste de Lagoa Santa-MG ou especialmente de Pains-MG (AULER & PESSOA, 2020; PILÓ & CRUZ, 2022; TIMO, 2022) onde é comum ocorrerem cavernas nestas condições. Neste contexto da APANRV, aonde predominam superfícies em exumação (carste coberto), as depressões são os elementos do ambiente superficial mais marcantes do carste local e potencialmente mapeáveis por sensoriamento remoto. Apesar de feições positivas também serem potencialmente mapeáveis com a mesma metodologia de preenchimento e subtração com MDE's (LYEW-AYEE et al., 2007), a correlação genética destas feições com a ocorrência de cavernas é bem menos direta. A presença de depressões no terreno em áreas carbonáticas tem alto potencial de indicar processos de carstificação e espeleogênese, sendo um fator muito mais propício que superfícies isoladas ou resultantes da erosão diferencial. Além disso, a possibilidade da identificação de cavernas ativas e conectadas a sistemas mais abrangentes do ponto de vista hidrológico enaltece a representatividade e importância desses achados, especialmente para análises posteriores sobre o comportamento desses sistemas frente a eventos extremos de chuva (mudanças climáticas), sobre vulnerabilidade e risco em áreas cársticas (HOFIERKA et al., 2018). No caso da APANRV, as cavernas com função hidrológicas ativas serão consideradas com maior cuidado tendo em vista os objetivos primordiais de criação da unidade de conservação, ou seja, a conservação das cavernas e dos recursos hídricos locais.

Já a questão das omissões, ou seja, a não previsão pelo modelo da ocorrência de depressões aonde de fato ocorrem, pode-se interpretar especialmente em função da escala da base utilizada e da sua baixa efetividade em representar o real nível do solo em ambiente de densa vegetação. O uso de MDE de alta resolução ou com sensores capazes de filtrar a vegetação (LiDAR, p.ex.) certamente geraria um número bem maior de alvos potenciais que representassem mais fidedignamente as dolinas (WU et al., 2016; UTLU & ÖZTÜRK, 2023; TELBISZ & SZÉKELY, 2024). Entretanto, essas bases são de difícil acesso ou com abrangência mais restrita que o necessário para a abordagem executada na área de estudo. Pelo conhecimento que se obteve neste projeto da geografia local, observou-se que as depressões cársticas mais importantes foram detectadas pelo modelo de elevação utilizado, estando muitas outras próximas ou sendo parte dos mesmos fenômenos representados (coalescência de objetos, normalmente).

Como visto, no geral, as cavernas identificadas neste projeto estão majoritariamente inseridas em áreas de mata e muito secundariamente em áreas de pastagens. A presença de água em quase metade da amostra ajuda a explicar melhor esse fenômeno na região. As vertentes e planaltos mais propícios à agricultura, originalmente associadas ao cerrado (campo aberto), foram sendo paulatinamente convertidos em pastagens, onde atualmente ainda se encontram algumas dolinas com cavernas. Outras provavelmente foram soterradas com o uso de maquinário agrícola. As áreas mais preservadas, normalmente com declividades maiores junto aos cursos de água, bordas de dolinas e exposição de rochas foram preteridas e abrigam a maior quantidade de cavernas, justamente onde há maior umidade que permite o desenvolvimento das matas galeria. Tudo isso também converge para a percepção de que a carstificação, mais acelerada nas franjas erosivas na interface entre os carbonatos do Grupo Bambuí e os sedimentos clásticos referentes ao desmonte do Grupo Urucuia na região, vem capturando as águas superficiais para níveis inferiores por meio das dolinas (CALDEIRA et al., 2021).

5. Conclusão

O estudo baseado em dados de sensoriamento remoto relativos a possíveis depressões cársticas no terreno a partir de MDE se revelou bastante útil para delinear alvos de grande potencial de ocorrência de cavernas. Áreas de carste coberto com poucas e esparsas exposições de rocha, como muralhas ou morros testemunhos, mas com grande potencial para dolinamentos podem ser beneficiadas com uso da metodologia proposta, com até 70% de acerto. Além disso, apesar de desejáveis bases em escalas mais detalhadas ou o uso de sensores capazes de penetrar o dossel (LiDAR, p. ex.), o MDE utilizado teve custo zero e uma boa taxa de retorno positivo. A base ALOS-PALSAR utilizada indica naturalmente áreas mais carstificadas em que há a possiblidade de achados acessórios não necessariamente atrelados aos polígonos de depressão. Ela, porém, não esgota métodos clássicos da prospecção espeleológica, como análise de imagens, fotos aéreas, demais fontes bibliográficas e sobretudo entrevistas junto às comunidades locais e pessoas com maior conhecimento do campo.

Como etapa subsequente ao trabalho aqui descrito almeja-se dar continuidade ao projeto de validação e tabulação dos dados referentes às demais depressões detectadas na metodologia que eventualmente não foram classificadas como alvos prioritários. Paralelamente as cavernas identificadas neste trabalho como de maior potencial espeleométrico, importância ambiental ou conveniência logística, serão listadas em níveis hierárquicos para priorização das atividades topográficas. Com isso espera-se também contribuir com a melhoria das informações presentes no CANIE, que terá os dados antigos ajustados ou incorporadas novas cavernas. O avanço do projeto também visa incrementar a base de informações qualificadas de campo relativo às demais feições do carste local, colaborando assim no resultado geral para um maior entendimento do quadro natural da APANRV e, possivelmente para subsidiar a elaboração do seu plano de manejo.

Agradecimentos

A todos os funcionários da APANRV/ICMBio que auxiliaram nas pesquisas; recursos obtidos por meio do Termo de Compromisso de Compensação Espeleológica - TCCE nº 01/2022, assinado entre o ICMBio e Vale.

Referências

AULER A. S. (2016) Cave protection as a karst conservation tool in the environmentally sensitive Lagoa santa karst, southeastern Brazil. Acta Carsologica, 45(2), 131–145. https://doi.org/10.3986/ac.v45i2.4429

AULER A. S., PESSOA P. (2020. Lagoa Santa Karst: Brazil's Iconic Karst Region. Retrieved from http://link.springer.com/10.1007/978-3-030-35940-9

BRASIL. (2008) Decreto nº 6.640, de 7 de novembro de 2008. Dispõe sobre a proteção das cavidades naturais subterrâneas existentes no território nacional e dá outras providências. Diário Oficial da União, Brasília, 7 nov. 2008. Seção 1, p. 1

BRASIL. (2022) Instituto Chico Mendes de Conservação da Biodiversidade (ICMBio). Cadastro Nacional de Informações Espeleológicas (CANIE).

Disponível em: https://www.gov.br/icmbio/pt-br/assuntos/centros-de-pesquisa/cavernas/cadastro-nacional-de-informacoes-espeleologicas/canie. Acesso em: 19 de dezembro de 2022.

CAHALAN M. D., MILEWSKI A. M. (2018) Sinkhole formation mechanisms and geostatistical-based prediction analysis in a mantled karst terrain. Catena, 165, 333–344. https://doi.org/10.1016/j.catena.2018.02.010

CALDEIRA D., UAGODA R., NOGUEIRA A. M., GARNIER J., SAWAKUCHI A. O., HUSSAIN Y. (2021) Late Quaternary episodes of clastic sediment deposition in the Tarimba Cave, Central Brazil. Quaternary International, 580(January), 22–37. https://doi.org/10.1016/j.quaint.2021.01.012

CARVALHO JUNIOR, O. A., GUIMARÃES, R. F., MONTGOMERY, D. R., GILLESPIE, A. R., GOMES, R. A. T., MARTINS E. S., SILVA N. C. (2014) Karst depression detection using ASTER, ALOS/PRISM and SRTM-derived digital elevation models in the Bambuí Group, Brazil. Remote Sensing, 6, 330–351. https://doi.org/10.3390/rs6010330

FERREIRA C. F., UAGODA R. E. S. (2020) Mapeamento De Dolinas: Desafios E Possibilidades Do Uso De Modelos Digitais De Elevação. Revista Brasileira de Geomorfologia, 21(3). https://doi.org/10.20502/rbg.v21i3.1645

FERREIRA C. F., HUSSAIN Y., UAGODA R. (2022) A semi-automatic approach for doline mapping in Brazilian covered karst: the way forward to vulnerability assessment. Acta Carsologica, 51(1), 19–31. https://doi.org/10.3986/ac.v51i1.10011

GUTIERREZ F., PARISE M., DE WAELE J., JOURDE H. (2014) A review on natural and human-induced geohazards and impacts in karst. Earth-Science Reviews, 138, 61–88. https://doi.org/10.1016/j.earscirev.2014.08.002

HOFIERKA J., GALLAY M., BANDURA P., ŠASAK J. (2018) Identification of karst sinkholes in a forested karst landscape using airborne laser scanning data and water flow analysis. Geomorphology, 308, 265–277. https://doi.org/10.1016/j.geomorph.2018.02.004

LONCAR N., GRCIC I. (2022) Gis-based analysis of doline density on Miljevci karst plateau (Croatia). Acta Carsologica, 51(1), 5–17. https://doi.org/10.3986/ac.v51i1.10465

LYEW-AYEE P., VILES H. A., TUCKER G. E. (2007) The use of GIS-based digital morphometric techniques in the study of cockpit karst. Earth Surface Processes and Landforms, 32, 165–179. https://doi.org/10.1002/esp

MIHEVC A., MIHEVC R. (2021) Morphological characteristics and distribution of dolines in slovenia, a study of a lidar-based doline map of Slovenia. Acta Carsologica, 50(1), 11–36. https://doi.org/10.3986/ac.v50i1.9462

MORENO-GOMEZ M., MARTINEZ-SALVADOR C., MOULAHOUM A. W., LIEDL R., STEFAN C., PACHECO J. (2019) First steps into an integrated karst aquifer vulnerability approach (IKAV). Intrinsic groundwater vulnerability analysis of the Yucatan karst, Mexico. Water (Switzerland), 11(8). https://doi.org/10.3390/w11081610

PILÓ L. B., CRUZ J. B. (2022) A região cárstica de Pains. Brasília: ICMBio.

SALLES L. Q., GALVÃO P., LEAL L. R. B., PEREIRA R. G. F. A., PURIFICAÇÃO C. G. C., LAUREANO F. V. (2018) Evaluation of susceptibility for terrain collapse and subsidence in karst areas, municipality of Iraquara, Chapada Diamantina (BA), Brazil. Environmental Earth Sciences, 77(16), 593. https://doi.org/10.1007/s12665-018-7769-8

TELBISZ T., MARI L., SZEKELY B. (2024) LiDAR-Based Morphometry of Dolines in Aggtelek Karst (Hungary) and Slovak Karst (Slovakia). Remote Sensing, 16(5). https://doi.org/10.3390/rs16050737

TIMO M. B. (2022) Caracterização geomorfológica da região cárstica Arcos-Pains e de seus sistemas cársticos. Caderno de Geografia, 32(68), 191. https://doi.org/10.5752/p.2318-2962.2022v32n68p191

UTLU M., ÖZTÜRK M. Z. (2023) Comparison of morphometric characteristics of dolines delineated from TOPO-Maps and UAV-DEMs. Environmental Earth Sciences, 82(7). https://doi.org/10.1007/s12665-023-10862-x

WU Q., DENG C., CHEN Z. (2016) Automated delineation of karst sinkholes from LiDAR-derived digital elevation models. Geomorphology, 266, 1–10. https://doi.org/10.1016/j.geomorph.2016.05.006

Genesis and chronology of the speleothems in La Rovellonera Hall (Avenc de Sabarín Cave, Tarragona, NE Spain)

Fernando Gázquez (1,2), Carlos Cantero (3), Luis Almela (4), Jesús Almela (4), Eneko Iriarte (5), Hsun-Ming Hu (6), Chuan-Chou Shen (6) & José María Calaforra (1,2)

(1) Department of Biology and Geology. University of Almería, Carretera de Sacramento s.n, La Cañada de San Urbano, Almería, 04120, Spain. f.gazquez@ual.es (corresponding author)

(2) Centro Andaluz para el Cambio Global - Hermelindo Castro (Engloba), University of Almería, 04120, Spain

(3) Unió Excursionista de Catalunya de Tortosa, Tarragona, Spain

(4) Espeleo Club Catelló, Castelló, Spain

(5) Laboratorio de Evolución Humana. Universidad de Burgos, Spain

(6) High-Precision Mass Spectrometry and Environmental Change Laboratory (HISPEC), Department of Geosciences, National Taiwan University, Taipei 10617, Taiwan, ROC

Abstract

We investigated the age (U-Th dating) and isotopic composition (δ18O and δ13C) of epiphreatic calcite speleothems (shelves, subaquatic crusts, and poolfingers) from La Rovellonera Hall in Avenc de Sabarín Cave (Tarragona, NE Spain). The Hall is located in the upper level of the cave, 33 m above the current aquifer base level. It has an oval shape, with a height of 15 m, a maximum diameter of 30 m and shows evidence of having hosted a large underground lake. Cave clouds and poolfingers are observed aligned at different heights relative to the base of the Hall, as well as large shelves with rounded edges indicating the maximum oscillation level of the lake. These were left hanging like “cornices” when the water abandoned the lake. U-Th dating of some of these speleothems indicates that the origin of the Hall dates back over 600,000 years and that the underground lake still existed 29,000 years ago. The oxygen isotopes of the speleothem carbonate suggest that they may have formed from waters with temperatures ranging from 7°C to 16°C, like the current cave temperature (~8.5°C), so with no influence of thermal water. Further studies on these speleothems may shed light on the paleohydrological evolution of the regional aquifer.

1. Introduction

Precipitation of subaqueous carbonate speleothems in caves occurs within phreatic and epiphreatic environments, either under low-temperature or hydrothermal conditions (e.g. KLUGE et al., 2014; GÁZQUEZ et al., 2018; KOLTAI et al., 2024). The presence of subaqueous speleothem in caves indicates total or partial flooding at the time of carbonate precipitation. Therefore, by determining the age of different subaqueous speleothems located at different depths, it may be possible to track the evolution of the water table over time in karstic aquifer hosting caves (e.g. GÁZQUEZ et al., 2018).

Besides, the oxygen and carbon isotope composition ($\delta^{18}O$ and $\delta^{13}C$) of speleothemic carbonate can provide information about long-term environmental changes in the cave, including water temperature oscillations in relation to paleohydrological variability (e.g. KLUGE et al., 2014; GÁZQUEZ et al., 2018; KOLTAI et al., 2024, among many others).

The recently discovered La Rovellonera Hall in the Avenc de Sabarín cave (Tarragona, NE Spain) (UEC TORTOSA et al., 2024), offers a unique opportunity to study subaqueous speleothem. The Hall, with a maximum diameter of 30 m and a height of up to 15 m, houses spectacular formations of subaqueous calcite speleothems that appear horizontally aligned at different levels, indicating past water-level paleo-positions.

In this study, the age of some of these speleothems was investigated by means of U-Th isotope dating, along with their oxygen and carbon isotopic compositions, in order to unearth the timing and environmental conditions in which they formed. The objectives were to determine the temporal framework of past water-level fluctuations in the Hall, the timing when the phreatic water abandoned this cave level, and to make a preliminary estimation of the water temperature at the time of speleothem formation.

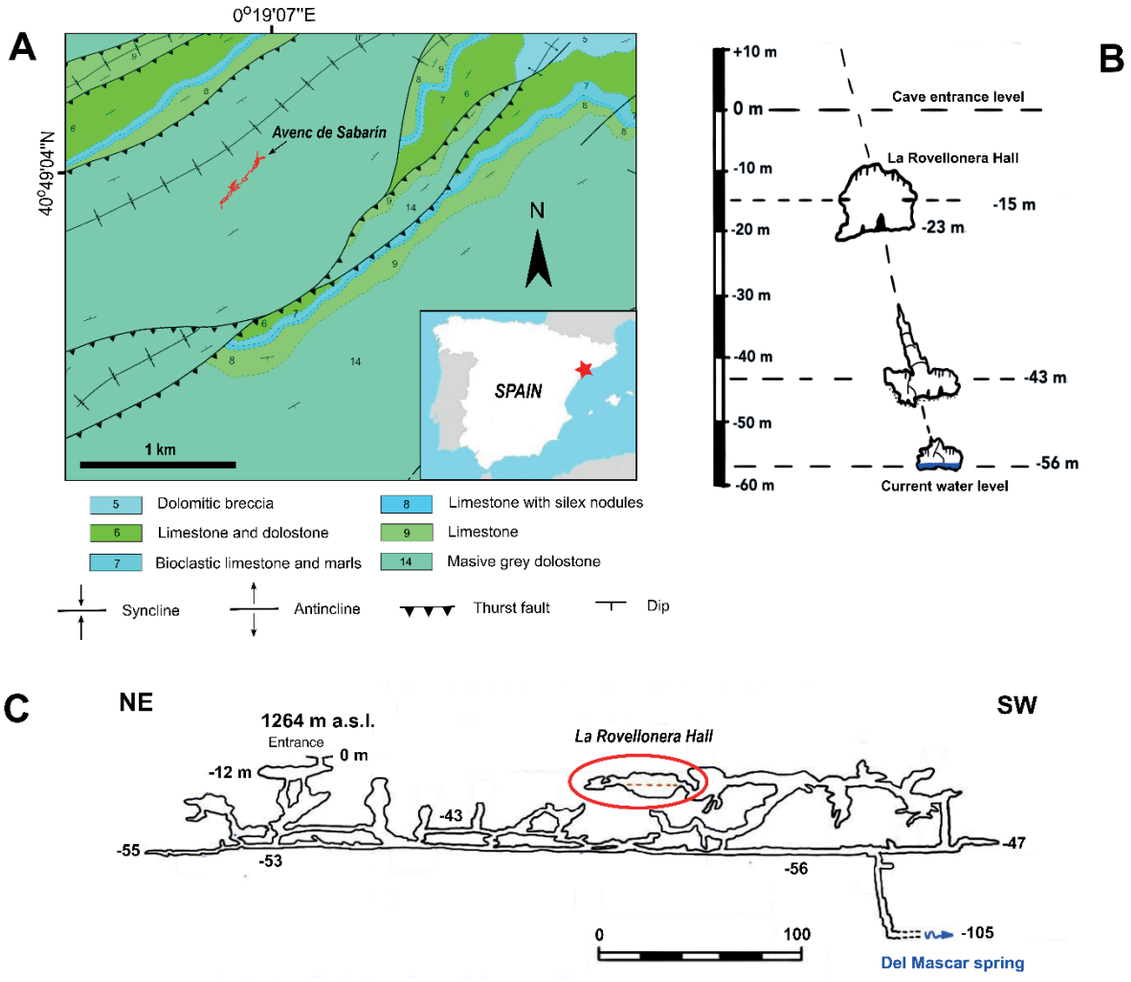

Figure 1: *A. Location of Avenc de Sabarín cave. The cave is developed in Jurassic dolostone. Geological map modified from MAGNA 1:50,000 (GARCIA DE DOMINGO & LOPEZ-OLMEDO et al., 1982). B. Location of the three main levels of galleries within the cave, including the level where La Rovellonera Hall is located. C. Cross section of Avenc de Sabarín cave.*

2. Geological setting and cave description

Avenc the Sabarín cave is located in the Massís dels Ports (S Tarragona province, NE Spain), at the contact between the Iberian Mountain Range and the Catalan Prelitoral Range. This massif consists of kasrtified Mesozoic carbonate materials. In particular, the cave is developed in Upper Jurassic dolostone (Figure 1). La Mola de Catí mountain, where the cave is located, has a maximum elevation of 1,326 m a.s.l. and sharp slopes. The massif is highly kartified, as evidenced by the presence of caves systems some of which exceed 1 km in length. Around the Mola de Catí mountain, various springs are found, Font del Mascar on the southeastern slope, being the most relevant.

In the heart of the Mola de Catí lies Avenc de Sabarín cave, which, with its 2,689 m of passages and a maximum depth of -105 m, has become a renowned cavity for speleological activities in recent years. The first references to this cave date back to 1945. More recently, between 2009 and 2020, it was surveyed and topographically documented.

The entrance lies at 1,219 m and the cave´s development occurs along a large NE-SW oriented fracture that dictates the alignment of its galleries. This results in a generally sub-horizontal pattern, spanning approximately 500 m in length. Broadly speaking, the cave can be divided into three sectors according to the sub-horizontal development of its passages: the upper levels (-10 to -20 m deep) that are composed of galleries and chambers with broader cross-sections and a notable abundance of speleothems, the intermediate levels (-20 to -50 m) with smaller galleries sometime not being interconnected, and the lower levels (-50 to -56 m and below), which is occupied by a perennial water course. This river plunges through several shafts before vanishing at the cavity's deepest point, at -105 m. The topographically lower cave passages are partially under water and can get completely flooded during heavy rain events (Figure 2). In 2020, within the upper cave level, the extraordinary La Rovellonera Hall was discovered (Figure 3).

Figure 2: *La Rovellonera Hall within Avenc de Sabarín cave. Note the level of shelves in the middle part of panel A. Subaqueous speleothems, like cave clouds, are found beneath this leve of shelves, as observed in panel B. Different levels of shelves (in the range of 50 cm in heigh) can be found at 8 m from the Hall´s floor (panel C).*

3. Materials and methods

Sampling of speleothems and water

In January 2023, eight carbonate samples were collected from different parts of the Rovellonera Hall at varying heights from the base, ranging from 0.25 to 8 m. Samples were primarily taken from shelves that mark levels of relative stability of water at 0.25 (ROV-01), 0.9 (ROV-02), 7.5 (ROV-07), and 8 m (ROV-04 and ROV-06) from the Hall´s bottom. A sample of calcite rafts (ROV-05) was collected from a still active pond located over the upper most shelves at 8 m from the base. In addition, 2 samples of subaqueous cylindrical speleothems with rounded tips, typified here as « pool fingers », that show up hanging from the walls at different heights were collected (at 1 m, ROV-03, and at 6.5 m, ROV-08, from the Hall´s bottom). Finally, a sample of a modern, actively growing self (NEO) at the lowest level of the cave (-56 m) where the current cave river flows, was collected. Water samples were taken at the sites where calcite samples ROV-05 and NEO were collected.

U-Th dating

The ages of carbonate samples ROV-03, ROV-04, ROV-07 and ROV-08 were determined by U-Th isotope dating at the High-Precision Mass Spectrometry and Environment Change Lab (HISPEC) at the National Taiwan University using resin column separation and a multicollector inductively coupled plasma mass spectrometer (MC-ICPMS). Details of the analytical protocol and isotopic parameters used for age calculations can be found in SHEN et al. (2012).

Stable isotopes

Ten powdered samples were analyzed for stable isotopes of carbonates, using a Gas Bench II (Thermo Scientific) sample preparation device coupled with a DELTA V Plus isotope ratio mass spectrometer (Thermo Scientific) at the University of Burgos (Spain). The isotopic composition of oxygen and carbon ($\delta^{18}O$ and $\delta^{13}C$) was standardized against the international V-PDB standard. The reproducibility of the method was ±0.03‰ (1σ) for $\delta^{13}C$ and ±0.05‰ for $\delta^{18}O$, based on the analysis of internal standards. The $\delta^{18}O$ values in the V-PDB scale were converted to V-SMOW (Vienna Standard Mean Ocean Water) using the formula provided by COPLEN (1995) to facilitate comparison with water values. The two liquid water samples were analyzed for $\delta^{18}O$ and $\delta^{2}H$ at the University of Almería using a Picarro L2140i isotope analyzer. Results are standardized against V-SMOW and given as ‰ units.

Sample	Description	^{238}U 10^{-9}g/g [a]		^{232}Th 10^{-9}g/g		$d^{234}U$ measured[a]		$[^{230}Th/^{238}U]$ activity[c]		$^{230}Th/^{232}Th$ atomic ($\times 10^{-6}$)		Age (kyr ago) uncorrected		Age (kyr ago) corrected [c,d]		$\delta^{234}U_{initial}$ corrected[b]		$\delta^{13}C$ ‰	$\delta^{18}O$ ‰
ROV-01	Shelf at 0.25 m																	-5.96	-5.96
ROV-02	Shelf at 0.9 m																	-5.20	-5.07
ROV-03a	Pool finger at 1 m	102.69	± 0.18	19.608	± 0.066	82.7	± 1.9	1.1198	± 0.0028	96.70	± 0.37	>600		>600		-		-3.88	-5.31
ROV-03b	Pool finger at 1 m																	-5.72	-6.14
ROV-04	Shelf at 8 m	79.70	± 0.14	7.436	± 0.023	1720.1	± 4.3	0.6752	± 0.0021	119.33	± 0.48	30.19	± 0.12	29.33	± 0.45	1868.6	± 5.3	-7.86	-5.23
ROV-05	Calcite rafts																	-9.71	-6.20
ROV-06	Shelf at 8 m																	-6.78	-6.30
ROV-07	Shelf at 7.5 m	149.55	± 0.19	14.427	± 0.051	32.8	± 1.6	1.0415	± 0.0026	178.00	± 0.74	583	± 72	581	± 71	169	± 47	-8.76	-6.86
ROV-08	Pool finger at 6.5 m	138.92	± 0.13	12.346	± 0.051	63.6	± 1.5	1.0652	± 0.0037	197.6	± 1.0	424	± 19	422	± 18	209	± 13	-7.80	-6.38
NEO	Modern shelf lower cave level																	-10.39	-6.02

Table 1: *U-Th ages and carbon and oxygen isotopes of carbonate. Analytical errors are 2σ of the mean. [a] $[^{238}U] = [^{235}U] \times 137.818$ (±0.65‰) (HIESS et al., 2012); $\delta^{234}U = ([^{234}U/^{238}U]_{activity} - 1) \times 1000$. [b] $\delta^{234}U_{initial}$ corrected was calculated based on ^{230}Th age (T), i.e., $\delta^{234}U_{initial} = \delta^{234}U_{measured} \times e^{\lambda 234 \times T}$, and T is corrected age. [c] $[^{230}Th/^{238}U]_{activity} = 1 - e^{-\lambda 230 T} + (\delta^{234}U_{measured}/1000)[\lambda_{230}/(\lambda_{230} - \lambda_{234})](1 - e^{-(\lambda 230 - \lambda 234) T})$, where T is the age. Decay constants are 9.1705 × 10^{-6} yr^{-1} for ^{230}Th, 2.8221 x 10^{-6} yr^{-1} for ^{234}U (CHENG et al., 2013), and 1.55125 x 10^{-10} yr^{-1} for ^{238}U (JAFFEY et al., 1971). [d] Age corrections, relative to 2023 C.E., were calculated using an estimated atomic $^{230}Th/^{232}Th$ ratio of 4 (± 2) x 10^{-6} (SHEN et al., 2008). Those are the values for a material at secular equilibrium, with the crustal $^{232}Th/^{238}U$ value of 3.8. The errors are arbitrarily assumed to be 50%.*

4. Results

U-Th dating

^{238}U content in the four analyzed samples ranged from 78 to 150 ppb. The $^{230}Th/^{232}Th$ activity ratio, which together with the error associated with the calculation of $^{238}U/^{234}U/^{230}Th/^{232}Th$ rules the uncertainties associated with the final ages, is relatively high (>95), indicating low detrital thorium contamination. As a result, the ^{230}Th corrected age differs by less than 5% to the "uncorrected" ages. The age of the pool finger collected from the lower part of the Hall exceeds the U-Th dating limit, indicating >600 ka (where ka is 1000 years). The shelf at 7.5 m from the bottom was dated to 581±71 ka, while the pool finger at 6.5 m was determined to be 422±18 ka. The youngest speleothem analyzed in this study is the upper shelf (8 m), dated to 29.3±0.4 ka.

Stable isotopes

The $\delta^{18}O$ values of carbonate samples (n=10), previously confirmed to be calcite by XRD analyses, ranged from -6.86 to -5.07‰, while $\delta^{13}C$ did from -10.39 to -3.88‰ (V-PDB) (Table 1). The highest $\delta^{18}O$ values correspond to the shelf at 0.9 m from the Hall´s bottom, whereas the shelf at 7.5 m show the lowest values. The highest $\delta^{13}C$ values were found in the poolfingers at 1 m, while the lowest were recorded by calcite shelves collected at the lowest cave passages, ca. 44 m below La Rovellonera Hall, likely of recent origin. The $\delta^{18}O$ of water in a gour at the Hall was -6.06‰ (V-SMOW), while the $\delta^{2}H$ value was -37.7‰. For the water from the underground river at the -56 m deep level, the $\delta^{18}O$ was -7.01‰ and the $\delta^{2}H$ was -42.1‰.

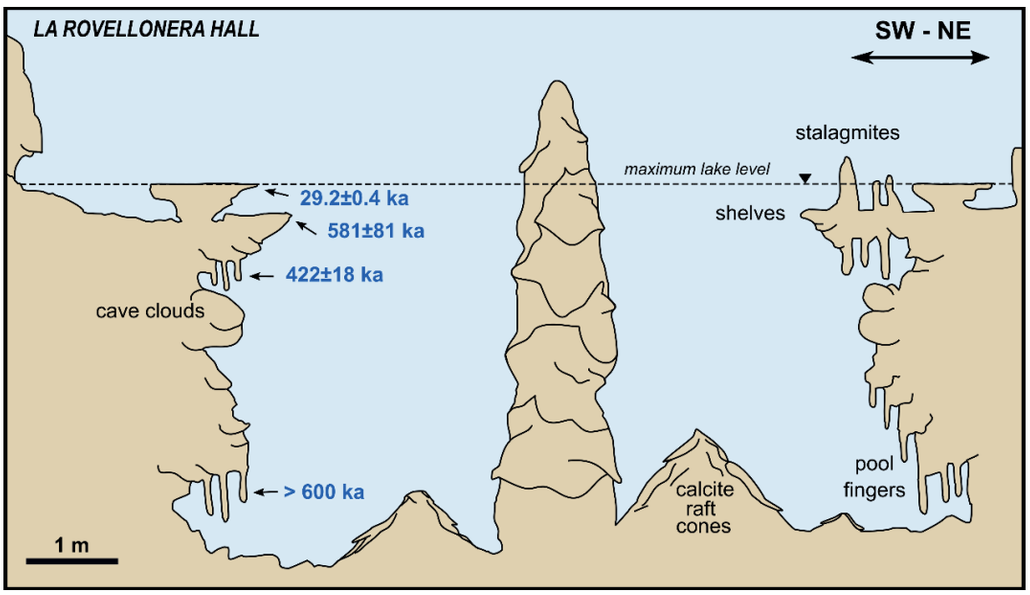

Figure 3: *Scheck of La Rovellonera Hall and approximated position of the main speleothems and their ages.*

5. Discussion

The age of the subaqueous speleothems in La Rovellonera Hall ranges from >600 to 29 ka. This suggests that the -12 m-deep cave level was occupied by water, continuously or discontinuously, for at least 570 ka. The oldest speleothems have been found in the middle and lower parts of the Hall. This includes cave clouds that coat its walls, and in pool fingers appearing at various levels of depth. Specifically, the pool fingers located in the lowest part, 1 m above the base of the paleolake, exhibit the oldest ages. The uppermost edge of the shelves, 8 m above the lower part of the chamber, shows the youngest age of 29 ka. This could indicate that the lake still existed during the last glacial period. However, given the limited number of samples in our study, it is difficult to determine whether it persisted continuously or discontinuously, with phases of fluctuating water levels.

The stable isotopes of carbonate have been analyzed to make a preliminary estimate of the speleothem formation temperatures. This approach considers that the fractionation of oxygen isotopes in equilibrium between the dissolved water and the precipitating carbonate depends on temperature (e.g., TREMAINE et al., 2011). Therefore, by knowing $\delta^{18}O_{calcite}$ and $\delta^{18}O_{water}$, and assuming carbonate precipitation occurred in equilibrium, it is possible to determine the mineral formation temperature.

The $\delta^{18}O_{water}$ values in the speleothems analyzed from La Rovellonera Hall are −5.9±0.6‰ (V-PDB). The past isotopic composition of the water ($\delta^{18}O_{water}$) in paleo-lake is unknown but can be approximated using the values of current cave waters, averaging −6.8±0.6 ‰ (V-SMOW). As shown in Figure 4, the combination of $\delta^{18}O_{calcite}$ and $\delta^{18}O_{water}$ suggests that the formation temperature of the speleothems in La Rovellonera Hall averaged 12°C, ranging from 7°C to 16°C, considering the range of values obtained for both carbonate and current cave waters (±1σ and ±2σ). The modern water temperature of the underground cave river is 8.6±0.1oC (five measurements between 2021 and 2023; UEC TORTOSA et al., 2024), in good agreement with the estimated paleo-temperatures. The inferred formation temperature of the speleothems likely encompasses the whole temperature variability expected for glacial–interglacial transitions during the Quaternary, so our approach does not allow for precise paleoenvironmental interpretations regarding changes in cave water temperature during speleothem formation. However, it has allowed us to rule out the contribution of hydrothermal flows to the formation of these speleothems, as such flows would have resulted in lower $\delta^{18}O_{calcite}$ values (e.g. GÁZQUEZ et al., 2018).

Our approach assumes that the$\delta^{18}O_{water}$ during speleothem formation was similar to the current value in the cave water. It is possible that this value has varied over time due to global and regional hydrometeorological changes. However, several studies suggest that the $\delta^{18}O$ value in meteoric water on a Glacial-Interglacial scale in the central and western Mediterranean may have changed by ~1‰ during last Glacial-Interglacial cycle (JASECHKO et al., 2015). An ±1‰ change in $\delta^{18}O_{water}$ when using the TREMAINE et al., (2011) paleothermometry equation results in a variability of ~5°C in paleotemperature calculations. Therefore, it can still be concluded that the epiphreatic speleothems in Avenc de Sabarín cave did not form at temperatures higher than 21°C or lower than 2°C, still supporting the hypothesis of no hydrothermal contribution to the cave formation. Further analyses of fluid inclusions and clumped isotope (Δ47) in these speleothems may result in accurate paleotemperature reconstructions (e.g. KLUGE et al., 2014; GÁZQUEZ et al., 2018; KOLTAI et al., 2024).

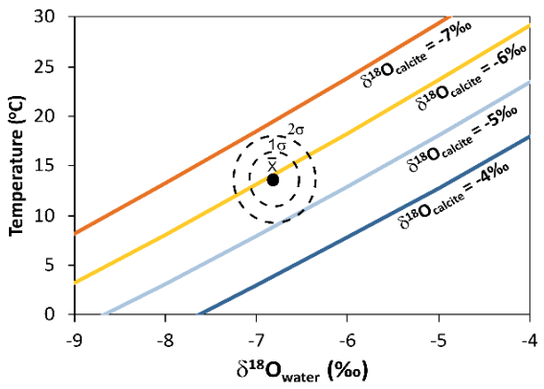

Figure 4. Relationship between $\delta^{18}O_{water}$, $\delta^{18}O_{calcite}$ and water temperature according to the paleotemperature equation by TREMAINE et al., (2011). The x value is the mean of the $\delta^{18}O_{calcite}$ (V-PDB) of the speleothems from La Rovellonera Hall analyzed in this study (n=9) and the mean $\delta^{18}O_{water}$ (V-SMOW) of the two water samples analyzed from the cave. The dashed-line ellipsoids represent the 1σ and 2σ of the mean for both isotope parameters.

6. Conclusions

The geochemical analyses of epiphreatic speleothems from La Rovellonera Hall in Avenc de Sabarín cave indicate that the shallower levels of the cavity (-12 to -20 m) were occupied by water at least between 600 and 422 ka, and later around 29 ka. The study of a continuous speleothem sequence extracted from the Hall, such as a core sample from a subaqueous flowstone or a cave cloud, could shed light on whether the hall was permanently or intermittently occupied by water during that period. Stable isotope analyses of the carbonate suggest that the water from which the speleothems formed had a temperature between 7 and 16 oC, indicating that the cavity did not receive hydrothermal water inputs for at least the last 600 ka. Additional fluid inclusion and clumped isotope analyses could refine these temperature estimates. Finally, the distribution of cave passages across three well-differentiated subhorizontal levels suggests three stages of relative stability in the aquifer's phreatic level, likely related to the paleogeographic evolution of the Ebro Delta. These stages may have been a consequence of the river's incision process and a response to tectonic history of the northeastern Iberian Peninsula. Studying the age of vadose and epiphreatic speleothems at different levels of the cavity could provide insights into the paleogeography of this region during the Late Quaternary.

Acknowledgments

This research was funded by the Project P_FORT_GRUPOS_2023/17 of the University of Almería and Junta de Andalucía Regional Government through European Union FEDER funds and the funds of the Water Resources and Environmental Geology Group (RNM-189) of University of Almería. Dr. Fernando Gázquez thanks the Ramón y Cajal contract (RYC2020-029811-I) and the PPIT-UAL grant from the Junta de Andalucía-FEDER 2022-2026 (RyC-PPI2021-01).

References

CHENG, H., EDWARDS, R.L., SHEN, et al. (2013). Improvements in 230Th dating, 230Th and 234U half-life values, and U-Th isotopic measurements by multi-collector inductively coupled plasma mass spectrometry. Earth Planet. Sci. Lett. 371-372, 82–91.

COPLEN, T.B. (1995) Reporting of stable carbon, hydrogen, and oxygen isotopic abundances. In: Reference and intercomparison materials for stable isotopes of light elements. International Atomic Energy Agency, TECDOC, pp. 31-34.

GARCIA DE DOMINGO, A. & LOPEZ OLMEDO, F. 1982. Mapa Geológico de España E 1:50000 n° 521 (Beceite). Segunda serie (MAGNA).

GAZQUEZ, F., COLUMBU, A., DE WAELE, J. et al., (2018). Quantification of paleo-aquifer changes using clumped isotopes in subaqueous carbonate speleothems. Chem. Geol. 493, 246–257.

HIESS, J., CONDON, D.J., MCLEAN, N., et al. (2012). 238U/235U systematics in terrestrial uranium-bearing minerals. Science 335, 1610-1614.

JAFFEY, A.H., FLYNN, K.F., GLENDENIN, L.F., et al., (1971). Precision measurements of half-lives and specific activities of 235U and 238U. Phys. Rev. C4, 1889-1906.

JASECHKO, S., LECHLER, A., PAUSATA, F. et al. (2015). Late-Glacial to late--Holocene shifts in global precipitation δ18O. Clim. Past. 11, 1375–1393.

KLUGE, T., AFFEK, H.P., DUBLYANSKY, Y. et al. (2014). Devils hole paleotemperatures and implications for oxygen isotope equilibrium fractionation. Earth Planet. Sci. Lett. 400, 251–260.

KOLTAI, G., KLUGE, T. & KRÜGER, Y. et al. (2024) Geothermometry of calcite spar at 10–50 °C. Sci. Rep. 14, 1553.

SHEN, C.-C., WU, C.-C., CHENG, H., et al., (2012). High-precision and high--resolution carbonate 230Th dating by MC-ICP-MS with SEM protocols. Geochim. Cosmochim. Acta 99, 71–86.

TREMAINE, D.M., FROELICH, P.N. & WANG, Y. (2011). Speleothem calcite farmed in situ: Modern calibration of $\delta^{18}O$ and $\delta^{13}C$ paleoclimate proxies in a continuously-monitored natural cave system. Geochim. Cosmochim. Acta 75, 4929–4950.

UEC TORTOSA, CARLOS CANTERO, LUIS ALMELA, et al. (2024). La Sala de la Rovellonera de l'Avenc Sabarín i els seus excepcionals espeleotemes subaquàtics. Revista de la Sociedad Catalana de Espeleología (EspeleoCAT).

Speleogenesis of Puntali Cave (Sicily, Italy): an example of flank margin cave in telogenetic limestones

Annalucia Gullo (1), Giuliana Madonia (1,2), Giovanna Scopelliti (1), Marco Vattano (3) & Cipriano Di Maggio (1)

(1) Department of Earth and Marine Science, University of Palermo, Italy, annalucia.gullo@community.unipa.it, giuliana.madonia@unipa.it (corresponding author) giovanna.scopelliti@unipa.it, cipriano.dimaggio@unipa.it

(2) National Biodiversity Future Center (NBFC), Palermo, Italy

(3) ANS Le Taddarite, Palermo, Italy marco.vattano@gmail.com

Abstract

Puntali Cave is located in the north-western sector of the Palermo Mountains (NW Sicily, Italy). This area recorded the interaction effects between Quaternary tectonics and sea-level fluctuations. Currently, the cave hosts one of the most populous bat colonies in Western Sicily. The analysis of the cave and surface morphologies, and the characterization of the cave deposits, support the hypothesis that Puntali Cave originated as a flank margin cave and later evolved into a continental environment until the present, when the biotic component boosts active speleogenetic processes. Furthermore, through comparison with literature data the age of the early evolutionary phases of the cave has been estimated.

1. Introduction

Flank margin caves are coastal mixing caves. MYLROIE & CAREW (1990) proposed a model to interpret the genesis of mixing caves in immature young carbonate coasts. These caves form by mixing dissolution processes in the distal margin of the freshwater lens, under the flank of the enclosing landmass. The development of caves is controlled by the position of the fresh-salt water mixing boundary, which in turn, is connected to sea-level position.

The flank margin caves model was later extended to similar caves in telogenetic carbonates where structural control becomes more evident (MYLROIE et al., 2008; OTONIČAR et al., 2010; RUGGIERI & DE WAELE, 2014; D'ANGELI et al., 2015; DE WAELE et al., 2025).

A flank margin cave is characterized by passages that are more developed in width than in height, from which smaller conduits branch, dead-ended passages, rounded and smooth wall morphologies that indicate the involvement of undersaturated solutions in slow flows under phreatic conditions. Lack of morphologies and deposits from fast and turbulent flow is diagnostic (MYLROIE et al., 2008; MYLROIE & MYLROIE, 2013).

Puntali Cave is located in the north-western sector of the Palermo Mountains (NW Sicily, Italy), at the western edge of the Carini Plain about 2.5 km from the coastline.

The Carini Plain is bordered by high degraded carbonate paleo-cliffs and is characterized by several orders of marine terraces, resulting from the interaction between Quaternary tectonic uplift and sea-level fluctuations. A post-Tyrrhenian uplift rate of 0.15 m/ky has been estimated for the plain (ISPRA, 2013). In this area, Palermo Mountains are affected by NW-SE, NNW-SSE, N-S and NE-SW fault systems.

Since the second half of the 19th century, Puntali Cave has been recognized as a site of significant paleontological and archaeological interest. It is renowned for its important late Middle and Upper Pleistocene vertebrate deposits (BADA et al., 1991); traces of human frequentation in prehistoric times ranges from the Upper Paleolithic to the Bronze Age (DI MAIDA et al., 2020).

For over than 20 years, Puntali Cave has been protected as a Regional Integral Nature Reserve due to its speleological interest and for hosting a large bat colony.

2. Materials and methods

A detailed geomorphological survey was carried out on the surface and inside the cave. To characterize the physical cave deposits, nine sediment samples were taken from the floor or from small pockets in the walls. Ten incrustation samples were also collected from the walls.

Sedimentological and mineralogical analysis were carried out at the DiSTeM Labs (Palermo, Italy).

Sediments samples were washed through a 63 µm sieved and dried at 70°C. The >63-µm size fraction was observed under a reflected light microscope and visual comparison charts were used to estimate the classifying or sorting σ, degree of roundness and sphericity. The sieve was decanted for at least 24h, dried at 70°C and weighed with a precision balance. Bulk mineralogy of all samples (sediments and crusts) was determined by powder X-ray diffraction (XRD) using a Philips PW14 1373 with a Cu-Kα radiation filtered by a monochromator crystal and a 2° 2θ/minute scanning speed. The color was defined on dry powdered samples using the Munsell Standard Soil Color Chart, then converted in RGB codes.

3. Results

Puntali Cave opens at about 100 m a.s.l., at the base of an approximately 10 m high NE-facing cliff which connects two subplanar surfaces. To the North of the entrance, the cliff is cut by cavities and notches arranged on three levels: at its base, roughly 2.5 m and 4.5 m above ground level. The middle and upper levels follow along two notches within the cave (Figs. 1, 3).

Figure 1: *The three levels of notches and cavities cutting the cliff where Puntali Cave opens.*

The cave extends horizontally for 290 m in Lower Cretaceous-Upper Jurassic forereef limestone, mainly in NW-SE and NE-SW direction. At two-thirds of the way from the entrance, a branch develops downward, reaching a depth of 21 m below the upper level (Fig. 2).

Puntali Cave has a single entrance with a larger dimension in width than in height. The cave is made up of large chambers in the first and middle sections, smaller galleries in the mid-inner portion and finally passages closed by collapse boulders or due to the progressive lowering of the roof. The cave floor slopes inward and is covered by different types of deposits varying in thickness (i.e., collapse debris and boulders, fine terrigenous material, and bat guano).

Currently, the cave is hydraulically connected to the outside by wall percolation and ceiling drip which cause localized water stagnation.

Walls and roof of the cave passages are show different dissolution morphologies. These are discrete parietal sculptures or have spatial continuity; they are mostly concave rounded forms, generally decimetric in width/length and in depth. Among these, small phreatic tubes, solution pockets, spongework morphologies, and large scallops were recognized. Niches and cupolas, cusps, and altered smooth walls and ceilings characterize most of the cave (Fig. 3).

Two sub-horizontal notches were identified at different levels along the walls of the cave. One develops at the base of the walls at the same height as the middle level of the cavities/notches on the outer cliff, the upper one cuts the cave walls about 2 m from the first and correlates with the upper level of the outer cavities/notches. The lower notch has greater continuity through the different rooms of the cave; its base is almost always hidden by the fine sediments that cover the cave floor (Fig. 3).

Various kinds of deposits were found in the Puntali Cave. Chemical deposits consist mainly of carbonate speleothems related to dripping and flowing water, and incrustations.

Speleothems are almost always heavily corroded (Fig. 3). The incrustations differ in terms of consistency (hard to dusty-earthy), shape (speckled, elongated in the discontinuity direction, irregular), color (black, brown, grey, yellow, rust), location (on the wall, inside or above fractures) and thickness (from a few millimeters to a few centimeters). XRD analysis showed a predominantly hydroxyl/fluoroapatite composition for most of the crusts, sometimes with smaller percentages of calcite, quartz and clay minerals. Only one sample has a brushitic composition, with smaller amounts of hydroxyl/fluoroapatite and gypsum. The color of the powders is in the brown, grey and white tones.

Physical deposits include collapse debris and fine sediments (Fig. 3). The latter are on the floor, at the base of walls protected by niches, or in pockets carved into the walls. Textural maturity is moderate to high. The pelitic fraction is prevalent. The color of the powders is in the brown and yellow tones. The mineralogical composition consists mainly of clay and quartz, with smaller percentages of iron oxides and phosphates.

Other deposits are vermiculations, thick biological deposits linked to the presence of bat colony (guano) and remains of Pleistocene faunas, and Anthropozoic deposits which can be attributed to man frequentation of the cave in prehistoric times.

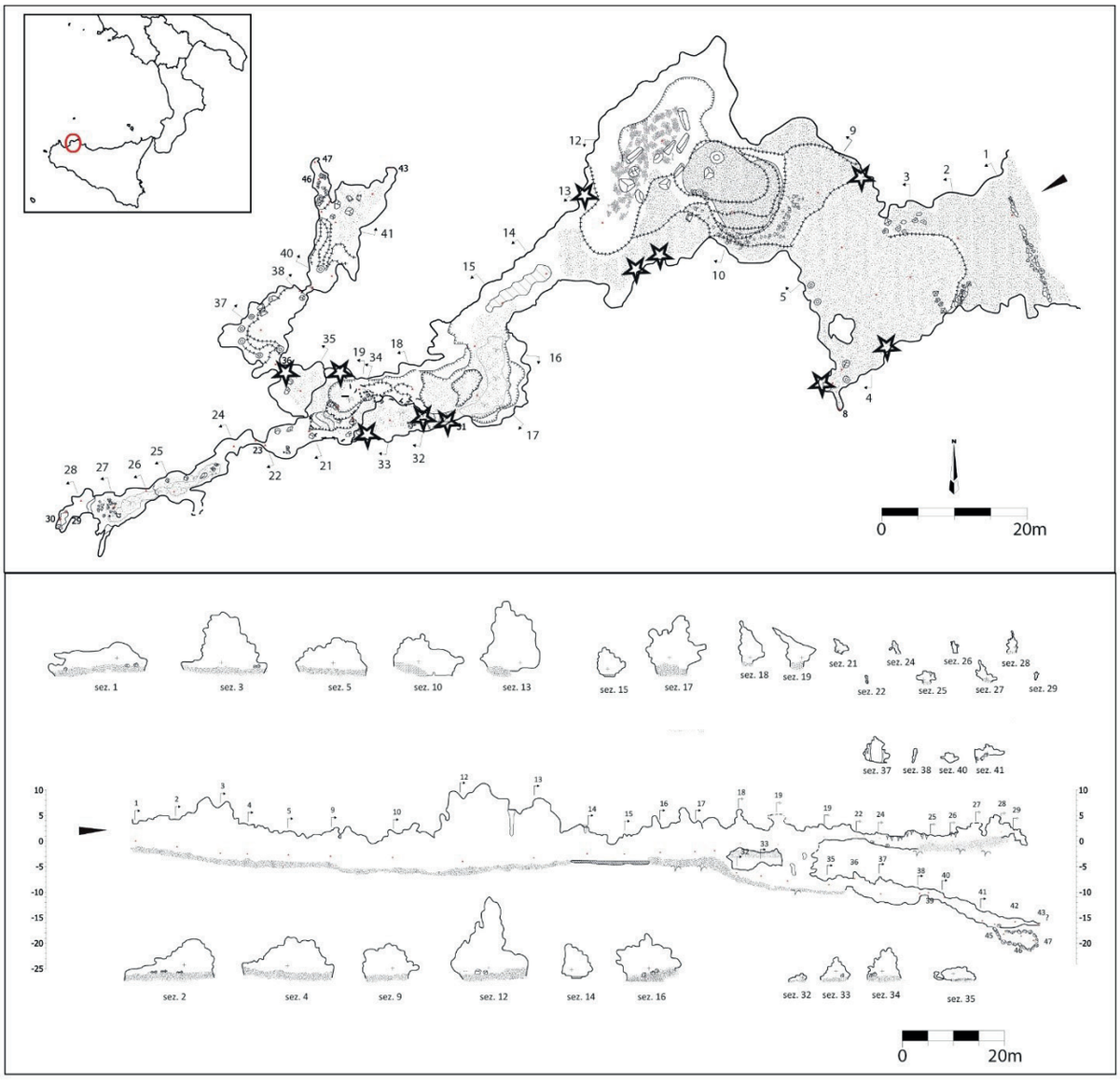

Figure 2: *Survey of Puntali Cave (redrawn after Grotta dei Puntali NR archive). Stars in the plan view indicate the sampling sites. Location of Puntali Cave in the box.*

4. Discussion

The results obtained allow us to identify a marine origin for Puntali Cave. A sequence of marine terraces occurs along the Carini plain in various orders, from sea level up to 200 m a.s.l. (DI MAGGIO, 2000). The inner edge of the V-order terrace lies at 100 m a.s.l.; the cliff base where the cave opens lies at the same altitude. This, together with the slope morphologies allows us to interpret the sub-horizontal surfaces as degraded marine abrasion platforms and the escarpment as a coastal paleo-cliff. The presence of the notches in the cave suggests the control of a standstill of the base level and their formation may be linked to the same phases of relative sea level standstill responsible for the cutting of the notches/cavities on the coastal paleo-cliff.

The rounded and smoothed wall morphologies in the cave as large scallops, solution pockets, spongework-like features, small phreatic tubes, can be related to mixing dissolution by slow flow. In contrast, evidences of fast and turbulent flows, such as scallops or canyons, are absent.

The development of the cave is roughly perpendicular to the paleo-cliff where it opens. The large environments in the first and middle portions and the branching of the cave in its inner part can be explained as the result of preferential dissolution at mixing interfaces compatible with the pseudo-lenticular configuration of a coastal freshwater aquifer. These clues lead to the conclusion that Puntali Cave originated as a flank margin cave, under phreatic conditions, when the piezometric level was at sea level.

A comparison between the plan development of the cave and the structural features of the region reveals a strong structural control, as predicted by the flank margin cave model in mature carbonate coastlines (MYLROIE et al., 2008).

The age of the cave was estimated from the available data. If an uplift rate equal to the post-Tyrrhenian (0.15 m/ka; ISPRA, 2013) is attributed to the pre-Tyrrhenian, the cave, which currently opens at 100 m a.s.l., should have been at sea level more than 450 ka, which is the time limit of most eustatic curves calculated by various authors (CAPUTO, 2007).

From the resolution of the equation of HANSEN et al. (2013) and with the help of δ18O values derived by COHEN & GIBBARD (2019), for the interglacial phases prior to 450 ka, an uplift rate compatible with the post-Thyrrenian rate is obtained for MIS 19.

Within MIS 19 itself, at least three phases of relative sea-level standstill occurred, as evidenced by the three levels of notches/cavities outside and inside the cave. The uplift tendency of the chain sector in this area would justify a downward rejuvenation of these notches.

Taking into consideration the uplift rate, the cave entered the continental phase starting from MIS 17. Since this stage, the cave probably has been subjected to processes currently active: enlargement by collapse, condensation/corrosion processes, vadose speleothems formation and filling by physical deposits.

The analysis of the physical cave deposits revealed their continental origin. Collapse debris, and fine sediments found inside pockets in the wall have an autochthonous nature. In particular, fine sediments have a grain size and composition compatible with those detected by DURN (2003) and MERLAK (2019) for the insoluble residue of carbonate rock. But the larger volumes of the physical deposits in the cave are certainly allogenic. Indeed, the analysis of fine terrigenous sediment samples taken from the floor and at the base of walls, revealed a predominantly quartz composition of the coarsest portion (Φ > 63 μm) and a good textural maturity of the quartz clasts. The predominantly pelitic grain size of the same samples can be related to deposition by settling from a suspension. This type of sedimentation is proposed to be the result of deposition in one or more water pools, fed by the filtration of material from the surface, carried by seepage water through the fracture network in the rock. Additionally, it is not excluded this fine material may also have an aeolian origin.

In most recent and current phases, the cave undergoes the effects of the condensation corrosion processes, mainly linked to the action of water vapor acidified by the digestion products of bat guano. The resulting wall morphologies mask and overlap the original morphologies, re-proposing the smoothed and rounded shapes of the mixing karst (large scallops, cupolas, niches, cusps) and making it difficult to attribute them to one phenomenon rather than the other.

The interaction between the acidic aqueous solutions thus derived and the carbonate substrate produces the incrustations with a predominantly hydroxyl/fluoroapatite composition, subordinately brushitic and gypsum in small percentages.

Figure 3: *The larger chamber of Puntali Cave. The notch correlated to the middle outer notch is visible. Walls and roof show different dissolution rounded morphologies as niches and cusps, cupolas, megascallops. Corroded carbonate speleothems hang from the ceiling. Brown fine sediments and collapse debris cover the floor (photo M. Vattano, Grotta dei Puntali NR archive).*

5. Conclusion

Puntali Cave originated in a phreatic environment as a flank margin cave between the Lower and Middle Pleistocene (MIS 19). Within the same isotopic stage, the interaction between uplift of the area and eustatic variation led to at least three episodes of sea-level standstill at different altitudes. Probably already since MIS 17, the cave has evolved under continental conditions.

The recent and current evolution of the cave is linked to dissolution condensation processes boosted by vapor acidified by the presence of bat guano, mineralization and vadose speleothems formation, and filling by fine terrigenous sediments.

Acknowledgments

We gratefully thank the Gruppi Ricerca Ecologica (GRE) Sicilia, managing body of the “Integral Natural Reserve of Puntali Cave” authorizing this study and Dr. P. Valenti for his help during the speleological survey and sampling. GM acknowledges the support of NBFC to University of Palermo, funded by the Italian Ministry of University and Research, PNRR, Missione 4, Componente 2, “Dalla ricerca all’impresa”, Investimento 1.4, Project CN00000033.

References

BADA J.L., BELLUOMINI G., BONFIGLIO L., BRANCA M., BURGIO E., DELITALA L. (1991). Isoleucine epimerization ages of Quaternary mammals from Sicily. Il Quaternario 4 (1a):49-54.

CAPUTO R. (2007). Sea-level curves: Perplexities of an end-user in morphotectonic applications. Global and Planetary Change 57(3–4):417-423.

COHEN K.M., GIBBARD P.L. (2019). Global chronostratigraphical correlation table for the last 2.7 million years, version 2019 QI-500. Quaternary International 500:20–31

D’ANGELI I.M., SANNA L., CALZONI C., DE WAELE J. (2015). Uplifted flank margin caves in telogenetic limestones in the Gulf of Orosei (Central-East Sardinia—Italy) and their palaeogeographic significance. Geomorphology 231:202-211.

DE WAELE J., SHEN C., VIGNA B., FIORUCCI A., MARINI P., HUANG, C., HU H. (2025). Speleogenesis of Valdemino Cave (Borgio Verezzi, Liguria, Northern Italy) shows very slow uplift of this coast since Middle Pleistocene. Geomorphology, 473:1-15

DI MAGGIO C. (2000). Morphostructural aspects of the central northern sector of Palermo Mountains (Sicily). Memorie Società Geologica Italiana 55:353-361.

DI MAIDA G., MANNINO M.A., ZILHÃO J., HOFFMANN D.L., GARCÍA-DIEZ M., PASTOORS A., STANDISH C.D., PIKE A.W.G., OLSEN J., SCHIMMENTI V., BATTAGLIA G., TERBERGER T. (2020). Radiocarbon and U-series age constraints for the Lateglacial rock art of Sicily. Quaternary Science Reviews 245:1-16.

HANSEN J., SATO M., RUSSELL G, KHARECHA P. (2013). Climate sensitivity, sea level and atmospheric carbon dioxide. Philosophical Transitions of the Royal Society A. 371: 20120294

ISPRA (2013). Carta Geologica d’Italia alla scala 1:50.000 - Foglio 594-585 “Partinico-Mondello”. Scientific Coordinator: Catalano R.

MYLROIE J.E., CAREW J.L. (1990). The Flank margin model for dissolution cave development in carbonate platforms. Earth Surface Processes and Landforms 15:413-424.

MYLROIE J.E., MYLROIE J.R., NELSON C.N. (2008). Flank margin cave development in telogenetic limestones of New Zealand. Acta Carsologica 37:15–40.

MYLROIE J.E., MYLROIE J.R. (2013). Flank Margin Caves in carbonate islands and the effects of sea level. In: Shroder J. (Editor in Chief), Frumkin A. (Ed.), Treatise on Geomorphology. Academic Press. San Diego, CA, vol. 6, Karst Geomorphology, 351-362.

OTONIČAR B., BUZIJAK N., MYLROIE J.E., MYLROIE J.R. (2010). Flank margin cave development in carbonate talus breccia facies: an example from Cres Island, Croatia. Acta Carsologica 39:79–91.

RUGGIERI, R., DE WAELE, J. (2014). Lower-to Middle Pleistocene flank margin caves at Custonaci (Trapani, NW Sicily) and their relation with past sea levels. Acta Carsologica 43 (1):11–22.

Insights from Cave Sediments Into Karst Evolution, Tectonics, and Climate Change

Nadja Zupan Hajna (1), Pavel Bosák (2) & Petr Pruner (3)

Dedicated to the memory of Andrej Mihevc (1),
whose contributions to karst studies remain invaluable.

(1) Karst Research Institute ZRC SAZU, Titov trg 2, 6230 Postojna, Slovenia, zupan@zrc-sazu.si (corresponding author)
(2) Institute of Geology of the Czech Academy of Sciences, Rozvojová 269, 165 00 Praha 6, Czech Republic, Bosak@gli.cas.cz

Abstract

Cave sediments provide important insights into the geological evolution, tectonic activity and climatic changes that characterize karst landscapes. In this study, sediment records from an unroofed cave above the active passages of Škocjanske Jame (Caves) in the Divaški Kras region, SW Slovenia, are investigated as an example. Using a multiproxy approach including sedimentological, mineralogical, paleomagnetic and chronological analyses, the depositional history and environmental evolution of the cave system were reconstructed. The results revealed sedimentary sequences that extend five million years, representing a transition of the cave from phreatic to vadose conditions. Allogenic deposits, including quartz-rich gravels, indicate external sources and high-energy environments associated with regional tectonic uplift, while authigenic speleothems reflect periods of groundwater fluctuations and climatic variability. The unroofing process, occurring within the last ~770 ka exposed these deposits and emphasizes the interplay between subsurface and surface processes. This research highlights the role of tectonic forces in regional base-level changes and sediment deposition as well as the sensitivity of karst systems to climatic fluctuations. Key findings include the timing of fluvial activity (~2.6 Ma), the formation of collapse dolines, and the denudation processes that influenced surface morphology. These results emphasize the value of integrated methods for understanding karst evolution over geological time scales.

1. Introduction

The dating of karst processes is a challenge due to the lack of surface sediments, especially in the Classical Karst region in southwestern Slovenia. Therefore, cave sediments found in the subsurface of karst landscapes or occasionally in exposed denuded caves often serve as a primary source of information for the study of past environments and processes such as climatic changes and tectonic activities (e.g. Zupan Hajna et al., 2020, 2021). Cave sediments are essential for deciphering the geological history and environmental changes in karst systems. These sediments are broadly divided into two main types based on their origin: allogenic and autogenic (e.g. Ford & Williams, 2007). Allogenic sediments are transported into caves from external sources such as rivers and streams and consist of materials such as quartz sandstone, gravel, clay and other detrital particles (e.g. Sasowsky, 2007; White, 2007; Farrant & Smart, 2011). These deposits usually accumulate during flood events or due to sustained water flow into the cave system. Conversely, autogenic sediments form in caves, primarily through the precipitation of minerals from the cave water. Speleothems reflect the chemical processes taking place in the cave environment and provide valuable records of paleoclimate conditions (e.g. White, 2007). Cave sediments reflect the changes in the internal environment of the cave and the influence of speleogenetic phases in different and successive hydrological karst zones (e.g. Ford & Williams, 2007; Audra & Palmer, 2011; Farrant & Smart, 2011; Zupan Hajna et al., 2024). Cave sediments are crucial archives of past geological, hydrological, and environmental conditions, particularly in karst systems where surface records are often sparse or absent. These deposits, formed by allogenic and autogenic processes, reflect changes in sedimentary environments and the dynamic interactions between climatic, tectonic, and hydrological forces over time. Allogenic sediments, such as quartz sandstone gravels and clays, are transported into caves by external water sources, while autogenic sediments, including speleothems, form within caves through chemical precipitation.

The unroofed cave above Škocjanske Jame offers a unique opportunity to study sedimentary records in a karst setting shaped by complex geological processes. Located in the Divaški Kras region of the Classical Karst (SW Slovenia), this system has undergone significant transformations due to regional uplift, denudation, and changes in hydrological regimes. The sediments in unroofed caves provide insights into the early stages of speleogenesis, subsequent environmental changes, and the long-term evolution of karst landscapes.

This paper represents a multiproxy approach, combining sedimentological, mineralogical, paleomagnetic, and chronological analyses, to reconstruct the depositional history and environmental evolution of the unroofed cave. By integrating different research methods, we aim to understand the interplay of tectonic activity, climatic variability, and hydrological dynamics in shaping the Škocjanske Jame system over millions of years.

2. Materials and methods

Unroofed cave in Risnik Industrial Zone was selected as an example of studied unroofed caves located in the Divaški Kras region, above the active passages of Škocjanske Jame (Fig. 1). This site, exposed during constructions in new industrial zone, provided an exceptional

opportunity to access sedimentary sequences documenting different depositional environments.

Two sediment sections were investigated at two nearby locations: Speleothem and Sediment sections (Fig. 2). The Speleothem Section (Fig. 2A) was located in a small cave at 455 m a.s.l., while the bottom of the Sediment section was located at 442 m a.s.l. (Fig. 2B). The cave floor was not reached at either site, and cave walls were only noted at two locations. Based on the locations and strata dips of the allogenic sediments, we presumed that the sediments in both sections represent the fill of the same cave passage. The thickness of unexposed sediments between the top of the Sediment section and the bottom of the pit containing the Speleothem Section can be estimated to 1–2 m, depending on the slight strata dip, the distance between the two sections and their height. The cumulative thickness of all units of the two sections was therefore about 16 m.

Sampling and analysis: 1) sedimentology included comprehensive field descriptions, photo documentation and macroscopic analyses were carried out to characterize the sediments. The sedimentary units were systematically classified based on their texture, composition and depositional structures. 2) The mineralogical composition of the sediment was determined by X-ray diffraction (XRD). The focus was on the identification of allogenic clastic materials transported by the Reka River. 3) Paleomagnetic investigations were carried out to determine the polarity of geomagnetic reversals in the sedimentary sequences. These analyses provided a framework for magnetostratigraphy and understanding the chronological sequence of the deposits. 4) Uranium-Thorium (U/Th) radiometric dating was used to determine the chronological sequence of the sedimentary deposits and to correlate paleomagnetic results with GPTS (Cande & Kent, 1995; Gradstein et al., 2020).

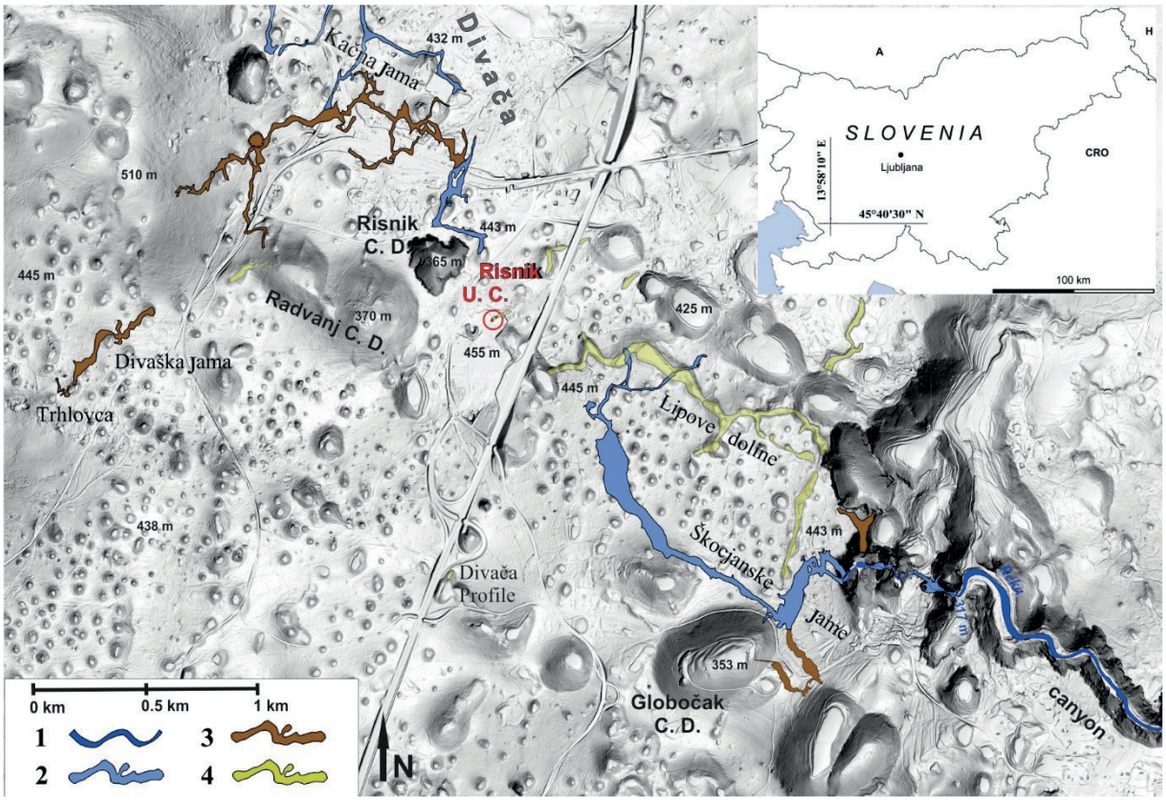

Figure 1: *Figure 1 Location of Risnik Unroofed Cave (two sampled sites) in Slovenia and on LiDAR DEM of Divaški Kras (Divača Karst) with solution dolines, collapse dolines (C.D.), sinking river and the largest caves. Legend: 1: Surface river; 2: Passages with active water flow; 3: Dry passages; 4: Unroofed caves. Source of Lidar data: Geodetski oddelek ARSO.*

3. Results

The sedimentary sequence in the unroofed cave in Risnik Industrial Zone (Zupan Hajna et al., 2024) comprises two separate sections (Speleothem and Sediment) with five distinct sedimentary units (Fig. 2). In Sediment section (Fig. 2B and 2C), Unit I consists of laminated fine-grained sediments indicating a low-energy phreatic environment. These sediments, consisting predominantly of clays and silts, were deposited under calm conditions with periodic input of fine sand, suggesting a stable hydrologic system. Unit II is characterized by cyclic sequences of sands and clays representing fluctuating water flow and sediment loading in epiphreatic to vadose environments. These cycles, characterized by rhythmic stratification, reflect episodic flooding and depositional pauses likely caused by external climatic factors. Unit III comprises matrix-supported quartz sandstone gravels deposited in a high-energy environment during regional tectonic uplift. The coarse nature of these sediments indicates increased erosional activity and rapid sediment transport. Unit IV (Fig. 2A) consists of coarse-grained limestone gravels reflecting significant fluvial incision and high-energy flow conditions, indicating intense hydrodynamic conditions capable of mobilizing large clasts, associated with tectonic uplift and base-level lowering. Unit V (Fig. 2A) comprises laminated micritic carbonates and speleothems deposited during intermittent flooding and groundwater fluctuations. These layers have clay intercalations and porous calcite and are evidence of alternating periods of deposition and erosion.

U/Th dating of speleothem layer (Fig. 2A) gave direct result but indicate that regarding equilibrium/disequilibrium state in 234U/238U isotopic ratio sample is older than 600 and younger than ~1,200 ka,

and as that the age should be of over 773 ka, as sample was in reversal polarized flowstone layer. This dating subsequently made it possible to compare the magnetic polarity zones with the GPTS in the upper part of the profile.

Basic magnetic and paleomagnetic properties of the Sediment and Speleothem Sections paleomagnetic directions were determined (Zupan Hajna et al., 2024) including magnetic susceptibility, natural remanent magnetization, declination, inclination and polarity (Fig. 2A and 2C). In Speleothem section were detected at least two normal and three reversal polarity magnetozones (Fig. 2A) and in Sediment section six normal and six reversal polarity magnetozones (Fig. 2C).

Based on paleomagnetic characteristic and U/Th data, the fill of the unroofed cave is estimated to be between approximately 5 Ma (probably 5.2 to 4.9 Ma) and > 773 ka old (Zupan Hajna et al., 2024). Our results reveal a complex interplay of allogenic and autogenic sediments, suggesting a stable catchment over several million years. The dating results indicate deposition in phreatic regime since at least 5 Ma, with the river flowing through the cave until about 2.6 Ma.

According to the research results, the regional uplifts most likely caused significant sedimentary changes, including mass flows and high--energy deposits as well as the vertical transition of active cave passages along the hydrological karst zones. The denudation (unroofing) of the cave occurred in the last 770 ka, exposing sediments and significantly affecting the morphology of the karst surface.

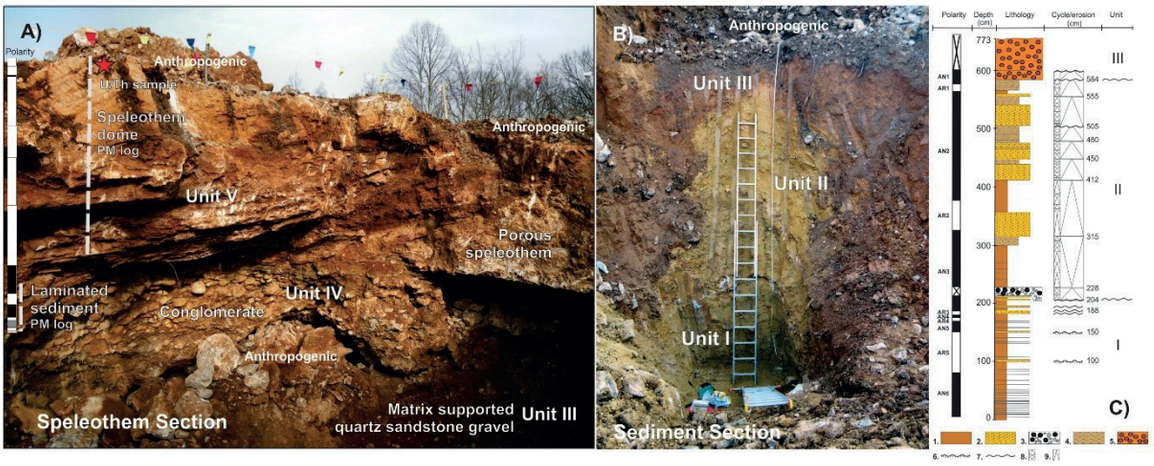

Figure 2: Risnik Unroofed Cave Sediment Sites (adapted from Zupan Hajna et al., 2024). A) Speleothem Section with identified Unit III-V. B) Sediment Section showing stratigraphic Units I-III. C) Complex log of Sediment Section with simplified paleomagnetic, lithological and cyclicity logs and Units; Legend: 1. clay layers; 2. silt layers; 3. limestone gravel and chert pebbles; 4. sand layers; 5. matrix-supported quartz sandstone gravel; 6. erosional boundary with weathering; 7. erosional boundary; 8. rhythms; 9: cycles. Polarity logs in 2A and 2C: black: N – normal polarity, white: R – reverse polarity.

4. Discussion

Our detailed multi-proxy studies of the sediments filling the unroofed cave in the Risnik Industrial Zone above the active passages of the underground Reka have revealed interesting sedimentary features, indicated speleogenetic processes, and determined the approximate time of sedimentation. The results also provided insights into the other processes that influenced changes in sedimentation characteristics, speleogenesis and the approximate timing of the formation of surface karst morphology (e.g. collapse dolines, solution dolines). The sedimentary record highlights the critical role of tectonic processes in the evolution of the unroofed cave. Multiple uplift phases in the region, beginning over 5 Ma ago, drove the lowering of the regional base level, which facilitated the incision of fluvial channels and the deposition of coarse allogenic sediments. The transition from phreatic to vadose conditions reflects the progressive impact of these tectonic events on the hydrological regime.

The coarse gravels in Units III and IV are direct evidence of high-energy depositional environments linked to these uplift phases. The presence of limestone clasts within these units suggests localized erosion of cave walls, while the quartz-rich gravels point to an external source in the Eocene flysch catchment of the Reka River.

Although secondary to tectonic activity, climatic variability played a significant role in shaping the sedimentary record. Cyclic deposits in Unit II, characterized by alternating sands and clays, are likely tied to climatic oscillations, such as changes in precipitation intensity and storm frequency. These deposits highlight the sensitivity of karst systems to external climatic influences, even when tectonic processes dominate. The intercalation of clay and carbonate layers in Unit V further underscores the interplay between climatic and hydrological factors. Periodic flooding events, driven by extreme weather conditions or seasonal variations, contributed to the deposition of these layers, while prolonged dry periods facilitated speleothem growth.

The evolution of the unroofed cave provides valuable insights into the early stages of the Škocjanske Jame system. Initial phreatic conditions allowed for the deposition of fine-grained sediments, while subsequent uplift and base-level changes transitioned the system to epiphreatic and vadose environments. The last time the river flowed through the now unroofed cave about ±2.6 Ma ago when paleo-flow was depositing fluvial sediments (gravel). Consequently, collapse dolines and the canyon in Škocjanske Jame (active water passage) and in front of the cave are younger (Fig. 1 and 3). The unroofing of the cave, occurring within the last 770 ka, exposed the fluvial sediments, revealing the intricate processes that shaped this karst landscape. The denudation process exposed the cave sediments but also influenced the development of surface karst features, such as dolines containing fluvial sediments (Fig. 1); i.e. intersection doline (Sauro, 2003). All these features, younger than 2.6 Ma, reflect the interplay between subsurface processes and surface geomorphology in the ongoing evolution of the karst system.

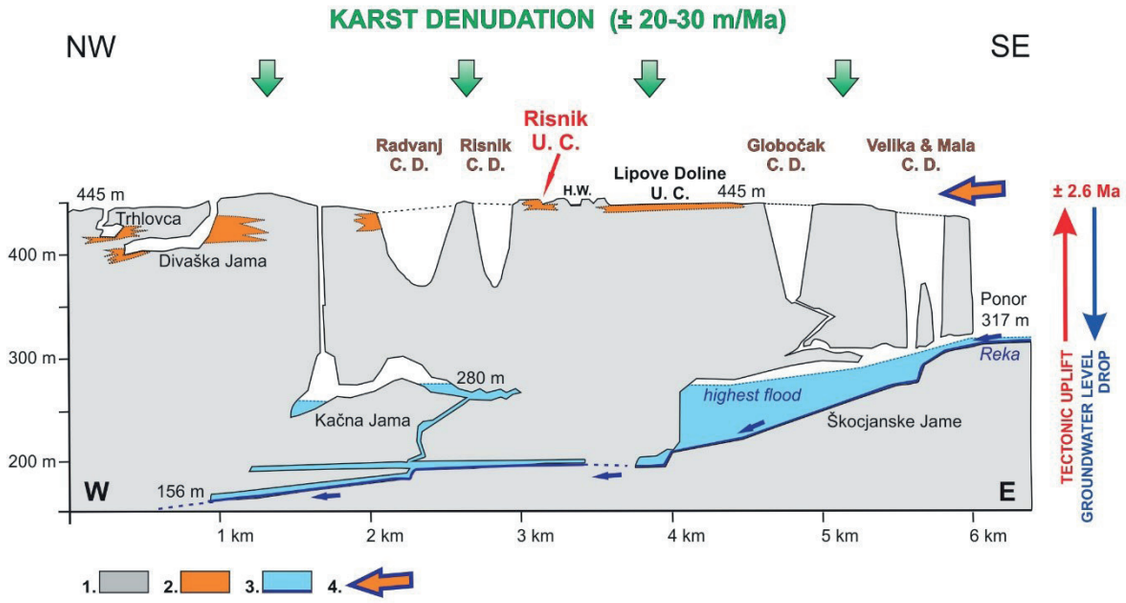

Figure 3: *Schematic cross section of Divaški Kras (adapted from Zupan Hajna et al., 2024) with main cave passages, unroofed caves (U.C.), underground river, actual flood zone level, and collapse dolines (C.D.). Legend: 1. carbonates, 2. relict cave sediments, 3. active river with flood level (epiphreatic zone), 4. direction of paleo flow.*

5. Conclusion

Unroofed caves and cave sediments are preserved on the surface above Škocjanske Jame. The allogenic sediments, including gravel, sand, silt and clay, were transported from the flysch catchment area of the Reka River, while limestone gravel and rubble originated from the erosion of the cave walls. The speleothems formed in the cave surroundings. The catchment area of the underground river has retained its character and location for at least five million years and has remained largely unchanged. This is confirmed by dating results and the presence of identical sediments at different surface and cave sites, which display varying degrees of weathering within the catchment area. All unroofed caves in this area are located about 200 meters above the present-day passages of the Škocjanske Jame and Kačna Jama representing a similar stage in the of the underground Reka drainage system.

This study also demonstrates the value of integrating sedimentological, chronological, and geomorphological approaches to unravel the history of karst systems. The most important findings include: 1) Sedimentary changes due to multiple tectonic regional uplifts since the Pliocene; 2) The early phase of Škocjanske Jame as an unroofed cave above the active cave; 3) Allogenic sediments deposited between 5 and 2.6 Ma indicate changes in the cave environment; 4) The last time the river flowed through the cave was about ±2.6 Ma ago; 5) Collapse dolines and the canyon in the active water cave are younger than ±2.6 Ma; and 6) Unroofing of the cave (denudation) occurred within the last 0.7 Ma.

This research underscores the importance of multiproxy studies in karst environments, offering insights into the interplay between geological, hydrological, and climatic factors in shaping karst landscapes.

Acknowledgments

We would like to thank to various colleagues for their help with fieldworks: F. Drole for geodetic survey and cave map, and M. Temovski R., Cerkvenik and M. Stupar for help with the sampling; and for laboratory analyses: D. Venhodová, J. Drahotová, O. Man, J. Petráček, P. Schnabl, S. Šlechta (paleomagnetic analyses and evaluation, drawings), M. Šťastný (XRD), Š. Matoušková (ICP U/Th dating); and H. Hercman with the staff of Uranium-Thorium Laboratory, Institute of Geological Sciences, Polish Academy of Sciences in Warsaw. The authors acknowledge the financial support from the Slovenian Research and Innovation Agency (research programme funding No. P6-0119), the Institutional Financing of Institute of Geology, Czech Academy of Science (No. RVO6798531), and MOBILITY PLUS project SAZU-24-04.

References

AUDRA P., PALMER A.N. (2011) The pattern of caves: controls of epigenic speleogenesis. Geomorphologie 4:359–378.

CANDE S.C., KENT D.V. (1995) Revised calibration of the geomagnetic polarity timescale for the Late Cretaceous and Cenozoic. J. Geophys. Res. 100(B4): 6093–6095.

FARRANT A.R., SMART P.L. (2011) Role of sediment in speleogenesis; sedimentation and paragenesis. Geomorphology 134:79–93.

FORD D., WILLIAMS P. (1989) Karst geomorphology and hydrology, Ed. Unwin Hyman Ltd. London, 601 p.

GRADSTEIN F.M., OGG J.G., SCHMITZ M.D., OGG G.M. (2020) Geological Time Scale 2020. Elsevier BV., Amsterdam. 1144 p.

SASOWSKY I. (2007) Clastic Sediments in Caves – Imperfect Recorders of Processes in Karst. Acta Carsologica 36(1): 143–149.

SAURO U. (2003) Dolines and sinkholes: Aspects of evolution and pro-

blems of classification. Acta Carsologica 32(2):41–52.

WHITE W.B. (2007) Cave sediments and paleoclimate. Journal of Cave and Karst Studies 69(1):76–93.

ZUPAN HAJNA N., BOSÁK P., PRUNER P., MIHEVC A., HERCMAN H., HORÁČEK I. (2020) Karst sediments in Slovenia: Plio-Quaternary multi-proxy records. Quaternary International 546:4–19.

ZUPAN HAJNA N., MIHEVC A., BOSÁK P., PRUNER P., HERCMAN H., HORÁČEK I., WAGNER J., ČERMÁK J., PAWLAK J., SIERPIEŃ P., KDÝR Š., JUŘIČKOVÁ L., ŠVARA A. (2021) Pliocene to Holocene chronostratigraphy and paleoenvironmental records from cave sediments: Račiška Pečina section (SW Slovenia). Quaternary International 605–606:5–24.

ZUPAN HAJNA N., PRUNER P., BOSÁK P., MIHEVC A. (2024) Temporal insights into karst system evolution: A case study of the unroofed cave above Škocjanske Jame, NW Dinarides. Geomorphology 461:109282.

The influence of microbial nitrogen cycling and subaerial dissolution on secondary speleogenesis in the caves of Gunung Mulu National Park, Malaysia

J. Max Koether (1), Andrew R Farrant (2) & Hazel Barton (1)

(1) University of Alabama, Department of Geology, Tuscaloosa, Alabama, United States
(2) British Geological Survey, Keyworth, Nottingham, United Kingdom.

Abstract

There is a growing recognition of the role of biological influences on chemical erosion. Secondary speleogenesis, such as condensation corrosion, can lead to post-speleogenetic passage enlargement, although the role of biology in these secondary processes is poorly understood in speleogenesis. The caves of Gunung Mulu National Park in Malaysia are especially unique in their size and morphology, which we believe could be explained by the influence of the extensive guano found throughout the caves. The impact of microbial metabolism within cave swiftlet and bat guano on the production of ammonia may explain some of the more unusual 'air scalloping' morphologies found in the caves, which is causing secondary passage enlargement. Using a combination of field chemical analysis, isotope ratio mass spectrometry, and fluorescent cell counting, we suggest that nitrogen-driven biogenic dissolution is common in tropical caves and may significantly enlarge cave passages following their initial formation.

1. Introduction

Gunung Mulu National Park in Sarawak, Malaysia, contains some of the longest and largest caves in the world, including Clearwater Cave (~256 km long), Good Luck Cave (which contains the world's largest cave chamber, the Sarawak Chamber, ~500 m in diameter and 80 m tall), and Deer Cave, which contains one of the world's largest cave passages at ~200m high) (GILLI 2021). Various dissolution features are found throughout the Mulu caves, but while small scallops are common in active river passages, they're notably absent in higher-level passages. In older passages, the small fluvial scallops are missing, and large (>1m length) scallops are often present. While traditionally seen as formed under slow phreatic flow, the size and occurrence of these large scallops alongside vadose notches suggest alternative formation processes apart from water flow (Fig. 1).

FARRANT et al. (in review) noted that the Mulu cave passage walls and boulders often develop a distinct weathering rind, ranging from a few mm to 1-2 cm thick, made of easily removable carbonate paste. Sometimes, this thickens and sloughs off, creating a 'cockling' texture on wet surfaces. During wet periods, it washes down, forming a thicker, bobbly crust resembling cottage cheese, often accumulating at the base of rock protrusions (Fig. 2).

Other cave formations resemble features formed by warm air sublimation found on glacier surfaces or in ice caves, suggesting they formed through air sublimation and ablation (BUSHUK et al. 2019, FARRANT et al. [in review]). These include streamlined fluting, where passage walls dissolve due to low viscosity fluid, leaving small irregularities like calcite veins, stalactites, or fossils standing with a distinctive bedrock ridge in the leeward of the irregularity (AUDRA et al. 2016). These formations suggest a subaerial mechanism of dissolution.

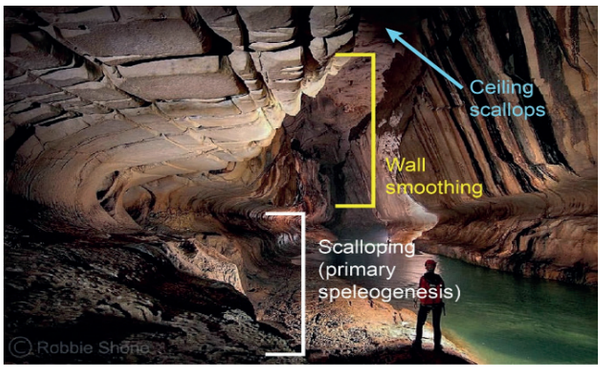

Figure 1: *Clearwater Cave passage displaying primary scalloping (white), secondary loss of the scalloping (yellow), and distinctly large ceiling scallops above (blue). Image courtesy of Robbie Shone.*

Figure 2: *Secondary dissolution and soft calcite rind deposits, exposing calcite ridges (left), and 'cockling' when deposited along wet surfaces (right).*

Our research suggests that the size of the passages in Gunung Mulu National Park, along with the unique passage morphology, is indicative of subaerial formation processes, which may be explained by previously undescribed microbial activity within the caves' guano-rich environment. The Mulu caves host large bat populations, but the caves are best known for their birds: millions of cave swiftlets, both black-nest (*Aerodramus maximus*) and white-nest (*Aerodramus fuciphagus*) swiftlets (HOBBS 2004). There has been limited research examining the impact of bird guano on stone, other than the effects of pigeon guano on masonry and concrete (SPENNEMANN & WATSON 2017). Guano is mildly acidic from the presence of uric and phosphoric (H3PO4) acids, and when fresh (<2 weeks), can etch stone (SPENNEMANN & WATSON 2017; FERNANDES 2006). These reactions have previously been linked to microbial activity shown to damage limestone monuments and produce ammonia (WARSCHEID & BRAAMS 2000). Ammonia is a volatile gas, which is highly soluble in water. If ammonia off-gases from the guano, it may sorb onto wet surfaces in the caves, including walls and other surfaces where water condenses. Oxidation by ammonia-oxidizing bacteria (in the phyla Betaproteobacteria and Gammaproteobacteria [ARP & STEIN 2003]) and Thaumarchaeota within the Archaea (KÖNNEKE et al, 2005]) have the potential to generate nitric and nitrous oxides, which would dissolve in water to form nitric acid (HNO_3), which reacts with limestone following the dissolution equation $CaCO_3 + HNO_3 \rightarrow Ca^{2+} + HCO_3 + NO_{3-}$. This subaerial dissolution would lead to dissolution of wet limestone surfaces exposed to ammonia, erasing some of the morphologies associated with speleogenesis, such as scalloping, and producing a nitrate byproduct. Following sufficient dissolution of cave walls, secondary collapse may be induced, subsequently enlarging the cave passages. LUNDBERG & MCFARLANE (2012) suggest that as much as 70-95% of the total volume of the nearby Gomatong Caves in Borneo may have been opened by direct subaerial biogenic dissolution and biogenically induced collapse. This mechanism of limestone dissolution through subaerial ammonia-generated dissolution would exhibit a novel process of secondary cave enlargement.

2. Materials and Methods

2.1. Field Research

Field work was conducted in 2022, 2023, and 2024, in cooperation with the UK Mulu Caves Project, with field work permitted through Gunung Mulu National Park. Easter Cave, Deer Cave, Cave of the Winds, Lagangs Cave, and Lang Cave were selected for retrieving samples of guano (these caves containing bird, bat, and mixed populations of birds and bats), and Stonehorse, Lagang, and Racer caves were selected for retrieving wall dissolution rind samples (these caves containing mixed populations of birds and bats).

2.2. Cell Counts

Direct cell counts were performed by collecting 5mL of samples from guano deposits from the top, middle, and bottom of the guano piles, as well as samples of wall rind. Samples are preserved with 4% Paraformaldehyde for 4 hours, stored at 4°C, diluted with dH2O until between 0 and 50 cells are visible during microscopy count, treated with SYBR Green and SlowFade Gold Antifade Mountant, and analyzed on black filter paper with a BX53 Olympus Fluorescence Microscope (with Prior OptiScan II stage controller, Mercury-100W bulb, and ExiAqua imaging).

2.3. Isotope Analysis

5mL of each sample (including guano at surface, middle, and bedrock heights; along with fresh guano and wall dissolution rind) were be stored in a 0°C fridge at basecamp in Gunung Mulu National Park, dried overnight, transported to the lab, homogenized with a mortar and pestle, weighed on a digital balance, measuring 1-1.5mg of sample material into silver Costech capsules, treated with water and exposed to vapHCl treatment (used to treat samples with large quantities of inorganic carbon, as would be expected in dissolution karst environments), dried overnight at 60°C, and analyzed (using Costech 4010 Elemental Combustion System interfaced with a Thermo-Fisher Delta V Isotope Ratio Mass Spectrometer using a Thermo-Fisher Conflo IV) for bulk carbon/nitrogen and carbon/nitrogen isotopes.

2.4. Field Chemistry Analysis

Hach DR 1900 and SL1000 instruments were used to study concentrations of ammonia, hydrogen peroxide, nitrate, nitrite, total nitrogen, and phosphorous in water, air, and guano, to understand the potential presence of nitrification cycling through these systems. Humidity and temperature readings were recorded using an Extech RH300 Digital Psychrometer, and drying treatments were conducted using a Fisher Scientific Isotemp Oven, Model 655F (60°C) overnight. Field pH measurements were taken using a SevenGo Pro Mettler Toledo pH/Ion reader.

3. Results

3.1. Field Chemistry

In the bat guano piles of Deer Cave, NH3 readings exceeded the upper range of detection (>50mg/L) even at 1000:1 dilution (Fig. 3). NO3- was present at the bat guano's surface (474mg/L), but much higher at depth (up to 13,740mg/L at 40cm depth). Total phosphate exceeded the upper range of detection at every depth of the bat guano column.

In the bird guano samples, NH3 readings were much lower than in bat guano (270mg/L at the surface and 9.7mg/L at the bottom [12cm depth]), along with lower concentrations of nitrate at depth (1,020mg/L and 1,030mg/L at the surface and 12cm depth respectively), though the concentration of nitrate was higher at the top of the bird guano column (2,060mg/L) compared to the top of the bat guano column (474mg/L). Phosphate was also detectable throughout the bird guano column (2,745mg/L and >5,000mg/L at the surface and 12cm depth respectively).

Geochemical readings throughout the cave in the absence of guano demonstrated low nitrate and phosphorous concentrations, with the highest levels of nitrate (0.7mg/L) and phosphorous (0.6mg/L) found in readings just downstream from Clearwater Cave. However, condensation on cave walls exhibiting dissolution rind exhibited much higher concentrations of nitrate, up to 5,410mg/L.

3.2. Isotope Analysis

Isotope fractionation is noted in nitrogen and carbon sample analysis (Fig. 4). δN^{15} was found to increase in bat guano deposits at increased depth and age, from 4.5 δ^{15}‰ average in fresh guano, to 5.5 δ^{15}‰ average on the surface layer of the bat guano column, to 19.8 δ^{15}‰ average

in the middle of the bat guano column (20cm depth), and up to 22.0 δ^{15}‰ average at the bottom of the bat guano column (40cm depth). In contrast, δN^{15} in bird guano is found to remain quite similar at increased depth and age, with δN^{15} noted to be heavier in shallow deposits (4.3 δ^{15}‰ average for fresh guano and 5.6 δ^{15}‰ average for guano on the surface of the guano column) when compared to deeper deposits (3.9 δ^{15}‰ average for guano in the middle of the column, 3.5 δ^{15}‰ average for guano at the bottom of the column at 12cm depth). δN^{15} is noted to be much lighter in samples retrieved from wall dissolution deposits, with an overall average for the wall δN^{15} of -2.7 δ^{15}‰.

δC^{13} is at its lightest in plant samples (average δC^{13} -35.0 δ^{13}‰), followed by guano samples (average δC^{13} -27.1 δ^{13}‰), and finally wall dissolution rind samples (average δC^{13} -9.6 δ^{13}‰).

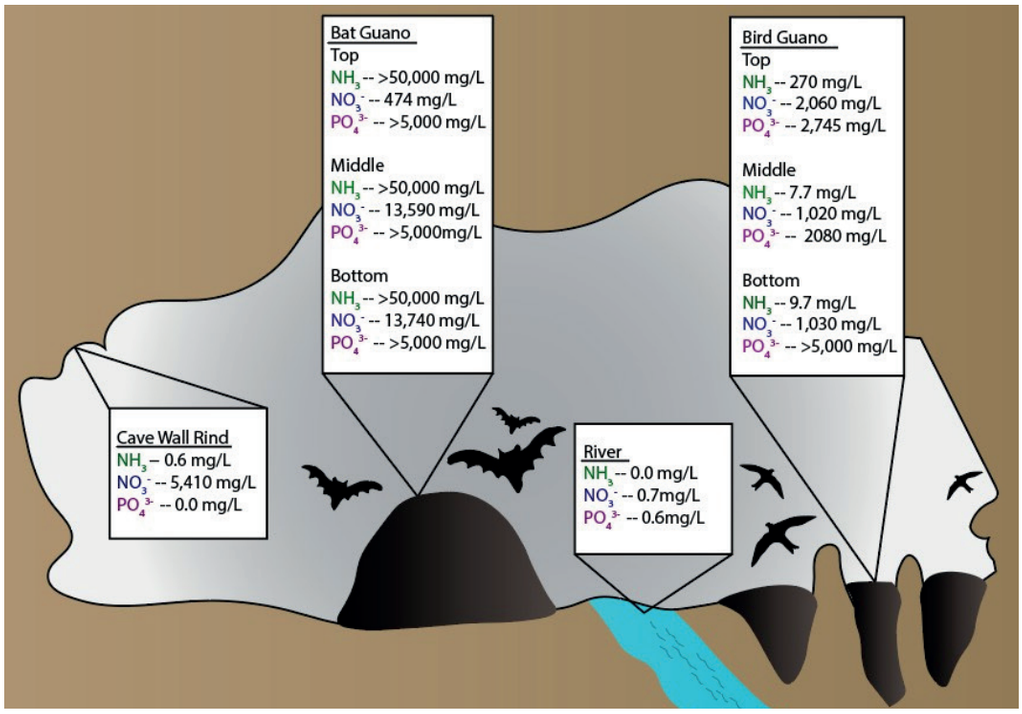

Figure 3: *Summary of field chemistry results from Mulu samples, including ammonia (NH_3), nitrate (NO_3), and phosphate (PO_4^{3-}) concentrations from cave wall rind, bat guano, bird guano, and river measurements.*

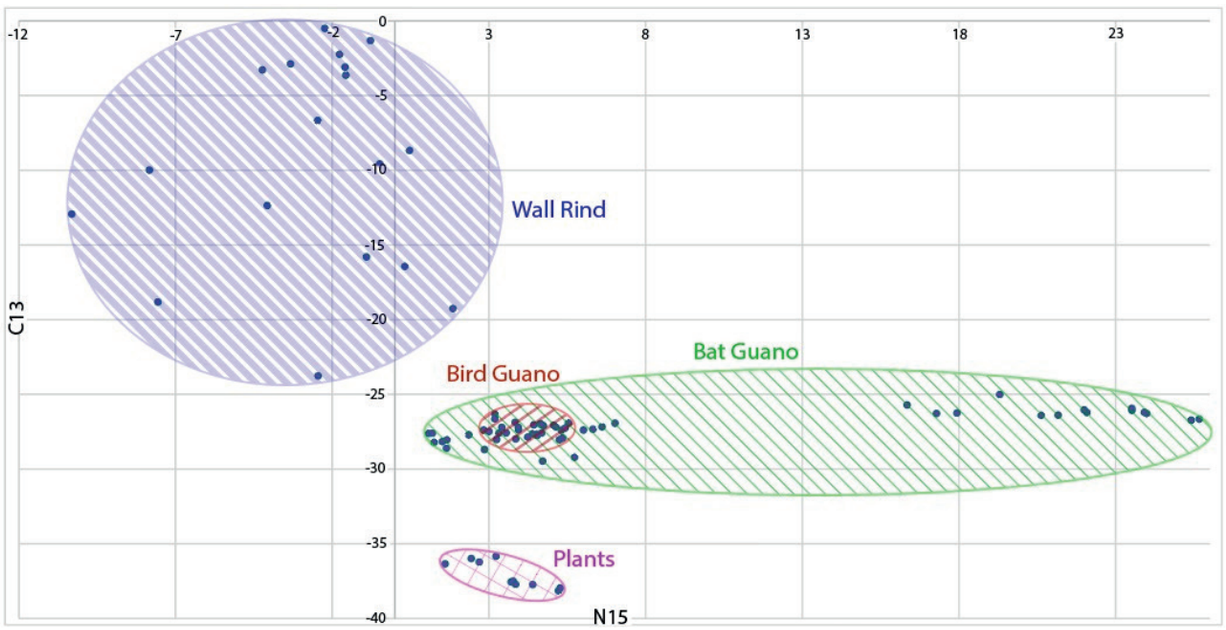

Figure 4: *Isotope data from Mulu samples, comparing δN^{15} and δC^{13} for plants (pink), bat guano (green), bird guano (red), and wall rind (blue).*

3.3. Cell Counts

All samples exhibited extremely high microbial numbers (Fig. 5). The dissolution rind in the Mulu caves exhibited 107-1010 cells/gram, and cell concentrations from Mulu guano samples were expectedly high, with similar cell concentrations between fresh bird and fresh bat guano of 1012 cells/gram. Microbial concentrations decreased 1,000x at depth in insectivorous bat guano (to 108 cells/gram at 40cm depth) while microbial concentrations decreased 10,000x at depth in insectivorous bird guano (to 109 cells/gram at 12cm depth).

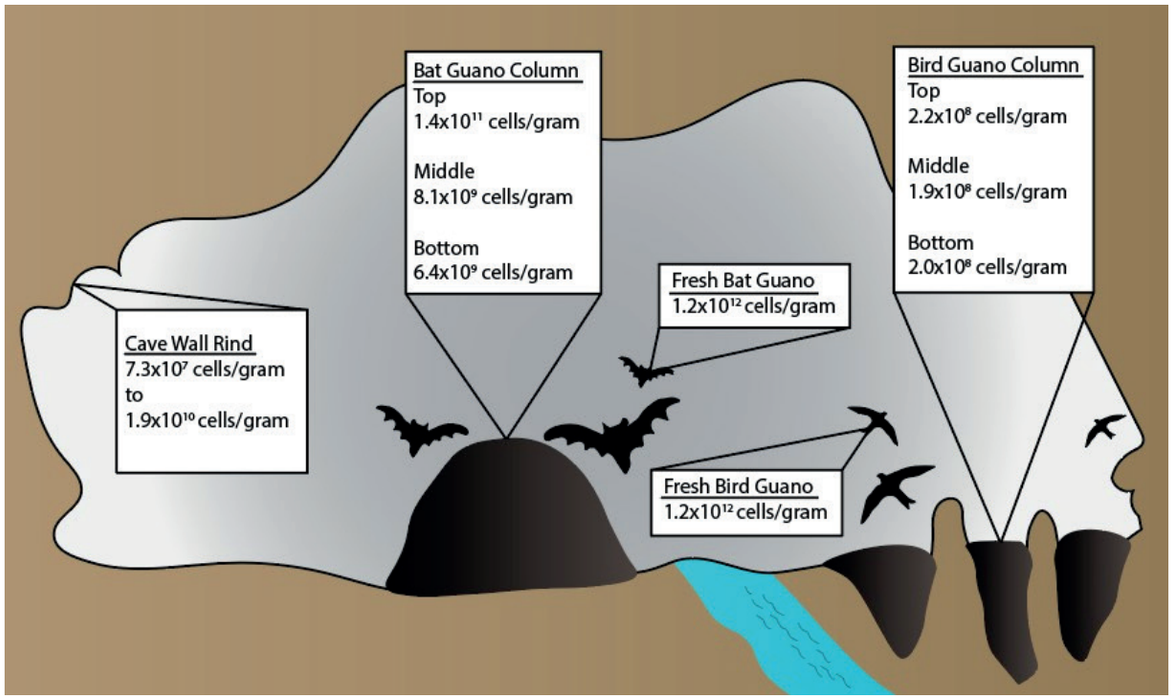

Figure 5: *Summary of cell count data from Mulu samples, including cave wall rind, bat guano, and bird guano, as a function of cells/gram of sample material.*

4. Discussion

The data collected from Gunung Mulu National Park is suggestive of the influence of microbial degradation of bird and bat guano in Borneo caves leading to subaerially-distributed, NOx-based dissolution. Though ammonia is present in both bird and bat guano columns, it appears at much higher concentration in bat guano. This may be due to the large amount of bat guano ammonia off-gassing (MCFARLANE et al. 2017; LUNDBERG et al. 2022). The greater accumulation of bat guano observed is due to bats clustering their roosting sites near cave entrances, while birds are found roosting deeper within the Mulu cave systems (BARTON & BRELEY 2019). Historic harvesting of swiftlet nests and disturbance of these sites may also have impacted the accumulation of fresh bird guano in established sites.

The increased concentration of nitrates in condensation on cave walls exhibiting dissolution is suggestive of nitrogen cycling and production of nitric acid (HNO_3), which would react with limestone to dissolve the bedrock and leave a nitrate chemical fingerprint. If the nitrate concentrations on the cave walls mirrored the concentrations found externally to the cave environment it could be argued that the nitrates were introduced to the system through intermittent flooding or fresh water recharge from the surface, but the observation that nitrate concentrations were below detection in these external samples, while >5,000mg/L in wall rind condensation is indicative of an independent mechanism for nitrate accumulation. That this dissolution mechanism may be biogenically induced is supported by the discovery of 107-1010 cells/gram in wall rind samples. Cell count concentrations from cave environments are usually low, often between 104-106 cells/gram (BUSQUETS et al. 2014; BARTON & JURADO 2007), and the dissolution rind on the walls of the Mulu caves exhibited up to $1x10^6$ fold greater cell count concentrations. Comparative 16S sequencing of the guano and scalloping microbial community capacity for nitrogen metabolism is an area of current investigation.

The isotopic fractionation data indicates that bat guano increases in δN^{15} with increased depth and age. This juxtaposes against the data collected from the bird guano column sample sites, which displays much less δN^{15} variability with increased depth and age. That δN^{15} is noted to be greater in shallow deposits of bird guano when compared to deeper deposits supports the hypothesis that the microbial metabolism of crystalline uric acid secretions occurs to a greater degree at the areas of the column with greatest access the O_2 necessary for urate oxidase enzymatic activity (WU et al. 1989), and that the deeper layers of the bird guano column may be older but less microbially active. Complimentary to the subaerial distribution hypothesis, the lower δN^{15} of condensation samples from areas of bedrock exhibiting dissolution is potentially indicative of the sorption of lighter isotopes of nitrogen in off-gassing ammonia to the cave walls. Additional evidence in support of the subaerial distribution hypothesis may be identified in the analysis of nitrogen isotope fractionation in the volatilized ammonia itself, which is an area of current investigation for this project.

The δC^{13} values in samples isolated from throughout the Mulu karst environment is noted to increase, as microbes metabolize the available δC^{12} carbon through the system. δC^{13} is at its lightest in plant samples via autotrophic CO_2 fixation, increasing in guano samples, and finally is at its highest δC^{13} values in wall dissolution rind samples. The higher δC^{13} values in the wall rind may represent the cycling of the organic carbon produced through autotrophic ammonia oxidation, or be indicative of the age of these rinds.

5. Conclusion

The more we understand how caves develop, the more we understand the impact that microbial metabolic processes have on dissolution. Our study explores a novel secondary subaerial mechanism of biogenic corrosion as a nitrogen-driven dissolution mechanism to explain the development of these caves. Microbial metabolism within bird and bat guano in the caves produces significant amounts of volatile ammonia, which is transported aerially and sorbed to the moisture on the cave walls, and is subsequently further oxidized by microbial activity, forming nitric acid and the resulting corrosion features. This explanation is further supported by the discovery of extremely high microbial cell counts and nitrogen isotope signatures that support ammonia oxidation on cave surfaces. This study suggests that nitrogen-driven biogenic dissolution may be common in tropical caves and may significantly modify and enlarge cave passages following their initial formation.

Acknowledgments

We would like to thank the University of Alabama for their support. We are also indebted to the Mulu Caves Project, British Geological Survey, British Cave Research Association, members of the Mulu Caves Project, and expedition team leaders Andy Eavis and Dr. Rostam Namaghi. We would like to thank the Gunung Mulu National Park team for their stewardship of the park and for supporting our scientific research.

References

ARP D.J., STEIN L.Y. (2003). Metabolism of inorganic N compounds by ammonia-oxidizing bacteria. Critical Reviews in Biochemistry and Molecular Biology. 38:471-495.

AUDRA P., BARRIGUAND L., BIGOT J.Y., CAILHOL D., CAILLAUD H., VANARA N., NOBÉCOURT J.C., MADONIA G., VATTANO M., RENDA M. (2016). L'impact méconnu des chauves-souris et du guano dans l'évolution morphologique tardive des cavernes. Karstologia. 68:1-20.

BARTON H.A., BRELEY G.J. (2019). Microbiology analysis of secondary deposits within Clearwater Cave. 2019 Mulu Caves Project. 1-15.

BARTON H.A., JURADO V. (2007). What's up down there? Microbial diversity in caves. The Microbe. 2:132-138.

BUSHUK M., HOLLAND D.M., STANTON T.P., STERN A., GRAY C. (2019). Ice scallops: a laboratory investigation of the ice–water interface. Journal of Fluid Mechanics. 873:942-976.

BUSQUETS A., FORNÓS J.J., ZAFRA F., LALUCAT J., MERINO A. (2014). Microbial communities in a coastal cave: Cova des Pas de Vallgornera (Mallorca, Western Mediterranean). International Journal of Speleology, 43:205-216.

DUCHENE H.R., PALMER A.N., PALMER M.V., MICHAEL QUEEN J., POLYAK V.J., DECKER D.D., HILL C.A., SPILDE M., BURGER P.A., KIRKLAND D.W., BOSTON P. (2017). Hypogene speleogenesis in the Guadalupe Mountains, New Mexico and Texas, USA. Hypogene Karst Regions and Caves of the World. 511-530.

FARRANT A., BARTON, H.A., KOETHER J.M., LAURITZEM S.E., PENNOS C., SMITH A.C., WHITE J., MCLEOD A., EAVIS A.J. (In review). Pervasive speleogenetic modification of cave passages by nitrification of biogenic ammonia. In review.

GILLI E. (2021). Study of Sarawak Chamber. Big Karst Chambers. 183-195.

HOBBS J.J. (2004). Problems in the harvest of edible birds' nests in Sarawak and Sabah, Malaysian Borneo. Biodiversity & Conservation. 13(12):2209-2226.

KÖNNEKE M., BERNHARD A.E., DE LA TORRE J.R., WALKER C.B., WATERBURY J.B., STAHL D.A. (2005). Isolation of an autotrophic ammonia-oxidizing marine archaeon. Nature. 437:543-546.

LUNDBERG J., MCFARLANE D.A. (2012). Post-speleogenetic biogenic modification of Gomantong Caves, Sabah, Borneo. Geomorphology. 157–158:153-168.

LUNDBERG J., MCFARLANE D.A., VAN RENTERGEM G. (2022). The nitrogen dynamics of Deer Cave, Sarawak, and the role of bat caves as biogeochemical sinks in Tropical Moist Forests. International Journal of Speleology. 51(3):4.

MCFARLANE D.A., LUNDBERG, J., VAN RENTERGEM G. (2017). Preliminary observations on tropical bat caves as biogeochemical nitrogen sinks. In Proceedings of the 17th International Congress of Speleology. 1:157-161.

SPENNEMANN D.H.R., PIKE M., WATSON M.J. (2017). Behavior of fresh pigeon excreta on masonry surfaces. Restoration of Buildings and Monuments. 23:15-28.

WARSCHEID T., BRAAMS J. (2000). Biodeterioration of stone: a review. International Biodeterioration & Biodegradation. 46(4):343-368.

WU X.W., LEE C.C., MUZNY D.M., CASKEY C.T. (1989). Urate oxidase: primary structure and evolutionary implications. Proceedings of the National Academy of Sciences. 86(23):9412-9416.

Predisposing Factors and Evolution Stages ff Sinkholes in Coastal Areasy

Isabella Serena Liso (1,2) & Mario Parise (1,2)

(1) Earth and Environmental Sciences Department, University Aldo Moro, Bari, Italy, serenaliso.uniba@gmail.com (corresponding author), mario.parise@uniba.it

(2) Centro Interdipartimentale di Ricerca sulla Dinamica Costiera, University Aldo Moro, Bari, Italy

Abstract

Sinkholes are the most significant geological hazard in karst, and strongly affects coastal areas, especially in low-topography settings. Through the example of a coastal stretch along the Adriatic side of Apulia (SE Italy), in this article we illustrate the predisposing factors at work in the susceptibility to sinkholes along the coasts, and describe three possible successive stages of evolution of the sinkholes. These include: a) formation of an individual feature, b) merging of nearby sinkholes, and eventually c) the formation of bays produced by coalescence of several individual features. This latter stage points out to the important role played by sinkholes, not only as a typical landform of the coastal karst landscape, but also in the changes of the coastline morphology.

1. Introduction

Karst environments can be affected by many typologies of geological hazards of natural origin, from flash floods, to seawater intrusion, and to gravitational movements of different categories (GUTIERREZ, 2010; PARISE, 2015). However, the most typical hazard in karst is definitely represented by sinkholes, that may be originated by a variety of mechanisms, as illustrated in the classification by GUTIERREZ et al. (2014). Understanding the conditions predisposing to sinkholes, as well as the preparatory processes that might intervene in their evolution, and the triggering factors starting them, is of great importance, aimed at better comprehending the phenomena, but also at identifying possible mitigation actions for human infrastructures and for safeguarding sites of cultural and historical heritage.

In coastal areas, sinkhole processes are even more significant, due to fragility of this zone of transition between land and sea, and to higher aggressivity of groundwaters toward soluble rocks, deriving from the mixing between freshwater and salt water (TULIPANO & FIDELIBUS, 2002; COTECCHIA, 2014; MASCIOPINTO & LISO, 2016).

At this regard, Apulia region in south-eastern Italy is among the most interesting areas of study, since it has widespread outcrops of soluble rocks (CIARANFI et al., 1988; FUNICIELLO et al., 1991; COTECCHIA, 2014, and references therein), with a variety of sinkhole processes (DELLE ROSE et al., 2004; PARISE & VENNARI, 2017; PARISE, 2019, 2022; VENNARI & PARISE, 2022). Most of the lithologies involved are bioclastic calcareous arenites of Pliocene and Pleistocene age, together with calcareous marls. These formations rest transgressively over the underlying limestone bedrock of Cretaceous age. The coastal landscape of the Adriatic side of Apulia is characterized by many marine terraces resulting from the combined action of regional uplift and glacio-eustatic sea level changes (BRUNO et al., 1995; MASTRONUZZI & SANSÒ, 2002). This article, taking as case study a coastal stretch in the vicinity of the town of Ostuni (Figure 1), extending between the localities of Gorgognolo and Torre Santa Sabina. The main goals are to illustrate the stages of evolution of sinkhole processes in the coastal karst of Apulia, and to describe the primary predisposing factors intervening in their formation and evolution.

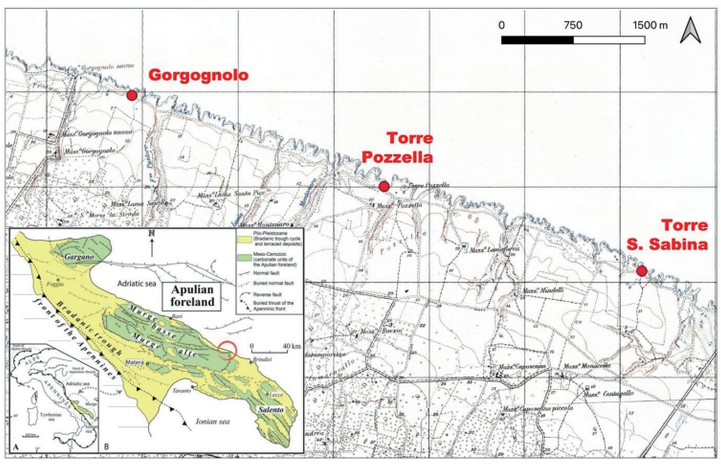

Figure 1: *Location map of the coastal stretch from Gorgognolo to Torre Santa Sabina, along the Adriatic side of Apulia. In the inset, the geological sketch map, modified by PIERI et al. (1997).*

2. Sinkholes in the coastal area of Ostuni

As regards the geological characters, the sector object of this research can be described as characterized by cropping out of Quaternary calcarenites and calcirudites consisting of poorly lithified and weathered bioclastic packstones, grainstones and floatstones belonging to the Calcarenite di Gravina Formation (CAMPANALE et al., 2025). They are classified as soft rocks having complex rock fabrics and diagenetic features (FESTA et al., 2017).

Morphologically, the area is a coastal plain bordered to the west by the Murge escarpment, the most important tectonic lineation in this sector of Apulia (SAURO, 1991; PIERI et al., 1997; FESTA, 2003; PARISE, 2011; TROPEANO et al., 2023). Continuity of the coastal plain is broken by SSW-NNE, slightly incised, valleys of fluvio-karst origin. These are locally named lame (COLAMONICO, 1953; PALAGIANO, 1965; PARISE et al., 2003), from a latin word indicating the shallowness of this morphological feature. The valleys appear to be strongly controlled by tectonics, in agreement with similar trends documented for karst and fluvio-karst landforms in many sectors of Apulia (PEPE & PARISE, 2014; MARGIOTTA et al., 2016; ZUMPANO et al., 2019; PISANO et al., 2020). Even though they are tipically dry, or with very limited water flow, for most of the year, the lame system may become able to transport huge amount of turbulent water and solid materials during the main rainstorms through flash floods (BISSANTI, 1972; PARISE, 2003; MOSSA, 2007; COTECCHIA & SCURO, 2010; MARTINOTTI et al., 2017; GENTILE et al., 2020).

3. Formation and evolution of sinkholes

The coastal stretch immediately north of Brindisi, where many diffuse submarine springs are present (LISO & PARISE, 2020), within an area intensely affected by seawater intrusion, shows as main features a succession of small bays mostly oriented in NNE-SSW direction; as it can be appreciated by the topographic maps, these resemble in plan view the merlons of a castle, from where the local name Costa Merlata comes (Figure 1). The coast is typically low, with cliffs limited to height not greater than 3-4 m. The bays are locally separated by intervening pocket sand beaches (CALDARA et al., 1998; MILLI et al., 2017).

The sector object of this work, from locality Gorgognolo to Torre Pozzella and, farther south-east, to Torre Santa Sabina, is a good example to document the different phases in sinkhole evolution, and the effects this has on development of bays and inlets.

As frequent along plains, both in intra-mountain environment (DEL PRETE et al., 2010) and in coastal settings (DELLE ROSE & PARISE, 2002; MARGIOTTA et al., 2012), the first step is the opening of an individual feature, typically due to collapse or cover-collapse mechanisms (sensu GUTIERREZ et al., 2014; PARISE, 2019, 2022). At Gorgognolo locality, the northernmost site of interest for the present article, a sinkhole appeared in 2021, about 15 m from the coastline. Generally circular in shape, individual sinkholes may range in size from tens of cm to several meters, with depth of 3-4 m; quite often, at their bottom it is possible to see karst conduits, clogged by the breakdown deposits, or too narrow to allow caving exploration. Nevertheless, these features indicate the presence of well-developed karst passages, at the origin of the collapse.

Following the sinkhole opening, its rims can be still unstable, producing further failures in the form of rockfall or topples, potentially enlarging the original sinkhole. If the sinkhole is an isolated landform in the karst landscape, its evolution may stop at this stage; such a situation is quite common when the sinkholes is formed at a distance of tens of meters from the coast. This is the case, again at Gorgognolo locality, of Puntore Cave (PU 377 in the regional cadastre of caves in Apulia, available at http://www.catasto.fspuglia.it), located half a kilometer from the Adriatic Sea (CAMPANALE et al., 2025). It is a cover-collapse sinkhole opening at 12 m a.s.l. (LISO & PARISE, 2023), with two natural small openings produced by collapses (Figure 2). To these, a third, artificial, opening, has to be added, that is used by local farmers to get water for irrigation. The cave walls show Lower Pleistocene soft carbonate rocks and carbonate breccias, passing downward to the Cretaceous limestones. The circular, 20-m wide, cave is largely filled by breakdown deposits, that leave space to a small lake with brackish water on its northern sector, that has recently been object of biospeleological research (GALMARINI et al., 2023).

The second stage of evolution of sinkholes in coastal areas of Apulian includes widening of individual features through failures and detachments of the rock mass at their rims, with consequent enlargement of the sinkholes. The later failures often occur following the main discontinuity systems, and cause the originally circular sinkholes to assume an elliptical shape.

Figure 2: *Puntore Cave, showing in the foreground the debris cone and, above, one of the openings.*

When two or more nearby sinkholes enlarge, the possibility of a merge brings to coalescing features, of greater size and with elongated or irregular forms (DELLE ROSE & PARISE, 2002; LISO & PARISE, 2023). This can be observed at Torre Pozzella (Figure 3), where the sinkhole of larger size opens inland, with many other smaller features between it and the bay. The sinkhole elongation often follows that of the bay itself. Merging of individual sinkholes, overall, determines a retreat of the coastline, with the formation of elongated bays or inlets.

Figure 3: *Sinkholes at Torre Pozzella: in green, the main one, and in yellow the minor sinkholes between the former and the bay (see text for explanation).*

Eventually, in case the process of coalescence among more sinkholes continues, the last phase of evolution brings the bay to deepen inland, typically with irregular but elongated shapes, where it is still possible to recognize some of the primordial circular sinkholes. When the bay becomes highly irregular, an overall protection from the direct arrival of sea waves can be obtained at its inner rims, and small pocket beaches formed, so that these sectors may be used by tourists. This, for instance, can be noted at Torre S. Sabina (Figure 4). In a setting like this, beyond the main bays, detailed surveys along the coast revealed many other minor sinkholes; their major axes (taking into account the sinkholes not of circular shape) are preferentially oriented in NE-SW direction, as shown in Figure 5, and roughly follow the prevailing direction of the bays, in turn coincident with those of the lame as well.

Figure 4: *Sinkholes at Torre Santa Sabina, showing the frequent detachment of rocks (A), and the use of the inner sectors of the sinkhole area by tourists (B).*

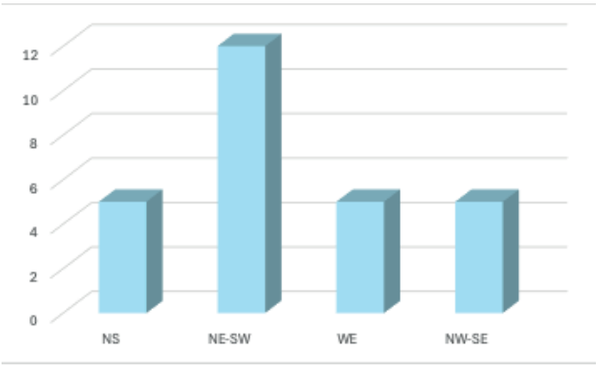

Figure 5: *Main directions of elongation sinkholes at Torre Santa Sabina: note the prevalence of NE-SW direction, corresponding to the main trend of lame.*

4. Predisposing factors of sinkholes

Development of coastal sinkholes occurs as the final result of the combination of a variety of factors, playing different roles in their origin. Such factors are generally discriminated on a temporal basis, with the predisposing factors that are invariable on the observation scale, mostly being related to the geological history at the site. Preparatory factors, instead, are related to time, and are characterized by different cycles (i.e., tides, sea waves, rainfall, etc.). Eventually, the triggering factor/process acts in a very short and well-defined time, typically representing the element causing the onset of the final, paroxysmal, stage in the development of the sinkhole.

Among the primary factors for sinkhole occurrence, lithology has definitely to be mentioned, since presence of soluble rocks is a prerequisite to start the process of karstification. Stratigraphy may have a crucial role, too, for possible differences in the geological and sedimentological succession, that might correspond to variations in permeability of the deposits. Changes in the stratigraphy, thus, might influence the flow of water and the erosional effects determined by such flow.

The mechanical resistance of rock masses is strongly influenced by its degree of karstification: in case of rock masses interested by deep karstification, this results in a high presence of voids, conduits and caves within the rock mass, potentially weakening it, and favoring the tendence toward a progressive failure, eventually leading to collapse.

Weathering controls the proneness to sinkholes, since chemical weathering can break down primary minerals in rocks, leading to a reduction in its cohesive strength, and making it more susceptible to detachment and failure from both vault and walls of the cave. To this, mechanical weathering, due to erosion by rapid inflow of water into underground voids, may be added, resulting in further degradation and enhancement of localized failures.

In coastal areas, in detail, the combined action of the physical setting and the possibility of water stagnancy or runoff at the ground surface, further increase the susceptibility to sinkholes: distance from the coastline represents a geomorphological factor controlling the

sinkhole occurrence, due to the mixing zone between freshwater and sea water, derived by marine intrusion in coastal aquifers. The deriving brackish solution strongly enhances the dissolution rate, potentially enlarging the size of karst caves and voids, and thus contributing to further predisposing the area to the final collapse. This is particularly true for low topography coastal plains, that allow higher advancement inland of the intrusion wedge (Ghyben Herzberg interface).

In addition, effects such as the turbulent action of running water (and of the solid materials therein transported), its mechanical erosion on the vault and walls of underground voids, and the increase in the degree of saturation of the hosting rock or soil, can be observed during sea storms for caves located along the coast or in its immediate proximity, within the zone potentially involved by the arrival of the waves with full energy.

5. Conclusion

Being Apulia a peninsula almost entirely with soluble rocks at the outcrop, sinkholes represent the most common geological hazard in its coastal areas. In this fragile environment, the combination of various factors accelerates sinkhole formation and evolution, starting from mixing of freshwater and salt water. Evolution of the sinkhole landforms is able to control the development of the coastal morphology, which more significant changes appear to be strongly dependent upon enlargement and merging of individual sinkholes. Given the high fragility of the Apulian coast, detailed studies about sinkholes should deserve greater attention by the authorities responsible for land management, also as concerns the risk to humans and infrastructures, that becomes particularly severe during the summer season, due to the high number of tourists frequenting the coastlines of Apulia.

Acknowledgments

This work was carried out within the RETURN Extended Partnership and received funding from the European Union Next-GenerationEU (National Recovery and Resilience Plan—NRRP, Mission 4, Component 2, Investment 1.3—D.D. 1243 2/8/2022, PE0000005). It has also been supported by the PRIN PNRR 2022 Project Fu.Co.Ka. — “FUture scenarios in COastal KArst: saltwater intrusion, loss of water resources and sinkhole development as effects of climate changes” (Project P2022JZHKM, Principal Investigator: M. Parise), funded by MUR—Ministry of University and Research. It.

References

BISSANTI A.A. (1972) L’alluvione del luglio 1972 a Manfredonia. Mem. Ist. Geogr. Fac. Econ. Comm., Univ. Bari 5:73 pp.

BRUNO G., DEL GAUDIO V., MASCIA U., RUINA G. (1995) Numerical analysis of morphology in relation to coastline variations and karstic phenomena in the south-eastern Murge (Apulia, Italy). Geomorphology 12: 313–322.

CALDARA M., CENTENARO E., MASTRONUZZI G., SANSO’ P., SERGIO A. (1998) Features and present evolution of Apulian coast (Southern Italy). Journal of

Coastal Research SI (26):55-64.

CAMPANALE F., LISO I.S., PARISE M., SPALLUTO L. (2025) Anatomy of a sinkhole near the Adriatic coast. Rendiconti Soc. Geol. It. Online.

COLAMONICO C. (1953) Lame e gravine in Puglia. Le Vie d’Italia 11:704.

CIARANFI N., PIERI P., RICCHETTI G. (1988) Note alla carta geologica delle Murge e del Salento (Puglia centro-meridionale). Mem. Soc. Geol. It. 41:449-460.

COTECCHIA V. (2014) Le acque sotterranee e l’intrusione marina in Puglia: dalla ricerca all’emergenza nella salvaguardia della risorsa. Mem. Descr. Carta Geol. d’It. 92:416.

COTECCHIA V., SCURO M.. (2010) Portrait of a Coastal Karst Aquifer: the City of Bari. Aqua Mundi:187-196.

DEL PRETE S., IOVINE G., PARISE M., SANTO A. (2010) Origin and distribution of different types of sinkholes in the plain areas of Southern Italy”, Geodinamica Acta 23(1/3):113-127.

DELLE ROSE M., PARISE M. (2002) Karst subsidence in south-central Apulia Italy. Int. J. Speleology 31(1/4):181-199.

DELLE ROSE M., FEDERICO A., PARISE M. (2004) Sinkhole genesis and evolution in Apulia, and their interrelations with the anthropogenic environment. Nat. Haz. Earth Syst. Sc. 4:747-755.

FESTA V. (2003) Cretaceous structural features of the Murge area (Apulian foreland, southern Italy). Eclogae Geol. Helv. 96:11–22.

FESTA V., FIORE A., LUISI M., MICCOLI M.N., SPALLUTO L. (2017) Petrographic features influencing basic geotechnical parameters of carbonate soft rocks. Engineering Geology 233. https://doi.org/10.1016/j.enggeo.2017.12.009

FUNICIELLO R., MONTONE P., PAROTTO M., SALVINI F., TOZZI M. (1991) Geodynamic evolution of an intra-orogenic foreland: the Apulia case history (Italy). Boll. Soc. Geol. It. 110:419-425.

GALMARINI E., VACCARELLI I., FIASCA B., DI CICCO M., PARISE M., LISO I.S., PICCINI L., GALASSI D.M.P., CERASOLI F. (2023) Regional climate contributes more than geographic distance to beta diversity of copepods (Crustacea Copepoda) between caves of Italy. Scientific Reports 13: 21243. https://doi.org/10.1038/s41598-023-48440-7.

GENTILE P., IAIA C., LISO I.S., PARISE M. (2020) Eventi alluvionali nell’ambiente carsico pugliese. Geologia dell’Ambiente, suppl. n. 1/2020:56-63.

GUTIERREZ F. (2010) Hazards associated with karst. In: ALCANTARA I., GOUDIE A. (Eds.) Geomorphological Hazards and Disaster Prevention. Cambridge Univ. Press, Cambridge: 161-175

GUTIERREZ F., PARISE M., DE WAELE J., JOURDE H. (2014) A review on natural and human-induced geohazards and impacts in karst. Earth Science Reviews 138:61-88. https://doi.org/10.1016/j.earscirev.2014.08.002.

LISO I.S., PARISE M. (2020) Apulian karst springs: a review. Journal of Environmental Science and Engineering Technology 8:63-83.

LISO I.S., PARISE M. (2023) Sinkhole development at the freshwater-saltwater interface in Apulia (southern Italy). Proc. 17th Multidisc. Conf. on Sinkholes and the Engng. and Environ. Impacts of Karst, Tampa, USA, NCKRI Symp. no. 9:229-238.

MARGIOTTA S., NEGRI S., PARISE M., VALLONI R. (2012) Mapping the susceptibility to sinkholes in coastal areas, based on stratigraphy, geo-

morphology and geophysics. Nat. Haz. 62(2):657-676.

MARTINOTTI M.E., PISANO L., MARCHESINI I., ROSSI M., PERUCCACCI S., BRUNETTI M.T., MELILLO M., AMORUSO G., LOIACONO P., VENNARI C., VESSIA G., TRABACE M., PARISE M., GUZZETTI F. (2017) Landslides, floods and sinkholes in a karst environment: the 1-6 September 2014 Gargano event, southern Italy. Natural Hazards and Earth System Sciences 17:467-480.

MASCIOPINTO C., LISO I.S. (2016) Assessment of the impact of sea-level rise due to climate change on coastal groundwater discharge. Sc. Tot. Environ. 569-570:672-680.

MASTRONUZZI G., SANSÒ P. (2002) Pleistocene sea-level changes, sapping processes and development of valley networks in the Apulia region (southern Italy). Geomorphology 46:19–34.

MILLI S., GIRASOLI D.E., TENTORI D., TORTORA P. (2017) Sedimentology and coastal dynamics of carbonate pocket beaches: the Ionian-Sea Apulia coast

between Torre Colimena and Porto Cesareo (Southern Italy). J. Mediterr. Earth Sci. 9:29–66.

MOSSA M. (2007) The floods in Bari: what history should have taught, Journal of Hydraulic Research 45(5):579-594

PALAGIANO C. (1965) Sulle lame e gravine della Puglia. Annali Fac. Econ. Comm. Bari 21:357-386.

PARISE M. (2003) Flood history in the karst environment of Castellana-Grotte (Apulia, southern Italy). Natural Hazards and Earth System Sciences 3(6):593-604.

PARISE M. (2011) Surface and subsurface karst geomorphology in the Murge (Apulia, southern Italy). Acta Carsol. 40(1):79-93.

PARISE M. (2015) Karst geo-hazards: casual factors and management issues. Acta Carsologica 44/3:402-404.

PARISE M. (2019) Sinkholes. In: WHITE W.B., CULVER D.C., PIPAN T. (Eds.), Encyclopedia of Caves. Academic Press, Elsevier, 3rd edition, ISBN 978-0-12-814124-3, p. 934-942.

PARISE M. (2022) Sinkholes, Subsidence and Related Mass Movements. In: SHRODER J.J.F. (Ed), Treatise on Geomorphology, vol. 5. Elsevier, Academic Press, 200–220. https://dx.doi.org/10.1016/B978-0-12-818234-5.00029-8, ISBN 9780128182345.

PARISE M., VENNARI C. (2017) Distribution and features of natural and anthropogenic sinkholes in Apulia. In: RENARD P., BERTRAND C. (Eds.), EuroKarst 2016, Advances in the Hydrogeology of Karst and Carbonate Reservoirs, Springer, pp. 27–34, ISBN 978-3-319-45464-1.

PARISE M., FEDERICO A., DELLE ROSE M., SAMMARCO M. (2003) Karst terminology in Apulia (S Italy). Acta Carsol. 32(2):65-82.

PIERI P., FESTA V., MORETTI M., TROPEANO M. (1997) Quaternary tectonic of the Murge area (Apulian foreland—Southern Italy). Ann. Geofis. 40:1395–1404.

PISANO L., ZUMPANO V., LISO I.S., PARISE M. (2020) Geomorphological and structural characterization of the “Canale di Pirro” polje, Apulia (Southern Italy). Journal of Maps 16 (2):479-487.

SAURO U. (1991) A polygonal karst in Alte Murge (Puglia, Southern Italy). Z. Fur Geomorphol. 35:207–223.

TROPEANO M., CALDARA M.A., DE SANTIS V., FESTA V., PARISE M., SABATO L., SPALLUTO L., FRANCESCANGELI R., IURILLI V., MASTRONUZZI G.A., PETRUZZELLI M., BELLINI F., CICALA M., LIPPOLIS E., PETTI F.M., ANTONELLI M., CARDIA S., CONTI J., LA PERNA R., MARINO M., MARSICO A., SACCO E., FIORE A., SIMONE O., VALLETTA S., D’ETTORRE U.S., DE GIORGIO V., LISO I.S., STIGLIANO E. (2023) Geological Uniqueness and Potential Geotouristic Appeal of Murge and Premurge, the First Territory in Apulia (Southern Italy) Aspiring to Become a UNESCO Global Geopark. Geosciences 13:131.

TULIPANO L., FIDELIBUS M.D. (2002) Mechanisms of groundwater salinisation in a coastal karstic aquifer subject to overexploitation. Proc. 17th SWIM, Delft:39-49.

VENNARI C., PARISE M. (2022) A chronological database about natural and anthropogenic sinkholes in Italy. Geosciences 12:200, doi.org/10.3390/geosciences12050200.

ZUMPANO V., PISANO L., PARISE M. (2019) An integrated framework to identify and analyze karst sinkholes. Geomorphology 332:213–225.

Digital models of caves for exploration in virtual reality

Rubson Pinheiro Maia (1), Caio Cavalcante de Souza Mota (2), Pedro Edson Face Moura (3), Anna Sabrina Vidal de Souza (4), Diego de Medeiros Bento (5), Jocy Brandão Cruz (6)

(1) Programa de Pós-Graduação em Geografia, Universidade Federal do Ceará, Brazil, rubsonpinheiro@yahoo.com.br
(2, 3) Departamento de Geografia, Universidade Federal do Ceará, Brazil caiocvlmota@gmail.com pedroedson18@gmail.com
(4) Programa de Pós-Graduação em Geografia, Universidade Federal do Ceará, Brazil, annasabrinavidal@gmail.com (corresponding author)
(5, 6) Centro de Estudos de Cavernas – Cecav – Icmbio (Instituto Chico Mendes da Biodiversidade) diego.bento@icmbio.gov.br
jocy.cruz@icmbio.gov.br

Abstract

This work addresses the applications of Terrestrial Photogrammetry in the generation of digital and virtual models of natural caves for immersive exploration in an interactive environment, which are useful tool in the education of Earth Sciences subjetcs. Two photogrammetric surveys were carried out in the Letreiro and Furna Nova caves, both within the Furna Feia National Park, northeastern Brazil. The methodological approach followed the photogrammetric acquisition protocol, and subsequent processing in the Agisoft Metashape Photoscan software through the Structure from Motion (SfM) algorithm, resulting in the generation of 3D digital models of referred caves. The models were then transferred to interactive 3D viewers (Unreal Engine Software), and a human avatar, in real scale, was inserted allowing the user to control the movements inside the virtual cave environment. In addition to this, a second mode of virtual exploration was related to virtual reality, as the models were uploaded in VR-type goggles (MetaQuest 2). Both forms of visualization allow users to move and explore the cave environments in an immersive and interactive way. This technology is a promising tool for the virtual presentation and exploration of natural environments, such as caves, which are frequently difficult to access.

1. Introdução

Caves are usually remote and low-light environments, which pose challenges regarding their access, mapping and exploration in the field. With the increasing use of digital mapping of natural spaces, the virtual exploration of caves then becomes a promising way of democratizing the knowledge about these spaces, as it enables any user, through an immersive experience, to explore them in virtual reality. The objective of this work is to report the application of virtual reality in facilitating general access to two caves located in the Brazilian semi-arid region. These caves (Furna Nova and Letreiro) were digitally reproduced for insertion into virtual reality. In addition to virtual exploration, the integration of advanced technologies in 3D modelling for education of Earth Sciences subjects has the potential to promote interactive and inclusive learning. In this regard, the manipulation of technological objects allows students to experience immersion, interaction, and imagination through Virtual Reality (ŠVEDOVÁ; KUBÍČEK, 2021; AZZURI et al., 2024). Technologies such as landscape visualization in VRs with 3D immersion goggles are resources that support the learning of complex concepts, as they offer immersive and hands-on experiences that allow students to explore and interact with representations of natural phenomena and environments in a more tangible way (FISHER et al., 2019; LAMPROPOULOS; KINSHUK, 2024).

Recent studies highlight the positive impact of these technologies, including augmented reality and virtual reality, gamification, and 3D landscape models, on new knowledge acquisition and student motivation, in addition to the inclusion of students with special needs (SILVA; MARTINS; ROCHA, 2025). This is particularly useful in the teaching of Geography and Cartography (CARRUBA; CALCAGNO; COVARRUBIAS, 2023).

In view of this, technological applications using Virtual Reality as a educational tool in lessons related to Earth Sciences, especially Geomorphology, were the focus of this work. The aim was to promote the visualization of geomorphological data in 3D digital models of landforms (caves).

2. Surveyed Area

The surveyed area is located in the state of Rio Grande do Norte, in northeastern Brazil, and comprises two caves (Furna Nova and Letreiro) within the Furna Feia National Park. The caves are carved in carbonate rocks of the Jandaíra Formation, which corresponds to the post-rift section of the Potiguar Basin. The exposed carbonates of the Jandaíra Formation tend to show a high level of karstification, with large fields of limestone pavements, collapse dolines, and numerous caves.

3. Materials and Methods

Photogrammetric surveys and subsequent processing result in the generation of three-dimensional virtual models of the natural objects being imaged, allowing for its manipulation, visualization, and data acquisition outside the field.

In caves, the technique emplyed is digital photogrammetry, which encompasses of two main stages, the first being the image capture

in the field (Figure 1). In this stage, sequential photographs are taken following the photogrammetric parameters of lateral and vertical overlap of at least 60%. For this work, about 2000 photos were captured with a Sony DSC-Hx300 digital camera, with a focal length of up to 215 mm. The photographs are taken sequentially and must cover 360° (acquisition globes, Figure 1A). Artificial white light is an essential factor for acquiring photos in this case, and this procedure is repeated along the length of the cavity. It is important to note that the camera's light meter should be set to "Low Light" to maximize the light capture on the sensor inside the cave. To assist the generation of homologous points during the cloud processing (e.g., identifying differences in the texture of the object), control points with different geometric shapes are positioned along the acquisition path inside the cave.

The subsequent processing steps - similar in both photogrammetry and aerial photogrammetry - result in the construction of the three-dimensional model with submetric resolution. The processing is performed in Agisoft Metashape Photoscan software (Geomorphology Laboratory - UFC) using the Structure from Motion (SfM) algorithm, which creates a computational model of points based on digital stereoscopic effects. The workflow consists of: adding photos and defining the geographic coordinate system (SIRGAS 2000); aligning figures; generating a point cloud. Afterwards, 3D models are generated from the interpolation of the point clouds, giving a high-resolution texture of the terrain. This visualization can be merged with the aligned photos in the model, giving a real appearance of the outcrop in the 3D model (Mesh). Subsequently, the Digital Terrain Model (DTM) and georeferenced orthomosaic are exported, and can be manipulated in other 3D data visualization and GIS (Geographic Information System) softwares.

These virtual models are adapted for three purposes: visualization of the model in open-source software (Cloud Compare), also used to obtain geometric data and production of virtual reality scenarios. After being generated in Agisoft Metashape, the models go through a process of mesh and texture optimization, where an algorithm (Optimize Alignment) is applied, which uses kriging to interpolate the points with gaps to reduce the number of artifacts in the product. This helps adapt the application to the graphical limitations of Meta Quest 2 devices (virtual reality headsets), without compromising visual fidelity to the real model. The Unreal Engine software, a 3D graphics engine, is employed to develop the interactive application, allowing for real-time exploration of the models. To ensure a smooth experience, gamification resources and graphic optimization techniques are used, ensuring interactivity and user immersion (COSTA, 2020; Figure 2C). These techniques involve rendering the models and their textures using Nanite technology, making the manipulation of heavy, high-resolution models easier, and also providing a more dynamic and realistic interface for viewing the immersive three-dimensional landscapes.

4. Results and Discussion

The resultant 3D models for exploration in virtual environments evidence the applicability of using virtual reality as an immersive experience, which can be utilized for various purposes.

In educational contexts, this immersion in the virtual environment contributes to a more direct interaction with subjects involving natural spaces. In this context, research has pointed out that virtual classroom activities allow students to develop conceptualizations of the environment in which they are immersed. Activities involving virtual reality learning environments (VRLE) enable immersion, interactivity, and imagination, as the virtual environment allows them to move and interact with the created environment (in this case, using the controls), stimulating the formulation of concepts and interpretations about the object they are engaging with (Figure 1).

Virtual reality (VR) and the use of immersive virtual environments (IVEs) provide a spatial experience that promotes the understanding and visualization of complex three-dimensional natural objects and a sensory experience of complex concepts, such as terrain formation and the climatic processes associated with cave genesis.

Virtual reality with 3D immersion headsets can be used both in Geoscience education and for scientific outreach purposes. Thus, virtual fieldwork using VRs not only constitutes methodologies that support traditional fieldwork but also becomes a potential tool for accessibility to anyone interested in experiencing an immersive cave experience.

Figure 1: *Cave scenario with a manipulable avatar in virtual reality, based on the gamification of the digital model generated by photogrammetry. This scenario is the view of the user with MetaQuest 2 glasses, where the user is the avatar, represented by a man in a blue jumpsuit and a yellow helmet, artificially inserted into the digital model for gamification. The avatar can move through the cavity using commands on the glasses' controller. A: Furna Nova Cave.*

Figure 2: *Cave scenario with a manipulable avatar in virtual reality, based on the gamification of the digital model generated by photogrammetry. This scenario is the view of the user with MetaQuest 2 glasses, where the user is the avatar, represented by a man in a blue jumpsuit and a yellow helmet, artificially inserted into the digital model for gamification. The avatar can move through the cavity using commands on the glasses' controller. B: Letreiro Cave.*

5. Conclusion

The use of virtual immersion in 3D models of cave environments can have a wide application and is a promising resource both in education and scientific outreach. Currently, technologies such as digital photogrammetry are becoming increasingly accessible, and their use for various purposes, including educational ones, has proven to be an efficient tool, especially allowing access and immersion in remote environments such as caves. We encourage the digitalization of caves and the availability of 3D for exploration in both digital and virtual modes, in order to expand knowledge and provide a more realistic immersive experience in caves. We highlight that these techniques can also foster the conversation of these relevant natural spaces.

Acknowledgments

We thank Cecav (Center for Cave Studies) – Icmbio (Instituto Chico Mendes da Biodiversidade) for financing this work through the Vivências 3D Project, carried out in partnership with the Geomorphology Laboratory of the Federal University of Ceará.

References

AZZURI, F.; DARFIANSA L. S.; BACHTIAR F. A.; TOLLE, H. The Development of Augmented Reality to Support Geomorphology Learning In Observing Landforms. In: 7th International Conference on Informatics and Computational Sciences (ICICoS), Semarang, Indonesia, p. 538-544, 2024. DOI: https://doi.org/10.1109/ICICoS62600.2024.10636826

CARRUBA, M.C.; CALCAGNO, A.; COVARRUBIAS, M. Google Earth in VR, for Students with Special Needs. In: DE PAOLIS, L.T.; ARPAIA, P.; SACCO, M. (Eds.). Extended Reality. XR Salento 2023. Lecture Notes in Computer Science, vol 14219, 2023. DOI: https://doi.org/10.1007/978-3-031-43404-4_1

COSTA, G. F. C. Fotogrametria 3D no Design de Jogos Digitais: estudo de caso da conceção de assets fotorrealistas em ambientes amadores. Dissertação (Mestrado em Design e Desenvolvimento de Jogos Digitais - 2º ciclo de estudos) - Faculdade de Artes e Letras, Universidade da Beira Interior, Covilhã (Portugal). 2020. 123 p.

SILVA, R. M.; MARTINS, P.; ROCHA, T. Virtual reality educational scenarios for students with ASD: Instruments validation and design of STEM programmatic contents. Research in Autism Spectrum Disorders, 119, 102521, 2025. DOI: https://doi.org/10.1016/j.rasd.2024.102521

FISHER, R.; HECKBERT; S.; MARIA, J.; SUTTON, S. Augmenting physical 3D models with projected information to support environmental knowledge exchange. Applied Geography, v. 112, 2019. DOI: https://doi.org/10.1016/j.apgeog.2019.102095

LAMPROPOULOS, G.; KINSHUK. Virtual reality and gamification in education: a systematic review. Educational Technology Research and Development, 72(3), p. 1691–1785, 2024. DOI: https://doi.org/10.1007/s11423-024-10351-3

ŠVEDOVÁ, H.; KUBÍČEK, P. The Use of Virtual Environments in Geoscience Education. In: International Cartographic Conference, 30, 2021, Florencia, Itália (ICC 2021) Anais [...]. Abstracts of the International Cartographic Association, 3, p. 1–3, 2021. DOI: https://doi.org/10.5194/ica-abs-3-281-2021

Preliminary characterization of karst in Baling, Kedah, Malaysia

Ros Fatihah Muhammad, Muhamad Akif Akwa Zaidi, Muhammad Afiq Hafifi Ngari & Mohamad Fahmi Mat Daud

Department of Geology, Universiti Malaya, 50603 Kuala Lumpur, rosfmuhammad@um.edu.my (corresponding author)

Abstract

The karst hill of Gunung Pulai in Baling (~512 m a.s.l.) forms a crescent-shaped ridge north of Baling town in Kedah, Malaysia. Along with Bukit Wang in the northwest, this limestone complex, trending approximately northeast to southwest, is believed to be the remnant of a doline, with its northwestern section completely denuded. This landscape results from the differential dissolution of the coarse sparry marble of the Baling Group and represents a tropical karst remnant tower, a common feature in Peninsular Malaysia. The area hosts at least 21 caves at various elevations, forming a network of channels and conduits that drain rainwater from the karst hills into Sungai Ketil. Springs emerge along the northwest flank, flowing northwestward before disappearing into a cave in Bukit Wang and re-emerging at the surface. Several cave springs also appear along the foothills at the southeast flank, especially during the wet season, when water resurfaces. These springs likely originate from rainwater within the karst system, contributing to Sungai Ketil through both surface and underground flows.

1. Introduction

Gunung Pulai, located in southeastern Kedah, Malaysia, lies on the boundary between Pulai and Baling districts. Baling town is situated 110 km from Alor Setar, the state capital of Kedah, and 410 km from Kuala Lumpur. This limestone hill range is prominently visible from Baling town. The central coordinates of Gunung Pulai are 5°40'15.8"N, 100°53'35.7"E. This limestone hill rises approximately 512 meters above sea level, forming 3.5 km long sharp ridge in a semi-spherical shape—resembling a crescent or horseshoe—that curves northwestward, with Bukit Wang, a smaller hill, to the north. The southeastern flank faces Baling town and appears gentler than the northwest side, which features a striking bare rock wall along the north bank of Sungai Ketil. Gunung Pulai is part of the Baling Group of Kroh Formation, dating back to the Cambrian-Ordovician period, which consists of argillaceous, calcareous, and arenaceous strata, with argillaceous layers being predominant (BURTON, 1970). The limestone member occurs in bands and lenses, ranging in thickness from a few millimeters to 1.6 km, but accounts for only 7% of the entire formation. One of these limestone lenses formed Gunung Pulai. Thermal metamorphism has led to the recrystallization of its calcareous strata into coarsely crystalline marble.

The northeastern section of the hill is currently being quarried, while the southwestern part faced a similar threat in recent years. However, strong opposition from the local community led to a halt in quarrying activities. Since then, the area has been promoted for tourism by locals and has attracted a steady flow of visitors who come to admire the karst wall facing Sungai Ketil. Despite this, most caves remain undeveloped for tourism, except for Gua Sireh in Bukit Wang, which is managed by the city council. This preliminary study aims to describe the morphology of Gunung Pulai, assess its potential for sustainable karst tourism, and explore conservation efforts. Additionally, the karst water, which partially feeds Sungai Ketil, may contribute to the domestic water supply stored in the Sungai Limau Reservoir, located 1.5 km west of the hill's westernmost tip. This research serves as a foundation for future karst management and preservation efforts.

2. Materials and methods

Site visits were conducted from 2018 to 2025 to identify caves and examine the drainage network within the karst area and its surroundings. The Sungai Ketil terraces were mapped in relation to cave elevations, which were determined using a Global Positioning System (GPS) and cross-checked with a Digital Elevation Model (DEM) generated in ArcGIS.

Cave characteristics are summarized in Table 1, including features such as stream occurrences, ceiling collapses leading to cave enlargement, and passage types. Additionally, key parameters used to analyze hill morphology—such as elevation, slope gradient, slope aspect, and stream order (WOHL, 2009)—were assessed using ArcGIS, particularly to determine drainage patterns within and around the karst complex.

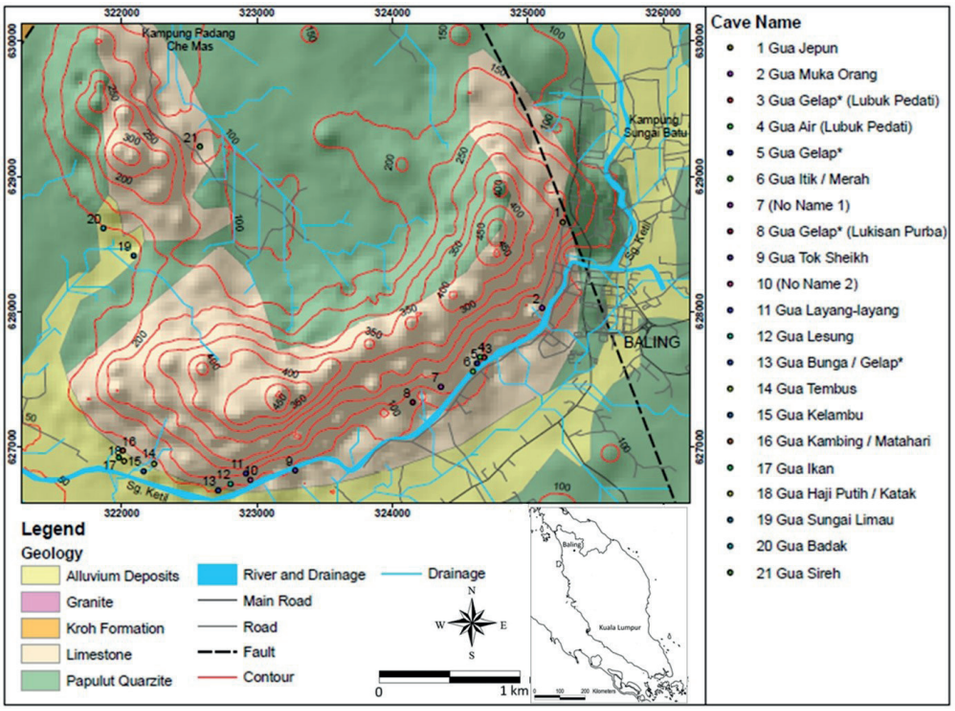

Figure 1: *The location, geology, drainage, and distribution of caves in Gunung Pulai. Most caves are situated along the T1 and T2 river terrace at elevations between 65 and 75 m above sea level, with some found at approximately 80 m and others exceeding 100 m. Karst springs emerge from within the hill, feeding Sungai Ketil along the southeast flank, while some merge to form second-order streams that flow northeast.*

3. Results

During preliminary scouting, a total of 21 caves were identified—18 on the southeastern flank of the hill and 3 in Bukit Wang. Their characteristics are detailed in Table 1. Along Sungai Ketil, three distinct river terraces were observed: T0, the active floodplain at approximately 60 m above sea level (asl), T1 at about 65 m asl, and T2 at 75 m asl. Most caves are situated at the T1 and T2 levels, with several higher-elevation caves exceeding 100 m asl. Lower-level caves typically preserve phreatic features, such as flat ceilings indicating former water table levels, and some contain active streams. In contrast, high-elevation caves have expanded due to ceiling collapse. Both the northwest and southeast flanks of Gunung Pulai feature drainage networks that originate from the limestone mass. Stream order analysis indicates that several first-order streams begin within Gunung Pulai, flowing into Sungai Ketil along the southeastern flank and northwestward along the opposite slope. Caves located at the lowest elevation on T1 function as intermittent springs. Their water source is allogenic, flowing through cracks, overflowing gour pools, and eventually draining onto the T1 terrace. These intermittent springs become active during the wet season, sometimes leading to severe flooding at T1, with the most recent major flood occurring in December 2020. A number of springs are observed along the northwest flank via the flow model generated in ArcGIS.

Figure 2: *The west-flowing Sungai Ketil seen in the background on the right forming T0 up to the house with the blue roof, followed by T1 that transition to T2 where the photograph was taken*

4. Discussion

The caves in Baling are generally categorized based on their elevation relative to the Sungai Ketil terraces. The lowest caves are located on the T1 terrace, another group is found around the T2 terrace, and the remaining caves are at higher elevations. In general, older caves tend to be at higher elevations, where the transition from the phreatic to vadose zone has occurred due to the progressive deepening of caves

alongside valley downcutting and river terrace evolution. In contrast, lower-level caves, which are typically younger, are found closer to the ground surface. These caves are relatively small, often preserve phreatic features, and contain abundant sediment transported by fluvial activity. Higher-elevation caves, on the other hand, are usually larger, with collapsed ceiling blocks scattered throughout. Some extend to the peak, forming skylights. The presence of both low- and high-level caves provides valuable insights for regional correlations, particularly in reconstructing Quaternary events through sediment transport and deposition records. This method has been widely applied in regional studies (PALMER, 1987).

A depression along the northwest flank acts as a water catchment, allowing water to accumulate before percolating into disappearing or sinking streams. These streams flow through underground limestone drainage systems, distributing water to smaller subterranean inlets.

According to PALMER (1991), as a karst depression expands, increasing amounts of water recharge the main drainage passages under hydraulic control in a self-accelerating process. The available water supply within the depression regulates the hydraulic gradient, which feeds the sinking streams and underground passages. As the underground drainage network evolves from small conduits into larger channels, water can be redirected through alternative routes. Additionally, sinking streams that feed water into the caves are often subject to intense flooding during periods of heavy rainfall. Increased precipitation temporarily raises water levels, causing overflow from underground drainage systems—a phenomenon observed in the study area.

No	Cave Name	Cave features																Passage type			Speleothems			Paleontology/ Archeology		
		Elevation (m asl)	Stream	Notches	Clastic cave infilling	Intermittent river	Former phreatic passages/tubes	Wide/High chamber	Block of limestone on caves floor	Rimstone dams	Cave Pool	Flat ceiling	Breccia	Ceiling collapse	Skylight	Multi-level	Cave marking	Guano deposits	Phreatic Zone	Epiphreatic zone	Vadose Zone	Low	Moderate	Intense	Artifacts	Fossils, dental remain	Ancient artwork
1	Gua Jepun	85.0						✓									✓				✓						
2	Gua Muka Orang	87.3																			✓						
3	Gua Gelap* (Lubuk Pedati)	105.0						✓		✓											✓		✓				
4	Gua Air (Lubuk Pedati)	110.0				✓		✓			✓					✓	✓	✓			✓		✓				
5	Gua Gelap*	70.0				✓			✓				✓	✓		✓					✓		✓	✓		✓	
6	Gua Itik / Merah	68.0																			✓						
7	Unknown (No Name)	63.0																			✓						
8	Gua Gelap* (Lukisan Purba)	75.3				✓		✓	✓				✓	✓		✓	✓	✓		✓	✓		✓			✓	✓
9	Gua Tok Sheikh	60.0				✓		✓		✓											✓	✓	✓		✓	✓	
10	Unknown (No Name)	80.0							✓												✓	✓					✓	
11	Gua Layang-Layang	154.0						✓	✓					✓	✓	✓		✓			✓	✓					✓	
12	Gua Lesung	80.0																			✓						✓	
13	Gua Bunga / Gelap*	82.0				✓		✓	✓	✓				✓			✓	✓		✓	✓		✓				✓	
14	Gua Tembus	93.3				✓			✓					✓							✓	✓			✓	✓	✓
15	Gua Kelambu	71.9				✓		✓	✓												✓	✓	✓			✓	
16	Gua Kambing / Matahari	81.7							✓					✓	✓						✓			✓	✓	✓	
17	Gua Ikan	70.0				✓			✓					✓		✓				✓	✓	✓	✓				✓	
18	Gua Haji Putih / Katak	69.8		✓	✓	✓	✓					✓							✓	✓	✓	✓					
19	Gua Sg. Limau	73.5	✓	✓	✓		✓	✓				✓					✓	✓		✓	✓	✓					✓	
20	Gua Badak	55.0				✓	✓	✓	✓			✓				✓	✓	✓	✓	✓	✓	✓	✓	✓				
21	Gua Sireh	86.7			✓	✓		✓		✓				✓		✓	✓	✓			✓		✓				✓	✓

Tavle 1: *List of caves in Baling karst , elevation in m above mean sea level, along with common features and indications of potential for paleontological and archeological aspects.*

5. Conclusion

Preliminary studies indicate that Gunung Pulai in Baling contains a significant number of caves with diverse morphology at various elevations. These features are crucial for further research on cave evolution, offering insights into the landscape development in the surrounding area. The karst system, with its surface and underground water networks, also serves as an important water source for the community. Given its tourism potential, proper management is essential to address associated challenges. These early findings highlight the need for detailed cave surveys, characterization, and effective karst water management.

6. Acknowledgments

We gratefully thank Roshasliza ABDULl RAZAK, Mohd Nazri HAMID and Mohd Tarmizi ABDUL AZIZ for the help during the fieldtrips. Thanks to Baling city council for facilitating the work in Gua Sireh and for partly funding the trips.

7. References

BURTON, C. K. (1970). Lower Palaeozoic rocks of Malay Peninsula: discussion. Am. Ass. Petrol. Geol. Bull. 54, 357-360.

WOHL, E. (2009). Streams. In G. E. Likens (Ed.), Encyclopedia of Inland Waters (pp. 756- 765). Oxford: Academic Press.

PALMER, A. N. (1987). Cave levels and their interpretation. NSS Bulletin, 49, 50-66.

PALMER, A. N. (1991). Origin and morphology of limestone caves. GSA Bulletin, 103(1), 1-21. doi:10.1130/0016-7606(1991)103<0001:oamolc>2.3.co;2

Estudo da Geomorfologia Cárstica na Região do Astroblema de Araguainha: Cavernas de Arenito no Município de Ponte Branca – Mato Grosso.

Isabella Martins Oliveira (1) & Ivaniza de Lourdes Lazzarotto Cabral (2)

(1) Estudante de Graduação em Geografia Bacharelado - UFMT, isabellamaria.profissional@gmail.com

(2) Professora associada do Departamento de Geografia - UFMT, ivanizacabral@hotmail.com

Resumo

No interior de Mato Grosso, está localizada um dos maiores eventos astronômicos da América do Sul – a cratera de impacto (Astroblema) de Araguainha, mais precisamente o Domo de Araguainha, e com ele a riqueza espeleológica da região. A pesquisa foca nas cavernas litológicas de arenito do município vizinho de Ponte Branca. O estudo foi realizado por meio de observações diretas em campo, nas quais foram estudadas as características geomorfológicas e ecológicas das cavernas e entorno. Complementando a análise, foi feito um levantamento bibliográfico sobre as formações e peculiaridades deste carste, buscando compreender suas interações, pois se trata de formações litológicas cársticas raras no País. Este estudo contribui para destacar a relevância para a conservação deste patrimônio natural e da biodiversidade da região, melhorando o entendimento da dinâmica geológica e proporcionando ideias e estratégias de proteção ambiental.

Abstract

In the interior of Mato Grosso, one of the largest astronomical events in South America is located – the impact crater (Astroblema) of Araguainha, more specifically the Araguainha Dome, along with the region's rich speleological heritage. The research focuses on the sandstone lithological caves of the neighboring municipality of Ponte Branca. The study was carried out through direct field observations, in which the geomorphological and ecological characteristics of the caves and their surroundings were examined. Complementing the analysis, a bibliographic survey was conducted on the formations and peculiarities of this karst, seeking to understand its interactions, as it involves lithological karst formations that are rare in the country. This study helps highlight the importance of conserving this natural heritage and the region's biodiversity, improving the understanding of its geological dynamics and providing ideas and strategies for environmental protection.

1. Introdução

A área de estudo está localizada na região do Astroblema de Araguainha, no município de Ponte Branca – MT, e é caracterizada pela presença de cavidades naturais em arenito. Carste litólogico de arenito são formações raras, principlamente no País. Processo pelo qual, levaram milhares de anos, foram esculpidas pela ação da água, do vento e do tempo. As cavernas selecionadas para a pesquisa são de arenito da Formação Aquidauana e Corumbataí, ambas da Bacia Sedimentar do Paraná. Elas estão posicionadas no norte da zona de impacto da cratera, sendo uma disposta sobre os anéis concêntricos do impacto. Este estudo procura trazer uma breveexplanação sobre estas cavernas, salientando sua geomorfologia cárstica. A metodologia utilizada foi a analise sistemica da paisagem. Como resultados iniciais estão a criação de uma carta imagem edo acervo fotográfico referente as cavernas pois, anteriormente, não havia registros dos referidos fatos na região.

2. Materiais e Métodos

A base teórica da pesquisa enfoca um estudo relacionado à Espeleologia e à Geomorfologia do Carste. As informações relacionadas às cavernas do município de Ponte Branca foram obtidas junto ao Centro Nacional de Estudo, Proteção e Manejo de Cavernas/InstitutoChico Mendes (CECAV/ICMBio), na Sociedade Brasileira de Espeleologia (SBE), na Companhia de Pesquisa de Recursos Minerais (CPRM) e no repositório de artigos acadêmicos do Google Scholar. Em campo a observação e análise das cavernas foram realizadas com a orientação das coordenadas geográficas e dados contidos no Cadastro Nacional de Informações Espeleológicas (CANIE), com os dados manipulados e visualizados por meio do Google Earth Pro (GEP) e com a colaboração do guia local Ruy Ojeda, arquivo fotográfico e georreferenciado por GPS (Global Positioning System), levantamento atualizado de da dos e coordenadas geográficos. A representação cartográfica utilizado foi através do software gratuito Google Earth Pro, resultando no desenvolvimento de uma carta imagem de localização e de um croqui feito pelo ArqGis versão 10.8.2, em escala 1:350.00, no qual mostra em que parte da estrutura dos anéis de impacto as cavidades estão. As coordenadas e shape files foram obtidas, gratuitamente na internet (CECAV/ICMbio, CANIE, IBGE) e também com material cientifico cedido por pesquisadores, sendo elaborados no software e contando também com ajuda do guia local.

Figura1: *Cavidade Casa de Pedra Barra do Casal.* **Fonte:** *Acervo pessoal. (2024).*

3. Resultados

Os resultados alcançados a partir das observações de campo, exibiram aspectos geomorfólogicos próprios do arenito nas cavernas. Foram selecionadas três cavernas de acordo com os dados obtidos e classificações dadas pelo Cadastro Nacional de Informações Espeleológicas (CANIE), parte integrante do Sistema Nacional de Informação do Meio Ambiente (SINIMA), desenvolvido pelo ICMBio, sendo o Centro Nacional de Pesquisa e Conservação de Cavernas (CECAV) o responsável pela sua gestão. Em campo foi constatado que todas as cavernas observadas são de litologia arenitícas. De acordo com o GeoSGB do Serviço Geológico do Brasil/CPRM - Carta Geológica da folha Goiânia, a estrutura geológica onde estão localizadas as cavernas são os arenitos do Grupo Itararé - Formação Aquidauana, pertencentes à Bacia Sedimentar do Paraná. As cavidades Casa de Pedra II, Abrigo das Mãozinhas e Casa de Pedra Barra do Casal foram as selecionadas para a pesquisa. Em duas delas o acesso foi por meio de condução própria e a terceira por meio de aula de campo do curso de Geografia da Universidade Federal de Mato Grosso – campus Cuiabá, contando com o apoio do guia local Ruy Ojeda. No contexto da cobertura vegetal as cavidades estão localizadas em meio ao Cerrado bem preservado, causando dificuldades no acesso a elas. No que se refere aos tamanhos as três cavernas representam formas de relevos cársticos de pequenas dimensões em arenito avermelhado e esbranquiçado, folhelhos e siltitos do Grupo Itararé e possivelmente arenito da Formação Corumbataí, como mostra a figura 1. As cavernas estudadas se localizam em uma das serras que representam uma parte de um dos anéis formados pela disperssão da energia durante o impacto do Astroblema. No detalhe, uma delas apresenta um ou dois pequenos salões principais conforme documentado nas figuras 1 e 4. Nesta foi possível verificar registros de inscrições rupestres em suas paredes. Eram registros compostos por símbolos semelhantes e em condições diferentes de preservação. Na ocasião, devido a ausência de um especialista no assunto, não foi possível obter maiores informações sobre tais símbolos. São cavernas secas, pois não apresentam circulação de água em seus interiores. Também foi possível perceber pouca diversidade na fauna e flora local, exceto o registro de uma grande quantidade de morcegos. Relacionado a dinâmica da formação das cavernas é possível perceber eventos relacionados a ação do intemperismo físico e químico nelas como, por exemplo, abatimento de porções de material rochoso e marcas de alteração nas superfícies das rochas. É importante destacar que nas próximas linhas de investigações destas cavernas está previsto a utilização de equipamentos especializados, ou seja, os Veículos Aéreos Não Tripulados – VANT para confirmar alguns dados presentes no Cadastro do CANIE. A utilização de imagens aéreas provenientes do referido equipamento é para averiguar a ocorrência de outras entradas, sumidouros e demais feições relacionadas as formas de relevo cárstico. A partir da análise e interpretação de imagens de satélite e os trabalhos de campo foi possível determinar que todas as cavernas consideradas neste trabalho estão localizadas em propriedades particulares, conforme apresentada na carta imagem da figura 2. E na figura 3, é mostrada onde estão concentradas as cavidades dentro dos anéis de impacto do astroblema.

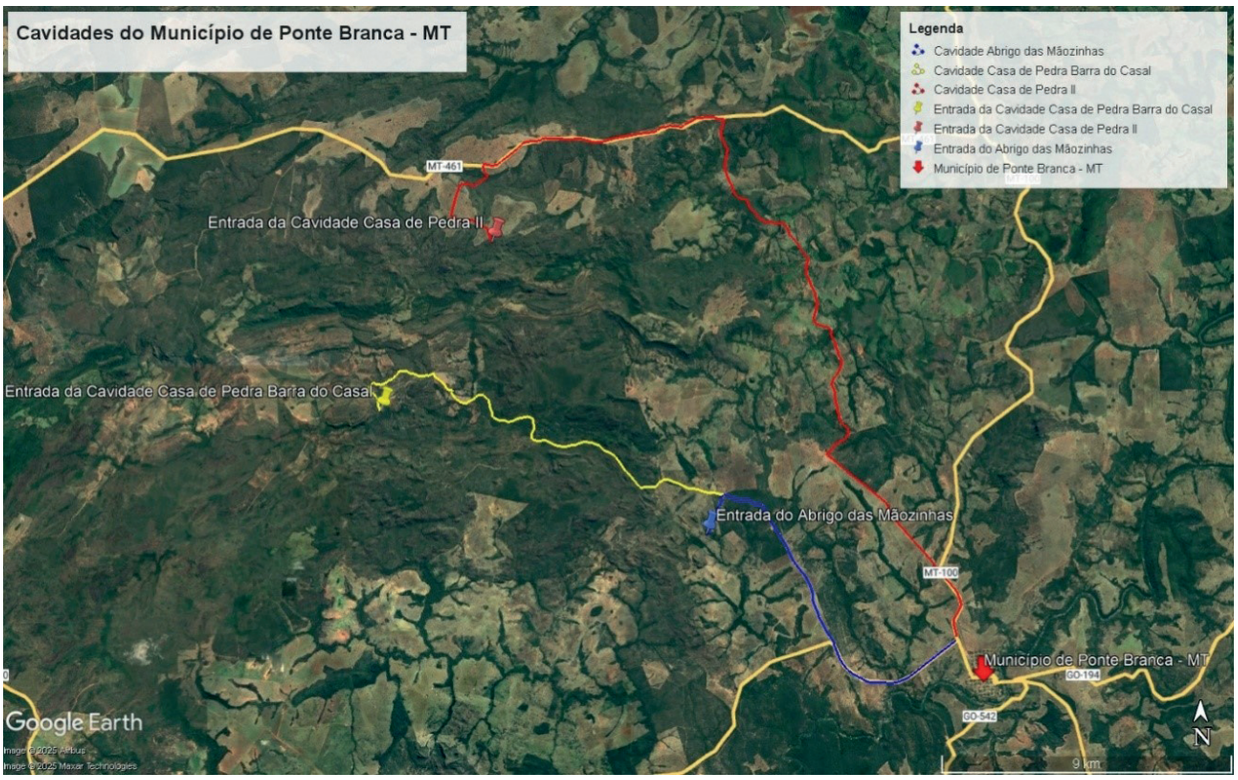

Figura 2: *Carta imagem mostrando a localização das cavernas no município de Ponte Branca/MT.*
Fonte: *Elaboração pela primeira autora (2024).*

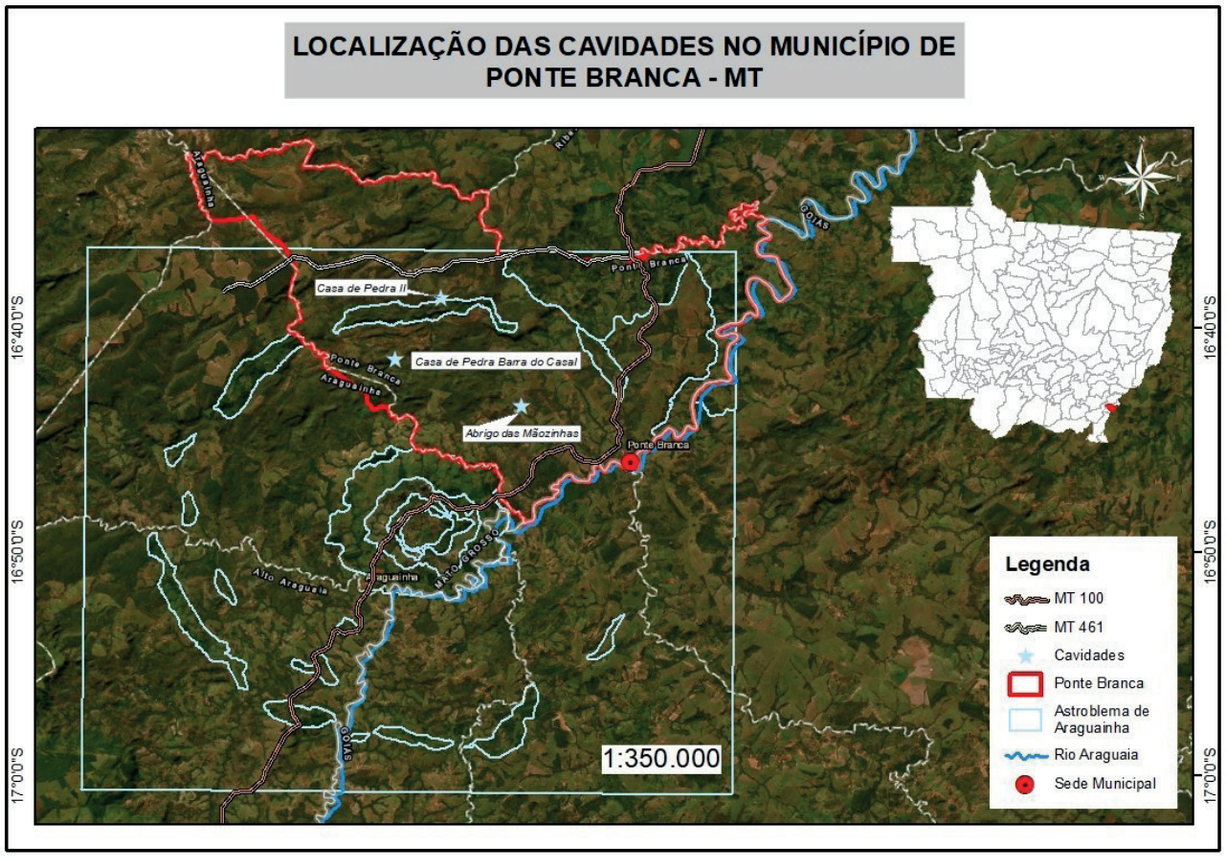

Figura 3: Croqui das cavidades no município.
Fonte: CECAV/ICMbio, CANIE, IBGE. Adaptado pela autora (2025), com dados disponibilizados pela Dra.Natalia Hauser (IG- UnB), Carolinna da Silva Maia de Souza, Lobo Uwe Reimold, Renato Borges Bernardes, Lucieth Cruz Vieira, Edi Mendes Guimarães e Manfred Gottwald.

4. Discussão

As inter-relações mútuas dos fatores ambientais, que são ainda mais complexas no caso das cavernas de arenito, podem ser comparadas à analogia do terreno cárstico descrito por Bertrand (1971). Como essas áreas cársticas serão afetadas por esses processos geomorfológicos, as estratégias de preservação devem ser planejadas levando em consideração esses processos, já que esses ambientes estão inter-relacionados com processos geomorfológicos. Embora, necessite de mais estudos e pesquisas, a descrição dos ambientes cársticos das cavidades aqui mencionadas, tem uma similiaridade com outros sistemas de cavernas da mesma litologia. Se faz necessário o aprofundamento da influência do impacto do corpo celeste com a área afetada.

A classificação destas cavidades é algo a se analisar pois, em alguns casos, uma mesma cavidade aparece na plataforma do CANIE com duas ou três entradas distintas e está registrada como se fossem cavernas independentes. No entanto, durante a visita a campo, foi possível perceber que se trata de uma única cavidade, o que evidencia a necessidade de revisão mais detalhada nas informações cadastradas.

Figura 4: *Cavidade Casa de Pedra II.*
Fonte: *Acervo pessoal. (2024)*

5. Conclusão

Embora a pesquisa tenha revelado aspectos importantes sobre a geomorfologia cárstica das cavernas estudadas, é imprescindívelnovos estudos e investigações tanto sobre estas cavernas quanto sobre as demais da região do astroblema de Araguainha, para uma aprofundada compreensão dessa dinâmica. A ausência de políticasde preservação e proteção ambiental para as cavernas e suas áreas do entorno, é uma questão urgente, uma vez que foram encontradas degradações provocadas por ações humanas em uma das cavernas visitadas. A ameaça representada pela pecuária e o desmatamento impacta seriamente a integridade do ambiente cárstico e os ecossistemas locais. É essencial que sejam implementadas estratégias de educação ambiental contínuas para sua conservação.

Figura 5: Inscrições rupestres Casa de Pedra II

Agradecimentos

Gostaria de expressar meus agradecimentos a minha mãe por sempre me motivar nos estudos e principalmente para escrever este artigo. E a minha professora Ivaniza de Lourdes Lazzarotto Cabral pelo incentivo e ajuda para esta pesquisa.

Referências

FREIRE, Luciana Martins; LIMA, Joselito Santiago de; VERÍSSIMO, Cesar Ulisses Vieira; SILVA, Edson Vicente da. Carste em Rochas Não Carbonáticas: contribuição ao estudo geomorfológico em cavernas de arenito da Amazônia Paraense (Karst in Non-Carbonate Rocks: contribution in geomorphological study in sandstones caves of the Paraense Amazon). Revista Brasileira de Geografia Física, [S. l.], v. 10, n. 6, p. 1829–1845, 2017. DOI: 10.26848/rbgf.v10.6.p1829-1845. Disponível em: https://periodicos.ufpe.br/revistas/index.php/rbgfe/article/view/234054. Acesso em: 10 fev. 2025..

FREIRE, Luciana Martins; LIMA, Joselito Santiago de; ULISSES VIEIRA VERÍSSIMO, Cesar; VICENTE DA SILVA, Edson. ESTUDO GEOMORFOLOGICO EM CAVERNAS DE ARENITO DA AMAZÔNIA PARAENSE. Revista de Geografia, [S. l.], v. 35, n. 4, p. 14–31, 2018. DOI: 10.51359/2238-6211.2018.238198. Disponível em: https://periodicos.ufpe.br/revistas/index.php/revistageografia/article/view/238198. Acesso em: 10 fev. 2025.

Souza, C. da S.M. de, Hauser, N., Reimold, W.U., Bernardes, R.B., Vieira, L.C., Guimarães, E.M., and Gottwald, M., 2024, Araguainha impact structure, Brazil: New insights into the geology of the central uplift: Meteoritics & Planetary Science, v. 59, p. 2577–2607, doi:10.1111/maps.14236.

CENE, V.R.; VITTE, A.C. A representação cartográfica da paisagem em Alexander von Humboldt: uma contribuição à história da geografia. In: Anais XII EGAL - Encuentro e Geógrafos de América Latina, Montevideo, p.1-16. 2009.

THEULEN, V. Estratégias para Conservação das Cavernas Brasileiras. Disponível em: <https://www.cavernas.org.br/wp-content/uploads/2021/02/26CBE_695-698.pdf>. Acesso em: 10 fev. 2025.

BERTONI, José; LOMBARDI, Maria. Teoria Geossistêmica: Contribuições para a compreensão dos processos naturaTeoria Geossistêmica: Contribuições para a compreensão dos processos naturais . São Paulo: Editora Acadêmica, 2006. p. 112.

Bertrand, J. (1971). Geossistemas e a evolução da geomorfologia . São Paulo: Editora Geosistêmicas

Geology, geomorphology and hydrogeology of the “Davorjevo brezno” cave, Classical Karst.

Rino Semeraro (1), Riccardo Corazzi (2) & Louis Torelli (2)

(1) CGEB (Hon. Mbr.), Gorizia, Italy, rinosemeraro0@gmail.com
(2) Commissione Grotte “E. Boegan” SAG-CAI Trieste (CGEB), Trieste, Italy,
[Corresponding author: Riccardo Corazzi, corazzi@iname.com]

Abstract

Davorjevo brezno is located on southeastern border of the Classical Karst in Slovenia. It is one of the largest caves in the Kras/Carso, currently depth -317 m and a spatial development of 6,660 m surveyed. The cave corresponds a system of “basal” galleries where hypogean streams flow: these inner streams are reached from the surface after a succession of shafts. A first monitoring cycle of two subterranean streams (Carbonari and Veneziano meanders) was carried out of two multiparameter probes recorded water level, temperature and electrical conductivity from 2020 to 2021. After the discovery of the stream of “Susy” gallery, a second monitoring cycle was carried out in years 2022 to 2024 on both three streams. Geological survey of the cave shows that it develops in the Alveolinid-Nummulitid Limestone (Ilerdian) and in the limestones of the Liburnia formation (Maastrichtian-Paleocene p.p.). Davorjevo brezno is characterized mainly by syngenetic galleries, paragenetic galleries and gorges. The “Veneziano” stream corresponds to approximately 17% (avg.) of the flow rates of the “Susy” water collector. The water collector, with maximum peaks of 1,107.5 L/s, from the hydrological and chemical data, would correspond to a larger basin with water reserves stored in the epiphreatic and karstic phreatic zone. The catchment, hypothetically, it could include the “Dane” endorheic basin and, externally, an eastern and north-eastern part of the area.

1. Introduction

The Davorjevo brezno 10060 SLO (number of Slovenia cave registry) (Davorjevo Abyss) develops partly internal and partly externally to the “Dane” basin (Fig. 1). The “Dane” basin, in the Classical Karst, is a karst depression located immediately south of the sinking of Reka river in Škocjanske jame (Škocjan Caves). In this basin two streams converge, originate from small watersheds on the northeastern slope of marly-arenaceous rocks of “Brkini” hills. The streams are absorbed into sinkholes and caves, deriving from a blind valley situated at the northern border of basin. The “Davorjevo brezno” is a subterranean complex of galleries, mainly with water courses apparently autogenics. The cave, discovered in 2009, is being explored and studied by the Commissione Grotte “E. Boegan” SAG-CAI Trieste (Italy) (CGEB) in collaboration with Slovenian speleologists, and it is one of the most important of the Classical Karst. Geological, geomorphological and especially hydrogeological investigations were carried out in Davorjevo brezno, which are the subject of this work.

Figure 1: *Geographical setting.*

2. The cave and the surveys

The entrance position (WGS84) is Lat. 45° 38’ 15.15” and Long. 13° 58’ 17.9”, at altitude of 511 m asl. The cave is currently –317 m deep with a spatial development of 6,660 m (planimetric 6,059 m) surveyed (Fig. 2). After the vertical zone of the main shafts, begins the “Tihe Vode” water meander, which receives the waters of “Carbonari” meander. The “Tihe Vode” meander flows into the “Veneziano” meander, which continues upstream with the “Papà” meander: this latter keeps going upstream and becomes the so-called “Marc’Aurelio” meander. The “Veneziano” meander ends with a siphon (“old bottom”) at an average of 232 m asl (depth –279 m). The system Veneziano meander, Papà meander and Marc’Aurelio meander goes back up in altitude reaching quote 417 m asl (depth –94 m). Ascending from the final part of the “Veneziano” meander, and then descending again, you reach a new watercourse: this is the “Susy” gallery, a water collector with a higher flow rate than previous streams. The “Susy” gallery leads to the second siphon at 207 m asl (depth -304m). Here a cave diver explored a submerged gallery

227 m long up to 194 m asl, from which he re-emerges at 207 m asl in a aerated descendant gallery, not yet explored.

Over many years of exploration, the CGEB has carried out a series of preliminary investigations. In 2020 a more complete hydrogeological study on the "Davorjevo brezno" were carried out by monitoring the "Carbonari" and "Veneziano" streams through the installation of multiparameter probes and weirs and also take a study of the spectral trends of atmospheric pressure and air temperature. Subsequently, in 2022-2024 the "Carbonari" and "Veneziano" meanders were monitored again, in association with the "Susy" gallery watercourse. This monitoring cycle was integrated with chemical analyzes of the water, the hydrogeological study of the basin and geological and geomorphological surveys.

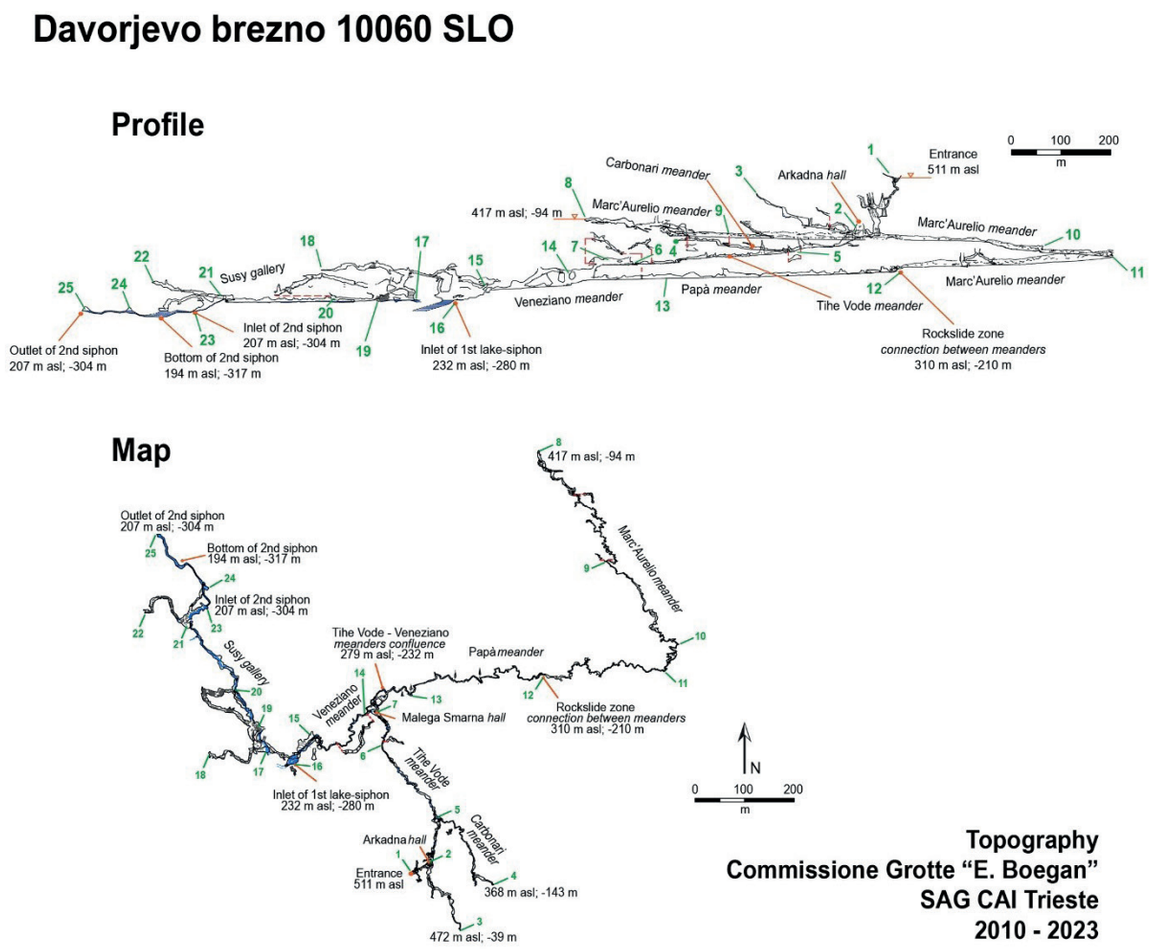

Figure 2: Topography of Davorjevo brezno.

3. Geology

The area of Davorjevo brezno (Fig. 3) is located at the transition between the Alveolinid-Nummulitid limestone [ANL] (Ilerdian), followed by the Transitional beds [TB] (Middle Ypresian-Lower Cuisian), and the Flysch of Brkini [F] (Upper Ypresian to Middle Lutetian), while to the north and south lays the Lipica formation [LI] (Upper Santonian-Campanian) and the Liburnia formation [LIB] (Maastrichtian-Paleocene p.p.) (JURKOVŠEK et al., 1996, 2016; DROBNE et al., 2009). This area is characterized by the border of the SSE-NNW gentle anticline dipping to SSE forming the east slope of "Danski" kras and "Dane" basin and the border of the SSE-NNW "Brkini" hills syncline.

In the area, the rock masses between the Lipica formation [LI] and the Alveolinid-Nummulitid limestone [ANL] are generally highly karstified, with the specification that the Liburnia formation [LIB] in the lower lithozone presents (on the karst outcrops) a lower degree of karstification, while in the upper lithozone (Slivje limestone (Middle-Upper Paleocene) the karstification is similar to that of the Alveolinid-Nummulitid limestone [ANL]. The Transitional beds [TB] and the marly-arenaceous Flysch [F] are non-karstified rocks.

Exploratory wells carried out by ARSA - SOCIETÀ ANONIMA CARBONIFERA (1937) for coal deposits research, shows the following stratigraphy for No. 5 and No. 6 drillings located in Kačiče, with old geological definitions. No. 5 – Elevation 465 m asl, Measure depth 639.59 meters, Stratigraphy: From 0 to 299 m depth "Nummulitico e Alveolinico", to 320 m "Miliolitico", to 590.75 m "Cosina", to end drilling "Cretaceo". No. 6 – Elevation 494 m asl, Measure depth 653.60 meters, Stratigraphy: From 0 to 325 m depth "Nummulitico e Alveolinico", to 364 m "Miliolitico", to 425 m "Cosina", to end drilling "Cretaceo".

Such stratigraphy were based on the old geology for the Classical Karst (STACHE, 1889): the correspondence with the current stratigraphy is as follows: "Nummulitico e Alveolinico": Alveolinid-Nummulitid limestone (Ilerdian), "Miliolitico": Liburnia formation, Slivje limestone (Middle-Upper Paleocene), "Cosina": Liburnia formation (Maastrichtian-Paleocene p.p.), "Cretaceo": Lipica formation (Upper Santonian-Campanian).

The main tectonic elements of the area, such as lineations, faults and fissured/crushed/broken zones, have been identified especially in the northern area (Škocjanske jame) and in the area of Davorjevo brezno. They

correspond to three main systems and one secondary system, identified as [F1] NNE/NE-SSW/SW subvertical (main), [F2] ENE-WSW subvertical (main), [F3] S/SSE-N/NNW subvertical/60° ENE-E (main), [F4] ESE-WNW/SE-NW subvertical (secondary). These tectonic structures correspond to those identified previously (GOSPODARIČ, 1983; ŠEBELA, 1994, 2009; ŠEBELA & NOVAK, 2023). In particular, the [F1] system is sometimes associated with sinistral transcurrents faults and little folds, while the [F3] system is mostly associated with fissured and broken zones. These are both Cretaceous-Paleogene structures and Neogene-Quaternary structures (JURKOVŠEK et al., 1996) and essentially all of them affected the speleogenesis in "Davorjevo brezno", as well as the strata, especially tectonized bedding plane and lithological differentiation as observed by KNEZ (1998) in Škocjanske jame.

The upper passages of the "Davorjevo brezno" develop into Alveolinid and Nummulitid limestone rocks, while the deeper parts are located in the Liburnia formations and here some layers present lenses and coal nodules typical of this formation (HAMRLA, 1959; CORAZZI et al., 2023).

Part of "Papà-Marc'Aurelio" meander is developed in limestones below the caprock of marly-arenaceous Flysch of Brkini syncline. The Alveolinid and Nummulitid limestones are highly karstified rocks represented by gray to hazelnut-colored limestones, locally dark gray, with generally decimeter-thick or sometimes indistinct layers, marly-limestone at the top. In the Classical Karst they host large caves. The rocks of Liburnia formation show a medium-high karstifiability and are represented by dark grey, blackish, brown limestones, often brecciated, with layers generally from 5 to 15-20 cm, sometimes lamellar, with carbonaceous levels. The upper lithozone (Slivje limestone) of Liburnia formation, represented by grey and dark grey stratified limestones with frequently Miliolidae, it has been observed, are more karstified than the limestones of the lower lithozone. These karstic characteristics of Liburnia formation are mainly observable on the surface outcrops, while at a depth they are rather homogeneous due to the fact that the cavities develop mainly on planes of preferential structure.

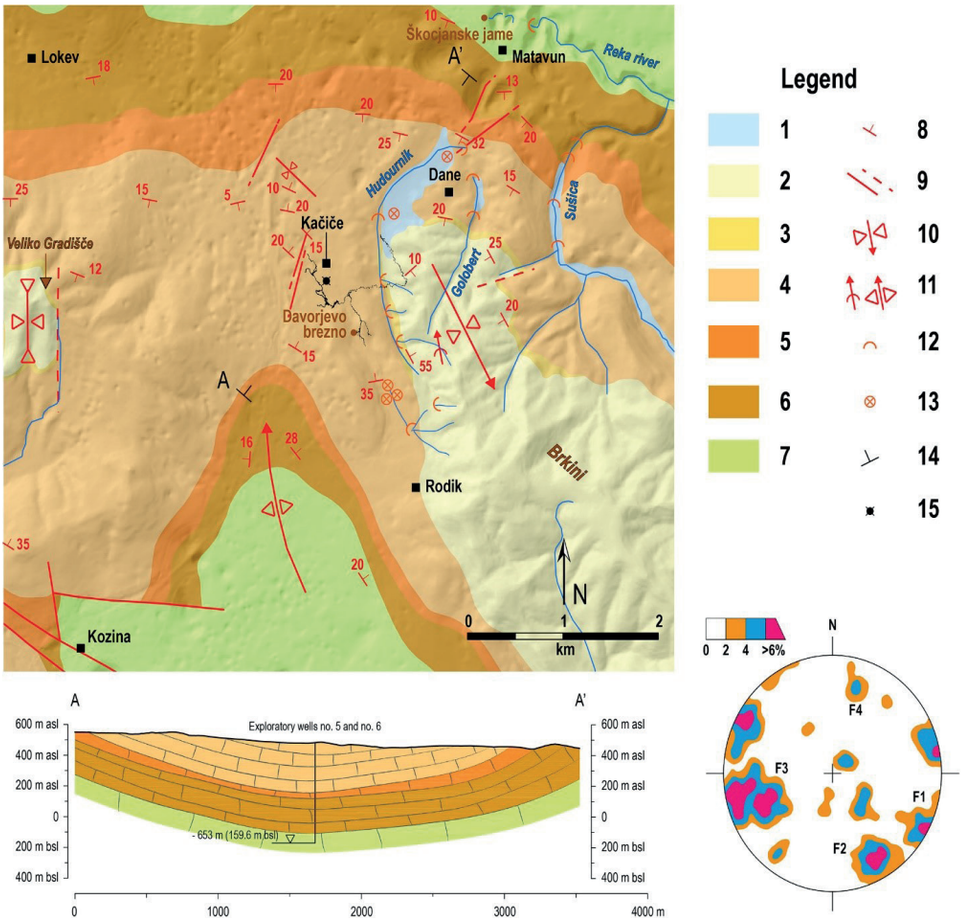

Figure 3: Synthesis geological map taken from PLENIČAR et al. (1973), JURKOVSEK et al. (1996, 2016), CORAZZI et al. (2023) and other geological surveys. Legend: 1. Alluvium (Quaternary). 2. Flysch (Eocene), alternations of marls, sandstones, breccias and conglomerates. 3. Transition beds (Middle Ypresian-Lower Cuisian). 4. Alveolinid-Nummulitid Limestone (Ilerdian), stratified limestones, generally light grey-grey, mostly dark in upper part. 5. Liburnian Formation, Slivje Limestone (Middle-Upper Paleocene), stratified limestones with frequently Miliolidae. 6. Liburnian Formation (Maastrichtian-Paleocene p.p.), stratified or slab-shaped limestones, marly limestones, brecciated limestones, locally carbonaceous layers (coal). 7. Lipica Formation (Upper Santonian-Campanian), stratified and massive limestones with Rudiste biostromes and bioherms. 8. Dip and strike strata. 9. Fault (established and covered). 10. Syncline (axis and plunging). 11. Anticline, major and minor (axis and plunging). 12. Sink stream (ponor) (in rock). 13. Sinkhole (in alluvium). 14. Cross section A-A'. 15. Exploratory wells no. 5 and no. 6 (average of stratigraphic contacts). Davorjevo brezno plan in black. Structural diagrams of 75 fault and fissured, crushed or broken zones (poles) of Škocjanske jame and Davorjevo brezno area, Schmidt net, lower hemisphere, equal density area and (F) main/secondary systems.

4. Geomorphology

Generally, "Davorjevo brezno" passages are structured mainly on the F1 tectonic system and secondarily on the F3 and F2 systems. It is common to see steps that are structured on bedding planes and dip to NE by 10°-20°, with cavities that have similar directions to those on F1 systems. In the hypogean karstifiability there are no strong differences between the passages developed in the rocks of the Alveolinid and Nummulitid limestone and the limestones of Liburnia formation. Since the deepest zone of "Davorievo brezno" is probably located where the cavities are now much less affected by the transition with the upper part of the water table contour, large conditioning phenomena attributed to the lithology are not appreciable. Furthermore, in this zone the lowering of the water table is evident, demonstrated by the development of large overlapping galleries due to the downward migration of the piezometric level.

"Davorjevo brezno" is characterized mainly by syngenetic galleries, paragenetic galleries and gorges. Syngenetic galleries are generally subelliptical shaped conduits, here mainly set on strata, and represent the initial phases of speleogenesis. These forms can be abandoned for subsequent evolution due to an abrupt change in water level and appear unmodified, or they can be deepened by erosion to form gorges. Paragenetic galleries, which correspond to the type prevalent in Classical Karst caves (FORTI & SEMERARO, 1983), in "Davorjevo Brezno" are mainly represented in the hydrologically inactive galleries, and are recognizable when the roofs are observable and not modified by collapses. Paragenetic galleries are especially visible between the altitudes of approximately 310-260 m asl. In the nearby Škocjanske, Jame, (MIHEVC, 2001) identified levels of paragenetic galleries between approximately 370 and 270 m asl. Paragenetic galleries generally shows corrosion cupolas on the roof and megascallop walls, while syngenetic galleries have mainly smaller scallops throughout the section but less on the floor. Vadose gorges show scallops mainly in the lower part.

The filling deposits in "Davorjevo brezno" are mainly coarse, consisting of sand and pebbles. This is mostly due to the contributions from the nearby marly-arenaceous rocks, and it's demonstrated by the almost ubiquitous presence of sandstone pebbles. Furthermore, a phase of calcitic sedimentation, apparently recent, is well represented. It is located in the lower part of the galleries, which is currently crossed by streams and cut by the current phase of erosion. The formation of flowstone is usually due to the formation of thin layers of yellowish to brownish calcite. These layers are very similar to those of the eroded flowstone studied in the nearby "Mejame" sinkhole, where Th/U analyses have dated ages of 42±28 Ka (ZUPAN, 1991) unlike a later dating of the same flowstone (MIHEVC, 2001) which gave a more recent age, as whose difference can be attributed to the error owed to contamination by 230Th. However, "Mejame" sinkhole concretions dates fall within the Upper Pleistocene, in a colder climate than the current one. In the surrounding area, west to "Davorjevo Brezno" (Divaški kras), paleomagnetic analyzes on cave sediments have indicated for the Divača profile (unroofed cave, 453 m asl) at the upper sequence (fluvial cycle) and lower sequence (calm and pulsed flow) a min age >1.77 Ma and max age >5.23 Ma. For "Divača jama" (cave levels between 410-350 m asl) in the upper sequence (clay) a Th/U age min 0.092 Ma and max 0.576 Ma and in the lower sequence (lacustrine, to calm river and pulsed flow), shows a paleomagnetic age min >1.2 Ma and max >5.0 Ma (ZUPAN HAJNA et al., 2008). These are sedimentary sequences ranging from the Pliocene to the Pleistocene. For the large paragenetic galleries of "Davorjevo brezno" (approximately 310-260 m asl) we can only suggest that they evolved within the most recent phase of this period.

5. Hydrogeology

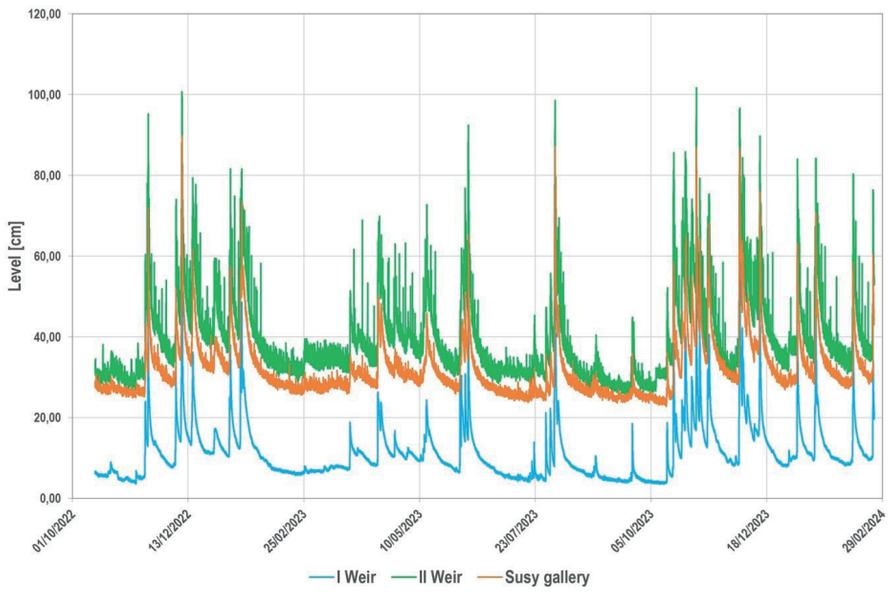

Figure 4: *2nd monitoring cycle. Water level comparison of I Weir, II Weir and Susy gallery.*

In the "Davorjevo brezno" abyss there are three subterranean water courses: the "Carbonari" meander, the "Veneziano" meander and the "Susy" gallery (water collector). The "Carbonari" flows into "Veneziano". It is assumed that the "Veneziano" flows into the "Susy" gallery, but the location is still unknown, although the distance between the first siphon ("old bottom") at the end of the "Veneziano" and the "Susy" gallery, which was reached going through a fossil bypass, is only about one hundred meters.

During the second monitoring cycle (from 15.10.2022 to 24.02.2024), parameters of temperature, hydrometric height and electrical conductivity of the three streams were checked with CTD Divers. For "Carbonari" (I Weir) and "Veneziano" (II Weir) the discharges were obtained with weirs,

while for “Susy” (due to the major difficulties given by the large shape of the gallery) by correlating a series of in situ discharges with ionic method and recorded logs of hydrometric heights. In this 2nd cycle, not specifically considering the flow rate of the “Carbonari” meander which is much lower than that of the “Veneziano” meander, but therefore considering the other two watercourses, it is estimated that the “Veneziano” meander has the following flow rates: min. 0.1 L/s, avg. 26.1 L/s, max. 766 L/s, while the “Susy” has min. 7.7 L/s, avg. 104.5 L/s, max. 1,107.5 L/s. Generally, “Davorjevo brezno” vadose and epiphreatic passages are subject to significant and rapid flow variations (Fig. 4), closely related to rainfall events and high rate flows from the Reka basin, as already observed during the 1st monitoring cycle (CORAZZI et al., 2023). This is clearly in the comparison between the water levels of the three hypogean streams. Temporal differences between the start of some piston flows, which precede the local meteoric inflows but already occurred in the area of the Middle Reka catchment, lead to consider hydraulic loads of the karst aquifer in its upstream zone which would cause, in the “Davorjevo brezno”, expulsion of waters with higher mineralization stored in the reservoir (SEMERARO et al., 2023). In another case, a modest rainfall event in the area in 2 days (25-26 February 2023) of 19.4 mm, with the Susy stream at minimum flow rates (26 L/s) typical of the cold winter low water, raised the EC K25 to 676 µS/cm after one day, indicating the expulsion of typically karst waters from the autogenic recharge of the Classical Karst stored in the aquifer. Considering the theoretical contour of karst water table of zone (HABIČ, 1984), the subterranean catchment, hypothetically, it could include the Dane endorheic basin and externally an eastern and north-eastern part of the area.

References

ARSA (1937) Sondaggi Roditti. Relazione “ARSA” Società An. Carbonifera, sondaggi geognostici alla scala 1:100. Archivio Regione Autonoma Friuli Venezia Giulia.

CORAZZI R., DIQUAL A., SEMERARO R., TORELLI L. (2023) Preliminary hydrogeological researches in Davorjevo brezno (Classical Karst). Atti e Memorie della Commissione Grotte “E. Boegan” 52:41–63,

DROBNE K., OGORELEC B., PAVSIC J., PAVLOVEC R. (2009) Paleocen in Eocen v jugozahodni Sloveniji. Paleocene and Eocene in south-western Slovenia. In: M. Pleničar, B. Ogorelec, M. Novak (eds.), Geologija Slovenije/ The Geology of Slovenia, Ljubljana, Geološki zavod Slovenije:311–372.

FORTI F., SEMERARO R. (1983) Sistema ipogeo del Carso Triestino: sedimentazione e speleogenesi. Atti del 4° Convegno di Speleologia del Friuli-Venezia Giu-lia:123–131.

GOSPODARIČ R. (1983) O geologiji in speleogenezi Škocjanskih jam. Geološki zbornik, Ljubljana 4:163–172.

HABIC P. (1984) Vodna gladina v Notranjskem in Primorskem krasu. Water table in Slovene karst of Notranjsko and Primorsko. Acta carsologica 12:37–78.

HAMRLA M. (1959) O pogojih nastanka premosišč na Krasu. On the conditions of origin of the coal beds in the karst region. Geologija 5:180–264.

JURKOVŠEK B., TOMAN M., OGORELEC B., SRIBAR L., DROBNE K., POLJAK M., SRIBAR L. (1996) Formacijska geološka karta južnega dela Tršasko-Komenske planote. Kredne in paleogenske karbonatne kamnine, 1:50.000. Institut geologijo, geotehniko in geofiziko, Ljubljana, 143 p.

JURKOVŠEK B., BIOLCHI S., FURLANI S., KOLAR-JURKOVŠEK T., ZINI L., JEŽ J., TUNIS S., BAVEC M., CUCCHI F. (2016) Geology of the Classical Karst Region (SW Slovenia–NE Italy). Map 1:50.000. Journal of Maps, 12 p., http://dx. doi.org/10.1080/ 17445647.2016.1215941

KNEZ M. (1998) The influence of bedding-planes on the development of karst caves (a study of Velika Dolina at Škocjanske jame Caves, Slovenia). Carbonates and evaporites 13(2):121–131

MIHEVC A. (2001) Speleogeneza Divaškega krasa. Založba ZRC SAZU, Ljubljana 27, 180 p.

ŠEBELA S. (2009) Structural geology of the Škocjan Caves. Acta carsologica 38(2/3):165–177.

ŠEBELA S. (1994) Določitev geološke zgradbe ozemlja nad Škocjanskimi jamami s pomočjo aerofoto posnetkov. Annales, serie historia naturalis, 4/94: 183–186.

ŠEBELA S., NOVAK U. (2023) Geological structure of karst stratigraphical windows at Škocjan Caves, Slovenia. SN Applied Sciences 5:104.

SEMERARO R., CORAZZI R., ARDETTI I., VALENTINUZ F. (2023) Signal examples from different aquifer source areas in the flood events of Davorjevo brezno. 30th International Karstological School, Karst Approaches and Conceptual Models, Abstracts and Guide Book, Postojna:150.

STACHE G. (1889) Die Liburnische Stufe und deren Grenz-Horizonte. 1. Uebersicht der geologischen Verhähaltnisse der Künstelländer von Oesterreich-Ungarn. Abhandlungen k.k. Geologische Reichsan- stalt 13(1) 170 p., karte 1:100.000, Wien.

ZUPAN N. (1991) Flowstone datations in Slovenia. Acta carsologica 20, Lju¬bljana:187–204.

ZUPAN HAJNA N., MIHEVC A., PRUNER P., BOSAK P. (2008) Paleomagnetism and Magnetostratigraphy af Karst Sediments in Slovenia. Carsologica 8, Založba ZRC/ZRC Publishing, Postojna Ljubljana, 266 p.

Cupolas associated with columnar stromatolites in the Vazante Group, MG - Brazil: characterization from 3D high-resolution models

Anna Sabrina Vidal de Souza (1), Rubson Pinheiro Maia (2), Marco Antonellini (3), Jo De Waele(4), Pedro Edson Face Moura (5), Vincenzo La Bruna (6), Augusto Sarreiro Auler (7) & Roberto Ventura Santos (8)

(1) Programa de Pós-Graduação em Geografia, Universidade Federal do Ceará, Brazil, annasabrinavidal@gmail.com (corresponding author)

(2) Programa de Pós Graduação em Geografia, Universidade Federal do Ceará, Brazil, rubsonpinheiro@yahoo.com.br

(3) University of Bologna, Department of Biological, Geological and Environmental Sciences, Bologna, Italy, marco.antonellini@unibo.it

(4) University of Bologna, Department of Biological, Geological and Environmental Sciences, Bologna, Italy, jo.dewaele@unibo.it

(5) Departamento de Geografia, Universidade Federal do Ceará, Brazil pedroedson18@gmail.com

(6) Programa de Pós-Graduação em Geodinâmica e Geofísica, Federal University of Rio Grande Do Norte, Natal, Brazil, vincenzolabruna@gmail.com

(8) Instituto do Carste, Carste Ciência e Meio Ambiente, Belo Horizonte, Brazil, aauler@gmail.com

(9) Laboratório de Estudos Geodinâmicos, Geocronológicos e Ambientais, Instituto de Geociências, Universidade de Brasília, Brazil robertoventurasantos@gmail.com

Abstract

The caves in the Vazante karst area are hosted in Mesoproterozoic carbonates, and some have well-preserved columnar Conophyton-type stromatolites. The VT-004 cave is in stromatolitic carbonates, and the roof is characterized by many cupolas. The smallest of these cupolas appear to have dissolved exclusively the stromatolite columns, whereas larger cupolas are the product of the coalescence of adjacent smaller ones. Stromatolite structures are exposed both in lateral view (along the cave walls) and in cross section. The stromatolitic columns have heights between ca. 1 and 4 m and widths of 0.30 to 0.65 m. Cross-sections are elliptical and only occasionally circular, with minor and major axes varying between 0.47 and 0.71 m and 0.31 and 0.37 m, respectively. Stylolites (mainly N-S trending) occur along the stromatolite major axis, whereas fractures and veins (striking mainly to NW and NE) also cross-cut their structures: both appear to have influenced fluid flow and consequent early phreatic karstification. Condensation-corrosion channels clearly show late vadose enlargement of the cave.

1. Introduction

Karst solutional features are commonly a result of the interplay between rock properties, including their mineralogy, petrography, age, stratigraphy and various types of fractures (FORD & WILLIAMS, 2007; DE WAELE & GUTIERREZ, 2022). These elements, along with the hydrological context in which the cave initiation occurs, are usually the guiding features and preferential pathways of karstification.

In view of the different scales in which karst features are developed, particularly local conditions and geological structures may assume a role in the shaping of wall and ceiling morphologies. Cupolas generally display a dome-shape and a circular to elliptical plan (OSBORNE, 2004), which can be fracture-guided or lack a clear structural control. Their morphology can be complex due to different processes acting on their development, both in vadose and confined conditions (DE WAELE & GUTIERREZ, 2022). Despite the reported mechanisms for cupola formation, case studies on morphological and morphometric parameters as well as local controls on their development are needed to shed light on the evolution of these forms, as a way of understanding the whole cave geomorphological evolution.

This paper deals with cupolas developed in stromatolitic rocks. Several caves were reported to have formed in Proterozoic carbonate rocks of the Minas Gerais state (Central-East Brazil) (AULER et al., 2016; AULER & SOUZA, 2017; VASCONCELOS et al. 2020). In this context the study site constitutes an exceptional example for studying cupola morphology and controls on their formation.

2. Study area

This paper concerns the VT-004 cave, located in the town of Vazante, Minas Gerais (Brazil) at the coordinates -46.75520194, -17.72307308, being part of the Vazante-Paracatu Karstic District (AULER & SOUZA, 2018). This area is situated in the tectonic context of the external zone of the Brasilia Fold Belt west of the São Francisco Craton (DARDENNE, 2000). The cave is developed in the mesoproterozoic rocks of the Vazante Group, a clay-dolomitic sequence, with the occurrence of stromatolitic dolomites in some formations (SOTERO et al., 2021). The studied location was described as a paleontological site (Cabeludo), characterized by Conophyton cilindricum stromatolites (DARDENNE, 2009). The stromatolites have a conical shape with cylindrical-conical lamination and have an age ranging between ~1300 and 950 Ma (MOERI, 1972). Previous works reported the occurrence of stromatolites in cave outcrops and particularly stromatolites associated with cupolas in VT-004, highlighting its unique

morphology and the importance for geoconservation (SOUZA & AULER, 2018; VASCONCELOS et al., 2020).

The morphological characteristic of this cave requires a detailed assessment of the mechanisms guiding the preferential karstification along columnar stromatolite structures and cupola formation, as previously suggested (SOUZA & AULER, 2018). In this work, preliminary analyses of high-resolution 3D LiDAR and photogrammetric models allowed for the collection of data on the cave morphology, dimensions and karstification volumes related to the cupolas and stromatolite columns, as a first step to characterize and interpret the controls on cave and speleothemes development.

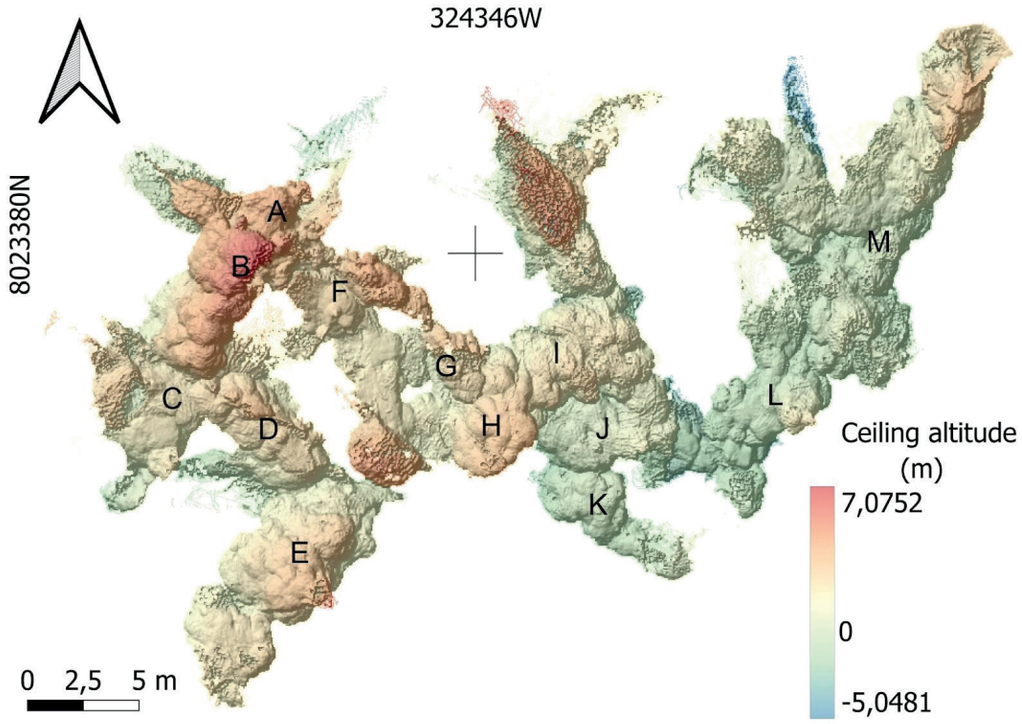

Figure 1: *LiDAR digital elevation model of cave VT-004 (MG, Brazil) showing the cave pattern and the typical morphology associated with the high density of cupolas, rendering an irregular aspect on the conduit 2D view . Note the two preferential conduit directions. Altitude values are relative. The codes A-M refer to the cupolas sectors identified by roughness analysis.*

3. Materials and methods

The laser scan survey was performed in all accessible cave chambers and conduits of VT-004 using the FARO GeoSlam mobile handheld LiDAR scanner. The surveying method is the walk-by scanning. The pre-processing of the collected data (point cloud, .las format) was carried out in the FARO Connected® software. Subsequently, the point cloud was segmented, and the floor and cave ceiling separated using the Cross Section Tool in Cloud Compare. This point cloud was then rasterized to generate a digital surface model, georeferenced in a GIS environment (QGIS). Raster analyses were performed, including roughness and isoline extraction from the DEM, which allowed us to identify the major and minor contours of cupolas in the cave. The measurement of the major cupola areas was also performed in the GIS software. The volumes of the karstified void (cave), the ceiling and individual cupolas was computed using the Compute 2.5D Volume Tool in Cloud Compare. Due to the high density of cupolas and their complex morphology, we organized 13 (A-M) cupola clusters to measure the whole volume of these sectors (Fig.1).

Photogrammetric surveys were also conducted in the two major rooms of the cave. A mirrorless Canon EOS R (24 mm) with a CMOS sensor was used to obtain the pictures, taken with a lateral overlap of approx. 70 % obtained in 360° acquisition globes. The processing occurred in the Agisoft Metashape software through SfM algorithm, following the workflow to generate among other products, a 3D mesh. The 3D model combining the mesh and the texture of the cave (images) allowed the visualization of different types of geological structures and geomorphological features. The photogrammetric model (.obj format) was further optimized in the MeshLab (CIGNONI et al., 2008) software to improve its visualization. These data were renderized and modified using software Unreal Engine 5 uploading both the model and texture given by the photos. “Nanite” technology facilitated the manipulation of the high-resolution and heavy model. With the dynamic interface in which a measuring mode is available, the collection of preliminary data on the dimensions of stromatolites and minor features such as rock protrusions from cave walls was possible, as well as characterize the detailed morphology of the cave, supplementing the previous observations done during field work.

4. Results

The VT-004 cave exhibits a general arrangement of conduits forming a network pattern, with main conduit directions trending NE-SW and NW-SE. The cave passages are relatively narrow, with rift-like shapes, and ~1.5 to 3 m wide and 0.4 to 5 m high, connecting two wider galleries (E and I, Fig. 1). The planimetric rectilinear aspect of the conduits is slightly lost due to the development of ceiling cupolas and notches.

Cupola cluster	Area (m²)	Volume (m³)
A	5.3	16.6
B	27,0	84.3
C	12.4	16.5
D	20.2	30.2
E	29.1	45.4
F	14.3	29,0
G	7,0	12,0
H	10.3	21.7
I	25,0	32.8
J	10.3	41,0
K	9.4	5,0
L	19.7	15,0
M	28,0	12.4

Figure 2: *Measurements of area and volume of cupola clusters in VT-004 based on LiDAR 3D model. Reference of clusters given in Figure 1.*

The 3D models allow us to visualize the widespread occurrence of ceiling features in the whole cave, particularly cupolas of various sizes. Based on roughness analyses, 13 main sectors or cupola clusters were defined; typically larger cupolas encompass smaller ones. The overall volume of these cupola clusters is given in Figure 2. The cupolas generally display a hemispherical morphology (sensu OSBORNE, 2004). One visible aspect observed in the cave is that smaller cupolas usually have their dimensions conforming to the dimensions of stromatolites (cross-section) (Fig.3A).

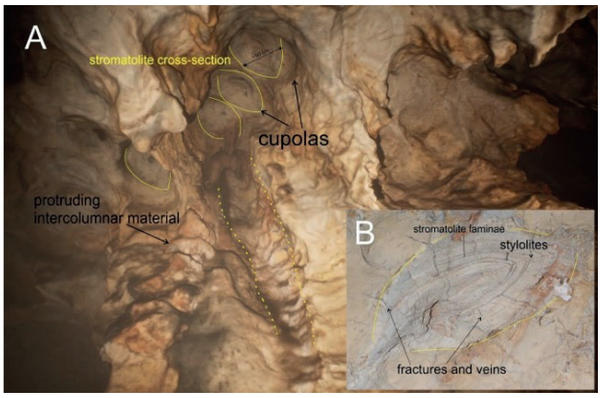

Figure 3: *A. 3D photogrammetric model of the VT-004 ceiling. A - Small cupolas associated with stromatolite structures can be observed. Note protruding material between stromatolites. B – Cross-section view of stromatolite with a deformed elliptical morphology, showing structural features such as stylolites, fractures and veins. Yellow contours show the cross-section outline of the stromatolites. Dashed line shows the wall concavity borders with a clear condensation-corrosion channel.*

The stromatolites in this cave are seen in both cave walls (longitudinal section) and ceiling (cross-section), displaying a typical conical morphology reported for the stromatolites in this area (DARDENNE, 2000). A yellowish, less soluble, intercolumnar rock between stromatolites often sticks out from the cave walls (protrusions varying between 0.2 and 0.6 m), because of the wall concavities generated by the dissolution of the former stromatolite structure (Fig. 3A).

Based on the 3D models, their longitudinal dimensions range from 106 x 30 cm to 397 x 65 cm. The cross-sections are elliptical and occasionally circular; the major and minor axes vary from 47 x 37 cm to 71 x 31 cm. Stylolites (mainly N-S trending) occur along the stromatolite major axis; fractures and veins (striking mainly to NW and NE) also cross-cut the cupolas (Fig. 3B).

5. Conclusion

The presented morphological characteristics allow us to infer that major fracture zones guided cave and conduit development as revealed by the structural-guided orientation of passages. The cupola clusters can be interpreted because of the coalescence of small stromatolite--controlled cupolas.

In addition to this, the occurrence of cupolas (of small dimensions) associated with the stromatolite structures points to the role stromatolites played in guiding preferential karstification in contrast to the other rock type which forms ledges between cupolas, being relatively less prone to dissolution. Structural features such as fractures and stylolites preferentially crosscutting stromatolites appear to have favored or facilitated the karstifying fluids along stromatolite columns. The cave void likely formed in confined (hypogene) settings, with fluids following the major available permeable features (fractures and open stylolites). These features were later further enlarged in vadose conditions, once the cave opened up to the surface and condensation-corrosion started working especially on the roof sectors of the cave. This led to the enlargement and deepening of the cupolas, and the creation of condensation-corrosion channels.

Acknowledgments

We thank the Brazilian Agency of Oil, Gas, and Biofuels (Agência Nacional do Petróleo, Gás e Biocombustíveis, ANP) and

Shell Brasil for the funding of the project POROCARSTE II: PROCESSOS E CARACTERIZAÇÃO DE ROTAS DE FLUXO DE FLUIDOS EM RESERVATÓRIOS CARSTIFICADOS, FRATURADOS E SILICIFICADOS DO PRÉ-SAL (ANP number 23505-1) which allowed the collection of the presented data.

References

AULER A.S., PERRONI G., SOUZA T.A.R. (2016) Parte II: Patrimonio Espeleológico, Arqueológico, Paleontológico. In: SOUZA T.A.R. & AULER A.S. (Eds.), Distrito Cárstico Vazante Paracatu: Patrimônio espeleológico, arqueológico e paleontológico, 442-717. Carste Ciência e Meio Ambiente, Belo Horizonte.

AULER A. S., SOUZA T. A. (2017) Hypogene Speleogenesis in the Vazante Group, Minas Gerais, Brazil. In: Klimchouk A.B., Palmer A.N., De Waele J., Auler A.S., Audra, P. (eds.), Hypogene Karst Regions and Caves of the World, 841-852. Springer, Cham.

AULER A.S., SOUZA T.A.R. (2018) Gênese de cavernas no Grupo Vazante. In: AULER A.S., SOUZA T.A.R. (Eds.) O Carste de Vazante-Paracatu-Unaí: Revelando Importâncias. Recomendando Refúgios, 149-175. Carste Ciência e Meio Ambiente, Belo Horizonte.

CIGNONI P., CALLIERI M., CORSINI M., DELLEPIANE M., GANOVELLI F., RANZUGLIA G. (2008) MeshLab: an Open-Source Mesh Processing Tool. https://doi.org/10.2312/LocalChapterEvents/ItalChap/ItalianChapConf2008/129-136

DARDENNE M.A. (2000). The Brasília Fold Belt. In: CORDANI U.G., MILANI E.J., THOMAZ FILHO A., CAMPOS D.A. (Eds.), Tectonic evolution of South America. XXXI Intern. Geol. Congress, Rio de Janeiro, SBG. p. 231-263.

DARDENNE M.A. (2009) Conophyton de Cabeludo, Grupo Vazante, MG Construções dolomíticas por cianobactérias no Proterozóico. Sítios geológicos e paleontológicos do Brasil, Brasília, Ministério de Minas e Energia 2, 515.

DE WAELE J., GUTIÉRREZ F. (2022) Karst Hydrogeology, Geomorphology and Caves. Wiley. Chichester. https://doi.org/10.1002/9781119605379.

MOERI E. (1972) On a columnar stromatolite in the Precambrian Bambui Group of Central Brazil. Eclogae Geologicae Helvetiae 65, 185-195.

OSBORNE R.A.L. (2016) The Troubles with Cupolas. Acta Carsologica 33(2), 9-36. https://doi.org/10.3986/ac.v33i2.289

SOTERO M.P., CAXITO F.DE A., DE ALVARENGA C.J.S., SANTOS R.V., PINHEIRO M.A.P., DIAS P.H.A. (2021) Isotope stratigraphy of the uppermost Vazante Group, Brazil: Insights on paleoenvironments and regional correlation. Journal of South American Earth Sciences, 108, 103156. https://doi.org/10.1016/j.jsames.2021.103156

SOUZA T.A.R., AULER A.S. (Eds.) (2018). O carste de Vazante-Paracatu-Unaí: revelando importâncias, recomendando refúgios. Belo Horizonte: Carste Ciência e Meio Ambiente. Artes Gráficas Formato Ltda. 279 p.

VASCONCELOS A.G., BITTENCOURT J.S., ELIZIÁRIO N.F., KRAEMER B.M., AULER A.S. (2020) Stromatolites in Caves in Southeastern Brazil and their Importance to Geoconservation. Geoheritage 12(2), 48.

Classification and Characteristics of Glaciovolcanic Caves

Christian Stenner (1), Lee Florea (2), Linda Sobolewski (3), Andreas Pflitsch (4)

(1) Alberta Speleological Society, Calgary, Alberta, Canada, cstenner@telus.net (corresponding author)
(2) Washington State Geological Survey, Department of Natural Resources, Olympia, Washington, USA
(3) Institute of Earth Sciences, University of Iceland, Reykjavík, Iceland
(4) Institute of Geography, Ruhr-University Bochum, Bochum, Germany

Abstract

Glacier caves have been known as a form of pseudokarst and have obtained increasing attention as changing climate influences glaciers around the world. Often discussed together with glacier caves are examples which formed due to geothermal influences. Volcanoes interacting with the cryosphere can host glaciovolcanic caves where thermal flux at the ice-rock boundary forms void spaces in the superimposed ice or firn substrate. We conducted a systematic literature review and fieldwork expeditions to catalogue known examples and demographics of glaciovolcanic caves and differentiate such caves formed along thermal gradients in volcanic environments from other landforms and from glacier pseudokarst. 80 individual examples of glaciovolcanic caves were identified and characterized. Glaciovolcanic caves are most often found on unconstrained glaciated volcanic edifices and primarily are formed in firn, and the principal mechanism of speleogenesis is fumarolic activity in combination with heated soil or bedrock substrate. Four subtypes were derived, all of which chiefly involve volcanically driven kinetics that initiate and maintain cave genesis from below the ice surface. Glaciovolcanic caves are an understudied element of pseudokarst and the cryosphere. Understanding their attributes, and discussion of their geomorphology and taxonomy within the ecosystem of volcano-ice interactions supports better understanding of the phenomena.

Résumé

Les grottes glaciaires sont connues comme une forme de pseudokarst et suscitent une attention croissante à mesure que le changement climatique influence les glaciers du monde entier. On évoque souvent, à côté des grottes glaciaires, des exemples qui se sont formés en raison d'influences géothermiques. Les volcans interagissant avec la cryosphère peuvent héberger des grottes glaciovolcaniques où le flux thermique à la limite glace-roche forme des espaces vides dans le substrat de glace ou de névé superposé. Nous avons mené une revue systématique de la littérature et des expéditions de terrain pour cataloguer les exemples connus et les caractéristiques démographiques des grottes glaciovolcaniques et différencier ces grottes formées le long des gradients thermiques dans des environnements volcaniques des autres formes de relief et du pseudokarst glaciaire. 80 exemples individuels de grottes glaciovolcaniques ont été identifiés et caractérisés. Les grottes glaciovolcaniques se trouvent le plus souvent sur des édifices volcaniques glaciaires sans contraintes et sont principalement formées dans le sapin, et le principal mécanisme de spéléogenèse est l'activité fumerolienne en combinaison avec un sol chauffé ou un substrat rocheux. Quatre sous-types ont été dérivés, qui impliquent tous principalement une cinétique volcanique qui initie et maintient la genèse des grottes sous la surface de la glace. Les grottes glaciovolcaniques sont un élément peu étudié du pseudokarst et de la cryosphère. Comprendre leurs attributs et discuter de leur géomorphologie et de leur taxonomie au sein de l'écosystème des interactions volcan-glace permet une meilleure compréhension des phénomènes.

1. Introduction

Glacier caves were categorized by HALLIDAY (2007) as glacier pseudokarst; one of eight pseudokarst typologies. Glacier caves are prevalent in glaciated environments, formed by ablation of ice by meltwater and maintained by atmospheric advection in the form of moulins, englacial conduits and as contact caves, or as sublimation caves (BADINO et al., 2007). The morphologies and genesis of glacier caves fit the defining elements of pseudokarst identified by HALLIDAY (2007) as subsurface drainage through conduit type voids.

One differing element from classical karst is that in glacier caves the karst-like morphologies are primarily produced by ablation and melt rather than dissolution. However, HALLIDAY (2007) also identified geothermal examples of glacier caves such as those at Mount Rainier, Mount Hood, and Mount Baker (USA) within the glacier pseudokarst typology.

The processes whereby volcanic heat from volcanic-magmatic systems interacts with ice is termed glaciovolcanism (SMELLIE & EDWARDS, 2016). Where speleogenesis resulting from glaciovolcanism creates void spaces, we have applied the term glaciovolcanic caves (SOBOLEWSKI et al., 2022). Categorizing them as glaciovolcanic caves recognizes them as a component of glaciovolcanism, spanning their overlap between volcanology and speleology, and highlights their volcanic genesis, which are vastly different from conventional glacier caves.

SOBOLEWSKI et al. (2022) discussed the limited distribution of glaciovolcanic caves across the world amongst the 245 geographic locations with potential for glaciovolcanic cave formation, and identified locations hosting caves confirmed in literature and locations requiring verification and further investigation. Studies over the past decade in the Cascade volcanoes of the Northwest USA have greatly added to our knowledge of glaciovolcanic caves, along with those further catalogued at Mount Erebus in Antarctica by CURTIS (2018). The most significant glaciovolcanic examples at present are the cave systems in the glaciers of the overlapping East and West craters at the summit of Mount Rainier. East Crater Cave is currently the longest glaciovolcanic cave in the world

at 3,593 m (FLOREA, et al., 2021; STENNER et al., 2022; STENNER et al., 2023). Further Antarctic examples have since been identified on Mount Melbourne (LIUZZO et al., 2018), and reports exist of glaciovolcanic caves in other locations via photos or anecdotal accounts. Table 1 reveals contemporary examples (confirmed in the past 15 years), and statistics from literature, while at their most extensive known development. Mount St. Helens caves appear to currently be in a state of regression (SOBOLEWSKI et al., 2025).

Six morphological patterns and passage types in glaciovolcanic caves have been identified, and those morphologies may result from mechanisms specific to glaciovolcanic cave subtypes (STENNER et al., 2024). Repeated here they are: 1) thermally influenced englacial conduits, where warm water initiates voids enlarged by atmospheric advection; 2) isolated 'steam domes', whose size and shape are dictated by the rate of convective fumarole emissions; 3) lateral conduits comprised of chains of steam domes positioned around fumaroles with an interannual size maintained by atmospheric advection; 4) chimneys and rising conduits that vent fumaroles with a size and shape guided by accumulation or ablation of firn; 5) heat enlarged crevasses and moulins that intersect glaciovolcanic caves; and 6) ice-margin melt at the ice-rock interface enhanced at the glacial margin and maintained by fluid movement but with highly variable morphology and persistence governed by bedload.

CURTIS (2016) defined the Mount Erebus examples as fumarolic ice caves, characterized by thermal flux originating from subglacial fumarole vents. The majority of presently documented glaciovolcanic caves appear connected to fumarolic activity; however, connections to thermally heated volcanic bedrock, subglacial lava eruptions, or subglacial hydrothermal springs are likely. These cave systems may also reveal diverse characteristics such as their location in relation to their volcanic edifices and the cryospheric substrates in which they form. This paper highlights examples of glaciovolcanic caves from around the world, and investigates the characteristics, genesis mechanism, and subtypes of these phenomena.

	Cave System	Location	Length (m)	Depth (m)	Reference
1	East Crater Cave	Mount Rainier, USA	3593	144	STENNER et al. (2022); (2023)
2	Sherman Crater Cave System	Mount Baker, USA	1220	-	KIVER (1978) [a]
3	Mothra Cave	Mount St. Helens, USA	797	72	SOBOLEWSKI et al. (2023)
4	Rodan Cave	Mount St. Helens, USA	775	82	SOBOLEWSKI et al. (2022b)
5	MC3 Ice Cave	Mount Melbourne, Antarctica	685	52	LIUZZO et al. (2018)
6	Warren Cave	Mount Erebus, Antarctica	524	23	CURTIS (2018); (2021)
7	Ghidorah Cave	Mount St. Helens, USA	434	30	STENNER et al. (2020)
8	West Crater Cave	Mount Rainier, USA	308	33	STENNER et al. (2022); (2023)
9	Crevasse Cave	Mount St. Helens, USA	276	56	STENNER et al. (2020)
10	Qwelqwélústen Cave	Mount Meager, Canada	258	59	CLANCE et al. (2024)
11	Hot Imagination Cave	Mount Hood, USA	273	58	PFLITSCH et al. (2017)
12	MC1 Aurora Ice Cave	Mount Melbourne, Antarctica	223	35	LIUZZO et al. (2018)
13	The Igloo	Mount St. Helens, USA	191	8	STENNER et al. (2020)
14	Kachina Cave	Mount Erebus, Antarctica	146	6	CURTIS (2010); (2021)
	Other notable systems:				
	Mammoth/Cathedral [b]	Mount Erebus, Antarctica	-	-	CURTIS (2021)
	Anchor Cave [b]	Mount Erebus, Antarctica	-	-	CURTIS (2021)
	Kverkfjöll Caves	Vatnajökull, Iceland	-	-	STORRIE-LOMBARDI et al. (2011

Table 1: *Table showing significant, contemporary glaciovolcanic cave systems identified in literature, (within the last 1.5 decades) and at their maximum known extents. – unknown/no data. a Recent observation in 2024 revealed this system is likely still present and extensive. b Mammoth/Cathedral system and Anchor cave at Mount Erebus are likely the longest in the region but are not surveyed. They are reported to be less extensive than the Mount Rainier system (CURTIS, personal communication, 2021).*

2. Methods

A systematic review was conducted which included our data, the Erebus caves database from CURTIS (2018) and relevant literature. Our data included cave surveys, photo monitoring of cave morphology, and environmental conditions in glaciovolcanic caves of the Pacific Northwest, USA, from 2017-2024, many of which were published in the literature included in the review. Literature inclusion criteria were peer-reviewed research papers, books, book chapters, and conference papers, relevant databases, and literature where clear glaciovolcanic parameters and data relevant to the discussion were present. Both contemporary and historical examples of glaciovolcanic caves were included, as data from caves which no longer exist were considered relevant to the phenomena.

A multi-step process for screening literature was used. The first step excluded literature with examples of glacier caves where no volcanic influence was found. Cave entrance locations in the Erebus cave database but without named, confirmed caves were excluded (n=46).

Second, the remaining literature was used to complete a synthesis list of individual glaciovolcanic caves, and review potential categories that could be assigned to each cave. Lastly, categorizations were assigned based on cave demographics recorded in the literature, including geographical location, volcanic edifice location (constrained in a crater or on the flank), type of cryospheric substrate (snow, firn, or glacier ice), and primary and secondary speleogenesis. As the depth of firn transition to glacier ice is dependent on factors such as mean temperature and differs throughout the world such as in temperate or polar locations (CUFFEY & PATERSON 2010), assigning the substrate as glacier ice was estimated based on cave depth and location. The results from the synthesis were tabulated to provide frequency distributions and data for discussion.

3. Results

Synthesis of the review revealed the following: Glaciovolcanic caves are concentrated around only a few volcanic areas and craters where glaciovolcanism is possible, and 80 individual cave examples were included in the synthesis. In Antarctica, Mount Erebus displayed the largest concentration in the data, n=38.

Mount Melbourne and Mount Rittman in Antarctica also hosted examples, while the Pacific Northwest USA volcanoes Mount Hood, Mount St. Helens, Mount Rainier, and Mount Baker each hosted caves. Additional examples were found in Kamchatka, Russia, and Iceland.

Substrates that contained the voids were nearly all in snow and firn layers, 92.5% (n=74). The remaining caves possibly transitioned from firn into layers of true glacial ice based on data reported in the literature or are estimated due to cave geographical location and passage depth under the glacier surfaces. Caves were found to be in glaciers constrained by topography in 24% of cases (n=19). The constrained cases were all located in volcanic craters. The remainder were located elsewhere on the volcanic edifice.

Three primary speleogenesis mechanisms were found. The predominant mechanism was the presence of subglacial fumaroles in conjunction with areas of heated bedrock or sediment surfaces. These two mechanisms were closely aligned and present in 94% (n=75) examples.

Outliers included two examples from Mount St. Helens, where caves in snow and firn formed independent of a known fumarole vent and only heated sediments were present. A distinctive mechanism was present in two examples and was a likely secondary mechanism in two additional examples, where subglacial hot springs were present and cave passages concentrated around them. These included the Snow Dragon and Hot Imagination systems at Mount Hood, where only thermal springs have been located sub glacially, and Kverkfjöll, where fumarolic influence is present but thermal springs are also a reported factor in introducing thermal flux in the subglacial environment. At Mount Baker, subglacial streams and a warm lake were reported in earlier studies (KIVER, 1978) while flowing subglacial streams with unrecorded temperatures were observed by authors recently.

4. Discussion

Caves in glacier pseudokarst may owe their origin to the advection of recharging melt from above and thermal flux from below. Glaciovolcanic caves reveal distinct patterns and common subtypes, reinforcing the view that glaciovolcanic caves have unique and diverse morphologies and genesis distinct from glacier caves and englacial conduits. The different morphologies between glaciovolcanic caves and glacier pseudokarst are analogous to the distinction between hypogenic and epigenic karst as expressed in STENNER et al. (2023). The synthesized examples here revealed the thermal speleogenesis mechanisms originating within the substrate below the superimposed ice and firn which contains glaciovolcanic caves.

Four primary mechanisms are relevant to glaciovolcanic cave genesis. The primary type is the fumarolic type, where degassing vents introduce thermal flux subglacially and result in voids of varying morphologies. However, observations in the Pacific Northwest and of the surveyed caves at Mount Erebus (CURTIS, 2018) revealed that additional passage formation is owed to areas of heated bedrock and substrate. Fumarolic activity was often combined with heated bedrock and substrate and all cases of fumarolic caves appear to have adjoining heated floors. Examples at Figure 1A and 1B reveal fumarolic types combined with heated substrates, 1A with primarily steam emitting fumaroles and 1B where steam and volcanic gas emitting fumaroles are present.

A second type exists were heated sediment and bedrock can create a contact void independent of fumarolic activity. These were observed in a few cases in the Mount St. Helens crater, where large areas of heated surfaces on the glaciated lava dome are kept snow free year-round (SOBOLEWSKI et al., 2023).

A third type is formed when subglacial thermal springs introduce thermal flux under the glacier. For example, a substantial cave system on Mount Hood was identified. Snow Dragon Cave, and a 273 m long remnant, Hot Imagination, presented heat flux derived principally from flowing thermal springs in the cave and advection of this thermal water through an englacial conduit (PFLITSCH et al., 2017). This represented a non-fumarolic example of the glaciovolcanic typology, Figure 1C. Cave type can be a hybrid of types such as in the fumarolic-heated substrate contact voids, but also where subglacial thermal springs and fumarolic activity coexist, such as at Kverkfjöll, and potentially at Mount Baker. These latter examples reflect challenges with classification, as the primary mechanism is not distinctive, and all three of the aforementioned types have passages which are maintained in combination with atmospheric advection once an exchange with external climate occurs thorough their entrances (FLOREA et al., 2021).

Subglacial eruption voids are a fourth type of glaciovolcanic cave, although studies of these were excluded in the systematic review. These voids fit the definition of glaciovolcanic caves as voids formed due to glaciovolcanism; in this case the extrusion of lava subglacially in an explosive or effusive manner, both of which create void spaces under ice. At Eyjafjallajökull during the 2010 eruption a subglacial lava flow was emplaced for 3.2 km along meltwater tunnels (ODDSSON et al., 2016). Such voids could be contained as subnivean voids or produce an entrance and could be filled with meltwater or drain at the ice-bedrock margin post eruption. Further review and synthesis to understand the prevalence and dynamics of this type would be beneficial.

Glaciovolcanic caves can be further differentiated by medium or permanence, or in geographic relation to a volcanic edifice. Caves can reform, be unroofed, or partly ablated seasonally (e.g., some firn caves such as Igloo Cave at Mount St. Helens, as well as likely most examples of glaciovolcanic caves formed in pure snow). Or they may be persistent features due to low levels of volcanism over decadal scales such as at Mount Rainier, STENNER et al. (2023).

Glaciovolcanic caves can be enclosed by a hybrid of mediums (e.g., snow, firn, and glacial ice), which is why terminology defining categories like “firn cave” isn’t necessarily appropriate. The mediums range from settled snow at 200-300 kg/m3 to glacier ice at 830-923 kg/m3, with firn caves in the middle of the range of possible strata for glaciovolcanic cave speleogenesis at 400-830 kg/m3 (CUFFEY & PATTERSON, 2010). Although ice density data was not available for most caves in the synthesis, the Antarctic caves are extremely unlikely to have formed in glacier ice due to their depth (VAN DEN BROEKE, 2008). However, examples such as in Gorshokov crater, Russia (SHIRAIWA et al., 2001) and Mothra Cave at Mount St. Helens (SOBOLEWSKI et al., 2022) revealed examples where cave depths extending into true glacier ice is possible. That 92.5% of known examples form in snow and firn layers reflects potential for the plastic creep of glacial ice to typically overcome the persistent low levels of thermal flux in stable glaciovolcanic settings, or a gap in the dataset reflecting unknown examples.

The caves are most commonly associated with volcanic edifices on active volcanic slopes where geothermal heating and fumarolic activity originating from the underlying substrate has created voids in the superimposed icy substrate. However, the most significant examples at Mount Rainier, Mount Baker, and Mount St. Helens (STENNER et al., 2023); SOBOLEWSKI et al., 2022b) exist in glaciers constrained by crater topography and where active low level and continuous geothermal activity is present.

In periods of apparent quiescence, the dynamic equilibrium resulting in persistent glaciovolcanic caves provides a window into their genesis. As glaciers on volcanoes ablate with changing climate the resulting deglaciation can cause increased volcanism due to a decrease in pressure over the mantle (CARRIVICK et al., 2009). Similar pressure decreases due to subglacial voids forming as a result of thermal flux and ablation is a concern. Characterizing glaciovolcanic interactions is important as they contribute to our shared language of geomorphology and to our understanding of volcano-ice interactions. Glaciovolcanism produces a number of distinct features which can help define the category of glaciovolcanic caves and assist our understanding of them as a distinctive pseudokarst.

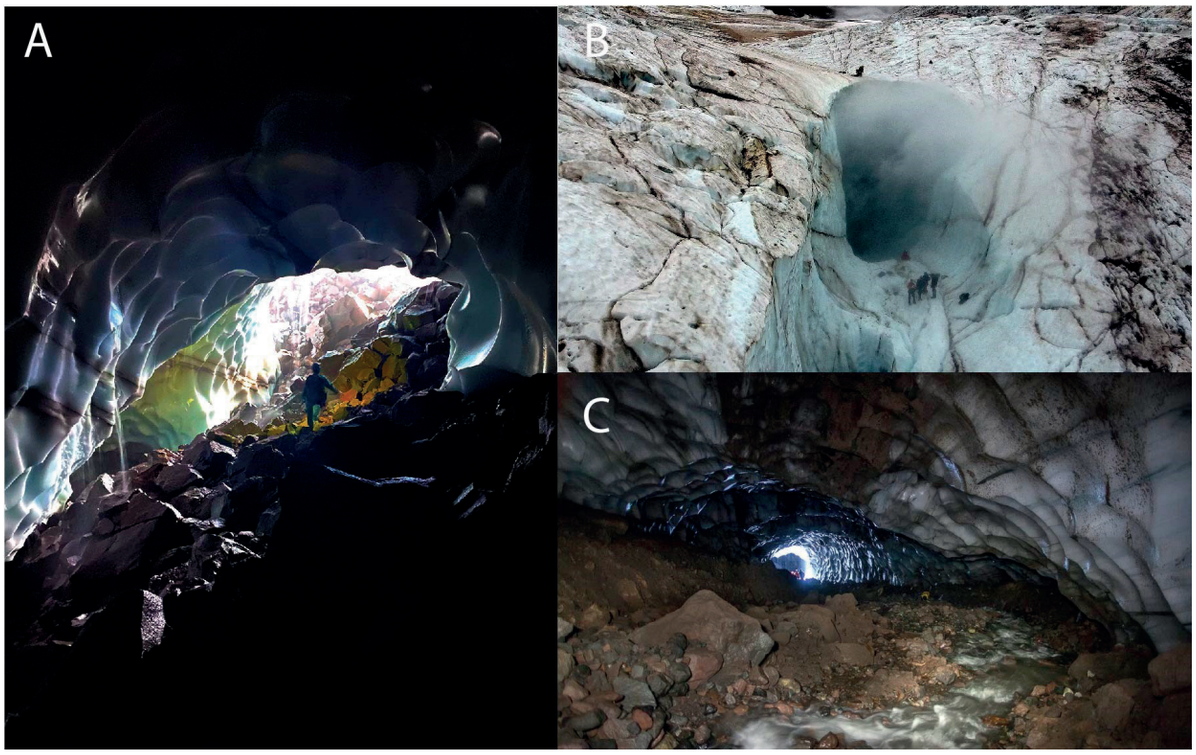

Figure 1: *Glaciovolcanic caves. A: Interior of Mothra Cave, Mount St. Helens, USA, 2022. A primarily fumarolic type characterized by release of warm steam from fumaroles and associated heated sediments and bedrock. B: An entrance to Q̓wel̓q̓welústen Cave, Mount Meager Volcanic Complex, Canada, 2019. A primarily fumarolic type characterized by release of warm volcanic gasses and steam. C: Snow Dragon Cave System, Mount Hood, USA, 2014. A primarily hydrovolcanic type characterized by warm spring water in addition to regular englacial conduit formation.*

5. Conclusion

Glaciovolcanic caves can exist in specific geographical settings and display common characteristics along with subtypes which relate to their primary mechanism of genesis and persistence. Glaciovolcanic caves are predominantly formed in firn and snow and do not typically reach depths where passage formation is in true glacial ice. Caves are most commonly associated with volcanic edifices on active volcanic slopes where geothermal heating and fumarolic activity originating from the underlying substrate has created voids in the superimposed icy substrate. However, the most significant examples exist in glaciers constrained by crater topography and where active low level and continuous geothermal activity is present. Glaciovolcanic caves can be further subdivided into four types. The primary and most common type is the fumarolic type, which is most often combined with areas of heated bedrock and substrate. Heated bedrock and substrate can also create a contact void independent of fumarolic activity. A third type is formed when subglacial thermal springs introduce thermal flux under the glacier, and a fourth type, a subglacial eruption void where melt from lava creates voids which can be filled with meltwater and may or may not become subaerial by breaching the surface. These types all reflect a style of glacier cave which is hypogene, and reflect a need for differentiation due to their evolution from volcanic subsurface influences which are independent of surface processes; until entrances are formed which introduce advection and exchange with surface climate and continues to maintain open passages. Glaciovolcanic caves are understudied and the potential to explore further relationships with their related edifices, the underlying hydrothermal systems, and surrounding glaciers, are a window into glaciovolcanism in both quiescent and escalating periods of volcanic activity.

Acknowledgments

Special thanks to Eddy Cartaya and all members of the Glacier Cave Explorers of the Oregon High Desert Grotto of the National Speleological Society who provided safety and surface support for fieldwork in the USA and Canada. Additional helpful support from Aaron Messinger, Special Projects Operations, Eugene Kiver, Bill Lokey, Glyn Williams-Jones, Kathleen Graham, Adam Walker, and Aaron Curtis. Support from the Royal Canadian Geographical Society, National Geographic, and the Trebek Initiative helped enable related fieldwork.

References

BADINO G., DE VIVO A., PICCINI L. (Eds.) (2007) Caves of sky: a journey in the heart of glaciers. La Venta, 153 p.

CLANCE, J., SHAFFER, J., CABLE, M., STENNER, C., WILLIAMS-JONES, G., SZYNKIEWICZ, A., PATON, M., GRAHAM, K., VINNES, O., MIKUCKI, J. (2024) Biogeochemistry of the rare sulfidic glaciovolcanic cave system on Mount Meager, British Columbia, Canada. Frontiers in Geochemistry, 2,1410338.

CARRIVICK, J.L., RUSSELL, A.J., RUSHMER, E.L., TWEED, F.S., MARREN, P.M., DEEMING, H. AND LOWE, O.J., 2009. Geomorphological evidence towards a de-glacial control on volcanism. Earth Surface Processes and Landforms, 34(8):1164-1178.

CUFFEY, K. & PATERSON, W. (2010) The Physics of Glaciers. Fourth Edition. Amsterdam, Academic Press. 704 p.

CURTIS, A. (2018) Erebus Cave and Fumarole Database. Available from: http://www.erebuscaves.com/ (Accessed Feb 4, 2025).

CURTIS, A. (2016) Dynamics and global relevance of fumarolic ice caves on Erebus Volcano, Antarctica. Ph.D. thesis, New Mexico Institute of Mining and Technology.

FLOREA, L., PFLITSCH, A., CARTAYA, E., & STENNER, C. (2021) Microclimates in fumarole ice caves on volcanic edifices—Mount Rainier, Washington, USA. Journal of Geophysical Research Atmospheres, 126(4).

HALLIDAY, W. (2007) Pseudokarst in the 21st century. Journal of Cave and Karst Studies, 69(1):103–113.

KIVER, E. (1978) Mount Baker's changing fumaroles. The Ore Bin, 40(8): 133-145.

LIUZZO, M., GIUDICE, G., GIUFFRIDA, A. (2018) Investigation of Ice-Caves on Melbourne and Rittman volcanoes, Antarctica [presentation]. European Geosciences Union General Assembly 2018, Vienna, Austria, 8-13 Apr. https://www.icevolc-project.com/presentations.

ODDSSON, B., GUDMUNDSSON, M.T., EDWARDS, B.R., THORDARSON, T., MAGNÚSSON, E. AND SIGURÐSSON, G. (2016) Subglacial lava propagation, ice melting and heat transfer during emplacement of an intermediate lava flow in the 2010 Eyjafjallajökull eruption. Bulletin of Volcanology, 78:1-17.

PFLITSCH, A., CARTAYA, E., MCGREGOR, B., HOLMGREN, D., STEINHÖFEL, B. (2017) Climatologic studies inside Sandy Glacier at Mount Hood Volcano in Oregon, USA: Journal of Cave and Karst Studies, 79(3):189-206.

SHIRAIWA, T., MURAV'YEV, Y.D., KAMEDA, T., NISHIO, F., TOYAMA, Y., TAKAHASHI, A., OVSYANNIKOV, A.A., SALAMATIN, A.N. & YAMAGATA, K. (2001) Characteristics of a crater glacier at Ushkovsky volcano, Kamchatka, Russia, as revealed by the physical properties of ice cores and borehole thermometry. Journal of Glaciology, 47(158):423-432.

SMELLIE, J., EDWARDS, B. (2016) Glaciovolcanism on Earth and Mars: Products, Processes, and Palaeoenvironmental Significance. Cambridge University Press, Cambridge, United Kingdom. 497 p.

SOBOLEWSKI, L., STENNER, C., FLOREA, L.J., MCWETHY, G., GOMEZ-PATRON, A.I., ZORN, E.U., IONESCU, A., CARTAYA, E. & PFLITSCH, A. (2025) Long-term development of lava dome morphology and thermal energy release in the crater of Mount St. Helens, Washington (USA). Journal of Volcanology and Geothermal Research, 108274.

SOBOLEWSKI, L., HANSTEEN, T.H., ZORN, E.U., STENNER, C., FLOREA, L.J., BURGESS, S.A., IONESCU, A., CARTAYA, E. & PFLITSCH, A. (2023) The evolving volcano-ice interactions of Crater Glacier, Mount St. Helens, Washington (USA). Bulletin of Volcanology, 85(4).

SOBOLEWSKI, L., STENNER, C., WILLIAMS-JONES, G., ANITORI, R., DAVIS, R. E., PFLITSCH, A. (2022) Implications of the study of subglacial volcanism and glaciovolcanic cave systems. Bulletin of Volcanology, 84(21).

SOBOLEWSKI, L., STENNER, C., HÜSER, C., BERGHAUS, T., CARTAYA, E., & PFLITSCH, A., (2022b) Ongoing genesis of a novel glaciovolcanic cave system in the crater of Mount St. Helens, Washington, USA, Journal of Cave and Karst Studies, 84(2):51-65.

STENNER, C., FLOREA, L., PFLITSCH, A., SOBOLEWSKI, L., WILLIAMS--JONES, G. (2024) Morphodynamics, morphology, and microclimate of glaciovolcanic cave systems. 10th International Workshop on Ice Caves, May 12-18, Werfenweng, Austria.

STENNER, C., FLOREA, L., PFLITSCH, A., CARTAYA, E., RIGGS, D. (2023) Morphodynamics of Glaciovolcanic Caves - Mount Rainier, Washington, USA. Journal of Cave and Karst Studies, 85 (3/4):65-85.

STENNER, C., PFLITSCH, A., FLOREA, L., GRAHAM, K., CARTAYA, E. (2022) Development and persistence of hazardous atmospheres in a glaciovolcanic cave system – Mount Rainier, Washington, USA. Journal of Cave and Karst Studies, 84(2):66-82.

STENNER, C., SOBOLEWSKI, L., PFLITSCH, A. AND CARTAYA, E. (2020) Morphology of a new system of glaciovolcanic caves—Mount St. Helens, Washington, USA. AGU Fall Meeting, Vol. 2020:C038-0001.

STORRIE-LOMBARDI, M.C., HALL, A.P., HANG, S., LYZENGA, G.A., CLARK, C.M., SATTLER, B.I., BEJ, A.K. AND HOOVER, R.B. (2011) Spectral profiling and imaging (SPI): extending LIFE technology for the remote exploration of life in ice caves (RELIC) on Earth and Mars. In Instruments, Methods, and Missions for Astrobiology XIV, Vol. 8152:355-366.

VAN DEN BROEKE, M. (2008). Depth and Density of the Antarctic Firn Layer. Arctic, Antarctic, and Alpine Research, 40(2):432–43.

An example of karst pavement in a tropical karst scenario at the Bodoquena National Park, Brazil

Luiz Eduardo Panisset Travassos (1), Darcy José do Santos (2) & Mauro Gomes (3)

(1) Researcher and Professor in the Graduate Program in Geography, PUC Minas, Av. Dom José Gaspar, 500, Coração Eucarístico, Belo Horizonte, MG, Brazil, 30535-610, luizepanisset@gmail.com

(Corresponding author)

(2) CECAV/ICMBio, Advanced Base of Minas Gerais, Av. Montreal, s/n, Nova Lima, MG, darcy.santos@icmbio.gov.br

(3) CECAV/ICMBio, Advanced Base of Minas Gerais, Av. Montreal, s/n, Nova Lima, MG, mauro.gomes@icmbio.gov.br

Abstract

The Serra da Bodoquena National Park (SBNP) in Mato Grosso do Sul hosts limestone pavements of high scientific and educational relevance. These geomorphological formations, shaped by chemical weathering and erosion, represent a remarkable example of a karst landscape in a tropical region, with similar morphologies in high-latitude and glacial activity areas. Studies indicate that such geological features, including fractures (grikes), depressions (kamenitzas), and karren, provide valuable insights into landscape evolution, climatic processes, and the interactions between geodiversity and biodiversity. This study uses a literature review, satellite imagery, fieldwork, and comparative analysis to understand local geomorphological processes. The results show that the Park's karst pavement developed under unique conditions and is impacted by human activities, such as cattle farming and unregulated tourism, particularly in areas outside the park's boundaries. Given its educational value, the site offers exceptional opportunities for environmental education, promoting hands-on learning about science and conservation. However, challenges such as land regularisation and environmental impact mitigation underscore the urgent need for protection. This study contributes to understanding tropical karst landscapes and reinforces the importance of conserving this unique geological heritage.

Resumo

O Parque Nacional da Serra da Bodoquena (PNSB), no Mato Grosso do Sul, abriga pavimentos calcários de alta relevância científica e educacional. Essas formações geomorfológicas, moldadas pelo intemperismo químico e pela erosão, representam um exemplo notável de paisagem cárstica em região tropical, com formações semelhantes em áreas de altas latitudes e atividades glaciais. Estudos indicam que essas características geológicas, incluindo fissuras (grikes), depressões (kamenitzas) e lapiás (karren), oferecem valiosos insights sobre a evolução da paisagem, os processos climáticos e as interações entre geodiversidade e biodiversidade. A pesquisa utilizou revisão de literatura, imagens de satélite, trabalho de campo e análise comparativa para compreender os processos geomorfológicos locais. Os resultados mostram que o pavimento cárstico do parque se desenvolveu sob condições únicas e é impactado por atividades humanas, como pecuária e turismo desregulado, particularmente em áreas fora dos limites do parque. Dado seu valor educacional, o local oferece oportunidades excepcionais para educação ambiental, promovendo aprendizado prático sobre ciência e conservação. No entanto, desafios como a regularização fundiária e a mitigação de impactos ambientais destacam a necessidade urgente de proteção. Este estudo contribui para a compreensão das paisagens cársticas tropicais e reforça a importância de conservar esse patrimônio geológico único.

Resumen

El Parque Nacional de la Serra da Bodoquena (PNSB), ubicado en Mato Grosso do Sul, alberga pavimentos calcáreos de alta relevancia científica y educativa. Estas formaciones geomorfológicas, moldeadas por la meteorización química y la erosión, representan un notable ejemplo de paisajes kársticos en una región tropical, en contraste con formaciones similares en áreas de alta latitud y actividad glaciar. Estudios previos indican que estas características geológicas, incluidas las fisuras (grikes), depresiones (kamenitzas) y lapiaz (karren), ofrecen información valiosa sobre la evolución del paisaje, los procesos climáticos y las interacciones entre la geodiversidad y la biodiversidad. La investigación realizada utilizó revisión bibliográfica, imágenes satelitales, trabajo de campo y análisis comparativo para comprender los procesos geomorfológicos locales. Los resultados muestran que el pavimento kárstico del PNSB se desarrolló bajo condiciones únicas y está impactado por actividades humanas, como la ganadería y el turismo no regulado, especialmente en áreas fuera de los límites del parque. Dado su valor educativo, el sitio ofrece oportunidades excepcionales para la educación ambiental, promoviendo el aprendizaje práctico sobre ciencia y conservación. Sin embargo, desafíos como la regularización de tierras y la mitigación de impactos ambientales subrayan la necesidad urgente de protección. Este estudio contribuye a la comprensión de los paisajes kársticos tropicales y refuerza la importancia de conservar este singular patrimonio geológico.

1. Introduction

The area within the Serra da Bodoquena National Park (SBNP) and its surroundings in Mato Grosso do Sul should be recognised for its significance in science and education, particularly in karst geomorphology. It represents an important example of a karst pavement in a tropical region (Figure 1).

A karst pavement refers to a unique geological surface feature in karst landscapes. Typically observed in carbonates such as limestone and dolomite, these formations result from the dissolution of these rocks. Such exokarst features are essentially exposed bedrock surfaces shaped and smoothed by chemical weathering and erosion processes associated with karst development. According to VERES (2010), the formation of this type of feature predominantly occurs in high-latitude and alpine regions where glacial activity has been prominent. Rock dissolution in these areas occurs due to the melting of accumulated snow during winter and direct rainfall on the rock surface.

As illustrated in Figure 2, notable examples of such features can be found in Spain (BARRÈRE, 1951; MARTÍN-VIVALDI CABALLERO, 2016), France (MAIRE, 1984; TÓTH, 2008; GAUDILLAT, 2008), Iraq (FORTI et al., 2021), Ireland (CORBEL, 1952), the United Kingdom (WARD; EVANS, 1976; LEMON; WATSON, 2014), Slovenia (TRAVASSOS, 2019), and many other countries (GUNN, 2004).

Limestone pavements are fascinating geological features that are important for understanding chemical weathering and erosion processes in karst landscapes. They are often studied to gain insights into the history and development of karst and the effects of geology and water on rock dissolution. According to WILLIAMS (1966), VINCENT (2004) and VERES (2010), limestone pavements develop in strata with a gentle slope and their surface is divided into cracks called “grikes”. Kamenitzas and karren commonly occur in these places.

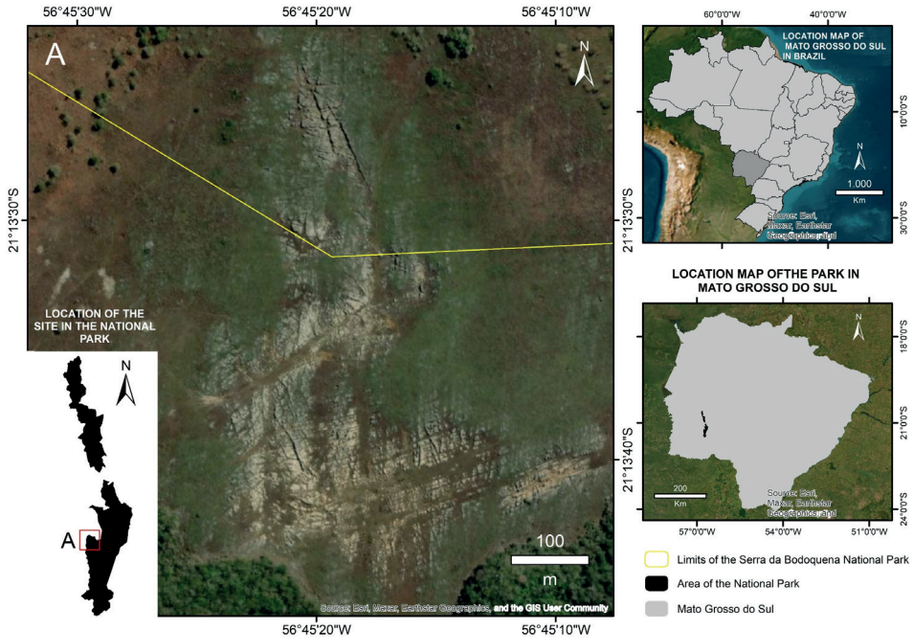

Figure 1: *Location map of the study área with the limits of the Serra da Bodoquena National Park.*
Source: *Elaborated by the authors.*

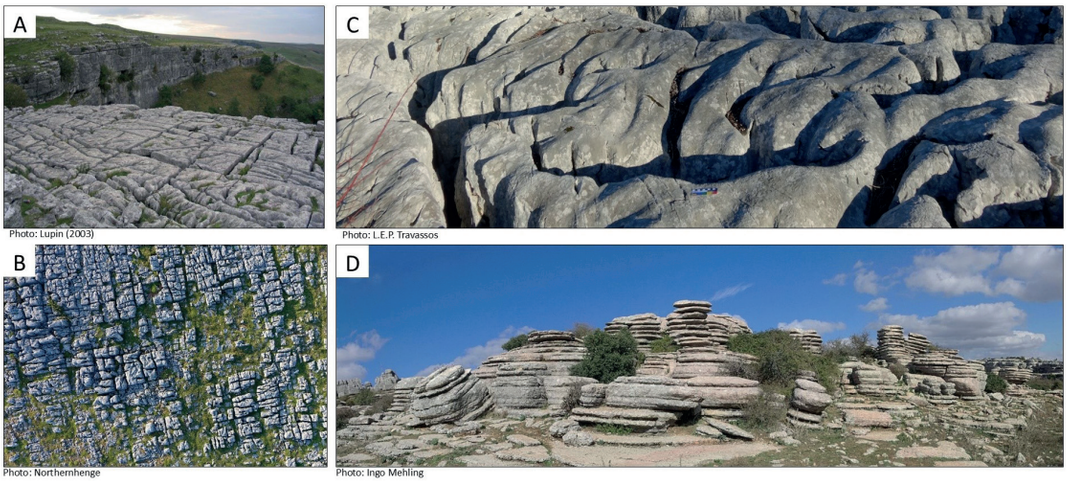

Figure 2: *Examples of karst pavements. A) Karst pavement above Malham Cove, Yorkshire, England. B) Karst pavement located in Orton Scar, Cumbria, England. C) Karst pavement located in Slovenia. D) Karst pavement in El Torcal de Antequera, Spain.*

2. Materials and methods

A comprehensive literature review on karst geomorphology was conducted, specifically focusing on limestone pavements and exokarst processes. Fundamental and contemporary works by authors such as WILLIAMS (1966), VINCENT (2004) and VERES (2010) provided the theoretical basis for understanding dissolution processes and the formation of grikes, kamenitzas, and karren in both tropical and temperate regions.

High-resolution satellite imagery was used to identify the area's surroundings. Direct observation, photographic documentation, and the use of GPS and photogrammetry via Remotely Piloted Aircraft (RPA) to collect the coordinates of key points of interest completed the fieldwork.

During the fieldwork, the main karst features associated with the limestone pavement were identified and classified, including Grikes (vertical fissures resulting from the dissolution of limestone), Kamenitzas (surface depressions caused by localised dissolution processes), and karren (grooves and irregular features shaped by the action of water on the rock surface). The collected data were analysed qualitatively to better understand local karstic processes' dynamics.

The findings were compared to documented limestone pavements in temperate and alpine regions, such as Malham Cove and Orton Scar in England, El Torcal de Antequera in Spain, and other sites in Slovenia. This comparison highlighted the limestone pavement's uniqueness in a tropical environment, providing a broader global context for the study.

The methodology combined geospatial analysis, field observations, and comparative studies to comprehensively understand the geomorphological processes shaping the limestone pavement in the Serra da Bodoquena.

3. Results

The relief of the Serra da Bodoquena National Park (SBNP) region is extraordinarily complex from an environmental perspective. The SW region of Mato Grosso do Sul comprises four distinct morphostructural domains, each subdivided into different geomorphological regions. As defined by IBGE (2006), these subdivisions include: i) the Interior Quaternary Sedimentary Deposits; ii) the Phanerozoic Sedimentary Basins and Covers of the Paraná River; iii) the Neoproterozoic Mobile Belts of Central Brazil; and iv) the Neoproterozoic Cratons of the Midwest.

The region is located in the SW sector of the Tocantins Province, where crystalline basement rocks, such as the Rio Apa Complex (southern portion of the Amazon Craton), outcrop alongside Proterozoic terrains. These include metavolcanic-sedimentary rocks of the Alto Tererê Metamorphic Association, the Acid Plutonic-Volcanic Suite of the Amoguijá Group and the Paraguay Fold Belt. The Coimbra Formation represents Palaeozoic terrains, while the Serra Geral Formation and São Bento Group characterise the Mesozoic terrains. Lastly, the Pantanal Plain is associated with significant Quaternary covers (GODOI et al., 2001; SALZO, I.; MATOS, 2013).

According to Boggiani et al. (2008), the Serra da Bodoquena developed within the Bocaina Formation of the Corumbá Group. The formation of Corumbá Group goes back to the fragmentation of the supercontinent Rodinia between 580 and 540 million years ago, forming other landmasses and oceans that led to the proliferation of primitive life forms. This calcium carbonate sedimentation led to the formation of the Corumbá Group. The Paraguay Fold Belt emerged between 530 and 520 million years ago when continental masses converged, folding the ocean floor. The carbonate deposits of the Corumbá Group were located on the ocean floor, subsequently exposing the rocks to folding processes.

Regarding the possible glacial origin of the limestone pavement described here, evidence of an Ediacaran (Vendian) glacial event has been confirmed in Mato Grosso do Sul (GONZAGA, 2001). However, this event occurred approximately 635 to 541 million years ago, during the Neoproterozoic. Although visual indicators are comparable to features described in other countries, studies on the carbonates of Serra da Bodoquena (ALVARENGA & TROMPETTE, 1992) suggest a more recent age than the aforementioned glacial event.

The region, located within the CLCP Geomorphological Unit (Labyrinth and Polygonal Karst) (SALLUM FILHO, 2005; SALLUM FILHO; KARMANN, 2007), exhibits fractures, corridors, depressions, and fluvial valleys. The limestone pavement is characterised by common fractures, corridors, and depressions (Figure 3) alongside flattened surfaces etched by various types of karren (Figure 4).

This karst area could be considered a valuable natural laboratory for scientific research: its unique environment provides a distinct perspective for understanding geological and environmental processes (past and present), natural cycles, and even climate change. The features, such as karren, caves, and depressions, make it an essential subject of study within a broader scientific context, addressing biodiversity and geodiversity preservation and conservation.

Figure 3: *General overview of fissures, corridors, and depressions on the Bodoquena Karst Pavement.*
Photos: *L.E.P. Travassos (2023)*

4. Discussion

The study underscores the urgent need for the limestone pavement area to be officially designated as an area of geological and geomorphological significance. Establishing such status would enable the implementation of appropriate regulations to control access and activities, ensuring the preservation of its unique geological and environmental features.

A scientific monitoring program is recommended to continuously evaluate the area's condition and provide essential data for future research. This would systematically track geomorphological and ecological parameters to understand ongoing processes and mitigate potential threats.

Educational programs and awareness are vital to fostering community involvement and visitor engagement in conservation efforts. By developing structured educational activities and raising awareness about the importance of karst, such an initiative can promote a culture of environmental stewardship among local populations and tourists.

The study highlights the need for partnerships and funding to enhance conservation efforts. The collaboration between research institutions, non-governmental organisations, and funding sources will be crucial for supporting protection measures and advancing scientific investigations in the area.

The limestone pavements of high scientific and educational value require immediate protection due to their critical role in understanding Earth's landscape evolution and environmental dynamics. These features, formed through chemical weathering and erosion, provide invaluable insights into ancient and modern geomorphological processes. Additionally, such features serve as habitats for various species, elucidating the interaction between geodiversity and biodiversity and guiding conservation efforts to protect fragile ecosystems.

Furthermore, limestone pavements hold significant clues to past climatic conditions. Features such as glacial striations and weathering patterns are essential paleoclimatic indicators, aiding in reconstructing historical environmental changes. In the case of the Serra da Bodoquena National Park´s pavement, the region's burial under soil—rather than glaciation—has facilitated rock dissolution and fracture widening, offering a unique perspective on karst processes.

Finally, the study emphasises the vulnerability of limestone pavements to human activities, such as poorly managed tourism, mining, and agriculture. These pressures highlight the necessity of protective measures to preserve this irreplaceable geological heritage while contributing to a broader understanding of landscape evolution, ecosystems, and Earth's geological and climatic history.

Figure 4: *Details of the various types of karren on the surface of the Bodoquena Karst Pavement. A) Kluftkarren; B) Rillenkarren, Trittkarren, and exposed subaerial karren; C) Mäanderkarren (meandering or sinuous karren); D) Rillenkarren, Trittkarren, and exposed subaerial karren; E) Elongated kamenitza on the right side of the photo with sinuous karren.*
Photos: *L.E.P. Travassos (2023)*

5. Conclusion

The research emphasises the critical role of the limestone pavement in Serra da Bodoquena National Park and the surrounding areas as a critical asset for ecological preservation, scientific research, and education. The karst formations serve as a unique natural laboratory, offering insights into the climatic history, biodiversity, and geomorphological processes, particularly in tropical environments where these structures are less common.

The results emphasise the pressing necessity of officially safeguarding this region by designating it as important to our Geoheritage. This would guarantee the enforcement of essential regulations to protect its geological and ecological integrity from the hazards posed by human activities, such as poorly managed tourism, mining, and agriculture.

It is imperative to implement a comprehensive scientific monitoring program to monitor the condition of karst pavement and produce data that will inform future conservation strategies and research. Additionally, implementing education and awareness initiatives would encourage community involvement and heighten visitors' perceptions of these distinctive karstic features, fostering sustainable utilisation.

Engaging in collaborative initiatives with academic institutions, NGOs, and funding agencies will be essential to advancing knowledge and guaranteeing the preservation of this irreplaceable geological heritage. This heritage is essential for understanding the Earth's landscape evolution, environmental dynamics, and biodiversity conservation.

Lastly, the investigation advocates establishing partnerships and funding to bolster research and protection initiatives.

Acknowledgments

This work was funded through the Speleological Compensation Commitment Terms (TCCE) No. 01/2020, signed between ICMBio and Mineração Ferro Puro, for which we are grateful. The authors are deeply grateful for the logistical support provided by the Serra da Bodoquena National Park team and the Research Productivity Fellowship provided by the National Council for Scientific and Technological Development (CNPq).

References

ALVARENGA C. J.S de, TROMPETTE R. (1992) Glacially influenced sedimentation in the Later Proterozoic of the Paraguay belt (Mato Grosso, Brazil). Palaeogeography, Palaeoclimatology, Palaeoecology 92(1-2):85-105. https://doi.org/10.1016/0031-0182(92)90136-S

BARRÈRE P. La morphologie karstique en Espagne. Revue géographique des Pyrénées et du Sud-Ouest. Sud-Ouest Européen 22(2):228-230, 1951. https://www.persee.fr/doc/rgpso_0035-3221_1951_num_22_2_1318.

BROOK G. A., FORD, D.C. (1980) Hydrology of the Nahanni karst, northern Canada, and the importance of extreme summer storms. Journal of Hydrology 46(1-2):103-121.https://doi.org/10.1016/0022-1694(80)90038-4

CORBEL J. (1952) Une région karstique d'Irlande: le Burren. Géocarrefour 27(1):21-33. https://www.persee.fr/doc/geoca_0035-113x_1952_num_27_1_1054

FORTI L. et al. (2021) Geomorphology of the northwestern Kurdistan Region of Iraq: landscapes of the Zagros Mountains drained by the Tigris and Great Zab Rivers. Journal of Maps 17(2):225-236. https://doi.org/10.1080/17445647.2021.1906339. .

GUNN, J. Encyclopedia of caves and karst science. Routledge, 2004.

GAUDILLAT V. (2008) Les «Pavements calcaires» («Limestone pavements»): Caractérisation et valeur patrimoniale d'un habitat complexe selon une approche pluridisciplinaire. Karstologia 51(1):25-32. https://www.persee.fr/doc/karst_0751-7688_2008_num_51_1_2620.

GINÉS A. et al. (2009) Karst Rock Features. Karren Sculpturing: Karren Sculpturing. Založba ZRC.

GONZAGA G. (2001) Glaciação Samburá (Neoproterozóico-Vendiano?) como possível agente transportador de diamantes no estado de Minas Gerais. Revista Brasileira de Geociências 31(4):597-604.

IBGE - Instituto Brasileiro de Geografia e Estatística. Diretoria de geociências (2006) Mapa das Unidades de Relevo do Brasil. Rio de Janeiro. 1 map, 1:5.000.000.

LEMON K, WATSON R. (2014) The evolution of a Global Geopark: challenges and achievements in the Marble Arch Caves Global Geopark. Atlantic Geology 50(1):297-379. https://www.erudit.org/en/journals/ageo/2014-v-50-ageo04779/1062333ar.pdf

MAIRE, R. (1984) Un exemple de karst haut-alpin: le Désert de Platé (Haute-Savoie). Carte géomorphologique au 1/25 000. Karstologia (3)1:25-33. https://www.persee.fr/doc/karst_0751-7688_1984_num_3_1_2067

MARTÍN-VIVALDI CABALLERO M.E. et al. (2016) Geomorphology of the Sierra Gorda karst, South Spain. Journal of Maps 12 (5):1143-1151. https://doi.org/10.1080/17445647.2015.1137790.

SALLUN FILHO W., KARMANN I. (2007) Geomorphological map of the Serra da Bodoquena karst, west-central Brazil. Journal of Maps 3(1):282-295. https://doi.org/ 10.1080/jom.2007.9710845.

SALZO I., MATOS A. M. (2013) Plano de Manejo do Parque Nacional da Serra da Bodoquena. ICMBio. Brasília: ICMBio. https://www.gov.br/icmbio/pt-br/assuntos/biodiversidade/unidade-de-conservacao/unidades-de-biomas/cerrado/lista-de-ucs/parna-da-serra-da-bodoquena/plano-de-manejo-/plano-de-manejo-pnsbd/plano-manejo-pnsbd-encarte-1.pdf

TÓTH G. (2008) Une nouvelle approche du système des lapiés alpins nus. Collection EDYTEM. Cahiers de géographie 7(1):147-156. https://www.persee.fr/doc/edyte_1762-4304_2008_num_7_1_1064

WARD S. D., EVANS, D.F. (1976) Conservation assessment of British limestone pavements based on floristic criteria. Biological Conservation 9(3):217-233. https://doi.org/10.1016/0006-3207(76)90011-2.

WILLIAMS P. W. (1966) Limestone pavements with special reference to western Ireland. Transactions of the Institute of British Geographers 40:155-172. https://doi.org/10.2307/621575

Morphostructural characteristics of the prealpine (isolated) karst: evidence from the Rovte region, Central Slovenia

Andrzej Tyc (1), Krzysztof Gaidzik (1), Filip Šarc (2), Dominika Bania (1), Kewin Rzadkowski (1) & Bojan Otonilćar (2)

(1) Institute of Earth Sciences, University of Silesia in Katowice, Będzińska 60, 41-200 Sosnowiec, Poland, andrzej.tyc@us.edu.pl (corresponding author)

(2) Karst Research Institute ZRC SAZU, Titov trg 2, Postojna, Slovenia

Abstract

This study presents the structural and geomorphological characteristics of the Rovte area in Central Slovenia. The region belongs to the pre-alpine (isolated) karst and is situated in the transition zone between the Dinaric and Alpine karst. The karst landscape in this area has developed in nearly latitudinal belts of Lower and Middle Triassic dolomites, limestones, and marly limestones, which are interbedded with sequences of siliciclastic rocks. Closed depressions of various sizes and shapes are a common landform in both dolomites and limestones, with a moderate to high doline density (40 dolines/km^2 in average). At the contact between marly limestones and dolomites, small-scale contact karst features have developed. Several caves occur here; studied Mravljetovo Brezno v Gošarjevih Rupah (MBGR) is the second longest in the entire region. Karst landforms and cave passages are primarily controlled by bedding planes dipping toward the S-SW, and by steeply dipping fractures and meso-faults with a direction of NNE-SSW to NE-SW (NE-SW to NW-SE dominated in the MBGR cave). Higher-order N-S faults influence the alignment of major cave passages, the direction of major axes of dolines, and the development of blind and dry valleys.

1. Introduction

Slovenia is well known for its karst landscapes, particularly in the Dinaric Karst, which includes the classical Kras plateau and Alpine karst, mainly in the Julian Alps. The study area (~32 km^2), located northwest of Rovte (Central Slovenia; Fig. 1), lies between these two major karst regions. According to GAMS (2004) and MIHEVC et al. (2016), this transitional area belongs to the pre-alpine or isolated karst. The landscape is characterized by rounded hills and plateaus with numerous closed depressions, incised by narrow valleys. The highest point in the study area is Vrh Svetih Treh Kraljev (Three Kings Hill) at 884 m a.s.l., while the lowest point, at 486 m a.s.l., is in the Poljanska Sora valley.

The Rovte region belongs to the frontal areas of the Trnovo Nappe, which represents the highest over-thrust of the Outer Dinarides in western Slovenia. It is situated northeast of the regional right-lateral strike-slip Idrija Fault (MLAKAR & ČAR, 2009; ČAR, 2010). Numerous faults in this extensive tectonic zone intersect the study area, the most significant being the Ravne Fault (Fig. 2). The lithology of the region consists of alternating Middle Permian to Middle Triassic carbonates and siliciclastics. The area's geology is highly diverse and varies over short distances, with belts and patches of various carbonate rocks (dolomites, limestones, marly limestones and marls) interbedded or laterally contact with clastic and siliciclastic rock formations (Fig. 2). A detailed description of the lithology of the Rovte region is provided by JOHNSTON et al. (2024).

Some caves in the study area, develop within the bedded Middle Triassic (Anisian) dolomite (Fig. 2). The longest (904 m) and deepest (73 m) cave within this unit is Mravljetovo Brezno v Gošarjevih Rupah (MBGR). Significant occurrence of dedolomitization is present in this studied site (OTONIČAR et al., 2013, 2016).

The geological and geomorphological studies conducted in this area aimed to identify the key relief features and morphostructural tendencies of the Rovte region. This region is characterized by heterogeneous carbonate lithology dominated by the contact between Lower and Middle Triassic dolomites and limestones or marly limestones. While the geomorphology of dolomite areas in Slovenia is well studied (KOMAC & GABROVEC, 2004), karst development in dolomitized rocks received less attention. This study highlights the specific karst features of the dolomites in the Rovte region, particularly the plateaus with a high density and depth of dolines, as well as the presence of large caves and small-scale contact karst.

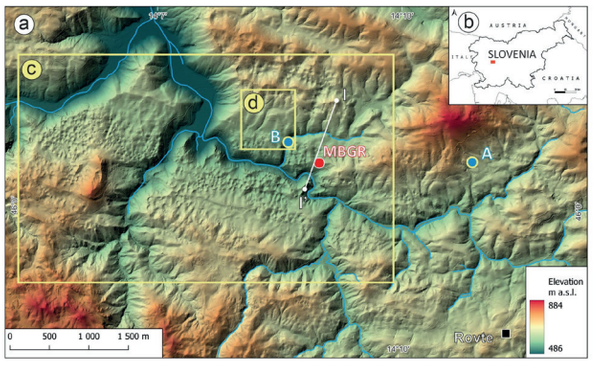

Figure 1: *Location of the study area. a) hypsometric map based on the open access digital elevation model (DEM) from the ARSO Geoportal, b) map of Slovenia indicating the Rovte region (red box), c) the area of detailed morphometric analyses of closed depressions, explanations in the text and in Fig. 3, d) the area of contact karst features shown in Fig. 4; MBGR – Mravljetovo brezno v Gošarjevih rupah cave; I-I' – morphological section line shown in Fig. 7; A, B – sites of structural studies carried out on the surface, shown in Fig. 5.*

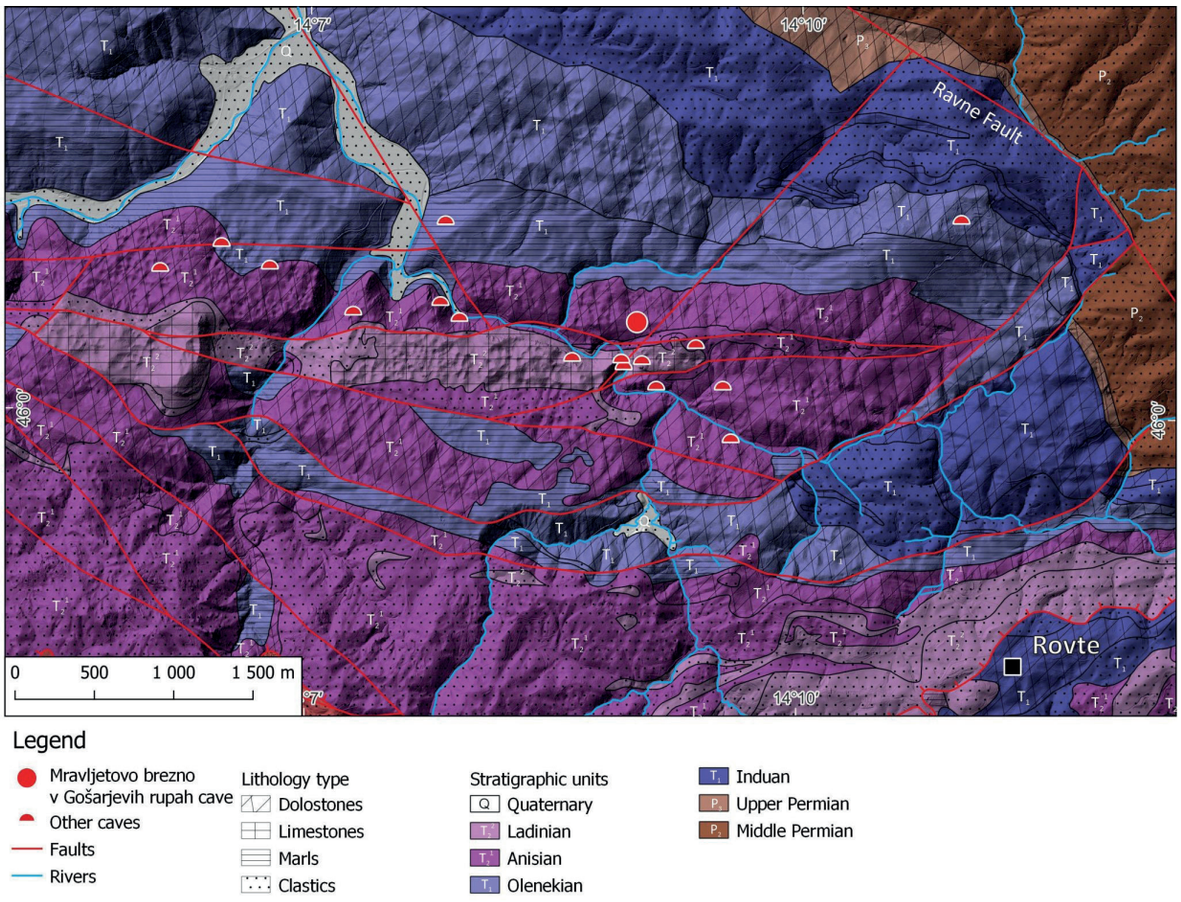

Figure 2: *Geological map of the Rovte region (after JOHNSTON et al., 2024, modified). Location of caves after https://www.katasterjam.si/.*

2. Materials and methods

In this study, we used a digital version of the geological map published by JOHNSTON et al. (2024), which was superimposed on a high-resolution digital elevation model (DEM) to visualize the geological context and cave locations in the Rovte region. Analyses of digital data were supplemented with geological and geomorphological field mapping, and observations in caves.

Morphometric studies of the Rovte region were conducted using open-source software – QGIS version 3.28.14 and SAGA GIS 7.8.2. The analysis was based on 1 × 1 m DEM obtained from the ARSO Geoportal (https://gis.arso.gov.si). Using this DEM, key morphometric characteristics of the study area were derived. For the analysis of closed depressions, a representative area of 11.38 km^2 was selected (see in Fig. 1). The delineation of dolines and other karst depressions was performed using the automatic Closed Depressions module within the Basic Terrain Analysis algorithm in SAGA GIS. Morphometric parameters and indices were calculated for all identified closed depressions, following the methodology presented in VERBOVŠEK & GABOR (2019), and summarized by DE WAELE & GUTIÉRREZ (2022). For non-circular depressions, orientation was assessed by determining the azimuth of the major axis. Using the Distance Matrix tool, as described by VERBOVŠEK & GABOR (2019). The directions of depression elongation were then analyzed using the Line Direction Histogram plug-in for QGIS and presented in a rose diagram.

Structural analysis was conducted in natural outcrops and road cuttings in the gorge of Gošarjev graben (west of the MBGR cave), in the Hlevni vrh quarry, and within the MBGR cave itself (Fig. 1). These studies focused on the geometric, kinematic, and dynamic analysis of minor tectonic deformation structures, including fractures, meso-faults with associated surface structures and kinematic indicators, and veins. The study primarily involved the geometric analysis of mesoscale structures, to assess the relation between their morphology, spatial orientation, and superpositional age. More than 1,500 structural orientation measurements were collected using a Freiberg biaxial geological compass. The data is visualized using structural diagrams (point plots, great circles and contour stereoplots) in an equal-area Lambert-Schmidt projection on the lower hemisphere, generated with SpheriStat software (STESKY, 1998). Additionally, rose diagrams were used to illustrate the strike direction of fractures measured in surface outcrops.

3. Results and discussion

The geological structure of the study area is complex due to its location in the frontal part of the Outer Dinarides over-thrust zone (Trnovo Nappe) and within the Idrija Fault zone. The area consists of carbonate, clastic, and siliciclastic formations ranging from the Middle Permian to the Middle Triassic (Fig. 2). The detailed lithological characteristics of the stratigraphic units are discussed in JOHNSTON et al. (2024), which

integrates data from previously published maps and reports (MLAKAR & ČAR, 2009; ČAR, 2010) with recent geological mapping (OTONIČAR et al., 2016).

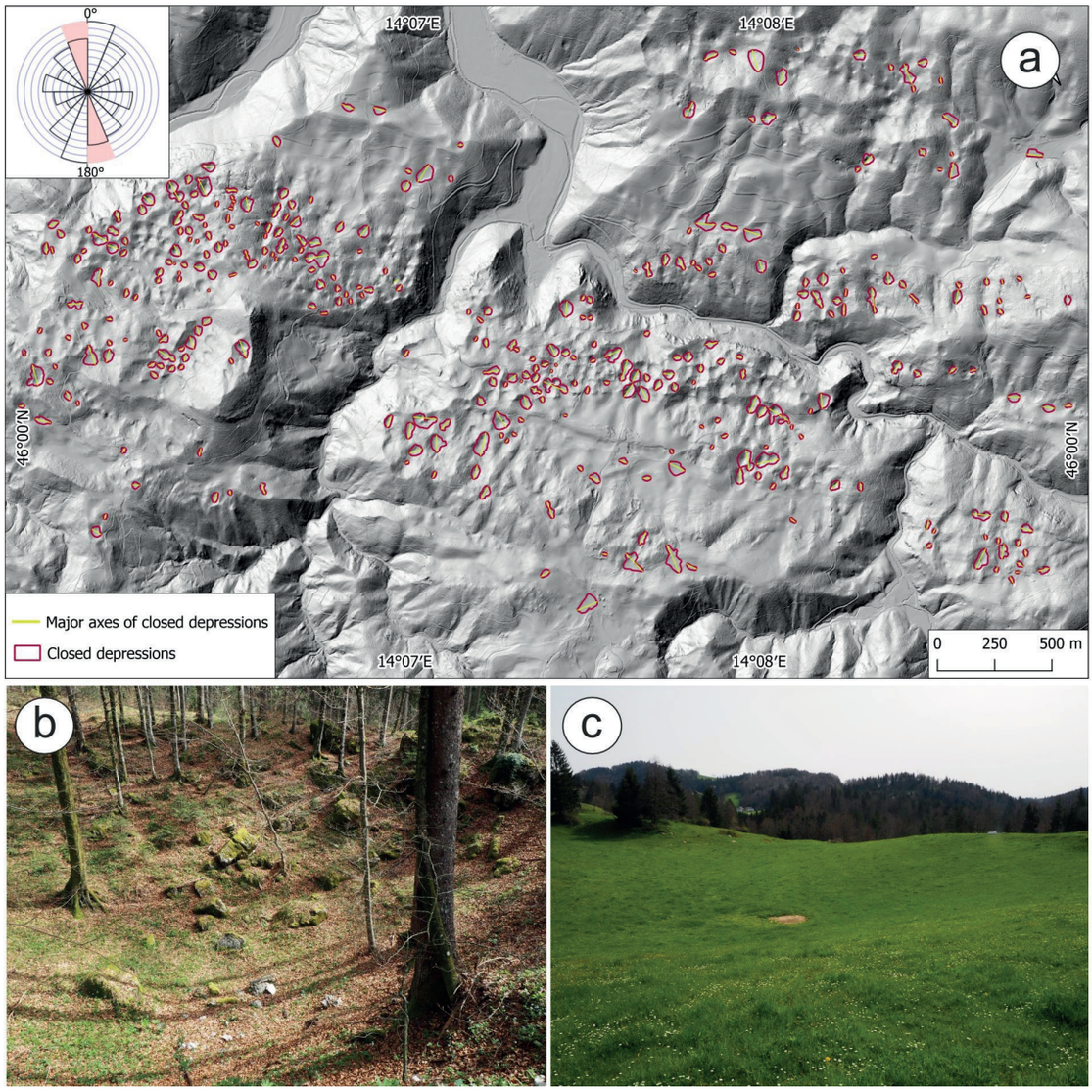

Figure 3: *Closed depressions in the Rovte region. a) orientation of the major axes of closed depressions with diagram of their main directions, b) doline in the Middle Triasic (Anisian) dolostone, c) shallow closed depression in the Lower Triassic (Olenekian) marly limestone.*

The central part of the study area is dominated by thick or indistinctly bedded Middle Triassic (Anisian) dolomites (Fig. 2), although the lithology of individual stratigraphic units is not homogeneous. Many transition zones exist between lithological types. These outcrops cover nearly 7 km^2 (21.3% of the total area). The lithology of this stratigraphic unit is dedolomitized. Indeed, it is noticeable, that the MBGR cave and other smaller caves are developed this unit. The surface is densely covered with dolines. The dolomite belt is bordered to the North by an extensive zone of Lower Triassic (Olenekian) marly limestones (4.5 km^2, 14.0%), while a much smaller area is occupied by bedded Lower Triassic (Olenekian) dolomites (3.7 km^2, 11.5%), forming a belt in the northern part of the study area. The only known cave within this unit is Jama pri Sv. Treh Kraljih (769 m long, 70 m deep), whose entrance was discovered during a tunnel construction (MIHEVC, 1991). A narrow belt of Middle Triassic (Ladinian) thick limestones (0.6 km^2) is located in the central part of the Rovte region (Fig. 2). Few caves are known in this unit, the largest and most famous being Matjaževe Kamre (300 m long, 14 m deep) (MIHEVC, 1989).

The primary karst surface in the study area are dolines. Such morphologies are concentrated in both dolomites and limestones rocks. Using the Closed Depressions algorithm in SAGA GIS, 447 closed depressions were identified within area underlain by different carbonate rocks. The majority are dolines of various size and circularity. Of these, 425 have an area of ≤5,000 m^2 and were included in further analyses. The remaining larger depressions likely consist of multiple interconnected smaller ones. The density of closed depressions classified as dolines is approximately 40 dolines/km^2, classifying the area in the moderate (10–40) to high (40–70) doline density class, following the classification of FAIVRE & PAHERNIK (2007). Most of the closed depressions (n= 365) are located in thick Middle Triassic (Anisian and Ladinian) limestones and dolomites. The largest depressions are located in marly limestones within the belt, North of the Anisian dolomites (Figs. 2 & 3).

The average area of all identified closed depressions is 1,737.9 m^2. The depth of depressions is up to 26.9 m, with an average depth of 4.5 m. The circularity ratio indicates that many depressions have an elongated shape, with an average index value of 0.83, significantly lower than the index value of a circular depression (e.g. circularity = 1). The study area contains depressions of various shapes, including 81 nearly circular forms

(circularity > 0.95), primarily developed in Lower and Middle Triassic dolomites. Excluding these circular dolines, direction parameters were determined for the remaining 354 ones. The dominant direction of their longest (major) axes is N-S (Fig. 3a).

Small-scale contact karst has developed at the interface between marly limestones and dolomites. This is evidenced by a blind valley terminating at a ponor below a permanent spring. Approximately 200 m downstream of the ponor zone, a 9 m deep shaft is developed in the dolomites (Fig. 4). Additionally, the dry valleys, with their mouths located above the bottom of the Gošarjev graben stream North of the MBGR cave (Fig. 2), likely represent remnants of former blind valleys that were incised by stream erosion.

Structural measurements taken at the Hlevni vrh quarry indicate monotonous bedding planes, dipping moderately to steeply toward the S-SW (Fig. 5a). A more complex setting was observed in the gorge, where bedding planes range from sub-horizontal to sub-vertical, dipping both South and North (Fig. 5b). Despite these variations, the fractures and meso-faults generally exhibit a consistent pattern, with a predominance of steep structures with NNE-SSW to NE–SW-direction.

Within the MBGR cave, bedding planes dip gently to moderately toward the S-SW, similar to the direction observed in the Hlevni vrh quarry. This trend remains consistent across all cave levels (Fig. 6a). Most observed fractures and meso-faults are steeply to vertically dipping, with two predominant strike orientations: NE-SW and NW-SE, though N-S and NNE-SSW directions are also common (Fig. 6b). A particular summary of the structural conditions of the relief and karst of the central part of the Rovte region is the context presented in the cross-section in Figure 7 (location in Fig. 1).

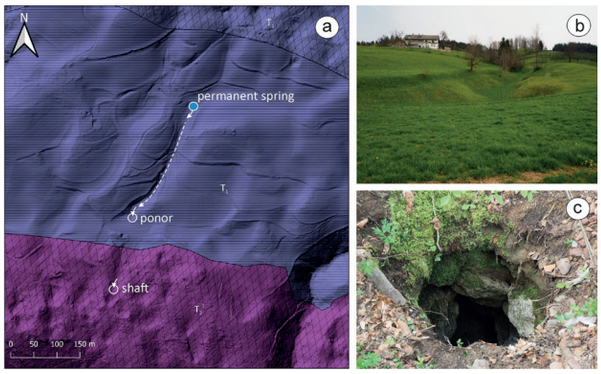

Figure 4: *Small-scale contact karst in the Rovte region (for location see Fig. 1). a) map showing geomorphological features on the contact between Lower Triassic (Olenekian) marly limestone and Middle Triassic (Anisian) dolostone (for explanation of lithology and stratigraphy see Fig. 2), b) short blind valley, c) shaft.*

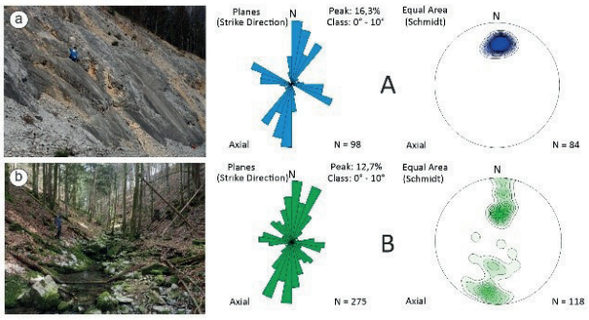

Figure 5: *Rose diagrams showing the strike orientation and number of fractures (at orientation intervals of 10 degrees) and the lower-hemisphere equal area projections of bedding for (a) Hlevni vrh quarry (blue diagrams, A in Fig. 1) and (b) Gošarjev graben gorge (green diagrams, B in Fig. 1).*

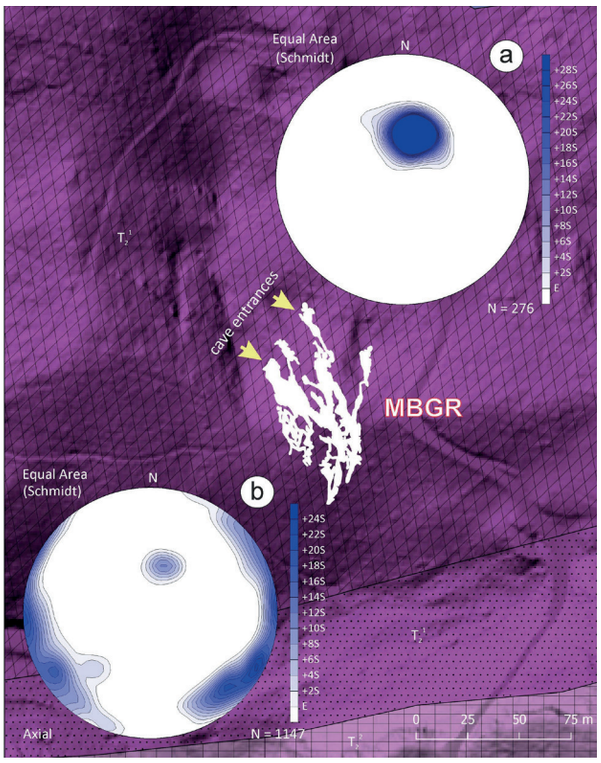

Figure 6: *Spatial orientation of bedding (a) and brittle meso-structures, including fractures and faults (b), in the Mravljetovo Brezno v Gošarjevih Rupah cave (MBGR). Stereoplots, projected onto the upper hemisphere, were generated using SpheriStat software (STESKY, 1998).*

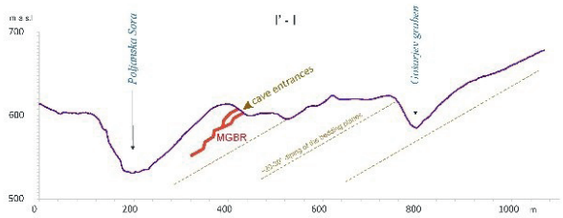

Figure 7: *Morphological profile (I'-I in Fig. 1) showing structural trend of the studied area. Profile generated from 1 m digital elevation model (DEM) from the ARSO Geoportal. The cross-section of the cave is approximate.*

4. Conclusion

The geomorphological setting and cave development in the Rovte region are influenced by the occurrence of alternating narrow belts of dolomite (up to several hundred meters wide), marly limestone, pure limestone (to a lesser extent), and siliciclastic rocks, which are dissected by faults associated with the Idrija Fault zone. Karst landforms and the passages of the Mravljetovo Brezno v Gošarjevih Rupah (MBGR) cave are controlled by bedding planes that dip moderately to steeply toward the S-SW, as well as by steeply dipping structures (fractures and meso-faults) with a NNE-SSW to NE-SW direction on the surface and a NE-SW to NW-SE direction within the cave.

A characteristic feature of the Rovte region, classified as a pre-alpine or isolated karst type in Slovenia, is the high density of dolines on the plateaus, composed primarily of Middle Triassic dolomites and limestones (Anisian and Ladinian) and, to a lesser extent, of Lower Triassic dolomites (Olenekian). The density of depressions reaches up to 40 dolines/km^2, a moderate category in comparison with other limestone areas of Dinaric Karst. However, it is considered a high density for dolomite regions in Slovenia. Another significant karst landform in the region is small-scale contact karst, including blind valleys with ponors and shafts at the boundary between marly limestones and dolomites.

Acknowledgments

The research was funded by the National Science Center (Poland), grant No. 2020/39/I/ST10/02357 and the Slovenian Research Agency (Slovenia), grant No. N1-0226.

References

ARSO Geoportal: Slovenian Environment Agency. Atlas Okolja, digital elevation model (DEM) of Slovenia. https://gis.arso.gov.si (access on January 2025).

ČAR J. (2010) Geological structure of the Idrija-Cerkno hills: explanatory book to the Geological map of the Idrija-Cerkljansko hills between Stopnik and Rovte 1:25.000. Geološki zavod Slovenije, Ljubljana, 125 p.

DE WAELE J., GUTIÉRREZ F. (2022) Karst hydrogeology, geomorphology and caves. John Wiley & Sons Ltd, 912 p.

FAIVRE S., PAHERNIK M., 2007. Structural influences on the spatial distribution of dolines, Island of Brač, Croatia. Zeitschrift für Geomorphologie, 51:487-503.

GAMS I. (2004) Kras v Sloveniji v prostoru in času. Založba ZRC SAZU, Ljubljana, 515 p.

JOHNSTON E. V., ŠARC F., WĄTOR K., OTONIČAR B. (2024) Hydrogeochemical data from carbonate springs as an aid for delimiting catchment areas in the Rovte region, Central Slovenia. Journal of Hydrology: Regional Studies, 56:1-24.

KOMAC B., GABROVEC M. (2004) Some characteristics of dolomite relief in Slovenia. Geografický Časopis, 56(3):187-201.

MIHEVC A. (1989) Matjaževe Kamre. Naše jame, 31:66-72.

MIHEVC A. (1991) Jama pri Sv. Treh kraljih. Naše jame, 33:28-37.

MIHEVC A., GABROVŠEK F., KNEZ M., KOZEL P., MULEC J., OTONIČAR B., PETRIČ M., PIPAN T., PRELOVŠEK M., SLABE T., ŠEBELA S., ZUPAN HAJNA N. (2016) Karst in Slovenia. Boletin Geológico y Minero, 127(1):79-97.

MLAKAR I., ČAR J. (2009) Geological map of the Idrija-Cerkno hills between Stopnik and Rovte 1: 25,000. Ljubljana.

OTONIČAR B., TYC A., OSBORNE R.L.A., BZOWSKA G. (2013) Dedolomit kot jamska prikamnina: Mravljetovo Brezno Gošarjevih rupah. Geološki Zbornik, 22:113-115.

OTONIČAR B., DUBLYANSKY Y., OSBORNE R.A., TYC A., PHILIPP S. (2016) Cave inception in dedolomite (a case study from central Slovenia). In: CHAVEZ T., REEHLING P. (eds.). Proceedings of Deep Karst 2016: origins, resources, and management of hypogene karst. Carlsbad, USA, 189–198.

PLACER L. (2008) Principles of the tectonic subdivision of Slovenia. Geologija 51(2):205-217.

STESKY R. M. (1998) SpheriStat user's manual. Pangea Scientific Software. Brockville, Ontario.

VERBOVŠEK T., GABOR L. (2019) Morphometric properties of dolines in Matarsko podolje, SW Slovenia. Environmental Earth Sciences, 78, 396.

The geomorphology of the caves in the Alunul Mare - Onceasa - Someșul Cald area, Bihor Mountains, Romania

Liviu Vălenaş (1), Emil Silvestru (2), George-Emil Pleş (3), Matei Cristian (4) and Ovidiu Guja (5)

(1) TU Bergakademie Freiberg, Lehrstuhl für Hydrogeologie und Hydrochemie, Gustav-Zeuner-Str. 12, 09599 Freiberg, Germany, liviu.valenas@gmail.com
(2) Geologist, #313-45513 Market Way, Chilliwack, BC, V2R 6A5, Canada, homospelaeus@gmail.com
(3) George-Emil Pleş, Universitatea Babeş-Bolyai, Departamentul de Geologie, Cluj-Napoca, george.ples@ubbcluj.ro
(4) Clubul de Speologie „Politehnica" Cluj-Napoca, matei.speopoli@gmail.com
(5) Societatea Națională de Speologie, Cluj-Napoca, snsro@intech.ro

1. Introduction

Alunul Mare Valley - Onceasa Plateau - Someșul Cald Valley is one of the important karst areas of Romania. It includes 4 long caves: the Avenul cu Vacă - Cerbului Cave System (6,212 m total length), Izbucul Alunului Mare Cave (3,109 m total length), Colțului Cave (3,526 m total length) and Pepii Cave (1,000 m total length). Another 12 smaller caves are in the same area, comprising a total of 14,269 m galleries. The deepest caves in the area are the Colțului Cave, -167 m and the Avenul cu Vacă - Cerbului Cave System, -124 m. The karst in the Alunul Mare - Onceasa - Someșul Cald area is a typical alpine karst of the Romanian Western Carpathians, both by the high altitude and the specific forms of relief. The caves were initially formed epiphreatic, then were remodeled vadose. The upper entrances also suffered the influence of gelifraction, one upper entrance, Avenul cu Vacă, still has a relatively large underground glacier. The fact that the Onceasa Plateau is relatively close to the deep valley of Someșul Cald, but also due to the fact that the Alunului Mare Valley goes directly to the Onceasa Plateau, did not allow the organization of a unique underground drainage. And thus three major drainages were formed in the area: Onceasa Plateau - Izbucul Alunului Mare Cave, Avenul cu Vacă - Cerbului Cave - Alunul Mare Valley and Colţului Cave - Pepii Cave. All the caves in the area were formed on faults and diaclases on two main directions: NE-SW and respectively NW-SE. Especially on the first direction the underground courses were organized.

The first exploration in this karst area, in the Pepii Cave, was undertaken by H. Roth in 1938, who explored approximately 300 m (VALENAS et al. 1977). In 1975-1978 L. Valenas, G. Drimba, N. Paul and N. Sasu mapped the underground river in the Pepii Cave (VALENAS 1976, 1978a, 1978b, 2022). Colţului Cave, which is the upstream continuation of Pepii Cave, was discovered in 1988 by C. Melnic, O. Guja and D. Croitoru from the Speleological Club „Politehnica" of Cluj- Napoca. The Izbucului Alunului Mare Cave was discovered by L. Valenas and H. Mitrofan in 1977 and it was explored only 11 m to an open sump. He was passed in 1986 by cavers of the Speleological Club „Politehnica", including S. Pătraș, C. Dobre, V. Grecu, M. Morărescu and O. Guja. In the years 1999-2001, together with cavers from GSM Grenoble, a system of fossil galleries was discovered, which led to the development of the cave to more than 3 km. Avenul cu Vacă was discovered by L. Valenas and I. Kövári in 1984, being explored up to -25 m, where a squeeze in the ice stopped the descent into depth. The Cerbului Cave was discovered in July 1988 by G. Frățilă, M. Gligan, C. Vodă and B. Ashbrook from the Speleological Club ‚Politehnica", which maped more than 3 km of galleries. After 1992, together with cavers from GSM Grenoble, the final halls are discovered and the junction with Avenul cu Vacă is made, 1994.

Figure 1: *Location of the Bihor Mountains (in white circle) in Romania.*

2. Materials and methods

The caves were surveyed before the year 2000 with Bézard or Sport 4 compasses, hip-chain and inclinometer, and after the year 2000 with DistoX. Cave entrances and karst springs were positioned with a Garmin 62s GPS. The geological map of Romania, Poiana Horea sheet, IGG publishing house (BLEAHU et al. 1980) was used as the geological base. The marking of two water losses from Poiana Onceasa was done, for each loss, with 500 g of fluorescein. Fluorescein was observed in springs visually. A LiDAR model was also used for the Onceasa Plateau.

3. Results

Almost all the caves in the area are developed in Upper Jurassic limestone (Oxfordian-Tithonian). They are bioclastic limestones (BLEAHU et al. 1980). Only Colțului Cave is, at least partially, also in Lower Cretaceous (Barremian-Aptian) lime- stone. Faults and diaclase are arranged in a „checkerboard", on two main directions: NE-SW and respectively NW-SE. The caves were formed in epiphreatic regime, the horizontality of the underground course support this hipothesis. Later, relatively recently, it was remodeled vadose. The horizontality of the underground streams of the main caves in the area was influenced by the proximity of the base level represented by the Someşul Cald valley.

Pepii Cave.

The entrance to the cave is on the left slope of Someşul Cald Valley, at 10 m relative altitude and at 1110 m altitude absolute, a few meters from the forest road going up from Ic Ponor towards the springs of Someşul Cald. The river underground that emerges from the cave forms beautiful small waterfalls before converging with the waters of Someşul Cald Valley. The main entrance is modest in size (3.5 m width, 2.5 m height) and gives access to a well-lit room, thanks to two natural windows. The underground course uses a unique, relatively small, highly meandering sectioned 2/3 m. The water mirror is from the wall in wall, forming a splendid winding lake, almost 450 m long. The streams often meander at right angles, caused by the successive passage along the two main directions of tectonic cracking, NE-SW and NW-SE. The cave has a total length of 1,000 m and VR +40 m (VALENAS 2022).

Colțului Cave.

The cave is fairly straight, oriented NE-SW, on an extend of 1,189 m. The cave is located 80 m above the Pepii Cave. The entrance to the cave is very modest, 3 m wide, 1 m high. After the entrance there is a larger hall. At the end of the entrance hall (40 m x 15 m), you reach a 15-meter pit, at the base of which the underground river appears. The gallery has a clear profile on the diaclase, up to 15 m high and 1.5 - 3 m wide. Above the upstream terminal sump, after climbing, a network of wells and parallel galleries was discovered, without succeeding in overcoming the sump. The upstream terminal sump was dived for only 30 m, with a maximum depth of 15.5 m. The downstream sump has an extension of 73 m and a restriction has until now prevented the direct junction with the Pepii Cave. The cave has a total length of 3,526 m and a depth of -167 m.

The Avenul cu Vacă - Cerbului Cave System.

This underground system is quite straight (extend 1,050 m) and also oriented in the NE-SW direction. The upstream entrance is Avenul cu Vacă, which starts from a large sinkhole and after three verticals of 15 m, 30 m and 25 m you reach a room with a permanent glacier. Through a very narrow gallery one descends to the main gallery, where an underground river flows. The gallery is generally wide, up to 30 m high. After passing an open sump, you reach the downstream terminal sump, which could not be explored. Cerbului Cave has an entrance from a collapse sinkhole, located in an area where limestones appear under non-karstifiable rocks. This entire underground system has a total length of 6,212 m and a depth of -124 m.

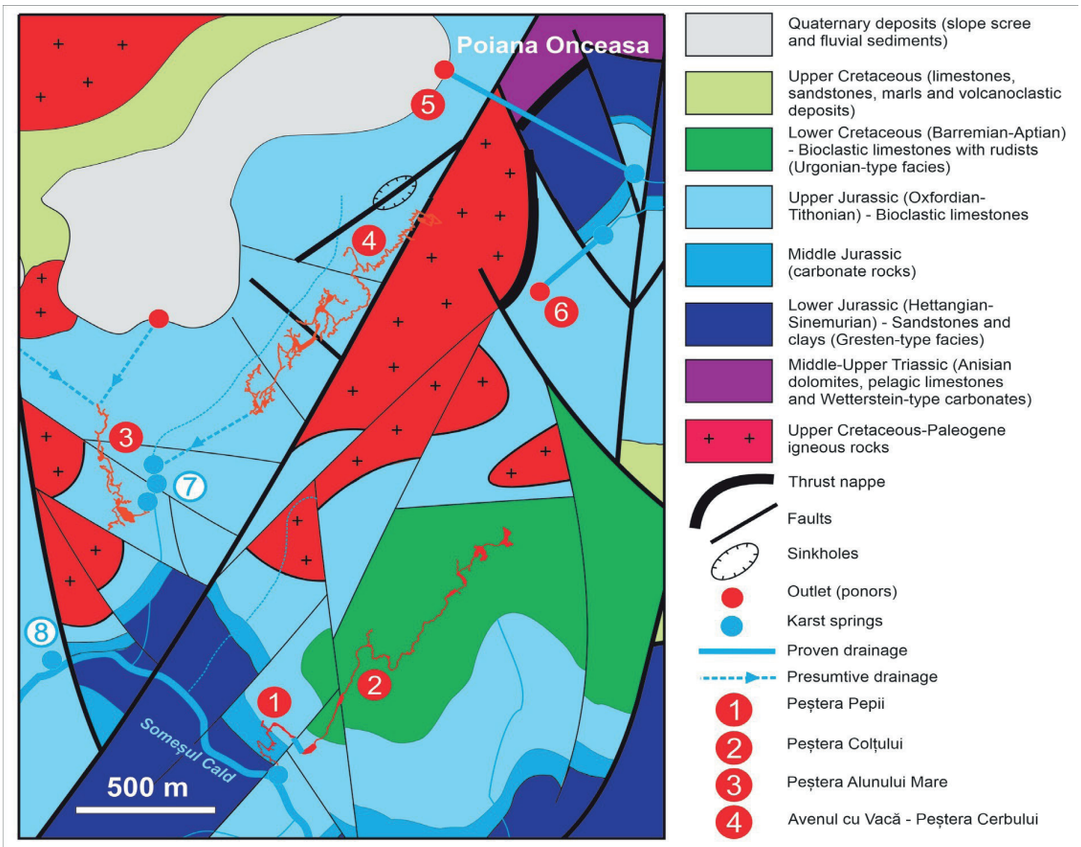

Figure 2: *Geological and hydrogeological map of the Alunul Mare-Onceasa-Someşul Cald area, modified by George-Emil Pleş and Liviu Valenas according to the geological map 1 50000, sheet 56b (Poiana Horea, BLEAHU et al. 1980). 1: Pepii Cave; 2: Colțului Cave; 3: Izbucul Alunului Mare Cave; 4: Avenul cu Vacă - Cerbului Cave System; 5-6: ponors in Onceasa Plateau; 7: springs in Alunul Mare Valley; 8: spring in Someşul Cald Valley.*

Izbucul Alunului Mare Cave.

The cave has two entrances, one through the spring. The upper entrance, rather narrow, opens into a deep sinkhole located on the right slope of the Alunului Mare Valley. After a few meters, the water course is intercepted, and continues through a low gallery through which it enters a large gallery. Downstream (to the left) the gallery continues upward and then closes, but continues slightly upward to the right, having a parallel path and above the water course. After about 800 m the sound of water can be heard again and through a jump of about 4 m it is possible to reach the water course again, a few meters downstream of the open sump, 64 m long, After this open sump, the upstream terminal sump is reached, explored over a length of 55 m, with a maximum depth of -9.5 m. In the terminal sector, a 10 m vertical climb leads to a maze made up of fossil galleries and several smaller halls. The cave has a total length of 3,109 m, VR: 89.1 m (+71.6 ; -17.5), extend 478 m.

The Onceasa Plateau is located in the north of the studied area, on the border with the igneous rocks of the Vladeasa massif. The Onceasa Plateau is partially covered by quaternary deposits. The Quaternary terrain has numerous suffosion sinkholes. Onceasa is not a polje, nor a closed basin, but a relatively horizontal karst plateau instead. At the boundary between the volcanic rocks or the Werfenian sandstones, several small surface valleys are lost in typical ponors. Many of them are impenetrable.

The plateau is full of sinkholes, some of them large. In a few places, the alignment of the sinkholes in the uvalas can be observed. In the western part of the plateau, in a wooded area, there are beautiful karst lakes in suffosion sinkholes. Until now, only 5 small caves havebeen explored in the Onceasa plateau (VALENAS 1978), with the exception of the Avenul cu Vacă, which continues with the Cerbului Cave..

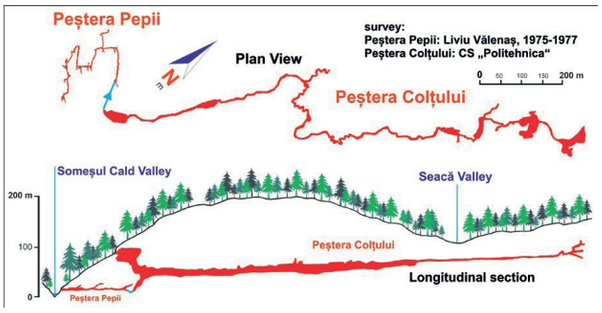

Figure 3: The plan and the longitudinal section in the Pepii and Colțului caves (cartography by the Politehnica Caving Club and Liviu Valenas).

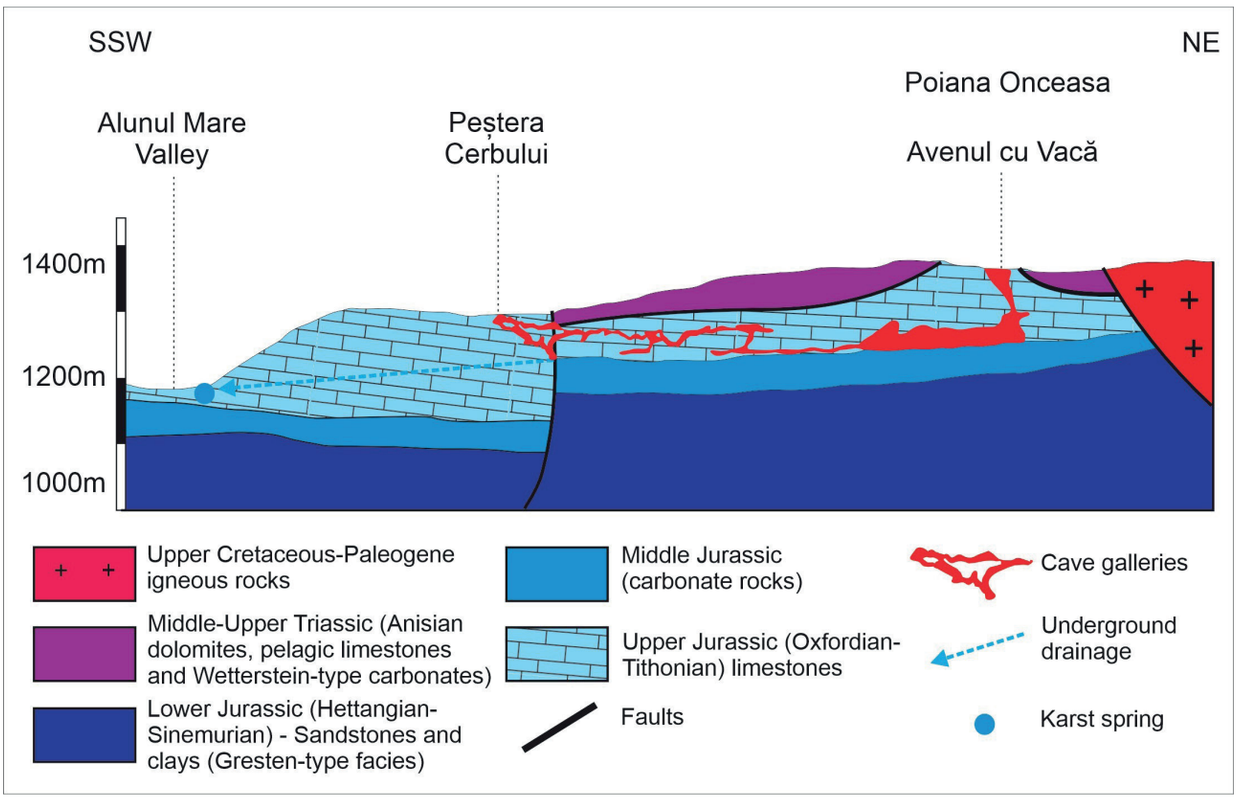

Figure 4: Stratigraphic profile between Onceasa Plateau and Alunul Mare Valley, modified by George-Emil Pleș after SILVESTRU et al. 1998.

4. Discussion

The Izbucul Alunului Mare Cave, the Avenul cu Vacă - Cerbului System and the Colțului Cave – Pepii Cave system have relative ly high flow underground rivers. The underground river in the Avenul cu Vacă - Cerbului Cave system could not be explored until the ressurgence, which are two springs, located 396 m in a straight line upstream of the Alunul Mare Valley. What is not known even to this day is the origin of these underground courses. It is more likely that the waters come from the Onceasa Plateau, from several ponors located there. In 1984, Liviu ponors located in the eastern part of the Onceasa Plateau, but, Vălenaș and Iuliana Kövári identified a ponor in the western part of the Onceasa Plateau, and it seems to be at the origin of the underground river in the Izbucul Alunului Mare Cave. In 1991, two injection tests with fluorescein were carried out in two surprisingly, fluorescein appeared after only a few hundred meters in small springs in the Onceasa Valley (SILVESTRU et al. 1998, ORĂȘEANU 2020).

5. Conclusion

The karst in the Alunul Mare - Onceasa - Someșul Cald area is a typical alpine karst of the Romanian Western Carpathians, both by the high altitude and the specific forms of relief. The fact that the Onceasa Plateau is relatively close to the deep valley of Someșul Cald, but also due to the fact that the Alunului Mare Valley goes directly to the Onceasa Pla teau, did not allow the organization of a unique underground drainage. And thus three major drainages were formed in the area. The age of the karst and endokarst in the area is recent. We appreciate that in the Lower Pleistocene, early phreatic drainages began to be organized. But only in the Middle Pleistocene we can talk about the formation of some caves, at first in epiphreatic regime and then vadose remodelled. The relatively recent age of the endokarst from Alunul Mare Valley - Onceasa Plateau - Someșul Cald Valley can be found in all the Romanian Carpathians.

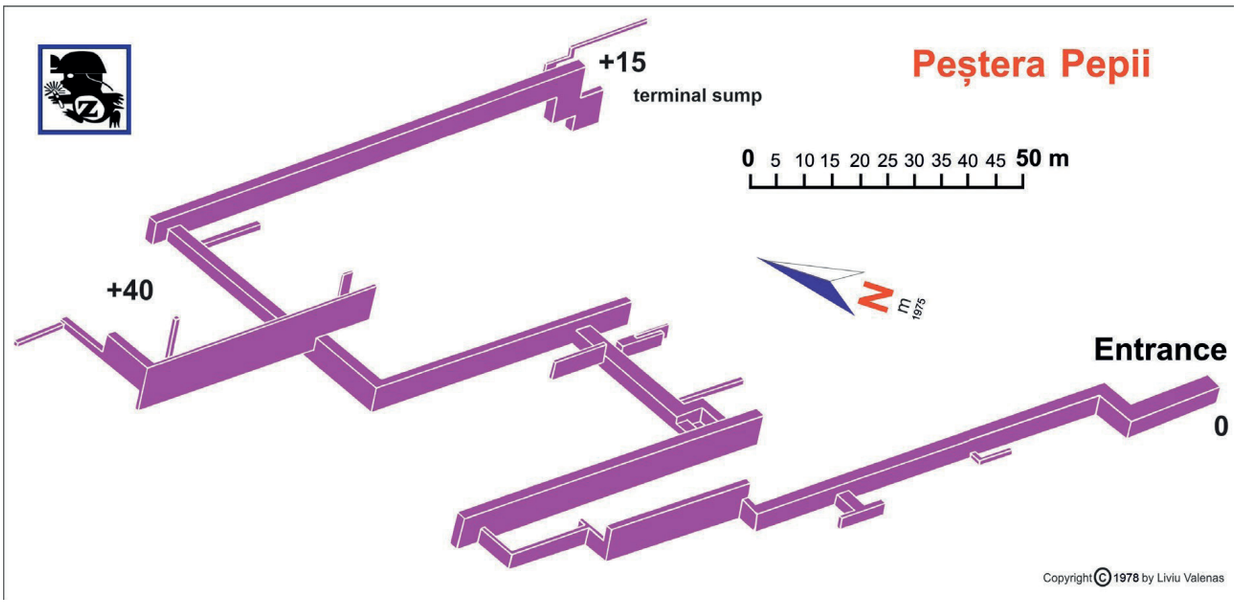

Figure 5: *Three-dimensional isometric representation of Pepii Cave (graphics Liviu Valenas).*

Figure 6: *Pepii Cave, the main gallery (photo Ovidiu Guja, assistant Dan Bogdan, August 2013).*

Figure 7: *Izbucul Alunului Mare Cave, the main gallery (photo Ovidiu Guja, assistant Daniel Ștefănescu).*

Figure 8: *Avenul cu Vacă, the vertical entrance (photo Matei Cristian, June 2024).*

Figure 9: *Cerbului Cave, the vertical entrance, photo Ruxandra Bocoș, June 2024).*

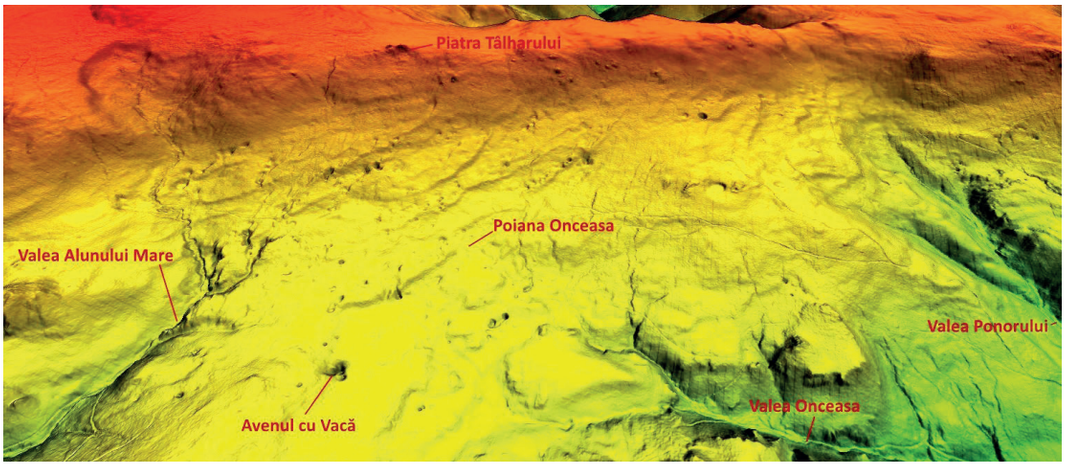

Figure 10: *Onceasa Plateau and Alunul Mare Valley with a LiDAR model. In the upper part, with red color, is the volcanic massif Vlădeasa. There are many sinkholes and ponors in the Onceasa karst plateau.*

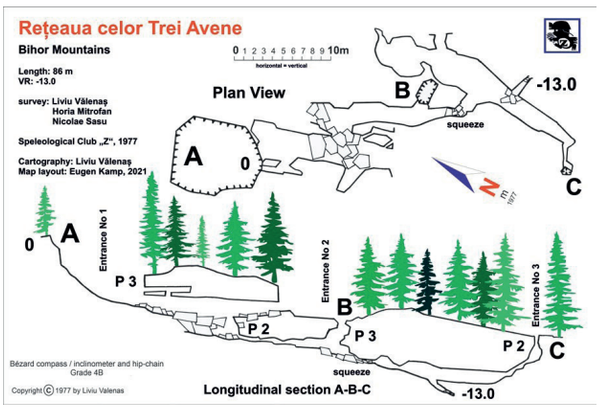

Figure 11: *Poiana Onceasa, Network of the Three Potholes, plan and the longitudinal section (cartography by Liviu Valenas).*

Figure 12: *Onceasa karst plateau (photo Matei Cristian).*

Figure 13: *Izbucul Alunului Mare Cave, the vertical entrance, (photo Ovidiu Guja).*

6. References

BLEAHU, M., DIMITRESCU, R., BORDEA, S., BORDEA, J., MAN- TEA, G. (1980) Harta geologică a României, Foaia Poiana Horea, Ed. IGG.

GORAN, C. (1982) Catalogul sistematic al peșterilor din România, CNE-FS-FRTA-CCSS, 496 p.

MANTEA, G. (1985) Geological Studies in the Upper Basin of the Someșul Cald Valley and Valea Seacă Region (Bi- hor-Vlădeasa Mountains), Ann. IGG, 66, 1-91.

ORĂȘEANU, I. (2020) Hidrogeologia carstului din Munții Apuse- ni, ediția a II-a, Ed. Belvedere, 349 p.

SILVESTRU, E., TĂMAȘ, T., FRĂȚILĂ, G. (1998) Preliminary data on the hydrogeology of karst terrains around the springs of Someșul Cald River (Bihor-Vlădeasa Mountains, Ro- mania), Theoretical and Applied Karstology, 8, 81-89.

VALENAS, L. (1976) Peștera Pepii, Bul. Com. Mun. de Tur., București, 36-37.

VALENAS, L. (1978a) Someșul Cald – 1977, Bul. Inform. FR- TA-CCSS, 2, 42-70.

VALENAS, L.(1978b) Reprezentarea tridimensională, Caietul CSER, București, 5, 306-313.

VALENAS, L. (2022) Peșterile Munților Bihor - Caves of Bihor Mountains, Romania, Ed. Clubului de Speologie „Z“, 264 p. VALENAS, L., BLEAHU, M., BRIJAN, P., HALASI, G. (1977) Inven-tarul speologic al Munților Bihor, Nymphaea, V, 209-335.

Distribuição dos afloramentos metacarbonáticos do carste do Legado Verdes do Cerrado e arredores, Centro-Oeste do Brasil

Márcio Henrique de Campos Zancopé (1), Rafaely Silva (2) & Renata Santos Momoli (3)

(1) Pequi Espeleogrupo de Pesquisa e Extensão e Instituto de Estudos Socioambientais, Universidade Federal de Goiás, Goiânia, Brasil, zancope@ufg.br (autor correspondente)

(2)Instituto de Estudos Socioambientais, Universidade Federal de Goiás, Goiânia, Brasil, rafaelysilva@discente.ufg.br

(3) Pequi Espeleogrupo de Pesquisa e Extensão e Instituto de Estudos Socioambientais, Universidade Federal de Goiás, Goiânia, Brasil, rsmomoli@ufg.br

Resumo

Regiões com afloramentos contínuos de rochas carbonáticas desenvolvem carstes cuja interação superfície-subsuperfície domina a morfogênese regional, enquanto que regiões com afloramentos descontínuos de carbonatos alternados por litologias menos solúveis desenvolvem carstes fragmentados de morfogênese multivariada. Este trabalho analisa a distribuição espacial e os tamanhos dos afloramentos de metacalcário na região da Reserva Legado Verdes do Cerrado, entre o Planalto Central e a Depressão do Alto Tocantins, sobre orógeno Neoproterozóico, no Centro-Oeste Brasileiro. O padrão de distribuição dos afloramentos foi obtido por geoprocessamento, a partir das unidades de metacalcários mapeadas (1:500.000), disponíveis na plataforma do Serviço Geológico do Brasil (https://geosgb.sgb.gov.br/) representado pelo mapa de isovalores dos tamanhos dos afloramentos. Destacou-se uma camada vetorial dos afloramentos, com o valor de área, transformando os polígonos em pontos, para interpolar pelo Inverse Distance Weight, gerando uma superfície contínua de valores discretos. A análise revelou que os afloramentos são dispersos e de extensão pequena em comparação com outros carstes de Goiás. Afloramentos entre 0,2 e 2,4 km2 compreendem 78% da área, cuja distribuição espacial decorre dos corpos metasedimentares lentiformes descontínuos e deformados do orógeno da Faixa Brasília da Província Tocantins que regionalizou as zonas de cisalhamento e os dobramentos, organizando a distribuição dos metacalcários.

Abstract

Regions with continuous outcrops of carbonate rocks develop karsts whose surface-subsurface interaction dominates regional morphogenesis, while regions with discontinuous carbonate outcrops alternating with less soluble lithologies develop fragmented karsts with multivariate morphogenesis. This work analyzes the spatial distribution and sizes of metalimestone outcrops in the Legado Verdes do Cerrado Reserve region, between the Central Plateau and the Alto Tocantins Depression, on the Neoproterozoic orogen, in Central-West Brazil. The distribution pattern of the outcrops was obtained by geoprocessing from the mapped metalimestone units (1:500,000), available on the Brazilian Geological Survey platform (https://geosgb.sgb.gov.br/) represented by the isovalue map of the outcrop sizes. A vector layer of the outcrops was highlighted with the area value transforming the polygons into points to interpolate by the Inverse Distance Weight, generating a continuous surface of discrete values. The analysis revealed that the outcrops are dispersed and of small extension compared to other karsts in Goiás, Brazil. Outcrops between 0.2 and 2.4 km2 comprise 78% of the area, whose spatial distribution results from discontinuous and deformed lentiform metasedimentary bodies of the Brasília Belt orogen of Tocantins Province which regionalized the shear zones and the folds, organizing the metalimestone distribution.

1. Introdução

Os terrenos cársticos são tradicionalmente reconhecidos por um relevo endêmico associado a um sistema subterrâneo, ambos resultantes do domínio da dissolução de rochas solúveis (GUTIÉRREZ et al., 2014; FORD & WILLIAMS, 2007). Embora seja admitido carstes sobre rochas pouco solúveis, este trabalho aborda os terrenos cársticos sobre rochas carbonáticas aflorantes e subsuperficiais em clima tropical úmido sazonal, no Cerrado do Centro-Oeste do Brasil.

Travassos (2019, p. 19) destaca a importância em se distinguir os terrenos cársticos sobre ocorrência contínua de rochas carbonáticas dos de ocorrência descontínua, visto que boa parte da população mundial ocupa esses terrenos e faz uso dos seus recursos. Para além disso, em razão do predomínio da dissolução geoquímica sobre os processos mecânicos, regiões com afloramentos contínuos de carbonatos desenvolvem terrenos cársticos cuja interação superfície-subsuperfície domina a morfogênese da paisagem. Por outro lado, regiões com afloramentos descontínuos de carbonatos, alternados por sucessivas litologias menos solúveis, desenvolvem terrenos cárstico igualmente descontínuos (KLIMCHOUCK & FORD, 2000 apud FERREIRA & UAGODA, 2019), resultando em paisagens regionais de morfogênese multivariada.

Terrenos cársticos descontínuos ocorrem na transição do Planalto Central Brasileiro para a Depressão do Alto Tocantins, no norte do estado de Goiás, área nuclear do Cerrado Brasileiro (ROCHA et al., 2022), entre a cidade de Niquelândia e o núcleo urbano de Assunção de Goiás (distrito do município de Vila Propício). A descontinuidade dos terre-

nos cársticos naquela região está condicionada aos afloramentos de lentes de metacalcários da sequência rítmica pelito-carbonatada do Grupo Paranoá (MOREIRA et al. 2008). Ao mesmo tempo, essas lentes constituem aforamentos com áreas restritas, apresentando paredões e maciços carbonáticos exumados que desenvolvem feições superficiais residuais como mogotes, humes e elevações ruiniformes, abundantes em feições de dissolução como campos de lapiás ou karrens (rillenkarren, wandkarren e schichtfugenkarren) e pináculos (spitzkarren). Muitos destes maciços carbonáticos apresentam cavernas registradas no Cadastro Nacional de Informações Espeleológicas (CANIE-CECAV/ICMBio). Posicionada no interior dessa região, está o Legado Verdes do Cerrado (LVC); uma reserva privada de desenvolvimento sustentável de Goiás, da Companhia Brasileira do Alumínio (CBA) e Reservas Votorantim. O LVC conta com 13 cavernas cadastradas no CANIE-CECAV/ICMBio até o momento, identificadas em litologias carbonáticas com o apoio do Pequi Espeleogrupo de Pesquisa e Extensão durante a realização dos projetos de pesquisa: i) Solos do Carste e ii) Espeleologia e biodiversidade no Legado Verdes do Cerrado entre 2019 e 2024 (CANIE-CECAV/ICMBio 2024; BRANDÃO & MOMOLI, 2022; MIRANDA et al., 2022).

Este trabalho tem por objetivo apresentar a distribuição dos afloramentos carbonáticos no LVC e arredores, e compreender a distribuição regional dos tamanhos das áreas dos respectivos afloramentos. Os resultados contribuem para a definição da tipologia do carste regional e a participação da carstificação na morfogênese da paisagem.

2. Materiais e Métodos

A área de estudo compreende a uma quadrícula entre os paralelos 14°04'S e 15°16'S e os meridianos 48°09'W e 48°52'W (Figura 1). Essas coordenadas permitiram posicionar o centro geométrico do limite territorial do Legado Verdes do Cerrado (LVC) próximo ao centro da quadrícula, abrangendo a maior quantidade de afloramentos circunvizinhos das lentes de metacalcários da região.

Integrante da Província Geotectônica Tocantins/Faixa Brasília, o Grupo Paranoá é uma sucessão psamo-pelítica Mesoproterozóica (1350 a 950 Ma) com participação frequente de rochas carbonáticas, que se estende pela área nuclear do Cerrado Brasileiro, desde o Distrito Federal até o sul do Tocantins. Na área do estudo em questão (Figura 1), predomina a última unidade dos megaciclos deposicionais (Unidade 4) do Grupo Paranoá (MPpa4), com sucessões rítmicas de metargilitos, ardósias, filitos carbonosos e quartzitos. Por entre estas sucessões, ocorrem lentes de metacalcários (MPpa4cc) e de mármores e dolomitos (MPpa4mm) (MOREIRA et al. 2008). As condições dos ambientes deposicionais e da paleotopografia do assoalho submerso produziram corpos rochosos lenticulares descontínuos lateralmente. Os subsequentes Ciclos Orogênicos Brasilianos (do Neoproterozóico ao Siluriano) causaram dobramentos, acavalamentos, soerguimentos e metamorfismos regionais, reposicionando as lentes de metacalcários em direções variadas e mergulhos elevados (SERAINE et al., 2021). "A relativa estabilidade tectônica subsequente favoreceu os ciclos denudacionais, que acentuaram as descontinuidades espaciais" dos metacalcários (ZANCOPÉ et al. 2023).

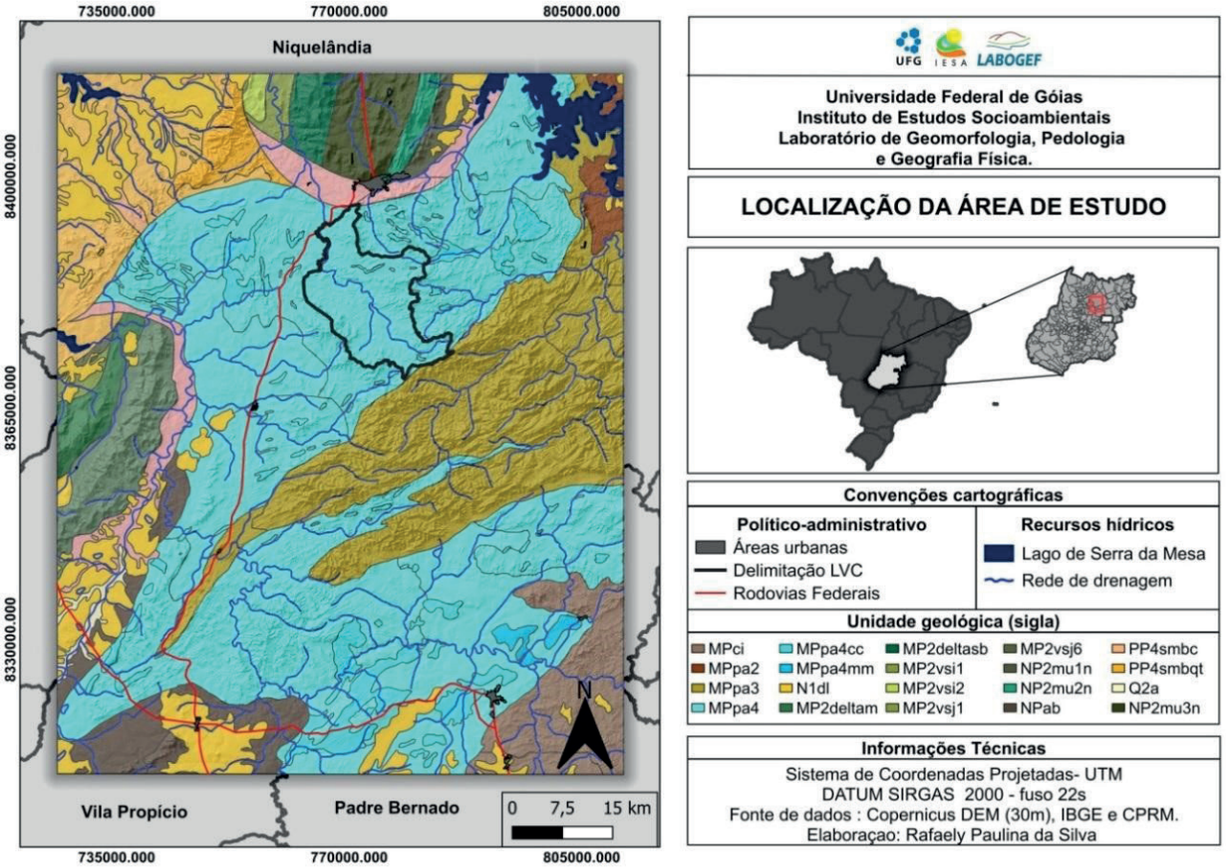

Figura 1: *Localização da área de estudo e das unidades geológicas regionais. Fonte dos dados: Moreira et al. 2008 e SGB/CPRM-GeoSGB*

O contexto geomorfológico compreende um planalto largamente entalhado e depressões intermontanas entre a borda ocidental da Chapada do Alto Rio Maranhão (900 a 1000 m de altitude) e a Depressão do Alto Tocantins (700 a 800 m de altitude). As serras e montanhas estão frequentemente alinhadas paralelamente entre si ou com os vales fluviais estreitos e profundos. Esses alinhamentos e paralelismos são

condicionados pela sequência estratigráfica das unidades litológicas e pela atitude das camadas de rocha (ZANCOPÉ et al. 2023), cuja direção, sentido e intensidade de mergulho são resultantes dos esforços orogenéticos Brasilianos (SERAINE et al., 2021). Nesse arcabouço litoestrutural é frequente a presença de combes e hogbacks em flancos de dobras. Mogotes, humes e maciços ruiniformes emergem topograficamente no interior dos vales entre os hogbacks e combes pela exumação das lentes de metacalcários das porções centrais das antiformas (ZANCOPÉ et al., 2023).

Para o desenvolvimento do trabalho, primeiramente, foram obtidos dados georreferenciados das unidades geológicas (1:500.000), de elevação (MDE) e hidrográficos para o recorte espacial da quadrícula escolhida como área de estudo (Figura 1), a partir das plataformas digitais do Serviço Geológico do Brasil (https://geosgb.sgb.gov.br/), Copernicus Europe's eyes on Earth (https://www.copernicus.eu/en) e IBGE (https://www.ibge.gov.br/), respectivamente. Em seguida, em ambiente SIG, foi destacada uma camada vetorial (SIRGAS 2000, UTM, Zona 22S) para os afloramentos das lentes de metacalcários (MPpa4cc) da Unidade 4 do Grupo Paranoá, permitindo determinar a área (km2) do polígono de cada afloramento mapeado pela base de dados.

Para encontrar o padrão espacial dos afloramentos das lentes de metacalcários (MPpa4cc) do Grupo Paranoá, foi elaborado um mapa de isovalores da distribuição dos tamanhos das áreas dos respectivos afloramentos. Para tanto, os polígonos dos afloramentos de MPpa4cc foram transformados em pontos, cada qual com o respectivo valor de área. A partir disso, aplicou-se o interpolador da média ponderada pelo inverso da distância (Inverse Distance Weight – IDW), que atribui maiores pesos para as amostras mais próximas, gerando uma superfície contínua baseada em valores discretos (APARECIDO et al., 2022; SOUZA & CAVALCANTI NETO, 2019)

3. Resultados

A partir dos dados disponíveis na plataforma digital do Serviço Geológico do Brasil (CPRM-GeoSGB) foi possível identificar 106 polígonos correspondentes aos afloramentos de metacalcários (Mppa4cc) da Unidade 4 do Grupo Paranoá (Mppa4) para o recorte de aproximadamente 8.896,7 km2 da área de estudo. Embora totalize uma área de 391,4 km2, a soma dos afloramentos não revela as características dos terrenos cársticos da região estudada. A diversidade de tamanhos e a distribuição dos afloramentos são as propriedades morfométricas mais relevantes.

Os afloramentos de metacalcários (MPpa4cc) apresentam uma variação muito elevada de tamanhos (Figura 2). O maior afloramento alcança 94,5 km2, sendo 2,8 vezes maior que o segundo maior, com 33,4 km2. Por outro lado, o menor afloramento, conforme a base de dados, não ultrapassa 0,084 km2 (8,4 ha). A Figura 2-A destaca que 78% dos afloramentos apresentam entre 0,2 a 2,4 km2.

A distribuição de frequência dos tamanhos dos afloramentos apresenta uma distorção muito elevada. A média (3,7 km2) é excessivamente maior que a mediana (1,1 km2), que é maior que a moda (0,38 km2 ; 38 ha), revelando uma assimetria positiva de alto grau. Os afloramentos de até 1 km2 dominam 47% da área de estudo, enquanto que entre 1 e 2 km2 constituem 29% dos afloramentos. Os afloramentos entre 5 e 100 km2 compõem 9,6% da área de estudo, os quais somam apenas 10 afloramentos (Figura 2-B). A concentração leptocúrtica e a assimetria muito elevada, com a cauda à direita muito longa da curva de distribuição permitiram agrupar os afloramentos de tamanho maior na última classe para melhor representar sua distribuição (Figura 2-B).

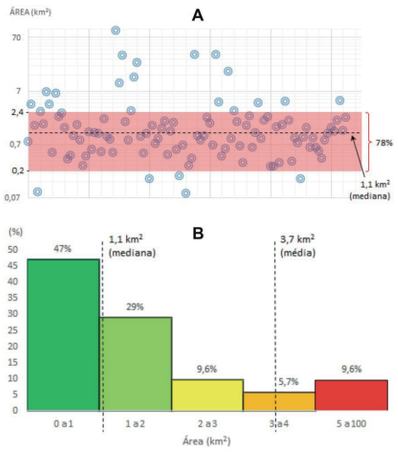

Figura 2: *Distribuição da frequência das áreas dos afloramentos de metacalcários (MPpa4cc). Fonte dos dados: Moreira et al. 2008 e SGB/CPRM-GeoSGB. Elaboração: os autores, 2024.*

Além dos tamanhos, a distribuição espacial dos afloramentos também é importante para compreender a ocorrência dos terrenos cársticos na área de estudo. A Figura 3 mostra que a distribuição dos afloramentos de metacalcários (MPpa4cc) está contida no interior da área das exposições da Unidade 4 (último megaciclo) do Grupo Paranoá (MPpa4) no recorte da região estudada. Lembramos que esses metacalcários constituem o litotipo responsável pelo desenvolvimento dos terrenos cársticos, com mogotes, humes e maciços ruiniformes, ricos em feições de dissolução, como lapiás e pináculos.

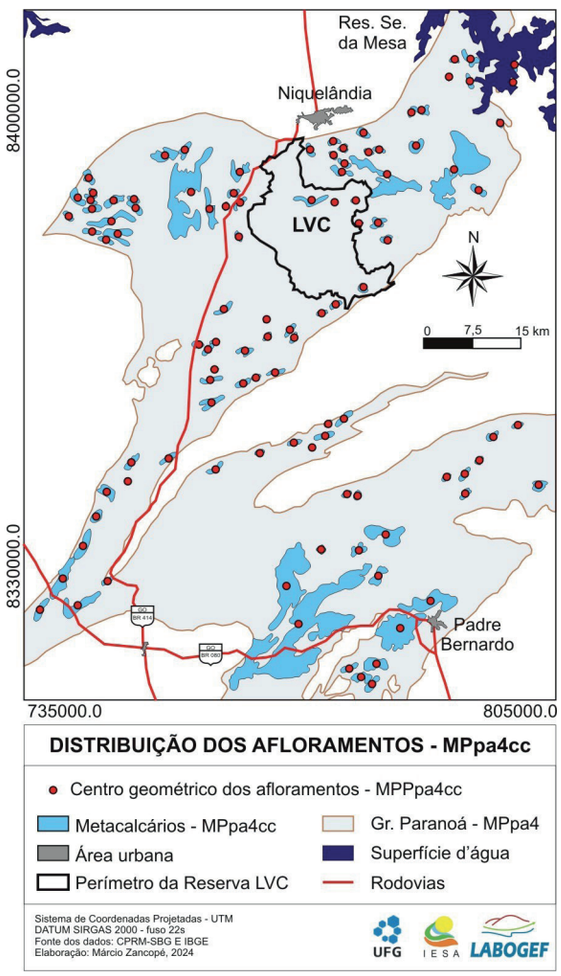

Figura 3: *Distribuição dos afloramentos de metacalcários (MPpa4cc). Fonte dos dados: Moreira et al. 2008 e SGB/CPRM-GeoSGB.*

Outros aspectos relevantes são a dispersão espacial e a descontinuidade dos afloramentos dos metacalcários. A Figura 3 permite perceber três agrupamentos principais dos afloramentos de metacalcários na área de estudo. O primeiro grupo forma uma zona posicionada na porção centro-sul da área de estudo. O segundo grupo ocorre na porção intermediária da área de estudo, constituindo uma faixa com direção preferencial NE-SW, aproximadamente. O terceiro grupo ocorre na porção norte, compondo uma faixa E-W ao sul de Niquelândia, englobando a metade norte da reserva LVC.

Embora seja possível observar esses três agrupamentos, os afloramentos dos metacalcários na área de estudo encontram-se desconectados, ou seja, não tangenciam uns aos outros. Essa descontinuidade dos afloramentos corresponde à forma lenticular de ocorrência dos metacalcários ao longo da sequência rítmica da MPpa4 do Paranoá.

O padrão de distribuição espacial dos tamanhos dos afloramentos (Figura 4) apresenta uma correspondência parcial com a distribuição das ocorrências dos mesmos (Figura 3). A zona centro-sul do recorte espacial estudado é dominada por afloramentos de área maior, entre 5 e 100 km2 (Figura 4). A porção intermediária da região estudada é dominada por afloramentos de área menor (entre 0 e 1 km2 e 1 a 2 km2), com duas direções preferenciais de distribuição: uma faixa de direção E-W na zona sul dessa porção intermediária; e outra faixa de direção NE-SW que atravessa a porção norte do recorte espacial estudado, alcançando o remanso do lago do reservatório da Usina Hidrelétrica de Serra da Mesa. Por sua vez, esta porção norte repete a faixa E-W, entre o sul de Niquelândia e a metade norte da LVC, tal como visto na Figura 3. Embora nessa faixa E-W da porção norte ocorra novamente os aforamentos de área maior (5 a 10 km2), ela é seccionada ao meio pela faixa NE-SW da porção intermediária com afloramentos menores (0 a 1 km2 e 1 a 2 km2). Ainda é possível observar a oeste desta porção norte a ocorrência de um grupo denso de afloramentos de áreas menores, entre 0 e 1 km2.

Por fim, vale destacar o predomínio de afloramentos de áreas menores no interior do território da Reserva Levado Verdes do Cerrado (LVC). Enquanto que nas porções leste e sul da LVC predominam afloramentos entre 0 e 1 km2, nas porções central e nordeste da LVC predominam afloramentos entre 1 e 2 km2.

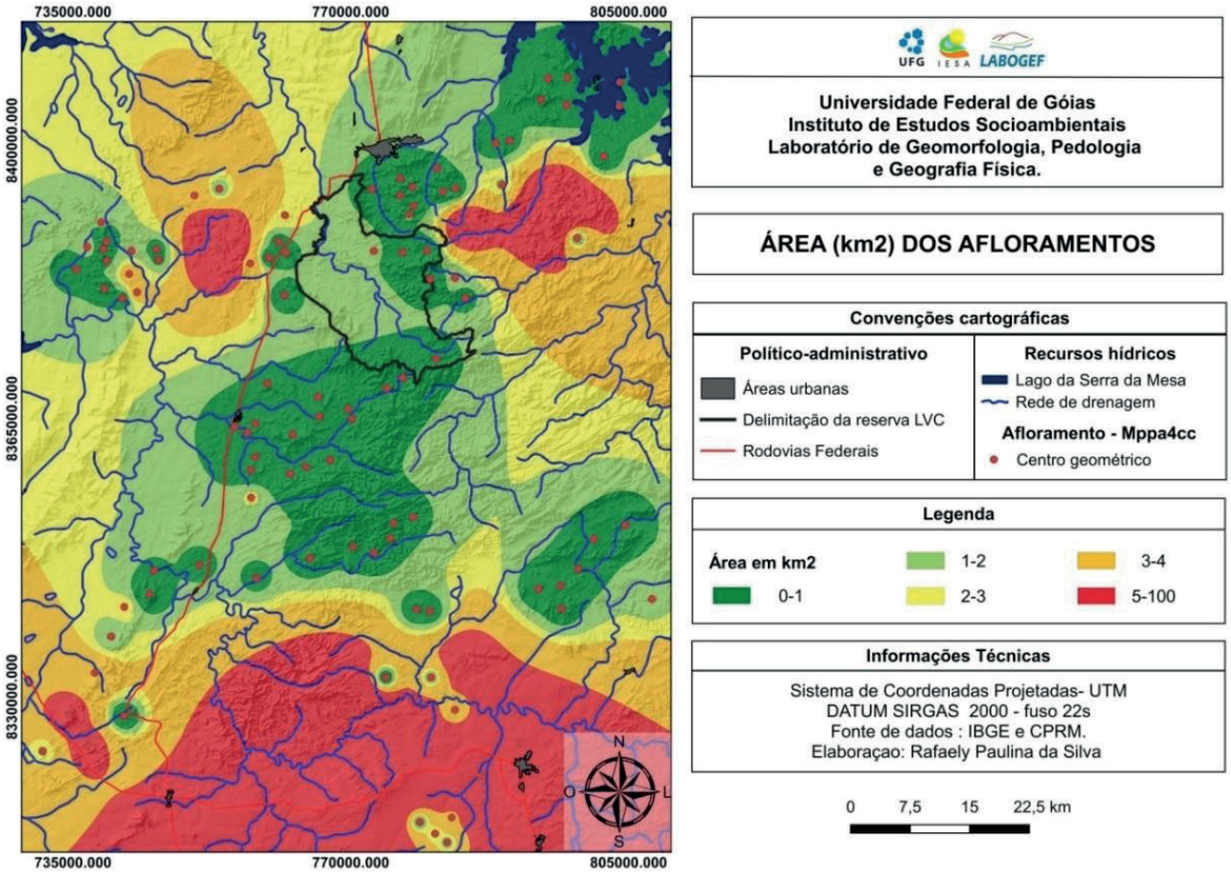

Figura 4: *Distribuição das áreas dos afloramentos de metacalcários (MPpa4cc). Fonte dos dados: Moreira et al. 2008 e SGB/CPRM-GeoSGB.*

4. Discussão

Os resultados mostram que na região estudada ocorrem afloramentos de metacalcários (MPpa4cc) descontínuos e com áreas de exposição pequenas. Esta característica é divergente de outros terrenos cársticos do estado de Goiás, como os carstes de São Domingos, Terra Ronca e Mambaí, internacionalmente conhecidos (AMARAL et al, 2023; FONSECA et al., 2023; NOGUEIRA et al., 2023), cujos afloramentos carbonáticos do Grupo Bambuí (Neoproterozóico) estão expostos de modo contínuo por ampla superfície. Essa distinção entre os terrenos cársticos do recorte espacial estudado e do nordeste do estado de Goiás decorre do contexto geotectônico de ambos casos. A região investigada neste trabalho situa-se sobre o orógeno da Faixa Brasília da Província Tocantins, cujas intensas deformações (do Neoproterozóico ao Siluriano) dobraram, acavalaram, soergueram e metamorfizaram as rochas. Os esforços geotectônicos, associado aos corpos sedimentares lentiformes dos protólitos dos metacalcários, produziram afloramentos de extensão restrita e de descontinuidade lateral elevada (MOREIRA et al. 2008; SERAINE et al., 2021; ZANCOPÉ et al. 2023). Por outro lado, o nordeste do estado de Goiás situa-se sobre a borda ocidental do Cráton do São Francisco, cuja

estabilidade geotectônica prolongada formou extensos corpos contínuos de carbonáticos do Grupo Bambuí (AMARAL et al, 2023; FONSECA et al., 2023; NOGUEIRA et al., 2023).

A distribuição espacial dos afloramentos dos metacalcários (Figura 3), bem como dos seus tamanhos (Figura 4), decorrem igualmente do contexto geotectônico. Os vetores dos esforços deformacionais regionalizaram as zonas de cisalhamento e os dobramentos, organizando a distribuição dos afloramentos (MOREIRA et al. 2008; SERAINE et al., 2021; ZANCOPÉ et al. 2023).

5. Conclusão

Os metacalcários do Grupo Paranoá (Neoproterozóico) constituem o substrato onde se desenvolvem mogotes, humes e maciços ruiniformes, abundantes em feições de dissolução, como lapiás e pináculos, na reserva Legado Verdes do Cerrado (LVC) e arredores. Os afloramentos desses metacalcários compreendem 4,4% do recorte espacial da área de estudo, fragmentados em 106 afloramentos mapeados. Além de descontínuos, eles apresentam áreas pequenas de exposição superficial, sendo que 78% desses afloramentos possuem entre 0,2 a 2,4 km2. Cerca de 47% do total dos afloramentos alcançam até 1 km2 e apenas 9,6% tem entre 5 e 100 km2.

O padrão de distribuição espacial dos afloramentos e dos seus tamanhos decorre do contexto geotectônico. Primeiramente, o ambiente deposicional neoproterozóico dos protólitos dos metacalcários produziram corpos rochosos lentiformes descontínuos lateralmente. Posteriormente, os esforços deformacionais (do Neoproterozóico ao Siluriano) do orógeno da Faixa Brasília da Província Tocantins regionalizaram as zonas de cisalhamento e os dobramentos, reorganizando a distribuição dos afloramentos.

Apesar de proporcionalmente representar uma fração pequena da área, a fragmentação dos afloramentos dos metacalcários na área de estudo impõe uma necessidade de manejo e conservação, considerando sua dispersão pela reserva LVC e arredores. Soma-se a isso o patrimônio cárstico e espeleológico de relevante geodiversidade diante do contexto geotectônico regional.

Agradecimentos

Agradecemos sinceramente à Reserva Legado Verdes do Cerrado (CBA/Votorantim) e ao Laboratório de Geomorfologia, Pedologia e Geografia Física (Labogef-IESA/UFG) pelo apoio logístico e instrumental e à Fundação de Amparo à Pesquisa do Estado de Goiás e a Votorantim S.A. pelo apoio financeiro (Chamada Pública 04/2018 e 10/2022 FAPEG-VOTORANTIM, respectivamente, processos n. 201810267001536 e 202310267000407).

Referências

AMARAL, A. K. N.; SILVA, G. B.; ROSA, L. E.; CHEREM, L. F. S.; MOMOLI, R.; ZANCOPÉ, M. H. C. (2023) Contamination vulnerability assessment of the Bambuí karst aquifer, in the Terra Ronca region - Goiás, Brazil. Journal of South American Earth Sciences 130: 104552. https://doi.org/10.1016/j.jsames.2023.104552

APARECIDO L. E. O., MORAES J. R. S. C., LIMA R. F., TORSONI G. B. (2022) Spatial interpolation techniques to map rainfall in Southest Brazil. Revista Brasileira de Meteorologia 37(1): 141-155 http://dx.doi.org/10.1590/0102-77863710015

BRANDÃO Z. C., MOMOLI R. S. (2022) Dinâmica da erosão em cavernas do grupo Paranoá, Niquelândia, Goiás In: MOMOLI, R. S.; STUMP, C. F.; VIEIRA, J. D. G.; ZAMPAULO, R. A. (org.) CONGRESSO BRASILEIRO DE ESPELEOLOGIA, 36, 2022. Brasília. Anais. Campinas: SBE. p.381-387. https://www.cavernas.org.br/wp-content/uploads/2021/02/36cbe_381-387.pdf

CANIE-CECAV/ICMBio CENTRO NACIONAL DE PESQUISA E CONSERVAÇÃO DE CAVERNAS. (2024) Cadastro Nacional de Informações Espeleológicas. https://www.gov.br/icmbio/pt-br/assuntos/centros-de-pesquisa/cecav/cadastro-nacional-de-informacoes-espeleologicas/canie.

FERREIRA C. F., UAGODA R. E. S. (2019) Tipologias do carste e classificação de dolinas: uma revisão. Caminhos de Geografia 20(7): 519-537 https://doi.org/10.14393/RCG207044169

FONSECA, M. R. S.; UAGODA, R. E. S.; CHAVES, H. M. L. (2023) Runoff, soil loss, and water balance in a restored Karst area of the Brazilian Savanna. Catena 222: 1066878. https://doi.org/10.1016/j.catena.2022.106878

FORD D, WILLIAMS P. (2007) Karst hydrogeology and Geomorphology. John Wiley & Sons Ltd. Chichester, 562 p. https://doi.org/10.1002/9781118684986

GUTIÉRREZ F, PARISE M, DE WAELE J, JOURDE H. (2014) A review on natural and human-induced geohazards and impacts in karst. Earth Science Reviews 138: 61-88. https://doi.org/10.1016/j.earscirev.2014.08.002

MIRANDA L. S., MOMOLI R. S., CORRECHEL V. (2022) Caracterização física de neossolos litólicos no entorno de cavernas, em Niquelândia-GO In: MOMOLI, R. S.; STUMP, C. F.; VIEIRA, J. D. G.; ZAMPAULO, R. A. (org.) CONGRESSO BRASILEIRO DE ESPELEOLOGIA, 36, 2022. Brasília. Anais. Campinas: SBE, p.342-348. http://www.cavernas.org.br/anais36cbe/36cbe_342-348.pdf.

MOREIRA M. L. O., MORETON L. C., ARAÚJO V. A. LACERDA FILHO J. V., COSTA H. F. (2008) Geologia do estado de Goiás e Distrito Federal. CPRM/SIB – Funmineral, Goiânia (mapa 1:500.000 e texto explicativo)

NOGUEIRA, A. M. CALDEIRA, D.; UAGODA, R. E. S. MENDES, L. C.; PUPIM, F. N. (2023) Sedimentary records in dry karstic valleys: The case of Mambaí, central Brazil. Journal of South American Earth Sciences 128: 104433. https://doi.org/10.1016/j.jsames.2023.104338

ROCHA A. B. A., BARBOSA V. R. F., FARIA K. M. S., MARTINS E. S., SOARES NETO G. B. (2022) Geomorphologic map of the Brasilian Cerrado by geomorphometric archetypes. Revista Brasileira de Geomorfologia 23(3): 1674-1684. https://doi.org/10.20502/rbg.v23i3.2132

SERAINE M., CAMPOS J. E. G., MARTINS-FERREIRA M. A. C., ALVARENGA C. J. S., CHEMALE JR F., ANGELO T. V., SPENCER C. (2021) Multi-dimensional scaling of detrital zircon geochronology constrains basin evolution of the late Mesoproterozoic Paranoá Group, Central Brazil. Precambrian Reserch 365: e106381. https://doi.org/10.1016/j.precamres.2021.106381

SOUZA J. R., CAVALCANTI NETO M. T. (2019) Espacialização das manchas de óleo e graxa na zona portuária de Natal – RN, através de técnicas de interpolação IDW e Krigagem. Holos 8: e9187. https://doi.org/10.15628/holos.2019.9187

TRAVASSOS L. E. P. (2019) Princípios de Carstologia e Geomorfologia Cárstica. ICMBio, Brasília.

ZANCOPÉ M. H. C., MOMOLI R. S., NUNES E. D., BAYER M., BUENO, G. T. (2023) Litoestruturas dobradas na dissecação da borda ocidental da Chapada do Alto Rio Maranhão, Planalto Central Goiano: o caso da Reserva Legado Verdes do Cerrado, Votorantim, Niqulândia/GO. Revista Brasileira de Geomorfologia 24(2): e2264. http://dx.doi.org/10.20502/rbg.v24i2.2264

Session 07

KARST HYDROGEOLOGY AND SPELEOGENESIS

Hypogene maze cave genesis in Irecê Basin, São Francisco Craton. Ioiô Cave, Bahia, Brazil

Philippe Audra (1), Luca Pisani (2), Marco Antonellini (2), Francisco Hilario R. Bezerra (3), Augusto S. Auler (4), Vincenzo La Bruna (3), Giovanni Bertotti (5), Fabrizio Balsamo (6), Cayo C.C. Pontes (3), Rebeca S. Lima (3), Marjan Temovski (7,8), Xianfeng Wang (9), Jo De Waele (2)

(1) Polytech'Lab UPR 7498, University Cote d'Azur, Nice, France, Philippe.AUDRA@univ-cotedazur.fr

(2) Bologna University, Department of Biological, Geological and Environmental Sciences, Italy, lucapiso94@gmail.com (corresponding author); marco.antonellini@unibo.it; jo.dewaele@unibo.it

(3) Programa de Pós-Graduação em Geodinâmica e Geofísica, Federal University of Rio Grande Do Norte, Natal, Brazil, bezerrafh@geologia.ufrn.br, vincenzolabruna@gmail.com, cayopontes@gmail.com, rebeca.seabra@hotmail.com

(4) Instituto Do Carste, Carste Ciência e Meio Ambiente, Belo Horizonte, Brazil, aauler@gmail.com

(5) Department geoscience engineering TU Delft, Netherlands, G.Bertotti@tudelft.nl

(6) University of Parma, Dep. of Chemical, Life and Environmental Sustainability Sciences, Italy, fabrizio.balsamo@unipr.it

(7) Isotope Climatology and Environmental Research Centre, ATOMKI, Debrecen, Hungary, temovski.marjan@atomki.hu

(8) Department of Mineralogy and Geology, University of Debrecen, Hungary

(9) Nanyang Technological University, Singapore, xianfeng.wang@ntu.edu.sg

Abstract

Ioiô Cave is a 4.7 km long maze cave in the south of the Irecê Basin (Bahia, Brazil). The earliest phases of carbonate alteration probably occurred during the Neoproterozoic Ediacarian deformation and Brasiliano orogeny. Deep rising hydrothermal fluids weathered the carbonates, creating dark ghost-rocks mainly in the anticlinal hinges and under the siliciclastic seals. Progressive exhumation of the carbonate reservoir favored meteoric water recharge of the aquifer, with sulfide oxidation at depth. The CO2 produced by Sulfuric Acid Speleogenesis rose along fractures and degassed at shallow depth, producing carbonic speleogenesis along the water table. This phase could be Plio-Quaternary, and possibly still active. This carbonic speleogenesis produced a maze network, by horizontal diffusion of aggressiveness from the feeders. Opening to the surface produced air flow activating degassing and supersaturation of the basins, with deposition of subaqueous calcite shelves, carved with bubble trails resulting from degassing by pyrite oxidation (localized SAS).

1. Introduction

Hypogene speleogenesis originating from rising flow and various deep-seated sources of aggressivity is at the origin of a minor part of known caves, compared to epigene caves, which are related to meteoric water infiltration and biogenic source of aggressivity from vegetation and soils (KLIMCHOUK et al., 2017, and refs. therein).

In the Irecê Basin and its vicinity many hypogene caves have been identified (KLIMCHOUK et al., 2016; CAZARIN et al., 2019; BALSAMO et al., 2020; BERTOTTI et al., 2020; SOUZA et al., 2021; PISANI et al., 2023). The hypogene speleogenesis phases were attributed to: the introduction of Si-rich fluids in deep-seated conditions during the late Proterozoic, to the Cambrian tectono-thermal event (~ 520 Ma), and to reactivation and hydrothermal events during the Pangea breakup (Jurassic-Cretaceous). Additionally, many caves have been subjected to late-stage SAS in shallow aquifer settings, resulting from the oxidation of sulfides contained in the carbonate beds (AULER & SMART, 2003).

We describe here the Ioiô Cave, a medium-sized (4.7 km long) maze. Thanks to its location at the SE edge of the basin where no allogenic runoff is present, original hypogene morphologies are still well-preserved. To understand its multiphase speleogenesis, we studied the structural context with detailed petrography and petrophysics, an early phase of ghost-weathering produced by rising deep fluids with specific mineralizations, the cave morphologies and speleothems.

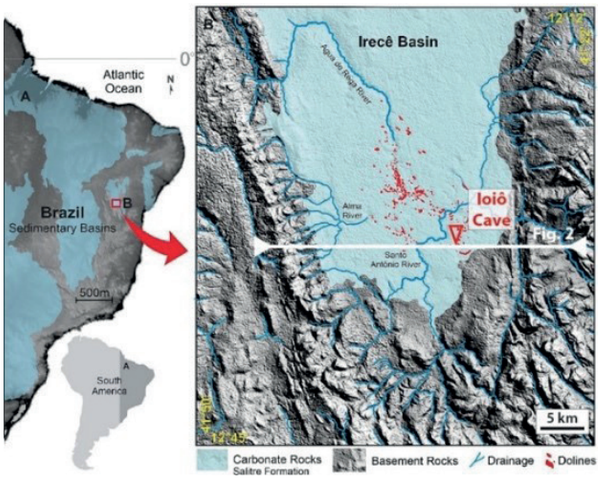

Figure 1: *Location of the of the Irecê Basin in the São Francisco Craton in Brazil (after MAIA et al., 2024)*

The Irecê Basin is located in the northern part of the São Francisco Craton, in the State of Bahìa (NE Brazil) (DE ALMEIDA et al., 2000) (Fig. 1).

It is composed of Neoproterozoic (670-600 Ma) carbonates of the Salitre Fm. (Una Group), overlying the Mesoproterozoic clastics of Bebedouro Fm. and the quartzites of the Chapada Diamantina Group. The basin formed due to extensional tectonics and subsidence that occurred during the fragmentation of the Rodinia supercontinent (ca. 950–600 Ma; D'ANGELO et al., 2019). The carbonate succession is 500 to 1000 m thick, made of laminated limestones with some intercalations of chert, siliciclastic, and heterolithic beds. A 2-phases contractional regime occurred during the late Brasiliano orogeny (ca. 650-510 Ma), creating E-W and NNE-SSW-verging folds and thrust belts. The most recent tectonic events during the Brasiliano orogeny (540-510 Ma) included some fissure magmatism and hydrothermal fluid flow along deep-rooted faults and fracture zones. Since the intensity of the contractional deformation decreased southward, in the southern tip of the Irecê Basin the Salitre Fm. is subhorizontal with only gentle, high-amplitude folds (PONTES et al., 2021) (Fig. 2).

Ioiô Cave (-12.393657°, -41.553533°, alt. 660 m) is located on the southern tip of the Irecê Basin, which displays as a low-lying plateau surrounded by quartzite ridges (Fig. 1). Together with the nearby Gruta do Impossível, it forms one of the most important fracture-guided maze systems of the area.

The Ioiô Cave opens at the bottom and northern margin of a large (ca. 100 m-wide semicircular) and 50 m-deep collapse doline. It develops in a well stratified carbonate sequence belonging to the Nova America Unit of the Salitre Fm. with very low permeability (0-7%, CAZARIN et al., 2019). The sequence is composed of dolomitized laminated carbonates with intercalation of sedimentary breccia and siltstone layers (PONTES et al., 2021). These less soluble siliciclastic units form seals on which the passage ceilings terminate. Bedding dips are very low (0 to 10°). The main passages develop along N-S, NW-SE, and NNW-SSE directed fold-related fracture corridors concentrated along anticline hinges in a 20-50 m module. Passages sometimes connect through almond-shaped windows separated by thin rock partings. Several large chambers are littered by collapse blocks. Most passages pinch out moving away from the main chambers. Most of the cave develops just above the water table as dry passages with rocky floor or thin sediment cover. Several lakes are present as large and deep rifts. Cave transverse profiles result in various combinations of almond shaped passages and rifts. In some places there are large domes of red soil seeping from the surface through fissures. Some ceiling cupolas show apatite crusts, produced by bat guano and urine. No alluvial sediments are present. In at least four areas, the walls show dark brown ghost-rock halos intersected by quartzite and dolomite veins.

These veins show a weathering halo of up to 30 cm thick. Their orientation cuts the cave passages at a slightly oblique angle, without having influenced the direction of karst development (Fig. 3).

The lakes are clearly associated with the feeders that extend at depth (Fig. 3). The main lake develops along a fracture for almost 100 m in length. It is over 27 m deep and the floor is not visible. The underwater V-shaped walls converge at about 12 m water depth to a 2 m-wide rift, then widens again. The submerged walls seem to be intensely corroded and the lake has no deposits except for calcite rafts.

Calcite rafts and re-sedimented calcite crystals (sand) are present in the dry entrance passage. Old hardened calcite rafts occur on perched terraces at 2 m height above present lake levels along the gallery, marking a recent higher water table, now probably lowered due to overexploitation of the aquifer; this high-water level roughly corresponds to the largest notch carved along the cave walls. At the same height, there are perched shelves of subaqueous calcite, the lower one carved by micro-bubble trails, which combine upwards in rising channels. These subaqueous calcite shelves, extend about 100 m on both sides of the lakes. On the higher shelves there are many hollow hardened raft cones, corroded on the inside by dripping. All lakes are covered with calcite rafts which accumulate on the shores; an island of calcite sand stands 2 m above the water.

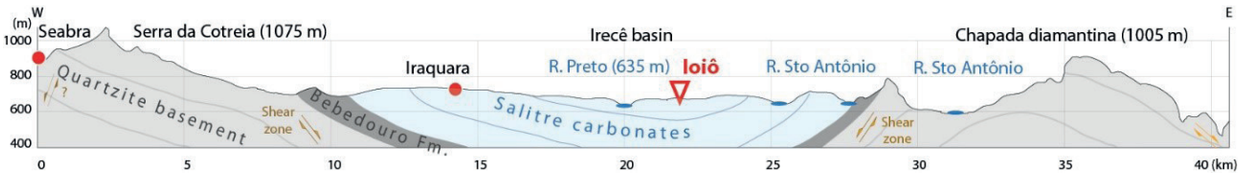

Figure 2: *Geological profile of the study area (indicated on Fig. 1). Vertical scale is exaggerated (after LAUREANO et al., 2014)*

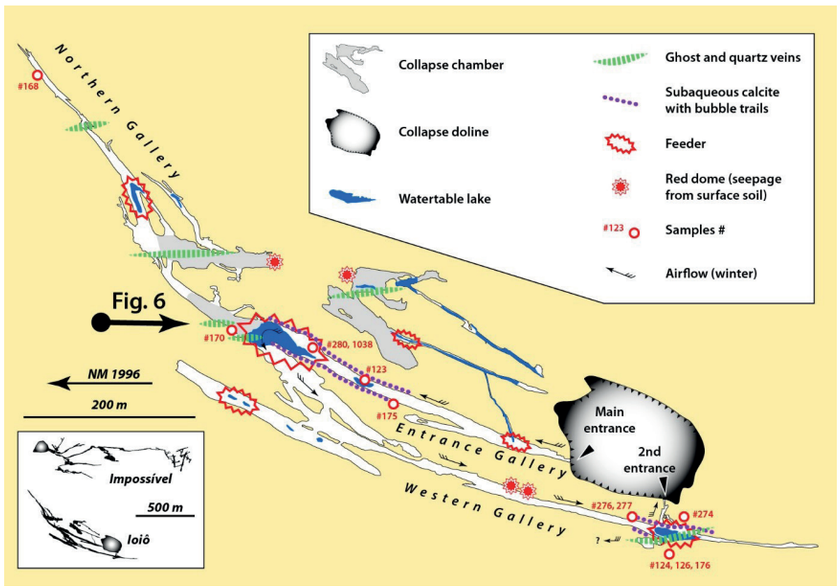

Figure 3: *Plan view of Ioiô Cave. The inset shows the outline of both Ioiô and Impossível caves. Samples location and main observed features are indicated. Cave map courtesy of Grupo Bambuí de Pesquisas Espeleológicas.*

2. Material and methods

Hand samples were collected for analyses (location on Fig. 3). Evaporation calcite was sampled for stable isotopes (18O, 13C) measurements: calcite sand accumulation under dripping zones (#123, 1038), and calcite rafts along the lake shores (#274, 280) where water temperature and specific electric conductivity were 24.5°C and 309 µS/cm, respectively. Four speleothem samples were sampled for U-series dating, two corroded subaqueous calcite linings (#175, 277) and two mammillary calcites carved with bubble trails (#124, 176). A sample of dark brown clay (#276) was collected in Western Gallery. Three brown bulk samples were taken from ghost-weathered zones: at the end of the W Gallery (#126), at the end of N Gallery with a crystallized dolomite core (#168), and beyond the first lake a silicified one with quartz (#170).

Structural analysis was carried out to characterize the type, kinematics, relative timing, and infilling material of the fractures. The cave pattern and morphological features were analyzed. XRD-XRF analyses were performed on selected cave sediments at the LTG-ER Laboratory, Natal, Brazil and Escola Politécnica da Universidade de São Paulo. Carbon and oxygen stable isotope composition of evaporative calcite were carried out at the Institute for Nuclear Research in Debrecen, Hungary. Uranium-series dating of subaqueous pool calcite was performed at Nanyang Technological University, Singapore.

3. Results

New high-resolution field structural measurements were taken (Fig. 4, location on Fig. 3). A persistent fracture zone, composed of open-mode N-S fractures, was documented along the central/axial portion of the cave conduit. A major and six minor faults striking NW-SE were also documented and display an oblique right lateral kinematic abutting against the aforementioned N-S fracture zone. A NNE-SSW striking joint set abuts against these NW-SE striking faults. Two sets of veins were measured (NW-SE and WNW-ESE), the second one cutting across the NW-SE faults and the NNE-SSW joint set.

Calcite sand and rafts (#123, 274, 280, 1038) show very similar stable isotope composition, with mean δ18O VPDB of -5.03±0.05‰ and δ13CVPDB of 7.83±0.29‰. SEM images of calcite sand (#123) show minute crystals made of blocky (bi)pyramidal rhombohedrons. The oldest corroded subaqueous calcite lining (#175, 277) yielded similar ages of 186.3 ± 3 and 191.5 ± 1.6 ka, whereas the fresher-looking calcite shelves (#124, 176) carved with bubble trails are younger (125.0 ± 4.7 and 87.0 ± 8.1 ka).

The ghost rock areas are composed of brown halos (#126, 168a, 170) cut by silica veins. #168b is made of a dolomite core with spongy silica overgrowth. The brown halo around the silica veins or the dolomite core is composed mainly of Fe and Mn oxides (up to 30% and 8%, respectively), secondary silica (up to 7%), and carbonates.

The SEM image shows bunches of cylindrical sticks (#170). In addition to Fe-Mn, metallic elements are present as traces (Ba, Cr, Al, Na, K, Sr), however with some significant concentrations of Cu (10%, #170) and Ta (5%, #168a) for some samples. EDS mapping shows a diffuse distribution of any element. The ghost halo is generally very hard with various degrees of alteration ("argillitic" brown halos or recrystallization). Finally, the dark brown mud observed on some pavements (#276) is composed of dominant silica, kaolinite, Fe oxides, Ca-Mg, and traces of PO4.

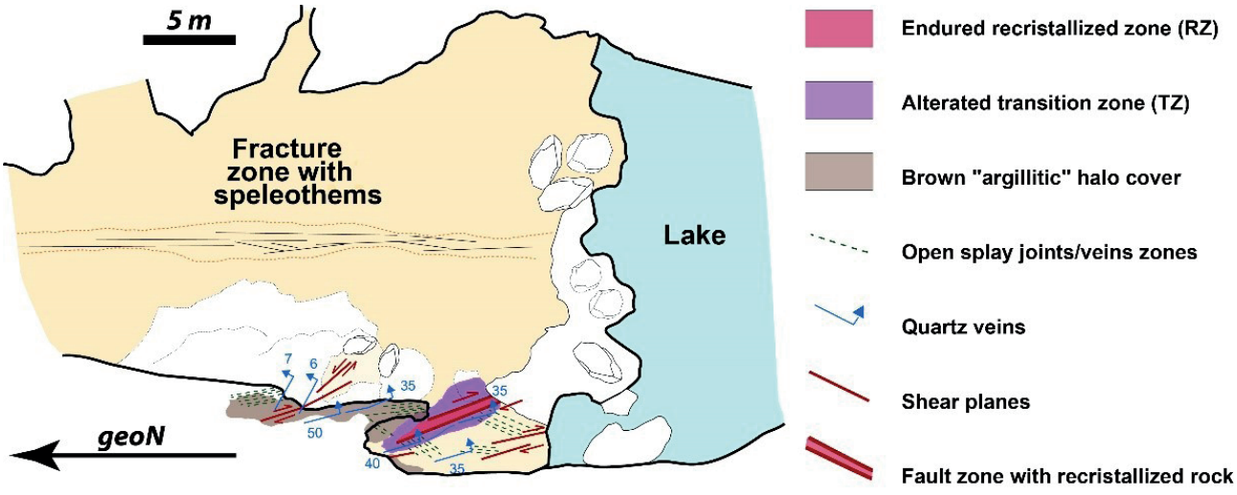

Figure 4: *Structural plan view of the zone after the lake (area located on Fig. 3).*

4. Discussion

A relative chronology could be reconstructed for the documented structural assemblage. The present conceptual model (Fig. 5) is characterized by four main stages or structural assemblages: (i) The first stage (Fig. 5a and e1) is associated to the background structural network documented by PONTES et al. (2021), and is composed of two stratabound and non-stratabound fracture sets respectively striking N-S and E-W; (ii) The second structural assemblage (Fig. 5b and e2) could be related to the Ediacaran contractional event (CRUZ & ALKMIM, 2007) and consists of a gentle folding which determined a N-S persistent through-going/non-stratabound fracture zone along the cave roof; (iii) The third stage (Fig. 5c and e3) is associated with N-S compression (D'ANGELO et al., 2019) that determined the development of a NW-SE striking right-lateral fault, and NNE-SSW to NE-SW striking tail joints localized at the fault extensional quadrants; (iv) Finally, the fourth structural assemblage (Fig. 5d and e4) is associated with the WNW-ESE striking quartz vein that cuts across the whole pre-existing structural assemblage.

The first phase of carbonate alteration produced dark-brown ghosts (with alteration halos) associated with veins of dolomite and quartz. Enrichment in Fe-Mn oxides and metals (Cr, Al, K, Cu, Ta...) reveals deep-seated fluid circulation, probably hydrothermal. Ta in unusual concentration (5%) is probably in the form of tantalite [(Fe,Mn)(Ta,Nb)2O6]. The origin of this element is generally associated with pegmatite veins surrounding plutons. Its occurrence in carbonates may be linked to the rising flow of acid magmatic fluids during the final stage of pegmatization, possibly during the Brasiliano orogeny. Finally, silica enrichment was acquired during migration through the quartzite and siliciclastic basement (BERTOTTI et al., 2020; LA BRUNA et al., 2021; PISANI et al., 2023).

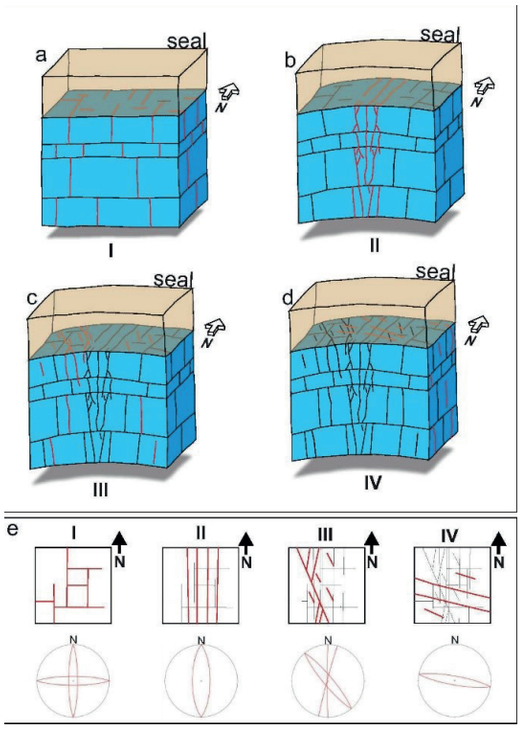

Figure 5: From (a) to (d) idealized block diagrams showing the overall structural assemblage evolution of the studied rock sequence. (e) from I to IV the documented structural assemblage sketched at a map view with the lower hemisphere projection of the fracture planes.

In such massive carbonate series, this initial phase of ghost-weathering concentrated along fractures, higher porosity-permeability beds, and below siliciclastic seals, prepared the reservoir for the second fluid flow phase at the origins of the conduits.

The geomorphological observations and cave deposits suggest a hypogene origin.

Parallel conduits connected by almond-shaped windows show development by expansion around the feeders, and limited linear development with abrupt terminations away from sources of aggressiveness.

Conduits running strictly along the water table, with no extension in height or depth apart from the punctual feeders, suggest development by CO2 degassing, diffusing aggressiveness laterally around the feeders.

As for the origin of the CO2, considering that the cave system is of "recent" formation (i.e. around Pliocene, LAUREANO et al., 2016), due to its adaptation to the water table controlled by the level of the Rio Santo Antônio, gaseous upwelling of deep origin is unlikely, although still possible as a minor contribution. The main source is to be found in the sulfides (mainly pyrite) present in abundance in the carbonate interval (AULER & SMART, 2003). Meteoric recharge of the aquifer thus enabled sulfide oxidation and the development of sulfuric acid speleogenesis (SAS) at depth (Fig. 6). Sulfate by-products contribute to the high ionic concentrations in the aquifer, while CO2 rises to the surface through large fractures. Maximum degassing occurs at shallow depth resulting in the expansion of conduits along the water table. The hyper-corroded walls of the Ioiô feeders, with no trace of carbonate deposits, suggest that attenuated carbonic degassing could still be active. Underwater calcite shelves carved by bubble trails are found above lakes, as well as in dry pools with associated calcite raft cones. Corrosion of the pool walls is produced by the oxidation of pyrites from the host rock in contact with water, which produces sulfuric acid and CO2 degassing. The sulfate by-products in solution and the ventilation of the conduit that favors CO2 degassing, lead to a high level of saturation in the pools and to crystallization as calcite rafts. Condensation drops falling from ceiling pendants focus the sinking of calcite rafts, which accumulate and gradually build calcite cones. This is a process of Sulfuric Acid Speleogenesis (SAS), localized in pools supersaturated by ventilation and sulfates, with a paradoxical neighboring area of strong corrosion as shown by the bubble trails. U/Th dating reveals at least two major periods of subaqueous calcite shelf development, during Marine Isotope Stages (MIS) 6e, 5e, and 5b. Some features are currently active.

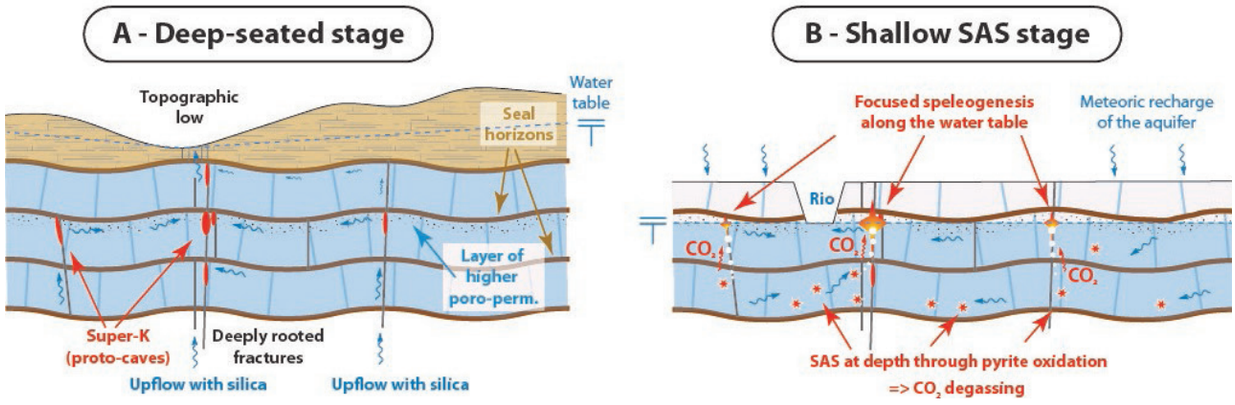

Figure 6: Conceptual model of hypogene speleogenesis. A) Deep-seated stage ending with late Brasiliano orogeny. Silica-rich Fluids rise along fractures and concentrate on anticline hinges below siliciclastic seals, producing ghost halos enriched in metallic mineralizations. Note that the cover thickness is not to scale, and probably very thick. B) Shallow SAS stage. Erosion of the cover and infiltration of meteoric water produces pyrite oxidation in the aquifer. CO2 rises along fractures and degassing below the water table enlarges rifts as feeders. Speleogenesis focuses along the water table by expansion of horizontal conduits. When they intersect older ghosts, dramatic enlargement produces large chambers and collapse dolines.

5. Conclusion

The study of the Ioiô Cave has made it possible to characterize the main karstification phases of the carbonate reservoir of the Salitre Fm. of the Irecê basin.

1) During the Neoproterozoic, carbonates underwent several stages of fracturing and deformation during the Ediacaran and under the stresses of the Brasiliano orogeny. Deep fluids, probably hydrothermal, loaded with silica as they pass through the siliciclastic and quartzite bedrock, rise through these fractures. They weathered the carbonates into dark brown halos concentrated in the anticlinal hinges and under the siliciclastic seals.

2) These weathered zones are enriched in quartz veins, dolomite geodes, Fe-Mn oxides and metallic elements. The source of Na-Ba-Sr-Mn is thought to correspond to sulfides present in abundance in the carbonate interval, while Cr, Al, K and Cu have a deeper origin. In particular, the high Ta concentration (5%) is associated with acid fluids from the final pegmatization stage of the basement.

3) Progressive exhumation of the carbonate reservoir favored meteoric water recharge of the aquifer, and sulfide oxidation with Sulfur Acid Speleogenesis (SAS). The CO2 produced rose along the fractures and degassed at shallow depth, producing carbonic speleogenesis along the water table. By affinity with nearby dated sites, this phase could be Plio-Quaternary, and possibly still active.

4) This carbonic speleogenesis produced a maze network, by horizontal diffusion of aggressiveness from the feeders. Conduit cross-sections are rifts or almond-shaped, depending on the combination of fracture and petrographic control. Crosscutting of ancient ghosts favored the widening of conduits into collapse chambers and dolines. Opening to the surface produced air currents activating degassing and supersaturation of the basins, with deposition of subaqueous calcite shelves, carved with bubble trails resulting from CO2 degassing related to pyrite oxidation in the basins (localized SAS). U/Th dating attests to at least 2 phases of shelve deposition, during MIS 6 and 5. Surface soils seeped along the fractures forming “red domes”.

6) The sub-actual phase is limited to the deposition of calcite sand and rafts by evaporation produced by winter air flows, biocorrosion by bat colonies lining cupolas with apatite and phosphate-rich guano deposits, and frequentation by present-day or Holocene troglophile species.

The Ioiô cave thus appears to be a major site for studying multi-phase creation of permeability by karstification of a carbonate reservoir. Precise dating of the Neoproterozoic veins, and further characterization of the sources of metallic enrichment of the weathering halo of the ghosts, would enable us to better constrain the modality of development of the pre-salt reservoirs of the Salitre Fm.

Acknowledgments

This research was carried out in the frame of the R&D project ANP 20502-1, “Processos e Propriedades em Reservartórios Carbonáticos Fraturados e Carstificados – POROCARSTE 3D” (UFRN / UNB / UFRJ / UFC / Shell Brasil / ANP) – Porokarst – Processes and Properties in Fractured and Karstified Carbonate Reservoirs, sponsored by Shell Brasil under the ANP R&D levy as “Compromisso de Investimento com Pesquisa e Desenvolvimento”. The cave survey was kindly provided by Grupo Bambuí de Pesquisas Espeleológicas. Cave sampling was performed through SISBIO permit 63178/1. Many thanks to Alisson Jordão, Uilson Teixeira and Vicente Antonio do Nascimento for helping during fieldwork. We sincerely thank landowners and the Brazilian Federal Environmental Agency, Inst. Chico Mendes, for providing the access to the cave and permission for sampling.

References

AULER A.S., SMART P.L. (2003) The influence of bedrock-derived acidity in the development of surface and underground karst: evidence from the Precambrian carbonates of semi-arid northeastern Brazil. Earth Surface Processes and Landforms 28(2):157-168. https://doi.org/10.1002/esp.443

BALSAMO F., BEZERRA F.H.R., KLIMCHOUK A.B., CAZARIN C.L., AULER A.S., NOGUEIRA F.C., PONTES C.C.C. (2020) Influence of fracture stratigraphy on hypogene cave development and fluid flow anisotropy in layered carbonates, NE Brazil. Marine and Petroleum Geology, 114:104207. https://doi.org/10.1016/j.marpetgeo.2019.104207

BERTOTTI G., AUDRA P., AULER A.S., BEZERRA F.H., DE HOOP S., PONTES C.C.C., PRABHAKARAN R., LIMA R. (2020) The Morro Vermelho hypogenic karst system (Brazil): Stratigraphy, fractures, and flow in a carbonate strike-slip fault zone with implications for carbonate reservoirs. AAPG Bulletin 104(10):2029-2050. https://doi.org/10.1306/05212019150

CAZARIN C.L., BEZERRA F.H., BORGHI L., SANTOS R.V., FAVORETO J., BROD J.A., AULER A.S., SRIVASTAVA N. K. (2019) The conduit-seal system of hypogene karst in Neoproterozoic carbonates in northeastern Brazil. Marine and Petroleum Geology 101:90-107. https://doi.org/10.1016/j.marpetgeo.2018.11.046

CRUZ S.C.P., ALKMIM F.F.D. (2007) A história de inversão do aulacógeno do Paramirim contada pela Sinclinal de Ituaçu, extremo sul da Chapada Diamantina. Rev. Bras. Geociencias 37:92–110.

D’ANGELO T., BARBOSA M.S.C., DANDERFER FILHO A. (2019) Basement controls on cover deformation in eastern Chapada Diamantina, northern São Francisco Craton, Brazil: insights from potential field data. Tectonophysics 772:228231. https://doi.org/10.1016/j.tecto.2019.228231

DE ALMEIDA F.F.M., DE BRITO NEVES B.B., DAL RÉ CARNEIRO C. (2000) The origin and evolution of the South American platform. Earth Sci. Rev. 50:77-111. https://doi.org/10.1016/S0012-8252(99)00072-0

KLIMCHOUK A.B., AULER A.S., BEZERRA F.H., CAZARIN C.L., BALSAMO F., DUBLYANSKY Y. (2016) Hypogenic origin, geologic controls and functional organization of a giant cave system in Precambrian carbonates, Brazil. Geomorphology 253:385-405. https://doi.org/10.1016/j.geomorph.2015.11.002

KLIMCHOUK A., PALMER A.N., DE WAELE J., AULER A., AUDRA P. (Eds.) (2017) Hypogene karst regions and caves of the world. Springer, Cham, 911 pp. https://doi.org/10.1007/978-3-319-53348-3_1

LA BRUNA, BEZERRA F.H.R., SOUZA V.H., MAIA R.P., AULER A.S., ARAUJO R.E.B., CAZARIN C.L., RODRIGUES M.A.F., VIEIRA L.C., SOUSA M.O.L. (2021) High-permeability zones in folded and faulted silicified carbonate rocks – Implications for karstified carbonate reservoirs. Marine and Petroleum Geology, 128, 105046. https://doi.org/10.1016/j.marpetgeo.2021.105046

LAUREANO F.V., KARMANN I., GRANGER D.E., AULER A.S., ALMEIDA R.P., CRUZ F.W., STRÍCKS N.M., NOVELLO V.F. (2016) Two million years of river and cave aggradation in NE Brazil: Implications for speleogenesis and landscape evolution. Geomorphology 273:63-77. https://doi.org/10.1016/j.geomorph.2016.08.009.

MAIA R.P., AULER A.S., BEZERRA F.H., BORGES S.V., LA BRUNA V., PUJONI D., dos SANTOS E.E., VIDAL, A.C. (2024) Fluid flow zones along fracture corridors inferred from collapse dolines in carbonates of the Irecê Basin, Brazil. Earth Surface Processes and Landforms, 49(13), 4506-4522. https://doi.org/10.1002/esp.5951.

PISANI L., KOLTAI G., DUBLYANSKY Y., KLEINE B. I., WHITEHOUSE M. J., SKRZYPEK E., CARBONE C., SPÖTL C., ANTONELLINI M., BEZERRA F.H., DE WAELE J. (2023) Hydrothermal silicification and hypogene dissolution of an exhumed Neoproterozoic carbonate sequence in Brazil: Insights from fluid inclusion microthermometry and silicon-oxygen isotopes. Basin Research 35(3):1102-1127. https://doi.org/10.1111/bre.12748

PONTES C.C.C., BEZERRA F.H.R., BERTOTTI G., LA BRUNA V., AUDRA P., DE WAELE J., AULER A.S., BALSAMO F., DE HOOP S., PISANI L. (2021) Flow pathways in multiple- direction fold hinges: implications for fractured and karstified carbonate reservoirs. J. Struct. Geol:146, 104324 https://doi.org/10.1016/j.jsg.2021.104324.

SOUZA V.H., BEZERRA F.H., VIEIRA L.C., CAZARIN C.L., BROD J.A. (2021). Hydrothermal silicification confined to stratigraphic layers: Implications for carbonate reservoirs. Marine and Petroleum Geology 124:104818 https://doi.org/10.1016/j.marpetgeo.2020.104818.

Speleogenesis of Gap-Gotan (Cupp-Coutunn) cave system, Köýtendag massif, Turkmenistan

Philippe Audra (1), Gaël Cazes (2), Xavier Robert (3), Lionel Barriquand (4), Yuri Dublyansky (5), Gabriella Koltai (5), Marjan Temovski (6,7), Victor Polyak (8), Cristina Carbone (9), Vasile Heresanu (10), Jean-Pierre Gruat (11), Jo De Waele (12)

(1) Polytech'Lab UPR 7498, University Cote d'Azur, Nice, France, Philippe.AUDRA@univ-cotedazur.fr (corresponding author)

(2) Geosciences Montpellier, UMR5243, Université de Montpellier, France, gael.cazes@umontpellier.fr

(3) Institut des Sciences de la Terre (ISTerre), University Grenoble Alpes, University Savoie Mont Blanc, CNRS, IRD, IFSTTAR, Grenoble, France, xavier.robert@univ-grenoble-alpes.fr

(4) University Savoie Mont Blanc, EDYTEM, UMR 5204, Le Bourget-du-Lac, France, lionel.barriquand@univ-smb.fr

(5) Institute of Geology, University of Innsbruck, Austria, yuri.dublyansky@uibk.ac.at, gabriella.koltai@uibk.ac.at

(10) HUN-REN Institute for Nuclear Research (ATOMKI), Debrecen, Hungary, temovski.marjan@atomki.hu

(11) Department of Mineralogy and Geology, University of Debrecen, Hungary

(8) Department of Earth and Planetary Sciences, University of New Mexico, Albuquerque, USA, polyak@unm.edu

(9) Department of Earth, Environmental and Life Sciences (DISTAV), Genoa University, Italy, cristina.carbone@unige.it

(10) Interdisciplinary Nanoscience Centre of Marseille (CINaM), CNRS – Aix Marseille University, France, vasile.heresanu@cnrs.fr

(11) Alpina Millau, France, bouysse67@yahoo.fr

(12) University of Bologna, Department of Biological, Geological and Environmental Sciences, Bologna, Italy, jo.dewaele@unibo.it

Abstract

The Gap-Gotan (Cupp-Coutunn) system (Turkmenistan) is known for its mineralogical wealth, thanks to the considerable work carried out by Vladimir Maltsev in the 80s. However, following fieldwork carried out in 2024, Maltsev's speleogenetic hypotheses have been revised, in terms of stages, chronology and processes. Several phases of speleogenesis can be identified. 1) Hydrothermal mineralizing fluids, leading to Pb-Zn deposits in the vicinity, and impregnation of the host rock with sulfides, fluorite, and calcite veins. 2) The formation of large horizontal phreatic conduits at shallow depth, fed by infiltration at high altitude, with dissolution produced by flows reacting with the sulfides in the host rock. This process has been repeated in stages as the base level fell, until the present day. Nowadays similar active phreatic conduits are presumed to exist beneath the gypsum collapses. 3) Once drained, the caves are decorated with gypsum speleothems mainly formed by sulfate-rich seepage from the surface (e.g., chandeliers), and filled with fluvial sediments injected locally from canyon sinkholes. Mapping, isotopic and mineralogical analyses, and U-series and U-Pb dating of the sediments are providing preliminary evidence for this model of speleogenesis in these unique and exceptional caves.

1. Introduction

The Köýtendag (or Kugitangtau) massif (Köýtendag meaning "mountain of canyons" in Tajik language) is the final western part of the larger Pamir-Alaï mountain range, located in the extreme southeast of Turkmenistan, forming the border with Uzbekistan. To the south the massif is bounded by the Amu Darya, a river that forms the border with Afghanistan, flowing at an altitude of around 260 m asl. To the west the massif is bounded by the Köýtendarya (a small tributary of the Amu Darya), fed by the numerous springs (often located in canyons) that dot the foot of the mountains. From the river, the plain rises slowly eastward reaching 350 m at the foot of the slope, then rising steadily culminating at the highest summit (Mt. Airibaba, 3138 m asl). On the Turkmenistan side, the western slopes of the Köýtendag are carved by over 100-m-deep (the deepest one reach 700 m!) and often dry meandering canyons, disrupting the longitudinal continuity of the slope. The climate is arid, with mean annual air temperatures in the plain between 5 and 30°C (down to -20°C in winter and up to 49°C during summer), and annual precipitation of ca. 120 mm in Köýtendag village, generally during winter and falling as snow at higher altitudes.

The massif is made of Upper Jurassic limestones (Callovian-Oxfordian) of the Kugitang Formation, reaching a thickness of over 400 m and characterized by reef limestones, grading upwards into more marly limestones and finally dolomitic limestones (Fig. 1).

Locally these limestones are slightly metamorphized and silicified, containing bituminous patches which may have contributed to the karstification (MALTSEV, 1997). The Kugitang limestones are covered in continuous sedimentation by 200 m of the Gowurdak (or Gaurduck) evaporites (gypsum) of Upper Jurassic (Kimmeridgian-Tithonian). These evaporites were spared from erosion on the lower slopes only. Adjacent to the massif in the footplains, the Garlyk mine exploits potash, and sulfur is extracted at Gowurdak (now called Magdanly). These evaporites are covered by green marls and red sandstones, forming superb ravine landscapes on the western slope of the Köýten valley. Finally, Neogene deposits fill the surrounding basins.

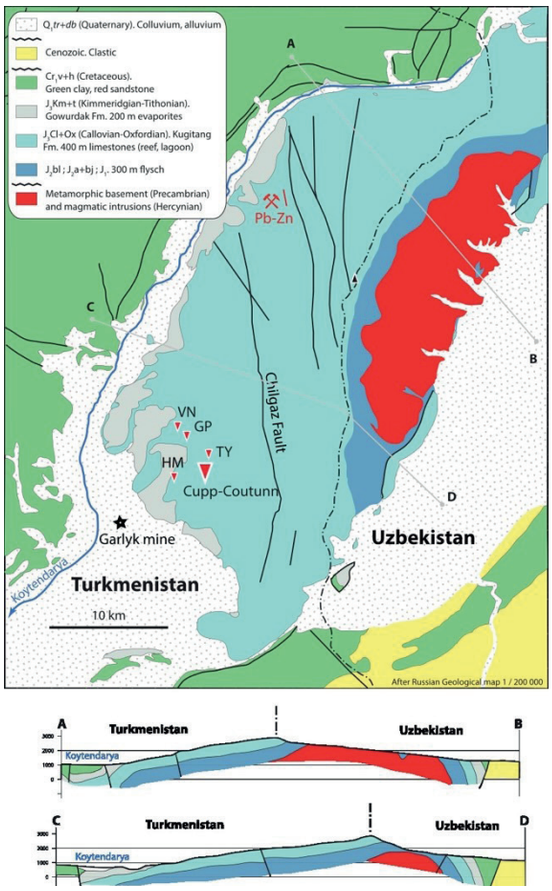

Figure 1: *Geological sketch map and cross-sections of the Köýtendag region (after Russian Geological map, scale 1:200,000). Red triangles indicate the caves: TY=Tush-Yurruck, HM=Hashim-Oyuk, GP=Geophysicalskaya, VN=Vertikalnaya.*

Köýtendag is an asymmetrical anticlinal dome, with gentle dips (approx. 7°) on its western (Turkmen) side. It is cut by large N-S oriented faults, the biggest of which, the Chilghaz Fault, divides the plateau into two morphological "steps". These N-S faults formed during the early phases of uplift. To the north, mines exploited Pb-Zn deposits in veins on one of these faults. Other secondary NW-SE and E-W faults play a role in organizing the cave systems located south (in the Gap-Gotan area). The massif was uplifted in several phases, from the beginning of the Tertiary (Paleocene) to the Middle Quaternary (MALTSEV & KORSHUNOV, 1998).

Surface karst morphologies are very scarcely developed on the limestones, given the arid climate, and the canyons appear to be related to past wetter climate. Underground karst development is active below the evaporites in the lowlands, as shown by large collapse sinkholes dotting the gypsum plains, testifying to important underground water flow fed by the mountains. This is not surprising, since the same limestones are the main reservoir rocks for the important gas and oil fields of Turkmenistan to the west, fed by the underlying marls (flysch) of Middle Jurassic (Bathonian-Bajocian) age. These marls are 300 m thick and interlayered with some volcanic strata. This sedimentary sequence overlies unconformably Precambrian metamorphic rocks composed of gneiss, and a large Hercynian granitic batholith [MALTSEV & SELF, 1992].

2. Previous studies

Besides the importance of the mountainous landscape, the Köýtendag massif is known for its marvelous caves, the most famous of which is Gap-Gotan (or Cupp-Coutunn Cave System, the junction of Gap-Gotan and Promeszutochnaya). This 56 km-long system, studied mainly by Vladimir Maltsev (1980-2000), is renowned for its minerals, with more than 30 identified species, some of which very rare, and for its extraordinary gypsum formations (chandeliers, hollow stalagmites, etc.), similar to those of Lechuguilla Cave in New Mexico (USA). Cupp-Coutunn Cave is listed as one of the most beautiful and interesting in the world (HILL & FORTI, 1997; MALTSEV, 1997). Besides Gap-Gotan, several other important underground systems were explored by Russians, including Hashim-Oyuk, Tush-Yurruck, Gulshirin (or Geophysicalskaya), and Vertikalnaya (Fig. 1). Based on his analysis, Maltsev identified 3 phases of development. A first deep phreatic phase, of Upper Cretaceous age, forming the labyrinthic maze, followed by clogging of the conduits by clays. The second phase results from the uplift of the massif during the Plio-Quaternary during which thermal and sulfidic waters rose into the cave system, truncating and exposing the first phase of mineralization (fluorite, sulfides, etc.). The third and final phase, still active, sees a continuation of mountain uplift, exposing part of the conduits, which now evolve in dry conditions. This latest phase is characterized by the oxidation of sulfides generating sulfuric acid and the typical associated secondary mineralization (mainly sulfates). Maltsev recognized that the evolution of karst continues at depth in drowned and partially blocked conduits, as revealed by the large collapse sinkholes in the evaporites, and by the presence of sulfate-rich springs near the foot of the slope.

3. Methods

To fill the lack of precise topographic data, several caves (Hashim-Oyuk (5.4 km), Tush-Yurruck (3.6 km), Geophysicalskaya (3.9 km), and Vertikalnaya (0.55 km)) were completely re-surveyed during the French speleological expedition "Koytendag 2024" (AUDRA et al., 2024). In the large Cupp-Coutunn-Promeszutochnaya Cave System, we measured the main center- and polygon line between the different entrances, and of the main cave branches. This enabled us to orthorectify the Russian survey of the 80-90s, and verify the altitudes of the different cave levels. Topographic data were processed with the Therion software (https://therion.speleo.sk/), allowing visualizations in 3D (https://github.com/robertxa/Turkmenistan).

A general geological and geomorphological mapping of the cave conduits and their mesomorphology, as well as more detailed surveys of significant sectors have been carried out with the objective of

associating the forms with different evolutionary phases of the caves (epigenic, hypogene, phreatic, hydrothermal, sulfuric, later condensation-corrosion, leaching of overlying evaporites), in order to specify the conditions specific to each phase.

Although mineralogy was largely performed by Maltsev in great detail, we have carried out mineralogical analyses (XRD, SEM) of the mineral associations sampled in most caves. Primary and secondary minerals can provide new information on their formation in relation to that of the caves and their environment.

Dating (U-series and U/Pb of gypsum and carbonate speleothems, 40Ar/39Ar of the by-products of sulfuric acid speleogenesis, etc.) will make it possible to better constrain the age of the different cave-forming phases and to link these to tectonic and paleoclimatic events.

An evaluation of the groundwater flow, physical (temperature, conductivity), and chemical (dissolved ions and notably sulfates) characteristics aimed to provide a better understanding of the karst aquifer.

Stable isotopes of oxygen and carbon, coupled with dating, provide insights into the climatic (temperature and precipitation) and environmental (vegetation) evolution during carbonate speleothem deposition. Sulfur and oxygen stable isotopes, on the other hand, will allow to get a better idea of the provenance of the sulfur in the secondary sulfates, sulfides (galena, pyrite) and in the water.

4. Preliminary results

4.1. Cave surveys and morphology

The most important caves are located in the southwestern tip of the Köýtendag range, in a military area, west of the major N-S Chilghaz Fault (Fig. 1). In this so-called “Lower Plateau” the upper beds of the Kugitang Fm. limestones crop out, covered with patches of the overlying gypsum rocks of the Upper Jurassic Gowurdak Fm. Most caves are cut by the deep canyons crossing this area, and do not appear to have a direct connection with the present-day surface morphology. Only Hashim-Oyuk opens up in the surface plateau in between canyons, as a collapse doline descending into a large labyrinthic network of galleries.

The new surveys show that the location of the cave conduits in the entire Cupp-Coutunn area is almost entirely controlled by the heterogeneities present in the rock mass (fractures, joints, bedding planes, petrographical changes with presence of more or less permeable beds), and by the position of the water table which controlled the altitude of the main underground drainage.

The Jurassic limestones of the Kugitang Fm. comprise thin beds at the top with thin marly intercalations, passing downward to thick beds separated by levels of green clay, some several cm thick. These lithological discontinuities played a major role in the location of the proto-conduits (Fig. 2). They also served as separation surfaces in later stages of cave development.

Figure 2: A typical lens-shaped cross-section in Geophysicalskaya, following a less resistant bedding plane surface. The cave walls are stained dark red because of the weathering residue known as “okher”, contrasting with the white calcite speleothems (Photo Philippe Crochet).

A significant part of the conduits follows the bedding planes with an average of 7° towards the SW (220-230°), in the direction of the dip, or obliquely to it.

On the other hand, many cave conduits develop horizontally, and record the altitudinal position of ancient base levels (i.e. water table) at the time of their formation (AUDRA & PALMER, 2015). Six main levels (or stages) have been identified in the study area (Fig. 3). Four of these levels are widely represented at current altitudes of 880, 800, 600, and 500 m, whereas two secondary levels were detected at 850 and 750 m (Fig. 3).

4.2. Speleothems and minerals

The caves around Cupp-Coutunn are known for their beautiful gypsum speleothem decorations and for their mineralogical variety (MALTSEV, 1997). Among common cave minerals, occurring in various typical forms, such as the carbonates aragonite, calcite, hydromagnesite, huntite and the rare (for caves) dolomite, siderite, cerussite and ankerite, and the sulfates including gypsum, celestite, barite, jarosite, epsomite, and thenardite, sometimes accompanied by native sulfur, of special interest are the silicates chrysotile, lizardite, and the very rare fraipontite and sauconite. Also, violet fluorite occurs in several caves and points to a thermal origin, as shown by fluid inclusion studies (MALTSEV & SELF, 1992; MALTSEV & KORSHUNOV, 1998). This fluorite is probably contemporary with corroded and old thermal calcite spar that has been found in many caves of the area and appears to predate the main cave enlargement phase. In some caves the yellow radioactive mineral tyuyamunite has been found.

4.3. Sulfur isotopes

We analyzed the sulfur isotopic composition ($\delta^{34}S$ and $\delta^{18}O$) of the Upper Jurassic Gowurdak gypsum rocks outcropping above the caves, of the sulfates in the waters at several springs (among which the main Gaynar Baba springs considered to be the main outlet of the active karst system), and of gypsum crusts, chandeliers and needles sampled in different caves. The mean isotope values for the Jurassic gypsum rocks were +15.7 ‰ (relative to VCDT) and +6.7 ‰ (relative to VSMOV) for $\delta^{34}S$ and $\delta^{18}O$ respectively, not very different from that of the secondary gypsum speleothems in the caves (+13.9 ‰ and +8.3 ‰, respectively), the two celestine samples (+15.3 ‰ and +9.7 ‰, respectively) and the sulfidic waters at the springs (13.0 ‰ and 8.0 ‰, respectively). Galena sampled in an abandoned mine gave a $\delta^{34}S$ value of +4.3 ‰.

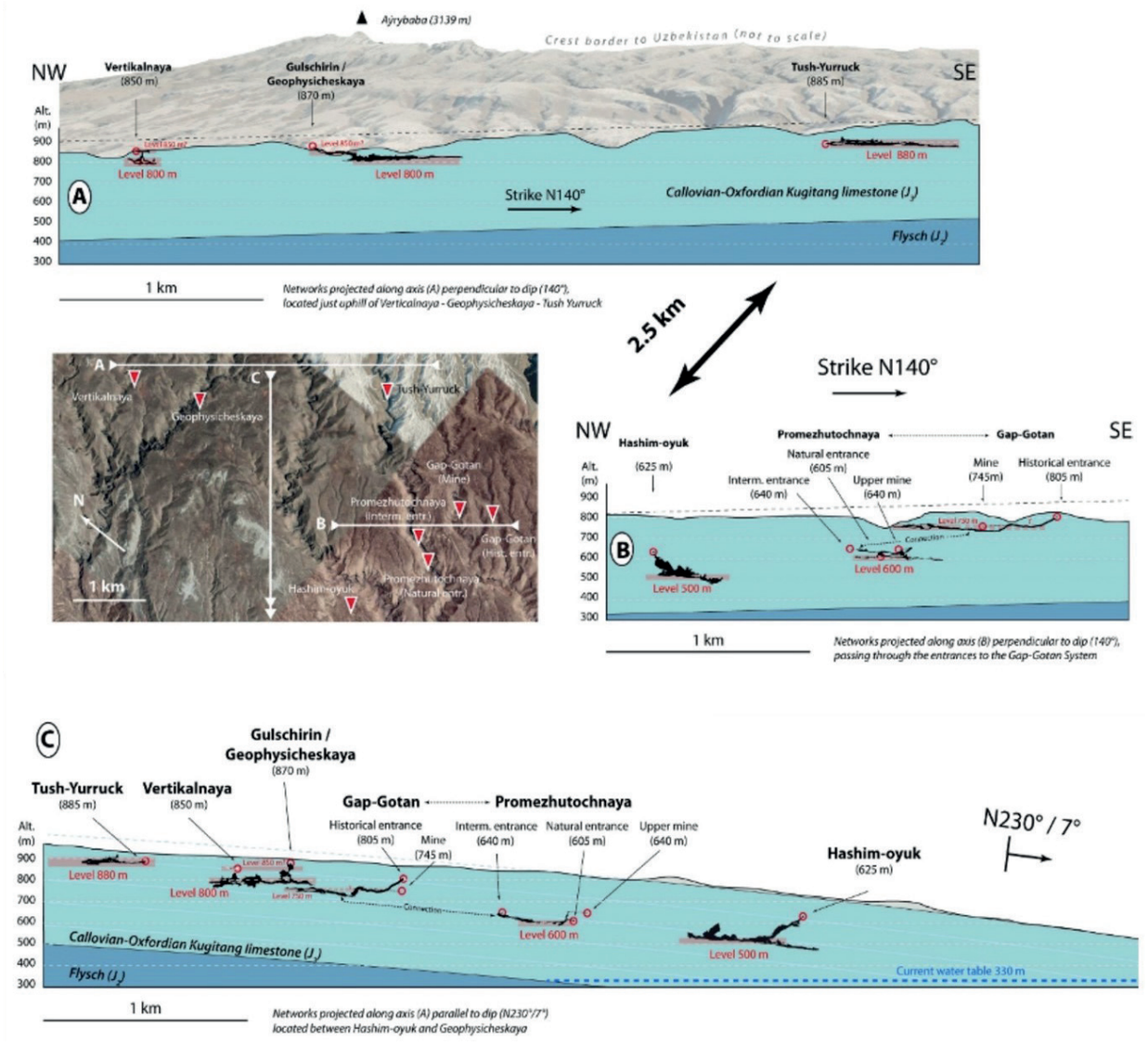

Figure 3: *The stepped levels of the Köýtendag caves. A-B) Caves projected along a dip-perpendicular profile. C) Caves projected along a dip-parallel profile. Location of profiles is shown on satellite image (not oriented to the N!)*

5. Discussion

The caves in the southern part of Köýtendag massif are remnants of an ancient karst system, now dissected by the canyons that characterize the western slopes of the mountain range. The caves appear to be carved in a phreatic regime in a low hydraulic gradient setting, and the fluids that carved the often large and low elliptical passages exploited weaknesses in the rock (Fig. 2), following mainly bedding planes dipping 7° towards the SW (220-230°N) or along strike, and some subvertical faults. The fact that part of these earlier phreatic conduits are following dip might indicate they formed prior to mountain uplift and tilting. Alongside these bedding-plane-guided conduits, there are also a set of close-to-horizontal cave levels, carved at or close to the water table and not determined by less permeable levels. These levels are sometimes connected by "soutirages", more vertical and small sections of cave carved in a vadose regime (HÄUSELMANN et al., 2003). Good examples of these can be seen in the Cupp-Coutunn-Promeszutochnaya Cave System, connecting cave levels from 805 m asl to 605 m asl.

As already mentioned by MALTSEV & SELF (1992), the caves appear to have formed in a phreatic regime. Our observations show that these caves cut thermal fluorite and calcite veins, which are clearly dissolved and corroded after their emplacement. We believe this hydrothermal stage to be prior to the main speleogenetic stage during which the main cave passages were carved. The age of the hydrothermal episode, and the following most important cave-forming stage is to be determined, but might even be Middle Cretaceous, and is possibly older than the age of the mountain uplift and the formation of the deep canyons, which is believed to have occurred since the Miocene. Our dating attempts will hopefully solve this question.

During or after the Köýtendag uplift, the hydraulic gradient increased and the caves were reactivated. Canyon downcutting appears to have occurred in phases, causing the water table to remain repeatedly stable over long periods of time, thus allowing the development of the four main cave levels (and additional two sublevels). Some of the caves were eventually cut by the canyons, opening up to the surface along the canyon walls.

Today the water table is well below the caves. Occasional flooding occurs in some cave passages closer to the canyon walls, as flood sediments indicate. The extreme thermal excursion (day-night, summer-winter) causes important seasonal (or even diurnal) condensation to occur in areas close to cave entrances or the exterior, and along main air currents, whereas the high internal temperatures cause evaporation of these condensation waters. This explains the widespread occurrence of condensation-corrosion morphologies, the deeply weathered rock walls (with reddish-orange residue called “okher”), and the massive precipitation of gypsum under different speleothem forms and crusts (Fig. 4). Most of this gypsum derives from seepage from the above lying Gowardak evaporites, as stable S and O isotopes indicate, and is not related to a sulfuric acid speleogenesis (as in Lechuguilla).

Figure 4: *Large gypsum chandeliers and hollow gypsum stalagmites, Geophysicalskaya (Photo by Philippe Crochet).*

Conclusion

During the French speleological expedition “Köýtendag 2024” many geological and geomorphological observations were made, and complete surveys were produced for several caves, whereas the large Cupp-Coutunn-Promeszutochnaya Cave System was partially resurveyed between entrances and along the main passages. These speleological and scientific activities aim to understand the genesis and evolution of these remarkable caves. Our preliminary investigations already led to the following observations: 1) we believe the fluorite and thermal calcite point to a hydrothermal diffuse event (most probably several phases) which occurred before the main cave formation; 2) the first cave network developed in a phreatic regime at low hydraulic gradient; 3) mountain uplift caused an increase in hydraulic gradient, and the formation of several horizontal cave levels; 4) all caves are now well-connected to the surface and characterized by extensive condensation-corrosion phenomena; 5) the large gypsum decorations are due to evaporation processes and mostly derive from the overlying Gowurdak evaporites and slow infiltrating waters, and are not related to a sulfuric acid speleogenesis.

Finally, an extensive part of time was dedicated to the documentation of these caves through photographs and 3D photogrammetry. Our work will hopefully help the Turkmen and Uzbek authorities to obtain the inscription of this area in the UNESCO World Heritage List.

Acknowledgements

The expedition has been made possible thanks to the help of his Excellency Maksat Chariev, Ambassador of Turkmenistan in France, the Ministry of Foreign Affairs and the Ministry of Environmental Protection of Turkmenistan, Ms. Chynar Rustemova, Executive Secretary of the Turkmen National Commission for UNESCO, Mr. Jumamyrat Saparmuradov, CEPF/CLLC Project Manager, Turkmenistan, Mr. Philippe Merlin, French Ambassador in Turkmenistan, Mr. Romain Gouvernet, Director of the French Institute of Turkmenistan, Mr. Shaniyaz Menliev, Head of the Scientific Department of the Koytendag Reserve, Mr. Saparklych Rahmanov, Director of Owadan Tourism, and Mrs. Dilora Geldiyeva, Sales Manager of Owadan Tourism.

6. References

AUDRA P., PALMER A.N. (2015) Research frontiers in speleogenesis. Dominant processes, hydrogeological conditions and resulting cave patterns. Acta Carsologica 44(3): 315-348.

AUDRA P., BARRIQUAND L., BRIFFON J.-M., CAZES G., CROCHET P., FALGAYRAC C., GRANDCOLAS J.-P., GREGO J., GRUAT J.-P., GUIRAUD A., HÉREIL J.-P-. LIPS B., LIPS J., POGGIA F., PONT A., ROBERT X., DE WAELE J. (2024) Expédition Köýtendag 2024 Turkménistan. Spelunca 175:3-24.

HÄUSELMANN P., JEANNIN P.-Y., MONBARON M. (2003) Role of epiphreatic flow and soutirages in conduit morphogenesis: the Bärenschacht example (BE, Switzerland). Zeitschrift für Geomorphologie 47(2): 171-190.

HILL C.A., FORTI P. (1997) Cave Minerals of the World. National Speleological Society, Huntsville.

MALTSEV V. (1997) Cupp-Coutunn Cave, Turkmenistan. In: HILL C.A. & FORTI P. (Eds.), Cave minerals of the world (2nd. ed.), 323-328. National Speleological Society, Huntsville.

MALTSEV V.A., SELF C.A. (1992) Cupp-Coutunn cave system, Turkmenistan, Central Asia. Proceedings of Bristol University Speleological Society, 19(2):117-150.

MALTSEV V.A., KORSHUNOV V. (1998) Geochemistry of fluorite and related features of the Kugitangtou Ridge Caves, Turkmenistan. Journal of Cave and Karst Studies 60(3):151-155.

The Monte Kronio hydrothermal cave system, Sicily, Italy

Philippe Audra (1), Marco Vattano (2,3), Giuliana Madonia (2,4), Didier Cailhol (5), Martina Cappelletti (3,6), Andrea Columbu (7), Gabriella Koltai (8), Marjan Temovski (9,10), Ángel Fernández Cortés (11), Fernando Gázquez-Sánchez (11), Christoph Spötl (8), Jean-Claude Nobécourt (12), Ermanno Galli (13), Jo De Waele (3,14), Francesco Sauro (3,5)

(1) Polytech'Lab UPR 7498, University Cote d'Azur, Nice, France, Philippe.AUDRA@univ-cotedazur.fr (corresponding author)
(2) Department of Earth and Marine Science, University of Palermo, Italy, marco.vattano@unipa.it, giuliana.madonia@unipa.it
(3) La Venta geographic exploration association, Italy
(4) National Biodiversity Future Center (NBFC), Palermo, Italy
(5) Traces Laboratory, University Toulouse Jean Jaurès, France, dcailhol@orange.fr
(6) Department of Pharmacy and Biotechnology - Fabit, University of Bologna, Italy, martina.cappelletti2@unibo.it
(7) Department of Earth Sciences, University of Pisa, Italy, andrea.columbu@unipi.it
(8) Institute of Geology, University of Innsbruck, Austria, gabriella.koltai@uibk.ac.at, christoph.spoetl@uibk.ac.at
(9) HUN-REN Institute for Nuclear Research (ATOMKI), Debrecen, Hungary, temovski.marjan@atomki.hu
(10) Department of Mineralogy and Geology, University of Debrecen, Hungary
(11) Department of Biology and Geology, University of Almería, Spain, acortes@ual.es, gsf751@ual.es
(12) Association française de karstologie, France, jcnobecourt@gmail.com
(13) Department of Chemical and Geological Sciences, University of Modena and Reggio Emilia, Italy
(14) Department of Biological, Geological and Environmental Sciences, University of Bologna, Italy, jo.dewaele@unibo.it
(15) Department of Geoscience, University of Padova, Italy, francesco.sauro@unipd.it

Abstract

The Gap-Gotan (Cupp-Coutunn) system (Turkmenistan) is known for its mineralogical wealth, thanks to the considerable work carried out by Vladimir Maltsev in the 80s. However, following fieldwork carried out in 2024, Maltsev's speleogenetic hypotheses have been revised, in terms of stages, chronology and processes. Several phases of speleogenesis can be identified. 1) Hydrothermal mineralizing fluids, leading to Pb-Zn deposits in the vicinity, and impregnation of the host rock with sulfides, fluorite, and calcite veins. 2) The formation of large horizontal phreatic conduits at shallow depth, fed by infiltration at high altitude, with dissolution produced by flows reacting with the sulfides in the host rock. This process has been repeated in stages as the base level fell, until the present day. Nowadays similar active phreatic conduits are presumed to exist beneath the gypsum collapses. 3) Once drained, the caves are decorated with gypsum speleothems mainly formed by sulfate-rich seepage from the surface (e.g., chandeliers), and filled with fluvial sediments injected locally from canyon sinkholes. Mapping, isotopic and mineralogical analyses, and U-series and U-Pb dating of the sediments are providing preliminary evidence for this model of speleogenesis in these unique and exceptional caves.

1. Introduction

Monte Kronio (or Monte San Calogero) is a 386m-high hill overlooking the Mediterranean Sea and Sciacca city, on the SW coast of Sicily, Italy. It was first mentioned by Diodorus Siculus in the 1st century BCE, and the upper cave (Grotta del Santo) is considered to have been the hermitage of San Calogero in the 6th century. However, the presence of Paleolithic artifacts and outstanding large Neolithic jars in upper Stufe di San Calogero (hereafter Stufe) demonstrate an even earlier frequentation (Fig. 1). The Commissione Grotte E. Boegan of Trieste has explored over 1 km of cave passages since the 1950s, including several caves that open along the hill slopes. They consist of subhorizontal passages connected by steep large passages or shafts including the giant 104 m deep "Pozzo Trieste" in the middle Cucchiara Cave (Fig. 2). However, the most unique character of the cave is its thermal environment. A powerful steam plume (37°C and 100% relative humidity) is emitted from the upper entrances (Stufe). It is supplied by the relatively cool intake of outside air through the lower openings (e.g., Cucchiara Cave). Consequently, the hot and moist cave air makes exploration extremely difficult, with a Humidex index (66) well above the "lethal" limit of 54 (Fig. 1).

The region is part of the Sicilian Maghrebides chain, characterized by south-verging thrust sheets, built of Jurassic to Paleogene dolomitic limestones originating from the sedimentary cover of an ancient passive margin. Monte Kronio emerged in the Upper Pliocene - Lower Pleistocene along normal faults. Recent uplift is evidenced by multiple marine terraces up to ≈250 m a.s.l. Their maximum elevation is located at Monte Kronio, forming a bulge from which the altitude of the terraces decreases on either side. OSL dating assigns ages of ≈80 ka for T1 located at ≈ 40 m a.s.l. and ≈197 ka for T5 located at ≈ 130-150 m a.s.l. This results in a high rate of uplift of around 0.5 m/ka, whereas estimates deduced from the oldest levels imply a very low uplift rate between 1.5 Ma and 400 ka (FERRANTI et al., 2021).

Figure 1: *Some of the large jars found in Stufe di San Calogero, lying on guano deposits. Explorers are equipped with a respirator delivering fresh air, enabling them to survive in the 37°C atmosphere showing 100% relative humidity (photo: G. Boldrini / La Venta).*

The main aquifer lies in Triassic-Jurassic carbonates, underlain at the foot of the massif by Cretaceous marly limestones (Fig. 3). The whole is topped by surficial aquifers, contained in Paleogene limestones and sandy limestones, themselves covered by Plio-Pleistocene marls with low permeability (aquiclude).

The Sciacca geothermal field reaches depths of over 2800 m, with a low geothermal gradient. Surface waters are recharged by local infiltration, and the spring flow is influenced by the sea and mantle-derived fluids associated to the active volcanism offshore (CAPACCIONI et al., 2011 and references therein).

2. Materials and methods

Seven calcite speleothems were collected in the uppermost level in Stufe and Fico Cave (≈340 m a.s.l.), in the middle level in Cucchiara Cave (≈280 m a.s.l.) at the upper window of the 104 m-deep Trieste Shaft that blows hot and humid air (35.7°C, almost 100% relative humidity, RH), and closer to the entrance in Cat Passage (La Gattaiola), a cooler side passage (≈18°C, ≈65% RH). Additionally, two calcite veins predating the cave passages were sampled in Cucchiara and in a quarry at the foot of the hill. Finally, a 30-cm tall, laminated stalagmite entirely composed of hydroxylapatite (unique in the world!) was collected in Cucchiara.

11 calcite speleothem samples were dated at ATOMKI, Debrecen, Hungary, using the 230Th method following EDWARDS et al. (1987) and CHENG et al. (2013). The $\delta^{18}O$ and $\delta^{13}C$ values of carbonate samples were analyzed following the method described in SPÖTL & VENNEMANN (2003). In addition, eight sulfate samples, mostly composed of gypsum, as confirmed by X-ray diffraction analysis and Raman spectroscopy, were collected for isotopic analyses. The $\delta^{34}S$ values of these sulfate samples were determined using the method described in TEMOVSKI et al. (2018) and are expressed in ‰ relative to the VCDT reference standard.

In December 2023, we measured air velocities at 18 spots, i.e. in most of the intaking or blowing holes, as well as inside Cucchiara Cave. For the latter, the passage dimensions were measured with a DistoX Leica laser distometer to calculate air discharge. We used a Testo 425 hot-wire anemometer to measure airflow velocity, a NKTECH TH1 thermo-hygrometer for cave air T and RH, and a X-am® 5600 Dräger gas detector for CO^2 and H_2S concentrations. The physical parameters (pH, electric conductivity (EC), T, discharge (Q) of nearby thermal springs were measured using WTW pH- and conductivity-meters and were compared to literature data.

Microbiological analyses of colored biofilms present on the wall of Cucchiara cave were carried out by DNA extraction, PCR amplification and sequencing of 16S rRNA gene V3-V4 hypervariable regions using Illumina and Oxford Nanopore sequencing technologies.

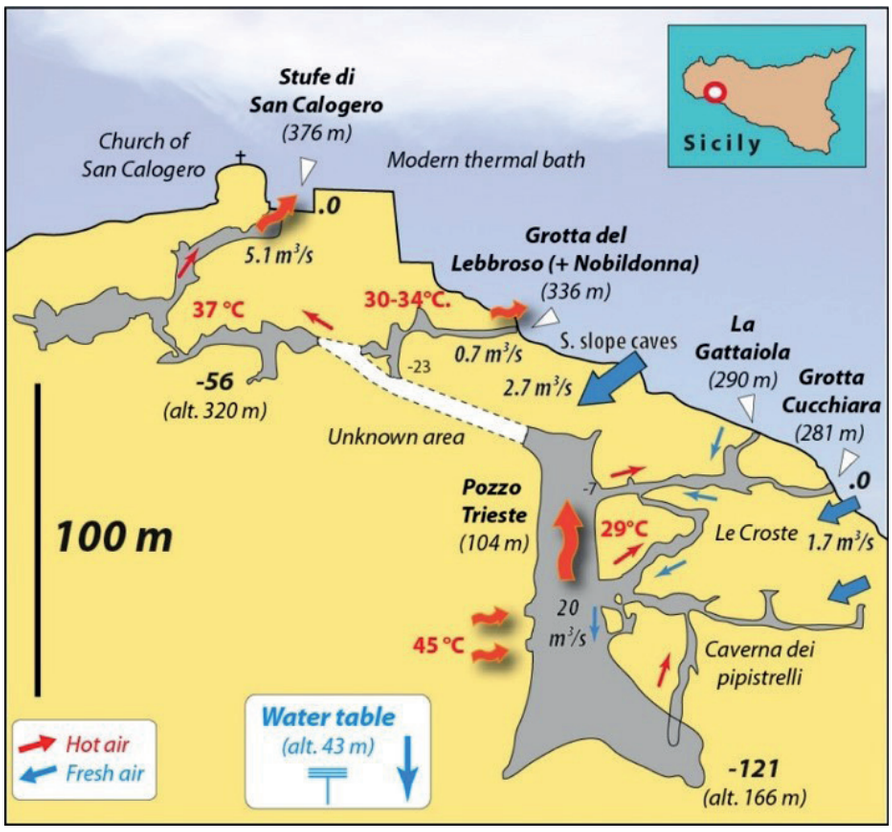

Figure 2: *Profile view of Monte Kronio caves (after Commissione Grotte E. Boegan). Air temperatures and airflow routes are indicated.*

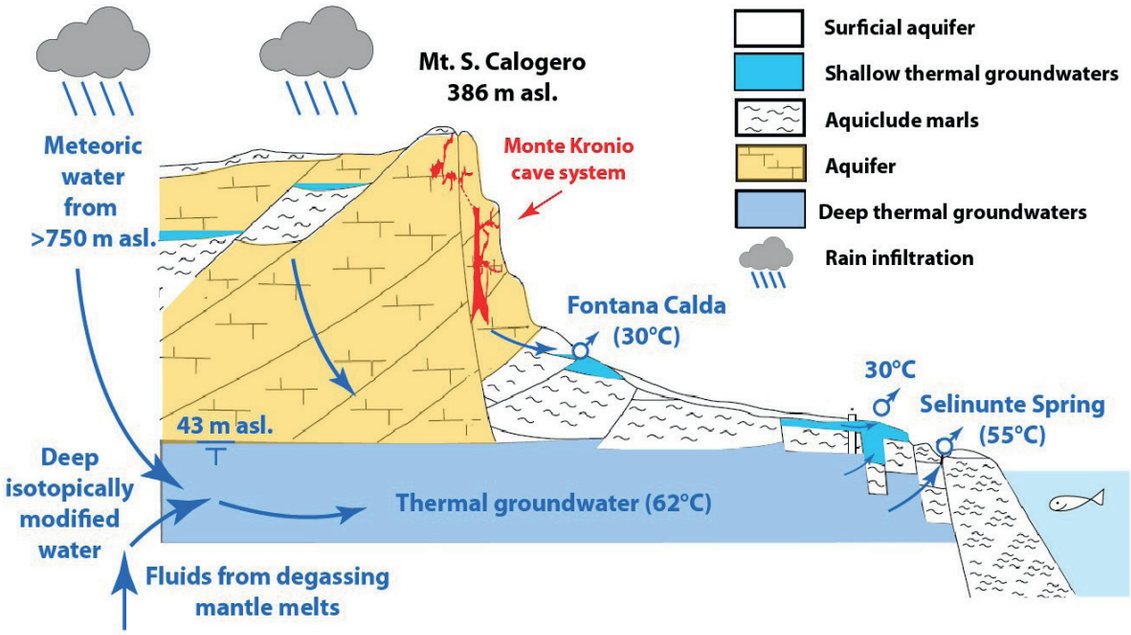

Figure 3: *Hydrogeological setting of the Monte Kronio and its thermal aquifers (after CAPACCIONI et al., 2011, modified).*

3. Results

The gypsum crusts yielded $\delta^{34}S$ values between +5.1 and +21.1‰. ^{230}Th-dating of subaerial speleothems yielded an age of about 346 ka for Stufe upper level, and ages comprised between 61 and 3 ka for Cucchiara, which is located in the middle level. Attempts to date the calcite veins failed due to the partial opening of the U-Th isotopic system. Except for one stalagmite, $\delta^{18}O$ and $\delta^{13}C$ values of the speleothems are similar and vary from -11.0 to -6.7‰, and -13.1 to -2.8 ‰, respectively.

In the upper entrances (Stufe, Lebbroso, Nobildonna), the total outgoing airflow is about 5.8 m^3/s, in the same range as reported by previous studies (BADINO & TORELLI, 2015). The highest measured temperature was 37°C and the RH was always close to 100%. In the lower entrances (Gattaiola, Cucchiara, Gallo, and several small fissures), the total measured incoming air was about 4.4 m^3/s. In Cucchiara Cave, complex air circulation and convection occur between the various branches. Intake airflows converging to Pozzo Trieste were about 20 m^3/s (Fig. 2). Due to strong airflow in the caves, the concentration of CO_2 always remained below 0.5% and no H_2S was detected (Pozzo Trieste was not visited).

Mineralogical analyses identified sulfates (gypsum, barite, chalcoalumite ($CuAl_4(SO_4)(OH)_{12}\cdot 3H_2O$)), carbonates (ankerite, sjögrenite (Pyroaurite-2H) ($Mg_6Fe_2^3+(CO_3)(OH)_{16}\cdot 4H_2O$)), bat guano-derived phosphates and nitrates (variscite, undifferentiated apatite, ardealite, crandallite, brushite, monetite, nitratine).

Microbiological analyses from Cucchiara cave samples indicate the presence of complex microbial communities with a composition that seems to be partially correlated with biofilm colors and the vertical gradient of temperature due to the mixing between thermal and external airflows (Fig. 4, 7). The microbial communities are dominated by bacterial taxa that are unclassified at low taxonomy levels. In particular, unclassified Actinobacteriota dominate several samples from white and yellow biofilms on Cucchiara walls and are probably involved in biomineralization processes. Different bacterial species were also identified that are involved in chemolithotrophic activities like N2 fixation and CH_4 oxidation.

Figure 4: *Sala delle Croste in Cucchiara Cave. Gypsum and barite crusts covering dry guano deposits. Condensation droplets with white biofilms dot the ceiling (photo: Ph. Audra).*

4. Discussion

Aeolianite patches on the surface suggest that detrital minerals (quartz and silicates, often associated with phosphates) could have been transported into the subsurface by seepage through the soil, aerosols, and especially bats. However, silica neoformation remains a possibility. Phosphates and nitratine are derived from the mineralization of bat guano. Apatite (undifferentiated) is typically found in contact with the carbonate host rock, occurring in well-crystallized forms and was also identified in a laminated stalagmite (#STM_CUCC). Variscite and crandallite result from the interaction of acidic guano with detrital clay minerals (AUDRA et al., 2019). Gypsum, ardealite, and brushite are precursors of guano mineralization, generally present on the surface of guano heaps (Fig. 5). Monetite occurs as a blackish crust associated to brushite close to dripping points. It is derived from brushite dehydration, from direct precipitation onto limestone, or from co-precipitation with hydroxylapatite (PUŞCAŞ et al., 2014). This mineral therefore requires very dry (and acidic) conditions, which is made possible by incoming airflow that dries as it warms up in Pipistrelli Chamber (34°C). We suggest that condensation dripping maintains brushite where moisture is present in guano, whereas it converts into monetite by dehydration in drier areas. The highly soluble nitratine requires the same environmental conditions. In the case of barite, the association with phosphate crusts suggests its formation during guano mineralization (Fig. 4).

Figure 5: *A cooler passage ("only" 28°C) in Stufe, whereas other places are 10°C warmer! Walls and ceiling are smoothed by condensation-corrosion. Thick guano deposits covered with gypsum crusts are present on the floor (photo: L. Imperio).*

Chalcoalumite, a Cu-Al sulfate, is a rare mineral found in only one other cave in South Africa (Mbobo Mkulu Cave, MARTINI et al., 1997). It occurs as a brown crust, associated with gypsum and ardealite. The source of Cu is probably hydrothermal. Ankerite and barite probably also have a hydrothermal origin.

Gypsum $\delta^{34}S$ values are within the range reported for local Messinian evaporites (+3.7 to +21‰; LONGINELLI, 1979). However, the wide range of values may also suggest a mixing of various sources, including hypogenic/volcanic sources (with $\delta^{34}S$ closer to 0‰), oxidation of hypogene sulfur gases, remobilization of marine gypsum in the case of the higher $\delta^{34}S$

values, and subsequent in-cave microbially mediated sulfur reduction/reoxidation, in the case of lower $\delta^{34}S$ values.

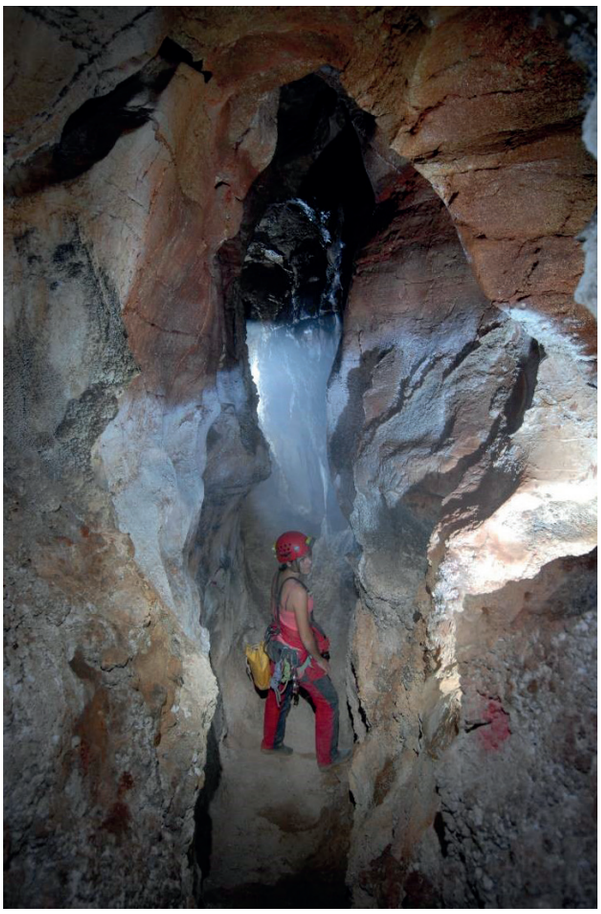

Figure 6: *Steep canyon-like passage in Cucchiara Cave. Evaporation occurs in the lower part of the section due to the sinking air from outside, whereas deep hot air rises along the ceiling where condensation-corrosion occurs (photo: M. Vattano).*

^{230}Th ages from Cucchiara and Fico cave speleothems indicate growth mainly from ca. 48 ka, but their older parts were not sampled. Speleothem growth near the upper window of the Trieste Shaft came to a halt at around 3 ka. For Stufe (≈340 m a.s.l.), one speleothem suggests a minimum age of about 346 ka for the draining for the upper-level caves, which is consistent with uplift rate calculated from marine terraces of about 0.5 m/ka (FERRANTI et al., 2021). In that case, the upper cave levels would have emerged at about 680 ka (if uplift was continuous) or about 1.2 Ma (if uplift before 400 ka was discontinuous).

Microbiological results indicate the presence of complex communities in the colored biofilms in Cucchiara cave whose formation seems to be associated to syntrophic relationships between chemolithotrophic and heterotrophic microorganisms. The presence of different bacterial species and metabolic interactions in the communities could contribute to the different colors and morphology of the biological patinas (Fig. 7).

The Kronio system probably initially developed along hydrothermal vents when the massif was uplifted. Its location is probably due to the presence of the structural bulge at the Kronio site, which allowed the early opening of a hydrogeological window at the highest point of the carbonate aquifer. Gradual karstification accentuated upward flow and focused aquifer permeability. The low geothermal gradient of the aquifer (10°C/km) could attest to homogenization by groundwater circulation along these deep karst routes. This hydrothermal chimney remained active during the uplift, which progressively drained the upper parts. The opening of lower entrances at the surface triggered an efficient air flow expelling hot and humid air through the upper entrances. This airflow led to the origin of specific mineralizations (e.g., monetite, nitratite) near the inlets. Importantly, it triggered pervasive condensation-corrosion resulting in wall weathering, rising ceiling channels, and a significant widening of the passages (Fig. 4, 5, 6, 7). Considering the very small size of the original hydrothermal conduits (visible in the quarry walls), the modern wide passages have only recently formed (i.e. after draining). The Trieste shaft measures 80 x 50 m at its base, for a total height of 104 m, and the Stufe galleries reach several meters in diameter. We suggest that late-stage condensation-corrosion is the main process of passage enlargement.

In addition to the water vapor expelled at the upper entrances, part of the condensation water is evacuated by the springs at the foot of the massif, such as at Fontana Calda (Fig. 3).

Figure 7: *Sala delle Croste in Cucchiara Cave. The air temperature near the floor is 24 °C due to cool air, whereas it reaches 32°C and 100% RH in the upper part of the passage as a result of air rising along ceiling channels, originating from the bottom of Trieste shaft. Most of the microbiological samples were taken in this chamber, displaying high gradients of temperature and humidity, and various patina colors (photo: M. Vattano).*

5. Conclusion

We hypothesize that the Monte Kronio system was formed during an early phase of uplift, in a phreatic environment driven by rising hydrothermal fluids. Subsequently, the conduits opened up to the surface, and significantly widened by condensation-corrosion during the Middle to Upper Pleistocene.

We identified chalcoalumite, a very rare Cu-sulfate mineral that was only mentioned once in a cave before, and the 2H polytype of pyroaurite (former sjögrenite), here for the first time mentioned as a cave mineral.

Research is ongoing, including exploration of the few accessible remote parts of the Trieste shaft.

We aim to better constrain the evolution of the site due to tectonic exhumation, by dating the early stage hydrothermal calcite veins, and various deposits related to phreatic and vadose stages. Calcite speleothems will be studied in order to characterize paleoclimatic and paleoenvironmental conditions. A more detailed study of the cave air currents should enable to quantify the extent of ongoing condensation-corrosion. Microbiological analyses are also ongoing to determine the bacterial contribution to biomineralization processes and the peculiar colored patinas that are present in Cucchiara cave.

Acknowledgements

The authors would like to thank all members of La Venta association and Comm. Grotte E. Boegan for the valuable data they shared and for their cooperation in cave activities. The scientific activities have been carried out within the Convention for the study of cave systems in the Riserva Naturale Integrale "Monte San Calogero (Kronio)" that involves the Assessorato Regionale Beni Culturali - Soprintendenza Beni Culturali ed Ambientali di Agrigento, Dipartimento Regionale dello Sviluppo Rurale e Territoriale, Servizio per il Territorio di Agrigento, Earth and marine Science Department (DiSTeM) of the University of Palermo, Department of Pharmacy and Biotechnology (FABIT) of the University of Bologna, Associazione La Venta Esplorazioni Geografiche APS, and Società Alpina delle Giulie (Sez. di Trieste del Club Alpino Italiano), Comm. Grotte E. Boegan.

References

AUDRA P., DE WAELE J., BENTALEB I., CHROŇÁKOVÁ A., KRIŠTŮFEK V., D'ANGELI I.M., CARBONE C., MADONIA G., VATTANO M., SCOPELLITI G., CAILHOL D., VANARA N., TEMOVSKI M., BIGOT J.Y., NOBÉCOURT J.C., GALLI E., RULL F., SANZ-ARRANZ A. (2019) Guano-related phosphates--rich minerals in European caves. International Journal of Speleology 48(1):75-105. https://doi.org/10.5038/1827-806X.48.1.2252

BADINO G., TORELLI L. (2014) The "Progetto Kronio": history and problems of an extreme exploration in an intact archaeological deposit. In GULLÌ D. (Ed.) From Cave to Dolmen: Ritual and symbolic aspects in the prehistory between Sciacca, Sicily and the central Mediterranean:31-42. Archaeopress. https://doi.org/10.2307/j.ctvqmp11h.6

CAPACCIONI B., VASELLI O., TASSI F., SANTO A.P., DELGADO HUERTAS A. (2011) Hydrogeochemistry of the thermal waters from the Sciacca Geothermal Field (Sicily, southern Italy), Journal of Hydrology 396(3-4):292-301. https://doi.org/10.1016/j.jhydrol.2010.11.015.

CHENG H., EDWARDS R.L., SHEN C.-C., POLYAK V.J., ASMEROM Y., WOODHEAD J., HELLSTROM J., WANG Y., KONG X., SPÖTL C., WANG X., CALVIN ALEXANDER E. (2013) Improvements in 230Th dating, 230Th and 234U half-life values, and U–Th isotopic measurements by multi-collector inductively coupled plasma mass spectrometry. Earth and Planetary Science Letters 371–372:82–91. https://doi.org/10.1016/j.epsl.2013.04.006

EDWARDS R.L., CHEN J.H., WASSERBURG G.J. (1987) 238U–234U–230Th –232Th systematics and the precise measurement of time over the past 500,000 years. Earth and Planetary Science Letters 81: 175–192. https://doi.org/10.1016/0012-821X(87)90154-3

FERRANTI L., BURRATO P., SELCHI D., ANDREUCCI S., PEPE F., PASCUCCI V. (2021) Late Quaternary coastal uplift of southwestern Sicily, central Mediterranean sea. Quaternary Science Reviews 255:106812. https://doi.org/10.1016/j.quascirev.2021.106812

LONGINELLI A. (1979) Isotope geochemistry of some Messinian evaporites: paleoenvironmental implications. Palaeogeography, Palaeoclimatology, Palaeoecology 29: 95-123. https://doi.org/10.1016/0031-0182(79)90076-2

MARTINI J.E.J., WIPPLINGER P.E. & MOEN F.G. (1997) Mbobo Mkulu cave, South Africa. In: C. HILL and P. FORTI (Eds.) Cave minerals of the World. National Speleological Society, Huntsville, Alabama USA: 336-339.

PUŞCAŞ C.M., KRISTALY F., STREMȚAN C.C., ONAC B.P. & EFFENBERGER H.S. (2014) Stability of cave phosphates: Case study from Liliecilor Cave (Trascău Mountains, Romania). Neues Jahrbuch fur Mineralogie Abhandlungen 191(2):157-168. http://dx.doi.org/10.1127/0077-7757/2014/0254

SPÖTL C., & VENNEMANN T. W. (2003). Continuous-flow isotope ratio mass spectrometric analysis of carbonate minerals. Rapid Communications in Mass Spectrometry, 17(9), 1004–1006. https://doi.org/10.1002/rcm.1010

TEMOVSKI M., FUTÓ I., TÚRI M., PALCSU L. (2018): Sulfur and oxygen isotopes in the gypsum deposits of the Provalata sulfuric acid cave (Macedonia). Geomorphology, 315, 80-90. https://doi.org/10.1016/j.geomorph.2018.05.010

The Jabal Al Qamar karst, SW Dhofar, Oman. Cave evolution and flashflood hydrodynamic

Philippe Audra (1), Nathan Rispal (1), Dominik Fleitmann (2), Frédéric Swierczynski (3), Hai Cheng (4), Abdul Hakim Amer Al Ma'ashani & Dhofar Adventure members (5)

(1) Polytech'Lab UPR 7498, University Cote d'Azur, Nice, France, Philippe.AUDRA@univ-cotedazur.fr (corresponding author), nathan.rispal@etu.univ-cotedazur.fr

(2) Department of Environmental Sciences, University of Basel, Switzerland, dominik.fleitmann@unibas.ch

(3) UnderWater eXperience, Le Rove, France, frederic.swierczynski@gmail.com

(4) Institute of Global Environmental Change, Xi'an Jiaotong University, Xi'an 710054, China & Key Laboratory of Karst Dynamics, MLR, Institute of Karst Geology, CAGS, Guilin, China, cheng021@xjtu.edu.cn

(5) Dhofar Adventure, Mirbat, Oman, dhofar.adventure@gmail.com

Abstract

Jabal Al Qamar, in southwest Oman, is a high plateau overlooking the Arabian Sea. Its semi-arid climate is mitigated by the foggy Khareef monsoon, while rare cyclones cause flash floods. The study resulted in a conceptual model typical of semi-arid karsts, illustrated by the Sha'at--Nakbat sinkhole-resurgence system, fed by rare rainfall events. It is embedded in a non-karst fissured carbonate aquifer, drained by perennial springs, depositing massive travertines, with a regular base flow at the origin of traditional irrigated agriculture. Dataloggers settled at the resurgence reveal underground transit velocities during the Khareef (44 m/h) and during cyclone Tej in October 2023 (400 m/h). The decay of organic matter introduced in sinkholes produces CO2, which concentrates in the confined cave atmosphere, maintaining powerful corrosion in the conduits long after flood phases. The Oteen porch is a unique case of a perched fossil level in Oman. U/Th dating of speleothems would allow to constrain the evolutionary stages of this slowly evolving system, which remains perched above the sea.

1. Introduction

Jabal Al Qamar (the Mountain of the Moon) (1,411 m) lies at the SW end of Oman, in the Dhofar province, on the border with Yemen (Fig. 1). Its relief is asymmetrical, with an 800-1000 m escarpment dropping down to the Arabian Sea, while inland a plateau intensely dissected by deep canyons gradually slopes down towards the center of the Arabian Peninsula. This relief corresponds to the passive margin of the Gulf of Aden, tilted towards the continent.

The pre-rift Paleocene-Eocene series incorporates the bioclastic platform limestones of the Umm er Radhuma Fm., up to 700 m thick and the main karstified interval. It rests unconformably on Cretaceous marls and sandy limestones, and is overlain by marly-chalk series (PLATEL et al., 1992; ROBINET et al., 2013). The emersion and uplift of the margin that began in the Oligocene was completed at around 15 Ma during the Miocene, and the morphology is considered to have been stable overall since then (PETIT et al., 2007).

While the interior of the Arabian peninsula belongs to the hyper-arid domain of the Najd desert, the narrow coastal fringe benefits from the attenuated influence of the monsoon (Khareef), with mainly occult precipitation, combining fog, drizzle, and low intensity rainfall (Fig. 2). In Salalah, capital of the Dhofar Governorate, rainfall is limited to 100 mm along the coast. On the edge of the Jbel, it is around 200 mm. However, some funnel valleys concentrate horizontal foggy precipitation, with the forest generating vertical precipitation through cloud interception, very locally reaching values in excess of 500 m, as at Tawi Atayr further E of Salalah (FRIESEN et al., 2018). Finally, and very randomly, cyclones can reach the coast, dumping huge quantities of water and triggering flash floods. In May 2018, cyclone Mekunu dumped 745 mm in 4 days at Qairoon Hairitti (alt. 880 m), the most exposed station on the edge of the plateau (MÜLLER et al. 2020). Cyclone Tej, a category 3 (Very Severe Cyclonic Storm, winds 178-208 km/h), hit the Yemeni coast on October 23-24, 2023, causing rainfall of 200-300 mm. Apart from these rare extreme events, the semi-arid climate favors high evaporation (≈75%), spasmodic runoff (≈20%), and very low infiltration (AL-HATRUSHI, 2013). Roughly equivalently, SHAMMAS & JACKS (2007) report 20-30% infiltration during the Khareef months. For the study area, with 200 mm of estimated rainfall, and for 5 and 20% infiltration, groundwater recharge would be between 0.25 and 1 L/s/km2, respectively. There is no permanent run-off, and only a few temporary streams reach the sea during the Khareef and, more exceptionally, after cyclones. On the other hand, numerous perennial springs gush out at the foot of the plateau, the only access to the resource that enabled local populations to settle there. The ionic load of these springs has a significant proportion of sulfates and chlorides (28%) from marine aerosols and surrounding rocks (STRAUCH et al., 2014), and a regulated flow regime typical of the slow draining of fissured aquifers (AL AMRI, 2006). The temperature and electrical conductivity drop is delayed by 4 months after Khareef recharge that confirms storage and slow flow in a non-karstic permeability system. Residence times and the presence of sulfate-chloride ionic charge are responsible for extensive travertine deposits at the system outlets.

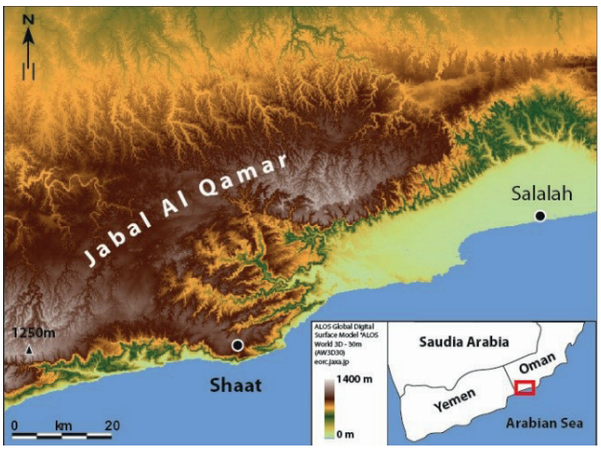

Figure 1: South Dhofar relief and location of studied area

In this semi-arid climate, karst morphologies are poorly developed: karren in "parmesan rappe", rare shallow dolines. Access to the underground network is exclusively via fluvio-karstic network, from deep-incised wadi canyons and deep sinkholes. The emergences are rarely penetrable beyond a few dozen meters, and can be identified by their travertine deposits, which are nevertheless less spectacular than those to the E of Salalah. Few caves have been recorded, with the exception of the area studied (AL KINDI et al., 2022). Our study focuses on the main underground system of Sha'at-Nakbat. We present the results of cave surveys, morphological and sedimentary studies, hydrogeology and, in particular, transfer dynamics obtained by recording at the emergence, which integrate the passage of cyclone Tej. Finally, we discuss the long-term evolution of underground networks and propose an atypical model of flow dynamics in semi-arid karst.

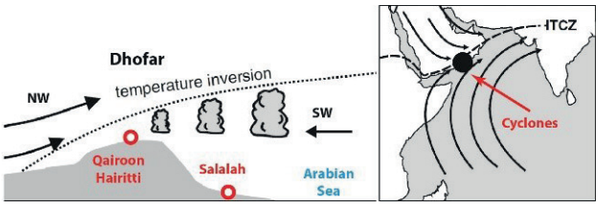

Figure 2: current position of the Intertropical Convergence Zone (ITCZ) determining the NE limit of the Monsoon (after FLEITMANN et al., 2007). Meteorological stations are indicated in red.

2. Materials and methods

The plan of caves explored by our predecessors (AUDRA, 2023) were surveyed with accuracy better than 5%, and their morphology was documented. Four speleothems were sampled for U/Th dating, which was performed at Xi'an Jiaotong University Isotope Laboratory, according to the method described by CHENG et al. (2013). During the January 2023 and 2024 missions, under winter low-flow conditions, the electrical conductivity (EC) of the flow was measured with a WTW 3110 conductivity meter (accuracy 0.5%) in the Nakbat South Tributary and in the main drain, upstream and downstream of the confluence, to account for the respective flows using mass conservation law. At the same times, C02 concentration in the cave atmosphere was measured using a Dräger X-am 5600 detector (resolution 0.01 vol.%). Stand-alone Sensus Ultra, Reefnet® loggers were installed at Nakbat resurgence for 1 annual cycle (March 2023 to January 2024), recording temperature and water depth (TD), as well as atmospheric temperature and pressure to enable barometric compensation. Temperature is resolved to 0.01 °C, with accuracy of ±0.8 °C. Depth is resolved to better than 1.27cm of water, with accuracy of ±30 cm. However, barometric compensation enables accuracy to be achieved to less than 1 cm.

3. Results

The Sha'at Sinkhole (16.7734°N, 53.5870°E, alt. 838 m) lies in a deep canyon draining a temporarily active catchment on marly limestone (Fig. 3). A 210 m shaft is followed by a steep gallery cluttered with large boulders. At -260 m, a permanent flow forms a river 850 m long, made up of a succession of long pools dammed by rimstones. It ends in a sump at -332 m. The resurgence of the system is the Nakbat spring (16.7667°N, 53.6076°E, alt. ≈460 m), which opens at the top of a 70 m-high travertine waterfall, mid-slope of the coastal escarpment, at the foot of the limestone wall. From the entrance, the first horizontal section consists of long pools dammed by rimstones. At 650 m from the entrance, the S. Tributary contributes around 1/3 of the flow, while the main course has incised a 50 m-high canyon that is climbed by a series of waterfalls. This is followed by a vast gallery leading to the upstream sump. Both Sha'at and Nakbat sumps are at the same altitude and 800 m apart. Our diving explorations from Nakbat have enabled us to progress 200 m into a phreatic conduit 20 m in diameter, where orientation is complex. Finally, the Oteen porch (16.7657°N, 53.6048°E, alt. ≈ 600 m), perched 130 m above Nakbat, harbors witness to the system's ancient flows (Fig. 3, 6). EC values, applied to the mass conservation law, show that the S. Tributary (680 µS/cm) has a discharge equivalent to half the main course from the upstream siphon (upstream confluence = 650 µS/cm; downstream confluence = 660 µS/cm). At low water (obs. January 2023 and January 2024) with ≈2 L/s in the S. Tributary, the discharge at the outlet would then be ≈ 6 L/s and that of the upstream sump ≈4L/s. The pattern features a single, monogenic conduit with no fossil level, which is a constant of sinkhole-resurgence systems throughout Oman. Almost the entire system is controlled by jointing, essentially parallel to the cliff, with those closest to the cliff opened by decompression. No stratigraphic control is apparent, even in the short sections connecting fractures. Two types of sediment are present: fluvial sequences and speleothems. Pebbles pass through the Sha'at-Nakbat system with each flood, and are locally cemented by active lateral flowstones fed by oversaturated seepage. We assume that these conglomerates are diachronic, as are the loose pebble bars reworked by each flood. The pools in the downstream section are lined with calcite shelves, dammed by rimstones. These subaqueous calcite deposits (shelves, rimstones) are currently being eroded by the aggressive water of the river. One of the reasons for this aggressiveness is the organic matter brought in during floods, trapped under the silts of the deep pools. Its anaerobic decomposition releases carbon dioxide, and probably methane and hydrogen sulfide with characteristic smell (CH4 and H2S not measured). The walls of the pools are etched into unusually large (≈10 cm), indented wall features (Fig. 4). As a result of degassing, the concentration of C02 in the cave atmosphere is high in the semi-confined zones (Fig. 3). In Nakbat, beyond the first low roof passage, the concentration reaches 2.4% (24,000 ppm). In Sha'at, below -260 m, the concentration rises steadily towards the bottom to 1.4% (14,000 ppm). In winter, these lower values are due to convection produced by the cold subsident air, which is effectively ventilated in the large inlet volumes, but is minimal in the semi-confined zone. These values remain moderate, compared with

the 4.5% (45,000 ppm) measured at -200 m in Qanaf Sinkhole, located further E of Dhofar. 130 m above Nakbat, the Oteen porch is filled with a fluvial sequence, made of pebbles at the base (L = 20 cm), followed by a 10 m-thick sandy-clay sequence with an interbedded flowstone, and capped by a flowstone (Fig. 5). This is the former emergence of the system, disconnected and currently perched. U/Th ages of flowstone bracketing a pebble bar upstream of Nakbat (NK.1, NK.2), and for the two Oteen flowstones (NK.3, NK.4) would help to better constraint the evolution of the system (Figs. 3, 5).

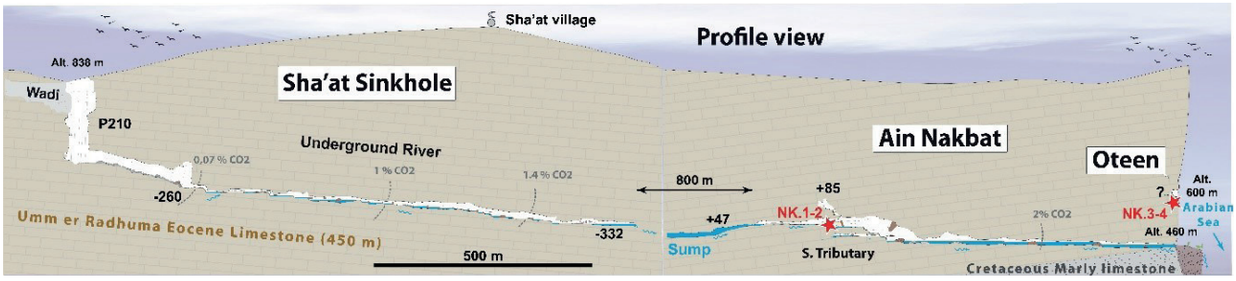

Figure 3: profile view of Sha'at-Nakbat system. Red stars indicate the location of calcite sampled for U/Th dating

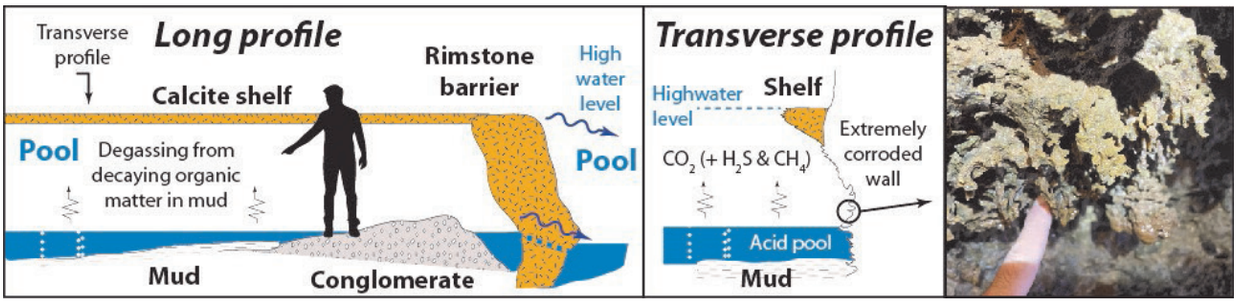

Figure 4: cave sediments along a pool in Nakbat, with outstanding etched indented walls due to high CO_2 provided by decaying organic matter.

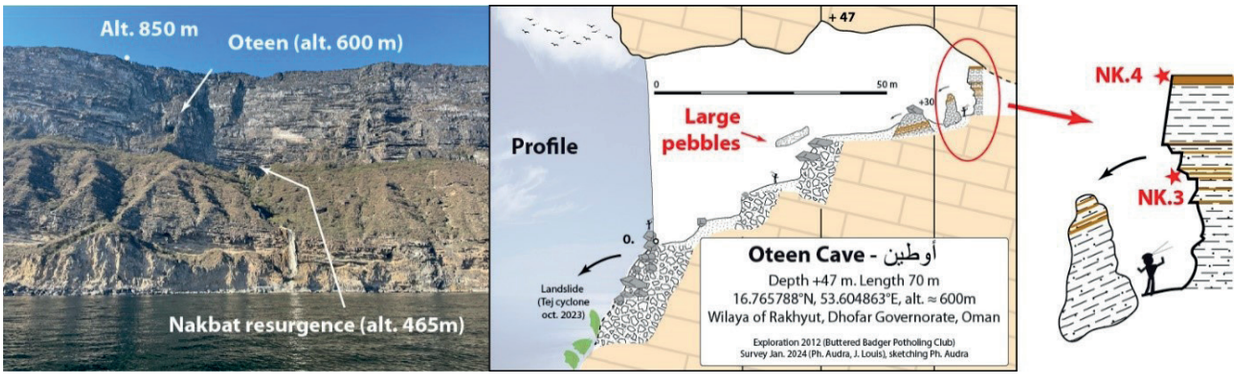

Figure 5: location, survey and speleothems sampled for U/Th dating of Oteen cave, the perched past outlet of the Sha'at-Nakbat system

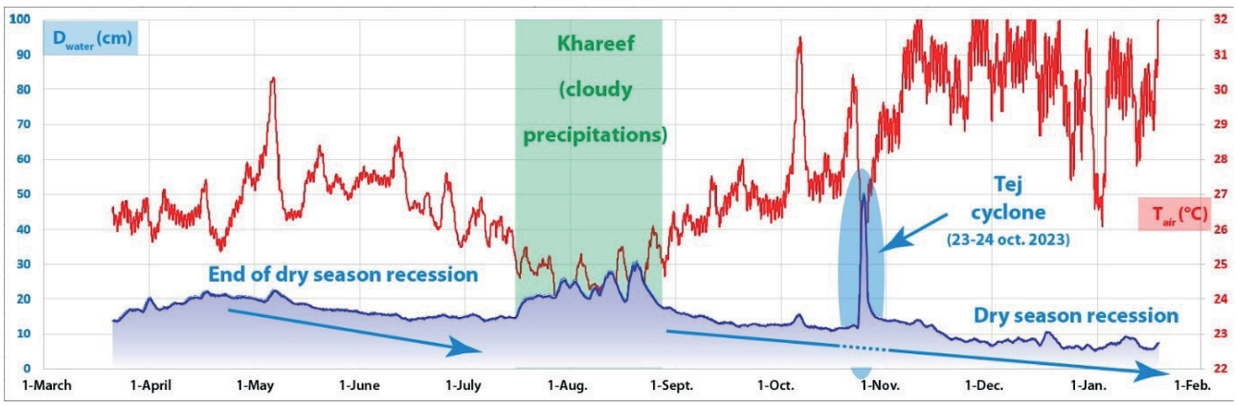

Figure 6: record of water depth (D) and atmospheric temperature at Nakbat resurgence from 2023

Temperature and water depth (TD) record in the Nakbat spring provide information on the seasonal dynamics of underground flow. Over the year (Fig. 6), the atmospheric temperature curve clearly shows the cooling effect of clouds during Khareef. Water depth shows a maximum during Khareef, and a secondary maximum in March-April, separated by two long dry periods, 3 months from mid-March to mid-July, and 5 months from September to January. At the end of October, the passage of cyclone Tej is clearly recorded.

Flow during the Khareef shows a series of peaks associated with rainfall events (Fig. 7). Water rises by a maximum of δD=32 cm, with a maximum rate of rise of 3 cm/h during the heaviest rainfall event in mid-August. Water temperature drops at the end of each peak, by δT= -0.35°C. Comparing the time of the first rise in D with that of the fall in T, the lag is 3 days. The arrival of the surface flow expels by piston flow the "hot" internal water stored in the reservoir. With a 3.2 km underground path length, made of torrential flow, phreatic passages and long pools, this corresponds to an average transit velocity of ≈44 m/h.

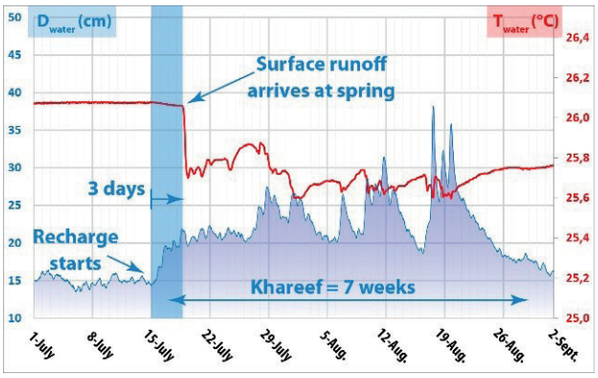

Figure 7: *record of water depth (D) and temperature (T) at Nakbat spring during wet season (Khareef), summer 2023*

Rainfall associated with the passage of cyclone Tej between the evening of October 23rd and the morning of the 24th reached 276 mm at the Rakhyut station, 17 km to the W on the coast. They probably exceeded 300 m in altitude over the study area. Their impact on the Nakbat flow was limited to 36 h (Fig. 8). The water rose by δD=1.35 m in 3 peaks of increasing height, implying considerable volumes in conduits averaging 10 m wide. The temperature dropped by δT=-3.15°C. The maximum instantaneous water rise is 1 m / 20 min. The return to base flow was extremely rapid, with the last peak showing the greatest and fastest decrease. The lag between the start of the water rise and the arrival of cold water is now only 8 h, corresponding to a flow velocity of ≈400 m/h, and decreases to 3 h and ½ h for the next 2 peaks. The origin of the 3 peaks is not defined and may correspond to two different situations: either 3 successive rainfall episodes, or a single episode having transited through 3 different pathways. In the latter case, with the calculated flow velocity, the first peak would come from the Sha'at Sinkhole at 3.2 km, the second from another sinkhole located 6 km away, which would correspond well with Ajdarawt Sinkhole (Fig. 9), with the third at 10 km remaining unknown.

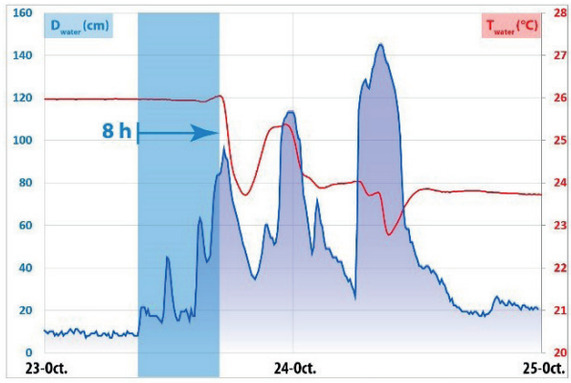

Figure 8: *record of water depth (D) and temperature (T) at Nakbat resurgence during Tej cyclone from 23 to 24 October 2023*

4. Discussion

The speleogenesis of this system is clearly associated with runoff previously concentrated on the surface in wadi rushing into sinkholes, such as Sha'at and Ajdarawt. Diffuse, supersaturated seepage probably does not contribute directly to the evolution of the conduits. The main drain mainly follows the fractures, but what is more unusual here is the apparent virtual absence of control by bedding planes. In this karst dammed by the impermeable substratum (Fig. 3, 9), the main drain has recorded the positions of successive base levels, in this case marine. However, the emergence should be now located 5 km further E, at the intersection of the aquifer with the current marine level, where it should have "slip" in response to the uplift of the plateau. This attests to the delayed adaptation of karst networks. It can be explained by the extremely low discharges, barely mitigated by flash floods whose powerful mechanical erosion by pebbles transport only lasts a few hours. Etched indented walls evidence of the current intense aggressiveness of the pools, but the rimstone dams that have barely been eroded suggest that this aggressiveness is recent, and that the water was previously rather oversaturated. The delay in adaptation implies a great antiquity and duration of activity for the Sha'at-Nakbat system, still active although perched by 465 m, and moreover for the fossil Oteen drain perched 600 m high.

The geological data allow us to constrain the limits of the Nakbat catchment area on virtually all sides (Fig. 9): to the S, the coastal cliffs; to the N, the low-permeability marly-limestone outcrops of the plateau following the watershed along Highway 47; to the E, the deep valley cutting into the limestone; and to the SW, beyond Ajdarawt Sinkhole, the dip inflection directing the waters in the opposite direction. The only uncertainty lies in a possible extension to the NW uphill of Ajdarawt Sinkhole. This corresponds to a catchment of ≈17 km2, third of which being covered by marly-limestone where temporary runoff occurs mainly on the surface. A third of this surface feeds the S. Tributary, located on the S rim of the cliff, of which Ajdarawt Sinkhole is probably the headwater.

During Khareef, transfer time is of the order of 3 days, with flow velocity of 44 m/h. During cyclone Tej, these values rise to 8 h and 400 m/h respectively, with water rises of 1.35 m in 30 min. in the outlet pools. The return to base flow within a few hours attests to the super-fast draining of an extremely transmissive conduit, and the absence of significant storage. This confirms that, as in the case of surface wadi, flash-flood flow is immediately dissipated and does little to recharge the aquifer. Recharge does occur, of course, through diffuse infiltration, but only over a very short, and therefore insignificant, period. True recharge occurs during the Khareef, which is more effective and longer-lasting despite the small quantities involved.

For these types of karst in semi-arid regions, we propose a conceptual model of double groundwater flow (Fig. 10). Large-scale drains fed by wadi sinkholes, particularly during cyclones, have an essentially transmissive function, with rare flash-floods of considerable discharge and very fast draining. Erosion in the conduits is mainly mechanical during floods, and the accumulation of CO2, partly from thin soils but

mainly from plant debris, prolongs the aggressiveness of the confined pools throughout the year, as they remain fed by diffuse seepage. The contribution of the conduits to aquifer recharge is thus generally insignificant compared with diffuse infiltration. In Dhofar, recharge is mainly due to the Khareef's moisture, which infiltrates diffusely and slowly into the fissured media, where it becomes saturated. In fact, this limestone aquifer remains in initial pre-karst conditions and maintains fissural-type flows and storage function, sustaining a base flow during the long dry season. Oversaturated springs build up travertine massifs. It is this slow draining of the fissured aquifer that enables the irrigated agriculture, thanks to the falaj system maintained by small traditional communities. In fact, karstification is strictly limited to the conduits. This is an extreme double-component model, with very limited exchanges between the conduits and the fissured media.

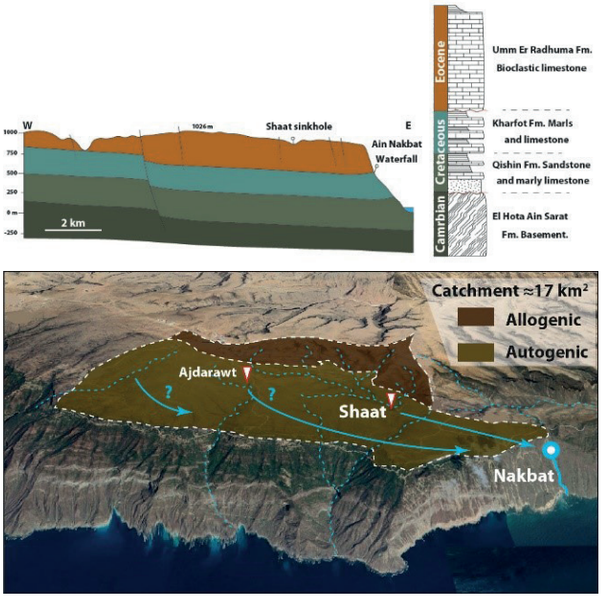

Figure 9: *Geological profile (after PLATEL et al., 1992) and hydrogeological catchment area of Nakbat resurgence (view to the N, the E-W length of catchment is about 6 km)*

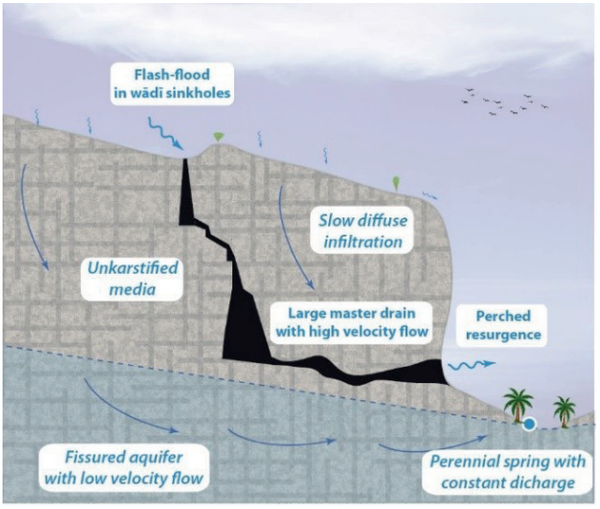

Figure 10: *conceptual model of double flow (fissured + large conduits) in semi-arid karst areas*

5. Conclusion

We present a conceptual model of karst flows in semi-arid environment, where recharge occurs mainly during the Khareef wet season, although misty precipitations are extremely limited. Water saturated from the subsurface flows slowly through the fissured carbonate aquifer, maintaining a permanent base flow at the springs where massive travertines are deposited. It is this type of non-karst flow that has enabled irrigated agriculture and the settlement of traditional communities. Fissured aquifers are interlocked by sinkhole-resurgence systems, where exchanges are however limited. These systems are fed by the temporary flow of surface wadi during Khareef, and more rarely during cyclones. The latter are the source of flash-floods, with transfer velocity of 400 m/h and lag times of 8 h or less, strong mechanical erosion through the transport of pebbles, and a contribution of plant debris. Their decay produces CO2, which concentrates in the confined cave atmosphere and acidifies the basins, prolonging the erosive effect of flood throughout the year, and forming outstanding etched indented pool walls. Curiously, bedding plane exerts no control over the cave flow path, which is almost entirely controlled by jointing. On the long term, the weakness of the underground flow results in a delay in the adaptation of the conduits, which remain perched several hundred meters above sea level. In a regional context where cave systems have no fossil level, for the time being Oteen Cave harboring a thick fluvial sequence represents a unique milestone, enabling us to study the ancient phases of cave systems development, in relation to climatic changes determining the nature of runoff and sedimentary deposits, as well as the uplift of the northern edge of the Aden rift. The opening of faults aligned along the cliff, preparing future landslides, is an identified risk. The spatial and temporal distribution of rainfall reconstructed from meteorological grids will enable us to refine the transfer functions highlighted by our record at Nakbat, particularly during cyclone periods. Studying the past and present dynamics of these atypical karst aquifers is vital for preserving water resources in semi-arid environments, where climate change is likely to significantly affect recharge.

Acknowledgements

Christophe Chellapermal for logistical support, Khaled Abdul Malak for friendly support, Mohammed Al Kindi of Oman Cave Exploration Team for enriching discussions.

References

AL-AMRI M. (2006) Hydrologic and hydrogeologic responses of springs to rainfall in Garziz and Arzat upper catchments, MSc. Thesis abstract, Sultan Qaboos University, Muscat. https://www.squ.edu.om/Portals/10/DNNGalleryPro/uploads/2019/4/25/CAMSResearchReport2006.pdf

AL KINDI M., ALL RIYAMI N., AL SAQRI N., CAHILL S., AL ZAKWANI N. (2022) A guide to the caves of Oman: the remarkable subterranean world of the Sultanate of Oman, Gilgamesh Publishing, London. 272 pp.

AL-HATRUSHI S.M. (2013) Assessment of the impact of climate change on water resources in the sultanate of Oman. UNCCD 2nd Scientific Conference, Bonn, https://www.researchgate.net/publication/260115532

AUDRA P. (2023) Le système Sha'at – Nakbat, Province du Dhofar, Sultanat d'Oman. Spéléo aquatique aux portes du désert. Spéléo Magazine, 121, 28-33. https://www.researchgate.net/publication/386089174

CHENG, H., EDWARDS, R.L., SHEN, C.-C., POLYAK, V.J., ASMEROM, Y., et al. (2013) Improvements in 230Th dating, 230Th and 234U half-life values, and U–Th isotopic measurements by multi-collector inductively coupled plasma mass spectrometry. Earth and Planetary Science Letters, 371–372, 82–91. https://doi.org/10.1016/j.epsl.2013.04.006

FLEITMANN D., BURNS S.J., MANGINI A., MUDELSEE M., KRAMERS J., VILLA I., NEFF U, AL-SUBBARY A.A., BUETTNER A., HIPPLER D., MATTERN A. (2007) Holocene ITCZ and Indian Monsoon Dynamics Recorded in Stalagmites from Oman and Yemen (Socotra). Quaternary Science Reviews 26(1):170-188. https://doi.org/10.1016/j.quascirev.2006.04.012

FRIESEN J., ZINK M., BAWAIN A., MÜLLER T. (2018) Hydrometeorology of the Dhofar cloud forest and its implications for groundwater recharge. Journal of Hydrology: Regional Studies, 16:54-66. https://doi.org/10.1016/j.ejrh.2018.03.002

Müller T., Friesen J., Weise S.M., Al Abri O., Bait Said A.B.A., Michelsen N. (2020) Stable isotope composition of Cyclone Mekunu rainfall, Southern Oman. Water Resources Research, 56, e2020WR027644. https://doi.org/10.1029/2020WR027644

PETIT C., FOURNIER M., GUNNELL Y. (2007) Tectonic and climatic controls on rift escarpments: Erosion and flexural rebound of the Dhofar passive margin (Gulf of Aden, Oman). Journal of Geophysical Research, 112, B03406. http://dx.doi.org/10.1029/2006JB004554

PLATEL J.-P., ROGER J., et al. (1992) Geological map of Raysut, Sheet NE 39-16C Scale: 1:100,000 + explanatory notes, 53 p., Sultanate of Oman, Ministry of Petroleum and Minerals, Directorate General of Minerals & BRGM.

ROBINET J., RAZIN P., SERRA-KIEL J., GALLARDO-GARCIA A., LEROY S., ROGER J., GRELAUD C. (2013) The Paleogene pre-rift to syn-rift succession in the Dhofar margin (northeastern Gulf of Aden): Stratigraphy and depositional environments. Tectonophysics, 607:1-16. https://doi.org/10.1016/j.tecto.2013.04.017

SHAMMAS M. I., JACKS G. (2007) Seawater intrusion in the salalah Plain aquifer, Oman. Environmental Geology, 53, 575–587. http://dx.doi.org/10.1007/s00254-007-0673-2

STRAUCH G, AL-MASHAIKHI K.S., BAWAIN A., KNÖLLER K., FRIESEN J., MÜLLER T. (2014) Stable H and O isotope variations reveal sources of recharge in Dhofar, Sultanate of Oman. Isotopes in Environmental and Health Studies, 50, 475-490. http://dx.doi.org/10.1080/10256016.2014.961451

Hypogene caves Atmos and Sulfur and the largest underground thermal lake in the world

Marek Audy (1), Vít Baldík (1,3), Richard Bouda (1), Jiří Bruthans (1,2), Jakub Mareš (1,2)

(1) Czech Speleological Society, audy@speleo.cz , boudar@me.com , jiri.bruthans@natur.cuni.cz
(2) Faculty of Science, Charles University, Albertov 6, Prague 2 CZ 12800 Czech Republic
(3) Czech Geological Survey

Abstract

In southern Albania, in the valley of the Sarandaporo River, members of the Czech Speleological Society discovered a hydrothermal karst connected to the sulphurous mineral waters of the Vromoner Valley. The area is defined by a massive limestone anticline that rises above the surrounding flysch. Here, thermal waters rich in hydrogen sulphide have created a series of massive hypogene caves with large domes, lakes and active streams.

In recent years, Czech speleologists have been carrying out speleological and hydrogeological research in the area, culminating in Lidar scanning and the creation of a 3D model of the subsurface and surface, including hydrology, in 2024. The largest caves in the area are Sulfur Cave, Shpella Breshkë (Turtle Cave) and Atmos Cave. A lake in the Atmos Cave was discovered, mapped and named Neuron Lake. This lake is the largest underground thermal lake in the world (known to date). All the springs in the valley have the same temperature and composition. The total yield of springs is 200 litres per second. Tracer tests have shown that the water from Lake Neuron polyfurcates into all the springs in the valley except the Old Spa Spring. Multidisciplinary international research of the hypogene area and biological research of the unique underground biotope continue.

1. Introduction

The South-Albanian fault, with rising warm waters and other fluids, follows the line Tomor–Qeshibesh–Bodar–Lëngaricë–Postenan–Melesin–Vromoner (Eftimi, Frashëri 2016).

Hypogene caves are located where this fault crosses the limestone outcrop at the surface. There are several such areas in southern Albania (fig.1)

Several hydrothermal areas are known in the Sarandaporo River valley between the Gramos and Pindos mountains. As early as the 14th century AD, the Pixaria Baths were built here (Audy et al., 2024).

The nearby Vromoner hydrothermal area, 1 km downstream of Sarandaporo, has been known since the 16th century. The Greek baths of Xomos were also built here.

The politically dark period of the second half of the 20th century prevented speleological research. The Vromoner area was a border zone with restricted access.

The geological setting of the Sarandaporo River is fairly straightforward, although the local tectonic setting, complicated by younger tectonics, tends to be quite complex. As a literal cross-section of the Albanides thrust belt (the Ionian Unit), it comprises a series of tectonic slices formed by a Jurassic to Eocene limestone sequence overlain by an Oligocene flysch sequence. These slices are separated by thrust faults/zones associated with steeply dipping bedding planes, representing the overturned limbs of SW-vergent asymmetric anticlines. These steeply dipping zones are usually associated with the presence of deep, narrow canyons separating sections of the mostly wide Sarandaporo River valley.

At the turn of the millennium, Albanian scientists described a cave from which a thermal stream flows (Eftimi, Frashëri, 2016).

Speleogenesis of caves in Vromoner was predominantly caused by hydrogen sulfide (H2S). H2S is derived from sulfates, which are common in groundwater, especially where evaporates occur at depth. When sulfate meets migrating oil and gas (mainly methane), the sulfates are reduced to H_2S. H_2S, together with residual sulfates, migrates with deep groundwater toward the ground surface. Here, it meets O_2 in shallow groundwater and, especially from the air (in fractures above the water table), and after its oxidation, sulfuric acid is produced. Sulfuric acid reacts with limestone and converts limestone to gypsum. Gypsum periodically falls from cave walls, exposing fresh limestone in a repetitive process. Part of H_2S is oxidized to native sulfur.

In 2021, Czech speleologists began exploring the Vromoner area and its sulphuric acid cave systems (SAS).

The first documented cave was the horizontal Sulfur Cave. The entrance to Sulfur Cave is located near the level of the Sarandaporo River on the Greek side of the border. Most of the area of this horizontal cave is already under Albanian territory. A 26°C warm thermal river flows from the base of the Universe dome (fig. 2) (Audy et al., 2022 and Audy, 2022). The presence of massive underground spaces is indicated by large dolines at the surface.

Figure 1: *The main tectonic faults in Albania with an indicated position of the Vromoner thermal springs.*

Entrances to other SAS caves have been found in these sinkholes. The Paleohypogene Horse Cave is filled with calcite and gypsum deposits.

Shpella Breshke (Turtle Cave) is particularly interesting. At the bottom of the cave, at a depth of 68 m, is an elliptical thermal lake with an 85 m circumference and a temperature of 26°C.

The most recent discovery was the Atmos sinkhole cave. The entrance, 150 metres from the hillside entrance, periodically emits clouds of steam that can be seen from a distance of 1 kilometre in winter. At the bottom of Atmos Cave, at a depth of 127 m, a large thermal lake was discovered and named “Lake Neuron” (Audy et al., 2023).

The Atmos and Sulfur Caves are located on the gently sloping limb of one of the above tectonic blocks. The whole sedimentary sequence generally dips gently SW but is folded into open folds with large wavelengths that dip gently SSE. A cleavage system has been detected that is genetically unrelated to the main folds. It is a subvertical, practically N-S striking cleavage, dipping steeply to the W. Four fracture systems can be distinguished. NE-SW and NNW-SSE striking fractures are the most dominant systems, accompanied by two minor systems: NNE-SSW and ENE-WSW striking systems.

Figure 2: *Mineral springs on the bottom of the giant dome Vesmír (Universe) in the Sulfur Cave. The Vesmír Dome was named after a Czech journal at the occasion of its 150th anniversary. (Photo by M. Audy & R. Bouda)*

2. Materials and methods

The SAS survey of the Vromoner Caves initially focused on mapping and hydrogeology. Various gas detectors were used to measure H2S concentrations, which ranged from 2 to 22 ppm in open areas. The air temperature in hydrothermally active caves ranges from 15° to 29°C, while inactive caves in the area maintain a temperature of 12° to 14°C.

DistoX and BRIC were initially used to map the caves. When researchers measured the massive lake dome in Atmos Cave, they could not fix points in the middle of the lake. A mobile lidar scanner, the Geoslam ZEB Horizon, was purchased in 2024 with a grant from the Neuron Foundation for Science Support. This device, capable of recording 300,000 points per second, This allowed us to create a 3D model of the entire hydrothermal area and obtain precise data on the dimensions of individual caves and thermal lake areas.

To obtain bathymetric data for the lakes in Turtle and Atmos Caves, we used the River Surveyor M9 sonar.

The yield and physico-chemical parameters of all springs in the area were measured. In order to detect the connection between the springs and the underground flows in the cave, a tracer test was performed using sodium fluorescein dye injected into the outlet of Neuron Lake in Atmos Cave.

3. Results

Lake Neuron at the bottom of the Atmos Abyss is currently the largest thermal cave lake in the world (Fig. 3). We used the most advanced measurement techniques to obtain dimensional data (Table 1, Fig. 4). These measurements will allow us to compare changes in the cave interior in the future.

The largest spring is the stream flowing from the Sulfur Cave, which reaches a discharge of up to 60 L/s. The total yield of the springs in the Vromoner area is 200 L/s. All the springs in the area have the same physicochemical parameters, which means that they originate from the same source. The water temperature is 26 °C, and the total dissolved solids are 1 g/L.

The tracer test has shown that water from Lake Neuron flows into all the springs in the area, indicating extensive polyfurcation. (Fig. 5) The only exception, where the tracer did not reach, is the Old Spa spring, which is probably fed by borehole.

	NEURON LAKE	ATMOS DOME
Perimeter	344,9 m	490,4 m
Area	3 200,6 m^2	5 268,6 m^2
Volume	8 335,0 m^3	138 544,6 m^3
Length	138,3	174,5 m
Width	42,0 m	42,6 m
Lake depth	-7,46 m	–

Table 1: *Dimensions of Atmos Cave obtained by lidar scanning.*

Figure 3: *The southern quarter of the gigantic thermal lake Neuron on the bottom of the Atmos Cave. Neuron Lake has a temperature of 26 °C. With a volume of 8335 m3 is the largest subterranean thermal lake in the world. (Photo by M. Audy and R. Bouda).*

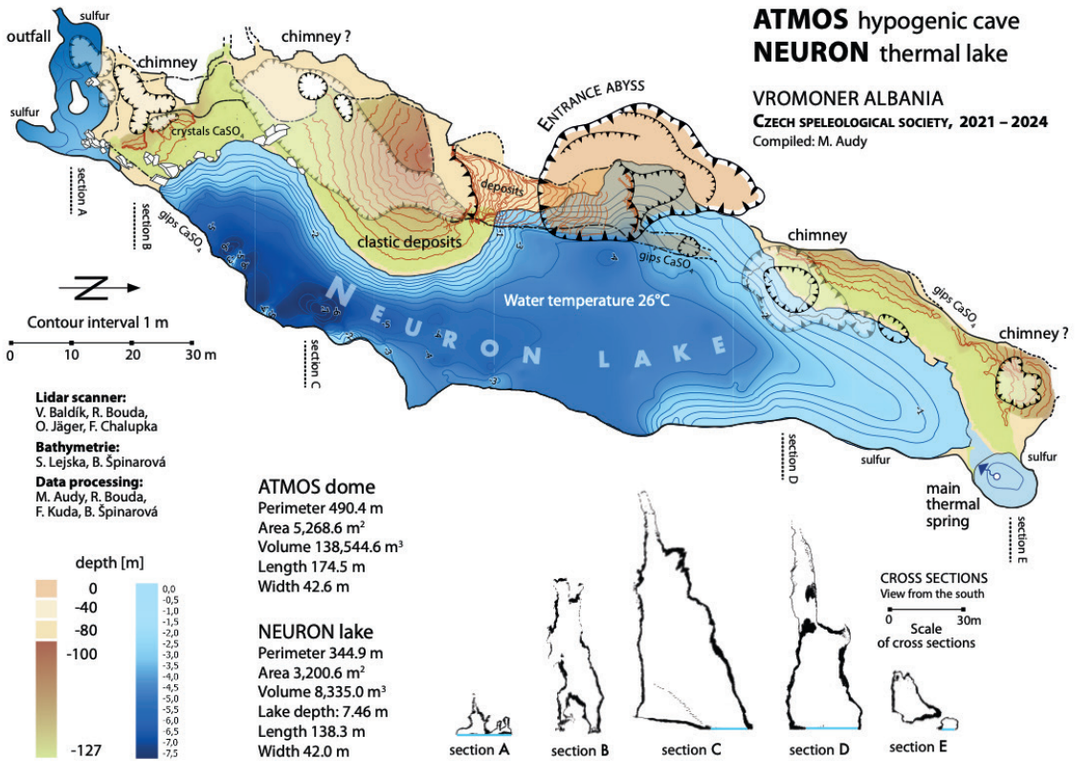

Figure 4: A map of the Atmos Cave generated from the point cloud obtained by a lidar scanner and sonar bathymetry.

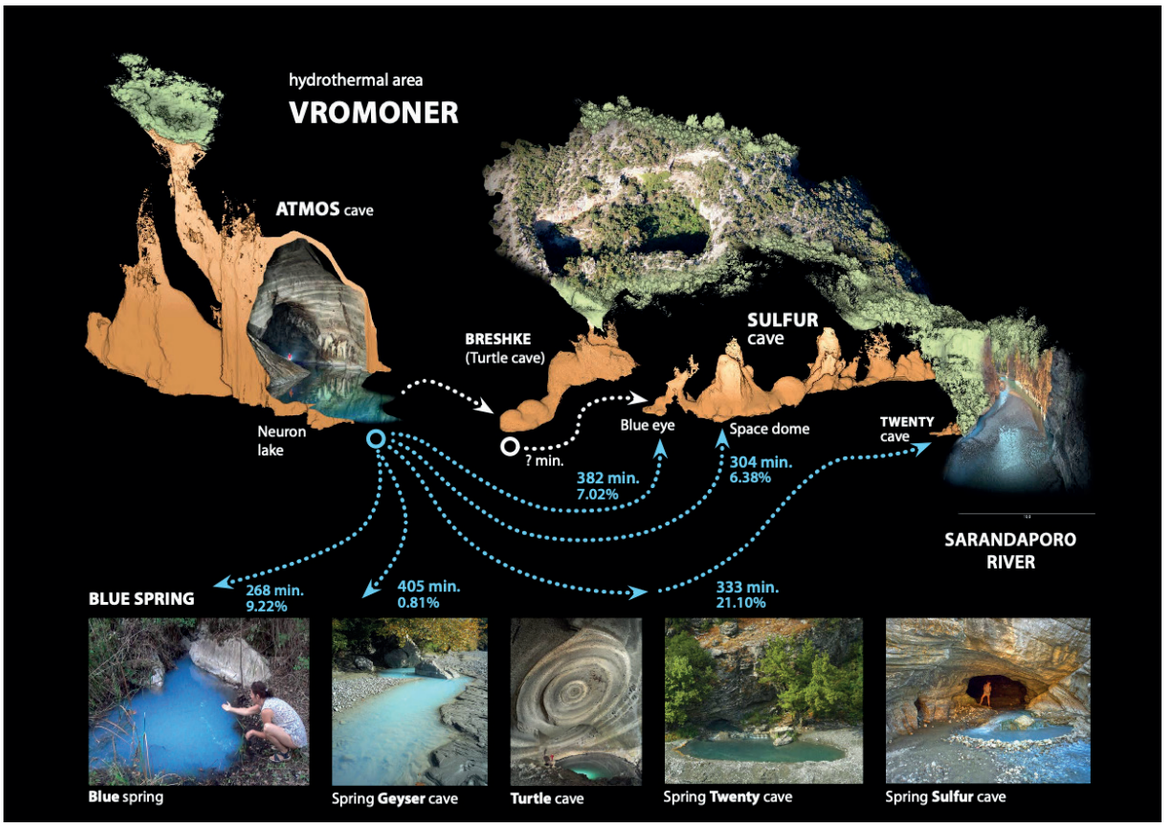

Figure 5: Situation of hypogene caves in the Vromoner area. Water from Lake Neuron (Atmos) flows into all springs in the valley (blue arrows), except for the outlets at the Xomos spa complex. Values indicate the time of first arrival in minutes. The percentage recovery of the tracer (fluorescein) is given.

4. Discussion

In the future, we hope to work in other SAS caves in nearby areas of Albania and Greece. The nearby thermal springs of Pixaria and Kavasila are related to the hydrothermal area of Vromoner. The Amarantos and Postemani hot steam vents, originating from limestone fissures high in the mountains, are of particular interest. The extensive SAS cave system, which has yet to be documented, is located on the Langarica River (alb. Lëngarica) near the town of Petran. One of the local caves, which has been listed as a cultural heritage site in Albania since 1983, is of significant importance. However, the extensive SAS cave system, with its active thermal flow, was only recently explored by Italian speleologists.

5. Conclusion

Intensive multidisciplinary research continues in the Vromoner area. We are also collaborating with local authorities. We are working towards having the hypogene caves included in the Vjosa National Park. Previously, Albanian hydrogeologists and historians succeeded in preserving the Bënjës geothermal area on the Langarica River by publishing information on the high heat flow of the vents and highlighting their potential for energy use (Frashëri 2013). Similarly, we aim to prevent the construction of a dam on the Greek side of the Sarandaporo River, as it could negatively impact the Sulfur Cave's habitat.

Acknowledgments

Thanks to the Neuron Foundation for supporting Czech science and the Atmos 2024 expedition, which allowed us to purchase a mobile lidar scanner and obtain precise data to verify the world's largest underground thermal lake, and to the Czech Hydrometeorological Institute for loaning the sonar.

References

AUDY M. (2022) Sulphur Cave. Une cavité thermale hypogénique exceptionelle en Albanie. Spelunca 165:6-13.

AUDY M., BOUDA R., BRUTHANS J., RUZICKA V. (2022) Hypogenní kras jižní Albánie. Speleofórum 41:42-51.

AUDY M., BRUTHANS J., KASTOVSKY J., BOUDA R. (2023) Atmos – nová hypogenní jeskyně (Shpella Avulit), Albánie. Speleofórum 42:72-78.

AUDY M., BRUTHANS J., MARES J., SARBU S., GALDENZI S., BOUDA R. (2024) Sulfur 2023, hypogenní jeskyně Albánie a Řecka – Kavasila, Vromoner, Langarica. Speleofórum 43:4-13.

Benassi A. (2023): Lengarices 2023 – Inseguendo il Respiro del Drago. https://www.scintilena.com/lengarices-2023-inseguendo-il-respiro--del-drago/05/13/

Eftimi R., Frashëri A. (2016): Ujërat Termale dhe minerale të Shqipërisë. SHBLB E RE: 1–224. (in Albanian) https://www.researchgate.net/publication/302914492

Frashëri A. (2013) Shpella prehistorike Bënjës, Tema. (in Albanian) https://www.gazetatema.net/2013/08/01/mos-shkaterroni-monumentet-e-natyres-dhe-te-historise

SARBU S. M., BRAD T., BANCILA R.I., STEFAN A. (2024) Exploring Biodiversity and Food Webs in Sulfur Cave in the Vromoner Canyon on the Greek–Albanian Border. Diversity 16:477

Sulphuric acid caves of Albania: state of the art

Marek Audy (1), Raluca Bancila (2), Andrea Benassi (3), Bouda Richard (1), Jiri Bruthans (1), Martina Cappelletti (4), Etmond Cauli (5), Luisa Dainelli (6),Teo Delić (7), Jo De Waele (4), Jean-François Flot (8), Sandro Galdenzi (9), Etleva Hamzaraj (10), Ettore Lopo (4), Alessandro Marraffa (11), Claudio Pastore (11), Serban M. Sarbu (2), Markos Vaxevanopoulos (12)

(1) Czech Speleological Society, audy@speleo.cz, boudar@me.com; jiri.bruthans@natur.cuni.cz
(2) "Emil Racoviţă" Institute of Speleology, Bucharest, Romania, bancila_ralucaioana@yahoo.com, serban.sarbu@yahoo.com
(3) Acheloos Geo-Exploring, Società Speleologica Italiana, benassiandr@gmail.com
(4) University of Bologna, Italy, martina.cappelletti2@unibo.it; jo.dewaele@unibo.it; ettore.lopo2@unibo.it
(5) Independent Albanian caver, etmond_cauli@yahoo.com
(6) University of Pisa, Italy, lu98.4692@gmail.com
(7) University of Ljubljana, Slovenia, teo.delic@bf.uni-lj.si
(8) Université Libre de Bruxelles, Belgium, jean-francois.flot@ulb.be
(9) University of Camerino, Italy, sandro.galdenzi@unicam.it
(10) University of Tirana, Albania, etleva.hamzaraj@fshn.edu.al
(11) Gruppo Speleologico Martinese, Italy, alessandro.marraffa97@gmail.com (corresponding author); claudio.speleo@gmail.com
(12) Volos Natural History Museum, Greece, vaxevanopoulos@gmail.com

Abstract

Over the last few years Albania has seen an explosion of discoveries of sulphuric acid caves. This country, rich in geothermal resources, has been the object of targeted speleological expeditions in the areas where thermal and sulphidic springs occur in contact with limestone outcrops. This has led to exploration and mapping of extensive maze of active sulphuric acid (SAS) caves in different areas of the country. These caves are hotspots of both geological and biological phenomenon, and multidisciplinary studies are being carried out in most of the newly discovered SAS cave systems. In Albania, rapidly developing country, scientific collaboration of speleological teams, coupled with involvement of local authorities and scientific collaborators, seems to be essential for documentation and protection of these sites. Especially as these unique geosites have high geological and biological importance, which can be properly protected only by scientifically based management and raising awareness among the local stakeholders and population.

1. Introduction

Carbonate rocks occupy almost 25% of Albania's land surface and are characterised by a widespread development of surface and underground karst phenomena (EFTIMI & ZOJER, 2015; EFTIMI, 2020). Before the fall of communism in Albania in the early 90s, speleological explorations in the country were carried out only by Albanian geographers and archaeologists (KRISTO, 1973; KRUTAJ, 1985; KRISTO et al., 1987). Most of the explored caves were easily accessible, archaeologically interesting, or known to local people. Nowadays, Albania still has poorly organized speleological community, with extremely low numbers of cavers. Therefore, it does not surprise that the most important cave discoveries since the 90s have been achieved by foreign cavers (for an overview see ZHALOV, 2015).

In recent years, explorer's attention was drawn by the uniqueness of sulphidic activity throughout the country. Strongly deformed inner and external Albanide regions are rich in geothermal waters, with many thermal springs reaching temperatures as high as 65°C. In addition to high temperatures, some of the springs are also characterised by Ca-SO4 chemistry (FRASHËRI, 2015), which is known to aggressively dissolve carbonate rocks. Potential aggressively based speleogenesis attracted Italian and Czech cave explorers in search of the first sulphuric acid cave systems (SAS) of this country.

SAS caves are widely present on the other side of the Adriatic Sea, in neighboring Italy (D'ANGELI et al., 2019), a country that hosts almost half of the currently known SAS caves in the world (DE WAELE et al., 2024). Due to similarities in regional development, Albania offers several geological settings where SAS caves might be expected to occur (KLIMCHOUK et al., 2022). Recently, important SAS cave systems have been discovered close to the border with Greece (BRANDOLINI, 2021; AUDY, 2022; MARRAFFA et al., 2022; AUDY et al., 2022, 2023, 2024; BENASSI, 2024) and were subject of initial biological and microbiological studies (SARBU et al., 2024). In addition to these, new SAS areas were recognized in the central part of the country, enhancing the need for an overview of SAS cave systems in Albania, accompanied with a summary of the ongoing scientific studies.

2. Materials and methods

In the last five years, several speleologists have wondered why in Albania there are no known active or fossil sulphuric acid caves. Their existence was especially expected since Albania shares some geological similarities with Italy and Greece (LAZARIDIS et al., 2011; D'ANGELI et

al., 2019; POPA et al., 2019), where sulphuric acid caves are widespread, and due to presence of numerous areas with thermal or even sulphidic springs (FRASHERI, 2015). Michele Sivelli (personal comm.) was one of the first to visit several of these sulphidic springs, at Holtas and at Vromoner, noticing the presence of important limestone outcrops characterized by the presence of cave entrances. Alexandra Bengel and Timo Hess photographed the first SAS cave in the Vromoner area in 2017 (ZUPNA HAJNA, 2021).

Several caving teams, mainly from Italy and the Czech Republic, started investigating these areas, based on geological maps and the position of known thermal springs, soon discovering important active sulphuric acid cave systems (Fig. 1). The scientific importance of these areas and caves became immediately clear, driving the caving teams to organize multidisciplinary expeditions involving geologists, hydrogeologists, biospeleologists and microbiologists. This holistic approach soon resulted in important scientific discoveries, mainly in the field of hydrogeology, biology, ecology and microbiology, some of which have already been published in a preliminary manner, while the others are being prepared and will be published soon.

Figure 1: *The four areas where SAS caves are being explored: 1. Holtas; 2. Langaricës; 3. Vromoner-Sarandoporo; 4. Fushë-Krujë (Map from Google Earth).*

3. Results

Presently, four cave areas are actually being investigated: Holtas Canyon (Gramsh District, Central Albania), Langarica's Canyon (Permet, Southern Albania), Vromoner-Sarandoporo Canyon (Leskovik, Greek-Albanian border), and Shpella e Zallës (Fushë-Krujë, around 15 km North of Tirana).

3.1. Holtas Canyon

In January 2018 a team of Italian cavers (Gruppo Speleologico Faentino (GSF) and Gruppo Speleologico Ariminum) started exploration in the area of the Holtas Canyon, close to the villages of Tervol and Kabash. Besides the Shpella Kabashit (shpella means cave in Albanian), known to local people, several additional sulphuric acid caves were explored. Among these, the Barutit-Kaceverrit system and the Avulit Cave, south and north of the gorge, respectively, were the most impressive. Shpella Avulit is an approximately 500-metre-deep cave system with several cave levels, characterized by extensive secondary gypsum deposits (Fig. 2).

In November 2018, scientific sampling was carried out in the framework of a bachelor thesis in Geology at the University of Bologna, finding the typical suite of secondary cave sulphates, the classical cave morphologic suite of rising flow and etching by sulphuric acid (e.g., replacement pockets), and trying to correlate different cave levels with river terraces (MARRAFFA et al., 2022).

In April 2023, thanks to the logistical support of the GSF and the Gruppo Speleologico Martinese (GSM), a multidisciplinary team carried out a sampling campaign, involving geologists, cave meteorologists, biospeleologists and microbiologists. The vast majority of collected samples are currently being studied, whereas some already led to interesting preliminary results.

Figure 2: *Sulphidic lake at the bottom of Shpella Avulit (Photo Orlando Lacarbonara).*

3.2. Langarica's Canyon

The initial research in the Kanioni i Langaricës canyon started in the 80s, when the first hypogean caves, Shpella e Pëllumbave (Pigeon Cave) and Shpella e Bënjës (Bath Cave), were described (FRASHËRI, 2013). The discovery of archaeological artefacts from the Illyrian and Neolithic periods led to the inclusion of these two caves in the list of cultural monuments of Albania. In 2023, Italian teams organized three expeditions in the area. They involved speleological clubs at national level as well as researchers from the Universities of Perugia, Bari, and Torino. In total, approximately 15 km of new cave passage were explored and documented in several sulphuric acid caves. Among them, the 12.7 km long and 116 m deep Langaricës System is the main cave here and longest known cave system in Albania (Fig. 3). It has four known entrances, with a very complex climatology and strong air circulation. The Dragon's Breath entrance is the highest and behaves like a smoking shaft in winter, with steam blowing out at temperatures of up to 26°C and with flow rates of over 5 m3/s. The cave develops over seven levels, the lowest of which has large active sections with sulphidic streams and big lakes reaching water temperatures of up to 30.4°C (BENASSI, 2024).

Preliminary biological investigations led to the discovery of rich subterranean biological communities, including endemic species of invertebrates, in both upper and lower levels of the cave. Large colonies of bats have been recorded throughout the cave, and the vast deposits of guano present the dominant food-base for the invertebrate communities. In the lower, sulphidic level of the cave, sulphur-oxidizing and -reducing bacteria and other acidophilic microorganisms form communities that cover the limestone walls as biofilms. Microbial activities and products seem to function as a food source for the cave invertebrate communities in the deepest sections of the cave.

Figure 3: *Large gypsum deposits in Regina Teuta gallery in the Langaricës Cave System. This level is located 20 metres above one of the active feeders, and is characterised by a strong flow of warm air which in winter rises towards the entrance named "Dragon's Breath" (Shpella Avullit) (Photo Andrea Massagli).*

3.3. Vromoner-Sarandoporo Canyon

Thermal springs in the Vromoner Canyon, on the Greek Albanian border, have been known from time immemorial. Due to their location in a strictly guarded border following the WW2, the hypogenic caves connected with these thermal waters have somehow skipped the attention of speleologist.

This area was explored in the last few years by the members of the Czech Speleological Society and now the research team has grown to include biologists from Romania, the US, Belgium, and Italy. Eight endemic invertebrate species have been identified in these caves to date.

Caves such as Sulfur (Fig. 4), Breshkë (Turtle), Twenty, and Atmos, contain warm sulphidic water and are actively evolving by hypogenic processes. In Atmos, one can observe one of the largest domes in hypogean caves in Europe, estimated to 200.000 m3. The huge dome is accompanied also by a thermal lake, which presents one of the largest known subterranean thermal lakes in the world. Somewhat harsh conditions for people seem not to affect the subterranean invertebrates, as eight endemic species have been identified in these caves to date.

In addition the caves in Vromoner Canyon, three additional active hypogean caves (New and Old Pixaria and Swallow Cave) have been mapped in the nearby Pixaria area, close to the Kavasila spa, Greece.

Figure 4: *Thermal sulphidic stream and gypsum accumulations covered in sulphur, in the Universe Dome in Sulfur Cave (Photo Marek Audy).*

3.4. Shpella e Zallës

Shpella e Zallës opens at the base of a limestone outcrop, located near to a cement factory in the Durazzo prefecture, 20 km north of Tirana. This area is known for its thermal springs known under the name of Uji Bardhe (white waters), alluding to the colour of the waters due to the presence of white microbial sulphur bacterial mats and streamers (Fig. 5). These thermal waters have been studied by several authors (EFTIMI & FRASHËRI, 2016; EFTIMI et al., 2024). This cave was explored by the GFS in 2018, and it was later surveyed by the GSM, reaching a total length of one kilometer. It has a horizontal level in which several feeders are present on the cave floor. These are full of fresh water that floats over the denser sulphidic one. A large sulphidic spring, with a flow rate of several litres per second, emerges just a few meters below the cave entrance.

Gypsum crusts cover the cave walls in a chamber located close to the entrance. Inside the cave, gypsum deposits are absent due to the recurring flood events which rapidly dissolve this mineral. Similarly to the caves in the Holtas Canyon, sampling of secondary minerals and sulphidic waters was carried out. Recent explorations (2023) have discovered some upper branches with extensive and beautiful gypsum crystals and crusts, and interesting microbial communities which are yet to be sampled. Future expeditions are planned to complete the survey of the entire cave, carry out sampling for microbiological analyses, and continue the exploration to some presently unknown branches.

Figure 5: *Shpella e Zallës, sampling the sulphidic spring below the cave entrance (Photo Jo De Waele).*

4. Discussion

The growing interest of foreign speleologists in the thermal and SAS cave systems in Albania has raised curiosity in both local inhabitants and authorities. One of the reasons of this lies in the fact that several of the cave systems are located in Natural Parks: Holtas Canyon is part of the Shebenik-Jabllanica National Park, while both Langaricës and Vromoner-Sarandoporo are parts of the Vjosa Wild River National Park. On the contrary, Shpella e Zallës is located in an industrialized area, largely devastated by the proximity of cement plants and quarries. The ongoing studies have shown all these active sulphuric acid caves, largely unknown to local or national authorities, to be extremely interesting places for geological and biological studies. Due to the prevailing extreme conditions, from a microbiological and ecological standpoint, these caves rank among the most interesting worldwide. In addition to the morphological phenomena largely developed under thermal and sulphidic activity, they all host specialized microbiological communities that serve as the basis for extremely adapted invertebrate communities. Many of these present new species for science and still need to be described. Specialized as they are, these ecosystems are also extremely fragile and depend on the presence of the rising sulphidic water and the peculiar conditions in which they thrive. None of the known SAS cave systems in Albania appear to be suitable for any kind of touristic or speleological exploitation, at the same time requiring human impact to be minimized to visits for scientific purposes.

5. Conclusion

Similarly to all other areas in the world where H2S-rich groundwaters emerge through springs harbored in soluble carbonate rocks, SAS caves are also present in the four Albanian regions known for the presence of thermal-sulphidic springs. The remarkable work done in the last seven years by specialized caving teams who searched for, explored, documented, and studied SAS caves in Albania, led to the discovery of extensive subterranean networks that display characteristic SAS morphological features and secondary gypsum deposits, as well as unusually abundant and diverse biological communities based on chemoautotrophy.

Alongside the continuation of work in the four sulphuric caves presently under exploration, further investigations will visit other areas known for the presence of thermal springs and sulphidic waters. It is expected that this will lead to further increase in number of sulphuric acid caves in Albania. Alongside exploring the SAS systems, and due to still poor organization of speleology in Albania, research teams are working towards involvement of local scientists of the University of Tirana and Albanian cavers, to establish a cooperation agreement for the biological research in the sulphidic caves in these areas. These activities were further enhanced by establishing the contacts with the Ministry of Tourism in Albania (responsible for the protection of nature in the country), to fulfill scientific research in compliance with both national and international legal acts (i.e. provisions of the Nagoya Protocol). By establishing these connections and following the legal framework, we tend to make a positive example, which will serve as a model for future explorers in Albania and will enable future scientifically-based protection of the country's karst peculiarities.

Acknowledgements

The explorations over the last five years were carried out with the contribution of dozens of cavers of many speleological associations, mostly members of the Italian Speleological Society, the Czech Speleological Society, and the Romanian Speleological Federation. Thanks to all.

References

AUDY M. (2022) Sulphur Cave. Une cavité thermale hypogénique exceptionelle en Albanie. Spelunca 165:6-13.

AUDY M., BOUDA R., BRUTHANS J., RUZICKA V. (2022) Albanian hypogene caves in the area of Vromoner thermal springs on the Sarandoporo River. Speleofórum 41:42-51.

AUDY M., BRUTHANS J., KASTOVSKY J., BOUDA R. (2023) Atmos – nová hypogenní jeskyne (Shpella Avulit), Albánie. Speleofórum 42:72-78.

AUDY M., BRUTHANS J., MARES J., SARBU S., GALDENZI S., BOUDA R. (2024) Sulfur 2023, hypogenní jeskyne Albánie a Recka Kavasila, Vromoner, Langarica. Speleofórum 43:4-13.

BENASSI A. (2024) Lengarices 2023: inseguendo il Soffio del Drago (Albania). Speleologia 89:4-6.

BRANDOLINI L. (2021) Albania 2009-2019. Ipogea Cronache speleologiche: 88-133.

D'ANGELI I.M., PARISE M., VATTANO M., MADONIA G., GALDENZI S., DE WAELE J. (2019) Sulfuric acid caves of Italy: A review. Geomorphology 333:105-122.

DE WAELE J., D'ANGELI I. M., AUDRA P., PLAN L., PALMER A.N. (2024) Sulfuric acid caves of the world: A review. Earth-Science Reviews 250:104693.

EFTIMI R. (2020) Karst and karst water recourses of Albania and their management. Carb. & Evap. 35(3):69.

EFTIMI R., FRASHËRI A. (2016) Thermal and Mineral Waters of Albania. PRINT-AL, Tirana, 214p.

EFTIMI R., ZOJER H. (2015) Human impacts on karst aquifers of Albania. Env. Earth Sci. 74(1):57-70.

EFTIMI R., LISO I.S., PARISE M. (2024) Hydrogeological Characteristics of the Makaresh Carbonate Karst Massif (Central Albania). Hydrology 11(2):29.

FRASHËRI A. (2013) Shpella prehistorike Bënjës, Tema. (in Albanian)

FRASHËRI A. (2015) Geothermal Energy Resources in Albania-Country Update Paper. Proc. World Geothermal Congress, 11 p.

KLIMCHOUK A.B., EFTIMI R., ANDREYCHOUK V. (2022) Hypogene karst in the External Albanides and its pronounced geomorphological effect. Karstologia Mémoires 24:205-208.

KRISTO V. (1973) Some aspects of karst in Albania. Collection of Studies 1:67-79 (in Albanian).

KRISTO V., KRUTAJ F., MEZINI B. (1987) Karst landscape of Albania and the problems of its rational exploitation. Studime Gjeografike 2:257-268 (in Albanian).

KRUTAJ F. (1985) Some features typical of the karst morphology at Kurvelesh. Studime Gjeografike 1:48-67 (in Albanian).

LAZARIDIS G., VASILIOS M., LAMBRINI P. (2011) The first cave occurrence of orpiment (As_2S_3) from the sulfuric acid caves of Aghia Paraskevi (Kassandra Peninsula, N. Greece). Int. J. Spel. 40:133-139.

MARRAFFA A., FABBRI I., POLETTI K., PASTORE C., VANDELLI W., SIVELLI M., DE WAELE J. (2022) The first important thermal sulphuric caves of Albania (Holtas canyon, Central Albania. Karstol. Mém. 24:201-204.

POPA I., BRAD T., VAXEVANOPOULOS M., GIURGINCA A., BABA S.C., IEPURE S., PLĂIAŞU R. and SARBU S.M., (2019) Rich and diverse subterranean invertebrate communities inhabiting Melissotrypa Cave in Central Greece, Trav. Inst. Spéol. «Émile Racovitza», 58:65–78.

SARBU S.M., BRAD T., BANCILA R.I., STEFAN A. (2024) Exploring Biodiversity and Food Webs in Sulfur Cave in the Vromoner Canyon on the Greek–Albanian Border. Diversity 16:477.

ZHALOV A.K. (2015) Bulgarian speleological studies in Albania 1991–2013. Berliner Höhlenk.Ber. 58:1-91.

ZUPAN HAJNA N. (2021) Karst, Caves and People. Založba ZRC, Ljubljana.

Speleogenesis in Quartzites in the Southwestern Ibitipoca State Park

Tiago Vilaça Bastos (1,2), Paulo Eduardo Santos Lima (1,4), Gabriel Lourenço Carvalho de Oliveira (1,3), Issac Daniel Rudnitki (1, 2); Pedro Henrique Assunção Silva (1, 3); Rafael Oliveira Silva (1,2).

(1) Universidade Federal de Ouro Preto, Programa de Pós-Graduação do Departamento de Geologia, Escola de Minas, Minas Gerais, Brazil, foxgeologia@gmail.com

(2) Sociedade Excursionista & Espeleológica dos Alunos da Escola de Minas, Universidade Federal de Ouro Preto, Minas Gerais, Brazil.

(3) Universidade Federal de Minas Gerais, Programa de Pós-graduação em Geologia, Instituto de Geociências, Departamento de Geologia, CPMTC-IGC, Laboratório de Estudos Hidrogeológicos (LEHID), Belo Horizonte, Brasil

(4) Universidade Federal de Ouro Preto, Departamento de Geologia da Universidade Federal de Ouro Preto, Escola de Minas, Minas Gerais, Brazil.

Abstract

The Ibitipoca Mountain Range, in southern Minas Gerais (Brazil), hosts an important speleological district that is part of the Andrelândia Speleological Province, where caves have developed in quartzites of the São Tomé das Letras Formation, Carrancas Group – Andrelândia Sequence. This study analyzed the speleogenesis of four caves in Ibitipoca State Park: Gruta Martimiano II, Gruta das Bromélias, Gruta Manequinho, and Gruta das Casas. Structural, petrographic, geochemical, and hydrochemical analyses were conducted. The results indicate that speleogenesis occurs mainly in fine-grained quartzite layers embedded between coarser quartzites. The incongruent dissolution of feldspars and micas, combined with the low solubility of silica, generates secondary porosity, favoring sandification and channeling processes. The caves follow regional fractures oriented NE-SW, NW-SE, and W-E and are also influenced by bedding (SE/21º) and an open fold (antiform) with an NNE-SSW axial plane. Groundwater shows low dissolved silica concentrations (1.67 to 3.22 mg/L) and acidic pH (3.0 to 5.8), indicating limited chemical dissolution and a predominance of mechanical erosion. Speleogenesis occurs in fine quartzite layers containing mica, feldspar, and kaolinite, with thicknesses ranging from 1.0 m (G. Martimiano II) to 11.3 m (G. Manequinho).

Résumé

La chaîne de montagnes d'Ibitipoca, située au sud du Minas Gerais (Brésil), abrite un important district spéléologique faisant partie de la Province Spéléologique d'Andrelândia, où des grottes se sont développées dans les quartzites de la Formation São Tomé das Letras, Groupe Carrancas – Séquence Andrelândia. Cette étude a analysé la spéléogenèse de quatre cavités du Parc d'État d'Ibitipoca: Gruta Martimiano II, Gruta das Bromélias, Gruta Manequinho et Gruta das Casas. Des analyses structurales, pétrographiques, géochimiques et hydrochimiques ont été réalisées. Les résultats indiquent que la spéléogenèse se produit principalement dans des couches de quartzite fin, intercalées entre des quartzites plus grossiers. La dissolution incongruente des feldspaths et des micas, associée à la faible solubilité de la silice, génère une porosité secondaire, favorisant les processus de sableification et de canalisation. Les grottes suivent les fractures régionales orientées NE-SO, NO-SE et O-E et sont également influencées par le litage (SE/21º) et un pli ouvert (antiforme) avec un plan axial NNE-SSO. Les eaux souterraines présentent une faible concentration en silice dissoute (1,67 à 3,22 mg/L) et un pH acide (3,0 à 5,8), indiquant une dissolution chimique limitée et une prédominance de l'érosion mécanique. La spéléogenèse se produit dans des couches de quartzite fin contenant du mica, du feldspath et de la kaolinite, avec des épaisseurs variant de 1,0 m (G. Martimiano II) à 11,3 m (G. Manequinho).

1. Introduction

Siliciclastic caves, although less studied than caves in carbonate rocks, exhibit speleogenetic features associated with differential dissolution and mechanical processes, representing a wide range of formations and processes (MARTINI, 1979; WRAY, 1997; SILVA, 2004; FABRI, 2014; WRAY & SAURO, 2017). The most recognized siliciclastic karst regions worldwide are located in Venezuela, South Africa, Australia, Brazil, and India, with large-scale features and caves (WRAY & SAURO, 2017). In Brazil, siliciclastic karst regions are found in the Amazon (states of Roraima, Amazonas, and Pará), Chapada dos Guimarães (Mato Grosso), Serra Geral province (Paraná and São Paulo), Serra do Caraça (Minas Gerais), and the Andrelândia Speleological Province (PEA) (Minas Gerais) (SILVA, 2004).

Ibitipoca State Park (PEIB) covers 1,488 hectares in southern Minas Gerais and hosts one of the largest concentrations of quartzite caves in Brazil, totaling 64 mapped cavities (SEE, 2024). It also has the highest density of large quartzite caves in the country (RUBBIOLI et al., 2019). Preliminary studies have contributed to understanding the speleogenesis of the cave system in the Ibitipoca Mountain Range. The processes of sanding and piping, controlled by lithological, structural, and hydrochemical factors, influence the formation of caves in the quartzites of the São Tomé das Letras Formation (Carrancas Group – Andrelândia Sequence) (CORRÊA NETO et al., 1993; CORRÊA NETO et al., 1997; CORRÊA NETO, 1997; CORRÊA NETO & DUTRA, 1997; OLIVEIRA, 2021). However, knowledge gaps still exist regarding the formation of this siliciclastic karst.

Thus, this study aims to analyze and discuss the speleogenetic processes of four caves located in the southwestern portion of PEIB. Through structural characterization, petrographic, geochemical, and hydrochemical analyses, this research seeks to understand the influence of geological structures, lithology, and hydrochemical interactions on the evolution of underground conduits and surface landforms.

2. Methods

Through field campaigns, geological (structural, petrographic, and lithological) surveys, hydrochemical analyses, and characterization of speleological processes and features were conducted. Four main caves within Ibitipoca State Park (PEIB) were selected for study: Gruta Martimiano II (4,170 m), Gruta das Bromélias (3,447 m), Gruta Manequinho (966 m), and Gruta das Casas (557 m) (Figure 1).

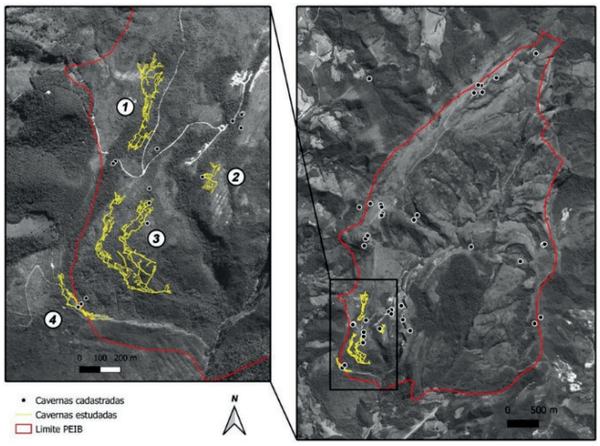

Figure 1: *Location of the Studied Caves in Relation to Ibitipoca State Park.*

2.1. Structural Characterization – Surface and Subsurface

Structural characterization involved measuring fractures, bedding, and foliation, totaling 1,705 structural attitudes. The data were analyzed using stereograms and plotted on maps to identify structural patterns controlling speleogenesis. Additionally, stratigraphic profiles were recorded to measure the thickness of fine-grained quartzite layers and assess their lateral continuity.

2.2. Petrographic and Geochemical Analyses

Twenty rock samples were collected for lithological and mineralogical characterization, analyzed using X-ray diffraction (XRD) and inductively coupled plasma optical emission/mass spectrometry (ICP-OES/MS) to determine major and trace element compositions.

2.3. Hydrochemical Analysis

Hydrochemical analyses were conducted at 23 groundwater sampling points, measuring physicochemical parameters such as pH, electrical conductivity (EC), resistivity (RES), temperature (T), oxidation-reduction potential (ORP), and total dissolved solids (TDS). These parameters were obtained using a Myron L Company Ultrameter II multiparameter instrument. Dissolved silica concentrations were determined using an Agilent 725 ICP-OES (Inductively Coupled Plasma Optical Emission Spectrometry).

2.4. Sediment Collection from Cave Walls and Ceilings

An innovative experiment was conducted in Gruta das Casas, where two 50×50 cm glass plates were placed in two fossil conduits: one beneath saccharoidal coarse-grained quartzite from the ceiling and another beneath fine-grained micaceous quartzite from the cave wall. These plates remained in place for one year, collecting sediments that naturally fell onto them due to gravitational forces, assisted by rock «breathing»—the expansion and contraction caused by water absorption and loss. The collected sediments were weighed using a precision balance at the Hydrochemistry Laboratory of DEGEO

3. Results

3.1. Structural Control

The caves exhibit strong structural control influenced by bedding, subvertical fractures, and folding. Three fracture families, an antiform, and bedding planes were mapped. The polydeformed quartzite presents penetrative fractures that allow meteoric water percolation and infiltration into deeper layers. Stereographic analysis indicates two main preferential fracture systems: NE-SW, NW-SE, and W-E, which govern the development of underground conduits. In the southwestern portion of PEIB, the rock bedding dips toward the SE at approximately 21° (Figure 2)

3.2. Lithostratigraphic Influence

Speleogenesis predominantly occurs in fine-grained micaceous quartzite layers, which are primarily composed of feldspar/kaolinite and muscovite, with accessory minerals such as lepidocrocite, glauconite, and jaffeite. These layers vary in thickness from 1.0 m to 11.3 m, with the thinnest layer in Gruta Martimiano II and the thickest in Gruta Manequinho (Figure 3).

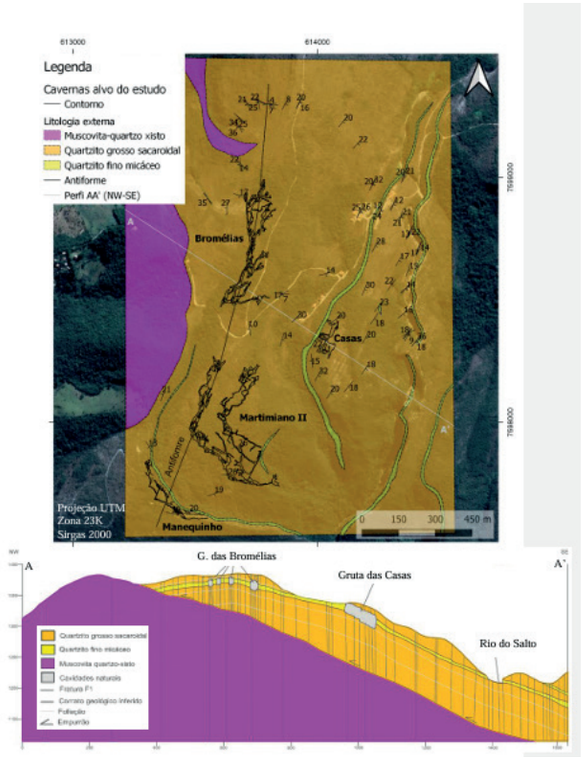

Figure 2: Geological map of the study area. The profile shows that the cavities develop in the fine micaceous quartzite found beneath the coarse saccharoidal quartzite. Fractures facilitate the percolation of rainwater, which accumulates in the fine quartzite and removes the material, thereby forming the cavities.

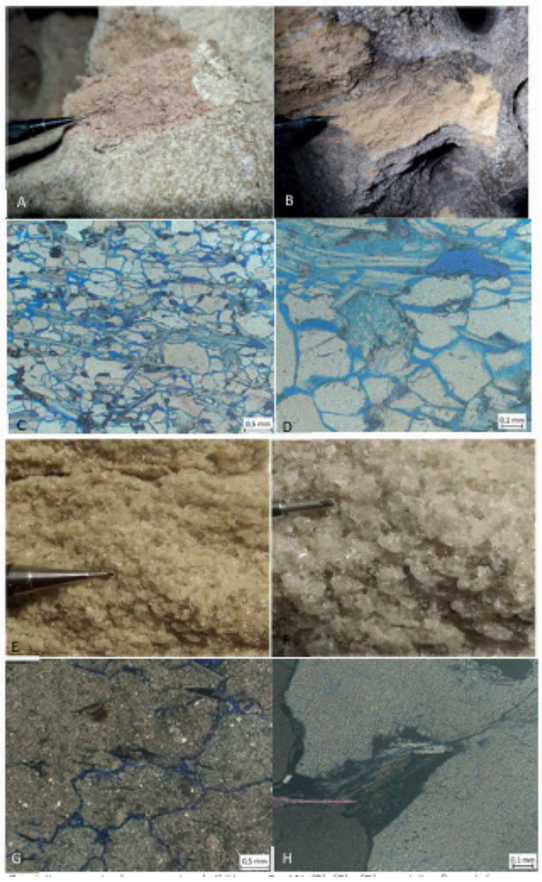

Figure 3: Quartzites found in the caves of Ibitipoca. In (A), (B), (C), and (D), fine micaceous quartzites with the presence of micas, feldspars, and high porosity (impregnated with blue epoxy resin). In (A) and (B), macroscopic view with colors ranging from white to pink; in (C), thin section with 0.5 mm zoom; and in (D), thin section with 0.1 mm zoom, both showing fine grain size, abundant micas, and secondary porosity. In (E) and (F), detail of the coarse grain size of the quartzite, whereas in (G) and (H), the thin section highlights low mica content, fractured grains, dissolution of quartz mineral edges, and low secondary porosity.

This lithology contains less resistant minerals such as feldspars and micas, which undergo incongruent dissolution, forming kaolinite. The dissolution along quartz grain boundaries due to water percolation is sufficient to initiate sanding processes, thus facilitating secondary porosity formation.

Conversely, coarse-grained saccharoidal quartzite, with SiO_2 content exceeding 94%, exhibits high resistance to dissolution, limiting speleogenesis progression. The fine quartzite layers, in contrast, contain SiO_2 ranging from 79% to 91% and Al_2O_3 between 3% and 13%, with the highest Al_2O_3 content (13%) found in Gruta Martimiano II, followed by Gruta das Bromélias (9%), and values below 2.01% in coarse quartzite samples.

As previously described, fine quartzite layers are interbedded within coarser quartzite layers. In some caves (Martimiano II, Bocão, and Rasteirinha), upper conduits developed within these fine-grained quartzite layers, revealing the repeated occurrence of this crucial lithological unit.

3.3. Hydrochemical Analyses

Hydrochemical analyses revealed low silica concentrations, ranging from 1.67 to 3.22 mg/L, and pH values between 3.0 and 5.8 (OLIVEIRA et al., 2023). Other elements detected in the analyses, such as Al, Ca, Na, Mg, and Fe, indicate the occurrence of additional hydrogeochemical processes, including the incongruent dissolution of feldspars and micas.

4. Discussion

4.1. Structural Control

Stereographic analysis indicates three main preferential fracture systems: NE-SW, NW-SE, and W-E, which govern the development of underground conduits. Bedding planes facilitate water percolation toward the Salto River (local base level), leading to the enlargement of conduits through dissolution and mechanical processes, which generate incasions followed by wall and ceiling collapses.

The mapped antiform in the northern portion of Gruta das Bromélias, located in the highest sector of the cave, contributes to the lateral expansion of conduits. The formation of entrances and skylights, associated with this structure, creates a direct pathway for rainwater infiltration into the system, accelerating dissolution and enhancing erosion processes.

4.2. Lithological Influence

The fine-grained quartzite layer is the primary lithological unit where speleogenesis initiates, either due to its composition, which contains more soluble minerals than coarse quartzite, or due to its finer grain size, making it more easily eroded.

Another active erosional process affecting fine-grained quartzite is the exudation-induced loss of water from the rock to the cave atmosphere, resulting in the disaggregation of sand grains that compose the quartzite. This process was confirmed by sediment collection using 50×50 cm glass plates installed in Gruta das Casas for one year. At sampling point CC1, 0.225 g of micaceous fine quartzite was collected from the cave wall, while at point CC2, 1.7074 g of quartzite sediment was collected from the ceiling.

This experiment demonstrates the volumetric loss of the cave without direct erosional agents and suggests that ceiling collapse may occur more rapidly than wall retreat. Once the fine quartzite layer is removed, collapse and conduit closure processes begin.

Additionally, vertical grooves ranging from centimeter to meter scales were observed in fine quartzite layers. These features result from gravity-driven movement of exudated water droplets, which emerge from cave walls and descend to the floor, forming vertical fluting. This mechanism gradually widens conduits and channels through mechanical quartz grain removal.

4.3. Hydrochemical Analyses

Hydrochemical data indicate that chemical dissolution plays a secondary but significant role in rock grain disaggregation and sandification, whereas mechanical erosion is the primary process driving conduit enlargement.

The characterization and analysis of subterranean water flow revealed hydraulic interconnectivity between the two largest caves of Ibitipoca (OLIVEIRA et al., 2023), forming an underground drainage system approximately 7.5 km long: the Bromélias-Martimiano II System, which also includes Gruta Vandinho, located between them.

5. Conclusion

The results of this study demonstrate that the speleogenesis of the caves in Ibitipoca State Park (PEIB) is controlled by three main factors:

Structural Control – The NE-SW, NW-SE, and W-E fracture systems dictate the orientation and development of underground conduits. Bedding planes, which dip SE at 21°, enhance erosional processes by directing water flow along the steepest slope toward the Salto River (local base level). Additionally, the antiform located in the northern portion and the main conduit of Gruta das Bromélias laterally expands the cave's area, resulting in the formation of five entrances. This expansion facilitates rainwater infiltration, increasing its microbasin contribution area and capturing part of the Rio Grande Basin flow into the Paraíba do Sul Basin.

Lithological Control – Speleogenesis initiates in fine-grained micaceous quartzites and progresses toward coarse-grained saccharoidal quartzites, which are less susceptible to dissolution but more prone to collapse. Dissolution features, such as channels, are only observed in fine quartzite layers, whereas in coarse quartzite, discontinuities are primarily enlarged by water erosion. Fine quartzite layers are enclosed above and below by coarse quartzite, and their complete removal triggers collapse processes, facilitated by bedding planes and fractures.

Hydrochemical Influence – The groundwater exhibits low silica concentrations, low levels of other dissolved elements, and acidic pH, indicating that chemical dissolution plays an essential role in sandification. This process allows mechanical erosion to act in conduit enlargement, transporting disaggregated quartz grains.

This study reinforces the importance of the Ibitipoca Mountain Range as a model for understanding quartzitic intra-stratal karst in Brazil. It highlights the interplay between lithology, structural controls, and hydrochemical processes in the formation of siliciclastic caves, where dissolution, erosion, and gravitational processes actively contribute to cave development.

Acknowledgments

The authors express their gratitude to the staff and collaborators of Ibitipoca State Park, especially to UC Manager Clarisse Silva, for her continuous support. We also extend our thanks to the cavers of SEE for their ongoing exploration efforts in Ibitipoca, which still holds much to be discovered. Our appreciation goes to our colleagues from the Department of Geology at UFOP and the Institute of Geosciences at UFMG, particularly to Professor Fabrício Caxito (Boni) and Dr. Lucas Padon de Sá Godinho (Rejeito) for their interest and valuable contributions. Special thanks to Professor Atlas Corrêa Neto (UFRJ) for insightful discussions and deepening the understanding of this topic.

We also acknowledge the National Center for Cave Research and Conservation (CECAV) of ICMBio – Chico Mendes Institute for Biodiversity Conservation, for funding support, and all the cavers who have contributed, directly or indirectly, to the studies of the Ibitipoca caves. Every mapped meter is part of this work!

References.

CORREA NETO, A.V., FILHO, J.B., 1997. Espeleogênese em quartzitos da Serra do Ibitipoca, sudeste de Minas Gerais. anu. Inst. Geocienc. 20, 75–87.

CORREA NETO, A.V.; ANISIO, L.C.C.; BRANDÃO, C.P. 1993. Um endocarste quartzítico na Serra do Ibitipoca, SE de Minas Gerais. Anais VII Simpósio de Geologia de Minas Gerais, p. 83-86.

CORREA NETO, A.V.; ANISIO, L.C.C.; BRANDÃO, C.P.; CINTRA, H.B. 1997. Gruta das Bromélias (mg-042), Serra do Ibitipoca, município de Lima Duarte, MG: Uma das maiores cavernas em quartzito do mundo. Espeleo-tema 18: 1-12.

CORREA NETO, A.V.; DUTRA, G. 1997. A Província Espeleológica Quartzítica Andrelândia, sudeste de Minas Gerais. Anais XXIV Congresso Brasileiro de Espeleologia, p. 57-64.

FABRI, F. P., AULER, A., & AUGUSTIN, C. H. R. R. (2014). Relevo cárstico em rochas siliciclásticas: uma revisão com base na literatura. Revista Brasileira de Geomorfologia, 15(3).

MARTINI, J.E.J., 1979. Karst in black reef quartzite near Kaapsehoop, eastern Transval. ann. s. afr. geol. surv. 13, 115–128.

OLIVEIRA, G. L. C. D. 2022. Processos hidrogeoquímicos como gatilho para a espeleogênese no setor sudoeste do Parque Estadual do Ibitipoca-MG.

OLIVEIRA, G. L. C. D. ASSUNÇÃO, P. H. S. LIMA, P. E. S. BASTOS, T. V. RUDNITZKI, I. D (2024). Conexão hídrica entre as cavernas quartzíticas Bromélias e Martimiano II na Serra do Ibitipoca, MG. Revista Brasieira de Espeleologia – RBEsp. V. 01, Nº01. – ICMBio/Cecav

RUBBIOLI, E., AULER, A., MENIN, D., & BRANDI, R. (2019). Cavernas-atlas do Brasil subterrâneo. Brasília, ICMBio/CECAV. 370p.

SILVA, S.M. Carstificação em rochas siliciclásticas: estudo de caso na Serra do Ibitipoca, Minas Gerais. MG. 2004. 143f. Dissertação de mestrado em geografi a, Instituto de Geociências, Universidade Federal de Minas Gerais, BH-MG.

SOCIEDADE EXCURSIONISTA E ESPELEOLOGICA – SEE (2024). Projeto Cadastro e Avaliação dos Aspectos Espeleoturísticos das Cavernas do Parque Estadual do Ibitipoca – MG (IBITITUR).

WRAY, R.A.L. 1997. A global review of solutional weathering forms on quartz sandstones. Earth-Science Reviews 42: 137-160.

WRAY, R. A., & SAURO, F. (2017). An updated global review of solutional weathering processes and forms in quartz sandstones and quartzites. Earth-Science Reviews, 171, 520-557.MAMMOLA S. (2019) Finding answers in the dark: caves as models in ecology ffty years after Poulson and White. Ecography 42(7):1331–1351.

On the genesis of caves in hardly-karstic rocks

Anatoliy Bulychov (1), Igor Novikov(1), Maria Bulychova (1) & Artem Barinov (2)

(1) Institute of Geology and Mineralogy, SB of RAS, Russia, Novosibirsk, climber.57@mail.ru (corresponding author)
(2) Krasnoyarsk Club of Speleologists, Russia, chairman, barinoff.t@yandex.ru

Abstract

Signs of abundant argillization (alteration of the initial substance by hypogenic processes and replacement of newly formed clay minerals) were found in the studied caves in conglomerates, marbles and silicified limestone. There are significant deposits of clay substrate (argillite) on the bottom of definite levels with uprising vertical tubes with dome-shaped dead-ends, change of rocks colour, shift of pH of solutions to acidic values, etc. The formation mechanism of the studied caves is offered: removal of the substrate argillized by low-hydrothermal processes along the fault zones, by groundwater without perceptible participation of karst processes.

1. Introduction

In the Altai-Sayan mountain region (southern Siberia of Russia), there are a number of caves developed in rocks in which karst processes are hardly possible to occur. In East Sayan, these are the Big Oreshnaya and Dudinskaya caves in conglomerates, the total length of which is more than 51 km and 41 km, respectively. Within the Altai Mountains, these are the Altaiskaya and Kek-Tash caves in marbled and silicified limestone with a total length of 4.7 and 3.2 km, respectively. 3-D mapping of the listed caves revealed that the morphology of their passages and the general structure differ significantly from those of caves in carbonate rocks. Their vertical extension is tens and more than hundred of meters, and lateral extension is up to hundred of meters. The structure of the passages of the studied caves resembles the structure of karst caves, rotated vertically by 90°. In general, the pattern of the passages is arranged as a system of disjoint extended subvertical planes with rare short subvertical planes connecting them. The revealed structure corresponds to the geometry of the structural pattern of Late Cenozoic fault systems formed as a result of subhorizontal compression and correlates with geophysical observations.

2. Methods and materials

During the study of caves, linear structures were identified: narrow, wide and at the same time high, rectilinear cave cavities, laid along the zones of crushing of Cenozoic tectonic disturbances. Linear structures have vertical or almost vertical walls with signs of slidingsides or without them due to erosion by draining watercourses. Associated crushing zones, breccias were identified and their tectonic origin was assumed. The height of the accessible part of faults was determined by mapping after wall ascents using

mountaineering equipment or laser surveys where it was possible. For a more detailed identification of the fault systems, instrumental mapping using a Leica HDS 7000 laser was necessary. On the surface, to identify areas of increased fracturing density, structural-tectonic profiling was carried out according BULYCHOV (2024), based on the assumption about wave nature of density distribution of fracturing. To detect near (3-20 m) surface cavities seismic-electrical measurements were carried out on the surface. The Big Oreshnaya and Dudinskaya caves are located in the Cambrian-Ordovician conglomerates of the Narva formation. The conglomerates are dislocated by Cenozoic extension faults, which are the feather structures of the system-forming faults of the right-lateral kinematic type (Novikov, 1998). The Big Oreshnaya cave has an amplitude of 234 m (according to the frontal projection), taking into account the new system system, which is located 44 m above the main entrance. The length of the cave is more than 51 km (Bulychov, 2021), but the three-dimensional labyrinth is extremely complex, so only 3-D cross-section is provided (Fig. 1).

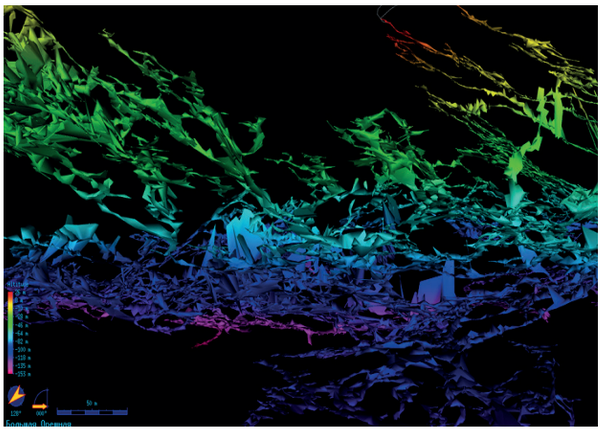

Figure 1 : *3-D cross-section of Big Oreshnaya cave.*

Similar observations were made on the Badjeysky massif, as a result of which a completely new cave, Dudinskaya, was discovered (Fig. 2).

There are more than 41 km of passages with chasms and a “lattice--box” labyrinth mapped in 2022-2024. Signs of disjunctive disturbances in the central part of the cave appear in crushed zones or linear structures located closer to the surface, but deeply embedded galleries are developed along distinct tectonic faults (Bulychov, 2024). The height of accessible part of the faults (either by means of topographic surveys after the ascents or by laser measurements) turned out to be from 20 to 80 m, the length from 90 to 250 m, the width from 0.5 m to 5 m.

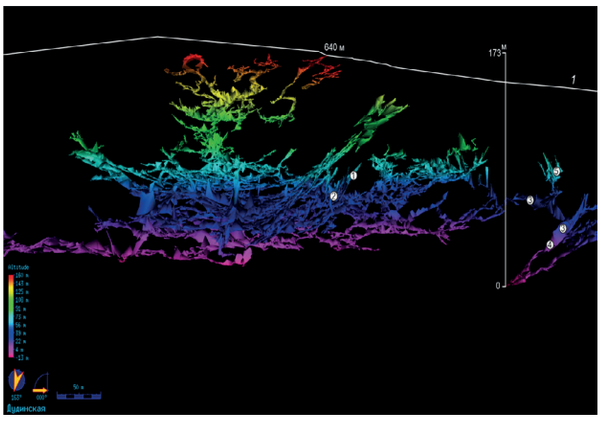

Figure 2 : *3-D cross-section of Dudinskaya cave : 1- day surface, 640 m-absolute height*

The Altayskaya Cave is the largest of the known caves in the Altai Mountains and has the most complex vertical structure among all the caves in the Far East and Siberia. It is located on the Metlevo plateau, 25 km from the village Kamlak. The Lower Cambrian marbled limestones of the Kayanchinskaya suite (400-500 m thick), in which the cave is located, are framed by acidic effusive, terrigenous-volcanogenic rocks, granites and faults of the right-lateral type with feathering extension structures. The final topographic survey and the map with a cross-section were made by the author of the article (Bulychov, 2021). Based on the results of structural-tectonic profiling and stereoscopic interpretation of aerial photographs, faults with extending of 0^0, 45^0, 315^0 were identified. A bright feature of the cave is a lot of ascending slit-like planes connecting the lower levels to the upper ones. Three wide cavities up to 180 m in height run into dome forms (Fig. 3) with quartzite crust, blocked from above by a layer of dense marbled limestones, while 15-20 m remains to the day surface.

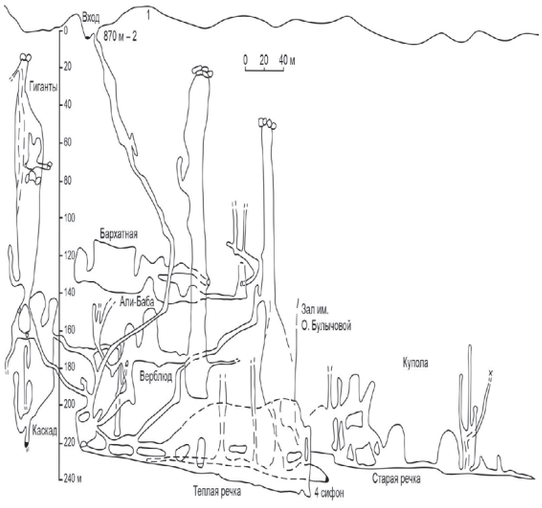

Figure 3 : *Cross-section of Altaiskaya cave : 1- day surface, 2-absolute height*

The Kek-Tash cave (Fig. 4) is located 17 km from the village Kamlak, has similar geological and tectonic conditions with the Altaiskaya cave: originated in dense marbled limestones of the Lower Cambrian of Kayanchinskaya suite by faults and cracking with extending of 0^0, 110^0, 230^0. The cave is the deepest in Siberia (Bulychov, 2021).

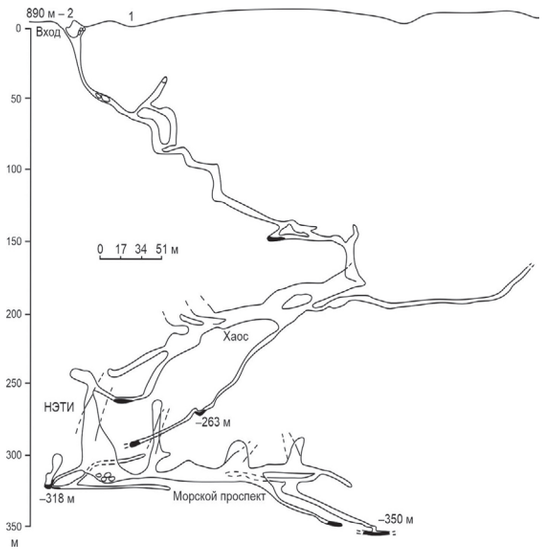

Figure 4 : *Cross-section of Kek-Tash cave : 1- day surface, 2-absolute height*

3. Results and Discussion

In all observed caves, signs of gypogenic argillization were found: light brown - yellowish argillizites, what corresponds to observations of RAZUMOVA (1977). The hydrogen index in the solution probe in a period of freatic flooding, measured by an autonomous pH-meter Ohaus ST300-B, occurred to be about 6.0. Significant deposits of argillizites were marked at the 2nd level of the caves: Old River and Sea Avenue, not wholly carried out by ground waters. The argillizites turned out to be close in composition to illite-smectite (according to results of X-ray phase analysis “Dron-8”) with inclusions of SiO_2 and feldspar, the grain size of which is no more than 0.02 mm (according to the results of granulometry). Ascending passages often run into dome-shaped dead ends (Fig. 5), what probably indicates their hypogenic origin and corresponds

to

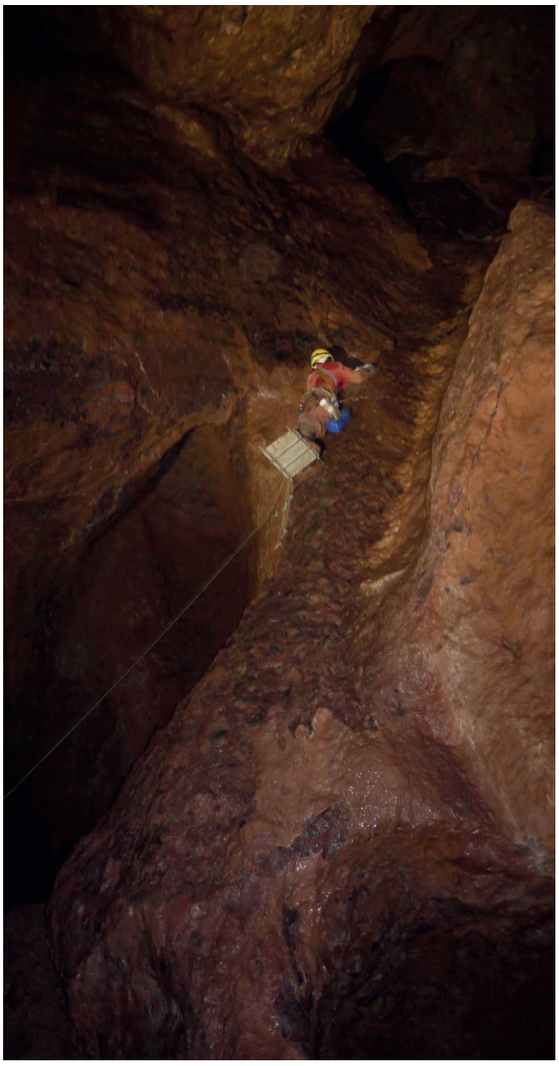

Figure 5 : *Climbing up to the dead-ends in Big Oreshnaya cave.*

The process of gypogenic argillization is a low-temperature hydrothermal weakly acidic leaching along zones of tectonic fractures, refer to Volostnykh (1972). Low-temperature hypobyssal emanations - gases: CO_2 (95%), H_2S (3%), H_2CO_3 (2%) - participate in the process. Carbon dioxide, when combined with ground water, forms H_2CO_3 acid, which is a very aggressive agent: the reaction rate increases up to tens of times according Palmer (1995) during the corrosion of rocks, including limestones and marbles: $CaCO_3 + CO_2 + H_2O \leftrightarrow Ca^{2+} + 2HCO_3$. Admixtures of mica, feldspars of silicified limestones and quartzites in the zones of deep faults are argillized by low-temperature metasomatism, according to Kazitsyn (1979), Dvornikh (2020):

$KA1_2(0H, F)_2[(AlSi)_3O_{10}] \rightarrow KAl_2(OH)_2[(AlSi)_3O_{10}] \rightarrow$
muscovite sericite -
$\rightarrow K_{0,5\text{-}0,7}Al_2(OH)_2[(SiAl)_3O_{10}] \bullet n\,H_20 \rightarrow A1_4(0H)_8[Si_4O_{10}]$,
hydromica kaolinite

what is also characteristic of argillization of plagioclases, micas in conglomerates.

We consider this process important in speleogenesis due to deep faults and the presence of igneous rocks in the studied area. There are a lot of evidences of hypogenic origin observed in the caves: dead-end dome arches, domes in the ceilings (Fig. 6), ascending blind chambers (Fig. 7), change of color of rocks, hydrothermal veins (Fig. 8, 9), suspended meanders (Fig. 10), etc.

Figure 6 : *Domes in the ceilings in Dudinskaya cave.*

Figure 7 : *Ascending blind chambers in Dudinskaya cave.*

Figure 8 : *Hydrothermal crystals of veins in Dudinskaya cave (Northern System).*

Figure 9 : *Crystals of hydrothermal creak in Dudinskaya cave.*

Figure 10 : *Suspended meanders in Dudinskaya cave.*

4. Conclusion

Mechanism for cavity formation proposed is based on the well-studied phenomenon of fault argillization. We distinguish three stages of cavity formation in hardly-karstic rocks: a) formation of crushed zones, b) processing by hydrothermal fluids (argillization) along crushed zones (confined system), which is proposed to begin in oligocen – miocen, c) removal of argillizite by ground waters. Cenozoic (golocen) fragmentation "opened" the deeply located cavities as a post-gypogenic process, according to Klimchouk (2009).

The proposed mechanism allows to take a fresh look at the prospects for discovering new large caves within the Altai-Sayan mountain region. Previously, when a karst mechanism for their formation was assumed, all exploration work was concentrated within the development fields of carbonate rocks. Now, when it is clear that the geological prerequisites for the formation of the considered caves are not associated with carbonates, the entire territory of plateau-like lowlands framing the alpine-type regions of the Altai-Sayan mountain region can be considered to be promising areas to plan discoveries.

Acknowledgments

We gratefully thank A.B. Klimchouk for consultations on hypogenic kastogenesis during our meetings at International Congresses of Speleologists beginning from Sweetzerland in 1997 and except Savoie Mont Blanc in 2022. Thanks a lot to B.R. Mavlyudov for ideas of karstogenesis in quarcites and marbles.

References

BULYCHOV A. (2024) Caves in slightly-karst rocks of Altai-Sayan mountain region : mechanism of formation and morphology. Geomorphology and paleogeography 2: 256-273.

BULYCHOV A. (2021) Speleology: rock-climbing and geomorphologic approach. South Florida Journal of Development (SFJD), ISSN 2675-5459, 2 (5): 6864-6881.

DVORNIKH G. (2020) Types of metasomatic rocks: temperature conditions of formation, compositional features, minerageny. News of UGGU 1(57): 63-72.

KAZITSYN Yu. (1979) Metasomatism in the Earth's crust. Leningrad: Nedra: 208 p.

KLIMCHOUK A. (2007) Hypogene speleogenesis: hydrogeological and morphogenetic perspective. National Cave and Karst Researxh Institute. Special paper #1. Carlsbad: 106 p.

KLIMCHOUK A. (2009) Morphogenesis of gypogenic caves. Geomorphology. 106: 100-117.

NOVIKOV I. (1998) The role of tectonics in the evolution of the relief of Mountainous Altai. Geomorphology 1: 82-91.

PALMER A. (1995) Geochemical models for the origin of macroscopic solution porosity in carbonate rocks.

Geochemical models for the origin of macroscopic solution porosity in carbonate rocks. Eds. Budd D.A., Harris P.M., Sailer A. American Association of Petroleum Geologists, Tulsa. Memoir 63: 77-101.

RAZUMOVA V. (1977) Ancient weathering crusts and the hydrothermal process. Moscow: Nauka: 156 p.

VOLOSTNYKH G. (1972) Argillization and mineralization. Moscow: Nedra: 240 p.

Defining the influence area on speleological heritage in the karst of Lagoa Santa: a case study of the Limeira Cave

Allan Calux (1), Moisés Perillo (2), Gisele Kimura (3) & Robson Santos (4)

(1) Carstografica Karst Applied Research Centre, Campinas/SP, Brazil, calux@carstografica.science (autor correspondente)
(2) Sigma 1 Geologia e Meio Ambiente, Itaúna/MG, Brazil, moisesperillo@hotmail.com
(3) Hidrovia Hidrogeologia e Meio Ambiente, Belo Horizonte/MG, Brazil, gisele@hidrovia.com.br
(4) TEC3 Geotecnia e Recursos Hídricos, Belo Horizonte/MG, Brazil, rsantos@tec3engenharia.com.br

Resumo

Delimitar a área de influência sobre uma caverna, sobretudo aquelas hidrologicamente ativas, implica em definir da melhor maneira possível as condições de contorno que influenciam a dinâmica de circulação de matéria e energia em determinado sistema cárstico. No Brasil, essa abordagem é especialmente importante porque tem aplicação direta na proteção e conservação das cavernas inseridas no contexto de empreendimentos minerários, geradores de energia hidrelétrica, de infraestrutura terrestre, entre outras, um avez que seus limites determinam as medidas de controle e monitoramento que devem ser realizadas durante a implantação, operação e fechamento destes empreendimentos. Por definição, a área de influência sobre uma caverna (ou sobre o patrimônio espeleológico) compreende os elementos bióticos e abióticos, superficiais e subteerrâneos, necessários à manutenção do equilíbrio ecológico e da integridade física do ambiente cavernícola, ao que acrescentamos também a necessidade de manutenção de sua dinâmica evolutiva. Este trabalho apresenta uma síntese dos resultados obtidos durante os estudos para definição da área de influência da Gruta da Limeira, localizada no contexto do Carste de Lagoa Santa, província espeleológica conhecida pela presença de lagoas cársticas e cavernas paragenéticas.

Abstract

Delimiting the area of influence over a cave, particularly those that are hydrologically active, involves defining as accurately as possible the boundary conditions that influence the dynamics of matter and energy circulation within a specific karst system. In Brazil, this approach is especially important due to its direct application in the protection and conservation of caves situated within the context of mining operations, hydroelectric power generation, terrestrial infrastructure projects, among others, given that their boundaries determine the control and monitoring measures that must be implemented during the installation, operation, and decommissioning of these ventures. By definition, the area of influence over a cave (or over speleological heritage) encompasses the biotic and abiotic elements, both surface and subsurface, necessary for maintaining the ecological balance and physical integrity of the cave environment, to which we also add the necessity of preserving its evolutionary dynamics. This paper presents a synthesis of the results obtained during studies aimed at defining the area of influence of Limeira Cave, located within the context of the Lagoa Santa Karst, a speleological province known for its karst lakes and paragenetic caves.

1. 1. Introduction

The area of influence of a cave, within the context of Brazilian environmental licensing, is defined by a resolution of the National Council for the Environment – CONAMA – as the area encompassing the biotic and abiotic elements, both surface and subsurface, necessary for maintaining the ecological balance and physical integrity of the cave environment (CONAMA 2004). However, although its definition is quite clear and objective, its application, given the continental extent of Brazil and, consequently, the immense diversity of environments and subterranean systems, faces significant complexity.

This paper presents the results of a comprehensive hydrogeological and hydraulic study conducted in the area of an intermittent karst lake located within the context of the Mina Limeira, in the municipality of Prudente de Morais, State of Minas Gerais (Figure 1). This lake occurs in the region known as the Lagoa Santa Karst, a speleological province characterized by a typical and diverse karst geomorphology, but which, according to Berbert-Born (2002), exhibits particularly striking features, among them the presence of lakes with varied hydrological behaviors, associated with doliniform depressions and lowered reliefs, and a complex network of subterranean conduits, often connected to the surface relief through passages accessible to humans.

The objective of this study was to understand the effective contribution of the waters from this lake to the evolutionary dynamics of Limeira Cave, located on the northwestern margin of this depression, which is occasionally subject to the effects of water level rise during high-magnitude rainfall events.

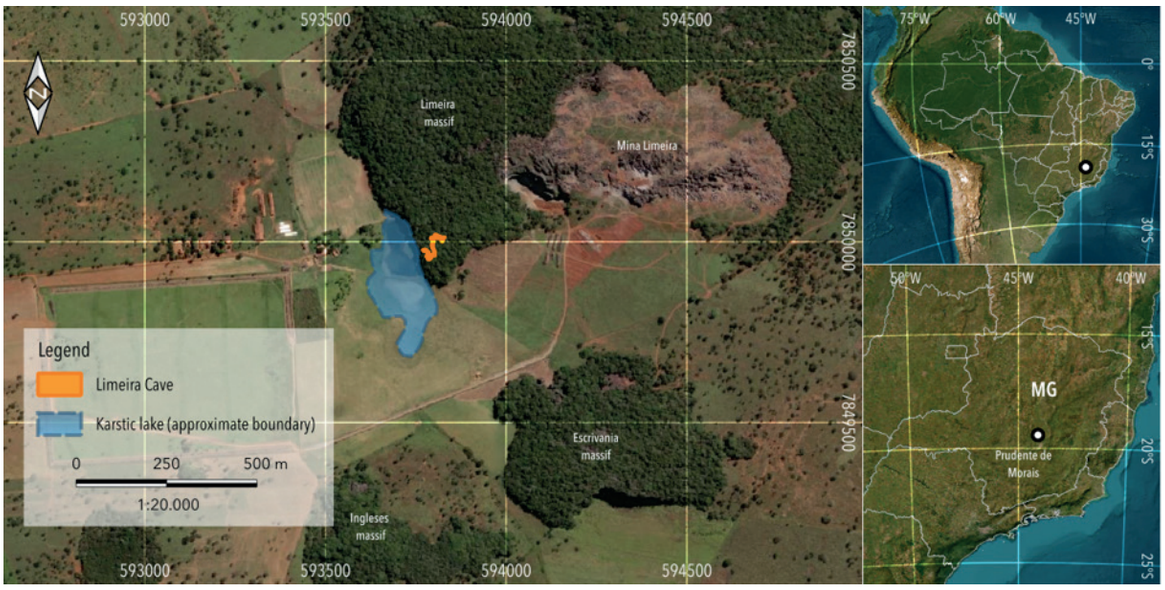

Figure 1: *Study area.*

2. Methods

Hydrogeological approach

The fieldwork was conducted during the months of September and November 2017 and aimed to identify local hydrogeological features, verify the wells listed in the available databases, conduct structural surveys, and evaluate the available drilling cores. These activities were integrated with secondary data collected (e.g., CPRM 2003, PESSOA 2005, IGAM 2017, SIAGAS 2017) for the development of the conceptual hydrogeological model.

Additionally, four percussion drillings were carried out to verify the depth of the water table and validate the geophysical model conducted in the area.

A potentiometric map was developed based on data collected from 30 registered tubular wells and springs in the vicinity of the study area, available in IGAM (2017) and SIAGAS (2017). The potentiometric levels were obtained through topographic leveling of the wells using the SRTM digital elevation model (spatial resolution of 30 meters) and measurements of the static water level depth at each point. Despite the limitations in altimetric resolution and the fact that measurements were taken at different times, an attempt was made to assess whether a qualitative and regional analysis of the main groundwater flow direction trends could be inferred from the existing data. The interpolation method used to generate the groundwater surface is called Topo-to-Raster, implemented in the QGIS 2.4 software.

Furthermore, in March 2019, three monitoring wells were installed in the study area. These, along with an existing tubular well in the area and the surface waters of the lake, were subjected to sampling for monitoring and hydrochemical characterization (Figure 2 and Figure 3).

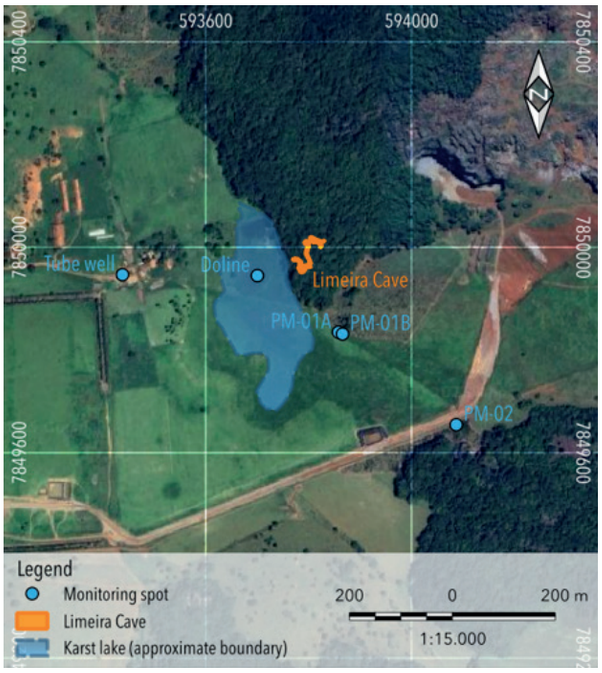

Figure 2 : *Monitoring and sampling spots.*

Spot	Location coordinates (SIRGAS 2000 23K)		Quantitative Parameters	Qualitative Parameters
	UTM E	UTM N		
PM-01A	593858	7849835	Water level	Bicarbonates Total Calcium Carbonates Chlorides Conductivity Total magnesium Nitrate Dissolved Oxygen Total Potassium Redox Potential Total Sodium Sulphates Ambient Temperature Sample Temperature
PM-01B	593866	7849831	Water level	
PM-02	594086	7849655	Water level	
Tube well	593438	7849947	Water level	
Doline	593700	7849945	-	

Figure 3 : *Location of monitoring and sampling spots.*

Hydraulic approach

For the development of the studies, the following materials were used:

- A topographic base with contour lines at submetric intervals;
- Hourly precipitation data obtained from a dedicated meteorological station installed at the same location as the tubular wells PM01 (A and B) between May 2019 and January 2020;
- Daily precipitation data from the Sete Lagoas rainfall station (code 83586), available in INMET (2020);
- Daily precipitation data for the Cercadinho and Pampulha stations, located in Belo Horizonte/MG, available in INMET (2020).

The methodology adopted for determining the inflow volumes as a function of precipitation (rainfall-volume model) was based on the rational method. Although this methodology is typically used to determine peak flow, its conversion to inflow volumes is entirely applicable using peak flow values and the duration of the precipitation event. The rationale behind the rational method is straightforward, as it incorporates the main factors contributing to stormwater runoff in a drainage area, including the drainage area itself, the precipitation for a given duration, and the runoff coefficient, which reflects the terrain's cover and its capacity to promote the portion of rainwater that effectively flows over the surface.

As a restrictive element, the application of this methodology should be limited to drainage areas of less than 1 km². However, it is possible to use this approach for areas of up to 10 km² by applying a delay coefficient determined according to the area and slope of the main channel, as shown in the equation below (Figure 4).

$$Qp = 0{,}278.C.i.A.\psi$$

Where :
Qp is the pick flow, in m^3/s
C is the runoff coefficient
i is the design rainfall intensity, in mm/h
A is the drainage area, in km^2
ψ is the delay coefficient

Figure 4 : Rational method equation with dalay coefficient.

Given that the area is karstic, meaning it is subject to the capture of surface waters, it was necessary to consider the effects arising from this hydrogeological component. In such cases, it is recommended to adopt a surface runoff loss factor to better represent the reduction in inflow volumes in karst regions. This factor is applied directly to the values (whether flow or volume) typically determined by traditional methods, thereby allowing the incorporation of runoff losses (due to infiltration) caused by the presence of karst features in the drainage area, particularly cavities and fractures. For this purpose, to better represent the contributed volumes, the adoption of the following loss factors (Figure 5) should be considered on the results of the Rational method, based on the return period, assuming the drainage area is entirely within a karst domain.

Return period - RT (years)	Loss factor
2	0
5	0
10	0
15	0
20	0
25	0
50	0
100	1
200	1
500	1
1000	1

Figure 5 : *Loss factors per return period.*

3. Results

From a geological perspective, the area is located within the Bambuí Group domain, composed of rocks formed by the transport and deposition of sediments in a predominantly marine environment approximately 600 million years ago. The stratigraphic stacking consists of interbedded pelites and limestones, with siliceous detrital rocks at the base and top. The area where the Limeira, Escrivania, and Ingleses outcrops are located lies within the Sete Lagoas Formation domain, where the calcite limestones of the Lagoa Santa Member outcrop. These are dark gray to black calcarenites, tending to lighter tones in altered portions. Their grain size ranges from fine to medium, with ooids observed at some points. The bedding is subhorizontal with a gentle dip to the south. Structurally, the main fracture family has a NE-SW orientation, although two other families occur in the area with NW-SE and N-S orientations, though they are less persistent.

Data from shallow drillings indicated that in the area of the karst lagoon, where there is no outcrop, the limestone is covered by a layer of yellowish to reddish clayey soil, with an average thickness between 13 and 25 meters. Additionally, a geophysical study was conducted using the electrical resistivity method to evaluate the characteristics of the sedimentary cover and the bedrock. The investigated depth was 100 meters below the surface, and this study was later validated with shallow drillings positioned at strategic locations to assess the nature of the material in zones of low and high resistivity, thereby supporting the geological interpretation.

By correlating the geophysical results with the geological knowledge of the area, interpreted geological profiles were developed based on the resistivity data, substantiated by the drillings. In the shallow portion of the area where the geophysical survey was conducted, up to an average depth of 20 meters, a zone of higher resistivity occurs. The interpretation of the high-resistivity zones at the top of the profiles was attributed to the unsaturated zone of the aquifer, characterized by high-porosity sediments without water saturation. This zone is likely

composed of clayey to silty-clay sediments. The low-resistivity zones located just below were interpreted as epikarst zones, defining a unit situated at the boundary between the unsaturated and saturated zones of the aquifers. This zone is of significant interest for fluid circulation, exhibiting high permeability and good storage capacity.

The doliniform depression where the karst lake develops is covered by a predominantly clayey soil with an average thickness ranging from 11 to 15 meters, according to drilling data from the area. One of the drillings, conducted in the lowest portion of this feature, penetrated an 18-meter-thick layer of yellowish-brown clayey soil, with the groundwater level located at a depth of 17.2 meters on November 22, 2017. Even under these conditions, the presence of water within the doline is observed during rainy periods. However, based on groundwater level depth data obtained from three points around the doline, this water does not correspond to the outcrop of the water table, as in this region, groundwater was situated at depths between 17 meters (in the drilling) and 23 meters (in the existing tubular well), according to data from November 2017. It is therefore evident that there are no direct hydraulic connection points between the bottom of the doline and the water table—a fact demonstrated by the accumulation of water on its surface while groundwater lies far below the terrain. If there were a connection point between the bottom of the doline and the underlying aquifer, rainwater would be rapidly drained to the local base level, preventing surface accumulation.

Even though groundwater levels might have been lowered due to the prolonged drought period between 2012 and 2017, past instances where anomalous rises in the water level accumulated in the doline were recorded—evidenced by flood phase marks on the limestone massif walls—also do not indicate an outcrop of the water table. If groundwater levels had risen close to the terrain surface, the water table would have emerged through the sinkholes identified at the edge of the Limeira massif, given the absence of other direct connection points with the aquifer at the bottom of the doline.

However, there have never been reports of water overflowing through these sinkholes, even during periods of extreme rainfall. All observations indicate that the sinkholes function effectively as water infiltration points, not as springs.

The potentiometric map developed indicates a groundwater flow direction from SW to NE, toward Córrego do Gordura, which represents the local base level. This flow direction was confirmed by water level measurements in piezometers P-01A, P-01B, and P-02, indicating that the groundwater flows from the Escrivania massif toward the Limeira massif.

The average difference of approximately 0.34 cm (ranging between 0.21 and 0.42 cm) between the water levels in wells PM-01A and PM-01B (with PM-01B levels being higher) suggests a connection between the shallow (water table) and deep (karst) aquifers, with a slight degree of confinement in the karst aquifer at this location. This behavior is expected, as the karst aquifer is overlain by a layer of clayey soil that acts as a partial confining layer, although this condition may vary depending on the thickness and granulometry of the soil at each location.

The results obtained confirm the understanding that groundwater levels lie below the terrain surface, with no connection to the water accumulated in the doline or to any surface runoff potentially identified in the cavities at the edge of the Limeira massif. The hydrochemical data, in general, point to a completely meteoric origin of the lagoon's waters.

Regarding the hydraulic approach, the application of the rational method resulted in a set of predicted water level elevations based on the return periods and durations of interest (Figure 6). The results suggest that the rise in the water level of the lake is more associated with long-duration events rather than extreme events (intense rainfall).

To address the importance of these periodic floods in dimensional development, as exemplified in Figure 7, an exercise can be conducted using the average denudation rate defined for the region by Auler (1994). Assuming continuous denudational evolution, with an average rate of 76 mm per thousand years, and considering the approximate thickness of the Limeira Massif in the section that hosts the 001L caves, it can be inferred that, in approximately 410 thousand years, chemical erosion would intercept and extinguish these cavities. As demonstrated by the hydrological model, periodic flooding is recurrent in the area. However, if we isolate the events with the highest probability of exceeding the cave entrance elevation, which occasionally functions as a sinkhole, and consider the longest period of cumulative rainfall, a return period of 25 years can be established. Over 410 thousand years, 16,400 flooding events would occur, which, individually, would account for a radial endokarst expansion of approximately 1.25 meters. In other words, in a highly summarized and simplified manner, within the same timeframe in which the massif enclosing the caves would eventually erode, the caves would evolve by 1.25 meters—a negligible value.

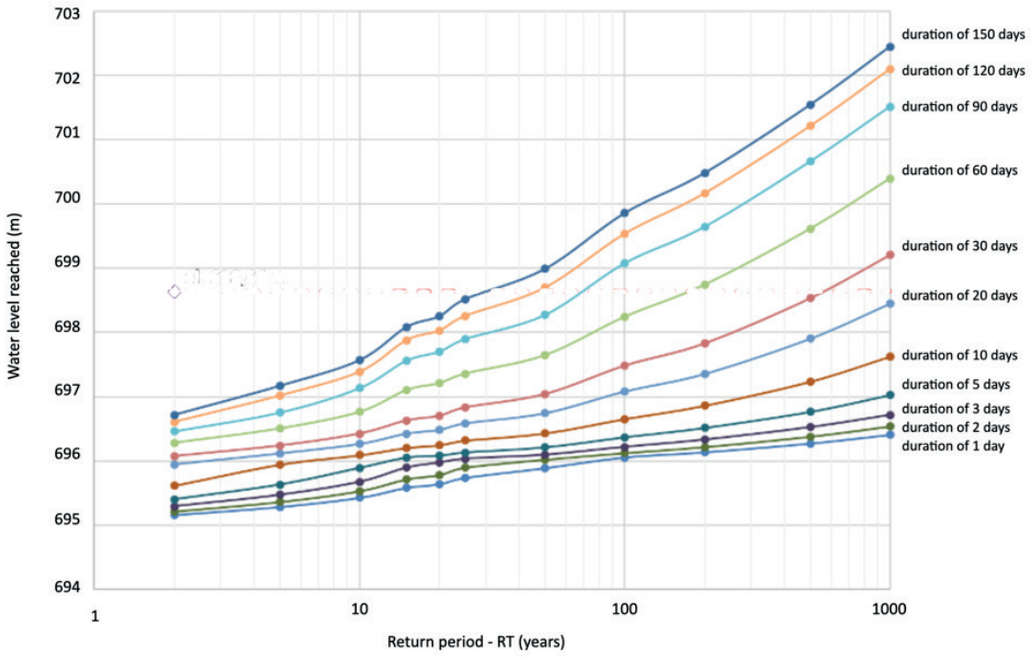

Figure 6 : *Simulation of the elevation of the lagoon water as a function of the return period obtained by the rational method.*

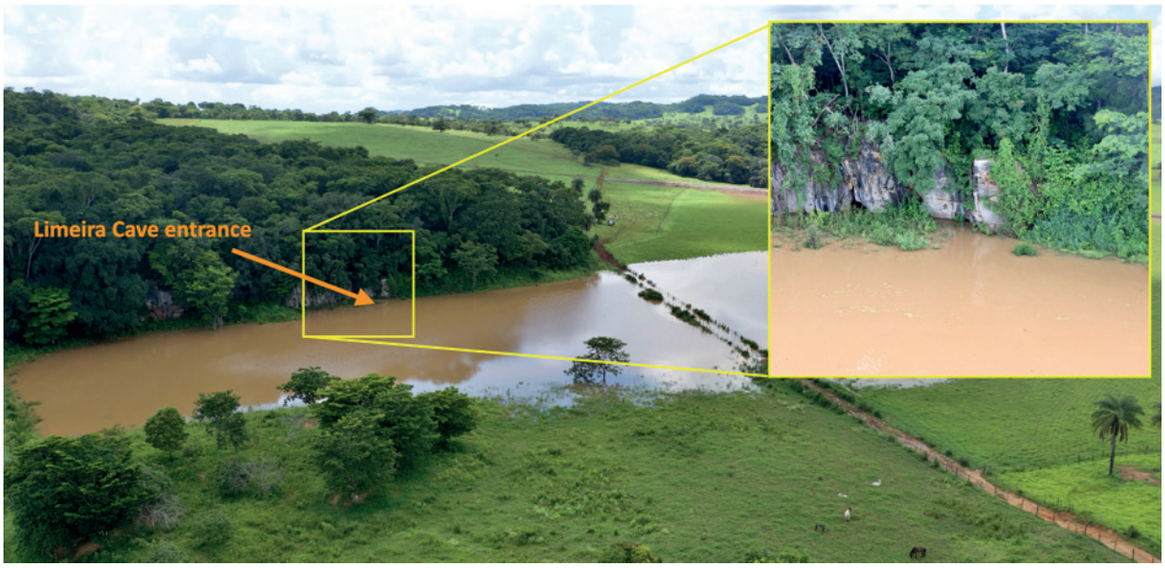

Figura 7 : *Limeira Cave sinkhole reactivated during long-term rainfall events in the summer of 2020.*

4. Discussion and conclusion

The obtained data demonstrated that, from an evolutionary perspective, the current hydrological context of elevated water levels in the karst lagoon has little influence on the expansion of the galleries and conduits of Gruta da Limeira. It was also demonstrated that the lagoon's waters are exclusively of meteoric origin, meaning the hydrological influence area is restricted to the fluctuation levels of these surface waters.

On the other hand, while the current hydrodynamic context does not significantly contribute to the speleogenetic expansion of the cave, these periodic water injections through the sinkhole of Gruta da Limeira, as observed during the summer of 2020, undoubtedly introduce sediments and trophic resources essential for structuring the cave-dwelling communities within.

Thus, we conclude that the approach used to validate the conceptual karst model of the area was not only appropriate but also fundamental for clearly delineating the limits of hydrological influence on this specific cave, Gruta da Limeira. In light of this, we emphasize the importance of monitoring the water level fluctuations of this lagoon to control and mitigate potential impacts caused by the mining operations occurring in its vicinity.

5. References

AULER, A. S. 1994. Hydrogeological and Hydrochemical Characterization of the Matozinhos-Pedro Leopoldo Karst, Brazil. Dissertação de Mestrado. Western Kentucky University.

BEERBERT-BORN, M. (2002). O Carste de Lagoa Santa, MG : berço da paleontologia e espeleologia brasileira. In : Schobenhauss et al. SIGEP : sítios geológicos e paleontológicos do Brasil. Distrito Federal : Brasília. Vol 1. P.415-430.

CPRM – SERVIÇO GEOLÓGICO DO BRASIL. (2003). Projeto Vida : Viabilidade Industrial e Defesa Ambiental – Relatório Final, Mapeamento geológico. Região de Sete Lagoas, Pedro Leopoldo, Matozinhos, Lagoa Santa, Vespasiano, Capim Branco, Prudente de Morais, Confins e Funilândia, Minas Gerais. Escala 1:50.000.

PESSOA, P. 2005 Hidrogeologia dos aquíferos cársticos cobertos de Lagoa Santa, MG. Tese de doutorado. Universidade Federal de Minas Gerais, 553p.

Sistema hídrico de cavernas em quartzito na Serra de Ibitipoca, Minas Gerais, Brasil.

Ana Eliza Medeiros Cândido (1,2), Pedro Assunção (2,3,4), Gabriel Lourenço Carvalho de Oliveira (2,4), Paulo Eduardo Santos Lima (1,2), Tiago Vilaça Bastos (2), Leandra Peixoto Nolasco Selos (1,2), Marcelo Taylor de Lima (2), Lucas Pereira Leão (1)

(1) Universidade Federal de Ouro Preto, Departamento de Geologia, Ouro Preto (MG), Brasil. ana.candido@aluno.ufop.edu.br

(2) Sociedade Excursionista e Espeleológica (SEE), Ouro Preto (MG), Brasil

(3) Espelogrupo Pains (EPA), Pains (MG, Brasil

(4) Universidade Federal de Minas Gerais, Programa de Pós-graduação em Geologia, Instituto de Geociências, Departamento de Geologia, CPMTC-IGC, Laboratório de Estudos Hidrogeológicos (LEHID), Belo Horizonte, Brasil

Abstract

Quartzite cave systems correspond to complex geological formations with dynamics distinct from traditional systems associated with carbonate rocks, and they have been gaining increasing scientific recognition. The Ibitipoca State Park, the study area of this work, stands out as an important Brazilian speleological province, housing extensive quartzite caves, including the Martimiano II Cave, the largest in the country in this lithology. The objective of this study is to investigate the potential hydro-karstic system of the Coelhos-Casas-Rasteirinha caves, using fluorescent dye tracers to map hydrological connections and delineate recharge and discharge areas. The results confirm the interconnection between the caves and reinforce the need for sustainable management of the area to preserve these unique environments.

Résumé

Les systèmes de grottes en quartzite correspondent à des formations géologiques complexes, dont les dynamiques diffèrent de celles des systèmes traditionnels associés aux roches carbonatées, et ils gagnent de plus en plus en notoriété scientifique. Le parc d'État d'Ibitipoca, zone d'étude de ce travail, se distingue comme une importante province spéléologique brésilienne, abritant de vastes grottes en quartzite, dont la grotte Martimiano II, la plus grande du pays dans cette lithologie. L'objectif de cette étude est d'explorer le potentiel système hydro-karstique des grottes Coelhos-Casas-Rasteirinha, en utilisant des traceurs fluorescents pour cartographier les connexions hydrologiques et délimiter les zones de recharge et de décharge. Les résultats confirment l'interconnexion entre les grottes et renforcent la nécessité d'une gestion durable de la zone pour préserver ces environnements uniques.

Resumen

Sistemas de cavernas em quartzito correspondem a formações geológicas complexas, com dinâmicas distintas dos sistemas tradicionais associados as rochas carbonáticas, e que vem ganhando cada vez mais notoriedade científica. O Parque Estadual De Ibitipoca, área de estudo deste trabalho, destaca-se como uma importante província espeleológica brasileira, que abriga extensas cavernas em quartzito, entre elas a gruta Martimiano II, a maior do país nessa litologia. O objetivo deste estudo está na investigação do possível sistema hídrico-cárstico das cavernas Coelhos-Casas-Rasteirinha, através da utilização de traçadores corantes fluorescentes para mapear conexões hidricas e delimitar áreas de recarga e descarga. Os resultados confirmam a interligação entre as cavernas, e reforça a necessidade de uma gestão sustentável da área para preservação desses ambientes.

1. Introduction

Sistemas de cavernas correspondem a parte da paisagem cárstica, que são relevos peculiares da crosta terrestre. Durante muito tempo, o termo carste associou-se exclusivamente às rochas carbonáticas (calcários e dolomitos), com cavernas e condutos geradas a partir da sua dissolução (FORD & WILLIAMS, 2007).

O avanço nos estudos em carstologia trazem novas perspectivas a respeito desse termo, visto que feições semelhantes e bem desenvolvidas ocorrem ao redor do mundo também em outras litologias, como em rochas siliciclásticas (WRAY, 1997). De acordo com a análise feita por Fabri (2014), existem consensos acerca do processo de formação de cavernas em rochas siliciclásticas.

A disponibilidade hídrica e o tempo necessário para que ocorra a dissolução, em virtude da baixa solubilidade da sílica, são importantes fatores consensuais entre diversos autores. Além disso, a estabilidade tectônica tem papel fundamental na dissolução, pois ela permite uma continuidade do processo ao longo do tempo geológico. Fatores geológicos-estruturais também são condicionantes importantes, pois a dissolução passa a ser eficiente também nos pequenos espaços vazios presentes entre os grãos e nas descontinuidades de rochas como o quartzito. Por fim, o processo mecânico erosivo conhecido como "piping" também aparece como um condicionante importante, a partir da abertura de espaços na rocha por meio da remoção física dos grãos

(WRAY, 1997; SILVA, 2004; FABRI 2014; WRAY & SAURO, 2017).

A geometria dos sistemas de cavernas em quartzitos pode passar por mudanças severas ao longo do tempo, como colapsos, preenchimento por sedimentos, oscilações da superfície freática e mudanças das direções de fluxo. Essas complexidades dificultam o entendimento da circulação da água subterrânea e na delimitação das áreas de contribuição hídrica destes sistemas. Dessa maneira, a técnica de traçadores fluorescentes tem se mostrado uma excelente ferramenta para determinar direções de fluxo/conexões hidráulicas, delimitar bacias de contribuição hídrica (áreas de recargas e descarga), além de estimar velocidades e tempo de trânsito do fluxo. Embora essa técnica seja bastante difundida em carste desenvolvidos em rochas carbonáticas, existem poucos estudos com sua aplicação em sistemas de cavernas quartzíticas (OLIVEIRA et al., 2024).

O Parque Estadual do Ibitipoca (PEIb) corresponde a uma unidade de conservação permanente com muitas cavernas formadas em quartzito, incluindo as maiores do país, sendo considerado uma importante província espeleológica brasileira. No setor sudeste do PEIb existe um sistema de cavernas cujas conexões hídricas e área de recarga são desconhecidas (Fig. 1). Diante deste contexto, este trabalho busca identificar as possíveis conectividades e a delimitação da contribuição hídrica do sistema da Gruta dos Coelhos, Grutas das casas e Gruta Rasteirinha, no sudoeste do PEIb, por meio da aplicação de traçadores fluorescentes e análise dos parâmetros físico-químicos.

2. Materials and methods

2.1. Revisão bibliográfica e dados pré-existentes

Constituiu-se da análise e busca por estudos prévios relacionados com a temática da pesquisa. Tais trabalhos, que envolvem artigos, trabalhos de conclusão de curso, dissertações e relatórios técnicos abordam pesquisas sobre a geologia/espeleologia do local (TEIXEIRA-SILVA et al., 2017). Também inclui a revisão e compreensão sobre os métodos que serão aplicados a fim de contribuir para seu desenvolvimento, além de dados espeleológicos fornecidos pela Sociedade Excursionista e Espeleológica – SEE.

2.2. Medições de vazão e análise físico-química

Para o monitoramento das vazões de descarga foi empregado o método volumétrico, que foi utilizado posteriormente para o cálculo da massa recuperada dos traçadores corantes fluorescentes. O método volumétrico feito se deu por meio da cronometragem do tempo gasto para encher um balde plástico com 30 litros e um cronômetro. As medições ocorreram em dois pontos diferentes, sendo um na gruta das Casas e o outro na Gruta Rasteirinha, onde foi realizado 5 medidas em cada um, para que fosse possível obter a média entre eles e um valor mais exato, visto que o fluxo da água estava alto e difícil se ser medido.

Os parâmetros físico-químicos foram obtidos por meio de um por meio de um multiparâmetro Ultrameter modelo IITM6p, onde foram obtidos os valores de potencial hidrogeniônico (PH) para as três cavidades.

2.3. Traçadores corantes fluorescentes

A técnica de traçadores é uma ferramenta muito importante utilizada na hidrogeologia cárstica. Por meio dela, é possível estabelecer os limites da bacia hidrográfica, determinar áreas de recarga, além de permitir estimar as velocidades de fluxo das águas subterrâneas (FIELD, 2002; GOLDSCHEIDER & Drew, 2007). A utilização desse método se deu a partir do estudo de background, que correspondeu a uma etapa inicial registrada 22 horas antes do início dos testes, para permitir a aplicação através da caracterização das condições naturais de fluorescência dos fluxos hídricos da área de estudo. Posteriormente, foi aplicado o teste onde a quantidade do traçador foi realizada com uma quantidade de injeção controlada, estimada a partir da equação proposta por Worthington & Smart (2003), sendo:

$$M = 1{,}9 \cdot 10\text{-}5\ (L \cdot Q \cdot C)^{0.95}$$

A partir disso, foi injetado 200 gramas de um traçador fluorescente (Fluoresceína Sódica) no ponto de recarga e monitoramento das curvas de recuperação dos traçadores nos pontos de descarga, por meio de um fluorímetro GGUN-FL30 modelo (1650) (SCHNEGG, 2002) com data loggers para análise quantitativa. O ponto de injeção ocorreu no sumidouro da Gruta Coelhos/Tio Nelson, e análise quantitativa com a instalação de dois fluorímetros de campo, sendo um na Gruta das Gruta Casas, programado para obter medidas a cada 15 minutos e na Gruta Rasteirinha, a cada 5 minutos (Fig. 1).

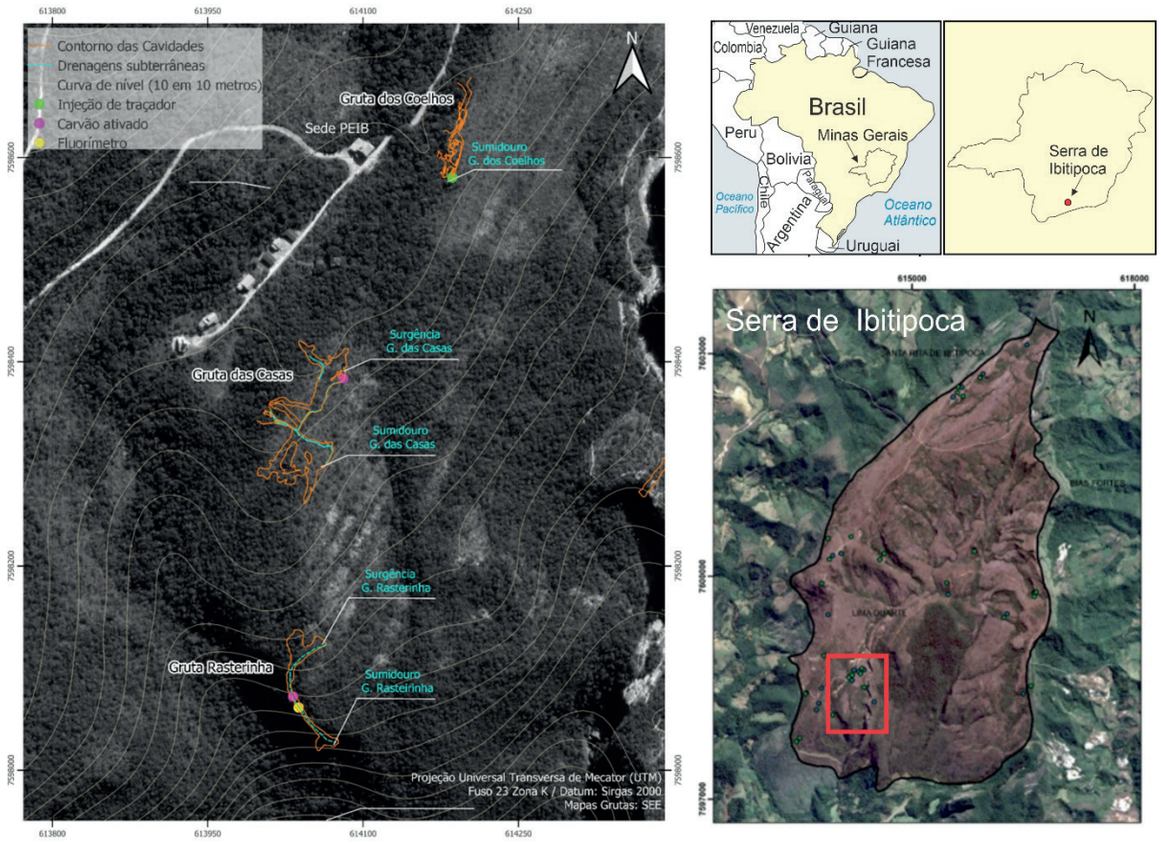

Figure 1: *Localização do sistema hídrico de cavernas estudado em relação ao Parque Estadual da Serra de Ibitipoca, no sul do estado de Minas Gerais, Brasil.*

3. 3. Results

A aplicação das metodologias foi facilitada pelo conhecimento prévio das cavidades, possibilitada a partir do mapeamento das cavidades já realizado previamente, pela Sociedade Excursionista e Espeleológica (SEE).

Os valores de vazão obtidos foram semelhantes para duas cavidades onde foi possível realizar a medição, sendo de 24,52 m^3/h para a gruta das casas e 25,48 m^3/h para a gruta rasteirinha. A coleta, realizada em período chuvoso, pode ter contribuído para os valores altos de vazão obtidos. Na gruta dos coelhos, não foi encontrado um ponto onde o método pode ser empregado para obter valores precisos.

A análise dos parâmetros físico-químicos foi realizada nas três cavidades com o objetivo principal de obter informações sobre o potencial hidrogeniônico (pH), sendo 4,45 para a Gruta dos Coelhos/Tio Nelson; 4, 39 para a Gruta das Casas e 4,26 para a Gruta Rasteirinha. Tais informações indicam um pH baixo, de característica ácida e que de acordo com Auler et al. (2020), apresentam influência para diminuição da intensidade da fluorescência e que envolve uma área também em quartzito e com condições baixas de pH.

A partir da análise quantitativa realizada com a fluoresceína, os dados obtidos apresentaram resultados associados aos parâmetros quantitativos, que passam pela fase de ascensão, pico e recessão, associadas ao tempo e concentração específicos, apresentados nas imagens 1 e 2. Essas fases incluem a análise do tempo em que o traçador foi detectado pela primeira vez após a injeção (t1); o momento em que a concentração atinge seu valor máximo (tp); o ponto em que o traçador retorna a níveis indetectáveis (tf) e o tempo necessário para que metade da massa total do traçador seja recuperada (tr/2) (Fig.2).

A partir disso, as concentrações ao longo da curva são definidas, com valor máximo de concentração atingido aos 90 minutos após a injeção, com concentração máxima de 189,14 ppb e 155 minutos com concentração máxima de 189,95 ppm na Gruta das Casas e Rasteirinha, respectivamente (Fig. 2).

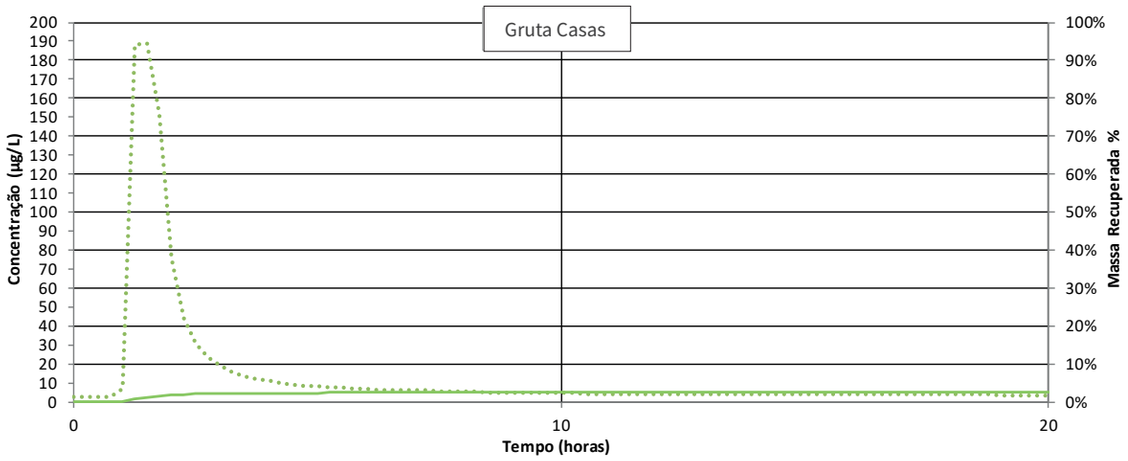

Parametros Iniciais			Curva de Restituição			Parametros Hidráulicos			Contudo e Fluxo	
Injeção	23/10/24-17:31:00		C0	2.77	(ppb)	tm	5.03	(horas)	V(m3)	123.25
Min	0.20	(kg)	t1	1.50	(horas)	Vm	71.95	(m/h)	A(m2)	0.34
Qin	0.00	(m3/h)	Cp	189.14	(ppb)	Vmax	241.50	(m/h)	Dc(m)	0.66
Qout	24.48	(m3/h)	tp	1.50	(horas)	Vf	28.76	(m/h)	ff	1.66
Δt	15	(min)	tR/2	1.50	(horas)	hL	0.005	(m)	Laminar	
X	315	(m)	Mout	0.01	(kg)	DL	191.21	(m2/h)	Pe	136.31
Xs	362	(m)		3%	(%)	α	2.66	(m)	Re	1698.44

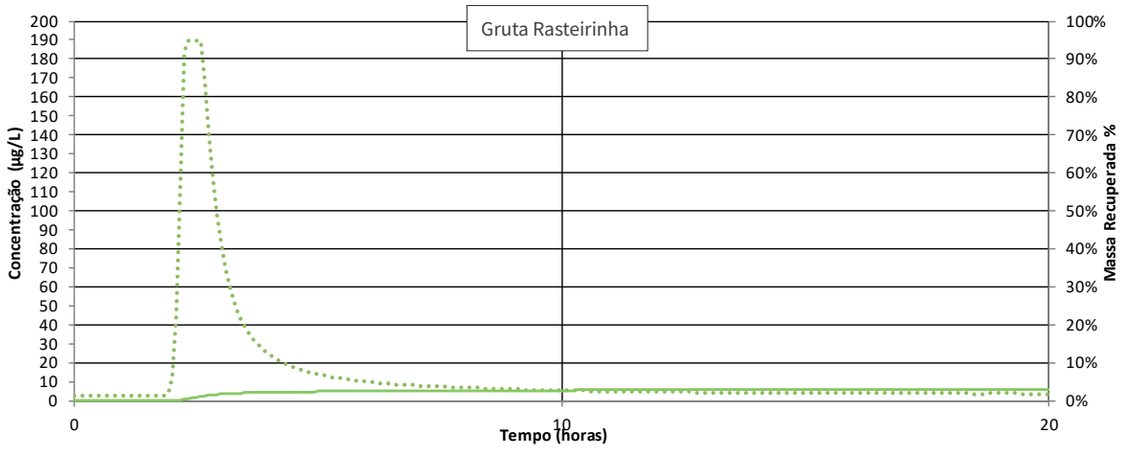

Parametros Iniciais			Curva de Restituição			Parametros Hidráulicos			Contudo e Fluxo	
Injeção	23/10/24-17:26:00		C0	2.40	(ppb)	tm	6.10	(horas)	V(m3)	149.45
Min	0.20	(kg)	t1	1.92	(horas)	Vm	101.72	(m/h)	A(m2)	0.24
Qin	0.00	(m3/h)	Cp	189.95	(ppb)	Vmax	324.00	(m/h)	Dc(m)	0.55
Qout	24.48	(m3/h)	tp	2.58	(horas)	Vf	46.23	(m/h)	ff	2.55
Δt	5	(min)	tR/2	2.83	(horas)	hL	0.024	(m)	Transição	
X	540	(m)	Mout	0.01	(kg)	DL	258.55	(m2/h)	Pe	244.32
Xs	621	(m)		3%	(%)	α	2.54	(m)	Re	2019.50

Figure 2: *Curvas de restituição da fluoresceína sódica para os pontos de monitoramento na Gruta Casas (superior) e na Gruta Rasteirinha (inferior) com os respectivos valores dos parâmetros iniciais, das curvas, hidráulicos e geométricos.*

4. Discussion

De acordo com os estudos realizados, foi possível obter dados importantes a respeito das três cavidades analisadas. Os resultados obtidos a partir do teste quantitativo mostram que existe uma conexão hídrica entre as grutas Coelhos-Casas-Rasteirinha formando um sistema hídrico-cárstico, no Parque Estadual de Ibitipoca.

A velocidade máxima do fluxo apresentou valores elevados, e que aumentaram da Gruta das Casas para a Gruta Rasteirinha, sugerindo uma contribuição do gradiente hidráulico presente no sistema.

Ademais, outros parâmetros obtidos abrem espaço para maiores discussões e busca por um melhor entendimento do comportamento do

sistema, como a baixa recuperação da massa do traçador, de apenas 3% nas duas cavidades monitoradas, levantando questões sobre a dinâmica do fluxo e possíveis vias de dispersão ainda não definidas.

5. Conclusion

O setor sudoeste do Parque Estadual de Ibitipoca (PEIB) abriga também o sistema hídrico das grutas Bromélias-Martimiano II, sendo o maior sistema hídrico de cavernas em quartzito do Brasil, com aproximadamente 7,5km de extensão (OLIVEIRA et al., 2023). Este estudo, que trouxe a confirmação do sistema hidríco-cárstico das grutas Coelhos-Casas-Rasteirinha no Parque é de extrema importância para a contribuição do entendimento espeleológico da região e reforça a relevância da área de estudo.

Cabe destacar que existe uma necessidade mais eficaz para a gestão de visitação turística, visto que a gruta dos Coelhos, aberta ao turismo e uma das mais visitadas do parque, integra-se a um sistema com outras duas cavidades de extrema importância e fragilidade, que demandam ações ainda mais específicas.

Para que se tenha uma compreensão ainda maior do sistema, é necessário que se tenha uma continuidade dos estudos na área e que outros parâmetros sejam analisados. Sabe-se que a formação dessas cavidades é fortemente condicionada por fatores estruturais, os quais também influenciam no fluxo hídrico. Investigações adicionas ampliarão o conhecimento científico da região, além de fornecer importantes informações que contribuem para uma gestão mais sustentável deste patrimônio natural único.

Acknowledgments

Esta pesquisa foi financiada por uma parceria com a Sociedade Excursionista e Espeleológica, e o Laboratório de Estudos Hidrogeológicos da UFMG (LEHID), coordenado pelos professores Paulo Galvão e Rodrigo de Paula, que cedeu os fluorímetros e traçador para realização do estudo. Os autores também agradecem ao Parque Estadual de Ibitipoca pela parceria firmada nos estudos desenvolvidos na região, a Universidade Federal de Ouro Preto e a todos os membros da Sociedade Excursionista e Espeleológica, que contribuem diariamente para possibilitar o desenvolvimento de trabalhos como este.

References

Auler, A. S., Meus, P., & Pessoa, P. F. (2020). Water Tracing Experiments in Low-pH Quartzite Karst Water, Chapada Diamantina, Northeastern Brazil. In Eurokarst 2018, *Besançon: Advances in the Hydrogeology of Karst and Carbonate Reservoirs* (pp. 183-191).

FABRI, F. P., AULER, A., & AUGUSTIN, C. H. R. R. (2014). Relevo cárstico em rochas siliciclásticas: uma revisão com base na literatura. Revista Brasileira de Geomorfologia, 15(3).

FIELD, M.S., (2002). The QTRACER2 program for tracer-breakthrough curve analysis for tracer tests in karstic aquifers and other hydrologic systems. National Center for Environmental Assessment–Washington Office.

FORD D., WILLIAMS P. (2007) Karst geomorphology and hydrology, Ed. Unwin Hyman Ltd. London, 601 p.

GOLDSCHEIDER, N., DREW, D., (2007). Methods in Karst Hydrogeology. Taylor and Francis. International Contributions to Hydrogeology, 9, 19, 65, 123; 130p.

OLIVEIRA, G. L. C., ASSUNÇÃO, P. H., LIMA, P. E. S., BASTOS, T. V., & RUDNITZKI, I. D. (2024). Conexão hídrica entre as cavernas quartzíticas Bromélias e Martimiano II, na serra de Ibitipoca, MG. Revista Brasileira de Espeleologia-RBEsp, 1(13), 318-338.

SCHNEGG, P.A., (2002). An inexpensive field fluorometer for hydrogeological tracer tests with three tracers and turbidity measurement. In Articles of the Geomagnetism Group, 1484-1488.

SILVA, S.M (2004). Carstificação em rochas siliciclásticas: estudo de caso na Serra do Ibitipoca, Minas Gerais. MG. 143f. Dissertação de mestrado em geografia, Universidade Federal de Minas Gerais, BH-MG.

TEIXEIRA-SILVA, C. M., PIRES, L. O., CONSTÂNCIO-JUNIOR, C. P., & VIEIRA, F. F (2017). Geoespeleologia da Gruta das Casas–Parque Estadual do Ibitipoca-PEI, Minas Gerais. In: Congresso Brasileiro de Espeleologia. p. 381-394.

WORTHINGTON, S. R. H. & SMART, C. C. (2003). Empirical equations for determining tracermass for sink to spring tracer testing in karst. In Beck, B. F. (Ed), Sinkholes and the Engineering and Environmental Impacts of Karst (pp. 287–295).

WRAY, R. A. L. (1997). A global review of solutional weathering forms on quartz sandstones. Earth-Science Reviews 42: 137-160.

WRAY, R. A., & SAURO, F. (2017). An updated global review of solutional weathering processes and forms in quartz sandstones and quartzites. Earth-Science Reviews, 171, 520-55.

Polygenetic Karstification in the Mammoth Cave Region

Mykah Carden & Patricia Kambesis

Center for Geo-Environmental Studies, Department of Earth, Environmental and Atmospheric Sciences, Western Kentucky University, Bowling Green, Kentucky, USA, mykah.carden118@topper.wku.edu, pat.kambesis@wku.edu

Abstract

The Mammoth Cave Region is one of the world's most extensively studied karst landscapes, with over 1,000 km of mapped cave passages and potential for further discoveries. Traditionally, all caves in the region are classified as epigenic, formed by top-down dissolution of limestone by meteoric water enriched with soil CO_2. However, emerging evidence suggests that hypogene processes may also have contributed to cave development. Several caves, particularly in the southern part of the region, exhibit extensive gypsum deposits, complex maze morphologies, hydrocarbon seeps, and sulfur-reducing microbial communities. Additionally, sulfurous springs emerging from a monoclinal structure suggest interaction with subsurface hydrocarbon deposits, reinforcing the possibility of bottom-up dissolution driven by hypogene speleogenesis. This study aims to determine whether these hypogenic characteristics indicate incipient hypogene karstification, hypogene overprinting on pre-existing epigenic passages, or both. The findings challenge the prevailing paradigm that karst development follows a strictly homogeneous trajectory with distinct epigenic or hypogene end members. Instead, they suggest a more complex, polygenetic model of cave evolution. Understanding these processes has significant implications for karst hydrology, geochemical cycles, and subsurface resource management, broadening our perspective on the interplay between epigenic and hypogene speleogenesis in large karst systems.

1. Introduction

The Mammoth Cave Region contains over 1,000 km of mapped cave passages, making it one of the most extensive karst systems in the world. The gently dipping, highly cavernous Mississippian-age limestones are protected from erosion by an impervious non-carbonate caprock, facilitating the development and preservation of vast cave systems. These include the Flint Ridge-Mammoth Cave System (685 km), Fisher Ridge Cave (216 km), and Whigpistle Cave (70 km), along with numerous smaller systems.

The region is drained by a complex distributary system of springs that resurge into the Green River. Beneath the area, eight groundwater sub-basins are defined by intricate cave conduit networks (Quinlan & Rowe, 1989). This study focuses on the Mill Hole sub-basin of the Turnhole Spring groundwater basin (Figure 1), which discharges through Turnhole Spring, an alluviated spring that resurges beneath the Green River. Within this sub-basin, key caves include the Whigpistle Cave System (70 km), portions of which extend into Mammoth Cave National Park (Glennon, 2001); the Parker Cave System (9 km), Beckners Saltpeter Cave (3 km), and several smaller caves. Parker Cave features five stream passages with varying water chemistry and a pronounced sulfur odor. The control site for this study is Great Onyx Spring, located in the Echo River groundwater basin upstream of Turnhole Spring.

All caves in this region have traditionally been classified as epigenic, formed by top-down dissolution driven by meteoric water enriched with soil CO_2 (Palmer, 2017). However, several caves in the southern part of the region exhibit strong hypogene characteristics, including extensive gypsum deposits, complex maze morphologies, hydrocarbon seeps, and purple sulfur-reducing bacteria. South of Park City, sulfurous springs emerge along a monoclinal structure, hinting at the presence of shallow hydrocarbon deposits in the subsurface. The combination of surface and subsurface indicators suggests the possibility of hypogene speleogenesis, where dissolution is driven by bottom-up processes (Jagnow et al., 2000; Florea, 2017; Klimchouk et al., 2017; Burgess et al., 2023).

The goal of this study is to determine whether these hypogenic features represent incipient hypogene karstification, hypogene overprinting on existing epigenic passages, or a combination of both. Understanding these processes is critical for refining karst evolution models and assessing the broader implications of hypogene contributions to cave development in the region.

2. Materials and Methods

This study is ongoing, and data collection is not yet complete. Geologic reconnaissance was conducted across the study areas to inventory and georeference surface and underground features associated with sulfur springs and seeps. Monthly water samples are collected from three sites—Parker Cave, Mill Hole, and Great Onyx Spring (control)—to analyze dissolved ion concentrations of δ^{13}C-DIC, δ^{18}O, and δ^{34}S (Figure 1). These data will help determine the provenance of sulfides.

In addition, gypsum hand samples from three locations in Whigpistle Cave have been collected for sulfur isotope analyses to trace the origin of sulfates. General water quality parameters, including temperature, pH, and conductivity—are recorded, and pressure transducers have been installed to monitor discharge. Cave mapping and direct observations document features indicative of hypogene processes.

Once sampling is complete, mixing models will be employed to assess carbon-sulfur cycle linkages, particularly the potential acceleration of carbon flux due to sulfuric acid dissolution in otherwise epigenetic settings (Burgess et al., 2023). Additionally, we will conduct statistical comparisons with ongoing geochemical analyses from the Great Onyx and River Styx-Echo River groundwater basins within Mammoth Cave National Park to provide broader regional context.

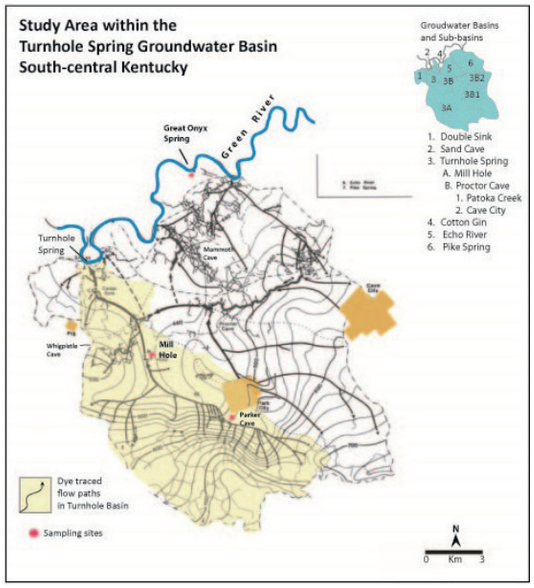

Figure 1 : Location map showing Mill Hole sub-basin (yellow), sampling sites and adjacent caves

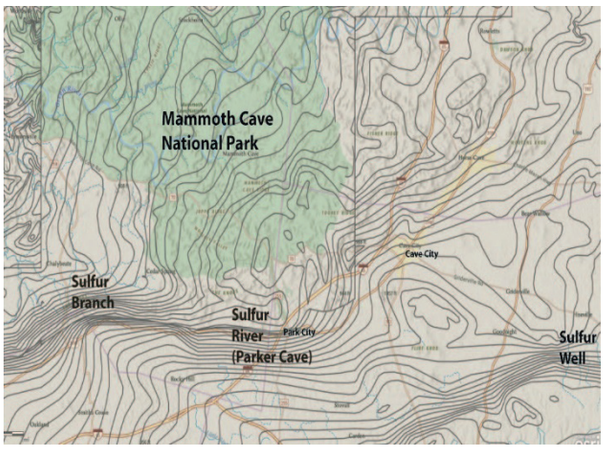

Figure 2: Monoclinal feature that marks various in-cave (Parker Cave) and surface sulfur springs and seeps

3. Results

Surface field reconnaissance identified a monoclinal structure strongly associated with sulfur seeps and springs (Figure 2). This structural feature is also significant in oil and gas exploration, as evidenced by numerous producing wells drilled in its vicinity (Figure 3). Cave survey data and maps reveal that Whigpistle Cave, particularly in its southern passages, exhibits strong hypogene characteristics, including complex maze-like morphology, extensive gypsum coatings, hydrocarbon seeps, and colonies of purple sulfur-reducing bacteria (Figure 4).

Among the five tributary streams in Parker Cave, Sulfur River exhibits the highest sulfate concentrations (600 mg/L), followed by Parker River (250 mg/L), suggesting a significant sulfur input. Similarly, Beckner Cave contains abundant gypsum deposits and sulfur-reducing bacteria, further supporting the influence of hypogene processes. Additionally, many domestic and decommissioned water wells in the region exhibit sulfur contamination, reinforcing the presence of deep-seated sulfur-rich fluids in the subsurface.

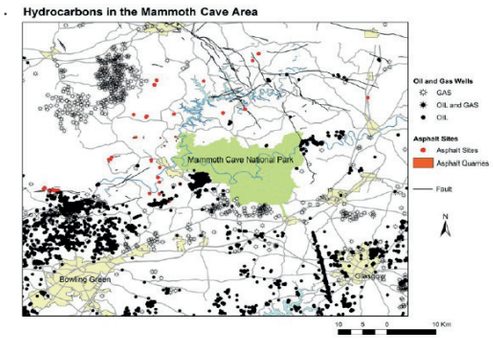

Figure 3: Oil wells, gas wells and asphalt mines. Map courtesy of Rick Toomey.

Figure 4 : Breakdown-floored borehole in Whigpistle Cave. Note the faint purple hue on the breakdown which is sulfur reducing bacteria that coats the bedrock. Photo by Joel Despain.

4. Discussion

The preliminary findings of this study suggest that while epigenic processes have traditionally been considered the dominant mechanism in the development of caves within the Mammoth Cave Region, hypogene influences are also present and may have contributed to localized cave formation and modification. The presence of hypogene indicators—including gypsum deposits, sulfurous springs, hydrocarbon seeps, and sulfur-reducing bacteria—suggests that bottom-up dissolution has played a role in certain areas.

The Mill Hole sub-basin, particularly within Whigpistle Cave, Parker Cave, and Beckners Saltpeter Cave, displays several features indicative of hypogene speleogenesis. The discovery of sulfur seeps correlated with monoclinal structures and hydrocarbon deposits strengthens the hypothesis that rising fluids have influenced cave formation in this area. The presence of purple sulfur-reducing bacteria, particularly in areas with high sulfate concentrations, suggests microbial mediation in sulfuric acid-driven dissolution. This aligns with previous research that has linked sulfuric acid dissolution to hypogene cave formation in other karst systems (Jagnow et al., 2000; Klimchouk et al., 2017).

Geochemical analysis of water and sulfate minerals will be critical in determining the exact provenance of the sulfur and identifying the extent to which deep-seated fluids have contributed to cave development. Initial sulfate concentration measurements from Parker Cave show elevated values (600 mg/L in Sulfur River and 250 mg/L in Parker River), reinforcing the likelihood of hypogene influences in these streams. The comparison of these values with the Great Onyx Spring control site, which lacks clear hypogene indicators, will provide further insight into the extent of hypogene overprinting.

Another important finding is the role of hydrocarbon seeps in cave modification. The correlation between sulfur-rich fluids and hydrocarbon deposits in the region suggests a petrogenic influence on karst development, a process observed in other hypogene cave systems (Florea, 2017; Burgess et al., 2023). The association of highly acidic waters with microbial activity in some cave streams suggests that sulfuric acid dissolution may not only modify existing passages but also promote localized increases in biodiversity by creating unique ecological niches.

A key question that remains is whether these hypogene characteristics represent incipient hypogene karstification or hypogene overprinting on pre-existing epigenic caves. Many of the observed caves, such as Whigpistle and Parker Caves, exhibit features associated with both processes, suggesting a complex polygenetic speleogenesis rather than a strict classification into epigene or hypogene end members. This challenges the conventional view of karst development as a homogeneous process and highlights the need for more nuanced models that incorporate mixed speleogenetic mechanisms.

5. Conclusion

This study provides evidence that hypogene processes have influenced cave development in the Mammoth Cave Region, challenging the traditional view that the region is solely shaped by epigenic processes. The presence of gypsum deposits, sulfur-rich springs, hydrocarbon seeps, and sulfur-reducing bacteria suggests that deep-seated fluids have contributed to localized cave dissolution and modification. Preliminary geochemical data indicate elevated sulfate concentrations in Parker Cave, supporting the hypothesis of

sulfuric acid-driven speleogenesis. While epigenic processes remain dominant, hypogene overprinting appears to have played a secondary but significant role in shaping certain passages. Further geochemical and hydrological analyses will be essential in refining our understanding of the interplay between these processes and their broader implications for karst development models.

Acknowledgments

We gratefully thank the Whigpistle Cave Project for sharing data and information, the Cave Conservancy Foundation's Charles W. Maus Undergraduate Karst Research Fellowship and Western Kentucky University for financial support, and all of the cavers, past and present, for their fieldwork and documentation without which this research would not be possible.

References

Burgess, S.A., 2021 *Sulfur Systematics and Carbonate Diagenesis in the Mitchell Plateau, Indiana*. Indiana University.

Florea, Lee J. , 2017, Sulfur-Based Speleogenesis in the Cumberland Plateau, USA.» *Hypogene Karst Regions and Caves of the World*: 683-690.

Glennon, John. 2001, «Application of morphometric relationships to active flow networks within the Mammoth Cave watershed.», (Masters Thesis, Western Kentucky University

Groves, Chris; Meiman, Joe; and Herstein, Shannon. 200). In-Cave Dye Tracing and Drainage Basin Divides in the Mammoth Cave Karst Aquifer, Kentucky. *U.S. Geological Survey Karst*

Jagnow, D.H.; Hill, C.A.; Davis, D.G.; DuChene, H.R.; Cunningham, K.I.; Northup, D.E.; Queen, J.M. (2000) History of the sulfuric acid theory of speleogenesis in the Guadalupe Mountains, New Mexico. J. Cave Karst Stud. 62, 54–59

Klimchouk, A.; Palmer, A.N.; De Waele, J.; Auler, A.S.; Audra, P. (Eds.) 2017, Hypogene Karst Regions and Caves of the World; Springer: Berlin/Heidelberg, Germany,

Palmer, A.N. (2017). Geologic History of Mammoth Cave. In: Hobbs III, H., Olson, R., Winkler, E., Culver, D. (eds) Mammoth Cave. Cave and Karst Systems of the World. Springer, Cham. https://doi.org/10.1007/978-3-319-53718-4_7

Quinlan, James F. and Rowe, Donald R., 1978 «Hydrology and Water Quality in the Central Kentucky Karst: Phase II Part A: Preliminary Summary of the Hydrogeology of the Mill Hole Sub-Basin of the Turnhole Spring Groundwater Basin» . *KWRRI Research Reports*. 203. 47.

Gypsum karst: a powerful CO_2 sink

Veronica Chiarini (1), Jo De Waele (2) & Paolo Forti (3)

(1) Department of Geosciences, University of Padua, Via G. Gradenigo 6, 35131 Padova, Italy, veronica.chiarini3@gmail.com
(2) Department of Biological, Geological and Environmental Sciences, Via Zamboni 67, 40126 Bologna, Italy, jo.dewaele@unibo.it
(3) Italian Institute of Speleology, Via Zamboni 67, 40126 Bologna, Italy, paolo.forti@unibo.it (corresponding author)

Abstract

In the past few years, rapid climate change induced by global warming has raised awareness towards the need to reduce carbon emissions worldwide. Besides this commitment, scientific research has been focusing on finding possible solutions to artificially capture and store greenhouse gases (GHG) (especially CO_2) to reduce the impact of climate disasters on nature and societies. Different methods have been identified which include CO_2 storage in subsurface geological formations and its mineralization into calcium and magnesium carbonates. However, none of the methods studied so far appears to be resolutive for this problem. It is thus important to study the naturally occurring CO_2 sinks to have a better comprehension of both natural processes involved in the CO_2 balance, and the actual possibility to artificially remove this GHG from the atmosphere.

The most well-known natural CO_2 sink is represented by marine and coastal environments, which are able to naturally store enormous quantities of carbon dioxide. However, CO_2 sequestration can occur also in continental environments, such as caves, even if at a lesser extent, through weathering of carbonate bedrock and speleothem deposition. But not all caves have the same potential for CO_2 sequestration. Indeed, while in limestone caves the CO_2 balance is variable (the gas is consumed to dissolve carbonate, but it is released into the cave atmosphere triggering speleothem formation), a different situation is found in dolostone and gypsum bedrocks. The calcium carbonate deposition in a cave formed in a dolostone bedrock potentially consumes CO_2 molecules. However, these types of caves are usually poorly decorated, thus making their role as CO_2 sink not very relevant. In addition, the potential of dolomite for CO_2 absorption has already been investigated by researchers. On the contrary, calcium carbonate deposition in gypsum caves is still poorly understood and has the potential to provide important insights into CO_2 sequestration in such environments.

1. Introduction

Global warming can be considered a major threat for current and future societies. The intensification of extreme meteorological events is obliging worldwide governments to face new challenges from both an economic and social point of view. The increased risk of climate catastrophes and the consequences of ocean acidification will enhance the already occurring biodiversity loss, challenging the survival of our species too.

The increased awareness towards these environmental problems has rose the attention to find a way to decrease the concentration of artificially produced greenhouse gases (GHG), which have been demonstrated to be the major trigger of current global warming (Filonchyk et al., 2024). Besides the commitment to reduce GHG emissions, research has been focusing also into the artificial sequestration of these gases from the atmosphere.

This process has been addressed mainly to CO_2, which is the most important GHG, and scientists are studying new methods to remove it from the atmosphere and store it in geological reservoirs over long periods of time (Carbon Capture and Storage, CCS).

The main approach to carbon dioxide sequestration involves its storage into subsurface geological formations such as saline aquifers, basalt formations, depleted oil and gas reservoirs and not-exploitable coal seams (Massarweh & Abushkaikha, 2024 and references therein). Another method, which is considered safer in the long-term, but less efficient, is represented by mineral trapping, consisting in CO_2 sequestration through the precipitation of carbonate minerals. This can be obtained by injecting this gas into basic siliciclastic aquifers (Bachu et al., 1994) and in basaltic rocks (Matter et al., 2016) or by the development of specific techniques able to sequestrate CO_2 directly from point-source emissions (e.g., Gadikota, 2020).

Considering that none of the cited methods is yet resolutive for the problem of long-term CO_2 sequestration and storage, it is important to study the natural processes which are able to remove CO_2 from the atmosphere. It will thus be of great importance to understand these processes and their role in the global balance of CO_2 sources and sinks, and to improve the development of artificial techniques to capture and store this GHG.

Marine and coastal environments play an important role in reducing the atmospheric CO_2 concentration (e.g., Raven & Falkowski, 1999; Puppin et al., 2024), but they are not the only ecosystems where CO_2 can be naturally removed from the environment.

Indeed, in continental caves an enormous quantity of newly formed calcium carbonate occurs: but can this naturally occurring phenomenon really lead to the subtraction of an equivalent quantity of carbon dioxide emitted into the atmosphere?

2. Calcite development in a carbonate environment

Enhanced rock weathering is considered a promising method for CO_2 sequestration (Xu et al., 2024). In karst environments, the well-known fundamental chemical reaction:

$$2CaCO_3\,[calcite] + CO_2 + 2H_2O \leftrightarrow 2Ca_2{+} + 2HCO_3{-} + H_2O$$

rules the mechanism by which the carbonate rock dissolves and $CaCO_3$ speleothems develop in caves (Fig. 1) within carbonate bedrocks.

Figure 1: *Hang Son Doong cave in Vietnam: giant calcite stalagmites (Photo by Dave Bunnel).*

This chemical equilibrium shows that if the chemical balance shifts to the right, the karst process will be active, and the carbonate rock will be dissolved: we will therefore have consumption of limestone rock and carbon dioxide. However, when the reaction changes direction we will have the deposition of calcium carbonate with the formation of speleothems and the release of carbon dioxide into the atmosphere.

It is evident that the weathering (dissolution) of carbonates is a way of removing CO_2 from the atmosphere, but the subsequent formation of calcite speleothems (induced by CO_2-degassing), and the loss of CO_2 at springs (especially when tufa deposits) counterbalances this carbon sink, leaving the balance of these reactions only slightly positive (WHITE, 2013). Thus, unfortunately, the karst process developing in calcite lithotypes cannot be considered an efficient CO_2 sink.

The situation is different for karst phenomena in dolomite: in fact, in this case a simple chemical balance as in the case of calcite does not control the global process. The karst process follows the same mechanism described before, thus leading to the consumption of an identical quantity of CO_2. But in the cave environment the formation of dolomite is strongly inhibited and therefore the quantity of calcite and/or aragonite speleothems that can develop corresponds to just a half while the Mg^{2+} and HCO^{3-} ions remain in solution because $MgCO_3$ is much more soluble than calcite and aragonite:

$$2MgCa(CO_3)_2 + 4CO_2 + 4H_2O$$
$$\updownarrow$$
$$2Ca^{2+} + 2Mg^{2+} + 4HCO_3^- + 2H_2O$$
$$\updownarrow$$
$$2CaCO_3 + 2Mg^{2+} + 4HCO_3^- + 2H_2O$$

Thus, caves within dolomitic rocks may be considered more efficient CO2 sinks. However, it must be considered that their effect is scarce at the global scale because they have (1) a relatively scarce global diffusion and, (2) they normally host few and less abundant calcite speleothems. It is woth noting that this mechanism has also been recently investigated by Urseguía et al. (2023) for carbon sequestration through industrial processes.

3. Calcite development in non-carbonate environment

Calcium carbonate speleothems may also develop in caves in a non-carbonate lithotype although, normally, they almost never reach the dimensions of those found in limestone or dolostone caves. In this respect, a very particular case is that relating to the lava tubes of Jeju Island in South Korea (Fig. 2) (FORTI, 2005; WOO et al., 2008). Indeed, in these basaltic caves, there is an exceptional display of calcite speleothems derived from the dissolution of the calcareous micro-coquina layer deposited above the lava flows, and its subsequent precipitation inside the cave through CO_2 degassing. In many other cases where calcite and/or aragonite speleothems form in non-carbonate caves, $CaCO_3$ always comes from the dissolution of above-lying limestone formations. Therefore, the general reaction, ruled by dissolution of limestone, allows for the development of calcite and/or aragonite speleothems in most non-carbonate environments and, as previously said, in all these natural caves there is only a slightly positive CO_2 sink effect.

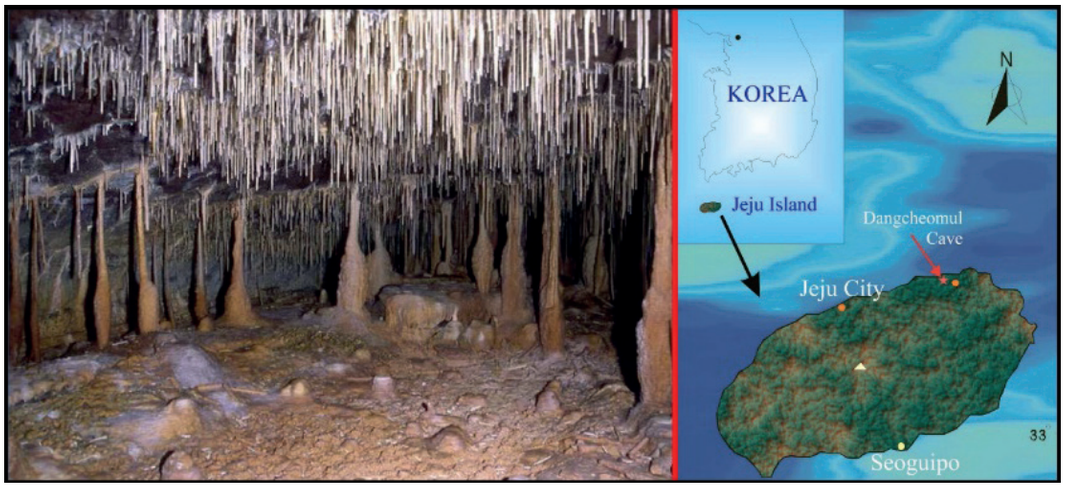

Figure 2: *Dangcheomul pyroduct (Jeju Island, South Korea): the astonishing display of calcite speleothems developed thanks to the "normal" karst reaction because the rain water comes in contact with a thin layer of carbonate microcoquina before reaching the below-lying lava tube.*

4. Calcite development in gypsum environment

Gypsum caves are different: in such caves, calcite speleothems are often abundant even if no overlying limestone formation exists above the caves. The development of calcite speleothems in gypsum caves is closely related not only to the climate of the geographical area in which they are found, but above all to the development of the vegetation cover at the surface (CALAFORRA et al., 2008; COLUMBU et al., 2015; CHIARINI et al., 2024). Their maximum development occurs in temperate continental and humid tropical zones, and rapidly decreases in cold and hot arid climate regions.

Excluding the presence of relevant carbonate layers in the gypsum outcrops which may provide the calcium carbonate, in the 80s of last century scientists started to develop the idea that the deposition of abundant calcite speleothems in epigenic gypsum caves could be the result of a process other than the simple dissolution of calcite from the overlying bedrock. In fact, there are other possible alternative mechanisms that directly involve CO2 in the reaction leading to the formation of calcite speleothems in gypsum caves (FORTI & RABBI, 1981). A process called «incongruent dissolution» was invoked, during which for each molecule of calcium carbonate that precipitates, one molecule of gypsum can dissolve, increasing the sulfate concentration and leaving that of calcium stable (Fig. 3).

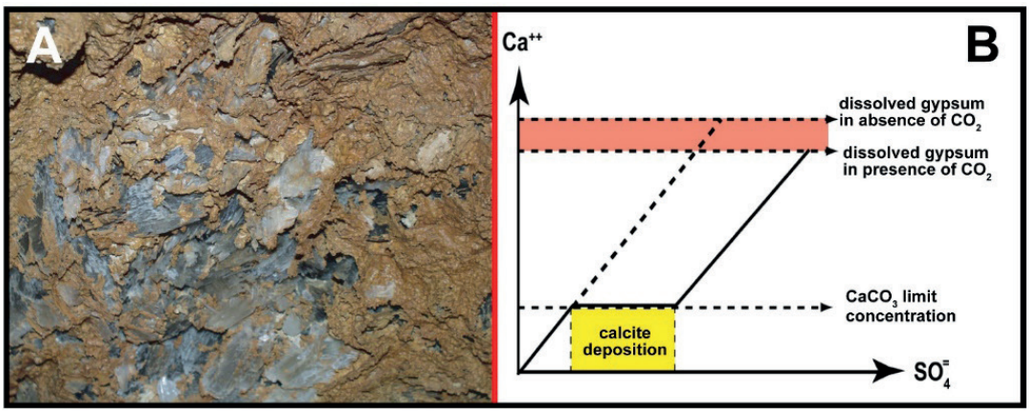

Figure 3: *A: Grotta Novella (Gessi Bolognesi) detail of the gypsum boulder on which the dripping simultaneously causes the rapid dissolution of the gypsum crystals and the formation of thin calcite crusts (Photo Paolo Forti). B: scheme of the simplified mechanism ruling the incongruent dissolution of $CaSO_4.2H_2O$, which causes the development of calcite speleothems inside gypsum caves (after CALAFORRA & FORTI (2021) modified). During a simple dissolution the ionic concentrations in the solution are necessarily equal to that of the substance that dissolves ($[Ca^{2+}]= [SO_4^{2-}]$) while during incongruent dissolution the ion in common with the substance that precipitates ($[Ca^{2+}]$) does not change its concentration in the solution while the concentration of the other ($[SO_4^{2-}]$) continues to increase (after CALAFORRA & FORTI (2021) modified).*

The problem was that this process (considering gypsum, CO_2, calcium carbonate and water only) cannot proceed towards the deposition of calcium carbonate due to the rapid decrease in pH, blocking its efficiency. One of the reactions that is potentially suitable for the development of calcite speleothems in gypsum environments is the so-called “dedolomitization”. According to this reaction, if dolomite is present, when it comes into contact with water extremely rich in Ca^{2+} and SO_4^{2-}, it releases Mg^{2+} into the solution thus transforming itself into calcite. This process lowers the concentration of Ca^{2+} in the solution, inducing the dissolution of additional gypsum, thus increases both Mg^{2+} and SO_4^{2-} in the solution:

Dolomite $[MgCa(CO_3)_2]$ + Gypsum $[CaSO_4 \cdot 2H_2O] + nH_2O \rightarrow$ 2 calcite $[CaCO_3] + Mg^{2+}_{aq} + SO_4^{2-}_{aq}$

It is also possible that, when a minimal part of carbon dioxide enters the gypsum-saturated water (from the cave atmosphere, for example), and pH is kept neutral (because of the presence of alkaline ions) the calcite immediately precipitates, again subtracting Ca^{2+} from the residual solution. Also, in this case an additional gypsum dissolution will occur. This reaction determines the maintenance of undersaturated conditions of the solution with respect to gypsum, thus favoring its dissolution. Finally, the dedolomitization process consumes calcium ions derived from the dissolution of gypsum, converting the dolomite into calcite and at the same time, thanks to the buffering power of the magnesium carbonate within the solution, allows the pH to be maintained in a neutral or slightly basic range.

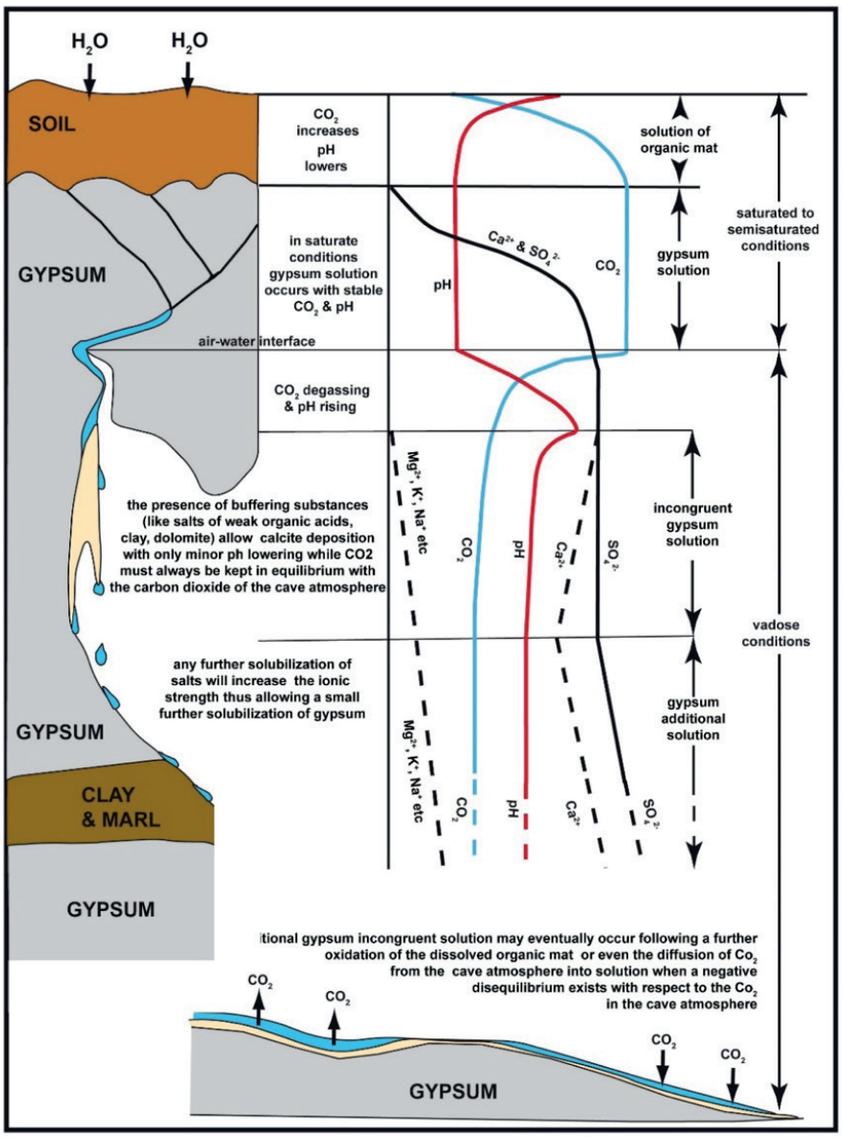

Figure 4: *Diagram of the progressive variations of pH and of main ion concentrations within the water from the moment it enters the semi-outcropping gypsum formation.*

However, this process alone can hardly explain the actual quantity of carbonate speleothems in the caves of Emilia-Romagna and Sicily (Italy) and, above all, it cannot completely justify the clear relationship existing between vegetation cover and their development (CALAFORRA & FORTI, 2021). In addition to this, the amount of dolomite present in the marly-clayey interbeds of the Messinian gypsum formations is normally rather low. Dedolomitization therefore must act in combination with other incongruent dissolution processes that directly involve other buffering substances – for instance other weak acids such as humic and fulvic acids – in addition to the carbonic acid and magnesium carbonate system. The presence of these acids (often evidenced by the bright reddish-brown color exhibited by the calcium carbonate speleothems developing in gypsum caves) and their salts with alkaline elements (first of all sodium and potassium) are therefore fundamental in the incongruent dissolution process of gypsum and, consequently, the development of large calcite speleothems contributing in making the pH of the solution higher (Fig. 4).

These organic acids are also weaker than H_2CO_3 and their combination with alkaline ions can develop even greater buffering effects. Indeed, the abundance of clays rich in sodium and potassium can contribute to maintaining the pH of the solution in a range close to neutrality, thus counteracting the acidifying effect of CO_2. The process of calcite precipitation in gypsum caves, which is much more complex than simple dedolomitization and involves an active role of the organic material coming from the soil, can continue as long as CO_2 is available and the pH does not lower too much.

It is evident that the CO_2 degassing from infiltrating water into the cave atmosphere has a scarce, if any, effect on the development of carbonate speleothems in gypsum caves. On the contrary, the reverse process – i.e., the diffusion from the cave atmosphere to a saturated solution of gypsum – can induce the formation of calcite deposits. This is the case of floating calcite rafts over small standing pools, or flowstones forming in running water: this type of deposition is observed even several kilometers from the point where water sinks into the gypsum rocks. The production of CO_2 by decomposition (oxidation) of organic material (leaves, wood chips, humic and fulvic acids) in the water that flows within the karst system is the “fuel” for “incongruent dissolution of gypsum”.

Finally, the incongruent gypsum dissolution is responsible for the development of not only the majority of most common calcite formations,

but also of a few peculiar ones. This is the case of the big subvertical calcite crusts almost completely detached from the highly dissolved gypsum wall. In the early 1960s, cavers from Bologna called them «calcite blades» as they are still anchored to the gypsum rock only in very few points. A curious characteristic of these blades is that they always have a thin layer of mud in their inner part (FORTI & RABBI, 1981). Subsequently, blades completely similar to those of the Bologna ones were also observed in the caves of the gypsum outcrop of Punta Alegre in Cuba and in Sorbas (Spain). Anyway, the largest of these «calcite blades» (14 m high, up to 3 m wide, but just 10 cm thick) is still the one discovered near Bologna (Italy) inside the Novella cave (Fig. 5).

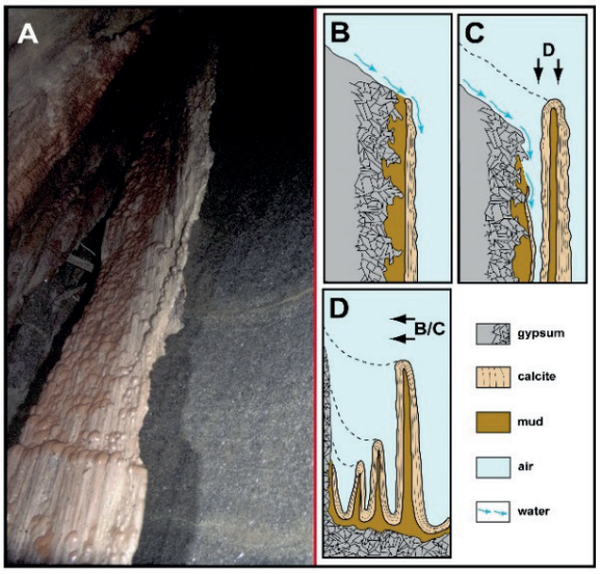

Figure 5: *A) The large "calcite blade" of the Novella cave (Parco dei Gessi Bolognesi): the progressive dissolution of the gypsum wall on which it originally began to form caused the wall to retreat by almost two meters (Photo by Sandro Mandini). B) The water flow causes the incongruent dissolution of gypsum and the deposition of calcite, while the mud remains trapped between the blade and the gypsum wall. C) The progressive retreat of the wall causes the evolution of a new calcite blade. D) The continuation of the process leads to the development of a series of subparallel blades (from CALAFORRA & FORTI, 2021 modified).*

5. Conclusion

The study of natural processes able to consume environmental CO_2 is of primary importance for the understanding of the CO_2 sources and sinks in a context of rapid climate warming related to GHG emissions. Furthermore, a deep understanding of these processes can contribute to the development of new techniques for the artificial sequestration and long-term storage of atmospheric CO_2. Carbon dioxide mineralization into $CaCO_3$ is one of these techniques and represents a naturally occurring process in cave environments. Although limestone caves cannot be considered efficient CO_2 traps due to a variable balance between the CO_2 consumed and produced during the bedrock dissolution and speleothem deposition, dolostones and gypsum caves present a stronger potential to store environmental CO_2 over long periods of time through the deposition of carbonate speleothems. While caves in dolostone bedrocks are usually poorly decorated, the incongruent dissolution of gypsum allows for the relatively fast deposition of massive calcite speleothems. This process involves the consumption of CO_2 produced within the soil overlying the gypsum bedrock and/or the diffusion of carbon dioxide from the cave atmosphere into the cave water saturated in gypsum. Environmental CO_2 is thus effectively trapped into these types of speleothems, making gypsum caves a powerful CO_2 sink.

The deposition of carbonate speleothems in gypsum caves is a complex process involving the actions of not only water, CO_2 and gypsum, but of other components (organic acids, dolomite and alkaline ions derived from the overlying soils and bedrock clay interlayers, which are common in most gypsum formations worldwide) able to higher the pH of the solution to allow for the precipitation of $CaCO_3$. This process is thus efficient in triggering calcium carbonate precipitation that allows for the deposition of massive calcite speleothems in gypsum caves, which can survive erosion and weathering over long periods of time (Fig. 6) (> 600 ka, CHIARINI et al., 2024) especially in areas with a temperate to warm humid climate. However, the exact process of calcite deposition in gypsum caves is still not fully understood and further investigation is needed as it may provide important results, which can be applied to the artificial sequestration of atmospheric CO_2.

Figure 6: *Fragment of a calcite flowstone found in the middle of the woods in the Ca' Monti area (Vena del Gesso Romagnola), which grew in a gypsum cave, now completely dismantled, about 350 thousand years ago (Photo by Elisa Ponti) (after CHIARINI et al., 2024)*

References

-BACHU S., GUNTER W. D., PERKINS E.H. (1994) Aquifer disposal of CO2: hydrodynamic and mineral trapping. Energy Conversion and Management 35(4):269-279.

CALAFORRA J.M., FORTI P. (2021) Speleotemi peculiari dei gessi e delle anidriti. Mem. Ist. It. Spel. 36:1-140.

CALAFORRA J.M., FORTI P., FERNANDEZ-CORTES A. (2008) The speleothems in gypsum caves and their paleoclimatological significance Env. Geol. 53(5): 1099-1105.

COLUMBU A., DE WAELE J., FORTI P., MONTAGNA P., PICOTTI V., PONS--BRANCHU E., HELLSTROM J., BAJO P., DRYSDALE R. N. (2015) Gypsum caves as indicators of climate-driven river incision and aggradation in a rapidly uplifting region Geology 43(6):539-542.

CHIARINI V., PISANI L., COLUMBU A., DE WAELE J. (2024) Evolgyps – Landscape evolution in the Messinian gypsum areas of Emilia- Romagna. Mem. Ist. It. Spel. 46B:1-182.

DALMONTE C., FORTI P. (1995) L'evoluzione delle concrezioni di carbonato di calcio all'interno delle grotte in gesso: dati sperimentali dal Parco dei Gessi Bolognesi. Sottoterra 102:32-40.

DE WAELE J. FORTI P. (2024) Il fenomeno carsico nei gessi. Mem. Ist. It. Spel. 45:45-82.

Filonchyk M., PETERSON M.P., ZHANG l., HURYNOVICH V., HE Y. (2024) Greenhouse gases emissions and global climate change: Examining the influence of CO2, CH4, and N2O. Science Total Environment 935:173359.

FORTI P. (2005) Genetic processes of cave minerals in volcanic environments: an overview. J. Cave & Karst Stud. 67(1):3-13.

FORTI P., RABBI E. (1981) The role of CO2 in gypsum speleogenesis: I° contribution. Int. J. Spel. 11:207-218.

Gadikota G. (2020) Multiphase carbon mineralization for the reactive separation of CO2 and directed synthesis of H2. Nature Reviews Chemistry 4(2):78-89.

MASSARWEH O., ABUSHAIKHA A. S. (2024) CO2 sequestration in subsurface geological formations: A review of trapping mechanisms and monitoring techniques. Earth-Science Reviews 253:104793.

Matter J.M., Stute M., Snæbjörnsdottir S.Ó., Oelkers E.H., Gislason S.R., Aradottir E.S., ... & Broecker W. S. (2016) Rapid carbon mineralization for permanent disposal of anthropogenic carbon dioxide emissions. Science 352(6291):1312-1314.

Puppin A., Tognin D., Paccagnella M., Zancato M., Ghinassi M., D'Alpaos C., ... & D'Alpaos A. (2024) Blue carbon assessment in the salt marshes of the Venice Lagoon: Dimensions, variability and influence of storm- surge regulation. Earth's Future 12(10): e2024EF004715.

Ursueguí, D., Faba L., Díaz E., Caballero R., Ordóñez S. (2023). Dolomite industrial by-products as active material for CO2 adsorption and catalyst for the acetone condensation. Waste Management 168:431-439.

WHITE W.B. (2013) Carbon fluxes in Karst aquifers: Sources, sinks, and the effect of storm flow. Acta Carsologica 42(2-3):177-186.

WOO K.S., KIM J.C., CHOI D.W., KIM J.K., KIM R., NEHZA O. (2008) The origin of erratic calcite speleothems in the Dangcheomul Cave (lava tube cave), Jeju Island, Korea. Quaternary International 176:70-81.

Xu Q., Zhang F., Song F., Guo H., Wang X., Bi F., Xu M. (2024) Investigating CO_2 sequestration via enhanced rock weathering: Effects of temperature and citric acid on dolomite and basalt. Journal of Cleaner Production, 144414.

CH^4 as the Carbon Source of the Biological Ecoystem in the Ayyalon Cave System

Shlomit Cooper-Frumkin (1), Itay J. Reznik (2) & Amos Frumkin (3)

(1) Geological Survey of Israel, 32 Yesha'ayahu Leibowitz, Jerusalem 9692100, Israel ; The Fredy and Nadine Herrmann Institute of Earth Sciences, The Hebrew University of Jerusalem, Jerusalem, Israel, Shlomit.frumkin@mail.huji.ac.il (corresponding author)

(2) Geological Survey of Israel, 32 Yesha'ayahu Leibowitz, Jerusalem 9692100, Israel

(3) The Fredy and Nadine Herrmann Institute of Earth Sciences, The Hebrew University of Jerusalem, Jerusalem, Israel

Abstract

A fundamental question in the research of the ecosystem of the Ayyalon Cave system, Israel, pertains to the carbon source sustaining the biological system in the subterranean environment, where photosynthesis is ruled out. It was previously suggested that HCO_3- provides the carbon source to the biological system. Carbon isotopic measurements ($\delta^{13}C$) of the microbial biofilm, the large arthropods and the HCO_3- showed values of -41.8, -33.5 to -36.3 and -12.2 ‰ VPDB, respectively. The gap in the isotopic values of $\delta^{13}C$ between the biological system and the HCO_3- was explained by biogeochemical fractionation during the assimilation of inorganic carbon. Here, based on the overlap between the $\delta^{13}C$ values of the CH_4 (-35 to -41.4 ‰ VPDB), sampled from the cave lakes, and the $\delta^{13}C$ values of the biological system, we suggest that the biological system can assimilate carbon from the methane. During this process, methanotrophic bacteria oxidize the methane and use it as an energy and carbon source for their metabolic processes. Further analysis of the isotopic values of the hydrogen in the methane is required in order to further determine the source of the methane, that can either originate from biogenic processes or from thermogenic processes in deeper underground sections.

1. Introduction

The Ayyalon and Levana caves terminate with warm, brackish groundwater lakes. These lakes which are part of the Ayyalon anomaly, within the Yartan aquifer, Israel, are characterized by warm water, rich in H_2S with low pH values (7) compared with the surrounding area (7.8). Within this isolated system of anoxic water, an endemic ecosystem has evolved, that includes a microbial biofilm and *arthropods* that feed on the biofilm (FRUMKIN et al., 2022).

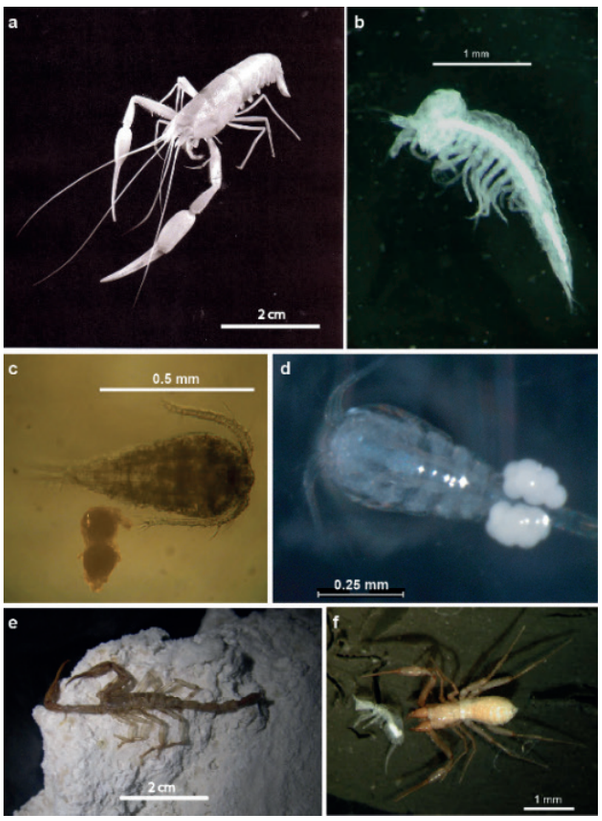

Figure 1: *The main aquatic (a-d) and terrestrial (e-f) arthropod fauna of Ayyalon anomly caves (after FRUMKIN et al., 2022). a. Typhlocaris ayyaloni (Photo D. Darom). b. Tethysbaena ophelicola (Photo N. Ben Eliahu). c. Metacyclops longimaxillis (Photo N. Ben Eliahu). d. Metacyclops subdolus (Photo Z. Ganem). e. Akrav israchanani (Photo I. Naaman). f. right: Ayyalonia dimentmani; left: Troglopedetes (Collembola) (Photo I. Naaman).*

2. Materials and methods

The water from the lakes in the caves was sampled from various depths in glass veils. After a quick recapping, 20% of sample was replaced by N_2 Ultra High Purity (UHP) to create headspace. This is done by using two syringes as one pushes N_2 UHP in and the other removes equivalent volume of water, slowly and while the vial is upside down. Samples were measured on Focus-GC (Thermo) FID detector (0.8 mL, replaced by N_2 UHP) after vigoursly shaken for 2 minutes (at that point all CH_4 moves to the headspace). Samples were kept in refrigiration until isotope analyses (3 weeks). Carbon isotopic values ($\delta^{13}C$) of CH_4 were measured using isotope-ratio mass spectrometry (IRMS). Further measurments of carbon stable isotopes were described in FRUMKIN et al. 2023.

Figure 2: *a. Cave rafts and microbial film, Ayyalon cave. Installing a monitoring EXO1 Multiparameter Sonde for continuous measurements of water properties b. Cave raft and microbial film at Levana cave with gas bubbles trapped underneath (photos: S. Cooper-Frumkin). c. Fallen rocks in the margin of the lake of Ayyalon cave. The biofilm/cave rafts remain on the rocks and serve as evidence of former water levels. Rock karrens formed by acidic water weathering by the aggressive H2S rich groundwater . (photo: A. Frumkin).*

3. Results and Discussion

During this study, the concentration of Methane (CH_4) in Ayyalon water system was analyzed (0.942-1.039 µM). The isotopic value of carbon within the CH_4 showed values of -35.2 to -41.4 ‰ VPDB. The $\delta^{13}C$ values of the microbial biofilm, the large arthropods and the HCO_3- showed values of -41.8, -33.5 to -36.3 and -12.2 ‰ VPDB, respectively . Previous studies suggested that HCO_3- is the carbon source of the biological system where the gap in the isotopic values of $\delta^{13}C$ between the biological system and the HCO_3- (Fig. 3) was explained by biological fractionation of chemotrophs (FRUMKIN et al., 2023). The discovered presence of CH_4, however, raised the possibility that methanotrophic bacteria oxidize the methane and use it as an energy and carbon source for their metabolic processes. Following the measurements of the isotopic value of carbon within the CH_4 and the overlap of $\delta^{13}C$ values between the CH_4 and the biological system (Fig. 3), suggests indeed that the carbon source of the system could be directly from the CH_4. Our findings can be compared with the CH_4 source of the similar ecosystem in the Movile Cave (SARBU et al., 1996). Further analysis of the isotopic values of the hydrogen in the methane in the system is required in order to see whether this conclusion can also be based on additional geochemical proxies.

The water in the Ayyalon anomaly has lower pH values compared to the surrounding aquifer, resulting in agressive water and the formation of the caves (FRUMKIN & GVIRTZMAN, 2006; GAVRIELI et al., 2002). However, due to yet to be determined physio-chemical changes over the year, low Mg calcite cave rafts are formed on the lake surfaces. Furthermore, the bubbling of gases from the bottom of the lakes results in their trapping beneath the buoyant cave rafts, which can facilitate the sampling of gas in future expeditions (Fig.2b).

4. Conclusion

The light isotopic values of $\delta^{13}C$ in methane corresponds to the light $\delta^{13}C$ values observed in the biological system in the Ayyalon cave and the surroundings, and therefore methane may indeed serve as the carbon source for this unique and endemic biological system.

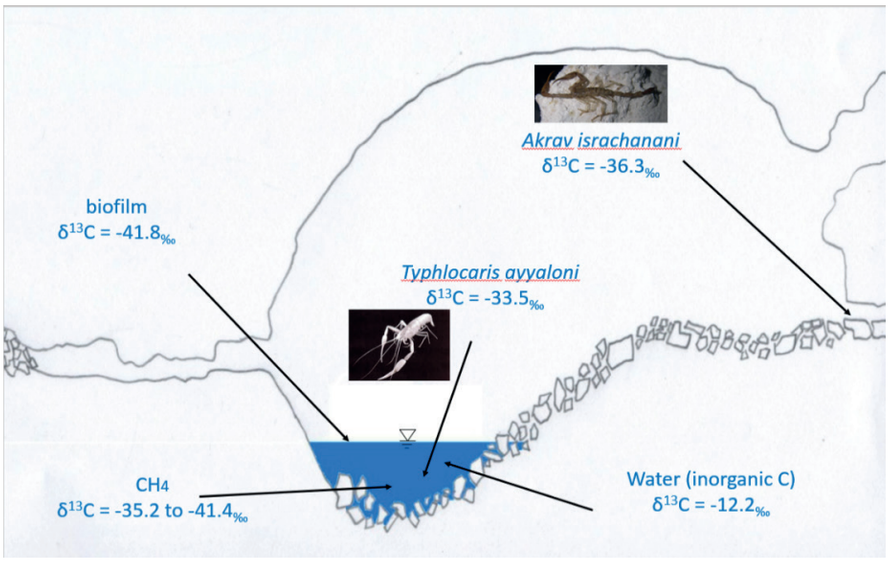

Figure 3: *Measurements of $\delta^{13}C$ VPDB from Ayyalon and Levana caves (Profile of Ayyalon cave by I. Naaman – Israel Cave Research Center (ICRC)).*

Acknowledgments

We gratefully thank Amitai Cooper (ICRC), Ilya Kutuzov, Hadas Ben-nun Levanon, Reuven Zakai and Boaz Langford (ICRC) for the help during the expeditions. We also thank Orit Sivan and Efrat Eliani for $\delta^{13}C$ measurments.

References

Frumkin, A., Chipman, A. D., & Naaman, I. (2023). An isolated chemo-lithoautotrophic ecosystem deduced from environmental isotopes: Ayyalon cave (Israel). Frontiers in Ecology and Evolution, 10. https://doi.org/10.3389/fevo.2022.1040385

Frumkin, A., Dimentman, C., & Naaman, I. (2022). Biogeography of living fossils as a key for geological reconstruction of the East Mediterranean: Ayyalon - Nesher Ramla system, Israel. Quaternary International, 624, 168–180. https://doi.org/10.1016/j.quaint.2020.11.036

Frumkin, A., & Gvirtzman, H. (2006). Cross-formational rising groundwater at an artesian karstic basin: The Ayalon Saline Anomaly, Israel. Journal of Hydrology, 318(1), 316–333. https://doi.org/10.1016/j.jhydrol.2005.06.026

Gavrieli, I., Burg, A., & Guttman, J. (2002). Transition from confined to phreatic conditions as the factor controlling salinization and change in redox state, Upper subaquifer of the Judea Group, Israel. Hydrogeology Journal, 10, 483–494.

Sarbu, S. M., Kane, T. C., & Kinkle, B. K. (1996). A Chemoautotrophically Based Cave Ecosystem. Science, 272(5270), 1953–1955. https://doi.org/10.1126/science.272.5270.1953

The relative importance of chemical and mechanical erosion in Sistema J2, Oaxaca, Mexico

Matthew D. Covington (1), Ethan W. Oleson (1), Max P. Cooper (2), Rogelio Hernándes-Vergara (3), María de los Angeles Verde-Ramírez (4)

(1) Department of Geosciences, University of Arkansas, Fayetteville, AR, USA, mcoving@uark.edu

(2) Lunasonde, Tucson, AZ, USA

(3) Instituto de Geología, Universidad Nacional Autónoma de México. Circuito Interior s/n, Coyoacan, C.U., 04510 Ciudad de México, México

(4) Asociación de Montañismo y Escalada de la Universidad Nacional Autónoma de México. Ciudad Universitaria, Coyoacan, C.U., 04510 Ciudad de México, México

Abstract

Mechanical erosion can be important within cave streams, but few studies have constrained the factors that control its importance. Here, we examine erosional features in a high-gradient cave stream and use percent feature coverage as a proxy for the importance of different erosion processes. We find that most sites within the cave are dominated by mechanical erosion features, particularly features that indicate abrasion by sediment. Erosion at sites with closely spaced fractures (<60 cm) is typically dominated by plucking of blocks. There are three sites where solutional features dominate. All of these sites are upstream of boulder chokes, where ponding occurs during large floods. During moderate floods, backflooding does not occur, and high velocity water drives mechanical erosion near the bed. During large floods, ponding reduces flow velocities and shuts off mechanical erosion. However, chemical erosion can proceed within the ponded reach. We interpret these results by considering how chemical and mechanical erosion rates scale with discharge or flow velocity. Overall, our results suggest that mechanical erosion is an important process within cave streams and should be considered when studying the later stages of speleogenesis.

1. Introduction

Early speleogenesis is primarily driven by chemical dissolution of the rock. However, mature cave systems often contain powerful streams that can transport coarse sediment and mechanically erode rock (FARRANT & SMART, 2011). While it has long been recognized that mechanical erosion is an important process within cave streams (NEWSON, 1971), few studies have attempted to quantify mechanical erosion within cave streams or to understand the factors that control its importance. Here, we observe diagnostic erosional features along a cave stream that indicate either chemical or mechanical erosion processes. We use coverage by these features as a proxy for the relative importance of different erosion processes and explore factors that may influence the relative importance of various erosion mechanisms.

The site for this study is Sistema J2, a cave system that is one branch of the larger Cheve Karst Hydrological System, located in the Sierra de Juárez of northern Oaxaca. J2 has an explored length of 14.4 km and a depth of 1,229 m. It has not been physically connected into Cheve, though it is probable that the water from both caves joins and drains to the resurgence, Cueva de la Mano, located in the Santo Domingo Canyon. The caves are developed in a fold-thrust belt that has deformed calcareous rocks of the Zongolica Basin.

2. Materials and methods

Nine sites were surveyed within stream channels in J2. Seven of the sites were in the main stream passage of J2, and the other two (Ptygmatic and J2LB44) were located in an infeeding stream that connects to another cave entrance called Last Bash. At each site, we quantified the percent coverage of different types of mechanical erosion features, including mechanical erosion flutes, potholes, and surfaces with recently plucked blocks. We also looked for evidence of dissolution, such as scallops, solution pockets, or sharp rough surfaces. Feature coverage was estimated to the nearest 5% along reaches that were approximately 10 m long.

To examine potential controls of erosional processes, we also quantified fracture spacing and recorded Schmidt hammer scores at each site. The Schmidt hammer provides

a measurement of elastic rebound, which is often used as a proxy for compressive strength and, therefore, mechanical erodibility (GOUDIE, 2006). At each site, 36 Schmidt hammer scores were taken to get a representative median value.

3. Results

The cave stream incises through two primary types of rock, a sandy limestone and a clayey limestone, both of which have been mylonitized to varying degrees during deformation within the fold-thrust belt. Results below are divided according to rock type. At the active stream level, all studied sites predominantly displayed mechanical erosion features rather than signs of dissolution (Fig. 1). Mechanical erosion flutes were particularly prevalent, though some sites also indicated a dominance of plucking. In Fig 1., sites are divided between those in the limestone and

clayey limestone. While flutes and potholes develop in both rock types, plucking was much more common within the clayey limestone than the purer limestone. No clear scallops were observed at any sites, and only three sites displayed clear chemical erosion features. However, these were not near the stream bed and will be described later.

Schmidt hammer scores ranged between 49 and 61, indicating a relatively narrow range in rock mechanical strength. There are also no clear trends between Schmidt hammer score and the types of erosional features that dominate at a site (Fig. 2).

Fracture spacing was related to the coverage of plucking features, where all sites with greater than a 10% coverage by plucking features had a fracture spacing of 60 cm or less (Fig. 3). The site with the greatest extent of plucking also had the smallest fracture spacing of 20 cm. The clayey limestone tended to have more closely spaced fractures. An example of a stream reach dominated by plucking (near BTBK26) is shown in Fig. 4.

Though no sites displayed clear dissolutional features at stream level, three sites (Donde Homek, C3 logger, and VSB27) displayed solutional surfaces beginning 2-3 m above the stream bed. All of these sites were located in the sandy limestone. The solutional surfaces typically consisted of solution pockets and sharp, jagged fins of rock (Fig. 5A,B). Many of these surfaces also contained dark coatings. Near stream level, the channel walls and bed were dominated by mechanical erosion flutes, potholes, and smooth polished surfaces (Fig. 5C,D). All three of these sites are upstream of boulder chokes that block the entire cave passage. At one site (C3 logger), a data logger indicated water depths of greater than 4 m during large flood events, suggesting that water ponds upstream of the boulder choke during floods.

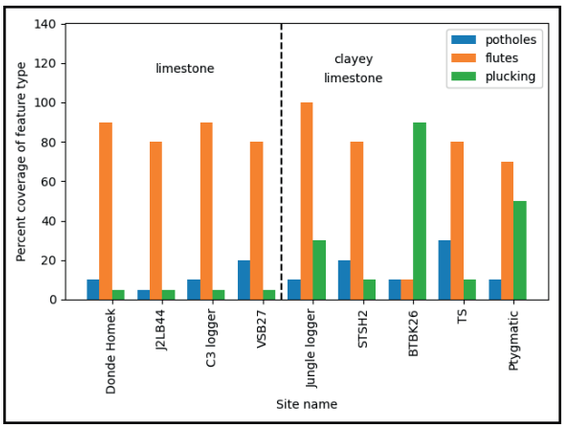

Figure 1: *Coverage of stream channel surfaces by different types of mechanical erosional features. Note that percentages may add up to greater than 100%, since a single surface can display more than one type of feature.*

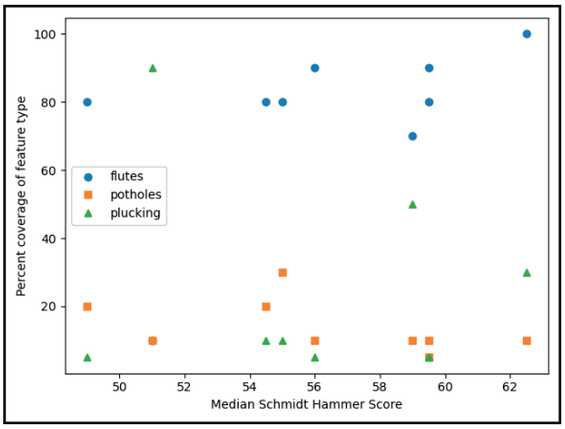

Figure 2: *Coverage of stream channel by erosional features as a function of Schmidt hammer score, which is a proxy for rock erodibility. There are no clear trends between Schmidt hammer scores and coverage by any of the feature types.*

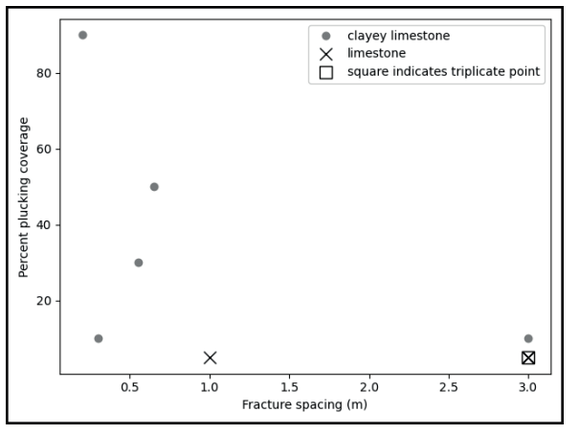

Figure 3: *Percent coverage by plucking at the stream sites as a function of fracture spacing. Plucking dominates at sites with fracture spacing <60 cm, which are all in the clayey limestone unit. Sites with greater than 3 meter spacing between fractures are depicted as 3 meters, and there is a triplicate point shown with a square.*

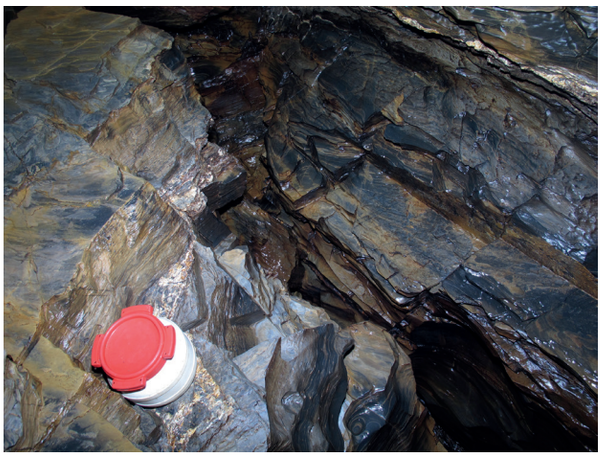

Figure 4: *An example site that is dominated by plucking, located near BTBK26.*

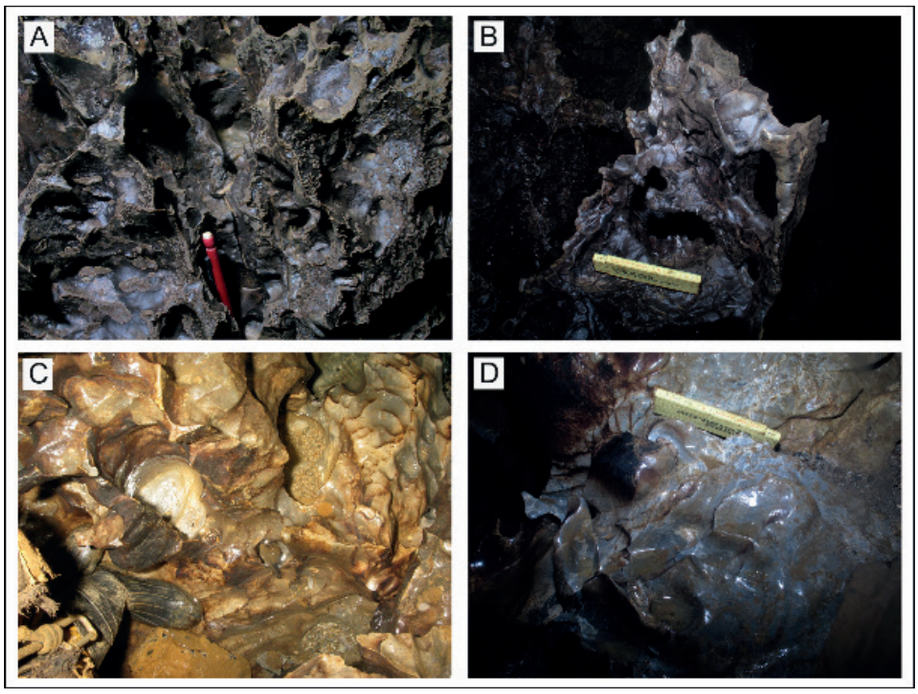

Figure 5: *Photos from VSB27 (A,C) and Donde Homek (B,D). The top row shows solutional surfaces that were located 2-4 m above the stream bed. These surfaces contain solution pockets and sharp jagged edges and frequently have a dark coating. The bottom row shows mechanical erosion surfaces located on the beds of these sites, including flutes, potholes, and polished surfaces.*

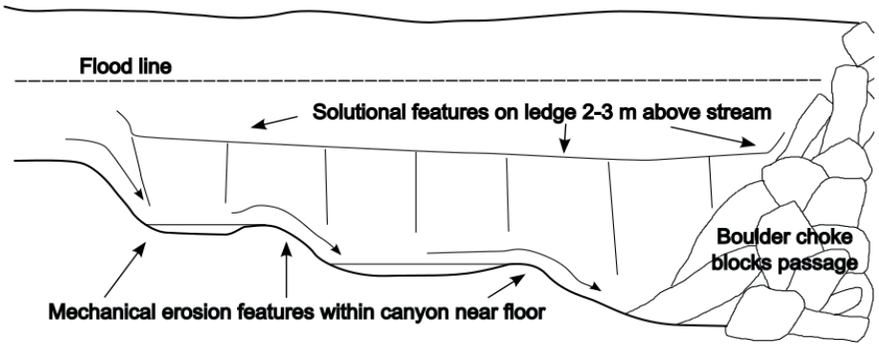

Figure 6: *A sketch of the configuration of features at the Donde Homek site. A narrow canyon is incised in the floor and filled with mechanical erosion features. Starting around 2 m above the stream bed, solutional features dominate. A horizontal line that is visible in the passage (dashed line) marks the level of backflooding during the highest discharges.*

4. Discussion

Even though caves initially develop from chemical dissolution, the cave stream of J2 displays few signs of chemical erosion and many signs of mechanical erosion. The stream channel has a high gradient, descending on average at a slope of around 15 degrees. The site is also influenced by a monsoonal climate, with heavy precipitation and intense flooding during the summer season.

The stream bed contains abundant coarse sediment, mostly in the sand to gravel size. Much of this sediment load likely travels as suspended load during flood events, enabling rapid abrasion of the rock. Even though the cave is autogenically recharged, some metavolcanic clasts are present, as well as the remnants of impurities within the carbonate rocks. Harder minerals, such as quartz, may contribute to the effectiveness of limestone abrasion. Though sediment is abundant in the channel, most of the bed is exposed bedrock, and there is insufficient sediment supply to produce much armoring of the bed (SKLAR & DIETRICH, 2004).

In general, abrasional features, such as mechanical erosion flutes and polished surfaces, dominate the stream channel (Fig. 1). The dearth of solutional features suggests that mechanical erosion processes dominate for much of the channel. This is perhaps not surprising given the high gradient, abrasive sediment, and intense flooding.

Plucking of blocks is also an important process in the cave, particularly in the clayey limestone, which is more densely fractured. This finding is similar to prior work that found a dominance of block plucking within bedrock channels when fracture spacing is below the meter scale (WHIPPLE et al., 2000).

The dominance of mechanical erosion, except at sites that experience backflooding, can be explained by considering a conceptual framework (Fig. 7) for the relative importance of chemical and mechanical erosion

in soluble bedrock channels (COVINGTON et al., 2015). Dissolution rates scale relatively weakly with discharge or flow velocity. In the case that rates are limited by kinetics, then they are independent of velocity. If transport controls the dissolution rates, then they scale with the square root of shear stress. Mechanical erosion processes scale more strongly with shear stress (WHIPPLE et al., 2000). However, mechanical erosion typically ceases below a threshold discharge, often the threshold for sediment transport. When mechanical erosion is active, it tends to have higher instantaneous rates than dissolution (Fig. 7). Therefore, the relative importance of the two processes largely depends on the amount of time that the stream spends above or below the threshold for mechanical erosion, and the extent to which the water is saturated with respect to calcite at lower discharges.

Under most flood conditions in J2, sediment transport is active and mechanical erosion outpaces chemical erosion. The cave is autogenically recharged, and therefore it is also likely that the stream is near saturation during low to moderate flow conditions. Therefore, dissolution is not active during these low flow periods. Consequently, mechanical erosion is dominant at most sites.

At the three sites where solutional features were observed, backflooding and ponding of water upstream of boulder chokes changes the situation. At the highest discharges, when backflooding occurs, stream velocity dramatically decreases within the ponded sections and mechanical erosion ceases. However, the water is undersaturated during these storms and can actively dissolve the surfaces that are in contact with the ponded water. During smaller floods, backflooding does not occur and mechanical erosion continues rapidly near the stream bed, creating the mechanical erosion features observed near the bed.

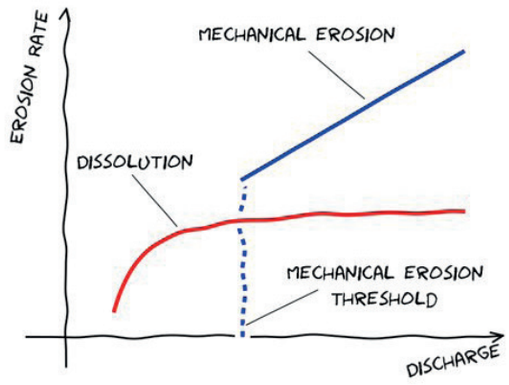

Figure 7: *Dissolution scales more weakly with discharge or flow velocity than mechanical erosion. Mechanical erosion is inactive below a threshold, but when it is active the instantaneous rates tend to be higher than dissolution. The relative importance of chemical and mechanical erosion is largely determined by the relative position of the threshold discharges under which each process activates and the time distribution of discharges in the stream (COVINGTON et al., 2015).*

5. Conclusion

Though most caves initially develop through chemical erosion processes, mature cave streams can also incise via mechanical erosion. Here, we studied erosional features in a high-gradient stream cave, Sistema J2, Oaxaca, Mexico. We find that this stream channel is dominated by mechanical erosion features, particularly features that indicate abrasion by suspended and bedload sediment. Some reaches also display a dominance of plucking features, where fractures are more densely spaced and blocks can be transported by the stream.

Three sites display solutional features. However, these are located several meters above the bed of the stream. Ponding at these sites, which are upstream of boulder chokes, enables active dissolution at high discharges, when mechanical erosion ceases due to the low flow velocity of the ponded water. Overall, our observations indicate that mechanical erosion can be a dominant process in cave evolution and should be considered when studying the later stages of speleogenesis. However, processes that produce ponding, such as blockage by breakdown, may elevate the importance of chemical erosion processes.

Acknowledgments

We thank the people of San Francisco Chapulapa for permission to access the cave. This work would not have been possible without the organizational efforts of expedition leader Bill Stone, Mexican caver 'Wicho' Diaz, and numerous other members of the Cheve Cave Project. We additionally thank Bill Stone, Vickie Siegel, Marcin Gala, Kasia Biernacka, and Elliot Stahl for assistance in collecting field data.

References

COVINGTON, M. D., GULLEY, J. D., & GABROVŠEK, F. (2015). Natural variations in calcite dissolution rates in streams: Controls, implications, and open questions. Geophysical Research Letters, 42(8): 2836-2843.

FARRANT, A. R., & SMART, P. L. (2011). Role of sediment in speleogenesis; sedimentation and paragenesis. Geomorphology,134(1-2): 79-93.

GOUDIE, A. S. (2006). The Schmidt Hammer in geomorphological research. Progress in Physical Geography, 30(6): 703-718.

NEWSON, M. D. (1971). A model of subterranean limestone erosion in the British Isles based on hydrology. Transactions of the Institute of British Geographers, 55-70.

SKLAR, L. S., and W. E. DIETRICH (2004). A mechanistic model for river incision into bedrock by saltating bed load, Water Resources Research, 40: W06301.

WHIPPLE, K. X., HANCOCK, G. S., & ANDERSON, R. S. (2000). River incision into bedrock: Mechanics and relative efficacy of plucking, abrasion, and cavitation. Geological Society of America Bulletin, 112(3): 490-503.

Speleogenesis and evolution of the Valdemino Cave (Borgio Verezzi, Liguria, Northern Italy)

Jo De Waele (1), Chuan-Chou Shen (2,3), Bartolomeo Vigna (4), Adriano Fiorucci (4), Paola Marini (4), Chun-Yuan Huang (2,3), Hsun-Ming Hu (2,3,5)

(1) Department of Biological, Geological and Environmental Sciences, Alma Mater University of Bologna, Via Zamboni 67, Bologna, Italy, jo.dewaele@unibo.it (corresponding author)

(2) High-Precision Mass Spectrometry and Environment Change Laboratory (HISPEC), Department of Geosciences, National Taiwan University, Taipei 10617, Taiwan, ROC, river@ntu.edu.tw, yuau0213@gmail.com

(3) Research Center for Future Earth, National Taiwan University, Taipei 10617, Taiwan, ROC

(4) DIATI Politecnico di Torino, Corso Duca degli Abruzzi 24, Torino, Italy, bartolomeo.vigna@formerfaculty.polito.it; adriano.fiorucci@polito.it; paola.marini@polito.it

(5) Atmosphere and Ocean Research Institute, The University of Tokyo, Chiba 277-8564, Japan, hsunming.hu@gmail.com

Abstract

Valdemino show cave (Borgio Verezzi, Northern Italy), is hosted in Triassic dolostones. It shows mixing corrosion morphologies and large collapses, lacking morphologies and sediments related to turbulent water flow. Speleothem samples were subjected to U/Th dating to constrain the timing of collapses, coastal mixing, and speleogenesis. The oldest speleothems indicate speleogenesis to have started over 630 thousand years ago (ka, before 1950 AD), probably during marine isotope stage (MIS) 17. Collapses appear to have taken place mostly during cold stages. Speleogenesis is mainly related to coastal mixing corrosion which dissolved lower lying portions of the rock mass during various periods of the Middle- to Upper Pleistocene up to today. During cold stages, when the sea retreated and the water table lowered, loss of buoyancy caused these lower levels to collapse, creating the cave voids accessible today. The cave appears thus to have been in the fresh-salt water mixing zone during several sea level highstands over the last 650 ka, in a slowly uplifting coast (ca. 0.05 m/kyr).

1. Introduction

Valdemino Cave is located in the Borgio Verezzi municipality, at an altitude of 32 m above sea level (asl) (WGS84 Lat. 44.16287988, Long. 8.30415604979)(Fig. 1). The cave was discovered and "explored" by three young boys, after a flash flood in 1933 caused a man-made hole, excavated to divert surface waters from a local brook, to enlarge and absorb most of the water (MORTARI & CHIARELLA, 2005). These boys left their signatures on the wall of the cave.

Twenty-two years later, some Royal Air Force soldiers discovered a new entrance penetrating around 400 metres into the cave (LAMBOGLIA, 1955). Subsequently local cavers started exploring and mapping the entire system of chambers and passages, and spent 15 years excavating and adapting the narrow parts and digging a new artificial gallery for its future adaptation for tourist visits. The cave eventually opened to the wider public in the early summer of 1970, and attracts around 50,000 visitors per year (DENTELLA, 1997).

Today, after e resurvey of Speleo Club Tanaro taking advantage of a long-lasting dry period, which lowered the internal lake levels by over 4 metres, the cave reaches a development of 1,442 m and covers an altitudinal range of 37 m (+38 m asl to 1 m) (CALANDRI & GRIPPA, 1990).

Figure 1: *Location of Valdemino Cave on a Google Earth image. The red lines show the plan view of the cave survey. The inset shows the location of Borgio Verezzi in Northern Italy.*

2. Preliminary investigations

From a geological point of view the cave is entirely carved in the dolostones of the San Pietro dei Monti Formation (Middle Trias), here in decametric beds, with some local levels of cemented carbonate breccia. These rocks are intensely fractured at a metric scale along several directions, mainly NE-SW and E-W.

The soluble rock formation extends in a NNE direction for over 2 km, where it borders the underlying Permo-Triassic quartzites and metavolcanics, and reaches the coastline to the S, where the dolomitic limestones are covered by a thin deposit of Quaternary alluvial and coastal sediments. Near Valdemino there are other smaller caves (Staricco, Renovo, Varicella caves), all reaching lakes that are always at the same altitude.

The cave is characterised by several rooms of up to 50 metres wide, connected by rather narrow (less than 2 m wide) passages. Its cave passages extend over a rather small area, around 250 m in the N-S direction and 160 m in the E-W direction. Some parts of the cave are at less than 600 metres distance from the present coastline. All known cave passages are very shallow, some parts having even less than 10 metres of rock to the surface. Large collapses characterise most of the cave, with old and thick broken and inclined flowstones and stalagmites, and large blocks fallen from the ceiling (CALANDRI, 1990). Collapses appear to have occurred in different periods. The entire cave appears to be mostly recharged by the diffuse network of fractures.

In the early 1960s a vertical fissure filled with bone remains was intercepted during the excavation of the artificial tourist gallery (FORNASIERO, 1989). This fossiliferous breccia was excavated and sampled by several geologists showing the presence of two fossil layers (upper and lower) separated by a sterile part.

Several fossil species typical of the Middle Pleistocene were found in the Lower layer (MIS 15, ca. 600 ka) (NOCCHI & SALA, 1997), the Upper layer, on the other hand, contained only Late Pleistocene species.

3. Methods

We visited Valdemino Cave several times between 2020 and 2024 to carry out geomorphological observations and sampling. All cave branches (including the lowest ones) were visited during these trips, thanks to the exceptionally low water levels, and pictures were taken of characteristic sites in the cave (lakes, rock falls, speleothem formations, etc.) from the same viewpoints during both very low and normal water levels, enabling their visual correlation.

Rock samples of the San Pietro dei Monti Formation were taken for mineralogical (X-Ray Diffraction, Raman spectroscopy) and geochemical analyses (X-Ray Fluorescence), and textural and structural observations were carried out using a petrographic microscope.

A total of 21 speleothem samples were taken throughout the cave, at various altitudes. Spatial and stratigraphic relationships of sampled speleothem fragments, when taken in situ or when the original position was known, were carefully signed, in order to attribute a relative chronology.

Fragments of speleothems have been dated by the U/Th method at the High-Precision Mass Spectrometry and Environment Change Laboratory (HISPEC) of the National Taiwan University following established protocols (for detailed methods see SHEN et al., 2012).

Water samples were taken at different times (during normal (high) and extremely low water conditions) from different points in the cave, and at the surface in the "Lavatoio" Spring, which drains the entire karst aquifer. These last analyses can be used as a reference for resident waters in contact with the dolostones. Waters were analysed at the DIATI laboratory, Polytechnic of Turin (Italy).

Lake levels and EC-T of waters in the cave were monitored using OTT instrumentation, measuring with a time interval of 60 minutes.

4. Results

Valdemino Cave is carved in the intensely fractured dolostones of the San Pietro dei Monti Fm. XRD, Raman spectroscopy and XRF confirm the rock and the veins crossing it to be composed of pure dolomite. The rocks in which the cave is carved are generally dark grey, from finely to thickly layered, and contain parts in which the rock mass is brecciated and cemented by micrite. The spacing between fractures is centimetric to metric, forming a dense network of permeable pathways that have been dissolved, in variable amounts, by infiltrating waters.

One of the most striking morphological characteristics of the cave is the widespread occurrence of collapsed material, with blocks that can reach the size of several metres. These giant collapses give a dome-shaped morphology to the upper and larger rooms in the cave. Collapsed blocks are angular, and variously covered with both recent speleothems, and older flowstones sometimes exceeding the metre in thickness.

In general, all Valdemino Cave voids are angular, with very few areas where the rock surfaces are smoothed. Phreatic tubes are completely absent, and so are wall sculpturing features such as scallops. Alluvial sediments are almost exclusively found in the palaeontological branch, whereas water flows exclusively after heavy rainfall from the original entrance (where the three kids accessed the first time the cave), which acts as a sinking point.

Figure 2: *One of the lakes in Valdemino Cave. Water level is at 5 m asl: note the submerged speleothems (Photo Bartolomeo Vigna).*

Analysing the cave survey, the largest voids are located in the altimetric range of 3-6 m asl, and 10-14 m asl, the last producing the largest rooms. These upper areas are mainly the product of collapse of the underlying voids.

The monitoring of water levels of the lakes showed very slow variations over time, demonstrating underground water circulation is occurring in a very extensive saturated zone with rather low permeability values. In detail, in some periods, daily fluctuations in water levels of a few millimetres are observed with recurrence interval of ca. 6 hours. These water level changes are influenced by tidal pumping which is felt up to 600 m distance from the coast. These data, together with the discovery of small eels in the lakes of the cave, seem to demonstrate the existence of an extensive freshwater aquifer that floats on the saline water that underlies the entire coastal area.

Figure 3: *Corroded speleothem (ca. 650 ka old), filling gaps between block on the roof of Valdemino Cave (Photo Bartolomeo Vigna).*

Underground lakes correspond to the local base level, and are in direct connection with the karst aquifer. All lake levels in the cave, even the most distant ones, are exactly at the same altitude, and vary their water level synchronously in response to rainfall or drought. In ordinary meteorological situations, water levels are located at an altitude between 5 and 6 m asl, but following the extreme drought period between November 2022 and December 2023, the levels dropped by over 4 metres reaching an altitude around 1 m above sea level. The chemical analyses of the waters of the Lavatoio Spring, which represent the waters draining the entire aquifer, has an identical geochemical fingerprint of the cave lake waters. All waters showed a bicarbonate-calcium-magnesium component, with a Mg/Ca ratio compatible with dolomite rocks. The specific electrical conductivity measured at the time of sampling was on average at around 650 µS/cm at 25°C, highlighting waters with a higher mineralisation than those normally circulating in carbonate rocks, due in part to the presence of marine aerosol and, in part, to the slow circulation in the rock mass.

Figure 4: *Old collapsed speleothems (ca. 47 ka old), and newly growing stalactites (77 ka) and stalagmites in Valdemino Cave (Photo Bartolomeo Vigna).*

The age of the speleothems ranges between 647 ± 149 ka and 25.84 ± 0.28 ka. U/Th dating targeted speleothems, which could bracket episodes of collapse, mixing corrosion, or older speleogenetic phases (Fig. 3-4-5).

The ages obtained allow to attribute an age of the cave of at least 700 ka, and the occurrence of repeated collapses during cold stages, when sea level and the local groundwater table lowered.

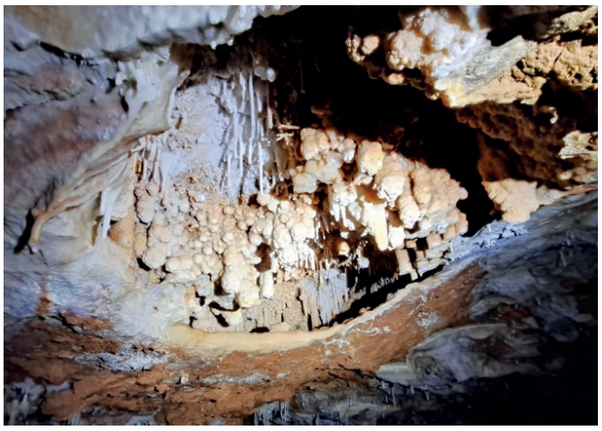

Figure 5: *Mammillary calcite (ca. 516 ka old) filling a large geode along the roof of Valdemino Cave. Note small stalactites that formed later in the geode (Photo Bartolomeo Vigna).*

The karstified dolostones of this area have been in or close to the salt-fresh water mixing zone repeatedly over the past 700 ka, with dissolution occurring by mixing corrosion during sea level highstands, and collapses happening after sea level retreated. This evidences how this part of the Ligurian coast has been relatively stable over the past 700 ka, with an average estimated uplift rate of only 0.05 m/ka.

5. Conclusions

Valdemino cave, a labyrinthic, more or less horizontal cave located close to the Ligurian coast, is a touristic site that attracts an important number of tourists because of its beautiful speleothems and the presence of a series of blue lakes. Geomorphological observations clearly allow recognising this cave to be of the coastal mixing type, with almost complete lack of alluvial or coastal sediments, no scallops or rounded phreatic morphologies, and the spongework organisation of cave passages. U/Th dating of speleothems throughout the cave, at various altitudes and in different settings, with oldest ages set in MIS 16, show the cave to have started forming probably during MIS 17 or earlier (Fig. 6A-B). Collapses, dated by overgrowths of speleothems on fallen blocks, all occurred during even MIS (cold stages), when sea level dropped and the loss of buoyancy triggered gravitational movements (Fig. 6C). These collapses created the voids that are still accessible today (the tourist paths are built on a floor made of giant collapsed blocks).

During warm and wet periods, on the contrary, the high sea levels often reached the altitude of the actual cave levels, causing mixing dissolution. Some old flowstones, now occurring at 6 m asl, appear intensely corroded, and must have been in the mixing zone at least once. This most probably occurred during the last interglacial (MIS 5e) (Fig. 6D): if this is true, this strip of coast must have uplifted very slowly (at rates of ca. 0.05 m/ka) over the last 630 ka.

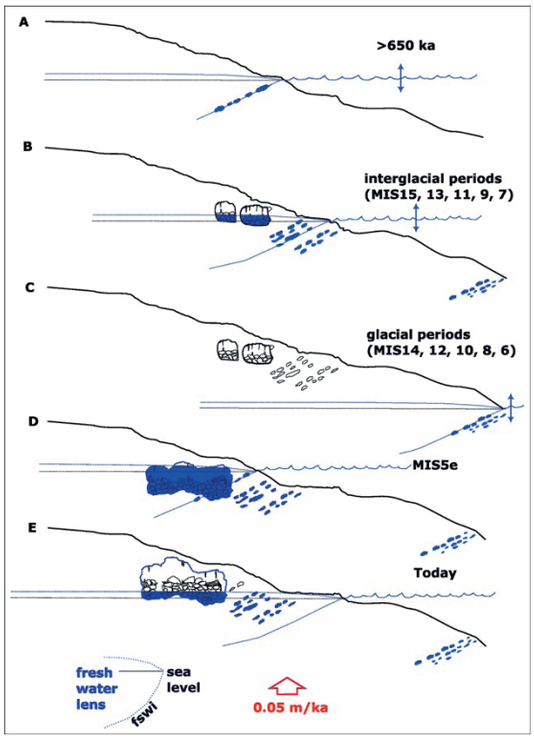

Figure 6: *Evolutionary model of Valdemino Cave. See text for details.*

Acknowledgments

Many thanks to the Municipality of Borgio Verezzi and the cave management and guides for the availability during our studies, and authorization to carry out these researches. Speleo Club Tanaro is thanked for the having made available the cave maps. U/Th dating was supported by grants from the NTU Cutting-Edge Steering Research Project (105R7625) and Core Consortiums Project (110L8907, 113L891902), Higher Education Sprout Project of the Ministry of Education (112L894202), and the projects under the National Science and Technology Council in Taiwan (110-2123-M002-009, 111-2116-M-002-022-MY3, 113-2926-I-002-510-G) and Academia Sinica (AS-TP-113-L04) (PI C-C Shen).

References

CALANDRI G. (1990) Le acque della Grotta di Valdemino (Borgio Verezzi, Sv): appunti idrogeochimici. Bollettino del gruppo speleologico imperiese 51:3-6.

CALANDRI G., GRIPPA C. (1990) Valdemino (SV): 1600 m di sviluppo. Speleologia 22:64.

DENTELLA G. (1997) Le Grotte di Borgio Verezzi. L'eccentrico 1:44-50.

FORNASIERO O. (1989) Cronostratigrafia di due giacimenti quaternari continentali a mammiferi della Liguria. MSc. Thesis, University of Ferrara.

LAMBOGLIA N. (1955) La scoperta di una nuova grotta a Borgio. Rivista Ingauna e Intemelia 10(3):84-86.

MORTARI, S., CHIARELLI, A. (2005) Le Grotte di Borgio Verezzi. Guida alle Grotte Liguri, Borgio Verezzi. Albenga: Tipografia Fratelli Stalla, 82 p.

NOCCHI G., SALA B. (1997) The fossil rabbit from Valdemino cave (Borgio Verezzi, Savona) in the context of western Europe Oryctolagini of Quaternary. Palaeovertebrata 26:167-187.

SHEN C.C., WU C.C., CHENG H., EDWARDS R.L., HSIEH Y.T., GALLET S., CHANG C.C., LI T.Y., LAM D.D., KANO A., HORI M., SPÖTL C. (2012) High--precision and high-resolution carbonate 230Th dating by MC-ICP-MS with SEM protocols. Geochimica et Cosmochimica Acta 99:71-86.

Quaternary deglacial speleogenesis on the Gower Peninsula, South Wales, UK

Trevor Faulkner

British Cave Research Association, trevor.marblecaves@gmail.com

Abstract

Renewed interest in the caves of the Gower Peninsula of southern Wales was sparked by the recent re-opening of Llethryd Swallet, the discovery of several other significant caves, and a new book. The latter proposes that the local water supplies are derived from precipitation falling on Gower, rather than from the northern limb of limestone in the South Wales Coalfield Syncline. However, claims are made that some of the existing caves are older than ten million years. This paper offers a simpler hypothesis, from considerations of cave passage sizes, morphologies and lacustrine sediments and of surface deposits at the southern coast. The caves remaining on Gower were probably initially developed during the deglaciations of the Anglian and/or Devensian icesheets. In particular, the Llethryd Swallet–Tooth Cave system was likely initiated by phreatic dissolution during the Anglian deglaciation, when an annular ice-dammed lake surrounded Cefn Bryn and perhaps extended eastwards beyond Hunts Bay, before collapsing at a jökulhlaup. Further development by vadose entrenchment, plus phreatic dissolution at lower levels, occurred during the subsequent interglacials, with renewed phreatic enlargement by similar processes during the Devensian deglaciation.

1. Introduction

Information about the caves on the Gower Peninsula of southern Wales, UK (Figures 1 and 2) was provided by JENKINS & WILLIAMS (1963) and EDE & BULL (1989), as summarized by WALTHAM et al. (1997). Recent field trips to Gower were in 2015 (SHAKESBY & HIEMSTRA, 2015) and 2017 (COOPER, 2023). The re-opening of Llethryd Swallet and the discovery of associated caves were reported by FREEM (2021). A book by KOKELAAR (2021) has discussed the geology, geomorphology, glaciology, hydrogeology and caves of Gower, as critically reviewed by WALTHAM (2021) and JOHN (2022). It demonstrates that the annual precipitations on Gower's local allogenic and karstic autogenic catchment areas exceed the annual discharge from Llethryd Swallet's resurgence. Similarly, autogenic precipitation into a perched shale aquifer on the northern slope at Cefn Bryn (Figure 2) exceeds discharge at local wells and only an exceptional drought lasting >140 days could cause the springs to run dry. Thus, there is no need to invoke a 30km flow of water from the North Crop through the limestone in the >3km-deep South Wales Coalfield Syncline to account for the discharges, as previously widely assumed. However, claims that some caves are 200, 60 or 10 million years old, based on highly complex deductions about Mesozoic and Tertiary landscape evolution, oppose the conclusion that "the overall character is typified by flow patterns more closely associated with surface topography than is commonly considered normal in limestone terrains" (EDE & BULL, 1989, p212). Because there is insufficient space to debate the justification of geologically ancient cave survival here, this author argues instead that the caves were developed mainly during and after the local Quaternary deglaciations of the Anglian and Devensian icesheets in Marine Isotope Stage (MIS) 12 at c. 426ka and in MIS2 after 26ka.

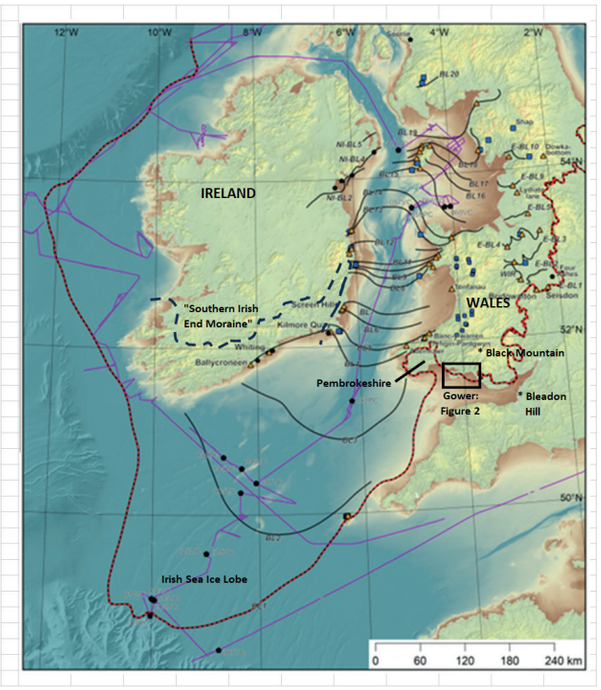

Figure 1: *Gower, within the reported LGM area of the Devensian glaciation (from Scourse et al., 2021, Fig. 1).*

2. The caves of Gower

About 200 speleological sites are noted on Gower (COOPER, 2023). More might be buried beneath glacial sediments. Caves up to 70m long are abundant on the southern sea cliffs, some containing Ipswichian (MIS5e) faunal assemblages. The longest hydrological system lies beneath Llethryd Cwm, where a stream sinks into the 610m-long Llethryd Swallet (Figure 2). The water flows from Sump 4 via an unknown route to Pot Sump in the lowest, Main Stream, passage of the 1550m-long Tooth Cave, before resurging >1000m farther south. Ogof Ffynnon Wyntog is a second significant system, with >300m of open cave passages. Its stream normally rises from a sump at Ogof Wyntog (Kokelaar, 2021). Both systems contain commonly small relict phreatic passages and chambers above the active streams. A third north–south flow system lies beneath the Bishopston Valley that has short caves and collapsed sections north of Pwlldu Head.

3. Geology and glaciology

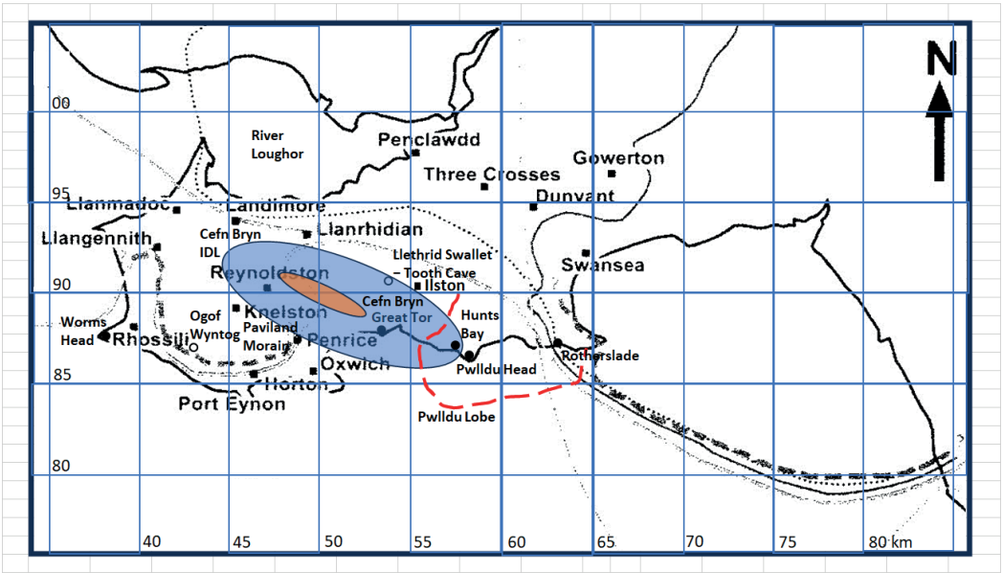

Figure 2: *The Gower Peninsula, showing some previous estimates of the southward extremity of the LGM, based on Cooper (2023, Fig. 3.1), and the Pwlldu Lobe (red dashes), according to Kokelaar (2021, Fig. 46). A hypothetical annular deglacial Cefn Bryn IDL is shown (in blue) around the Cefn Bryn ridge (in brown) when the lake edge reached Llethryd Swallet.*

Gower comprises the South Crop of the South Wales Coalfield Syncline, with rocks of Silurian to Jurassic ages including karstic Carboniferous limestones, with a history of later uplifts, erosion surfaces and varying adjacent sea levels (KOKELAAR, 2021). Its Quaternary glaciations were discussed by SHAKESBY & HIEMSTRA (2015). From the nature of the erratics and tills, only the Anglian icesheet, with a thickness of a few hundred metres, and that at the Devensian Last Glacial Maximum (LGM) advanced onto Gower. Based on evidence of sparse Anglian weathered erratics and thin widespread coastal glacigenic sediments containing Devonian Old Red Sandstones, red Triassic fragments and identifiable igneous rocks, the Anglian glaciation probably covered the whole peninsula. The erratics were likely derived from north Pembrokeshire or an Irish Sea ice lobe in the west, and might extend east beyond Swansea Bay (JOHN, 2024). This ice possibly deposited an enigmatic morainic gravel deposit on Bleadon Hill in Somerset (HUNT, 2006; Figure 1). Locally, these deposits underlie or mix with, reach farther south and occur at higher altitudes than, Ipswichian Interglacial (MIS5e, 126–115ka) Patella Beach deposits that themselves underlie younger Devensian tills that range in thickness to >10m.

Studies of the pathways of glacigenic sediments and glacial erratics have prompted proposal of many different southern limits for the Devensian icesheet on Gower (Figure 2). At the LGM, three ice lobes transported erratics (including distinctive quartzites and tough white sandstones from the North Crop) and till c. 30km southwestwards to Gower from the Black Mountain area (Figure 1). An LGM ice limit covering all of eastern Gower was proposed by KOKELAAR (2021, Fig. 46). It extended eastwards from a Paviland Lobe ice stream at the Paviland Moraine, c. 110m above sea level (asl), near the present southern coast, to an Ilston Lobe at the north slope of the Cefn Bryn ridge, and then to his proposed Pwlldu Lobe (Figure 2). It had previously been argued by SHAKESBY et al. (2018) that the Paviland Moraine was of Devensian, rather than Anglian, age. From considerations of possible sea floor moraines, KOKELAAR (2021) speculated that the Pwlldu Lobe extended 3–4km farther south than the ice that reached the present coastal cliffs at Hunts Bay (MCCARROLL & MCCARROLL, 2015). Thus, it was contiguous with the widely accepted ice lobe in Swansea Bay. Development of collapsed chambers at Higher and Lower Daw Pit and the 35m-deep Gwynspar Pit in the Bishopston valley was presumably triggered by the weight of the LGM ice.

The LGM ice limit proposed by KOKELAAR (2021, Fig. 46) is, however, unconvincing, because the highest parts of the ridge from Llanmadoc Hill (186m asl) to Rhossili Down (193m) and the Cefn Bryn ridge (70–188m), and all the land around Oxwich Bay, were shown as being clear of ice. Thus, KOKELAAR (2021, p110) assumed that, in contrast with the Anglian, degraded tors at several western high points and on Cefn Bryn, and some limestone pinnacles on the eastern side of the Ilston Lobe (p86), remained as nunataks at the LGM. That would indicate continuous exposure since MIS11, although the only reported cosmogenic nuclide exposure age is 23±2ka, for Arthur's Stone on Cefn Bryn (PHILLIPS et al., 1994). Seemingly, these assumptions were based on an LGM ice thickness between c. 100m (in the north and in the Paviland Lobe) and 10–20m (near Ilston) (KOKELAAR, 2021, p83). Furthermore, the proposed limits of the Paviland and Ilston lobes coincidentally mirror the present sea cliff at Paviland and the brow of Cefn Bryn. For the Paviland Lobe, this was just 20km east of the wide Irish Sea Ice Stream, which took the Irish

LGM limit beyond the Scilly Isles, 550km to the southwest, at 25.5ka (SCOURSE et al., 2021; Figure 1), but which retreated 300km northwards by 25.0ka. The Ilston Lobe ice stream was powerful enough to deposit Devensian till at 140m asl on the northern side of Cefn Bryn (KOKELAAR, 2021, p201), to carry the nearby 35-tonne Arthur's Stone erratic for 30km up to 147m asl, and to transport other large local erratics to 155m asl. Thus, the ice itself likely flowed c. 0.5km farther south over the western brow of Cefn Bryn at a height of 167m asl, to join the Paviland Lobe. Following the suggestion that the ice might have reached 170m asl on Llanmadoc Hill (KOKELAAR, 2021, p112), it seems likely to this author that there were no nunataks on Gower at the LGM, even at the eastern brow of Cefn Bryn at 188m asl, as supported by the exposure age for Arthur's Stone. However, in contrast to Kokelaar' view (2021, p95), uncertainly about the existence of nunataks does suggest that the Gower ice was thin enough to have a permanent cold, rather than warm, base in the low temperature at the LGM. Such relatively thin ice probably left little surface evidence of its presence, so that the tors could survive uneroded, frozen beneath cold ice.

The southern limits of erratics and till might also mark only the minimum extent of each ice lobe, if thin stationary cold basal ice was unable to deposit any subglacial material. As well as LGM ice flowing across Gower from the north, it could initially have been nourished and then supplemented on higher ground by local precipitation from Atlantic storms, which nowadays cause the high NaCl content of Gower waters (KOKELAAR, 2021). Like the Pwlldu Lobe, the Paviland and Ilston lobes probably also extended on land beyond the present coastline, when eustatic sea level was 130m lower than now. It therefor seems likely that the entire peninsula was glaciated at the LGM, as suggested by MCCARROLL & MCCARROLL (2015). If so, the Paviland Moraine represents a recessional, rather than a terminal, moraine, perhaps associated with the short slight warming during Greenland Interstadial 2 (GI2) at 23.3ka. It could be analogous to the so-called "Southern Irish End Moraine" (Figure 1). An LGM limit at 26ka on Gower was still shown as being c. 6km north of the Paviland Moraine by SCOURSE et al. (2021, Figs. 1 and 7) and in the final report of the BRITICE-CHRONO Project (CLARK et al., 2022, Fig. 6). These authors also showed an unlikely ice-free enclave over southern Pembrokeshire and the retreating southern limit of the icesheet as being well north of Gower by 24ka (Figure 1), but they did not discuss Gower and the Devensian age of the Paviland Moraine suggested by SHAKESBY et al. (2018). Strong evidence that LGM ice covered the whole of Pembrokeshire was subsequently provided by JOHN (2023). Unfortunately, any relevant sea-floor deposits south of Paviland are masked by modern sand deposits (KOKELAAR, 2021, p91), which were not cored by the BRITICE-CHRONO Project (Chris Clark, pers. comm., 2019). This author concludes that the local LGM probably covered all of Gower, but only for a few millennia, before Arthur's Stone was deglaciated at 23±2ka.

4. Deglacial speleogenesis, especially in the Llethryd Swallet–Tooth Cave system

The setting along the southern Gower coast, with some relict cave entrances and phreatic passages in implausibly high locations (lacking catchment areas), seems analogous to that at Giggleswick Scar in Yorkshire. There, MURPHY et al. (2015) deduced that the caves formed by phreatic dissolution when fractures in the Carboniferous limestone were flooded by the waters of a deglacial ice-dammed lake (IDL) for several hundred years, soon after local nunataks emerged above the icesheet as it downwasted. A similar process explains the speleogenesis of >1000 caves in central Scandinavia (FAULKNER, 2018, 2024). There, isostatic uplift caused by the reducing weight of ice produced or re-activated fractures in metalimestone, as appears also to be demonstrated by a c. 5cm neotectonic movement along a bedding plane in a relict passage in Ogof Ffynnon Wyntog (KOKELAAR, 2021, Fig. 74). Then, dilute unsaturated meltwater from lowering deglacial IDLs flowed through the fractures. This dissolved and eroded the marble walls mechanically at a total rate of c. 1mm per year for typically 1000 years, forming phreatic passages up to 2m in diameter during each deglaciation (FAULKNER, 2006). LiDAR was used by BLOMDIN et al. (2021) to identify >36,000 landforms associated with the evolution of high-level IDLs during deglaciation of the Weichselian Fenno-Scandinavian Ice Sheet in Jämtland in Sweden. This was confirmed by REGNELL et al. (2023), who also reported >4500 relict shorelines, deltas and meltwater channels in Jämtland, related to 30 deglacial IDLs. Their paper reviewed and supports the >100-year-old hypothesis (REGNELL et al., 2023) that deep extensive glacial lakes were dammed in Scandinavia during icesheet downwasting, and shows that their production is a typical deglacial process.

Deglacial speleogenesis that involved metalimestones in Scandinavia could equally affect sedimentary limestones, as deduced at Giggleswick Scar. Assuming that the whole Gower Peninsula was covered by ice during the Anglian glaciation and at the LGM, the same process would have applied there during both deglaciations. IDLs probably formed around the higher summits and ridges of Llanmadoc Hill, Rhossili Down and Cefn Bryn, and possibly merged as the ice surface down-wasted, but endured for only a few centuries (see below). That would explain the small sub-metre size of most Gower phreatic passages. The reports of clay in the Paviland till (KOKELAAR, 2021, p95) and in sediments on the south coast (SHAKESBY & HIEMSTRA, 2015) and of waterlain silt and/or clay in high banks in the Annex in Llethryd Swallet, in its Main Chamber and Mud Chamber (EDE & BULL, 1989) and in the Tooth Cave Main Stream Passage (KOKELAAR, 2021) suggest possible deposition below one or more deglacial IDLs. The near-vertical 1m-diameter "pothole" at Worms Head (Figure 2; KOKELAAR, 2021, Fig. 10a) appears to have cupulas, indicating formation by upward flow. It probably formed by deglacial meltwater from an IDL around Rhossili Down flowing upwards into a moulin in the ice, as at Gully Cave, Cave Ha 1 and Cave 1 at Giggleswick Scar (MURPHY et al., 2015). There is no suggestion that any caves on Gower were formed by slow hypogenic processes that also cause upward flow (as expected if the Gower catchments were 30km to the north). Ogof Wyntog probably formed during the Anglian deglaciation, before Patella-bearing gravels were deposited on thick older, but undated, speleothem in MIS5e (KOKELAAR, 2021, p118). Vadose entrenchments and its resurgence sump probably developed during the interglacials that succeeded MIS12.

An exceptional anomaly is the size of the relict Main Chamber in Llethryd Swallet, which is up to 30m high and 45m wide (COOPER, 2023). At rates that caused wall retreat of c. 1mm/year, that would require 15,000–22,500 years of phreatic dissolution and erosion to form. Unless Main Chamber was initiated earlier than the Anglian glaciation, it must have developed under mainly phreatic conditions during its deglaciation, later interglacials, and the LGM deglaciation. It lies above the vadose Lower Stream Passage, which is therefore younger, and probably formed after the LGM. Other evidence that most of the small phreatic cave development on Gower occurred during LGM deglaciation is derived from the small sizes of the speleothems. Most show no evidence of separate growth stages in interglacials or interstadials and are so small that they probably grew entirely during the Holocene. Only the larger speleothems in Llethryd Swallet Main Chamber, Ogof Wyntog and the substantial flowstone in Leather's Hole (KOKELAAR, 2021, Fig. 27) at Great Tor (Figure 2) must be older. Indeed, the only pre-Holocene speleothem age is 426,250±14,380 years, at Leather's Hole (KOKELAAR, 2021, p41). Additionally, the archaeological deposits on Gower are of MIS5e age or younger (DINNIS et al., 2013), and so require speleogenesis no earlier than the MIS6 deglaciation. Small inaccessible conduits at the lowest cave levels (KOKELAAR, 2021, p114) probably derive from relaxation fractures formed during post-LGM deglacial isostatic uplift that have had insufficient time and flow rates to grow larger in the Holocene.

In Tooth Cave, c. 12cm-long scallops on phreatic passage walls (KOKELAAR, 2021, Fig. 91c) indicate dissolution by aggressive water flowing at c. 33cm/s, if close to 0°C (CURL, 1966). However, fluvioglacial cobbles derived from >200-million-year-old Old Red Sandstone strata entered Tooth Cave catastrophically and scratched the walls of Main Stream Passage (KOKELAAR, 2021, p137). A Hjulström curve shows that such large cobbles are transported only at a speed >1.5m/s, probably during a jökulhlaup, as discussed below. The cobbles overlie 0.5m of horizontally-bedded fine sands and silts, previously deposited in tranquil water flowing at <2cm/s, which display extremely regular layers (KOKELAAR (2021, Fig. 90), suggesting that they are annual varves. The apparent scale of Kokelaar's image suggests that each lamination is c. 5mm thick, implying that the whole sediment bank was deposited in c. 100 years. It also has c. 15 regularly-spaced darker layers, which could indicate a 7-year cyclicity of unknown association.

5. The deglaciations of the Gower Peninsula

During the deglaciations of both the Anglian and the Devensian icesheets, the Cefn Bryn ridge became exposed as a nunatak during slow down-wasting, firstly at ≥188m asl. It is hypothesized here that a long narrow, initially static, ring of summer meltwater must have formed around it each time, as the bedrock warmed. These annular IDLs were dammed by the surrounding ice stream of the Anglian glaciation and by the Ilston Lobe at the LGM. If the post-LGM Gower deglaciation was triggered by the GI2 warming at 23.3ka, then this Cefn Bryn IDL formed c. 3.6ka before Glacial Lake Severn, which existed after 19.7±2.5 ka (CHIVERELL et al., 2021). Because the surfaces of deglacial IDLs lowered annually and had low initial flow rates with only small amounts of fine suspended sediments, they left little early or high-level depositional evidence, or such deposits can be confused with loess. During downwasting, the melting ice widened the IDLs as their local meteoric catchment areas, flow rates and transported sediment grain sizes all increased, whilst the water inundated fractures and any existing conduits in the limestone below. The IDLs likely kept roughly triangular cross-sections down to bedrock and, initially at least, remained full to the ice surface level, overflowing as supraglacial streams. There were no suitable outlet cols on Gower to stabilise IDL water levels temporarily, and hence no erosional or depositional terraces were formed. CLARK et al. (2022, Fig. 13) indicated that the rate of terrestrial glacial retreat from its maximum extent at the local LGM was 5–40m/year in the Gower area, with much higher rates at marine ice-margin contacts. If Cefn Bryn was exposed at c. 23ka, the temperature would have remained low and the mean rate at which each side of the post-LGM Cefn Bryn IDL widened by melting a near-vertical wall of ice is speculated to be c. 10m/year. If so, it took c. 230 years for the northern limb of the IDL to reach the Llethryd Swallet entrance, 2.3km north of Cefn Bryn (Figure 2). In Norway, LANE et al. (2020) calculated that the ice surface at Snøhetta lowered at a rate of 0.23–1.68m/year from the start of the Younger Dryas (YD) at 12.9ka to the early Holocene after 11.7ka. A mean lowering rate of 0.25m/year is assumed for Gower, in the cold conditions at 23ka. Hence, after 230 years, the surface of the Cefn Bryn IDL would have lowered by c. 58m from the eastern 188m asl summit of Cefn Bryn to c. 130m. This is c. 91m above both the Llethryd Swallet entrance and the now-blocked lower entrance into Tooth Cave.

When the post-LGM Cefn Bryn IDL reached Llethryd Swallet, it surrounded a 5.5km-long and 0.6km-wide island ridge, with a maximum depth >91m and a width of c. 2km each side of the island. Its total length was c. 12km (Figure 2), if records of "0.5–1.0m of massive sand-silt-clay sediment (Unit 6)" in Hunts Bay west and "an overlying Unit 6" in Hunts Bay east (SHAKESBY & HIEMSTRA, 2015, Table 11.1, pp104 and 108) relate to lacustrine deposits beneath the same IDL. Such an assumed elliptical IDL around a narrow Cefn Bryn island would have had a surface area of c. 40km2 and a possible volume >2km^3. Lower sub-horizontal 2–2.5m-thick 'red bed' sediments of yellowish- red sand-silt-clay comprise Unit 2 above the beach in Hunts Bay west and east coves (Figure 3; SHAKESBY & HIEMSTRA, 2015, Figs. 11.3 and 11.13). This suggests that they were deposited beneath a similar IDL that formed during the Anglian deglaciation. No clay deposit was reported at Rotherslade, 4.5km east of Hunts Bay, hinting that the Cefn Bryn IDLs did not extend that far. Units 2 and 6 were dated at 201.7±20.4ka and 15.0±0.9ka (SHAKESBY & HIEMSTRA, 2015, p114) by Optically Stimulated Luminesce (OSL). These ages seem compatible with burial after the Anglian and LGM deglaciations, although the Unit 2 age is difficult to reconcile with an MIS5e age for the lower Patella Beach. Although SHAKESBY & HIEMSTRA (2015, p116) interpreted the fine sediment in Unit 2 as predominantly a colluvial deposit produced by slopewash action re-working an Ipswichian terra rossa soil, there is no mention of organic materials in Unit 2. Thus, the term "soil" might refer to "soil-like" material, and if these sediments are abiotic, they could instead be IDL deposits.

Figure 3: *Apparent lacustrine 'red bed' sediments, including clay layers, of Unit 2 at Hunts Bay east cove, possibly deposited in a Cefn Bryn IDL during the Anglian deglaciation. Photo by the author in October 2015.*

Part of the growth of the Llethrid Swallet–Tooth Cave phreatic passages to their present sizes occurred when aggressive water from the Anglian and post-LGM Cefn Bryn IDLs flowed through the fractures and conduits. Related karst water exits were back into the lakes and then out into either a supraglacial stream or englacial conduits (MURPHY et al., 2015, Fig. 15). A frozen 'lid' would form on the post-LGM IDL each winter, so the flow that deposited red mud in Llethryd Swallet and laminated fine sands and silts in Tooth Cave reduced seasonally. The passages continued to enlarge by upward paragenetic dissolution by dilute, but aggressive, meltwater. If post-LGM IDL lowering continued at the same rate after reaching Llethryd Swallet, this allowed a maximum of 364 years for phreatic enlargement before the lake surface reached 39m asl and the system started to drain and revert partly to vadose conditions. OSL and 26Al/10Be dating of lacustrine sediments in Llethryd Swallet and Tooth Cave and at Horton and Hunts Bay and dating of underground cobbles should determine when they were last exposed to daylight and cosmic rays and whether they were deposited synchronously during one or both deglaciations. It is likely that Leather's Hole, 1km south of the Cefn Bryn ridge and high in the coastal cliffs at 35m asl, was initially formed beneath the Anglian deglacial IDL, as supported by its flowstone age. The "peculiar karstic dissolution of the limestone near the entrances" (KOKELAAR, 2021, Fig. 27 caption) suggests that Leather's Hole was submerged again by the post-LGM Cefn Bryn IDL. The deglacial karstic

dissolution and surface and underground sedimentation continued until the IDL pressure breached the thinning ice dam to the south. The resulting jökulhlaup drew some of the IDL water through Tooth Cave to deposit the cobbles on top of the laminated sediments and block the previous entrance. Despite the high water velocity, such a brief event had no effect on the size of the dissolutional wall scallops. This type of jökulhlaup was thus comparable with that proposed by MURPHY et al. (2015), which produced the gorge at Cave Ha 4 at Giggleswick Scar. Although the exact age of the post-LGM jökulhlaup remains uncertain, it must have occurred before the ice and IDL surfaces lowered to the blocked Tooth Cave entrance, i.e. after a maximum time of c. 600 years, if at a lowering rate of 0.25m/year.

Limestone diamicts forming Unit 3 in Hunts Bay east cove might partly comprise deposits by a similar Cefn Bryn IDL jökulhlaup during the Anglian deglaciation. The overlying limestone and glacigenic diamicts with glacial erratics in places in Units 4 and 5 (SHAKESBY & HIEMSTRA, 2015, Table 11.1) could result from later transport during the local LGM. These are overlain by Unit 6 sediments, assumed above to be deposits beneath a post-LGM Cefn Bryn IDL. In this case, as yet there appears to be no record of diamicts above Unit 6 at Hunts Bay, brought there by a post-LGM jökulhlaup. Diamicts at Horton, 8km west of Hunts Bay, overlie fine 'red bed' sediments with clay that appear similar to Unit 2 (SHAKESBY & HIEMSTRA, 2015, Fig. 10.2). Those sediments could also signify deposition beneath an Anglian deglacial IDL. Units 3, 4 and 5 angular diamicts elsewhere on the southern coast could also comprise jökulhlaup debris, rather than resulting from periglacial action or proglacial outwash on the rapidly eroding coastline (SHAKESBY & HIEMSTRA, 2015, pp116−119). Dry valleys on Gower were likely incised by summer streams in periglacial conditions when the ground was frozen (WALTHAM et al., 1997), probably during glacials and stadials with glaciers that terminated north of Gower. Several post-glacial Rock Slope Failures of limestone blocks occur on the west side of Pwlldu Bay (KOKELAAR, 2021). Some blocks contain phreatic tubes, of which some contain partial infills of laminated sediments, originally of Triassic age. The phreatic tubes probably formed beneath an Anglian deglacial IDL that contributed the sediments.

6. Conclusion

The KOKELAAR (2021) assertions, without dating evidence, of the long survival of pre-Quaternary caves, are disputed. Although caves probably did form then, they are by now "palaeo caves in the sky" (FAULKNER, 2013), having been removed by erosion. Caves on the southern coast have probably been truncated by cliff retreat and might demonstrate a hybrid development, where entrances of initial phreatic passages were enlarged by marine erosion, if coincident with sea level (FAULKNER, 2018). Instead, working from simple assumptions that the Anglian and Devensian LGM icesheets both covered Gower without leaving nunataks exposed, an alternative hypothesis is deduced: the phreatic passages were formed by deglacial speleogenesis, during the wastage of one or both of these glaciations. Dissolution enlarged karst fractures and conduits during deglaciation, when the land above was covered by flowing ice-dammed lakes, until their demise as the dams collapsed at jökulhlaups. High-level post-Anglian and post-LGM Cefn Bryn IDLs have not previously been interpreted from surface evidence. However, absence of evidence is not evidence of absence. Although this might be regarded as a novel hypothesis, to resolve many current questions and anomalies about karst speleogenesis in glaciated areas, it is necessary to 'think outside the box' and derive new approaches to find solutions. Such approaches include interpreting the significance of size, morphology, hydrology and contents of karst caves, where they fortunately still exist to provide museums containing archival evidence of previous landscape evolution (FAULKNER, 2013).

References

BLOMDIN R. & 6 others (2021) Beskrivning till geomorfologiska kartan. Jämtlands Län. Sveriges Geologiska Undersökning, K705, 57pp.

CHIVERELL R.C. & 12 others (2021) The evolution of the terrestrial-terminating Irish Sea glacier during the last glaciation. Journal of Quaternary Science 36(5):752-779.

CLARK C.D. & 37 others (2022) Growth and retreat of the last British−Irish Ice Sheet, 31000 to 15000 years ago: the BRITICE-CHRONO reconstruction. Boreas 51(4):699-758.

COOPER J.S. (Ed.) (2023) Exploring the Karst and Caves of the Gower Peninsula: A walking guide to Gower's Caves. British Cave Research Association, 86pp.

CURL R.L. (1966) Scallops and flutes. Transactions of the Cave Research Group of GB 7:121–160.

DINNIS R. & 7 others (2013) Archaeological excavations at caves in Bishopston Valley, Gower, South Wales, UK. Cave and Karst Science 40(1):17–21.

EDE D.P., BULL P.A. (1989) Swallets and caves of the Gower Peninsula. In: FORD T.D. Limestones and Caves of Wales. Cambridge University Press, 211-216.

FAULKNER T. (2006) Limestone dissolution in phreatic conditions at maximum rates and in pure, cold, water. Cave and Karst Science 33(1):11–20.

FAULKNER T. (2013) A methodology to estimate the age of caves in northern latitudes, using Toerfjellhola in Norway as an example. 16th International Speleological Congress Proc. Vol. 3:342-348.

FAULKNER T. (2018) The ages of the Scandinavian caves. Norsk Grotteblad (70):15-33.

FAULKNER T. (2024). Comment on "Ice-dammed lakes and deglaciation history of the Scandinavian ice sheet in central Jämtland, Sweden" by REGNELL et al. (2023). Quaternary Science Reviews 328, 108487.

FREEM A. (2021) The Llethrid saga. Descent (283):32-38.

HUNT C.O. (2006) An enigmatic gravel deposit on Bleadon Hill. In: HUNT C.O. & HASLETT S.K. Quaternary of Somerset Field Guide. Quaternary Research Association, 53-56.

JENKINS D.W., WILLIAMS A.M. (1963) Caves in Wales and the Marches. Dalesman, 80pp.

JOHN B.S. (2022) Holocene book review: Peter Kokelaar: All Our Own Water (2021). The Holocene 32(4):346-347.

JOHN B.S. (2023) Was there a Late Devensian ice-free corridor in Pembrokeshire? Quaternary Newsletter 158:4-15.

JOHN B. (2024). An igneous erratic at Limeslade, Gower, and the glaciation of the Bristol Channel. Quaternary Newsletter (162):4-14.

KOKELAAR P. (2021) All Our Own Water: Landscape Evolution, Caves and Hydrogeology of Gower. Published privately, 281pp.

LANE T.P. & 9 others. (2020) Elevation changes of the Fennoscandian Ice Sheet interior during the last deglaciation. Geophysical Research Letters 47(14) e2020GL088796.

MCCARROLL D., MCCARROLL B. (2015) Watch-house Bay and Foxhole Cove, Southgate. In: SHAKESBY R.A., Hiemstra J.F. (Eds.) The Quaternary of Gower: Field Guide. Quaternary Research Association, 120-130.

MURPHY P.J., FAULKNER T.L., LORD T.C., THORP J.A. (2015) The caves of Giggleswick Scar – examples of deglacial speleogenesis? Cave and Karst Science 42(1):42-53.

PHILLIPS F.M., BOWERN D.Q., ELMORE D. (1994) Surface exposure dating of glacial features in Great Britain using cosmogenic chlorine-36: preliminary results. Mineralogical Magazine 58A:722-723.

REGNELL C. & 10 others (2023) Ice-dammed lakes and deglaciation history of the Scandinavian Ice Sheet in central Jämtland, Sweden. Quaternary Science Reviews 314, 108219.

SCOURSE J.D. & 23 others (2021) Maximum extent and readvance dynamics of the Irish Sea Ice Stream and Irish Sea Glacier since the Last Glacial Maximum. Journal of Quaternary Science 36(5):780-804.

SHAKESBY R.A., HIEMSTRA J.F. (Eds.) (2015) The Quaternary of Gower: Field Guide. Quaternary Research Association, 145pp.

SHAKESBY R.A., HIEMSTRA J.F., KULESSA B., LUCKMAN A.J. (2018) Re-assessment of the age and depositional origin of the Paviland Moraine, Gower, south Wales, UK. Boreas 47(2):577-592.

WALTHAM A.C., SIMMS M.J., FARRANT A.R., GOLDIE H.S. (1997) Karst and caves of Great Britain. Geological Conservation Review 12. Chapman Hall, 358pp.

WALTHAM, T. (2021) Book Review: Peter Kokelaar: All Our Own Water (2021). Cave and Karst Science 46(3); p130.

Speleogenesis of the calcareous littoral caves on the Island of Lismore, Scotland

Trevor Faulkner

Grampian Speleological Group, trevor.marblecaves@gmail.com

Abstract

About 90 littoral caves and indentations are now known on the island of Lismore in Loch Linnhe in the Grampian Highlands of Scotland at altitudes up to 35m above sea level, mostly on the west coast. There are many wells and small sinks, springs and dolines inland, but no enterable karst caves. It is confirmed that the entrance floors of the great majority of the caves occur at the point where one of several inclined raised beaches or platforms meets the base of the next cliff inland. The association with present and previous sea levels suggests that the caves were mainly formed by marine abrasion, during a time when the beach was being produced by a stable sea level after Lismore was deglaciated at the start of the Lateglacial Interstadial. On the west coast, however, nine caves occur above the bases of the cliffs. These perhaps formed when isostasy caused sea level to rise or fall continuously. Other speleogenetic processes to consider include inception by phreatic karstic dissolution beneath glacial lakes during deglaciation, with possible later vadose entrenchment, and some caves being formed by Rock Slope Failures. The two longest caves and their speleothems could have formed before or during the MIS5e Interglacial. They were probably partly unroofed at the Last Glacial Maximum, to create calanques (unroofed caves) in front of their entrances that were then invaded temporarily by the sea.

1. Introduction

The 16km-long and 1.6km-wide weakly metamorphosed limestone island of Lismore is aligned in Loch Linnhe, a sea loch SW of Fort William in the Grampian Highlands of Scotland, UK (Figure 1), which lies between the Great Glen Fault (GGF) and the Firth of Lorn Fault. Lismore comprises mainly the >1km-thick Lismore Limestone Formation, which forms the longest tract of coastal limestone in northern Scotland. Reports of c. 155 sites with tufa and speleothem deposits on the island in June 2018 and June 2022 were provided by FAULKNER & CRAE (2018; 2022) and FAULKNER (2023a; 2025), following reports of speleothems in littoral cave entrances by GRAY & IVANOVICH (1988). These visits, one by CORBEL (1957) and others by the Grampian Speleological Group in 1974, 1983 and 2019 (TILLSON, 1974; SALVONA, 1983; CRAE, 2018, 2020), revealed many short littoral caves in the coastal cliffs, as tabulated by FAULKNER (2023b). This article summarises the cave sites, whilst making observations of relevance to local glaciation, sea level change, and speleogenesis. For an introduction to the calcareous geology, geomorphology, Quaternary glacial history, karst and hydrogeology of Lismore, and the types of tufa and speleothem found, see Faulkner and Crae (2018) and its references.

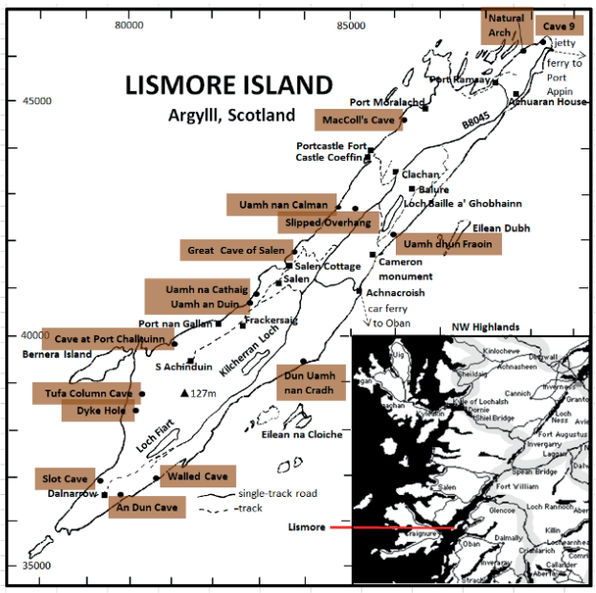

Figure 1: Larger littoral cave locations and some place names on Lismore Island.

2. The littoral caves on Lismore

Ridges and the lithological strike are aligned NE–SW along Lismore, parallel to the GGF. The low-grade greenschist facies metacarbonate was deformed during the Ordovician Grampian Orogeny. The surviving bedding is commonly near-vertical or contorted. The entire outcrop is intruded orthogonally by dense swarms of vertical igneous dykes of various ages and lithologies and up to 3m wide. These have created small ravines or protruding linear stacks, some being close to littoral caves and/or tufa deposits. CORBEL (1957: Figs. 60–62) reported marine lapiaz at the coasts.

Elsewhere in Scotland, littoral caves in metalimestones are rare, but 89 such indentations and caves (mainly single passages, only 30 being ≥3m long) are known above raised beaches and platforms on Lismore (FAULKNER, 2023b). Some contain large tufa-like speleothems in the daylight zone, which is also rare globally (FAULKNER, 2025). On the west and east coasts respectively, there are 71 and 18 caves, with lengths up to 36m and 10m and heights up to 10m and 5m. Because of their commonly short lengths, caves on Lismore are defined as “places where a dog can

shelter from rain that is falling vertically". Floor-level altitudes vary from below sea level (bsl) to 35m above sea level (asl) on the west coast and mainly from 10–20m asl on the east coast, although difficulty in easily measuring low altitude elevations (ROVERE et al., 2016) reduces these accuracies to ±5m asl. Plots of cave floor altitude against British National Grid north coordinate for the west and east coasts are shown in Figures 2 and 3. The absence of any inland karst caves is confirmed from visits described in the Introduction. However, there are 17 known inland karst hydrological features (wells, sinks, risings, seepages, intermittent stream flows and dolines). The longest allogenic underground stream courses are 300m and 200m long, with vertical ranges ≤15m. Many houses and farms extract abundant supplies of hard water from wells and boreholes ≤40m deep. No coastal resurgences are known, but some water probably resurges invisibly under the sea (CORBEL, 1957, p278). A similar west coast, east coast and inland decline occurs among the recorded caves and karst features (71, 18 and 17) as occurs for the numbers of tufa deposits (117, 26 and 12) recorded by FAULKNER (2023a). Both trends are probably more a function of climate and geomorphology than investigation bias. As illustrated in Figure 4, the great majority (47, where noted) of the cave entrance floors on the west coast, and all those on the east coast, coincide with a cliff base (CB), where it meets an inclined raised beach or platform at its inner margin (Figures 5, 6, 7, 8), as occurs elsewhere at Scottish coasts (GRAY, 1974a). They can therefore indicate late Quaternary sea levels (MYLROIE & CAREW, 1988). However, nine caves on the west coast occur in less accessible mid-cliff locations (M: Figures 5 and 9). No cave entrances on the island occur within the incline of a raised beach. The indentations do not resemble the coastal horizontal C-shaped notches in carbonate cliffs in Israel (SHTOBER-ZISU et al., (2015).

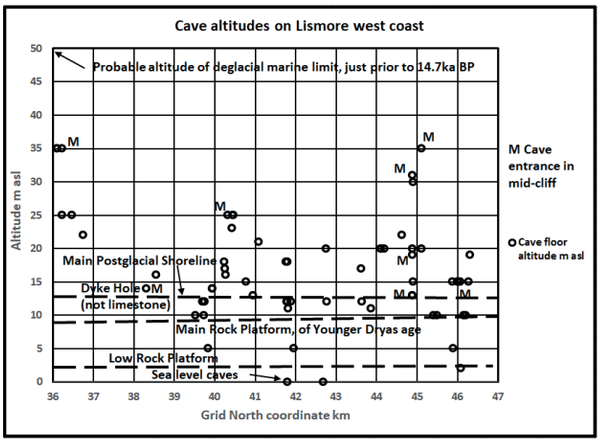

Figure 2: Cave floor altitudes on the west coast

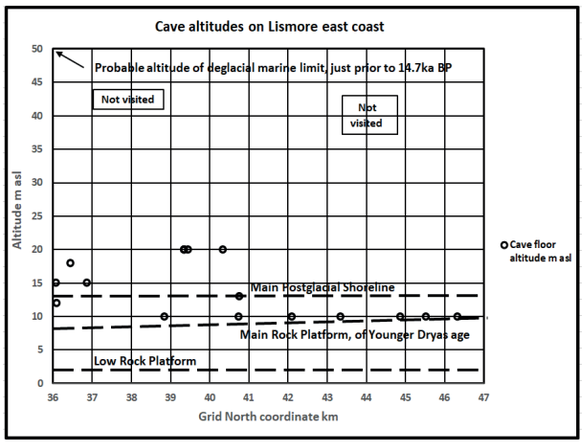

Figure 3: Cave floor altitudes on the east coast.

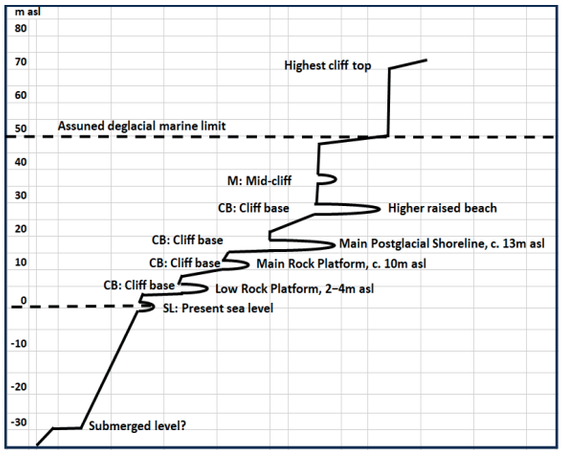

Figure 4: Diagrammatic locations of littoral caves on the Lismore west coast.

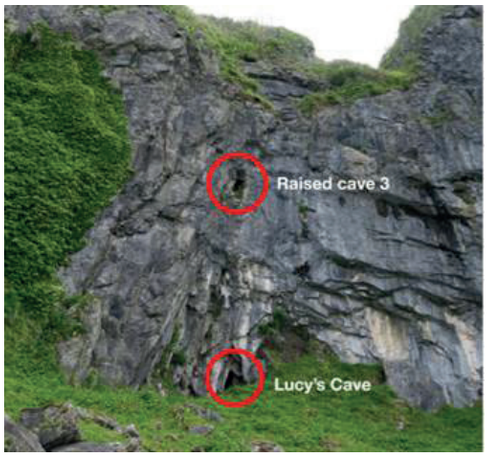

Figure 5: Caves at locations M (Raised Cave 3) and CB (Lucy's Cave). Photo by Noel Williams.

3. Speleogenesis and Lismore shorelines

At least six cave-forming processes might have acted individually or in concert at each cave during and after each major Quaternary deglaciation. These are: creation of inception fractures by tectonic movement during isostatic rebound; phreatic chemical dissolution beneath deglacial ice-dammed lakes or in subglacial waterways along Nye channels during deglaciation; marine abrasion, including of dykes (GRAY, 1974a); phreatic dissolution during interglacials; vadose dissolution and mechanical erosion during interglacials; and openings created by gravitational Rock Slope Failures (RSFs), which occurred throughout Scotland as valley sides re-adjusted to the removal of ice after the Last Glacial Maximum (LGM: 27–18ka). Dissolution deep below sea level after deglaciation is unlikely, because most sea water is saturated with calcium carbonate. However, dissolution in brackish water during deglaciation was possible. There are also tiny constructional 'caves' on Lismore, under banks of tufa 'speleothems' (FAULKNER, 2025).

The location of most Lismore caves at a platform inner margin

suggests formation mainly by marine abrasion, whilst relative sea level (RSL) remained constant. Caves orthogonal to the coast commonly have inward tapering walls, floors and ceilings. These caves lengthened along fractures and lines of weakness, some being beside dykes, faster than the rate of cliff retreat. Other littoral caves in non-karstic lithologies along the western Scottish coast, including Dyke Hole on Lismore itself (Figure 9), are uniform single passages through headlands. Similar passages through limestone headlands on Lismore, such as the Natural Arch (Figure 10), thus likely formed mainly by marine erosion. It was assumed by CORBEL (1957) that such arches and the cave in his Fig. 57 (probably the Little Cave of Salen: Figure 6 herein) were formed by underground water and enlarged by marine abrasion. Probably, the inland superficial endokarst flow systems developed mainly after deglaciation, assisted by open fracture creation during isostatic rebound. A postglacial 2-metre neotectonic movement in the centre of Lismore has created a long, wide, sharp Slipped Overhang (Figures 11 and 12), which would not have survived glacial erosion. About eight caves on the west coast have narrow vertical or inclined entrance profiles, such as Slot Cave (Figure 7) that might have formed partly as RSFs.

Figure 6: *Little Cave of Salen (W coast). Photo by Alan Marshall.*

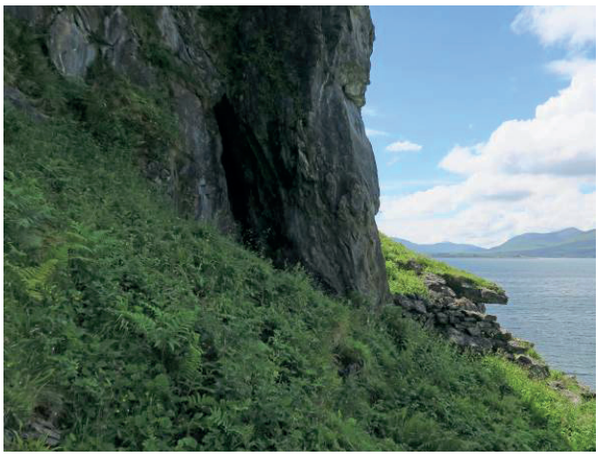

Figure 7: *Slot Cave on the west coast. Photo by Noel Williams.*

Figure 8: *An Dun Cave (E coast). Photo by Trevor Faulkner.*

Figure 9: *Dyke Hole on the west coast, formed at location M in an igneous dyke, not limestone. Photo by Alan Marshall.*

The glacial cycles and varying RSLs during the later part of the Quaternary determined the speleogenetic history of Lismore. These involved 3-way competitions among terrestrial ice cover, isostasy, and eustatic sea level during glaciations and deglaciations and during stadial–interstadial changes. Intact surface deposits from glaciations older than the LGM no longer exist, having been overridden by the Loch Linnhe ice stream. It deposited many far-travelled erratic granite boulders with diameters up to one metre, carved a limestone roche moutonée beside the primary road, and deepened depressions in the limestone that underlie the three lakes of Loch Balnagowan, Kilcheran Loch and Loch Fiart. There are few moraines, drumlins or till deposits, perhaps indicating some re-working by the sea. Being in a climatically sensitive location, western Scottish ice sheets waxed and waned in a complex manner as RSL fluctuated. Many confusing shoreline platforms of disputed ages were described, before dating became more reliable. This section discusses the relationships of caves to the platforms, starting at the lowest, as illustrated in Figures 2 and 3. The relationships of coastal features to palaeo RSLs can be difficult to interpret, but the level floor of a cave entrance commonly provides an RSL marker (ROVERE et al., 2016). The absence of broad entrances taller than 5m suggests that they enlarged at a time of falling sea level (FAULKNER, 2018).

3.1. Submerged level: 30m bsl

HALL & RASHID (1977) reported a submerged platform of unknown age, 30m bsl near Oban (Figure 1), which is less sharply defined than local raised beaches. It clearly formed when there was substantial global glaciation, whilst western Scotland was unglaciated. No submerged levels or caves are reported around Lismore, which awaits investigation by diving. Diving has revealed several deep *submerged* marine caves off the islands of St. Kilda and North Rona. There is also a broad platform 120m bsl of probably LGM age farther west in the Atlantic.

3.2. Present sea level

Although parts of both Lismore coasts have low cliffs up to the Low Rock Platform that descend into the sea, other parts have a wide beach. There are three known caves in the cliffs on the west coast and one on the east coast that are within the local tidal range of 1–4m (Figures 2 and 3). Probably more await discovery, by using canoes and kayaks.

Figure 10: *The Natural Arch on the west coast.*

Figure 11: *The Slipped Overhang, viewed from the north.*

Figure 12: *At the Slipped Overhang. Photos by Trevor Faulkner.*

3.3. Low Rock Platform (LRP): 2–4m asl

A wide level LRP at 2–4m asl in the Lismore area (GRAY, 1974a: Fig. 7; 1978: Fig. 3) might be comparable to the Norwegian strandflat (DAWSON, 1984). This suggests that it developed during many interglacials, with its present level partly set in the Ipswichian/Eemian Interglacial at MIS5e, when eustatic sea level was a few metres higher than in the Holocene. Three tiny caves lie near the edge of this platform on the west coast (Figure 2). They are backed by low cliffs ≤5m high, which probably formed in the Holocene, but none occur on the east coast at this level.

3.4. Main Rock Platform (MRP) of Younger Dryas (YD) age: 7–10m asl

GRAY (1974a: Figs. 7 and 9) levelled the altitudes of the MRP that forms an almost continuous raised beach along the coasts and islands of southern Loch Linnhe. GRAY & IVANOVICH (1988) reported that the MRP surrounds Lismore, where it is typically 20–100m wide, unglaciated without till, and commonly backed by steep cliffs 15m high. It rises from 7–10m asl along the island, towards the centre of Scottish isostatic uplift, 55km to the NE at Rannoch Moor. Following the LGM, Lismore was deglaciated before the start of the Lateglacial Windermere Interstadial at 14.7ka, but not re-glaciated during the YD (THORP, 1986), as also discussed by MATTHEWS et al. (2021) and DAWSON (2021). There are several littoral caves at the MRP level (Figures 2 and 3), some containing massive calcite deposits, some of which appear to be degraded by subsequent marine erosion when submerged below the Main Postglacial Shoreline (see below). GRAY & IVANOVICH (1988) used some samples to date the MRP by the U-series method. Most were contaminated with detrital thorium, yielding assumed Holocene ages. STONE et al. (1996) used the 16Cl exposure age of the bedrock to confirm that the MRP (and therefore the caves at that level) formed by marine abrasion during the severe periglacial conditions of the YD.

3.5. Main Postglacial Shoreline (MPGS): 13m asl

Following the uplift caused by the melting of the nearby YD ice cap, RSL then rose faster than uplift at low YD isobases in western Scotland. This caused a Holocene transgression that created the MPGS at 13m asl near Lismore at c. 7.4ka (GRAY, 1974b: Figs. 5 and 6). This is also the highest shoreline farther east, where reglaciated in the YD. This marine abrasion probably produced several tall towers of limestone and protruding dykes (Figure 9) above the MRP on the Lismore west coast, which could not have survived glacial over-riding, and many cave entrances near this level (Figures 2 and 3).

3.6. Higher shorelines: >13m asl

SISSONS & DAWSON (1981: Fig. 1) and DAWSON (1984: Fig. 3) levelled the altitudes of higher platforms and shorelines from 18–51m asl on the western Scottish coast. The tops of the highest cliffs on the west coast of southern Lismore reach c. 70m asl, above bases at c. 50m asl, but no known caves occur above 35m asl. A high Scottish post-LGM deglacial marine limit (dml) is 41m asl, at the 1m YD isobase, c. 40km to the west of Lismore (DAWSON (1984, p. 352), perhaps equivalent to an unrecognised dml of c. 50m asl at Lismore. Thus, platforms from 50–13m asl on Lismore probably formed during the Lateglacial Interstadial from 14.7–12.9ka, contemporary with the marine erosion of the many caves at higher cliff bases on the west coast (Figure 2) and several up to c. 20m asl on the east coast (Figure 3). The nine west coast mid-cliff caves perhaps formed whilst sea level rose or lowered continuously without a hiatus. If any platforms higher than 50m asl at the 10m YD isobase at

Lismore (or lower, at lower isobases farther west) exist, they must have formed prior to being eroded at the LGM. This could apply to cliff tops and cliff bases at 70 and 50m asl in southern Lismore. They perhaps formed during MIS5c and 5a, after stadial glaciations in MIS5d and 5b caused deep isostatic depressions, before other growing northern hemisphere icesheets caused eustatic sea levels to fall by greater amounts.

4. Discussion

Peaks on each side of Loch Linnhe reach c. 900m asl, suggesting up to 1000m of glacial erosion in the Quaternary, i.e. c. 20m per glacial cycle, so that the land probably rose by several metres by erosional isostasy after each deglaciation. Interglacial eustatic sea levels depended on the extent of remaining polar ice, which has varied by several metres of sea level equivalent. Thus, it seems unlikely that the present paleo sea level platforms on Lismore, or elsewhere in Scotland, would be at a similar altitude to any platform that formed prior to the LGM, except by chance.

GRAY & IVANOVICH (1988) reported that a tufa sample from a deep undercut at the north of the west coast of Lismore gave an apparently reliable but imprecise age of 103.3+28.4/-20.0 ka. That would indicate growth at some time from the MIS5e Interglacial (129–115ka) until after MIS5c (104–90ka) and a surprising survival during the subsequent LGM. The two longest caves are both on the west coast. Cave 9 (36m long and 19m asl) is at the north end. It contains a substantial vegetated stalagmite inside its entrance, which is at the head of a 10m-deep dry gorge leading to the sea. Uamh na Cathaig (20m long and 13m asl) is in the middle of the coast, with a large tufa column that splits the entrance into two parts. A 5m-deep dry gorge starts about 30m in front of the cave that also leads to the sea. (See FAULKNER & CRAE, 2018 for entrance photos). It seems possible that these two gorges represent cave passages that used to extend back to the existing caves. If so, they were later unroofed by glaciation and then submerged by the high RSL after deglaciation, to create narrow, steep-walled, calanques (unroofed caves submerged temporarily by the sea) as reported at two different unidentified coastal sites on Lismore (Corbel, 1957: Figs. 58 and 59). In this case, these two sites and perhaps the deep undercut (above) are examples of unroofed caves and calanques, which have rarely and nowhere else, been reported in Britain.

The longer palaeo Cave 9 and Uamh na Cathaig were perhaps formed originally by phreatic karstic dissolution during the MIS7 Interglacial, if they remained flooded by meteoric water below the level of their resurgences, with sinks farther inland to the east. Or perhaps they formed later, by dissolution during the MIS6 deglaciation, if subject to flows from submerging glacial lakes. Many windgaps cross the main NE–SW ridges on Lismore. These suggest that the western side of the island supported high-level ice-dammed lakes during the MIS2 deglaciation that collapsed at jökulhlaups and flowed out to the east through spillway cols, as the ice margin retreated eastwards, perhaps repeating a similar MIS6 deglacial process. The large speleothems themselves then probably grew in MIS5e in vadose conditions, part way along longer cave passages. The existing cave passages avoided being eroded away by the MIS6 glaciation (if formed at MIS7) and by the MIS5d–MIS2 glaciations, which would have removed some of the bedrock above them and created the two calanques. The speleothems survived marine abrasion during all the occasions when the caves were at or below sea level after final deglaciation at c. 14.7ka, perhaps by chance as the cliffs at their entrances were eroded back. They clearly avoided erosion when the MRP was cut below them in the YD.

MYLROIE & MYLROIE (2009) discussed a "Carbonate Island Karst Model" to explain the formation of flank margin karst caves by mixing-zone dissolution. This occurs when freshwater meets sea water to create a mixing chamber that is subsequently breached by surface erosion after uplift, where speleothems can form when in the vadose zone. This model seems unlikely to apply to the caves on Lismore, after considering methods to differentiate between flank margin caves and sea caves formed by marine erosion (WATERSTRAT et al., 2010).

5. Conclusions

The c. 90 littoral caves and indentations on the calcareous island of Lismore occur mainly where an inclined raised beach or platform meets the base of the next cliff inland. Most are on the western coast, ≤35m above sea level, rather than the east coast at ≤20m asl. Nine caves are located part way up a steep cliff, but only on the west coast. The smaller altitude range and numbers of caves and tufa deposits on the east coast probably reflect its location, even more sheltered from westerly winds. Thus, although perhaps initiated by karst dissolution along fractures, the caves commonly formed by marine abrasion after deglaciation at c. 14.7ka, synchronously with the raised beaches. The more-vertical caves on the western coast perhaps formed by Rock Slope Failure. Cave 9 and Uamh na Cathaig likely formed in MIS5e or earlier, but were partly eroded at the Last Glacial Maximum to create two calanques, or unroofed caves. These were submerged temporarily beneath the sea, and then became gorges in front of the present entrances.

With the much clearer understanding of Scottish deglaciation (Clark, et al., 2022), the ages and levels of the raised platforms need to be reconsidered. Dating of calcite from Lismore speleothem bases would provide minimum ages of speleogenesis. Accurate levelling of cave floor altitudes on Lismore and the western Scottish coast could also be important for Scottish Quaternary science. They would provide more evidence of palaeo deglacial relative sea levels and isostatic uplift, to confirm how the altitudes of the raised beaches increase towards the centre of glaciation at Rannoch Moor. Similarly, confirmations of the floor depths of submerged marine caves, by diving off the islands of St. Kilda and North Rona, could provide information about the extent of isostatic depression in the forebulge area beyond the hinge line. Combining these data would enable more accurate isobase maps to be constructed.

6. References

CLARK C.D. & 37 others (2022) Growth and retreat of the last British-Irish Ice Sheet, 31000 to 15000 years ago: the BRITICE-CHRONO reconstruction. Boreas 51(4):699-758.

CORBEL J. (1957) Autour du Ben Nevis. In: Les Karsts du Nord-ouest de l-Europe, Université de Lyon, 276-278.

CRAE J. (2018) Lismore – an investigation. Grampian Speleological Group Bulletin 2(5):47-53.

CRAE J. (2020) Lismore 2019. Grampian Speleological Group Bulletin 3(3):26-32.

DAWSON A.G. (1984) Quaternary sea-level changes in western Scotland. Quaternary Science Reviews 3:345-368.

DAWSON A. (2021) The Main Rock Platform in Western Scotland. In: PALMER et al. The Quaternary of the West Grampian Highlands: Field Guide. Quaternary Research Association, 33-40.

FAULKNER T. (2018) The ages of the Scandinavian caves. Norsk Grotteblad 70:15-33.

FAULKNER T. (2023a) Additional tufa sites on Lismore island, Argyll, Scotland. Cave and Karst Science 50(2):55-62.

FAULKNER T. (2023b) More cave hunting on Lismore. Grampian Speleological Group Bulletin 4(4):38-47.

FAULKNER T. (2025) More exotic tufa deposits on the island of Lismore, Argyll, Scotland. Submitted to the 19th ICS.

FAULKNER T., CRAE J. (2018) Distribution of tufa and speleothem deposits on the island of Lismore, Argyll, Scotland. Cave and Karst Science 45(3):101-110.

FAULKNER T., CRAE J. (2022) Exotic tufa and speleothem deposits on the island of Lismore, Argyll, Scotland. 18th International Speleological Cong. Proc. Vol. 5:55-58.

GRAY J.M. (1974a) The main rock platform of the Firth of Lorn, western Scotland. Transactions of the British Institute of Geographers 61:81-99.

GRAY J.M. (1974b) Lateglacial and postglacial shorelines in western Scotland. Boreas 3(4):129-138.

GRAY J.M. (1978) Low-level shore platforms in the south-west Scottish Highlands: altitude, age and correlation. Trans. of the British Institute of Geographers NS 3:151-164.

GRAY J.M., IVANOVICH M. (1988). Age of the main rock platform, western Scotland. Palaeogeography, Palaeoclimatology, Palaeoecology 68:337-345.

HALL J., RASHID B.M. (1977) A possible submerged wave-cut platform in the Firth of Lorne. Scottish Journal of Geology 13(4):285-288.

MATTHEWS I.P., PALMER A.P., LOWE J.J. (2021) Proposed ice limits and the deglaciation of Loch Linnhe and the Firth of Lorne. In: PALMER et al. The Quaternary of the West Grampian Highlands: Field Guide. Quaternary Research Association, 41-49.

MYLROIE J.E., CAREW J.L. (1988) Solution conduits as indicators of late Quaternary sea level position. Quaternary Science Reviews 7:55-64.

MYLROIE J.E., MYLROIE J.R. (2009) Caves as sea level and uplift indicators, Kangaroo Island, South Australia. Journal of Cave and Karst Studies 71(1):32-47.

ROVERE A.W. & 9 others. (2016) The analysis of Last Interglacial MIS5e) relative sea-level indicators: Reconstructing sea-level in a warmer world. Earth-Science Reviews 159:404-427.

SALVONA J. (1983) Diary of an itinerant Scottish caver. Grampian Speleological Group Bulletin 4(2):28-30.

SHTOBER-ZISU N., AMASHA H., FRUMKIN A. (2015) Inland notches: implications for subaerial formation of karstic landforms – An example from the carbonate slopes of Mt. Carmel, Israel. Geomorphology 229:45-59.

SISSONS J.B., DAWSON A.G. (1981) Former sea-levels and ice limits in part of Wester Ross, northwest Scotland. Proceedings of the Geologists' Association 92(2):115-124.

STONE J., LAMBECK K., FIFIELD L.K., EVANS J.M., CRESSWELL R.G. (1996) A Lateglacial age for the Main Rock Platform, western Scotland. Geology 24(8):707-710.

TILLSON J. (1974) A visit to Lismore Island. Grampian Speleological Group Bulletin 1(1): p. 37.

THORP P.W. (1986) The mountain icefield of Loch Lomond Stadial age, W Grampians, Scotland. Boreas 15: 83-97.

WATERSTRAT W.J., MYLROIE J.E., OWEN A.M., MYLROIE J.R. (2010) Coastal caves in Bahamian eolian calcarenites: Differentiating between sea caves and flank margin caves. Cave and Karst Studies 72(2):61-74.

Piping e dolinas na gênese da Caverna do Pinheiro Torto, Passo Fundo/RS: processos geomorfológicos e implicações

Luis Paulo Fragomeni (1), Vagner Perondi (2), Juliana Soares (3) Cristiane Voltolini (4), Ismael Voltolini (5), Maricélio de Medeiros Guimarães (6) Marcus Paulo Alves Oliveira (7)

(1) geólogo, Universidade de Passo Fundo e Fundação Casa de Cultura de Marabá,lpfragomeni@gmail.com
(2) arquiteto, Universidade de Passo Fundo e Fundação Casa de Cultura de Marabá,cumeprojetoeconstrucao@gmail.com
(3) arqueóloga, cume.arqueologia@gmail.com
(4) bióloga, crisguep@yahoo.com.br
(5) médico, cem_voltis@yahoo.com.br
(6) biólogo, Fundação Casa da Cultura de Marabá, trilhas.virtuais@gmail.com
(7) biólogo, BioEspeleo Consultoria Ambiental,marcus@bioespeleo.com.br

Resumo

O presente trabalho apresenta características de uma cavidade em Passo Fundo/RS, cujo registro no ICMBio/Cecav indica tratar-se de uma paleotoca. Dados coletados em campo, avaliação do entorno e consulta à bibliografia indicaram que a cavidade pode ter sua gênese vinculada com processos de erosão subterrânea denominados de piping, não se tratando propriamente de um icnofóssil. O embasamento da região está associado aos arenitos da Formação Tupanciretã, cujo solo arenoso é suscetível à erosão possibilitando a ocorrência de tais fenômenos.

Abstract

The present paper presents characteristics of a cavity in Passo Fundo/RS, registered with ICMBio/Cecav as a paleoburrow. Field data, environmental evaluation and literature review indicated that the cavity's genesis might be linked to underground erosion processes known as piping, rather than being a true ichnofossil. The region's bedrock is associated to sandstones from the Tupanciretã Formation, whose sandy soil is susceptible to erosion, allowing for the occurrence of such phenomena.

1. Introdução

A Caverna do Pinheiro Torto é uma cavidade natural que ocorre na área do Parque Natural Municipal do Pinheiro Torto - PNMPT, em zona urbana de Passo Fundo, RS. O PNMPT é uma Unidade de Conservação (UC) criada pelo Decreto Municipal 43/2011, com área de 31,88 ha inserida em zona urbana de Passo Fundo. O gestor do Parque Natural Municipal do Pinheiro Torto é a Secretaria do Meio Ambiente da Prefeitura Municipal de Passo Fundo. O Parque Natural Municipal do Pinheiro Torto tem o objetivo de preservar os ambientes naturais ali existentes, realizar pesquisas, atividades de educação e recreação em contato com a natureza. O Plano de Manejo foi aprovado no ano 2016. O Quadro 1 apresenta a Ficha Técnica da Unidade de Conservação Municipal (BUDKE et alii, 2016). Neste artigo, apresentamos discussão sobre a gênese da cavidade considerando dados observados em recente visita técnica de campo realizada em agosto de 2024.

Figure 1: *Location of the Parque do Pinheiro Torto in southern Brazil.*

Nome da Unidade: **Parque Natural Municipal do Pinheiro Torto** Gerência Executiva, endereço: **Secretaria Municipal de Meio Ambiente – SMAM. Rua Uruguai, Nº 760, Centro – Passo Fundo, RS – CEP: 99010-110** Telefone para contato: **(54) 3312-9201** Endereço Eletrônico: **smam@pmpf.rs.gov.br; cmma@pmpf.rs.gov.br** Unidade Gestora Responsável: **Divisão de Licenciamento e Fiscalização Ambiental**		
Endereço da sede (SMAM)		**Rua Uruguai, Nº 760, Centro – Passo Fundo, RS**
Telefone		**(54) 3312-9201**
E-mail		**smam@pmpf.rs.gov.br**
Site		**http://www.passofundo.rs.gov.br/secretaria.php?c=467**
Superfície da Área (ha)		**31,88 ha**
Perímetro da área (km)		**3,6 km**
Superfície da ZA (ha)		**389**
Perímetro da ZA (km)		**9,73 km**
Município que abrange e percentual abrangido pela Área		**Passo Fundo – 0,0049%**
Estado que abrange		**Rio Grande do Sul**
Coordenadas geográficas (latitude e longitude)		**28°14'7.84"S; 52°27'14.21"O (Sede da Unidade)**
Data de criação e número do Decreto		**Decreto Nº 43 de 15/04/2011**
Marcos geográficos referenciais dos limites		**Decreto Nº 43 de 15/04/2011**
Biomas e ecossistemas		**Bioma: Mata Atlântica** **Ecossistemas: Floresta Ombrófila Mista**
Atividades ocorrentes	**Uso Indireto**	**Conservação Biodiversidade**
		Pesquisa Científica
		Educação Ambiental, Lazer e Recreação

Figure 2: *Unit Datasheet.*

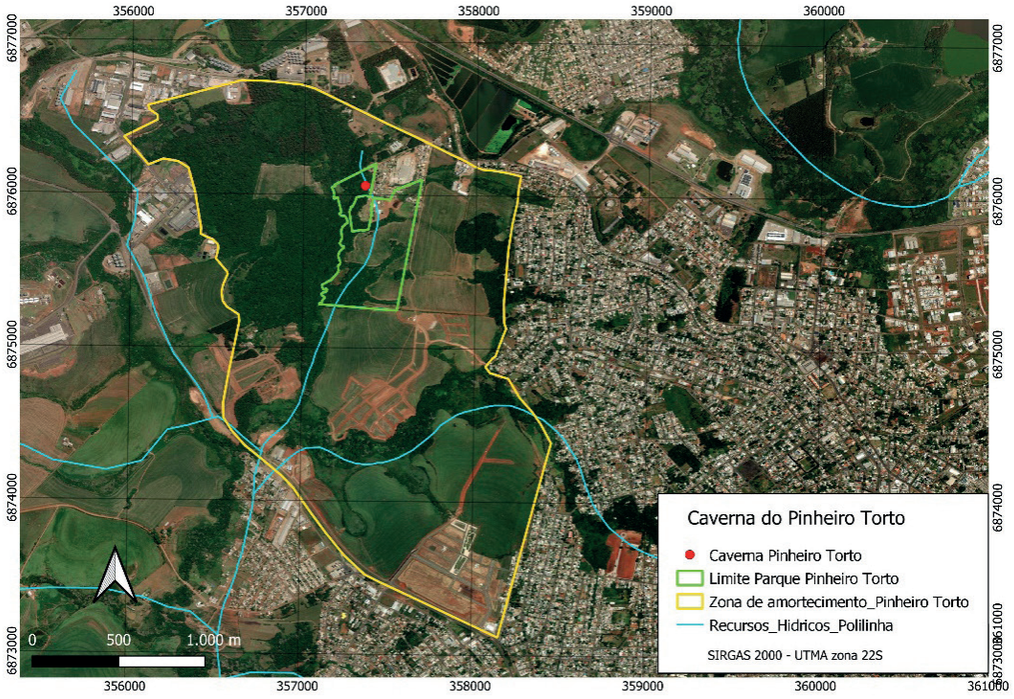

Figure 3: *Location of the Caverna do Pinheiro Torto, area of the conservation unit (park), buffer zone and water resources present in the area.*

2. Discussão

Discussões sobre a gênese da cavidade

Embora a Caverna do Pinheiro Torto esteja registrada no Cadastro Nacional de Informações Espeleológicas - CANIE/CECAV como paleotoca, com o número 019688.00001.43.14100, apontamos que algumas de suas características não suportam esta classificação, sendo que que sua gênese está vinculada a processos de erosão subterrânea denominados de piping. A caverna soma 17,00 m de comprimento acessível, com formato retilíneo e altura que pode chegar a três metros, e mais um desenvolvimento não medido formado por duto de pequeno diâmetro e formato irregular, que não permite o acesso.

Não são conhecidas cavernas na região de Passo Fundo e nas áreas dos municípios do entorno, o que justifica a sua classificação como de isolamento geográfico. Mesmo sendo globalmente conhecidos processos de piping em vários tipos de solos e variados ambientes climáticos,

existe pouca informação disponível sobre erosão subterrânea (BERNATEK-JAKIEL et alii, 2018), o que torna esta ocorrência rara. De acordo com o regramento expresso no Decreto da Presidência da República nº 6.640/2008, a Caverna do Pinheiro Torto é classificada com o grau de relevância Máximo, em função de ser uma ocorrência única/rara e por seu isolamento geográfico.

A Caverna do Pinheiro Torto está registrada no CANIE/CECAV como uma paleotoca porque os seus primeiros 17 metros de comprimento realmente se assemelham a uma escavação executada por animais da megafauna extinta, sendo que seu desenvolvimento neste trecho é de formato retilíneo, ovalado, com média de 2 m de largura e 3 m de altura. A continuidade da caverna a partir deste trecho inicial, se mostra bem diferente e remete à ocorrência de processos erosivos. Paleotocas são escavações na forma de túneis produzidas por vertebrados extintos para habitação, refúgio ou estivação, constituindo um registro indireto da presença de grupos taxonômicos onde fósseis corpóreos são inexistentes (RUCHKYS et alii, 2014). Uma paleotoca se constitui de um grande icnofóssil e a descrição dos traços fósseis que se encontram em seu interior ajudam a identificar o agente escavador. Os icnofósseis são produzidos em sedimento ainda inconsolidado e em diversos tipos de rocha (como siltitos, arenitos e basaltos alterados) e permitem que sejam feitas algumas inferências sobre a morfologia do animal bem como sobre o seu modo de vida (SCHNEIDER et alii, 2014).

A Caverna do Pinheiro Torto apresenta em seus metros iniciais o aspecto de uma paleotoca, mas apresenta, em sua continuidade, feições que são indicativas de um processo dinâmico de *piping*, com desenvolvimento formado por um duto com formato irregular e quebras bruscas de direção, com menos de 0,50 m de largura e 2,00 de altura, em solo hidromórfico da Formação Tupanciretã. Há um curso de água que corre no seu piso e que é responsável pelo processo de exumação dinâmica que ocorre atualmente, aprofundando o nível de base. Observa-se vários locais da caverna com sinais de abatimento do teto e, no terreno do entorno, algumas dolinas vinculadas a processos semelhantes e não necessariamente associadas a ela. A ocorrência de alguns dutos pequenos em conexão com o duto principal da caverna, com extensão variando de poucos centímetros a mais de dois metros de comprimento, de desenvolvimento irregular e quebras bruscas de direção, são evidências de processos de erosão subterrânea.

O embasamento rochoso no local onde está localizada a Caverna do Pinheiro Torto é classificado como de arenitos da Formação Tupanciretã. Embora não haja afloramento rochoso no interior da caverna, no entorno são encontrados afloramentos no fundo de drenagens e cortes de terreno. Os sedimentos da Formação Tupanciretã encontram-se discordantemente assentes sobre as efusivas da Formação Serra Geral. O pacote litológico que constitui essa formação é composto por arenitos conglomeráticos, conglomerados basais e finas camadas de argilas, sendo que a litologia predominante é representada pelos arenitos. São, geralmente, de cor avermelhada, às vezes amarelo-esverdeados, com granulação variável de fina a média, mal classificados, eventualmente conglomeráticos e constituídos essencialmente de quartzo e, subordinadamente, feldspato alterado a caulinita. Apresentam-se, de modo geral, muito friáveis e, às vezes, endurecidos por silicificação epigênica, sendo o cimento mais comum o óxido de ferro. São geralmente maciços, podendo, entretanto, exibir estratificação plano-paralela e cruzada do tipo fluvial. É de ocorrência restrita ao estado do Rio Grande do Sul, embora correlacionável à Formação Bauru em São Paulo.

Constatou-se que os maiores problemas de erosão acelerada, tanto em expressão como em extensão, encontrados na Unidade Geomorfológica Planalto de Santo Ângelo – onde se insere a região da Caverna do Pinheiro Torto, estão associadas aos arenitos da Formação Tupanciretã, cuja alteração resulta em solo arenoso, mais suscetível à erosão. Verificou-se, generalizadamente, a ocorrência de sulcos, ravinas e voçorocas nas vertentes suaves das colinas, por vezes transpondo-as. Geralmente desenvolvem-se próximo aos canais fluviais, sendo que alguns até já se interligam com a rede de drenagem organizada, dando origem a novos braços fluviais, procedendo a ampliação dela. Os fenômenos de erosão acelerada nos arenitos da Formação Tupanciretã são por vezes tão violentos que chegam a desenvolver imensas voçorocas, com a abertura de extensos e profundos anfiteatros de erosão, em meio a áreas de campo com criação de gado. Essa ocorrência de intensos problemas de erosão acelerada não tem termo de comparação com nenhuma das outras unidades geomorfológicas mapeadas no estado do Rio Grande do Sul (IBGE, 1986).

CULSHAW et alii, 2005, expressam que, embora a vasta maioria dos processos erosivos tipo pipes e dolinas sejam encontrados em rochas solúveis, tais como calcários, dolomitos e gipsitas, estas feições podem ocorrer em outros tipos de rochas. Além dos tubos de lava em basaltos, paisagens que lembram dolinas em seus processos e morfologia tem sido descritos em arenitos e siltitos, onde a drenagem passa por condutos vazios ou pipes. Estas feições de pseudokarst diferem daquelas do karst verdadeiro e são formadas por outros processos que não envolvem dissolução. Estruturas tipo pipes em rochas inconsolidadas, alteradas ou pobremente consolidadas, são amplamente distribuídas e desenvolvem uma forma de pseudokarst onde as dolinas que se formam sobre cavidades de solo instáveis podem constituir perigo significativo. A feição mais comum é a de lavagem das partículas finas de solos granulares em um processo que aumenta em escala progressivamente, e materiais mais grosseiros são retirados até que a cavidade do pipe é formada. Eles se estendem formando a partir do exutório, em locais onde os gradientes hidráulicos têm declividade suficiente para iniciar o fluxo em solos inconsolidados, e apenas alcançam tamanhos significativos quase que exclusivamente em ambientes de clima semiárido. Em qualquer tipo de solo em que ocorrem pipes, existe a possibilidade de colapso de solo em sistemas de pipes não visualizados. Os arcos de solo formados são tão frágeis que é esperado colapsem naturalmente com a continuidade do processo erosivo. Novos pipes e dolinas podem ser formados durante um único evento de tempestade. Desta forma, para prevenir o aumento do processo erosivo, é essencial controlar as águas de superfície e assegurar que as águas pluviais não infiltrem nestes locais.

Sítios arqueológicos x dolinas

Na região do Planalto Sul-brasileiro é comum a ocorrência de sítios arqueológicos identificados como casas subterrâneas, que se tratam de escavações no solo em formato circular que compunham parte da moradia das populações indígenas Proto-Jê Meridionais no período aproximado de 1.800 anos A.P., até a chegada do colonizador europeu (Copé, 2015). Tais registros arquitetônicos assemelham-se à fenômenos de dolina, onde ocorre o abatimento do solo, seja por eventos lentos de ação da água ou por fenômenos de colapso. Aproximadamente a 35 m da Caverna do Pinheiro Torto encontram-se 03 estruturas circulares que remetem a casas subterrâneas, mas, no entanto, trata-se de dolinas das quais emerge água e que, possivelmente, ligam-se por meio de canais com a cavidade em estudo.

Figure 4: *1. Surge, 2.4. Irregular duct, 3. Depositional processes of the Tupanciretã*

3. Conclusão

Existe uma percepção, disseminada por vários setores da população de Passo Fundo, de que as dolinas que ocorrem no Parque Natural Municipal do Pinheiro Torto são "buracos de índios", ou seja, vestígios de casas subterrâneas e, portanto, sítios arqueológicos. No ano de 2003 uma indústria (Cervejaria Colônia) foi impedida de se instalar no local para não haver interferência nos sítios arqueológicos. Embora atualmente os setores da sociedade mais esclarecidos e o Poder Público já tenham a informação técnica de que não se trata de casas subterrâneas, não são raros os comentários sobre a ocorrência de sítios arqueológicos naquela região.

Os solos da Formação Tupanciretã, naturalmente friáveis, a presença de solo hidromórfico na Caverna do Pinheiro Torto ocorrência de ambiente pedogenético saturado de água), e a irregularidade dos condutos indicam que este local não foi construído por animais escavadores da megafauna para instalar sua habitação.

A forma irregular dos condutos que ocorrem para além dos metros iniciais a partir de sua boca, a presença de solos

hidromórficos em embasamento rochoso da Formação Tupanciretã, a ocorrência de dolinas nas proximidades e a revisão de literatura que apresenta diversas situações de erosão subterrânea em variados tipos de solos, convergem para a indicação de que a gênese da Caverna do Pinheiro Torto está ligada a mecanismos de piping.

Em observância ao Decreto da Presidência da República nº 6.640/2008, que dispõe sobre a proteção das cavidades naturais, a Caverna do Pinheiro Torto é classificada com o grau de relevância Máximo, em função de ser uma ocorrência única/rara e por seu isolamento geográfico.

Figure 5: *Conduit inspection; sinkholes.*

Figure 6: *1. External area close to the mouth; 1. Topographic mapping; 3. spalling caused by roots; 4. garbage carried by water. 5.Irregular duct.*

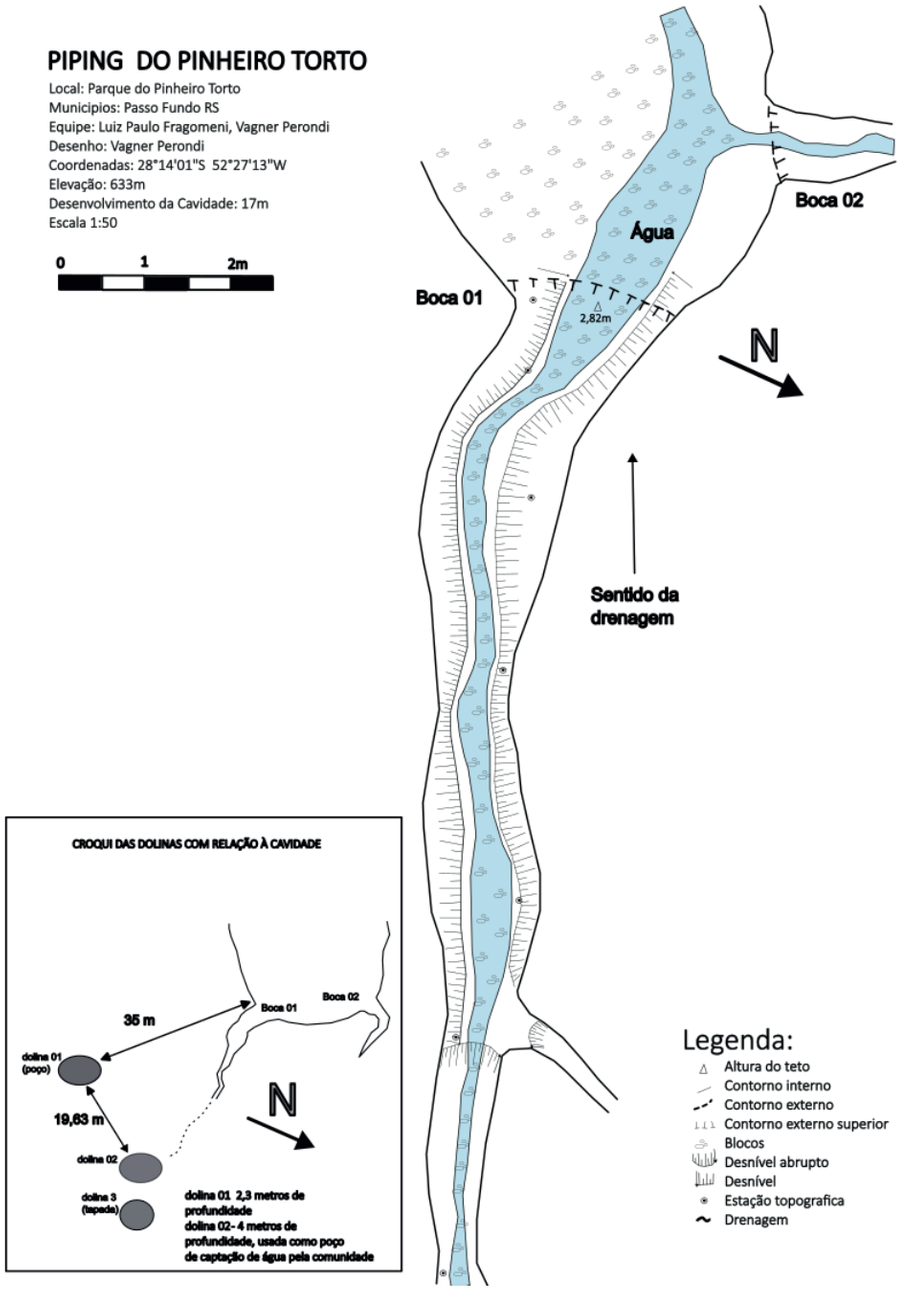

Figure 7: piping topography

Referências

BERNATEK-JAKIEL, A., POESEN, J. (2018) Subsurface erosion by soil piping: significance and research needs. Earth-Science Reviews 185, 1107-1128.

BUDKE, J.C. (2016) Plano de Manejo – Parque Natural Municipal do Pinheiro Torto. Passo Fundo.

COPÉ, S. M. (2015) A gênese das paisagens culturais do planalto sul-brasileiro. Estudos Avançados 29 (83).

IBGE – FUNDAÇÃO INSTITUTO BRASILEIRO DE GEOGRAFIA E ESTATÍSTICA. (1986) Levantamento de Recursos Naturais, v. 33.

SCHNEIDER, B. C., CORREA, R. C., PINTO, M., URBAN, C., ADAMI_RODRIGUES, K. (2014) Icnofósseis (Paleotoca) atribuídos à fauna pleistocênica na região de Pelotas, Monte Bonito, RS, Brasil. XXIII Congresso de Iniciação Científica da Universidade Federal de Pelotas.

RUCHKYS, Ú. de A., BITTENCOURT, J. de S., BUCHMANN, F. S. de C.. A Paleotoca da Serra do Gandarela e seu potencial como geossítio do Geoparque Quadrilátero Ferrífero, Minas Gerais. Caderno de Geografia, v2.

Newly discovered caver under Zadar Airport

Davor Garašić (1,2) & Mladen Garašić (2,3)

(1) Faculty of Civil Engineering, University of Zagreb, dgarasic@grad.hr
(2) The Society for the Research, Surveying and Filming of Karst Phenomena Zagreb, Croatia (corresponding author)
(3) Karst Committee, Croatian Academy of Science and Arts, Zagreb, mgarasic@grad.hr

Abstract

During the works for the extension of the tarmac at Zadar Airport, two caverns were discovered. Since this is a karst area, it was important to conduct speleological research of these caves. The goal of the research was to determine the hydrogeological function and other geological factors that could affect the stability of the aforementioned tarmac. Since the caverns were discovered just 2 months before the deadline for completion of the works, it was extremely important to conduct the research quickly and thoroughly. After the speleological research, the best solutions for remediation of these caves were proposed and accepted and the construction works were completed on time.

1. Introduction

At the end of 2023, Zadar Airport started the reconstruction, which in the next six years will completely change the airport in Zemunik as we know it today. A new passenger terminal building, an expanded tarmac, and a runway will be rebuilt in several stages. During the excavation works for the extension of the tarmac, two relatively small vertical caverns were discovered and immediately explored by speleologists and geologists. These narrow vertical shafts transition into horizontal channels and extend northeast. Detailed engineering-geological survey of the caverns suggests that they were developed along a set of faults or a fault zone in karstified Eocene limestones (MAJCEN et al. 1973). There is no constant water flow in these caves. It depends highly on the climate on the terrain surface. In most cases, water seeps into the underground through joints and faults. The depth of the weathering zone in these caves is estimated at 100 to 200 meters, which spreads well under the sea level. The zone of vertical circulation varies from 40 to 60 metres. Horizontal circulation brings fresh water to the submarine springs (Vruljas) in the Adriatic Sea. The explored caves showed signs of gravitational karstification and in their lower parts also the traces of regressive karstification i.e. aggressive weathering towards the surface (GARAŠIĆ, 1989, 1991, 1995). Since the foraminiferal Eocene limestones are, in a hydrogeological sense, water permeable due to their intense secondary porosity, it is expected that in the continuation of this fault zone several other similar caves might appear.

2. Materials and methods

Detailed speleological, engineering geological, and hydrogeological survey of caves found under Zadar airport was conducted by the team of experts in February 2024. The research aimed to establish the engineering geological and hydrogeological functions of caves that extend under the Zadar Airport tarmac for their remediation. Since these are vertical caves, it was necessary to use the caving equipment and techniques intended for such exploration; ropes, descenders, and ascenders (Fig 1.). The research was carried out in the late winter period, during windy days (Bura wind) when air temperatures on the surface spanned between +8°C to +15°C, while in the deeper parts of the cavern, between 9.3°C and 9.5°C. A weak airflow was measured using the digital anemometer. It should be mentioned that before the beginning of construction work at the Zadar Airport, there were no known caves in this area.

Figure 1: *Entrance to the northern cave at Zadar Airport*

Detailed engineering-geological maps of both newly discovered caves were created, which served as the basis for finding the best rehabilitation solution. The entrances to the caves K-1 (northern cavern) and K-2 (southern cavern) were opened during the excavation of the terrain to the projected level (Fig 2). Cavern K-1 was discovered on February

1, 2024, and cavern K-2 on February 3, 2024. Back then, the entrances were small and narrow. The entrance to cavern K-1 was 0.3 x 0.5 m, and to cavern K-2 0.3 x 0.3 m. They were later expanded for research purposes on February 14, 2024. The entrance to the speleological object K-1 (northern cavern) has an irregular, elliptical shape, with two vertical pit channels that connect after 1.30 meters. It is noticeable that the covering rock that separated the surface of the former terrain from the cavern in the area of today's entrance was no more than 1.5 meters thick. To descend into the interior of the cave, the northern entrance to the K-1 cavern was used because it was slightly larger than the southern entrance. It should be emphasized that both entrances to the K-1 cavern were extremely unstable and narrow at the time of the survey, and that at the time of the survey, constant attention had to be paid to this for the safety of speleologists. Since the rocks of the entrance parts of the caverns were intensively fractured and cracked due to intensive karstification processes and works on the tarmac construction site, it was not possible to anchor the rope with wedges in the nearby primary rocks. Therefore, during the described speleological research, anchoring was done by tying to heavy construction machines. In order to be able to meet the deadlines for the construction of the new tarmac, the time allotted for speleological exploration work was reduced to a minimum.

Figure 2: *Entrance to the southern cave at Zadar Airport*

3. Results

The rocks in which the cavern was formed belong to the contact area near the axis of the north-western wing of the sinkhole, in the bottom of which there are Eocene foraminiferal limestones ($E_{1,2}$), which are deposited discordantly on the Upper Cretaceous Senonian limestones (K_2^3). They are characterized by a white to grey-white colour. Deposits of Fomaminiferous limestones of Eocene age in the area of the Zadar Airport terminal are in transgressive contact with Senonian Cretaceous limestones that form the deeper bottom of the syncline. Their thickness can be up to 200 meters. These are miliolid, nummulitic and alveolitic limestones, which geologically later, in other nearby localities, gradually transition into Middle Eocene clastites. Structurally, foraminiferal limestones ($E_{1,2}$) are part of the south-western wing of the syncline. The thickness of limestone layers are decimetres to meters, and are inclined at an angle of 25o to 30o degrees towards the northeast. Eocene deposits are relatively poorly layered in calcareous breccias, but layering is noticeable in foraminiferal limestones. The entire lithological-tectonic micro-unit is characterized by tangential types of deformations, i.e. reverse faults and in connection with thrusting and micro-flaky structures. The faults are almost perpendicular to the Dinaric direction of the syncline, i.e. the southwest-northeast direction. In the immediate vicinity and in the speleological facility itself, the slope of the carbonate deposits (limestones) is between 15o and 20o, and the direction of the slope is towards the northeast (from 45o to 65o). The cracks observed in the building are up to ten centimetres wide, flat and smooth. This is the main phase of speleogenesis (GARAŠIĆ D. 2021). In the immediate vicinity of the cavern (on the surface), the fractures are mostly filled with hard clay, reddish-brown in colour. In the deeper parts of the caverns, there are some carbonated calcite binders, in crystalline or amorphous form. Speleothems appear rarely on the rocks. They come in the form of thin crusts. In the lower parts of caverns, there is more clay. At the location of the caves, there are more intensive fracture and fault zones with a width of about 2 to 3 meters, which, in addition to the lithological and hydrogeological conditions, played a significant role in the genesis (origin) of the main parts of the investigated caverns. No mylonitic fault zones were observed in the caves. The assessment of this speleological research is that this is a relatively younger, but now inactive fault or fault zone, as evidenced by the thin silty and clay layers that freely cover the paraclase of the fault in the pit, without being naturally broken or deformed. The main fault of both caverns extends in 45o - 225o direction, with subvertical paraclase. The fracture system is approximately at an angle of 60o to the main fault and has a position of 150o - 330o with an average dip between 75o and 85o (slope to the northeast). The corrosion of the surrounding rocks is very intense. Edges and small underground karrens have very sharp edges, measuring 1 to 2 cm. In the engineering-geological sense, we are talking about limestones whose uniaxial compressive strength of the substrate (limestones at the level of the pit) is estimated at 80-120 MPa, RQD varies, but is mostly above 40%, the distance between discontinuities is on average about 30 cm, in the upper parts with clay filling. Fracture systems are over 10 meters long, with an average length of 5 to 10 meters. Their width varies from 1 to 10 cm, they are rough, wavy and smooth in the upper parts, and smooth in the lower parts of the cave.

A cave survey at the construction site of the Zadar Airport tarmac provided data on the location, dimensions, and morphology of the caves. These are vertical caves, simple to knee-shaped morphological types (GARAŠIĆ, M., 2021). The depth of both caverns is over 10 meters and it most likely extends deeper (Fig. 3).

Figure 3: *Vertical shaft in the southern cave at Zadar Airport*

However, the exact depth remains unknown due to the narrow passages that prevented further exploration. Caverns are about 15 meters apart and are not connected. Their shape and morphology are very similar since both cavers extend along the fault lines from the same set, meaning the same dip direction and angle. No permanent active water flows were observed in the caves, but drip water is present in some places, creating small speleothems. The possible occasional water flow, which could be somewhat more abundant in the rainy season, belongs to the Adriatic catchment area and transports groundwater vertically to the permanent groundwater level at approximately 25 m/asl. In the geological past, underground water acted aggressively on rocks through erosion and corrosion. Caves are generally developed in the southwest-northeast direction, corresponding to the fault set's spatial orientation, which plays a significant role in their genesis (GARAŠIĆ D., 2021). As a result of speleological research, an engineering-geological map of both caverns was made, which served as a basis for finding an adequate solution for their remediation (Fig 4.).

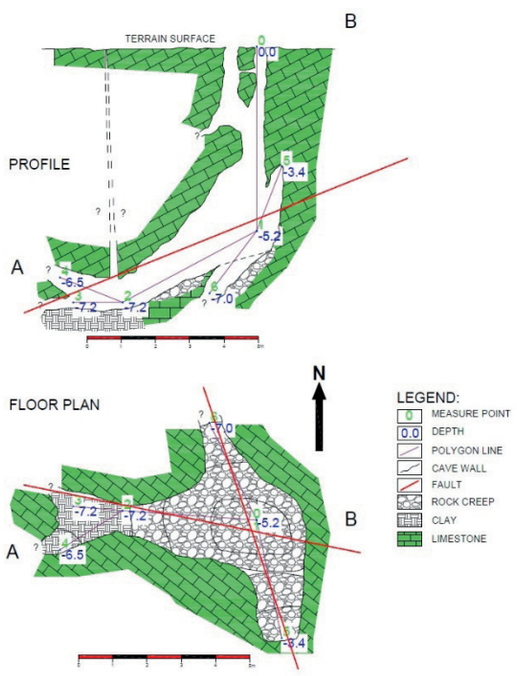

Figure 4: *Profile and floor plan of the cavern K-1.*

4. Discussion

Speleological and engineering geological research of karst caves always poses a problem and danger for researchers. One of the biggest challenges for speleologists is the instability of the rock mass at the very entrance to the cave. The instability is caused by the intensive work that led to the discovery of the cave, whether it was mechanical digging or blasting. Experience has shown that a longer stay of speleologists in such unstable caves can lead to further instability that can be fatal for researchers. For this reason, research must be carried out quickly. Since speed is of utmost importance, some other factors fall into the background. Figure 1 shows a rope rubbing against the rock. In ideal conditions, this situation would be avoided by installing an additional anchor or deviator, but given the instability and danger of staying in the cave for a long time, this step was skipped. Nowadays, with the existence of precise geodetic instruments, it is possible to conduct detailed measurements in caves. It is possible to obtain three-dimensional representations of cave channels and main discontinuities. In the case of the mentioned caverns, it was not possible to conduct such research due to the narrow channels, instability of the rock mass and the short time frame set for speleological research. Measurements carried out using the traditional polygon train method gave satisfactory results and offered optimal solutions.

5. Conclusion

The mentioned caves extended under the construction site of the Zadar Airport tarmac and represented a problem in the stability of the rock masses. Due to the importance of the location and the short time frame, research and remediation plans needed to be fast and efficient. Since no permanent water flows were noted in the caves, lower parts were filled with concrete. Reinforced concrete slabs are placed above both caverns. With their size, they cover the floor plans of the explored parts of the caves and extend 1 meter over. They are 30 cm thick. Zadar Airport is currently fully operational with the new tarmac.

Acknowledgments

We would like to thank Ivan Krpina and Tomislav Gospodinović for their great contribution during field work. We would also like to thank the Zadar airport for the assistance and trust they showed to the members of The Society for the Research, Surveying and Filming of Karst Phenomena Zagreb, during this research.

References

GARAŠIĆ D. (2021) The Relationship Between Speleogenesis and Discontinuities in Tunnels. PhD Dissertation, University of Zagreb.

GARAŠIĆ M. (1989) New conception of the morphogenesis and hydrogeology of the speleological objects in karst area in Croatia (Yugoslavia). 10. International Congress of Speleology, Proceedings, vol.1, str.234-236, s1.8, Budapest, Hungary.

GARAŠIĆ M. (1991) Morphological and Hydrogeological Classification of Speleological Structures (Caves and Pits) in the Croatian Karst area. Geološki vjesnik, vol. 44, str.289-300, fot.3, sl.4, Zagreb.

GARAŠIĆ M. (1995) Speleogeneza u okviru hidrogeologije krša i procesa karstifikacije. 1. Hrvatski geološki kongres, Opatija, Zbornik radova, Proceedings, 177-182, Zagreb.

GARAŠIĆ M. (2021) The Dinaric Karst system of Croatia - Speleology and Cave Exploration. 1-462, Springer International Publishing.

MAJCEN Ž, KOROLIJA B. SOKAČ B. NIKLER L. (1970) Osnovna Geološka Karta SFRJ 1:100000, list Zadar, L33-L39, str.1-44, Beograd.

MAJCEN Ž, KOROLIJA B. (1973) Tumač za OGK, list Zadar, L33-L39, str.1-44, Beograd.

Pliocene-Holocene evolution of a cratonic, sandstone covered karst system: NE Brazil

Lucas Padoan de Sá Godinho (1), Ivo Karmann (2), Darryl Granger (3), Fernando Verassani Laureano (4), Tom Dias Motta Morita (5), Gabriela Duarte (6)

(1) Instituto de Geociências, Universidade de São Paulo, São Paulo, Brazil (corresponding author), lucaspsgodinho@gmail.com
(2) Instituto de Geociências, Universidade de São Paulo, São Paulo, Brazil, ikarmann@usp.br
(3) Department of Earth and Atmospheric Sciences, Purdue University, West Lafayette, Indiana, USA, dgranger@purdue.edu
(4) Instituto de Geociências, Universidade de São Paulo, São Paulo, Brazil, verassani@gmail.com
(5) Instituto de Geociências, Universidade de São Paulo, São Paulo, Brazil, tomdmmorita@gmail.com
(6) Instituto de Geociências, Universidade de São Paulo, São Paulo, Brazil, gduart@usp.br

Abstract

Large cave systems in northeastern Brazil record ancient and modern karstification events associated to different tectonic uplift and subsidence cycles. Low uplift and denudation rates in the craton environment allowed multiple base level fluctuation events to rework cave passage levels at approximately the same elevation. Paleokarst landscape and interstratal karstification were recognized as early phases of dissolution since the Paleozoic and the Paleogene to Neogene transition (i.e. before and after burial of the major limestone unit by sandstone rocks). The analysis of modern karst landscape features, cave passage morphology and geology, lithostratigraphic relations, hydrochemical analysis of karst waters and geochronological analysis of cave deposits (cosmogenic ^{26}Al and ^{10}Be, OSL and U-Th dating) were applied in this study. This allowed to reconstruct a complex evolution history of the major phase of karst development since the Pliocene, after the second evidenced limestone exposure cycle. Multiple episodes of local base level fall and rise interpreted from cave erosion and deposition features suggest climate change control on surface river power increase (incision trends) and vegetation cover weakening (aggradation trends).

1. Introduction

Base level change is one of the major controls in the evolution of a karst system (Ford, 1971; Ford and Williams, 1989). Tectonic and climatic dynamics can influence base level fluctuations, so cave passages may record aggradation and erosion trends as they search equilibrium with a new established base level (Farrant and Smart, 2011; Calvet et al., 2024). Thus, erosion and deposition features in cave conduits allow the interpretation of past environmental conditions associated with aquifer and landscape evolution (Palmer, 1987, 2007).

Most karst systems in Brazil develop in limestone rocks deposited during the Neoproterozoic in a cratonic environment. The stable tectonic conditions imply in slow rates of uplift, denudation and regional groundwater lowering. This favors the development of single level, wide, and low gradient cave passages. Deposition and erosion records in cave passages tend to be superimposed at the same elevation, giving rise to a complex cave stratigraphy, characteristic of the tropical karst in stable terrains (Audra and Palmer, 2015).

In the São Desidério karst area (Figure 1), northeastern Brazil, large limestone cave systems develop at the margins of a sandstone covered plateau and preserve sedimentary records that indicate successive base level fluctuations. The causes associated with those changes in base level are not well understood, so careful study of cave geology, karst geomorphology and hydrogeology may help to connect local and regional aspects of the karst system evolution.

The aim of this research was to recognize major stages of evolution in the São Desidério karst system, taking into account modern groundwater recharge and discharge landscape features, cave passage morphology, and geochronological analysis of cave deposits.

Figure 1: *Collapse sinkholes with limestone cliffs, aligned in the ENE-WSW direction, parallel to a major cave system. The low gradient landscape that surrounds the sinkholes is covered by sandstone. The major axis of the sinkhole in the foreground is 180 m, and its depth is 90 m. Photo: Gabriel Lourenço.*

2. Materials and methods

Open access satellite images, topographic maps and digital elevation models (SRTM – USGS, BDGEX - Brazil) where used to delineate topographic divides and drainage basin geometry in an area of approximately 600 km^2. From this, surface recharge karst features were define, and morphometric parameters of enclosed depressions were defined (Williams, 1972).

Spring inventory was carried out in the field in order to identify aquifer discharge points in this area (Feitosa and Feitosa, 2008). Hydrochemistry analysis of karst waters (springs, drippings, and cave rivers) was conducted to investigate the origin of the acidity responsible for cave enlargement. Geological map analysis (SBG - Brazil) and the survey of 8 cross sections in the field (rock exposures and pumping well data), ranging from 1 to 60 km in extension, where used to characterize the lithostratigraphy, typify karst recharge styles and recognize paleokarst features.

Survey data (Bambuí and GGEO caving clubs) from representative caves were used to analyze 6.8 km of passage morphology. Cave geology research (Palmer, 1987, 2007) in the field was carefully performed in order to identify erosion and deposition conduit features that indicate base level fluctuation.

Finally, 40 samples for geochronological analysis (cosmogenic ^{26}Al and ^{10}Be, OSL and U-Th) were sampled from quartz rich clastic sediments and calcite speleothems in the caves (Granger, 2006; Rhodes, 2011; Richards and Dorale, 2003). Major stages of evolution of the karst system was interpreted from this multiple method approach.

3. Results

Geological cross sections revealed that the erosive contact surface between the Bambuí Group limestones (Neoproterozoic, lower unit) and the Urucuia Group sandstones (Cretaceous, upper unit) is characterized by a paleovalley morphology. Sinkholes developed on the sandstone are ubiquitous in the covered karst zone, indicating that subjacent limestone caves drag large volumes of quartz sands to the underground limestone conduit system.

The limestone rock is exposed to the surface near the base and mid hillslope elevations of the São Desidério River valley (local base level). Allogenic recharge from the sandstone drainages form blind valleys at the contact with the limestone. Authogenic recharge through sinkholes is widespread when the limestone rock is exposed to the surface. Spring inventory showed that 21 intermittent and 22 perennial springs are responsible to the discharge of the limestone karst and the insoluble sandstone aquifers.

Mapping of surface karst depressions and springs showed that the longest cave system in the area (named João Rodrigues) has its recharge on surface coming from the Tamanduá River watershed (sandstone covered karst zone), while the discharge spring drains to a different surface watershed, at the margins of the São Desidério River.

Cave morphology is characterized by wide, low gradient phreatic passages (cave levels) oriented parallel to the intersection between the strike of the limestone bedding planes (NE-SW to NW-SE) and prominent normal faults (ENE) (Figure 2). The limestone beds are folded and show average dip angle equals to 21°, as a consequence of the Brasiliano Orogeny that affected the borders of the São Francisco Craton during the Neoproterzoic.

Figure 2: *Upper cave passage level in the Sopradeira cave. Fluvial bars covered by calcite (to the right), wall notches (to the left), remnants of quartz sand deposits in the walls (top left), and ceiling channels (at the top) indicate fluvial aggradation reworking of the passage (base level rise) after phreatic passage development and subsequent vadose incision (base level fall).*

Two major cave levels where recognized: the lower at 525 m.a.s.l. and the upper at 555 m.a.s.l. Those are connected by vadose canyon passages that follow the dip direction of the limestone strata.

Plan view morphology of the cave systems is characterized by a dendritic pattern, locally superimposed by network or anastomosing flood maze passages, depending on the dip of the strata and the occurrence of prominent vertical angle fault zones.

Hydrochemical analysis of karst waters showed that Ca^{2+} and HCO_3^- represents 60-80% of the ionic species in solution, while SO_4^{2-} usually constitutes <20% of dissolved species. Average Ca^{2+} concentrations in the karst waters was 80 mg/l. Linear regression analysis of the Ca^{2+}, Mg^{2+} and HCO_3^- concentrations show a good correlation (r = 0,93). High concentrations of SO_4^{2-} (20 mg/l) occur in the deep phreatic zone (≈ 60 m depth in pumping wells) and some cave drippings. Saturation index analyses showed that karst springs are saturated all over the water year, except during major flooding events.

The burial ages of clastic cave deposits vary from 3.03 ± 0.19 My (^{26}Al and ^{10}Be) to 1.8 ± 0.1 ky (OSL). Minimum ages of cave formation in three different cave systems gets progressively younger in the upstream direction of the surface river (base level). Cave deposits at the top (2.15 ± 0.18 My, ^{26}Al and ^{10}Be age) and bottom (1.16 ± 0.18 My, ^{26}Al and ^{10}Be age) of a major vadose canyon with vertical amplitude of 30 m mark the timing of a major base level drop.

Calcite flowstone speleothems that cover fluvial river bars in the upper passage level shows a wide range of crystallization ages (337.9 ± 15.6 ky, 228.2 ± 3.5 ky, 85.8 ± 6.2 ky, U-Th age). Subaquatic speleothems with stromatolitic lamination (speleomicrobialites) locally form thick crusts (≈ 10-30 cm) on the sinkhole cliffs and all-around collapsed cave passage walls and ceiling (Figure 3). The subaquatic speleothems occur up to 40 m above the modern cave river level and they consist of interchanged vadose (soda straw) and phreatic (stromatolitic lamination) facies. Ages of deposition vary from 4.3 ± 0.052 ky to 2.2 ± 0.248 ky.

Figure 3: *Speleomicrobialites preserved on the cliff of a large collapsed sinkhole (the same as in the background of Figure 1). Major axis of the larger speleothems on the top left corner of the picture are approximately 4 m long.*

4. Discussion

The older karstification event corresponds to the Paleokarst formed between the erosive contact of the Bambuí Group and the Urucuia Group. This karstification phase is characterized by the paleovalley morphology, and its formation is associated to the erosive hiatus between the Ediacaran and the upper Cretaceous (a gap of approximately 400 My).

After the deposition of the Urucuia Group, continental uplift took place in the interior of the South American Platform (Almeida et al., 2000), giving rise to a regional plateau landscape in the Cenozoic (Valadão, 2009). Interstratal karstification was triggered by the new established hydraulic gradient of the plateau escarpment (≈ 1,000 m relief). The evidences of the interstratal karstification are the sandstone sinkholes in the covered karst zone.

Limestone exposure occurred during the incision of the São Desidério River valley. Carbonic acid dissolution was dominant to cave passage enlargement in the phreatic and vadose zones. Punctual pyrite oxidation in interlayered mudstone and limestone successions is interpreted to have influenced dissolution by sulfuric acid in the vadose zone, as indicated by higher SO_4^{2-} concentrations in cave drippings and pumping wells.

The saturation index from karst springs suggests that cave enlargement by dissolution is active only during major floods. During most of the water year, waters are saturated chemical with calcite and corrosion is predominantly inactive.

The extension of the longest underground cave system flow route and the average dip of the limestone strata were used to estimate the maximum depth of groundwater flow in conduits between 150-270 m from the surface, following the equation proposed by Worthington (2001).

Acidic water infiltration in the sandstone to limestone contact along the Tamanduá River created an alternative underground flow path and head gradient to the São Desidério River. Due to the large catchment area of the Tamanduá River (long watershed axis ≈ 100 km), the João Rodrigues cave system developed large underground galleries and eventually pirated the Tamanduá River flow to the São Desidério River. The time constrain for this stage is indicated by the minimum age of karst conduit formation in the area (3.03 ± 0.19 My, ^{26}Al and ^{10}Be age).

Knickpoint migration along the São Desidério River is responsible for the erosive retreat of the sandstone plateau escarpment. Cave systems get progressively younger to the upstream direction, as suggested by cosmogenic burial ages, indicating that new limestone exposures are formed during the knickpoint migration process.

An important base level drop event occurred approximately between 2-1 My, leading the caves to entrench vadose canyons down to a new elevation. The São Desidério River is the local base level, so this event represents an increase in the surface river power and erosion capacity.

After the base level drop and the development of the lower cave passage level, successive fluvial erosion reworking and aggradation events were superimposed, affecting the lower and upper cave passages. The wide range of cave deposit ages younger than 500 ky, in different elevations, is the evidence to the interpretation of constant base level fluctuation. The cause for an erosion to aggradation trend shift is interpreted as a transition from more humid climatic conditions to drier periods. This climate change leads to less developed vegetation cover and a more efficient hillslope transport of sediments to the bottom of the surface valleys, as the process described by Langbein and Schumm (1958) and Acosta et al. (2015), ultimately causing cave passages to fill up with clastic sediments.

Breakdown reworked cave passage morphology, and this process is associated to different causes: cave floods and weakening of fracture planes by dissolution at high hydraulic gradients; vadose infiltration and precipitation of secondary carbonate and sulphate minerals in the fractures (crystal wedging); erosion of the land surface and removal of cave roof support, leading to collapse sinkhole development.

Subaquatic speleothems cover breakdown walls in the caves. They are preserved as scattered crusts along entire cave systems (> 10 km of cave passages). Three major vadose growth phases of the speleomicrobialites, interlayered with subaquatic growth phases, indicate that the regional water table varied in a 3-40 m amplitude during the last 6 ky.

5. Conclusion

The São Desidério karst system was formed during different phases of exposure and burial of the Bambuí Group limestones. The earlier phase of evolution is related to the erosive unconformity between the Bambuí Group limestone and the Urucuia Group sandstone (Paleozoic to Mesozoic hiatus), where a paleokarst is evidenced by a buried paleovalley landscape. Interstratal dissolution followed after the uplift of the continental crust and the formation of a regional plateau, probably in the Paleogene to the Neogene transition. The most prominent phase of cave systems development started in the Pliocene, after the modern exposure of the limestone rocks to the surface.

Several base level change episodes were recognized in the cave systems during the last 3 My. They reflect the increase of the river power and erosion capacity of the major river on surface (local base level) when base level drops, and a change from more humid to drier climatic conditions leading to aggradation when the base level rise.

Acknowledgments

We extend our gratitude to the Brazilian research funding agencies Fapesp, process nº 2018/15774-5, CAPES and CNPq for sponsoring this research. We also thank to the Bambuí and GGEO caving clubs from Brazil, for giving access to the cave maps. Finally, we thank to the many caver friends who participated in the field trips, for so many hours of fun and science in the underground.

References

ACOSTA, V. T., SCHILDGEN, T. F., CLARKE, B. A., SCHERLER, D., BOOKHAGEN, B., WITTMANN, H., von BLANCKENBURG, F. (2015) Effect of vegetation cover on millennial-scale landscape denudation rates in East Africa: Lithosphere, v. 7, n. 4, p. 408-420.

ALMEIDA, F. F. M., NEVES, B. B. B., CARNEIRO, C. D. R. (2000) The origin and evolution of the South American Platform: Earth-Science Reviews, v. 20, p. 77-111.

AUDRA, P., PALMER, A. N. (2015) Research Frontiers in Speleogenesis: Dominant Processes, Hydrogeological Conditions and Resulting Cave Patterns: Acta Carsologica, v. 44, n. 3, p. 315.

CALVET, M., GUNNELL, Y., DELMAS, M., BRAUCHER, R., JAILLET, S., HÄUSELMANN, P., DELUNEL, R., SORRIAUX, P., VALLA, P. G., AUDRA, P. (2024)

Valley incision chronologies from alluvium-filled cave systems: Earth--Science Reviews, v. 258, 40 p.

FARRANT, A. R., SMART, P. L. (2011) Role of Sediment in Speleogenesis: Sedimentation and Paragenesis: Geomorphology, v. 134, n. 1, p. 79-93.

FEITOSA, E. C., FEITOSA, F. A. C. (2008) Metodologia Básica de Pesquisa de Água Subterrânea, in, Feitosa, F. A. C., Manoel Filho, J., Feitosa, E. C., Demetrio, J. G. A. Hidrogeologia: Conceitos e Aplicações, Rio de Janeiro, CPRM, LABHID, 812 p.

FORD, D. (1971) Geologic Structure and a New Explanation of Limestone Cavern Genesis, in The Transactions of the Cave Research Group or Great Britain: Symposium on the Origin and Development of Caves, v. 13, n. 2, p. 81-94.

FORD D., WILLIAMS P. (1989) Karst geomorphology and hydrology, Ed. Unwin Hyman Ltd. London, 601 p.

GRANGER, D. E. (2006) A Review of Burrial Dating Methods Using 26Al and 10Be: Geological Society of America Special Papers, v. 415, p. 1-16.

LANGBEIN, W. B., SCHUMM, S. A. (1958) Yield of Sediment in Relation to Mean Annual Precipitation: Transactions, American Geophysical Union, v. 39, n. 6, p. 1076-1084.

PALMER, A. N. (1987) Cave Levels and Their Interpretation: The NSS Bulletin, v. 49, p. 50-66.

PALMER, A. N. (2007) Cave Geology: Cave Books, Dayton, 454 p.

RICHARDS, D. A., DORALE, J. A. (2003) Uranium-series chronology and environmental applications of speleothems: Reviews in Mineralogy and Geochemistry, v. 52, n. 1, p. 407-460.

RHODES, E. J. (2011) Optically stimulated luminescence dating of sediments over the past 200,000 years: Annual Review of Earth and Planetary Sciences, v. 39, p. 461-488.

VALADÃO, R. C. (2009) Geodinâmica de superfícies de aplanamento, desnudação continental e tectônica ativa como condicionantes da megageomorfologia do Brasil oriental: Revista Brasileira de Geomorfologia, v. 10, n. 2, p. 77-90.

WILLIAMS, P. W. (1972) Morphometric Analysis of Polygonal Karst in New Guinea: Geological Society of America Bulletin, v. 83, p. 761-796.

WORTHINGTON, S. R. H. (2001) Depth of Conduit Flow in Unconfined Carbonate Aquifers: Geological Society of America, v. 29, n. 4, p. 335-338.

Project MIKAS (Most Important Karst Aquifers' Springs): Progress and request for information

John Gunn(1), Zoran Stevanović(2), Augusto Auler(3), Avihu Burg(4), Seifu Kebede(5), Neven Kresic(6), Peter Malik(7), Junbing Pu(8), Benjamin Tobin(9)

(1) School of Geography, Earth and Environmental Science, University of Birmingham, United Kingdom
(2) Centre for Karst Hydrogeology, University of Belgrade-Faculty of Mining & Geology, Serbia
(3) Instituto do Carste / Carste Ciência e Meio Ambiente, Belo Horizonte, MG, Brazil
(4) Geological Survey of Israel, Jerusalem, Israel
(5) School of Agricultural, Earth and Environmental Sciences, University of KwaZulu-Natal, South Africa
(6) Independent Consultant and Director, Karst Waters Institute, Warrenton, VA, USA
(7) Geological Survey of the Slovak Republic, Bratislava, Slovakia
(8) School of Geography and Tourism, Chongqing Normal University, P.R.China
(9) Kentucky Geological Survey, University of Kentucky, Lexington, KY, USA

Abstract

The MIKAS (Most Important Karst Aquifer's Springs) project was launched by the Karst Commission of the International Association of Hydrogeologists in 2022 and is intended to be concluded by the end of 2025. The first aim is to identify, and provide a list of, the most important karst springs at the global, but also at the national level (NIKAS). Subsequently, it is intended that a Code of Practice for their utilisation and protection will be drawn up and the springs will be promoted by labelling them in-situ and publicising them on the Internet. The project has an advisory board whose members recruited National Experts who agreed to compile information on karst springs in their country. As of January 2025, over 100 national experts had been recruited and 175 springs in 40 countries had been evaluated. This paper provides background to the project, a summary of the results to date with examples from the four UK MIKAS, and an appeal for assistance from speleologists carrying out exploration in remote areas where springs may be poorly documented.

1. Introduction

Globally, the majority of large springs discharge from karst groundwater systems and karst springs provide the base flow to many rivers and form important sources of potable supply, including to some large cities. Springs with lower discharges may also be important because of their aesthetic, cultural, ecological, economic, historic or scientific values. Some lists have been published showing the largest springs (for example, FORD & WILLIAMS 1989, Table 5.6 and 2007, Table 5.9) but there is no consensus on which springs are the most important. Hence, the aim of the MIKAS (Most Important Karst Aquifer's Springs) project is to identify, and provide a list of, the most important karst springs at the global, but also at the national level (Nationally Important Karst Aquifer's Spring ;NIKAS). Subsequently, it is intended that a Code of Practice for the utilisation and protection of these springs will be drawn up and the springs will be promoted by labelling them in-situ and publicising them on the Internet. The project was launched in June 2022 at the annual meeting of the International Association of Hydrogeologists (IAH) Karst Commission (KC). The MIKAS project team leader is Zoran Stevanović and the Project Advisory Board (PAB) consists of the team leader, five regional representatives, and the three rotating chairs of the KC. These individuals are co-authors of this paper.

During preliminary discussions, the PAB decided that the project would best be accomplished by appointing national experts who would be responsible for identifying the most important karst springs in the countries for which they were responsible. It was also decided that national experts should have the option of producing a list of Nationally Important Karst Springs (NIKAS) although only the MIKAS are reviewed by the Advisory Board. A set of Guidelines has been agreed that include selection criteria for MIKAS and NIKAS together with a template for the Spring Survey Form (discussed below). The PAB also agreed that spring selection would be on the basis of five criteria: the cultural, ecological, economic, historic and scientific value of the spring. However, it was recognised that all five criteria will not be present at all springs. This approach provides built-in flexibility allowing MIKAS and NIKAS lists to be created based on a set of common criteria, but adapted to local conditions, recognising that something that is important in one country does not have to be important in others.

2. The Survey Form

Initially, it was planned to have as much information about the proposed springs as possible. However, the PAB recognised that the amount of information available varies widely from country to country and decided to simplify the Survey Form to facilitate the work of national experts. The form requests certain mandatory basic information for each of the proposed springs together with other optional information. One of the parameters that was initially thought of as being mandatory is the spring regime. However, it has become apparent that surprisingly

few of the springs that meet other MIKAS and NIKAS criteria have their flow measured on a continuous basis and for some the flow has only ever been estimated as opposed to being measured using recognised hydrometric techniques. A case in point is Tobio in Papua New Guinea which was listed in FORD & WILLIAMS (1989, Table 5.6 and 2007, Table 5.9) as being the world's largest karst spring with a mean discharge of 85 – 115m^3s^{-1}. The main reference given (MAIRE, 1981) states that "*the huge Tobio emergence has been reckoned by Beck to [sic] 85 – 115 cubic metres per second*". No reference is given but the actual source is thought to be BECK (1975) who states that "*at Tobiu something like 3000 – 4000 cusecs (85 – 113 cumecs) was thundering from an entrance 55m high by at least 24m in width*". The lead author of the present paper was able to contact Beck (pers. comm., 8 January 2025) who provided the following information: "*On route to Pulupare the Iaro River which emerges from Tobio is crossed on a bridge about 16km upstream… our estimate of water flow at the cave had no scientific basis, other than attempting to gauge volume from the banking at this crossing. I would think this would be the only safe place where a proper measurement might be attempted, but it was beyond our remit and abilities at the time. The river could well of course have picked up other unknown tributaries between bridge and resurgence*". This is entirely reasonable and Beck is to be commended for at least making an estimate but it illustrates the problems of assembling data on world karst spring regime.

The template (Figure 1) can be downloaded from the project website (https://mikasproject.org/), which also has more information about the project, including the Guidelines, Instructions for completion of the Survey Form and the list of engaged experts.

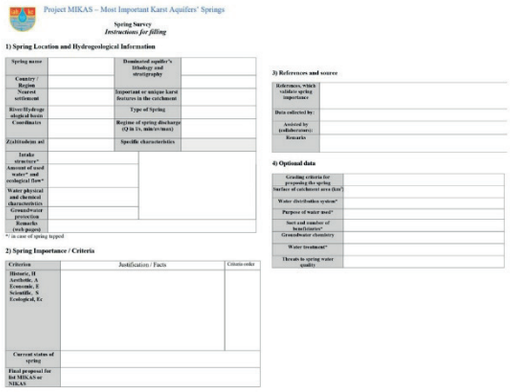
Project MIKAS – Most Important Karst Aquifers' Springs

Spring Survey
Instructions for filling

1) Spring Location and Hydrogeological Information

Spring name		Dominated aquifer's lithology and stratigraphy	
Country / Region and settlement		Important or unique karst features in the catchment	
River Hydrographical basin / Coordinates		Type of Spring	
		Regime of spring discharge (Q in l/s, min/ave/max)	
Exhibitions and		Specific characteristics	
Intake structure*			
Amount of used water* and ecological flow*			
Water physical and chemical characteristics			
Groundwater protection			
Remarks (web-page)			

* in case of spring tapped

2) Spring Importance / Criteria

Criterion	Justification / Facts	Criteria order
Historic, H Aesthetic, A Economic, E Scientific, S Ecological, Ec		
Current status of spring		
Final proposal for list MIA AS or NIKAS		

3) References and source

References, which validate spring importance	
Data collected by	
Assisted by (collaborators)	
Remarks	

4) Optional data

Grading criteria for preparing the spring surface of catchment area (km²)	
Water distribution system*	
Purpose of water used*	
Sort and number of beneficiaries*	
Groundwater chemistry	
Water treatment*	
Threats to spring water quality	

Figure 1 : *Project MIKAS Spring Survey Form*

3. Results to date and a request for assistance from speleologists

As of January 2025, over110 national experts had been recruited and 175 springs in 40 countries had been evaluated. Countries and their MIKAS springs are presented in alphabetical order on the project website (https://mikasproject.org/mikas-list/). Those countries for which NIKAS have been proposed are listed on a separate website (https://mikasproject.org/nikas-list/). The MIKAS list is preliminary and has been created based on evaluations by the Advisory Board. A final list, possibly containing only 200 springs, will be announced at the end of the project and it is intended to publish a monograph with the assembled information. The United States of America has by far the largest number of MIKAS (26) with France second (14). In part, this is due to the excellent historical documentation of karst springs in both countries and for the United States this is reflected in a free-to-download book by Kresic (2024). In contrast, there are some countries that are known to contain spectacular karst areas in which there are large caves and springs but for which very little information is available. For example, and as discussed above, Tobio in Papua New Guinea is listed as the world's largest spring on the basis of a single estimate made on a caving expedition in 1975. The site is very remote and it is possible that since then it has not been visited other than by indigenous peoples. There have been a greater number of caving expeditions to the Nakanai Mountains, an area of spectacular karst on the Papua New Guinea Island of New Britain (Gabriel et al., 2018) and information from cavers (Jean-Paul Sounier, pers. comm. 2024) has been used to compile survey forms for candidate MIKAS and NIKAS sites. Similar information is sought from speleologists visiting remote areas containing important karst springs that are not already listed on the MIKAS website. Information can be sent to the corresponding author of this paper or via the website (https://mikasproject.org/contact-us/).

4. Examples of MIKAS in the United Kingdom

The United Kingdom comprises Great Britain (England, Scotland and Wales) and Northern Ireland and within Great Britain there is a greater temporal range of carbonate rock outcrops per unit area than anywhere else on earth: Quaternary freshwater carbonates (tufa); limestones and dolostones of Cretaceous, Jurassic, Permian, Carboniferous, Devonian, Silurian, Ordovician and Cambrian ages and Cambrian to Neoproterozoic metacarbonates (marbles). Groundwater is present in all of these carbonate rocks and there are many hundreds of springs, most of which have a relatively small average annual flow (<1 m^3s^{-1}) as a consequence of limited catchment area. Information on springs in the different lithologies was reviewed by three National Experts (Farrant, Gunn and Maurice) and whilst many were thought to qualify as NIKAS, only four were proposed as MIKAS: Bath Hot Springs, Bedhampton & Havant springs, the Castleton spring group, and Wookey Hole spring.

The Bath Hot Springs were selected on the basis of their Historic, Economic and Scientific values. The springs were developed as a spa in Roman times and the baths gave their name to the city of Bath, which is a UNESCO World Heritage Site, designated for its cultural values. They were of economic value to the Romans and this continued from mediaeval times to the present when they are a key tourist attraction to this day, bringing more than 1 million visitors each year to the city. Scientifically, the Bath springs discharge from Carboniferous limestone and are an unusual example of hot springs (44-47°C; the highest in the UK) in a karst aquifer because the water is thought to be of Holocene age (at least 1,000 years) with a small modern component. The springs have been the subject of many studies, most recently summarised in an Environment Agency (2020) report which discusses the hydrogeological settings of deep springs (fed by groundwater from >400m), and the Bath Springs in particular, with the aim of illustrating how best to assess their provenance.

The Bedhampton and Havant spring complex was also selected on the basis of Historic, Economic and Scientific values. The springs discharge from the Cretaceous Chalk and there are multiple (at least 28) outlets with an average combined discharge of 1110 Ls^{-1} and a range of 610-1960 Ls^{-1}. Based on the average flow, they are amongst the largest karst springs in the UK although there are many springs discharging from the Carboniferous limestones that have higher peak flows. The springs are an important source of potable water and currently supply

approximately 250,000 people, the largest Chalk spring supply in Western Europe. There are very few caves in the English Chalk and this contributed to an erroneous assumption that the rock, and aquifer, are not karstic. This has remained to the present when much hydrogeological work and groundwater management and protection still fails to consider karst. However, early work on karst at the Bedhampton and Havant springs, including water tracing experiments from sinks, contributed to the recognition and development of conceptual ideas about chalk karst (Atkinson et al., 1974). The springs continue to be an important site for improving understanding of chalk karst and its importance for groundwater protection (e.g. Farrant et al., 2023; Maurice et al., 2023).

The Castleton spring group was proposed as MIKAS primarily because of the springs scientific value but also due to their historic, aesthetic and ecological values. There are three springs that emerge within a 100m radius from Carboniferous limestone: Peak Cavern Rising (PCR), Slop Moll Rising (SMR) and Russet Well (RW). They drain an extensive (>16km) vadose - phreatic cave system of Quaternary age that has intersected large hypogenic voids of putative Carboniferous age. Over 50 sumps (water-filled conduits) have been explored by cave divers, the deepest descending over 70m with a complex profile. Under low to average flows RW and SMR, the 2 lower elevation springs, discharge mixed-allogenic/autogenic recharge and PCR discharges only autogenic recharge. As flow increases the capacity of the conduits feeding RW and SMR is exceeded and PCR becomes dominant. RW and SMR display complex periodicities related to siphons and flow switching between conduits at a range of flows but PCR only displays such complex behaviour at times of high flow. The rhythmic and episodic changes in discharge at RW and SM (and at PCR during high flow) are more complex than in any other spring globally. They are largely due to variations in flow from two phreatic conduits (Main Rising (MR) and Whirlpool Rising (WR)) that enter, and pass through, Speedwell Cavern en route to the springs. The short-term temporal variability in water depths at both MR and WR is greater than any documented in previous studies. This is attributed to conduit bedrock geometry and changes in conduit permeability due to sediment accumulation in phreatic loops, which together influence the response to recharge (Gunn & Bradley, 2023). Within the catchment and at the springs there has also been research into bacterial water quality, clastic sediment dynamics and geochemistry.

Peveril Castle was established directly above PCR soon after the Norman Conquest of 1066. The Domesday Book (1086) mentions 'William Peveril's castle of Pechesers' ('Peak's Arse') and by medieval times the cave was known as "The Devil's Arse" because the gurgling sound made by a siphon inside the cave was likened to the Devil breaking wind. It is the largest cave entrance in the British Isles, 100m long, 20m high and 35m wide, and contains the remains of a village used from 1642 to 1880 by rope makers, who supplied rope for the lead mining industry around Castleton. The cave has been visited by tourists for over 400 years and was described by Martel following a visit in 1897. The aesthetic value lies in PCR emerging at the foot of an impressive gorge (Figure 2) and the ecological value relates to observations of depigmented fish in the springs by cave divers and by this being one of only a few springs systems in UK in which there have been detailed studies of the aquatic invertebrate community.

Wookey Hole spring, the final UK MIKAS, was nominated for its Aesthetic (Figure 3), Historic, Economic and Scientific values. Unlike the other three sites, the discharge is through a single outlet developed in Triassic calcareous breccias, although some water has been traced to a second spring 1 km downstream of the main outlet. The first part of the cave behind the spring has also developed in breccia but the inner passages and most of the catchment are in Carboniferous limestones. The cave has been developed for tourism and contains material with prehistoric archaeological significance. Water from the spring was used by a mill that dates from the 1600s, and the spring itself is of historical significance for cave diving. It was the site of the first cave dive in the UK (1935) and was instrumental in the development of deep cave diving, with the deepest explored sump in the UK (c. -90m). Globally important studies of karst hydrogeology have been conducted at the spring, most notably the widely cited work of Atkinson (1977).

Figure 2: *Peak Cavern Gorge. Slop Moll Rising is at bottom right. Path on right leads to entrance of tourist cave "The Devil's Arse". Peak Cavern Rising is mid-left. Photo by John Gunn.*

Figure 3: *Wookey Hole Resurgence in context (photo by Andrew Farrant).*

5. Conclusion

The MIKAS projectect provides an opportunity for the global cave and karst community to recognise and protect globally, and nationally, important karst springs. Good progress has been made and it is hoped that the proect will be concluded by the end of 2025.

Acknowledgments

Thanks are due to all those who have contributed to the MIKAS project as National Experts, and particularly to Dr. Andrew Farrant and Dr. Lou Maurice for their work on the UK MIKAS.

References

ATKINSON, T.C. 1977. Diffuse flow and conduit flow in limestone terrain in the Mendip Hills, Somerset (Great Britain). *Journal of Hydrology*, 35(1-2), 93-110.

ATKINSON, T.C. & SMITH, D.I. 1974. Rapid groundwater flow in fissures in the Chalk: An example from South Hampshire. *Quarterly Journal of Engineering Geology and Hydrogeology*, 7(2), 197-205.

BECK, H.M. 1975. Iaro River Cave, Southern Highlands District. *Niugini Caver*, 3(1), 4.

ENVIRONMENT AGENCY. 2020. *Perspectives on protection of deep groundwater*. Environment Agency, Bristol, UK (https://www.gov.uk/government/publications/perspectives-on-protection-of-deep-groundwater).

FARRANT, A.R., MAURICE, L., BALLESTEROS, D. & NEHME, C. 2023. The genesis and evolution of karstic conduit systems in the Chalk. *Geological Society, London, Special Publication*, 517, 15-37.

FORD, D.C. &WILLIAMS, P.W. 1989. *Karst Geomorphology and Hydrology*. Unwin Hyman, London, UK.

FORD, D.C. &WILLIAMS, P.W. 1989. *Karst Hydrogeology and Geomorphology*. John Wiley & Sons, Chichester, UK.

GABRIEL, J., SPECHT, J., LEAVESLEY, M., KELLY, M., WOOD, M., FOALE, S., FILER, C., MCINTYRE-TAMWOY, S., BOURKE, R.M., GILL, D., & SOUNIER, J-P. 2018. *The Nakanai Ranges of East New Britain, Papua New Guinea*. James Cook University, Cairns, Australia.

GUNN, J. & BRADLEY, C. 2023. Characterising Rhythmic and Episodic Pulsing Behaviour in the Castleton Karst, Derbyshire (UK), Using High Resolution in-Cave Monitoring. *Water*, 15, 2301.https://doi.org/10.3390/w15122301.

KRESIC, N. 2024. *Notable springs of the United States*. https://iah.org/wp-content/uploads/2024/12/Notable-Springs-of-US_Kresic-1.pdf

MAIRE, R. 1981. Inventory and general features of PNG karsts. *Spelunca*, supplement 3, 7.

MAURICE, L., FARRANT, A.R., MATHEWSON, E. AND ATKINSON, T. 2023. Karst hydrogeology of the Chalk and implications for groundwater protection. *Geological Society, London, Special Publications*, 517, 39-62.

Geological and structural configuration of Cheve cave, Oaxaca, Mexico

Rogelio Hernández Vergara (1), Matthew D. Covington (2) & María de los Ángeles Verde Ramírez (3)

(1) Instituto de Geología, Universidad Nacional Autónoma de México. Circuito Interior s/n, Coyoacán, C.U., 04510 Ciudad de México, México, rogeliohernandezvergara@gmail.com

(2) Department of Geosciences, University of Arkansas, USA, mcoving@uark.edu

(3) Asociación de Montañismo y Escalada de la Universidad Nacional Autónoma de México. Ciudad Universitaria, Coyoacán, 04510 Ciudad de México, México, angelesverde@gmail.com

Abstract

The Cheve Karst System (CKS) is one of the deepest known karst systems in the world. The most recent exploration reached a depth of -1530 m; however, the elevation difference between the highest cave passages and the resurgence in the Santo Domingo River is greater than 2600 m. If connected by exploration this would currently be the deepest in the world. The current explored extent of Sistema Cheve lies in the region between Concepcion Papalo and San Miguel Santa Flor (SMSF) in southern Mexico. The preferential conduit orientation is NW-SE, the same as nearby J2 and Charco caves. The complex geological-structural configuration in this region led to the development of the CKS in a series of folded and faulted sandy limestone, dolomite and mylonitized limestone beds. These rocks are cut by NNW-SSE regional normal faults with inclination to the SW, related to the normal fault of Oaxaca, and by local strike-slip faults with NW-SE and SE-NW orientations. Here, we compare the results of surface geological mapping focused in the SMSF area with structural and geological mapping in Jornada de Trabajo Cave, a new entrance to Sistema Cheve. The main results show that Jornada de Trabajo developed in a NW-SE orientation corresponding to tensional T faults that cut the carbonate beds, generating small vadose galleries that connect with the larger main passages of Cheve. The passages in Cheve near the current terminus are developed in mylonitized limestone affected by the normal fault plane that coincides with the Oaxaca cortical normal fault. Statistical fracture analysis, and its comparison with the mapped conduits shows that the preferential development of the CKS may continue to the north in small passages interconnected by R, R´ and T faults.

Resumen

El Sistema de la Cueva Cheve (SCC) es uno de los sistemas más profundos del Hemisferio Occidental, y las exploraciones más recientes han alcanzado una profundidad de -1530 m. Sin embargo, el gradiente hidráulico muestra una diferencia de nivel de alrededor de 2600 m desde la entrada hasta el nivel base del río Santo Domingo, lo que haría de esta cueva una de las más profundas del mundo. El SCC se desarrolla entre Concepción Pápalo y la zona de San Miguel Santa Flor (SMSF) en el sur de México. La orientación preferencial de los conductos es NW-SE, la misma que las cuevas J2 y Charco. La compleja configuración geológico-estructural de esta región genera que el SCC se desarrolle en una serie de capas de roca caliza arenosa, dolomita y caliza milonitizada plegadas y con corrimiento capa a capa, que son cortadas por fallas normales regionales NNW-SSE con inclinación hacia el SW, pertenecientes a la falla normal de Oaxaca, y fallas latérales locales con orientaciones NW-SE y SE-NW. Este trabajo presenta un análisis multiescalar mediante el mapeo geológico superficial enfocado en la zona de SMSF y su comparación con el mapeo estructural y geológico de la cueva Jornada de Trabajo, una nueva entrada del SCC. Los principales resultados muestran que la cueva Jornada de Trabajo se desarrolló en dirección NW-SE correspondiente a fallas tensionales T que cortan las capas carbonatadas, generando pequeñas galerías vadosas que se conectan con el conducto principal del SCC, desarrollado en caliza minoritaria afectada por el plano de falla normal que coincide con la falla cortical normal de Oaxaca. El análisis estadístico de fracturas y su comparación con los conductos desarrollados muestra que el desarrollo preferencial del SCC puede continuar hacia el norte en una sección de pasajes pequeños interconectados por fallas R, R´ y T.

1. Introduction

The Cheve Karst System is one of the deepest known karst hydrological systems in the world. The hydrological connection between Sistema Cheve and the resurgence, Cueva de la Mano, was proven by dye tracing (SMITH, 1991). There is an elevation difference of over 2600 m between the highest and lowest known cave passages within the cave system (STONE et al., 2023). Despite the global significance of the Cheve Karst System, relatively little is known about its geological context and speleogenesis. A brief description is provided by SMITH (2002), though the main focus of that study was Sistema Huautla. A few observations were also reported by HOSE (1995). Further exploration in the region over the past 20 years has led to the discovery of many additional kilometers of cave passages, including several other deep caves and a substantial extension to the end of Cheve itself (STONE et al., 2023). A high-resolution geologic quadrangle was also recently produced for the area (SGM, 2014). Here we provide a preliminary report of an ongoing project to understand the speleogenesis and tectonic context of Sistema Cheve. We focus on the region near the current terminus of the cave, where complex interacting faults have influenced the development of the system.

2. Geologic framework

Cheve Cave System is located in southern Mexico in the Sierra de Juárez in the state of Oaxaca. The cave is developed in a calcareous rock sequence that belongs to the Zongolica basin near the boundary between the basin and the Sierra de Juárez Metamorphic Complex (SJMC). The SJMC is a polymetamorphic crystalline basement block that hosts rocks from the Precambrian to the Mesozoic, which outcrops in a 15 km wide and 60 km long belt oriented NNW–SSE. (Alaniz-Álvarez et al., 1994, Espejo-Bautista et al., 2022). This belt is mostly composed of mylonitic rocks with different protoliths such as pelitic gneiss with abundant biotite, orthogneiss with blue quartz, marble, meta-anorthosite, and mafic orthogneiss. In addition, metagranites, migmatites, metagabbros, and metavolcanic rocks have been described as part of the complex (Ángeles-Moreno, 2006; Espejo-Bautista et al., 2022). The western boundary of the SJMC block is the Oaxaca Fault, a major lithospheric structure, while the eastern boundary is the Siempre Viva Fault (Centeno-García, 1988; Alaniz-Álvarez et al., 1996).

The Zongolica basin stratigraphy includes the Tepexilotla, Xonamanca, Tamaulipas Inferior, Calpolucán, Tamaulipas Superior, Orizaba, Maltrata, Tecamalucan, and Guzmantla formations (Ortuño-Arzate et al., 2003). The Upper Jurassic-Upper Cretaceous marine sedimentary sequence is composed principally of limestone, calcareous shale, dolomite, shale, siltstone, and tuffs exposed in the Sierra de Zongolica and Sierra de Juárez (Ortuño-Arzate et al., 2003). These units grade laterally into reef facies toward the Cordoba platform (Nieto-Samaniego et al., 2006).

The Berriasian-Valanginian Xonamanca Formation, which according to the Servicio Geológico Mexicano constitutes the principal host rock of the Cheve Karst System (SGM, 2014, Figure 1), is mainly composed of limestones, clayey limestone, calcareous sandstone, and calcareous shale. The reported thickness of this unit varies between 250 to 1400 m (PEMEX, 1988; Ortega-González and Lambarria-Silva, 1991), and the sedimentary environment has been interpreted as shallow marine (González-Ramos et al., 1997).

The sedimentary rocks of the study area belong to the southern part of the Mexican Orogen (Fitz-Díaz et al., 2018), a fold-thrust belt developed during the Late Cretaceous to Early Paleogene. The deformation was transferred from the Zongolica Basin to the Cordoba Platform and ultimately to the Veracruz Basin in the Paleogene (Ortuño-Arzate et al., 2003).

3. Materials and methods

This study conducted detailed fieldwork on well-exposed outcrops to update the geologic map, focusing on the distribution of rock assemblages, geological contacts, and structures such as faults and folds. Structural measurements were taken on the surface and within the cave, collecting data for bedding (S0), foliations (S1 and S2), fractures, and faults. Dominant structural patterns were identified by comparing the orientations of major and minor geological structures with the cave conduit orientation. Structural data were processed in Stereonet software.

Cave surveying followed standard mapping techniques. Data were collected using a DistoX2 device and the TopoDroid app (Android). Data reduction and plotting were performed in Walls v2 B8 software.

4. Results

4.1. Description of the Local Geology

The Cheve Karst System is located in southern Mexico (Figure 1a). In this region, a fold and thrust belt forms the Sierra Mazateca, extending northwestward to the Sierra Negra in Puebla and the Sierra de Zongolica in Veracruz. Its main characteristic is the generation of highly deformed zones that create folds bounded by thrusts that transport the hanging wall to the east, supported by lateral fault systems, which are transfer faults that dislocate blocks at various scales. This same region is affected by the Oaxaca Fault, oriented NNW-SSE, which has a complex deformation history of strike-slip faulting with a major reactivation of normal faulting that influences a zone several tens of kilometers.

The surface projection of the Cheve Cave system expresses a trend of 20° NW for 8 km, with a maximum width of up to 2.5 km. This same orientation is seen in J2 and Charco caves, located just 1 km to the NE of Cheve (Figure 1b). Data from geological mapping in the San Miguel Santa Flor area shows a little over 50% of the rocks where these caves are developed to be massive limestone with 1 to 4-meter-thick strata, showing evident intra-formation shear zones. In the northern sector, these rocks display intercalations of dolomitized and mylonitized limestone layers at the base. In western of the study sector these rocks are overlaid by a sequence of clayey limestone, with a thrust vergence to the east, generating frictional layer-by-layer sliding in the strata.

These rocks are further overlaid by calcareous sandstone and calcareous silt through thrust faults. From the perspective of brittle deformation, there are three main fault systems. The first is a normal fault system with N-S orientation, which brings clayey limestone into contact with limestone. In the SMSF locality, this fault is cut by the Agua Ceniza fault with dextral kinematics with NE-SW orientation, showing the same contact relationships. In the northern sector, there is a smaller system of lateral faults-oriented NW-SE that also produce lateral contacts.

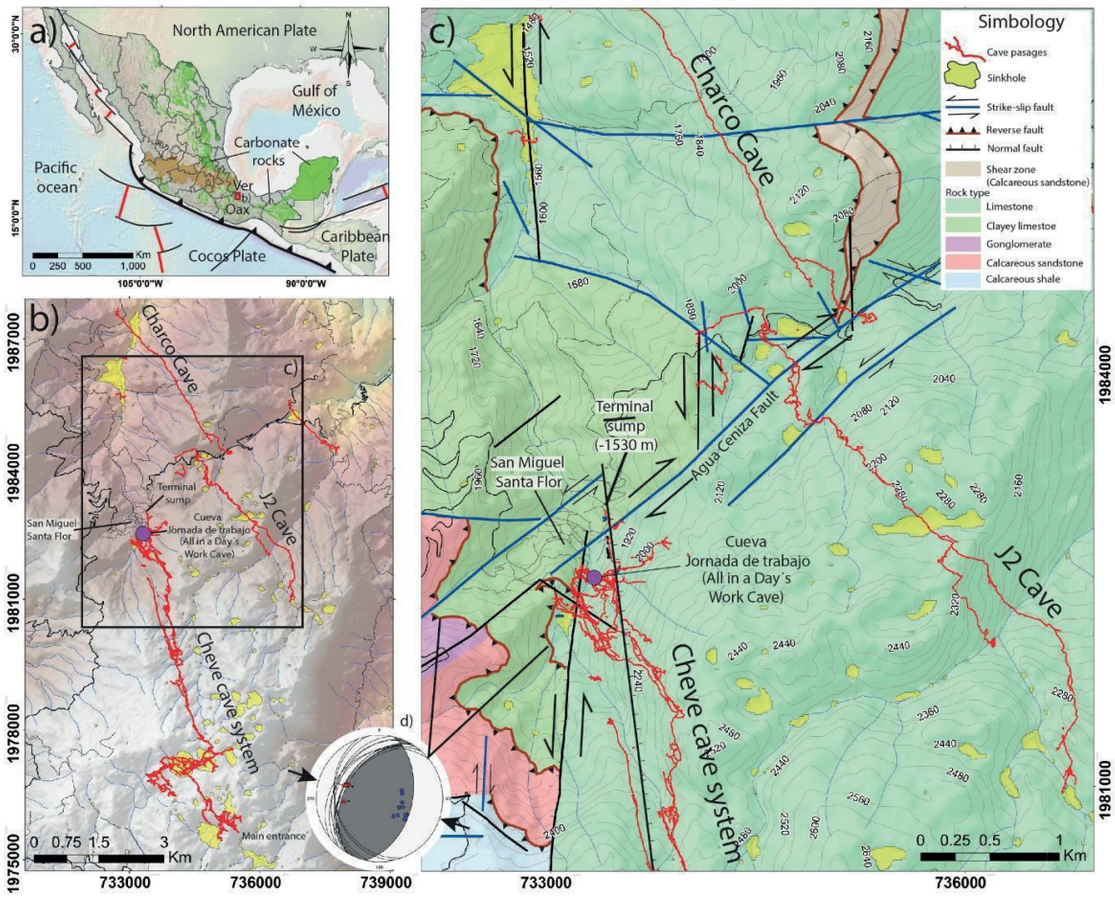

Figure 1: *a) Tectonic setting of Mexico and the study area locations, b) surface projection of Cheve Cave System and its relationship with J2 and Charco Caves. C) geologic map of San Miguel Santa Flor area and d) thrust faults that shows the transport of haging wall to the E.*

4.2. Structural observations in Jornada de Trabajo Cave

The main entrance of Cheve is in the SE of the study area. However, there are several entrances to the system, including Jornada de Trabajo (All in a Day's Work Cave), which is located in the village of San Miguel Santa Flor near the current end of exploration in Cheve (Figure 1c).

Jornada de Trabajo is developed within a structural geological profile which helps us understand the geological configuration of the Cheve System.

Jornada de Trabajo features vertical shafts and narrow canyon passages along a NW-SE orientation. The internal

geology reveals four main lithologies. From the entrance to the upper SE passage, this cave has developed along the contact between massive limestone (on the ceiling) and clayey limestone (on the floor).

The thickness of the clayey limestone ranges from 30 to 50 meters, with thin and slightly folded limestone layers, mostly inclined to the NW. Below the clayey limestone, the cave cuts through 200 meters of dolomitized limestone with strata between 1 and 3 meters thick, forming tight, closed folds with vergence to the E. In the lower part of the cave, these dolomitized limestones begin to show isoclinal folding and intense deformation that generates mylonitization, which dominates down to -1530 m, where the terminal sump of the Cheve Cave system is found.

Here, the stratification remains with dips to the NW (Figures 2 a, b, c). Fracture measurements within Jornada de Trabajoshow three main families. The most dominant is E-W oriented, followed by NNW-SSE and NW-SE orientations (Figure 2d).

Furthermore, the analysis of faults reveals a dominance of normal faults-oriented NNW-SSE, with left-lateral kinematics and normal reactivation. These faults are cross-cut by a dextral fault system-oriented NE-SW and E-S (Figures 2e and f).

5. Discussion

We conducted a multiscale analysis of the main faults and fractures on the surface and compared them to structural observations and passage orientations in Jornada de Trabajo and the deepest portion of the Cheve Cave System.No To compare structures with cave passages, we consider the shear fracture arrangement proposed by PETIT (1987), oriented 20° to the NW (which coincides with the Oaxaca Fault plane) and applied to a left-lateral fault system showing the development of synthetic R and P faults, antithetic R' and P' faults, and tensional T faults (Figure 3a).

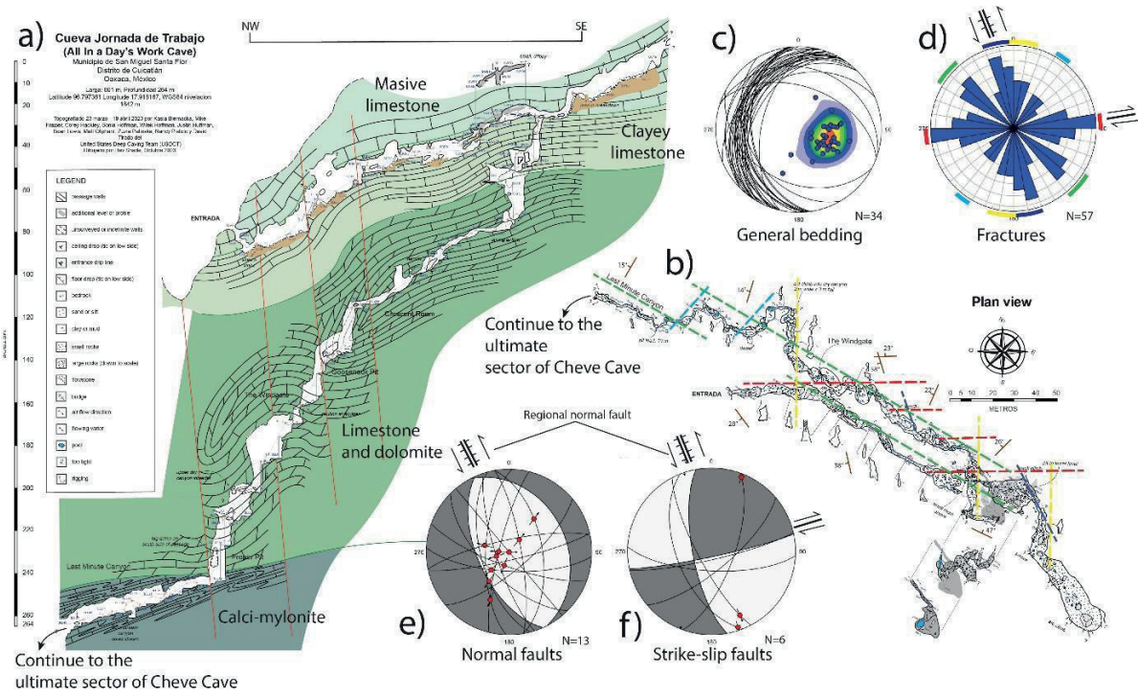

Figure 2: *a) Jornada de Trabajo Cave (All in a Day´s Work Cave) geological cross-section. b) Plan view map with structural data and main fault orientations, c) structural analysis of bedding in all passages, d) fracture date analysis, e) and f) beach -balls generated by measurements of fault planes and processes through Angelier analysis.*

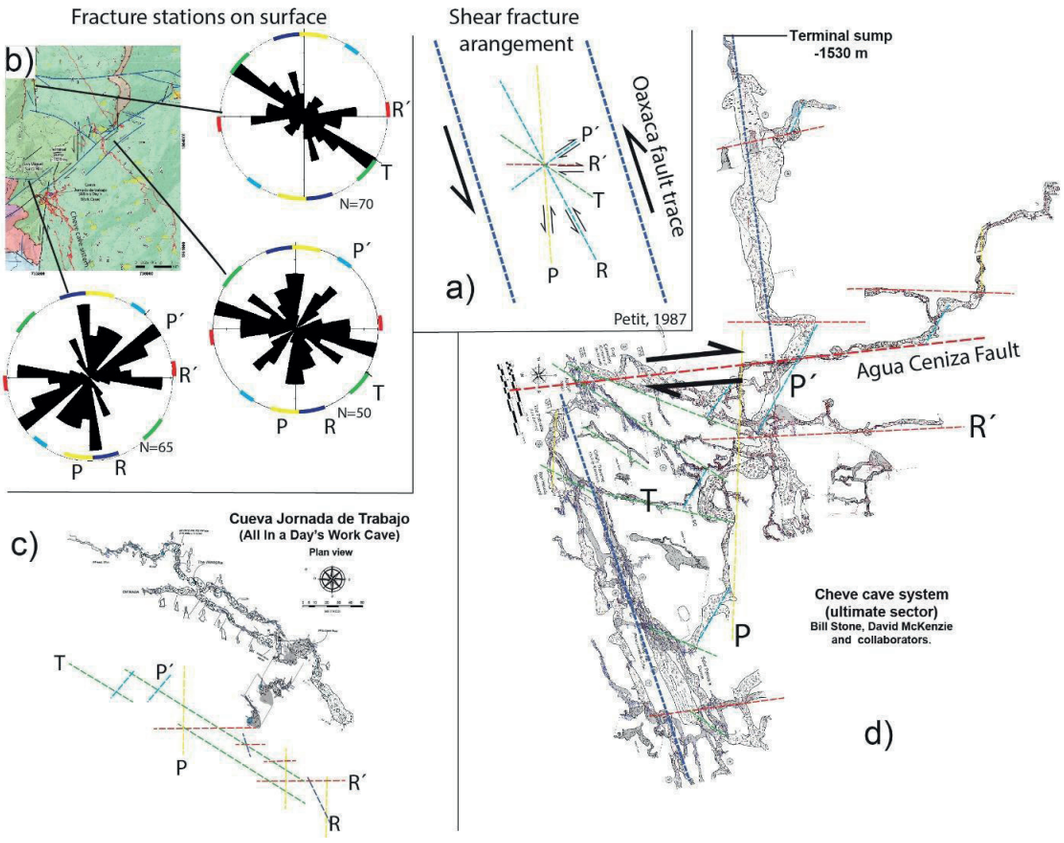

Figure 3: *Multiscale comparative analysis. a) shear fracture arrangement model sinistral fault PETIT, (1987). b) Surface fracture analysis, c) Jornada de Trabajo cave fracture tendencies, and d) Cheve Cave System fracture tendencies.*

The fracture data taken from the surface in the western sector show a dominance of synthetic and antithetic fractures (P, P', R, and R'). In contrast, the central and northern sectors have dominantly tensional faults (T). In Jornada de Trabajo, the main development is controlled by T faults bounded by R faults, with connections occurring in conduits associated with R', P, and P'.

6. Conclusions

The Cheve Cave System developed in an area with a complex geological-structural arrangement where folds and thrusts converge with shear zones that reach a degree of mylonitization. Subsequently, the rocks were later affected by normal fault systems-oriented NNW-SSE, NE, SW, and E-W.

The multiscale structural analysis of faults and fractures helped to define the characteristics of the deepest portion of the Cheve Cave System, which matches the surface geological map arrangements. However, the main faults divide several blocks with fracture and minor fault arrangements.

One example is the Jornada de Trabajo cave, located within a block where the main fault system is oriented NW-SE and corresponds to the tensional fault system (T). These structural and geological observations can help to define the new connections and focus human efforts in future expeditions to find new deep passages of the Cheve Cave System.

Acknowledgements

We thank Dr. Bill STONE for inviting us to work on the Cheve Cave exploration project and the 2024 expedition. Thanks to Mari and Juan, the San Miguel Santa Flor residents, for their support during the expeditions.

Thanks to Dra. Elisa Fitz Díaz from the Institute of Geology of UNAM, for support with technical equipment for the expedition.

References

ALANIZ-ALVAREZ, S.A., Nieto-Samaniego, A.F., Ortega-Gutiérrez, F. (1994). Structural evolution of the Sierra Juárez Mylonitic Complex, state of Oaxaca, Mexico. Revista Mexicana de Ciencias Geológicas, 11(2): 147–156.

ALANIZ-ALVAREZ, S. A., van der Heyden, P., Samaniego, A. F. N., & Ortega-Gutiérrez, F. (1996). Radiometric and kinematic evidence for Middle Jurassic strike-slip faulting in southern Mexico related to the opening of the Gulf of Mexico. Geology, 24(5): 443-446.

ÁNGELES-MORENO, E. (2006). Petrografía, geología estructural y geocronología del borde noroccidental del terreno Cuicateco, sierra Mazateca, estado de Oaxaca. [Ms. Thesis]. Universidad Nacional Autónoma de México.

CENTENO-GARCÍA, E. (1988). Evolución estructural de la Falla de Oaxaca durante el Cenozoico. [Ms. Thesis]. Universidad Nacional Autónoma de México.

ESPEJO-BAUTISTA, G., Ortega-Gutiérrez, F., Solari, L. A., Maldonado, R., & Valencia-Morales, Y. T. (2022). The Sierra de Juárez Complex: a new Gondwanan Neoproterozoic-early Palaeozoic metamorphic terrane in southern Mexico. International Geology Review, 64(5): 631-653.

FITZ-DIAZ, E., Lawton, T. F., Juárez-Arriaga, E., & Chávez-Cabello, G. (2018). The Cretaceous-Paleogene Mexican orogen: Structure, basin development, magmatism and tectonics. Earth-Science Reviews, 183, 56-84.

GONZÁLEZ-RAMOS, A., Arceo-Cabrilla Francisco Armando, González-Ramos, A. (1997). Carta geológico-minera Oaxaca E14-9 escala 1:250,000 estado de Oaxaca.

HOSE, L. D. (1995). World's deepest karst hydrologic system documented in Sierra Juárez, Oaxaca, Revista Mexicana de Ciencias Geológicas, 12 (1): 108-111.

NIETO-SAMANIEGO, A. F., Alaniz-Álvarez, S. A., Silva-Romo, G., Eguiza-Castro, M. H., & Mendoza-Rosales, C. C. (2006). Latest Cretaceous to Miocene deformation events in the eastern Sierra Madre del Sur, Mexico, inferred from the geometry and age of major structures. Geological Society of America Bulletin, 118(1-2): 238-252.

ORTEGA-GONZÁLEZ, J. V, and LAMBARRIA-SILVA, C. (1991). Informe geológico del prospecto Hoja Oaxaca. Coordinación Divisional de Exploración, Gerencia de Exploración Región Sur, Subgerencia de Geología superficial y Geoquímica.

ORTUÑO-ARZATE, S., H. Ferket, M. C. Cacas, R. Swennen, and F. Roure (2003). Late Cretaceous carbonate reservoirs in the Cordoba Platform and Veracruz Basin, eastern Mexico, in C. Bartolini, R. T. Buffler, and J. Blickwede, eds., The Circum-Gulf of Mexico and the Caribbean: Hydrocarbon habitats, basin formation, and plate tectonics: AAPG Memoir, 79: 476– 514.

PEMEX, Petróleos Mexicanos (1988). Estratigrafía de la República Mexicana, Cenozoico. Subdirección de Producción Primaria, Coordinación Ejecutiva de Exploración, 136 p.

SERVICIO GEOLOGICO MEXICANO (2014). Carta geológico-Minera Cuicatlán E14-D17. Scale 1:50:000.

SMITH, J.H., (1991). Hydrogeology of the Sierra Juárez, Oaxaca, Mexico. AMCS Activities Newsletter, 18: 82–87.

SMITH, J.H. (2002). Hydrogeology of the Sistema Huautla Karst Groundwater Basin, AMCS Bulletin 9: pp 156.

STONE, B., SHADE, B., and J. TOLES, eds. (2023). Sistema Cheve, Oaxaca, Mexico - Reporte de la Expedición 2023. https://www.usdct.org/downloads/2023_Cheve_Expedition_Book.pdf.

Thoughts about dispersion in karst – a bit too late

Sid Jones (1)

(1) University of Tennessee Knoxville, sjones5@utk.edu

Abstract

Groundwater tracing studies are fundamental to karst hydrology, but the type of information that might be used to better understand subsurface mass transfer processes in karst settings is usually collected only at springs. Tracer recovery data at springs can often be fit reasonably well to analytical solutions of the advection dispersion equation or to transient storage models, but there is usually little opportunity to check the degree to which assumptions inherent in such models are valid. Dispersion coefficients derived from fitting tracer recovery curves to these models depend on many parameters, including the scale of the test. Dispersion may be less than anticipated when groundwater velocities are unexpectedly high, when mass transfer between flowing water and stagnant zones is minimal, and when tracer is released directly into a cave stream or in other situations where hold-up and loss of tracer mass during the injection is negligible. In such cases, peak concentrations of tracer at points of groundwater discharge may be higher than desirable, as happened during a dye study with fluorescein from Helm's Deep Cave to Boiling Spring in Perry County, Tennessee in 2024.

1. Introduction

A practical reason to develop a better understanding of dispersion in groundwater in karst areas is to aid in the design of tracer tests that avoid high concentrations of fluorescent dyes or other tracers at springs used for water supply. Although tracer tests are commonly used to study karstic flow régimes, dispersion in groundwater in karst environments has been less studied than dispersion in surface streams or in porous media. With a few exceptions (DEWAIDE et al., 2016) tracer recovery data are available only at springs or other points where groundwater discharges to the surface. Even the channel geometry and velocity distribution are usually unknown over much of the flow path. Consequently, there is less information available to quantify the relative importance of processes responsible for dispersion and to study the spatial distribution of parameters used to describe dispersion quantitatively.

Some studies have nevertheless provided a basis for understanding solute transport processes affecting dispersion in groundwater in karst environments. Dispersion in karst conduits was described and analyzed in work by MULL et al. (1988). Quantitative tracer tests from the same sinking stream to a spring were repeated under different hydrologic conditions, and the authors observed that the coefficient of dispersion and normalized peak dye load increased with discharge, while the normalized peak concentration decreased with discharge.

More recent studies have provided a framework for understanding the effects of tracer hold-up in the source, in pools, or in zones of relatively stagnant water adjacent to active flow zones. To better account for skewed tracer recovery curves, models incorporating transient storage of solute in zones of relatively stagnant water were introduced by FIELD & PINSKY (2000). More recently, GOEPPERT & GOLDSCHEIDER (2019) have studied dispersion of particles during transport in a karst setting. JONES (2013) pointed out that minimal holdup of tracer in pools or in wells at the source of tracer injection can potentially change the characteristics of recovery curves when groundwater velocities are very rapid.

The equations for nonequilibrium solute transport in porous media are essentially identical to those for tracer migration in karst flow systems with transient storage zones (FIELD & PINSKY, 2000), so time constants defined for transport in porous media are applicable in the analogous karst flow regime. Thus, the characteristic time for advection (convection), τ_a, is x/v, where x is the distance from the point where tracer is introduced, and v is the velocity of the flowing water. The characteristic time for dispersion, τ_d, is D/v^2 where D is the coefficient of dispersion. Note that this time constant for dispersion is related to the time constant for advection by $\tau_d = \tau_a/P$ where P is the dimensionless Peclet number, vx/D. The Peclet number is a ratio of the parameter controlling the rate of advection (v) to parameters controlling the magnitude of dispersion (D/x).

SARDIN et al. (1991) compare the relative effects due to mass transfer of solute migrating into adjacent stagnant water to those due to convective and dispersive processes in flow through porous media. They show that transient storage becomes the dominant process for broadening the residence time distribution of a tracer when a characteristic time constant for exchange between mobile and immobile regions exceeds τ_d.

JEANNIN & MARECHAL (1997) discuss the effects of pools on tailing of dye recovery curves. JONES (2013) showed that holdup in an area where tracer is introduced may contribute significantly to the subsequent spread when the residence time at this source, τ_s, becomes greater than τ_d. This should be anticipated since at a distance x when $\tau_d = \tau_a$, tracer has migrated far enough for the Peclet number to reach unity, corresponding to the time when driving forces for advective transport should, in theory, become the dominant mass transfer process. When the residence time in the source is less than the time constant for dispersion, dispersive processes spread the tracer more than the delay in release from the source. As holdup time in the source becomes larger than τd, the delayed release from the source contributes relatively more to the spread of the advected tracer than dispersive processes.

2. Peclet numbers and the effects of scale

The studies cited above are primarily theoretical in nature, presenting only a few data sets to demonstrate applications of the theory. While they provide insight into processes that may contribute to dispersion, they do not provide adequate data to assess the effects of scale on dispersion in

a variety of karst environments. Some generalizations may be possible, however, using the limited data from many tracer tests performed over a wide range of distances and times. When holdup in regions with very large residence times or exchange with stagnant zones does not significantly alter the characteristics of tracer dispersion, the unidimensional advection-dispersion equation (ADE) may provide an adequate approximation for modeling the transport of solute. Assuming an instantaneous injection of a conservative tracer into a flow field with constant velocity v and no transient storage or permanent losses, a convenient form of the solution to the advection dispersion equation is given by:

$$\frac{C(x,t)}{M} = \frac{v\ exp\left[-\frac{1}{4Dt}(x-vt)^2\right]}{2Q(\pi Dt)^{1/2}} \quad \text{Equation 1}$$

Equation 1 is in the form of the solution where C (*x, t*) is given as the tracer concentration in the resident fluid as defined by KREFT & ZUBER (1978), modified only by using the ratio of the discharge to the mean fluid velocity, *Q/v*, for the cross-sectional area of the flow field. It is worth noting that others GOEPPERT & GOLDSCHEIDER (2008) used a form of the solution to the ADE based on concentration as measured in the fluid flux for both injection and detection. Given the various methods used for tracer introduction into groundwater used in karst studies and the possibility of significant mixing in springs prior to sampling, there would not appear to be an obvious preferred choice among the various equations presented by KREFT & ZUBER. Fortunately, for tracer transport dominated by advection, as is typical in karst conduits, the differences between models should not usually result in significant differences in the calculation of the dispersion coefficient.

Equation (1) was used by HAUNS et al. (2001) to estimate dispersion coefficients from recovery curves collected at several locations in a cave stream for over 1 kilometer downstream of the point where tracer was introduced. In their study, dispersion coefficients increase with distance traveled downstream by the tracer, as would be anticipated from what is known about solute transport in streams. JEANNIN & MARECHAL (1997) presented a larger data set from studies in the same cave stream and showed that dispersivity, defined as the dispersion coefficient divided by the velocity, also increases with distance traveled. However, any dependence of the Peclet number on either distance traveled or average velocity of the stream was less obvious.

WORTHINGTON & SMART (2016) published empirical equations based on over two hundred tests for predicting the ratio of the injected mass of tracer to the peak concentration of tracer. They find the form of the equation with the best fit to the data for traces from sinking streams to springs is:

$$\frac{M}{C_{peak}} = .76\left(Qt_{peak}\right)^{.99} \quad \text{Equation 2}$$

Here C_{peak} is the peak concentration and t_{peak} is the elapsed time corresponding to the peak concentration. Note that the exponent in Equation 2 is almost unity, so

$$\frac{C_{peak}}{M} \cong 1.3\left(Qt_{peak}\right).^{-1} \quad \text{Equation 3}$$

When the approximation $t_{peak} = \tau_a$, = x/v is valid, the exponential in Equation 1 reduces to unity. As pointed out long ago by LEVENSPIEL & SMITH (1957),

$$t_{peak} \cong \tau_a\ (\ 1 - P^{-1} + \tfrac{1}{2}\ P^{-2} + O(P^{-4})\ ) \quad \text{Equation 4}$$

so $t_{peak} \approx \tau_a$ when *P* is large, and

$$\frac{C_{peak}}{M} \approx \frac{v}{2Q\left(\pi Dt_{peak}\right)^{1/2}} \approx 1.3\left(\frac{1}{Qt_{peak}}\right) \quad \text{Equation 5}$$

Then since $t_{peak} \approx$ x/v for large Peclet numbers, this equation yields P ≈ 22. While this approximation is crude, it is based on much more data than individual Peclet numbers published in studies that analyze results from a single trace or a few traces. The result suggests that the dispersion coefficient scales linearly with distance and with the mean flow velocity. Peclet numbers calculated from the results given by MULL et al. (1988) show no clear trend with hydrologic conditions, but all exceed 100 and vary by over a factor of two. Results from eight traces with lithium injected under different hydrologic conditions in two swallow holes draining to well-developed karst systems and discharging at single springs yield Peclet numbers that average about 65 but vary over an order of magnitude (MORALES et al., 2010). Plots of the data used for regression analysis by WORTHINGTON & SMART (2016) confirm two orders of magnitude in the relative efficacy of dispersion processes during solute transport in karst groundwater might be anticipated, even when tracer is introduced only into sinking streams and recovered at springs.

3. Possible reasons for variation in dispersion in tracer tests in karst

As discussed in the previous section, dispersion coefficients in karst apparently depend on the scale of the test and vary with hydrologic conditions. Peak tracer concentrations at a point of groundwater discharge may be unexpectedly high when transit times are shorter than expected and/or the tracer disperses less than anticipated. This is most likely to occur when the tracer is introduced directly into a sinking or subsurface stream that contributes a significant percentage of the water at the point of discharge. Depending on the number of results included in the computation, Peclet numbers taken from the various studies cited above where tracer was introduced under such conditions average between 150 and 200, an order of magnitude larger than the Peclet number deduced from the data used for predicting peak concentration. Moreover, most of these Peclet numbers were computed based on the straight-line distance between the point of tracer introduction and the point of tracer recovery. If the actual path is more tortuous, the Peclet number based on the true distance travelled by the tracer will be larger by a factor of the path tortuosity squared.

Given the large Peclet numbers that seem to characterize tracer transport through the major conduits of a karst aquifer, the corresponding time constant for dispersion, τ_d, in these conduits would be two orders of magnitude less than the travel time to reach the peak concentration. If τ_a or t_{peak} is from a day to a week, as might be expected for traces on the scale of one to ten kilometers, τd would be expected to be a few minutes to an hour. At these high Peclet numbers, the hold-up of tracer in a source might be expected to noticeably affect the shape of the recovery curve when the residence time in the source reaches about five times τ_d (JONES, 2013). If t_{peak} is a day or two, a delay of an hour or two in reaching a major conduit due to migration through the vadose zone could be sufficient to add to the spread of tracer, increasing the apparent value of the dispersion coefficient, even when tracer was introduced into a sinking stream.

Unless information is available to allow detailed characterization of the flow path, it may be optimistic to characterize dispersive contributions to solute transport in karst settings for even an individual tracer test with a single dispersion coefficient. The use of advection-dispersion models or nonequilibrium models that assume instantaneous injection at the source may not be appropriate except when tracer is introduced directly into a cave stream or into a sinking stream that conveys most of the tracer to a major stream conduit within times that are small compared to the time to peak concentration. Empirical equations for estimating tracer mass

that are developed using results from tests where tracer must migrate for some time before reaching a master conduit may overestimate the mass needed to produce the desired peak concentration when tracer is injected directly into a cave stream.

There are additional reasons why dispersion might be lower in some cases than would be predicted from equations derived from a large data set. For a given travel time, peak concentration normalized by the mass of injected tracer in surface streams appears to increase with discharge (JOBSON, 1996). The results of MORALES et al. (2010) indicate that Peclet numbers in karst groundwater increase with the mean groundwater velocity. Higher discharge should correspond to less tracer mass lost in stagnant regions of the flow field in most cases. One might expect if the velocity along the flow path remains consistently high and very little exchange with transient storage zones takes place, dispersive processes may be relatively smaller when compared with advective transport.

4. Examples

In the experience of the author and anecdotally from the stories of others, most examples where peak tracer concentrations at a spring were much lower than anticipated have been when there was significant tracer hold-up at the source or somewhere along the flow path. Peak concentrations significantly higher than those predicted by empirical equations such as equation 12 of WORTHINGTON & SMART have been observed when there was no indication of significant tracer hold-up during injection and when groundwater velocities were unexpectedly high. Sometimes rapid velocities might have been anticipated because gradients along potential flow paths from the injection point were steep. In some cases, however, it seems that the tracer may be migrating through conduits that are more hydraulically efficient, resulting in rapid velocities under lower gradients. Dye recovery curves at two springs in Tennessee where the tracer migrated with little dispersion are presented in Figures 1 and 2. Here, the gradient inferred from estimates of the elevation change between the dye injection points and the springs is low. Both springs discharge under artesian pressure, as implied by the names given to them locally, the Boils in Jackson County and Boiling Spring in Perry County. Discharge at the Boils was about 4 cubic meters per second and discharge at Boiling Spring was about 0.5 cubic meters per second during dye recovery. The Boils is a single large rise pool with an average discharge of about 2.5 cubic meters per second and is one of Tennessee's largest springs. Tracing at the Boils took place in October of 2015 shortly after a rain event, with about 300 grams of fluorescein dye introduced into a swallow hole 1.5 kilometers upstream on Roaring River.

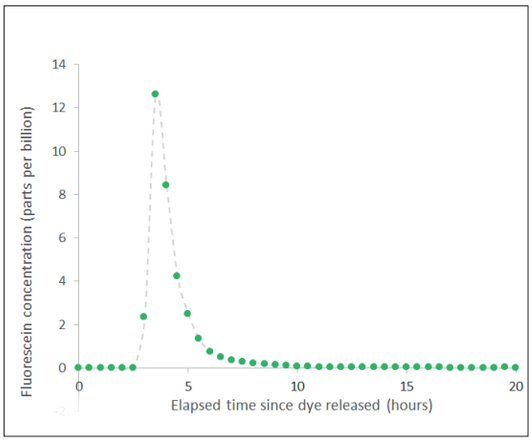

Figure 1 : *Dye released at swallow hole on Roaring River, recovered at the Boils, Jackson County, Tennessee.*

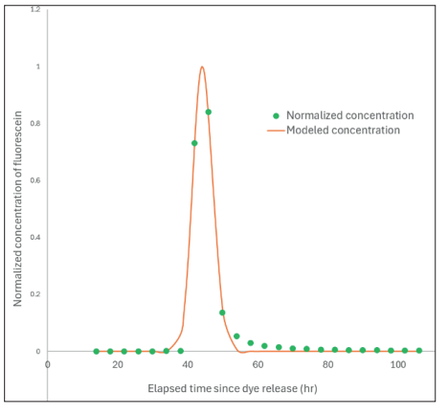

Figure 2 : *Dye released in Helm's Deep Cave stream, recovered at Boiling Spring, Perry County, Tennessee.*

Peak concentration of fluorescein at the Boils was 13 ppb as opposed to 3 ppb predicted using equation 12 of WORTHINGTON & SMART (2016). However, much of this discrepancy was apparently due to a rapid groundwater velocity of about 0.12 meters per second. The empirical equation based on travel time rather than distance (equation 13) of the same publication predicted peak concentration to be 8 ppb.

In contrast, equation 12 predicted 0.15 ppm and equation 13 predicted 0.08 ppm for a dye trace through the Bangor Limestone on the Cumberland Plateau escarpment in Van Buren County, Tennessee. Reported peak concentrations were about 1.1 ppm, an order of magnitude greater than those predicted by either equation (EPA, 2003). The ratio of the mass of dye released (115 grams) to peak concentration (1.1 ppm) for the discharge measured at two adjacent springs where dye emerged, the distance traveled by the tracer, and the elapsed time to the peak concentration lies further below the empirical fits than any of the nearly 200 data points used by the authors for the regression analysis.

A tracing study with fluorescein dye at Boiling Spring was conducted during low flow conditions in October of 2024, and the inability to predict peak dye concentration impacted residents using the spring as a source of drinking water. The predicted peak concentration given by both empirical equations was about 30 ppb. However, the dye dispersed very little during transit to the spring, and the chosen sampling interval was too large to determine the peak concentration with accuracy. In addition, Boiling Spring has multiple orifices, and dye concentrations may not have been identical in all outlets. The overall peak concentration was clearly over 1 part per million based on visual observations of Hurricane Creek, which at the time of the dye trace, was fed exclusively by Boiling Spring. Unfortunately, several residents using the water that discharged from Boiling Spring as a source of drinking water discovered green color in their water supply, as shown in Figure 3. They discontinued use of water until the dye cloud had passed and explanations were offered.

To adequately fit the sparse data on the recovery curve in Figure 2 to Equation 1, it was necessary to assume a Peclet number of about 500, but the mean velocity based on the time constant for advection was only about 0.03 meters per second. It appears that the 5-kilometer

flow path from the cave stream to the spring provided little opportunity for dispersion even though the average groundwater velocity was not significantly higher than was anticipated.

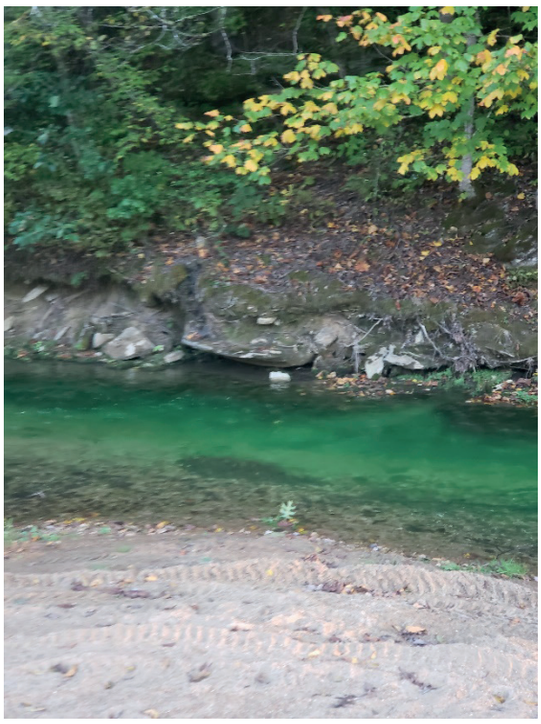

Figure 3 : *Visible fluorescein in Hurricane Creek.*

In retrospect, both discharge measurements and water chemistry in the cave stream and at the spring might have alerted those planning the tracer test to the possibility that peak dye concentrations at the spring could be in the visible range. The discharge in the cave stream was over 80 percent of the total discharge from the spring group during dye recovery, so the dye was evidently released directly into the main conduit providing water to the spring. Major ion concentrations in water discharged at the two largest springs in the Boiling Spring group were very similar to those in the cave stream. Despite the water in the cave stream being far from saturation with respect to calcite and dolomite, total dissolved solids increased by only about 10 ppm from the cave stream to the springs, indicating very little opportunity for mass transfer between mobile fluid and groundwater with a longer residence time.

Karstification at Helm's Deep Cave, now over 100 kilometers in length, is concentrated at the unconformity between the lower Mississippian age Fort Payne formation and underlying Silurian age carbonates. There is no written record of previous tracer tests in this geologic setting. Water chemistry at all major springs in the area that are developed on this unconformity or in the underlying Silurian limestones appears similar to chemistry at Boiling Spring. There appears to be much less seasonal and event driven variability in both flow and water chemistry at these springs, and swallow holes or sinkholes in the Fort Payne formation that overlies the known caves and springs in the Silurian limestones are conspicuously absent. During baseflow conditions, concentrations of major ions in these springs are typically

less than half the value of major ions in springs issuing from other Tennessee limestones. Thus, both geomorphology and water chemistry suggest that other karst springs in these rocks might be recharged similarly to Boiling Spring. Transit of dye along major conduits to these spring could occur with minimal dispersion, leading to unacceptably high dye concentrations at the spring.

5. Conclusion

Dispersion in groundwater in karst environments is a function of many variables, complicating the design of tracer tests. In general, the groundwater flow paths cannot be anticipated, and except in the rare case where tracing occurs in an accessible cave stream, the geometry of the flow field is unknown. Such constraints on information limit the use of physically based models for planning tracer studies. Empirical equations have been developed from past tracing studies that can provide guidance on one critical aspect of the design, the mass of tracer. However, they should be used with caution in situations where concentrations in a groundwater discharge need to remain beneath some threshold value. Less mass might be used if tracer is to be released directly into a major conduit providing flow to a spring or groundwater velocities are likely to be more rapid than those typical for karst. Other clues, such as artesian conditions at springs indicative of pipe-full conditions along some flow paths or spring water chemistry suggesting little exchange or mixing with groundwater having a longer residence time than that in the major conduits, should be considered when selecting the tracer mass to be used.

Acknowledgments

Many thanks to Audrey Patterson and Annette Engel of the University of Tennessee for chemical analyses on water from Helm's Deep Cave and nearby springs. Thanks to Steve Anderson for sharing the fluorescein analyses for tracing we did at the Boils.

References

DEWAIDE L., BONNIVER I., ROCHEZ G., HALLET V. (2016) Solute transport in heterogeneous karst systems: Dimensioning and estimation of the transport parameters via multi-sampling tracer-tests modelling using the OTIS (One-dimensional Transport with Inflow and Storage) program. Journal of Hydrology 534:567-578.

FIELD M.S., PINSKY P.F. (2000) A two-region non-equilibrium model for solute transport in solution conduits in karstic aquifers. Journal of Contaminant Hydrology 44:329-351.

GOEPPERT N., GOLDSCHEIDER N. (2019) Improved understanding of particle transport in karst groundwater using natural sediment as tracer. Water Research 166:1-10.

GOEPPERT N., GOLDSCHEIDER N. (2008) Solute and colloid transport in karst conduits under low- and high-flow conditions. Groundwater 46 (1):61-68.

HAUNS M., JEANNIN P.-Y., ATTEIA O. (2001) Dispersion, retardation and scale effect in tracer breakthrough curves in karst conduits. Journal of Hydrology 241 (3-4):177-193

JEANNIN P.-Y., MARECHAL J.-C. (1997) Dispersion and tailing of tracer plumes in a karstic system (Milandre, JU, Switzerland). Proceedings of the 12th International Congress of Speleology, La Chaux-de-Fonds,

Switzerland. 2:149-152.

JOBSON H.E. (1996) Prediction of traveltime and longitudinal dispersion in rivers and streams. Water-Resource Investigations Rep. 96-4013, US Geological Survey, Reston, Virginia

JONES S. (2013) Analytical models to describe the effects of tracer mixing before and after advection and dispersion. Proceedings of the 16th International Congress of Speleology, Brno, Czech Republic, 2:349-353.

KRERFT A., ZUBER A., Physical meaning of the dispersion equation and its solution for different initial and boundary conditions. Chemical Engineering Science 33 (11):1471-1480.

LEVENSPIEL O., SMITH W.K. (1957) Notes on the diffusion- type model for longitudinal mixing of fluids during flow. Chemical Engineering Science 6(4):227-235.

MORALES T., DE VALDERRAMA I.F., URIARTE J.A., ANTIGUEDAD I., OLAZAR M. (2007) Predicting travel times and transport characterization in karst conduits by analyzing tracer- breakthrough curves. Journal of Hydrology 334:183-198

MULL D.S., LIEBERMAN T. D., SMOOT J.I., WOOLSEY L.H. (1988) Application of dye tracing techniques for determining solute transport characteristics in ground water in karst terranes. Technical Report # EPA 904/6-88-001, U.S. Environmental Protection Agency, Atlanta, GA, 103.

SARDIN M., SCHWEICH D., LEIJ F. J., VAN GENUCHTEN M. TH. (1991) Modeling the nonequilibrium transport of linearly Interacting solutes in porous media- a review. Water Resources Research 27(9):2287-2307.

WORTHINGTON S.R.H., SMART C.C. (2016) Determination of tracer mass for effective groundwater tracer tests. Carbonates Evaporites 31:349-356.

US Environmental Protection Agency (2003) Final report of Lick Branch Dye Study, submitted to Tennessee Department of Environment and Conservation, Division of Water Pollution Control.

Polygenetic Speleogenesis and Karst Aquifer Evolution in the Southwestern Highland Rim of Tennessee. USA

Patricia Kambesis & Mykah Carden

Center for GeoEnvironmental Studies, Department of Earth, Environment and Atmospheric Sciences, Western Kentucky University, Bowling Green, Kentucky 42101 USA, pat.kambesis@wku.edu; mykah.carden118@topper.wku.edu

Abstract

The Highland Rim of Tennessee hosts karst aquifers traditionally attributed to epigene speleogenesis, where acidic meteoric water drives dissolution and permeability development. However, recent explorations in the Helms Deep cave system in Perry County, Tennessee have revealed a polygenetic karst system with both hypogene and epigene characteristics. Over 120 km of cave passages have been mapped, including a dense relict maze in the lower Fort Payne Formation and an active conduit in underlying Silurian strata. Geological mapping, mineralogical analyses, and hydrological studies indicate hypogene speleogenesis in the maze system, characterized by the presence of diadochite, jarosite, natrojarosite, and gypsum—suggesting subsurface acidity influences. In contrast, the active stream conduit exhibits linear morphology with no in-feeding side conduits, indicating epigene formation via sinking streams. The combination of these features challenges traditional models of karst development as strictly hypogene or epigene and instead supports a polygenetic model.

1. Introduction

Karst aquifers of the Highland Rim of Tennessee are thought to be products of epigene speleogenesis, where acidic meteoric water, fortified with soil CO_2, acts as the dissolutional agent in the self-organization of permeability structures. Classic karst features, such as sinking/losing streams, sinkholes, caves, and springs, are abundant in this region. The morphological characteristics of local caves suggest sinking stream and sinkhole recharge, with carbonic acid dissolution occurring along fractures and bedding planes. However, in the southwest Highland Rim, the surface karst is not as well developed as its spatial counterparts (MORAN 1980). Karst features are subtle, and the overall landscape exhibits a fluvial nature, though some caves are present.

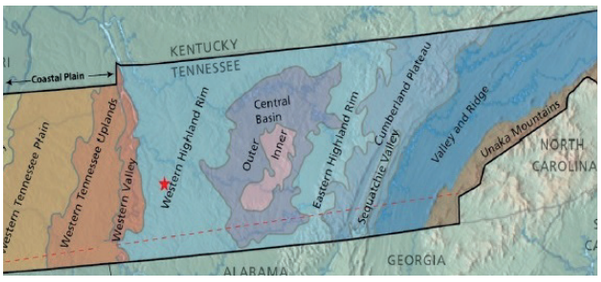

Figure 1: *Physiographic map of Tennessee with red star showing the location of Helms Deep*

A breakthrough and new surveys in a previously known cave, Helms Deep (Figure 1), revealed a relict maze of extensive proportions (120 km mapped so far), formed in the lower reaches of the Fort Payne Formation. Directly underlying the maze by 25 meters, and connected by collapse in only two sections, is an active conduit formed in upper Silurian strata. Results from cave surveys, geological mapping, mineralogical analyses, karst feature mapping, and dye tracing indicate that the maze exhibits characteristics of hypogene development (sensu stricto PALMER 2017), while the conduit is definitively epigene in origin. This combination of hypogene and epigene features challenges the traditional model of homogeneous karstic processes as either hypogene or epigene end--members in speleogenesis and instead suggests that karstification can be a polygenetic process.

2. Site and Setting descriptions

To investigate the polygenetic development of Helms Deep, a combination of geological mapping, mineralogical analysis, cave surveying, hydrogeological monitoring, and dye tracing were employed.

Site Description : Helms Deep is located in Perry County, Tennessee which is in the southwest portion of the Western Highland Rim physiographic province of Tennessee (BRADLEY 2021) (Figure 1). The difference in number of mega-kilometer caves on the Cumberland Plateau vs Perry County caves is likely due to the absence of the cave-rich upper Mississippian-age carbonate sequences common to other Tennessee karst

areas. In the southwest Highland Rim, the lower Mississippian-age Fort Payne Formation is exposed at the surface and karstification typically extends from the lower Fort Payne Formation down through Devonian to Silurian age strata (BURCHETT 1977).

Helms Deep has been known since the middle seventies and consists of a steep breakdown-strewn entrance slope formed in the Fort Payne Formation leading to a kilometer of stream passage formed in Silurian limestone. In 2020 a breakout at the unconformity separating the Mississippian from Siliurian strata revealed a dense anastomotic maze formed in the lower Fort Payne Formation. Over 120 km of cave passages have been discovered and mapped since 2020 with a vertical extent of 56 meters.

Geological Setting : Helms Deep is formed in two distinct chronostratigraphic sections. The Fort Payne Formation of lower Mississippian age is exposed at the cave entrance. However, noncomformities at the base of the Fort Payne Formation make it a challenge to determine the transition from the lower Mississippian to the Silurian strata (Figure 2). The maze section occurs within this transition zone. The maze appears to have three distinct levels: an upper “level” shale, middle level limestone, and a lower level of limestone/shale. The Chattanooga Shale which is ubiquitous in most of Tennessee appears to be missing locally but the Maury Shale is present. The stream level is formed in upper Silurian limestones.

Mineralogy: Mineralogical analyses of sediments from the maze section showed the presence of jarosite and natrojarosite (jaronite--alunite supergroup). These minerals form under acidic conditions where pyrite or other sulfides oxidize, leaving sulfuric acid that leads to local sulfuric acid speleogenesis (SAS) (EGEMEIER 1981, PALMER 1991, POLYAK & PROVENCIO 2001). Diadochite, was also detected. Though not a major speleogenetic driver, it can contribute to localized dissolution of carbonate rocks by producing sulfuric and phosphoric acids when reacting with water (HILL 1997. PALMER 2000). Gypsum is present in all levels of the maze and is associated with the oxidation of pyrite and the formation of hydrogen sulfide. Large gypsum crystals found within the muds of the lowest maze level (Mirkwood) likely formed as a result of oxidation of sulfides by calcium-rich ground water. The Fort Payne is known to contain pyrite which might contribute to local SAS.

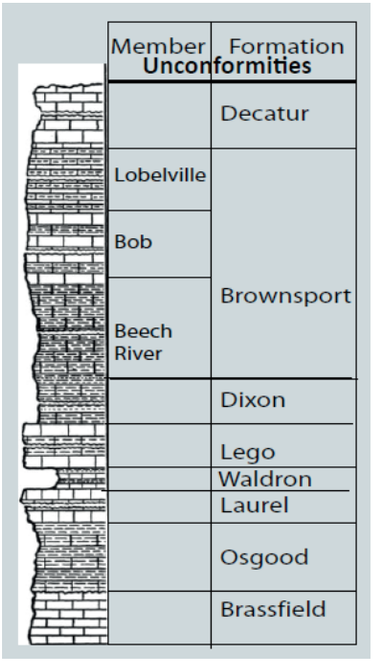

Figure 2: *Silurian Stratigraphy of Helms Deep.*

Hydrogeology: Maze section : The upper and middle maze sections of Helms Deep are relict in that they are no longer hydrogeologically active. The lowest maze level does appear to be active though points of hydrologic input are difficult to discern through the mud-coated floor. Morphologically the maze is anastomotic in pattern which is indicative of confined (phreatic) conditions where water is under pressure and dissolves limestone uniformly across a large area. Widespread dissolution forms multiple passages that grow at similar rates creating a dense complex of interconnected passages. (PALMER 1991, Gabrovšek, & Perne 2015).

Stream passage : The stream passage is a kilometer of linear conduit with no infeeders – a configuration characteristic of bedding-plane controlled conduit recharged by sinking or loosing streams (PALMER 2007). The conduit, formed in Silurian carbonates, is situated 25 meters directly below the maze complex. It is connected to the maze in only two places via breakdown. The stream rises in the floor of the passage, flows for almost a kilometer and then sinks. In 2024 dye was injected in the stream passage and was detected within 24 hours at spring resurgences located 3 km west of the cave. The recharge area is likely a series of losing streams located 5-6 km from the cave. Time series data from a logger installed in the stream shows the stream to quickly respond to precipitation events.

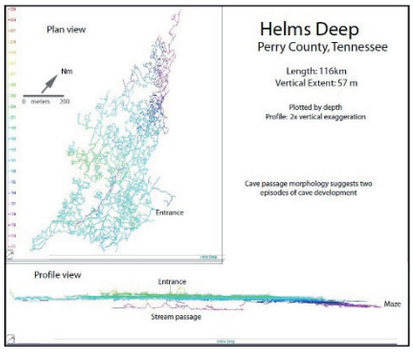

Figure 3: *Map of Helms Deep. Data from Helms Deep Project*

3. Results

The results of field and in-cave mapping, surface karst feature inventory, mineralogical analyses of sediments, morphometric analysis of passage morphology, and dye tracing, and stream monitoring suggest polygenetic (epigene and hypogene) aquifer development based on the following :

Hypogene characteristics:

a. Mineralogical occurrence of diadochite, jarosite, natrojarosite, and gypsum are all indicators of SAS acidity generated from subsurface strata. (Fort Payne Formation)

b. No obvious connection between maze level and current surface hydrology.

c. Connection to stream level by upper passage collapse in only two places

d. Anastomotic maze pattern indicative of confined phreatic hydrologic conditions

Epigene characteristics:

a. Distinct connection to the surface via loosing streams

b. Linear morphology of active stream conduit displaying no in-feeding side conduits

c. Anastomotic

d. Loosing surface streams are likely source of in-cave stream rise.

e. Discharge from spring resurgences commensurate with discharge measured in cave stream. Dye trace results pending

f. Preliminary water chemistry indicates very low conductivity – similar to that of local surface stream.

4. Discussion

To relate the findings of this study to karst aquifer evolution, we focus on the polygenetic development of karst aquifers and how both hypogene and epigene processes contribute to their formation over time. Following are key points to establish this connection.

Karst Aquifer Evolution Framework

Karst aquifers evolve through various stages influenced by geological, hydrological, and geochemical factors. The traditional models categorize karst development into epigene (surface-driven) or hypogene (geochemistry driven) processes (KLIMCHOUK 2017, PALMER 2011). This study challenges this binary classification by demonstrating polygenetic evolution, where both processes are active in different time frames and depths within the Helms Deep system. diadochite,

Hypogene Contributions to Evolution

The presence of jarosite, natrojarosite, Diadochite, and gypsum suggest past episodes of hypogene speleogenesis due to sulfuric acid. The anastomotic maze morphology, found at the unconformity between the Fort Payne Formation and Silurian strata, suggests that dissolution occurred in a confined phreatic environment with limited direct connection to surface waters. The lack of an apparent connection between the maze and modern hydrology suggests phases of isolated karstification before later integration into an epigene system.

Epigene Contributions to Evolution

The active stream passage formed in Silurian carbonates represents an ongoing epigene process, where surface-derived waters infiltrate, dissolve limestone, and contribute to aquifer recharge. The linear conduit morphology with no infeeding tributaries indicates that losing surface streams recharge the cave system, a key characteristic of epigene karst evolution. The dynamic hydrological responses, including precipitation-driven flow changes, suggest that modern karst development is driven by meteoric water.

Evolutionary Model for Helms Deep

Our study supports a multi-phase evolution model for karst aquifer development:

- *Hypogene Stage:* Speleogenesis was initiated by interstitial sulfuric acid-rich fluids that mixed with confined phreatic waters to dissolve limestone and form an anastomotic maze. Mineralogical evidence (diadochite, jarosite, natrojarosite) indicate past episodes of closed system karstification.
- *Transition Stage (Breakdown & Collapse):* Over time, tectonic adjustments and stratigraphic changes destabilized the hypogene system, leading to partial collapse and connection with shallower formations.
- *Epigene Stage (Surface Connection & Active Flow):* Karstification processes reshaped the landscape establishing losing streams that formed a single conduit system recharged by sinking and losing streams with spring resurgences that drain the system.

Implications for Karst Aquifer Evolution

Our findings reinforce that karst systems are not static but evolve through multiple speleogenetic pathways. The interaction between hypogene and epigene speleogenesis creates complex aquifer architecture, affecting groundwater storage, flow paths, and contaminant transport. Understanding this polygenetic evolution is crucial for groundwater management, resource exploitation, and predicting hydrological behavior in karst regions.

5. Conclusion

This study highlights the polygenetic nature of speleogenesis within the Helms Deep karst system, demonstrating the interplay between hypogene and epigene processes in karst aquifer evolution. Mineralogical and hydrological analyses confirm that hypogene speleogenesis, driven by sulfuric acid dissolution, contributed to the formation of an extensive anastomotic maze, while later epigene processes facilitated the development of an active stream conduit through surface water infiltration. The findings challenge traditional models that categorize karst development as either exclusively hypogene or epigene, emphasizing instead a dynamic, multi-phase evolution. This research enhances the understanding of karst hydrology, with implications for groundwater resource management, aquifer behavior prediction, and further investigations into complex karst systems.

Acknowledgments

We gratefully thank the Helms Deep Project, Tennessee Cave Survey, and Cleveland Grotto for supporting this research.

References

Bradley, M., 2021. A Summary of Karst Regions in Tennessee. US Geological Survey Karst Interest Group Proceedings, October 19–20, 2021, 19, p.18.

Burchett, C.R., 1977. Water resources of the upper Duck River basin, central Tennessee: Tennessee Division of Water Resources. Water Resources Series, (12), p.103.

Egemeier, S. J. (1981). Cavern development by thermal waters with a case study of the Black Hills, South Dakota, U.S.A. Journal of Hydrology, 54(3-4), 285–315.

Gabrovšek, F., & Perne, M. (2015). Morphology of karst conduits under different speleogenetic processes. Environmental Earth Sciences, 74, 7511–7525

Hill, C. A., & Forti, P. (1997). Cave Minerals of the World (2nd ed.). National Speleological Society

Klimchouk, A., 2017. Types and settings of hypogene karst. Hypogene karst regions and caves of the world, pp.1-39.

Moran, M.S., 1980. Aquifer Occurrence in the Fort Payne Formation ab. Groundwater, 18(2), pp.152-158.

Palmer, A. N. (2000). Hydrogeologic control of cave patterns. In Klimchouk et al. (Eds.), Speleogenesis: Evolution of Karst Aquifers (pp. 77–90). National Speleological Society.

Palmer, A.N., 2011. Distinction between epigenic and hypogenic maze caves. Geomorphology, 134(1-2), pp.9-22.

Palmer, A. N. (2007). Cave Geology. Cave Books

Palmer, A. N. (1991). Origin and morphology of limestone caves. Geological Society of America Bulletin, 103(1), 1–21.

Polyak, V. J., & Provencio, P. P. (2001). Byproduct materials related to H_2S–SO_4 speleogenesis in à karst environment. Journal of Cave and Karst Studies, 63(1), 23–32.

Seasonal Variability in the Rudice Sinkhole – Býčí skála cave system Waters

Veronika Kršková (1,2), Vít Baldík (1), Roman Hadacz (1), Eva Kryštofová (1), Jiří Faimon (1,2), Pavel Pracný (1,2), Roman Novotný (1), Jiří Nečas (1), Stanislav Lejska (3)

Czech Geological Survey, Klárov 131/3, 118 21 Praha 1, Czech Republic. veronika.krskova@geology.cz
Masaryk University, Faculty of Science, Kotlářská 267/2, 60200 Brno - Veveří, Czech Republic
Czech Hydrometerological Institute, Na Šabatce 2050/17 143 06 Praha 4-Komořany, Czech Republic

Abstract

The Rudice Sinkhole – Býčí skála cave system is the second largest cave system in the Czech Republic. The environmental impact of pollutants is a well known problem in and nearby the system. This paper is oriented on seasonal and hydrological influence on the chemical composition of Jedovnice stream. Results show a difference between vegetative and nonvegetative seasons. The highest concentration of nitrates is observed during dry periods with a low flow rate of Jedovnice stream and an increased proportion of groundwater. Phosphate concentrations are elevated near the wastewater treatment plant (WWTP), indicating anthropogenic influence. The surface sampling sites have more variable chemical composition as parameters such as agricultural activities and pollution, different hydrological conditions, and pond waters enter the system. The chemical composition of water within the karst system is more stable, with the lowest nitrate concentrations recorded in drip water, emphasizing the filtration potential of the epikarst. This study highlights the importance of an integrated approach to managing water resources in karst areas and underscores the need for further research into the impact of individual inflows on the overall chemistry of the system.

1. Introduction

The Rudice Sinkhole – Býčí skála cave system (the RS–BSC system) is the second largest cave system in the Czech Republic, with a length of 13 km. The Jedovnice stream flows through the whole system. It sinks through a ca. 110 m deep cascade system into the cave. Its groundwater tributaries are the Tipeček stream (water source for the Rudice village), Stará řeka stream, and Žegrov stream. These waters mix with other inflows and proceed to flow to the Býčí skála cave, after which they spring into the Křtiny valley. Basic karst processes are reflected in the composition of the water, based on which the complex protection of the karst areas is designed. Karst is a sensitive area because of its geological and hydrogeological features. When researching an anthropogenic influence on karst, we have to look not only at its own area but also at the area outside of karst, where most of the water flowing into the karst is infiltrated. The anthropogenic impact in the area of interest is significant (Baldík et al. 2020) and was the topic of many investigations. Extensive water sampling confirmed the presence of nitrates, phosphates and organic contaminants, let alone modern pesticides, which were not a part of this research. Alarmingly, the water quality in the drainage area of the RS–BSC system was found to be worse than in the Rudice Sinkhole streams entering the system. This finding required a detailed evaluation of all inflows into the system to identify the source of the contamination.

2. Materials and Methods

Site description

The Moravian karst is the largest karst area in the Czech Republic, covering an area of almost 92 km2, 3–6 km wide and 25 km long. It is located NE of Brno in a part of the Drahany Highlands (Balák et al., 2020). It varies between 250-550 m asl. Moravian Karst is formed by middle Devonian to lower Mississippian limestones (Carboniferous strata), overlaying Brunovistulian basement (Kadomian). The limestones were formed in two formations. Macocha formation formed by shallow-water carbonate sediments is characterized by more than 1000 m of cyclic reef and lagoonal limestone (Vilémovice and Lažánky Lms.) (Hladil, 1983). The transition from carbonate sedimentation to siliciclastic sedimentation is recorded by the younger Líšeň Fm. It comprises calciturbidites of the Hády-Říčka Lms. and more shallow-water Křtiny Lms. (Musil, 1993). This sequence is overthrust by a Variscan flysch stack (Culmian facies) represented by Viseán Rozstání nad Myslejovice Fms. The sedimentary cover originated during the Mesozoic (Jurassic), Tertiary, and Quarternary Era (Gregor, 2015).

The Moravian Karst is hydrologically divided into three parts – North, Central, and South. The area of interest, the Rudice Sinkhole – Býčí skála cave system, lies in the central part as a part of the Rudice Plateau (Fig. 1). The area was shaped during tropical weathering in the Lower Cretaceous and throughout subsequent karst cycles (Musil et al., 2020). The Plateau contains various karst forms and phenomena. Recent karst drainage is related to an underground erosional base 300-340 m above sea level. From this information, the significant thickness of the karstified limestones is evident, which allowed for the formation of deep karst depressions, massive sinkholes with underground waterfalls, and extensive cave systems with enormous chambers and tall chimneys (Baldík et al., 2021). The Jedovnický stream forms the outflow of the Olšovec pond, which probably lies on a Neogene basin. It then flows through Devonian limestones on the eastern edge of the Moravian Karst. The hydrogeological dynamics of Jedovnice Creek are notably influenced by upstream ponds.

Without an increase of mineralization, the hydrochemical water

type flowing into the Rudice Sinkhole (CaNa–HCO3SO4Cl) changes into simple Ca–HCO3 water type at the outflow from Jedovnice Stream Spring near Býčí Skála cave entrance, suggesting that the Jedovnický stream has significant underground inflow (Baldík et al. 2021).

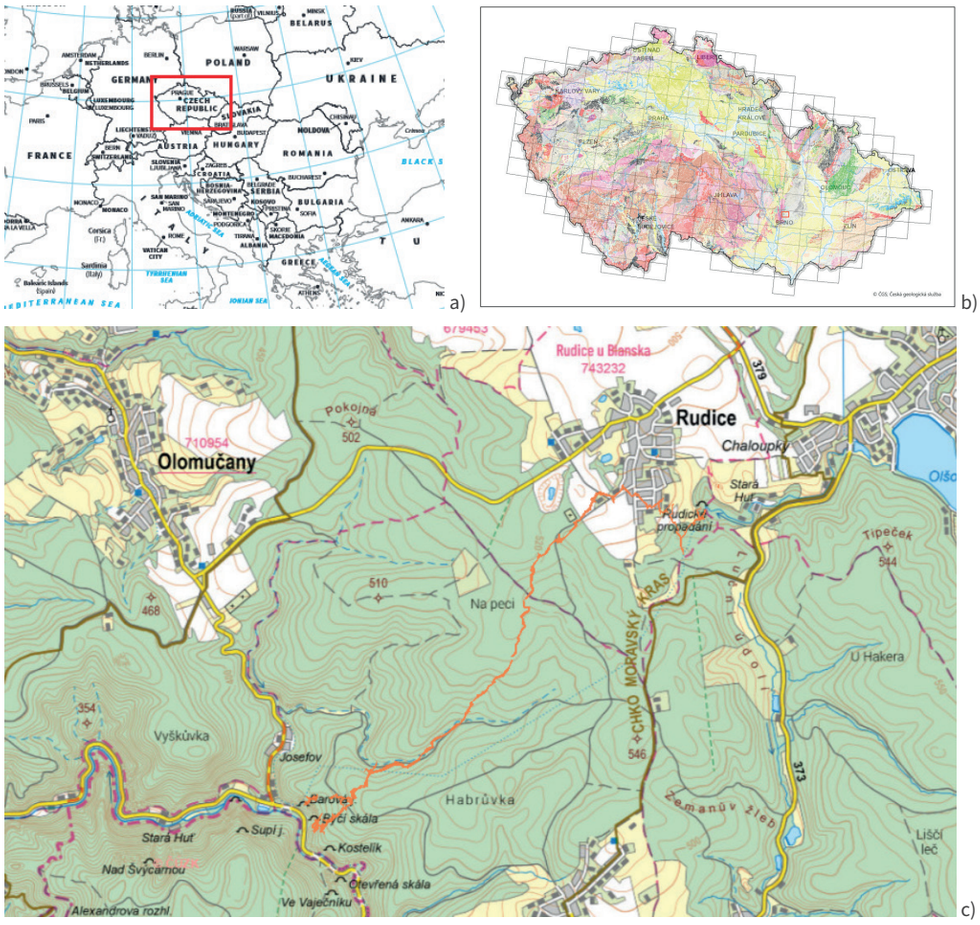

Figure 1: *Localisation of the studied area.*

Figure 2: *Sampling in Velká síň Chamber in Býčí Skála cave.*

Fig. 4 One of the sampling points

Figure 3: *Sampling of the Jedovnice Stream Spring at the end of the cave system near Býčí Skála cave entrance.*

Methods

The presented results are based on a preliminary analysis of a 2-year monitoring campaign. A basic network of 13 sampling points was established. Each site represents a specific part of the cave system, including more distant areas (such as Svážná studna cave) and samples from the direct outflow from the Jedovnice Wastewater Treatment Plant. The network connects the whole system from the Rudice Sinkhole to the Jedovnice Stream Spring, including tributaries inside the cave system (Fig. 4). Sampling was conducted monthly with a broader quarterly sampling (a total of 12 sampling events). The water samples were sent to laboratories for comprehensive physical-chemical analysis. Water samples from the outflow of the Jedovnice wastewater treatment plant

were subjected to microbiological analysis. The samples were plotted using Excel and Aquachem charts, focusing on nitrates and phosphates, which are key indicators of pollution and environmental impact on the karst system. To better interpret the data, the samples were categorized into vegetative and non-vegetative seasons, with their concentrations analyzed in relation to rainfall and flow rates.

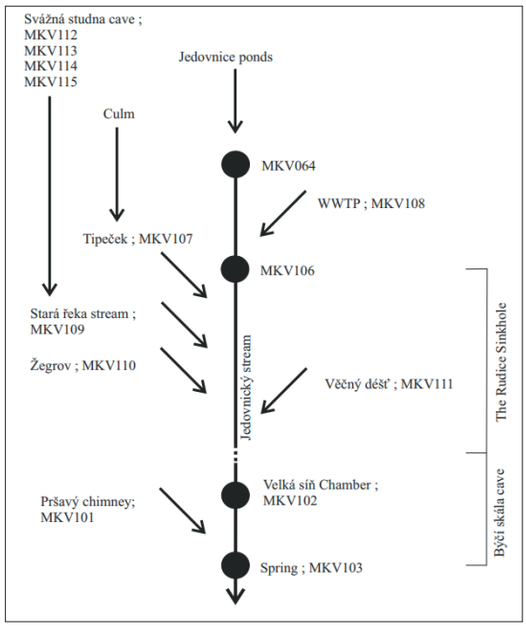

Figure 4: *Scheme of the sampling points.*

3. Results

During the non-vegetative period, an increase in nitrate concentrations was observed, with extreme values recorded primarily after periods of low flow. The highest value was recorded upstream of the wastewater treatment plant (56.8 mg/l), and the lowest in Jedovnický stream before the Rudice Sinkhole (< 3.0 mg/l). During the vegetative period, nitrate concentrations were generally lower, with maximum values (22.0 mg/l) mainly at the system's outlet (MKV 102, MKV 103 – Fig.2, Fig. 3) and the lowest before the Rudice Sinkhole (MKV 064, MKV 106). The variability of concentrations differed significantly across sampling stations. Surface flow stations (MKV064, MKV106) exhibited substantially greater variability than stations monitoring groundwater (e.g., MKV102). This difference highlights the fluctuating dynamics of nitrate concentrations based on surface and groundwater flow (Fig. 5).

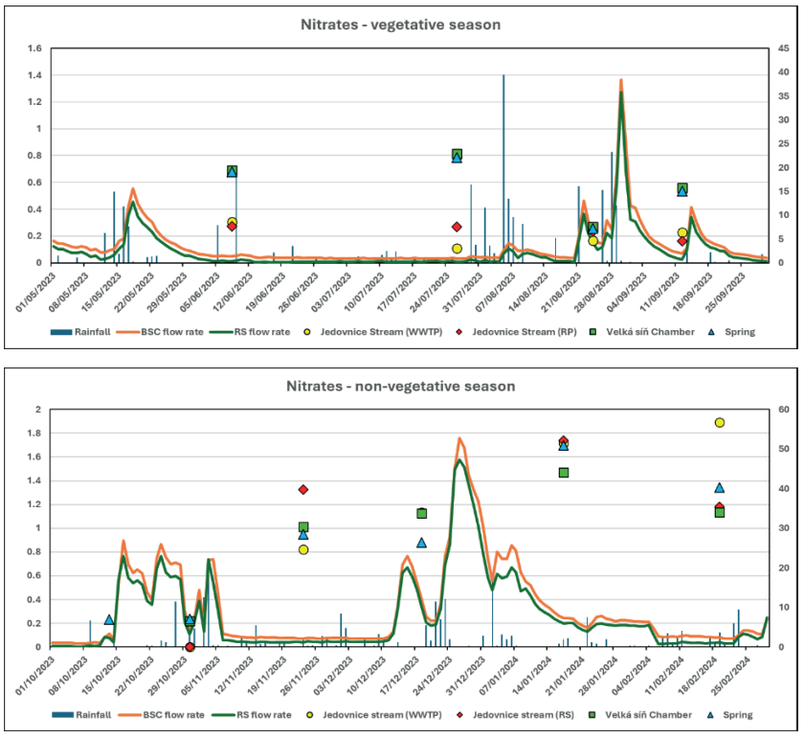

Figure 5: Concentration of nitrates during vegetative (a) and non-vegetative (b) season.

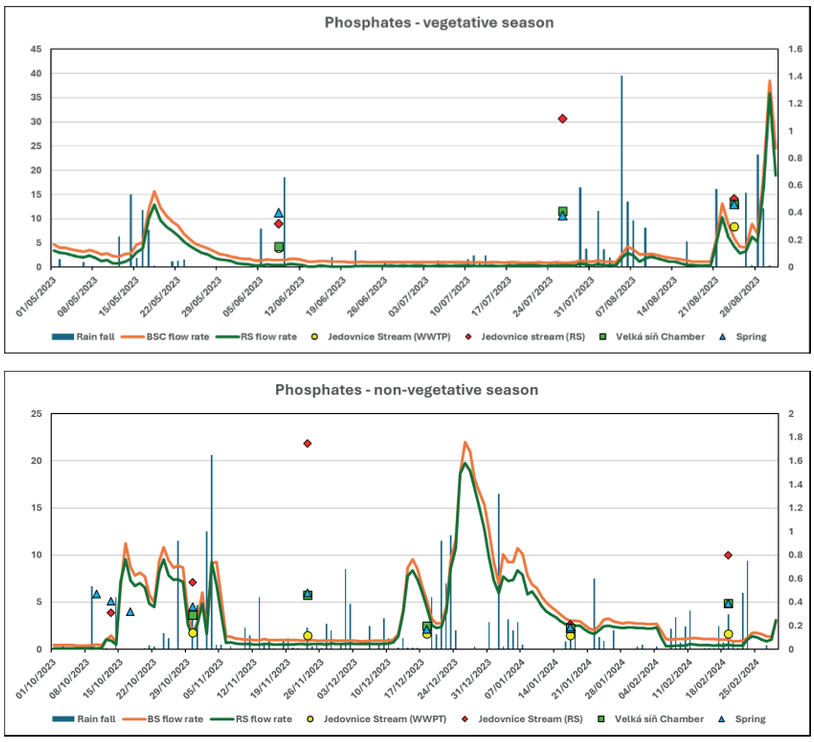

Figure 6: *Concentration of phosphates during vegetative (a) and non-vegetative (b) season*

The analysis of phosphates revealed elevated concentrations at the point where waters enter the karst system from the WWTP. Phosphate concentrations showed the most significant variability during the vegetative period (maximum 1.09 mg/l at sampling site MKV 106 and minimum 0.14 mg/l at sampling site MKV064). During the non-vegetative period, the highest phosphate concentration (1.75 mg/l) was recorded after a period of low flows, indicating the influence of hydrological conditions on phosphorus transport (Fig. 6). To better understand the chemical composition of the stream within the cave system, inflows of Jedovnický stream (Fig. 4) and drip waters (Pršavý chimney - MKV 101, and Věčný déšť drip - MKV 111) were included in the graphs. The lowest nitrate value in MKV 101 was < 3.0 mg/l, while the highest was 4.90 mg/l during the vegetative period, rising to 4.70 mg/l in February of the non-vegetative period. Phosphate concentrations never exceeded <0.05 mg/l. Among the inflows, Stará řeka stream exhibited the highest nitrate values (68.5 mg/l), which did not fall below 50 mg/l in any of the measurements. Inflows from Svážná studna cave contribute certain amounts of nitrates to the RS-BSC system, though they do not exceed 41.6 mg/l in surface water samples near Svážná studna cave.

4. Discussion

The results demonstrate the influence of seasonal factors and hydrological conditions on nitrate and phosphate concentration changes. During the cold months (non-vegetative period), nitrate concentrations increased, driven primarily by low flows, rainfall, and subsequent nitrate accumulation. Nitrate concentrations are also dependent on soil nitrogen uptake by plants, which is significantly lower during cold periods. Annual drainage of Jedovnice ponds plays a significant role in this trend, as increased flow rates dilute nitrate concentrations. Simultaneously, higher levels of microbiological contamination enter the karst system during this period.

During the vegetative period, nitrate concentrations are generally lower, with the highest concentrations measured in the system's terminal parts (Velká síň Chamber and the spring). Graphs show that waters within the karst system are more stable, whereas surface waters exhibit greater variability in nitrate concentrations. Phosphate analysis revealed elevated concentrations, mainly in the stream before the Rudice Sinkhole, attributed to WWTP discharges. The excessive loads during the summer, which is also the peak tourism season, might result from an increased equivalent population (EP) in the Jedovnice area exceeding the capacity of the WWTP.

To better understand water chemistry in the karst system, it is essential to consider inflows that chemically influence the main stream. Drip water from Pršavý Chimney and the Tipeček water source exhibited the lowest nitrate concentrations. Surface waters showed relatively high variability in concentrations, influenced by several factors, including seasonal fertilizer application, pond drainage, and WWTP discharges. Waters from Svážná studna cave, contributing to the Stará řeka stream inflow, demonstrated less variability in nitrate concentrations, except for surface samples strongly affected by anthropogenic agricultural activities. Stará řeka stream's and Žegrov›s inflows are distinctly different from other sampling sites.

Additional inflows contribute further along the RS-BSC system (between MKV 110 and MKV 102), which are more challenging to access but are assumed to impact the overall chemistry of the Jedovnice Stream's waters. These relationships will be part of the future research.

5. Conclusion

The analysis results demonstrate significant seasonal and hydrological influences on the chemical composition of Jedovnice Stream and the karst system. Elevated nitrate concentrations during the non-vegetative period indicate accumulation caused by low flows and the presumed higher proportion of groundwater. The annual drainage of Jedovnice ponds highlights the importance of hydrological regulation in influencing water quality, particularly through nitrate dilution. Conversely, it seems that nitrate concentrations are lower during the vegetative season due to increased biological activity.

Phosphates exhibit higher concentrations near the WWTP, signaling the influence of anthropogenic sources. The variability in phosphate and nitrate concentrations at surface sampling sites indicates high dynamics influenced by agricultural activities, rainfall, and WWTP discharges. Waters within the karst system have a more stable chemical composition, with the lowest nitrate concentrations recorded in drip water from Pršavý Chimney, emphasizing the filtering capacity of the epikarst.

To comprehensively understand chemical processes in this karst system, it is crucial to study inflows that significantly influence stream chemistry. These findings emphasize the need for an integrated approach to managing water resources in karst areas, particularly in the context of seasonal fluctuations and anthropogenic impacts.

Acknowledgments

Financial support through the project „Rock Environment and Natural Resource RENS" (SS02030023) is gratefully acknowledged.

References

BALÁK, I. – HOFMANN, E. – SVOBODOVÁ, H. – DURNA, R. – KOLEJKA, J. (2020): Moravský kras a okolí: Atlas pro terénní výuku a outdoorové aktivity.

BALDÍK, V. – BALÁK, I. – BURIÁNEK, D. – ČÁP, P. – DOSTALÍK, M. – FAIMON, J. – HADACZ, R. – JANDERKOVÁ, J. – KRUMLOVÁ, H. – KRYŠTOFOVÁ, E. – KYCL, P. – MALÍK, J. – MÜLLER, P. – NEČAS, J. – NOVOTNÁ, J. – NOVOTNÝ, R. – REZ, J. – ROHÁČ, J. – SEDLÁČEK (Brno), J. – TŮMA, A. (2021): CHKO Moravský kras – šíření strusky jeskynním systémem „Rudické propadání – Býčí skála" a Josefovským údolím: Studium mechanických a geochemických vlivů na kalcitové speleotémy a ekologii v oblasti.

BALDÍK, V. – BALÁK, I. – BURIÁNEK, D. – DOSTALÍK, M. – FAIMON, J. – HADACZ, R. – HORNOVÁ, H. – JANDERKOVÁ, J. – KNOZOVÁ, G. – KOTYZOVÁ, M. – KRUMLOVÁ, H. – KRYŠTOFOVÁ, E. – KŮRKOVÁ, I. – KYCL, P. – LEJSKA, S. – MALÍK, J. – MÜLLER, P. – NEČAS, J. – NOVOTNÁ, J. – NOVOTNÝ, R. – ROHÁČ, J. – SEDLÁČEK (Brno), J. – TŮMA, A. (2020): Aktuální negativní vlivy/procesy v CHKO Moravský kras.

GREGOR, V. A. (2015): The Jedovnice Creek cave system of the Rudice Plateau in the Moravian Karst – the Rudice Swallow Hole, Bull Rock and Bar caves. – Retrieved from https://www.byciskala.cz/MaRS/index.php?show=clanek&id=554.

HLADIL, J. (1983): The biofacies section of Devonian limestones in the central part of the Moravian Karst. – Sborník geologických věd, Geologie, 38, 71–94.

MUSIL, R. – CIHLÁŘ, J. – CIHLÁŘ, Z. (2020): Moravský kras: Průvodce Josefovským a Křtinským údolím. – Masarykova univerzita.

MUSIL, R. (1993): Moravský kras: Labyrinty poznání.

From Hypogenic to Biogenic Speleogenesis in Semi-Arid Climate: Bat Guano-Driven Carbonate Weathering and Cave Modification in Chariton Cave, Israel

Boaz Langford (1,2), Anton Vaks (2), Ilya Kutuzov (1,2), Jonathan Keinan (1,2), Tzahi Golan (2), Tami Zilberman (2), Gal Yasur (2), Navot Morag (2), Yael Ebert (1), Omri Gaster (1), Raz Ben-Yair (1), Micka Ullman (3), Amos Frumkin (1)

(1) The Institute of Earth Sciences, The Hebrew University of Jerusalem, Jerusalem, Israel
(2) The Geological Survey of Israel, Jerusalem, Israel
(3) The Institute of Archaeology, The Hebrew University of Jerusalem, Jerusalem, Israel
Corresponding author: boaz.langford@mail.huji.ac.il

Abstract

This study investigates the influence of bat guano on the development of Chariton Cave, the largest known hypogenic cave in the Levant. We examine the cave morphology, sediments, and moisture sources to understand post-speleogenetic processes in a vadose environment. Cave passages with keyhole cross-sections suggest secondary incision, where apatite deposits, formed through the interaction of guano leachates with bedrock, indicate a guano-related weathering area, which enables us to estimate the weathering volume attributed to this process as approximately 30% of the entire cave volume. This significant weathering occurs in semi-arid conditions, with limited infiltration of meteoric water from the surface. However, this moisture recycled within the cave, activating condensation corrosion weathering of the cave walls and ceiling, and also provides the moisture required for weathering associated with guano. U-Pb dating of calcite, which was deposited on secondary apatite, indicates bat activity in the cave since at least 5.19±0.85 Ma. This age also enables the calculation of guano-related incision rates of ~0.05 to ~0.07 mm/ka, and subaerial incision rates of 19.2 mm/ka. 14C dating of guano shows bat activity and guano accumulation 3360-3620 years ago, which continues to the present. This research highlights the importance of biogenic processes in reshaping hypogenic caves after their disconnection from formative environments, contributing to our understanding of karst evolution.

Visual Abstract

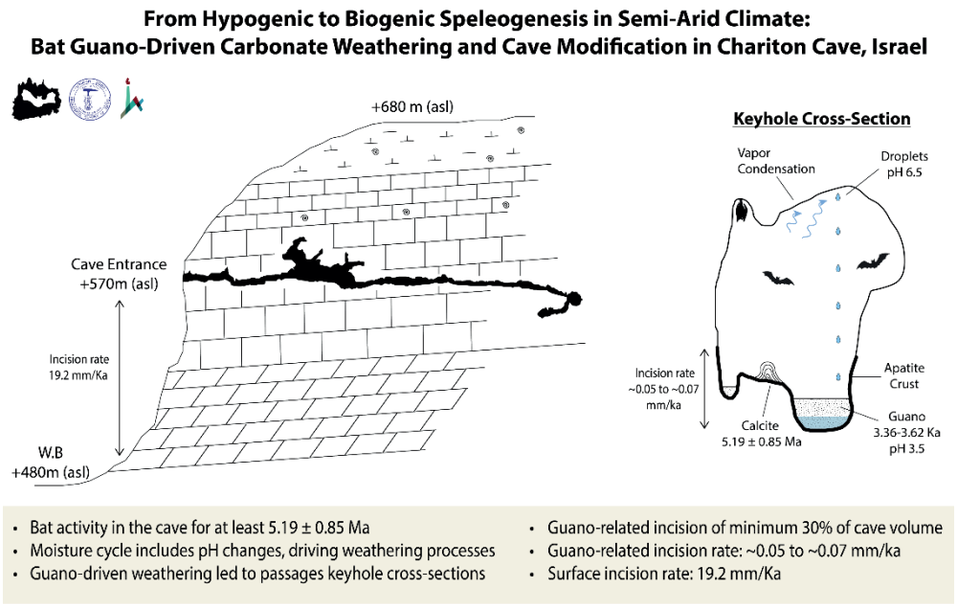

1. Introduction

Hypogene caves have received significant study in the last three decades, especially during the last decade (Klimchouk et al., 2017). Previous research has primarily focused on the processes forming these caves, the relationship between hypogenic karst and large hydrological systems, characteristic morphologies, and characteristic sediments (Klimchouk et al., 2017). Researchers have given less attention to processes of expansion and development of hypogenic spaces after disconnecting from the environment of their formation and moving into the vadose zone.

Study Site

Chariton Cave is the longest known limestone cave in Israel and the largest known hypogenic cave in the southern Levant (Langford et al., 2013; Frumkin et al., 2017). Its length and depth are 4185 m and 20.6 m respectively while its volume is 4019 m3.

The cave has a structure of a mostly 2D maze, with additional levels locally making it a 3D maze (Fig. 1). The width and height of the maze passages are tens of cm up to 3m. In addition, several chambers developed at passages intersections. The chamber structure is normally rounded, sometimes elongated. So-called phreatic morphology, mainly including elliptical cross-sections and smooth dissolution surfaces, has been preserved along all passages. The chambers present a similar phreatic morphology of smooth walls and rounded pockets, but boulders and collapsed material are common, indicating later modifications. Other morphologies related to late modifications of the cave spaces are cupolas, smoothing of the collapse boulders, collapse wall marks, and a passage keyhole cross-section.

The cave is structurally situated at the eastern flank of the Hebron monocline, which developed in the Upper Cretaceous. According to previous research, the cave was formed during the Oligocene - Early Miocene and uplifted above the groundwater during the Miocene (Frumkin et al., 2017). Dead Sea Rift, led to the exposure of the cave as it was cut by incision of the nearby canyon. The cave entrance includes three horizontal openings that are exposed on the west bank of the Chariton canyon, 570 m AMSL. The cave openings are located ~100 m below the local water-divide and similar elevation above the canyon stream bed.

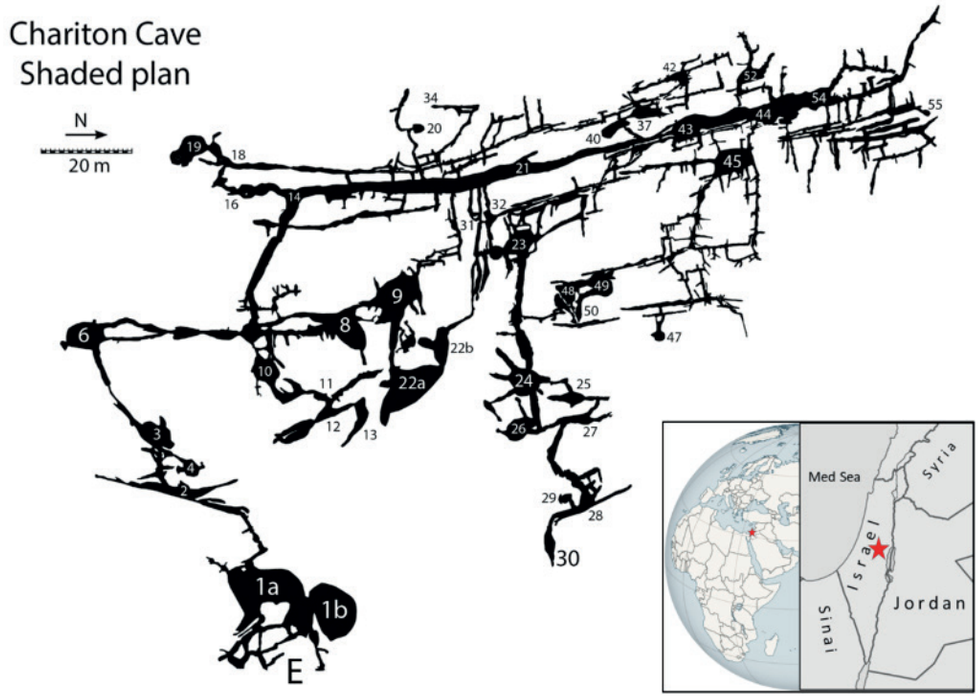

Figure 1: *Chariton Cave plan (horizontal projections, modified after Langford and Frumkin, (2013)). Chamber numbers in white within the plan or in black next to it. Cave entrance at the panel lower part, next to E. Right small panel : Cave location.*

2. Materials and methods

Field Measurements

Cave measurements were conducted using a Leica Laser Distance Meter X-310, converted to DistoX for paperless mapping. Cave length was calculated by summing all galleries and chambers, with volume determined using 3D modeling in Therion software.

Climate Monitoring

Continuous temperature and relative humidity monitoring was performed using HOBO® data loggers at four strategic points in the cave. Loggers were placed in chambers 1, 6, 44, and 49, (chamber location in : Fig 1) configured to record measurements hourly over 12 months.

Analytical Techniques

Several analytical methods were employed:

- U-Pb chronology using Laser Ablation-Inductively Coupled Plasma Mass Spectrometry (LA-ICPMS)
- 14C dating of bat guano
- Stable isotope analysis (oxygen and carbon)
- X-ray Diffraction (XRD)
- X-ray Fluorescence (XRF)
- Scanning Electron Microscope (SEM)

3. Results

Temperature and Relative Humidity

There is a notable spatial variations in the cave atmosphere. Temperature near the cave opening was 19°C with 34% relative humidity (RH). Upon entering, temperature stabilized at 22-23°C with RH rapidly increasing to ~80% at chamber 6. In inner parts of the cave, temperature reached up to 24.4°C and RH up to 93%.

Continuous monitoring at chamber 1 showed temperature variations from 19.7°C to 22.3°C and RH from 55.3% to 84%. Inner chambers (6, 44, and 49) exhibited stable conditions around 21°C with 100% RH.

Moisture Sources

Multiple moisture sources were identified:

- Humid air in chambers beyond chamber 6
- Water condensation on chamber walls
- Moist sediments
- Small water pools in chambers 30 and 49

Condensation droplet pH ranged between 6.5 and 7, while guano-rich sediment pH was acidic at 3.5. Isotopic analysis of available water sources showed consistent $\delta^{18}O$ values.

Guano Deposits

Bat guano deposits were found throughout the cave (Fig 2 A+C), with varying characteristics:

- Compressed in accessible areas
- Layered sediment with distinct horizons
- Thickness varying laterally
- Acidic pH of 3.5-4

Apatite Deposition

Prominent mineral deposits were observed along cave walls (Fig 2), characterized by:

- Thickness up to few centimeters
- Layered structure
- Mineralogy comprising hydroxyl-apatite
- Associated with guano deposits

Chronology

- U-Pb dating of calcite deposits overlying guano-related apatite indicated bat activity since at least 5.19±0.85 Ma.
- ^{14}C dating of guano revealed activity between 3360-3580 years ago.

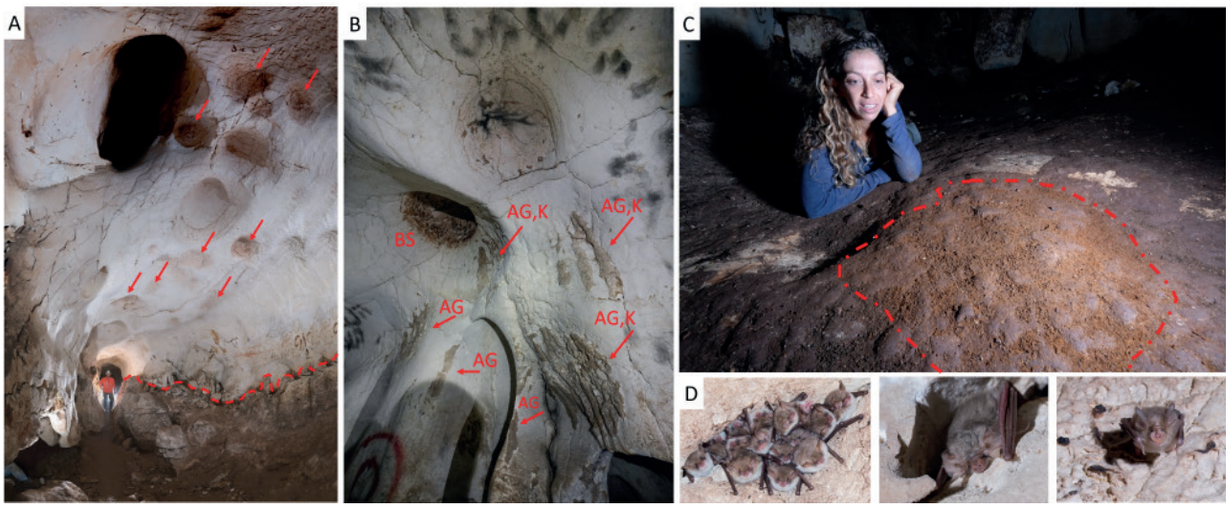

Figure 2: *Bats and indications for their presence (guano and urea) in Chariton Cave. A: passage in chamber 43 (see location in Fig. 1). Red arrows point on brown surface, associated with urea on the ceiling, concentrated in shallow domes. Red line marks apatite cover at the bottom. B: Marks related to bats activity on the cave walls. AG – Apatite and Gypsum, K – Karren, BS - Brown Surface. C: guano cover on the cave floor. Fresh guano is marked with a red line. D: insectivorous bats. From left to right: Myotis Nattereri, Plecotus, Rhinolophus blasii.*

4. Discussion

U-Pb dating of calcite deposited on apatite yielded an age of 5.19±0.85 Ma for the earliest deposition, indicating bat activity and guano-related weathering prior to this time. Subsequent calcite units were dated to 1.42±0.28 Ma and 1.08±0.31 Ma. These dates align with regional drainage system development and canyon incision patterns occurring after 6 Ma (Chaldekas et al., 2021). The cave documented bat occupation history extends into the Bronze Age, as evidenced by ^{14}C dating of guano deposits from 3360-3580 years BP.

Volumetric analysis of cave cross-sections reveals that guano-induced weathering accounts for ~30% of the current cave volume, primarily affecting the lower portions of passages. This estimate represents a minimum value, as it excludes additional volume modifications from condensation corrosion enhanced by guano-derived volatile compounds (Dandurand et al., 2019). Weathering rates calculated from dated cross-section indicate floor retreat of 29 cm over 5.19±0.85 Ma, yielding rates of ~0.05 to ~0.07 mm/ka.

Cave entrance elevation is 570 m AMSL, and it is located ~100 m below the local water divide and about the same distance above the

canyon bed. The dating results here indicate that by ~5.2 Ma, at least half of the local relief was already existing, allowing bats to enter the breached cave, while the remaining incision occurred during the last 5.2 Ma. This data indicate incision rates of ca. 19.2 mm/Ka, consistent with Ryb et al., (2014) who measured weathering rates of 19±1 mm/Ka in a similar climatic and lithological location.

Cave moisture derives from multiple sources, with isotopic analysis ($\delta^{18}O$) of available water sources showing values between -4.4 to -4.9‰, consistent with local rainfall patterns (Goldsmith et al., 2017). While direct water infiltration is not evident, condensation processes maintain 100% relative humidity in inner chambers, creating active dripping and shallow pools. The moisture system demonstrates pH variations, with neutral condensation water (pH 6.5) becoming acidic (pH 3.5) upon contact with guano before returning to neutral conditions through bedrock interaction (Fig. 3).

Mineralogical analyses reveal hydroxylapatite as the primary component of guano-derived deposits, with varying laminar structures exhibiting different hardness levels. The formation mechanism involves calcite-apatite replacement, where dissolution and crystallization rates control the process (Xia et al., 2009). XRF scanning showed higher concentrations of P and Zn with lower Ca content in harder layers compared to softer ones, while stable isotope analysis indicated that softer laminae retain partial carbonate signatures.

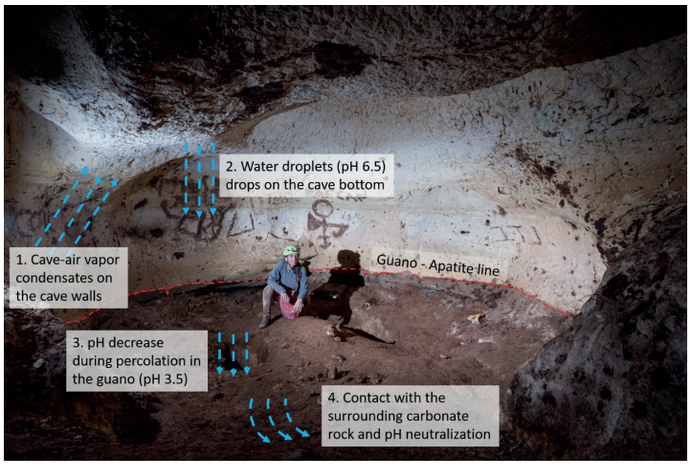

Figure 3: *Schematic representation of humidity path in the cave shown in chamber 49.*

5. Conclusion

This study demonstrates the significant impact of bat guano on the post-speleogenetic development of Chariton Cave, a hypogenic cave in a semi-arid environment. Our findings reveal that guano-related weathering has substantially modified the cave, accounting for at least 30% of its current volume. This process began at least 5.19±0.85 Ma and continues to the present day. The interaction between bat guano and the limestone bedrock has led to the formation of distinctive features such as keyhole cross-sections and apatite deposits. Despite the semi-arid surface conditions, high humidity levels are maintained in the cave, with a condensation-evaporation cycle. Interaction of the moisture with the guano leads to a pH change and to carbonate weathering. This cyclical process drives ongoing modification of the cave morphology.

Our results highlight the importance of biogenic processes in reshaping hypogenic caves after their disconnection from formative environments, contributing to our understanding of karst evolution in semi-arid regions. Furthermore, this study underscores the need to consider long-term biogenic influences when interpreting cave morphologies and speleogenesis in similar settings worldwide.

Acknowledgments

Fieldwork have done with volunteers from the Israel Cave Research Center: Yonatan Mashal Golan, Reuven Zakai, Shir Perelmuter, Dani Beilinson, Sergei Alimov, Shirli Gazit.

For assistance with laboratory analyses, my gratitude goes to Raanan Bodzin (Geological survey of Israel), Yonatan Goldsmith and Uri Ryb (The Institute of Earth Sciences, The Hebrew University of Jerusalem, Jerusalem, Israel).

References

CHALDEKAS, O., VAKS, A., HAVIV, I., GERDES, A., ALBERT, P., 2021. U-Pb speleothem geochronology reveals a major 6 Ma uplift phase along the western margin of Dead Sea Transform. GSA Bulletin 135, 1571-1584. https://doi.org/10.1130/B36051.1.

DANDURAND, G., BOURGES, P., & HOBLÉA, F. (2019). The impact of guano on cave wall weathering: A geochemical perspective. International Journal of Speleology, 48(2), 201-215.FRUMKIN, A., LANGFORD, B., LISKER, S., AMRANI, A. (2017). Hypogenic karst at the Arabian platform margins: Implications for far-field groundwater systems. GSA Bulletin 129, 1636-1659. https://doi.org/10.1130/B31694.1.

GOLDSMITH, Y., BROCARD, G.,ANTAL, D., & SCHUSTER, R. (2017). Isotopic signatures in semi-arid cave environments. Journal of Cave and Karst Studies, 79(3), 211-225.

KLIMCHOUK, A., PALMER, A. N., DE WAELE, J., AULER, A., & SYLVESTER, P. (2017). Hypogene karst regions and caves of the world. Springer International Publishing.

Ryb, U., Matmon, A., Erel, Y., Haviv, I., Benedetti, L., Hidy, A.J., 2014. Styles and rates of long-term denudation in carbonate terrains under a Mediterranean to hyper-arid climatic gradient. Earth and Planetary Science Letters 406, 142-152. https://doi.org/10.1016/j.epsl.2014.09.008.

XIA, Y., LIU, X., ZHANG, B., & WANG, J. (2009). Apatite formation and mineral replacement processes. Mineralogical Magazine, 73(4), 561-572.

LANGFORD, B., FRUMKIN, A., FILIPPI, M., BOSAK, P., 2013. The longest limestone caves of Israel. Czech Speleologicl Society. The 16th International Congress of Speleology, Prague, Czech Republic, pp. 105-109.

Long term alluviation and its contribuition to the development of distributary cave systems

Fernando Verassani Laureano (1), Ivo Karmann (2)

(1) Vale, Diretoria de Reparação, Nova Lima, MG, Brazil, fernando.laureano@vale.com (corresponding author)
(2) Instituto de Geociências USP, Rua do Lago, Cidade Universitária, ikarmann@usp.br

Abstract

This study characterizes an extensive sedimentary record occurring in Lapa Doce and Torrinha caves, NE Brazil. With more than 40 km of surveyed passages, these caves integrate a distributary cave system fed by allogenic recharge from the surrounding sandstone plateaus. Sediment petrography together with descriptions of depositional facies and architectural elements shows four depositional units related to fluvial and standing water environments. These include, from bottom to top: (1) a channel unit including lateral bars deposited during an ordinary flood regime; (2) a sandy flood unit including minor channel and scour fills derived from bank-full equivalent flood events; (3) mud caps deposited in standing water that often reach the ceiling; and (4) intraclast breccias associated with collapse of the mud caps under saturated conditions. Long term alluviation of the cave system seems to be important in forming passages, determining their configuration, and setting up a general distributary pattern evident in passage morphology and sedimentary sequences.

1. Introduction

Cave systems offer a unique environment for sediment transport, deposition and preservation. Because cave sediments are protected from weathering and bioturbation, caves often act as sediment repositories that may provide records of geomorphic events even where no river terraces can be found in the surface. Although there has been progress in understanding sediment transport through karst aquifer systems (Herman et al., 2012) there is still an enormous gap when compared to knowledge about clastic deposition in surface alluvial systems (Miall,2006; Bridge and Demicco, 2008).

In this study we characterize an extensive sedimentary record occurring in Lapa Doce and Torrinha caves, NE Brazil. Sediment petrography, facies descriptions and architectural elements of the deposits are presented. This work contributes to an understanding of clastic sediment transport and deposition within karst aquifers, especially those fed by surface fluvial systems.

2. Materials and methods

The Chapada Diamantina is an elevated region in the central Bahia state (Brazil) at the drainage divide separating waters flowing toward the São Francisco River from those flowing direct toward the South Atlantic Ocean. The region comprises a set of ranges and plateaus mainly formed on folded Proterozoic sedimentary rocks. The study area is located where Neoproterozoic rocks from Una Group and Mesoproterozoic sequences from Espinhaço Supergroup are folded into a narrow synform (CPRM, 1999).

The study area is drained to a local base level controlled by the Santo Antônio river and its main tributaries, which include intermittent and ephemeral streams as well as karst springs. The Santo Antônio is in turn tributary to the ocean-ward flowing Paraguaçu river. The Santo Antônio river flows out of the study area as a superposed drainage cutting toward the east through the siliciclastic rocks. Local streams include the Agua de Rega and Almas creeks, which sink into the west flank of the synform to form blind valleys. Although they behave at present as ephemeral streams, they were in the past major suppliers of sediment to the cave systems. Most of the drainage is confined to canyons with a flat alluvial floor. Despite the absence of a floodplain and terraces these streams store large amounts of sediments in the valley floor, especially when cutting through carbonate rocks.

Lapa Doce cave system is one of the most visited caves in Brazil. The whole system contains 25.8 km of surveyed galleries with multiple entrances associated with collapse dolines. It is characterized by a sinuous trunk passage and distributary branches generally associated with network maze sectors (Cruz JR, 1998; Auler, 1999). Scallops on the passage walls confirm a signature of divergent flow. The downstream decrease in trunk passage dimensions and increase in branching density is analogous to surface distributary rivers (Nichols and Fisher, 2007).

In both caves the profiles of trunk galleries often have a planar roof that cuts across carbonate bedding planes suggesting dissolution under a high water table in the past (Auler, 1999). The cross-sectional shape varies over those caves but remarkable wall notches can be observed as a result of lateral dissolution atop a sedimentary fill (Farrant and Smart, 2011). Some trunk galleries still contain a ceiling half-tube right above a sediment fill. Distributary branch arms and associated network sectors usually share the same flat sediment floor, but their ceilings are always lower than the ceiling of the adjacent trunk conduits. They are preferentially narrow passages not wider than a few meters. Pendants, cupolas, anastomosed half tubes and wall grooves are common features of these passages.

Six stepped trenches were excavated to expose the original sedimentary fill, where descriptions and sampling were preferentially performed. Five of them were located in trunk passages trying to follow general flow direction. Yet, in Torrinha cave, another excavation was made to characterize sediments in a minor passage that cuts across both trunk and

mazes passages. Sedimentary successions were synthesized by stacking descriptive facies (Anderton, 1985) recognized over all vertical risers. In addition, exposures on the sides of the trenches were used to constrain the internal geometry and unconformities. Facies nomenclature and the hierarchy of erosional boundary surfaces were adapted from Miall (2006). Sand samples were impregnated with resin for further analysis under a petrographic microscope. Fine sediment grain size was analyzed by low angle laser diffraction using a Malvern Mastersizer S facility and mineral content was determined using total sample X-ray diffraction.

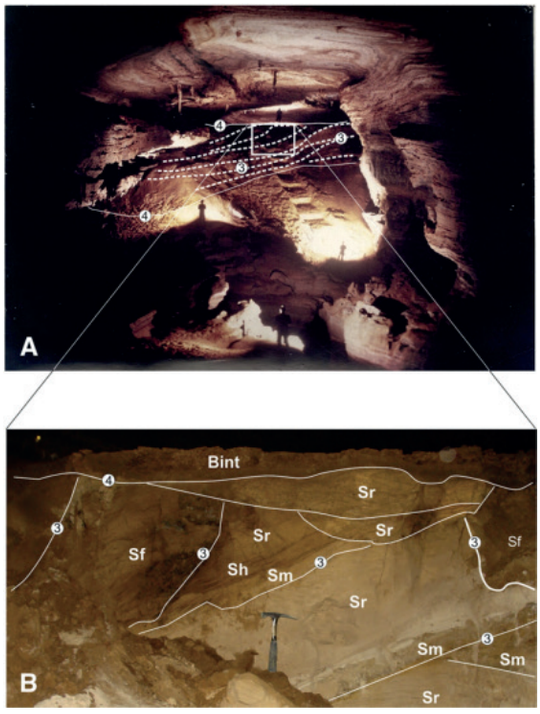

Figure 1 : *A – Step trench digged in Lapa Doce II, Sifão de Areia, where sediment were partially removed. B – Flood facies : 3rd order erosional surfaces showing lateral accretion of channel cutting structures within scours fill Circumscribed numbers are related to hierarchy of bounding surfaces.*

3. Results

The bulk sedimentary data allows the identification of four distinct depositional units bounded by 4th order (or higher) erosional surfaces. Two of them are assumed to be the result of sedimentation under fluvial conditions while the others are related to standing water deposition within conduits under phreatic to epiphreatic conditions (Figure 2).

Those derived from fluvial processes can only be distinguished in terms of architectural elements. Standing water depositional units are single descriptive facies successions located at the top of the sedimentary column, often reaching the ceiling of the passages and sometimes blocking them.

Channel deposits are present at the bottom of all trunk galleries; the basal contact with bedrock was recorded in both caves, and it is not much deeper than the general sandy, flat cave floors. From bottom to top, channel facies begin with one or more fining upward cycles or co-sets of cross-bedded sand, both followed by laminated silt. Where exposed along the cave wall, which is rare, this basal part of channel deposits has internal erosional surfaces suggesting downstream accretion. At the location of the cross-section, third order surfaces propagate from basal sand beds into superposed laminated silt, showing that they are part of a common macroform, in this case, a lateral bar. Internal fourth order erosional surfaces in upper laminated silt package reveal that the river channel has abandoned and reoccupied the same passage, leading to a superposition of two successive bars.

Flood depositional units comprise sand beds that were recognized in the middle of the sediment piles in trunk galleries of both caves and at the bottom of minor passages in Torrinha . Horizontal, plane laminated centimeter scale sand beds accumulated over climbing ripples often showing a high angle of climbing. Fine sand with horizontal lamination is present as well as massive sand. They are represented by approximately 3 m-thick rippled and massive sand showing an abundance of internal erosional surfaces. The cross-section views of these two sites reveal concave up 4th order erosional surfaces derived from successive minor ephemeral channels (Figure 1). However, these sediments are strictly composed of channel related bedforms. Descriptive facies succession and three-dimensional arrays of erosional surfaces suggest deposition related to minor channels or scours that filled during bank-full flood events. This would lead to deposition over active channel bars and galleries previously abandoned from the main river channel. This interpretation is also supported by another important distinctive element: a topmost flat surface developed independent of conduit morphology, level or size. Top flat surfaces usually derive from deposition in floodplains in surface fluvial systems (Bridge and Demicco, 2008) and although one should not expect to observe a floodplain in cave passage containing a stream; a flat surface would be the result of recurrent and successive flood events occurring in laterally displaced but interconnected passages. In the study caves, this top flat surface is also concordant with wall notches in some trunk galleries, and the general ceiling elevation of adjacent single or maze conduits.

Massive to finely laminated well-sorted mud caps occur upon fluvial deposits, sometimes reaching >4 m thick. They systematically lay over the top flat surface of flood deposits with an abrupt contact, although in Torrinha successive interbedding of rip-pled fine sand and massive mud suggests a gradual transition. Except for light brown discontinuous lamination, the red to dark brown mud package does not preserve significant syn-sedimentary structures, and is otherwise intensely cracked. Clods are often covered by post-depositional iron/manganese precipitates and show remarkable gypsum crystal growth in between. Unlike fluvial deposits, mud packages may regularly be observed interbedded and superposed by calcite crusts, or even showing diverse erosional relationships with flowstones and speleothems. This is important because it indicates that the mud caps are not derived from a single depositional event. Nevertheless, these events should be longer than the flood events previously described. There must be sufficient time for base level to rise and stand, sustaining the caves in phreatic or epiphreatic conditions. This facies often fills passages near to the ceiling and is closely associated with paragenetic features such as ceiling half-tubes and anastomoses.

Ungraded, matrix-supported intraclast breccias are found on the top of all 3 sections from Lapa Doce (Fig. 3). Away from the trenches, this facies transitions laterally to mud caps and it is a clear result of gravitational reworking of the mud caps. It may reach 2 m in thickness

and is quite different from gravitational diamictons described elsewhere (Gillieson, 1986; Bosch and White, 2007). This sediment is interpreted to be derived from slide or fall events that disrupted the original mud caps. Clast shape and fabric point to limited displacement and the presence of unsorted muddy matrix indicates water availability. The detachment of saturated muddy sediments could be triggered by rapid water table lowering or ceiling breakdown, but it clearly demonstrates that sediment piles were higher than at present and there was available space in aggraded conduits for sediment migration.

Depositional unit	Depositional environment	Distinctive elements	Interpretation
Channel	Fluvial system	Accretion of channel mesoform (dunes) and macroform (bars)	Migration of channel and lateral bars during ordinary floods in active river passages.
Flood		Accretion of scour and minor channel fills; overbank top flat surface	High sediment load influx during episodic bank full flood events affecting the whole cave system.
Mud caps	Standing waters	Absence of bedload deposits	Suspended load deposition on epiphreatic conduits. May experience moments of aerial exposure.
Intraclast Breccia		Ungraded angular intraclasts breccia	Slide or fall of saturated cracked mud packages due to slope instability or breakdown.

Figure 2 : *Distinctive elements and interpratation for recognized depositional units.*

4. Discussion

The role of sediments in speleogenesis has been reviewed by Farrant and Smart (2011) who recognized two main processes: paragenesis and alluviation. The first is a phenomenon relevant to phreatic conduits where sediments restrict their cross-sections, forcing upward dissolution (Renault, 1968). The second is derived from alluviation of passages in a vadose environment, where enhanced lateral corrosion sculpts wall notches. Paragenesis and alluviation processes may also develop simultaneously in a given evolving cave system. An example could be the sediment fill of loops within phreatic zone and the development of a bypass passage at upper vadose zone (Ford and Ewers, 1978). Both paragenesis (ceiling half tubes, pendants and cupolas) and alluviation (wall notches and bypass passages) derived features can be recognized in the studied caves, but the timescale and ordering of processes cannot be solved without an understanding of clastic deposition.

Together, the downstream decrease in trunk passage dimensions, the increase in branching density, the distributary flow signature recorded by scallops in cave walls, and the sedimentary record group to represent the medial to distal zones of a subterranean fluvial distributary system (Nichols and Fisher, 2007).

Cosmogenic burial dating fo these deposits (Laureano et al., 2016) has show that during the Early and Middle Pleistocene, the Lapa Doce and Torrinha cave system were linked to surface drainage in terms of water and sediment transport, which in turn was governed by the flood regime in Agua de Rega creek and Santo Antonio river (base level). As observed presently, because the Santo Antonio river has a larger watershed it rises and blocks groundwater flow during floods, sometimes promoting back flooding in the karst aquifer (Auler and Farrant, 1996). This backwater effect in part explains why sediments have aggraded within caves and also can be invoked to understand the maze network and narrow passages that are associated with trunk passages (Palmer, 1975).

Cave alluviation took course during at least 1.5 million years with successive input and flush of fluvial sediments. It seems to have been interrupted during the Middle Pleistocene, the two youngest burial ages point to a timeframe around 300 ky (Laureano et al., 2016). When studying sediments in caves fed by sinkholes in Brazil, Auler et al. (2009) have argued for a climate control for sediment input, but that should not be assumed in relation to the long term cave alluviation recorded here because depositional units related to fluvial deposits may be derived from ordinary flood regime (Herman et al., 2012).

5. Conclusion

Fluvial deposits can be distinguished in two units: the first is related to channel meso and macroforms deposited during base flow, the second is associated with scours and minor channel fills deposited in bank-full flow conditions. This long-term alluviation of cave systems is important in generating passages, determining their configuration, and setting up a general distributary pattern evident in passage morphology and sedimentary sequences.

Acknowledgments

Cave sediment studies presented in this document were funded by Fundação de Apoio à Pesquisa do Estado de São Paulo (FAPESP), grants 96/05686-0 and 2010/20560-2. Sampling of cave sediments was performed under permission by Instituto Chico Mendes de Biodiversidade (ICMBio/CECAV), license number 27341-2.

References

ANDERTON, R. (1985) Clastic facies models and facies analysis. In: BRENCHLEY, P.J., WILLIAMS, B.P.J. (Eds.), Sedimentology: Recent Developments and Applied Aspects. Blackwell, Oxford, pp. 31–47.

AULER, A.S., FARRANT, A.R. (1996) A brief introduction to karst and caves in Brazil. Proc. Univ. Bristol Spelaeol. Soc. 20: 187–200.

AULER, A.S. (1999) Karst Evolution and Paleoclimate of Eastern Brazil (PhD Thesis) University of Bristol.

AULER, A., SMART, P.L., WANG, X., PILO, L.B., EDWARDS, L., CHENG, H., 2009. Cyclic sedimentation in Brazilian caves: mechanisms and palaeoenvironmental significance. Geomorphology 106 : 142–153.

BOSCH, R.F., WHITE, W.B. (2007) Lithofacies and transport of clastic sediments in karstic aquifers. In: SASOWSKY, I.D., MYLROIE, J. (Eds.), Studies of Cave Sediments – Physical and Chemical Records of Paleoclimate. Springer, Dordrecht, pp. 1–22.

BRIDGE, J.S., DEMICCO, R.V. (2008) Earth Surface Processes, Landforms and Sediment Deposits. Cambridge University Press, New York, 815p.

CPRM - Companhia de Pesquisa e Recursos Minerais (1999) Carta geológica SEABRA (SD-23-V-A). Escala 1:250.000. Programa Levantamentos Geológicos Básicos do Brasil. CPRM, Salvador, Brasil.

FARRANT, A.R., SMART, P.L. (2011) Role of sediment in speleogenesis: alluviation and paragenesis. Geomorphology 134: 79–93.

FORD, D.C., EWERS, R.O. (1978) The development of limestone cave systems in the dimensions of length and depth. Can. J. Earth Sci. 15: 1783–1798.

GILLIESON, D. (1986). Cave sedimentation in the New Guinea Highlands. Earth Surf. Process.Landf. 11: 533–543.

HERMAN, E.K., TORAN, L., WHITE, W.B. (2012) Clastic sediment transport and storage in fluviokarst aquifers: an essential component of karst hydrogeology. Carbonates Evaporites 27: 211–241.

LAUREANO, F. V., KARMANN, I., GRANGER, D. E., AULER, A. S., ALMEIDA, R. P., CRUZ, F. W., NOVELLO, V. F. (2016). Two million years of river and cave aggradation in NE Brazil: Implications for speleogenesis and landscape evolution. Geomorphology, 273: 63-77.

MIALL, A.D. (2006). The Geology of Fluvial Deposits: Sedimentary Facies, Basin Analysis andPetroleum Geology. 4th rev. ed. Spring Verlag, Berlin.

NICHOLS, G.J., FISHER, J.A. (2007). Processes, facies and architecture of fluvial distributary system deposits. Sediment. Geol. 195: 75–90.

PALMER, A.N. (1975) The origin of maze caves. Natl. Speleol. Soc. Bull. 37: 56–76.

RENAULT, P. (1968) Contribuition a l'etude des actions mécaniques et sédimentologiques dans la spéléogenèse. Ann. Spéléol. 23: 529–596.

Influence of brittle deformation on waterflow and retention observed in a cave (Hochschwab, Eastern Alps)

Richard Michtner (1), Eva Kaminsky (2,3), Barbara Funk (2,4), Helene Bauer (5), Kurt Decker (1), Lukas Plan (2)

1 University of Vienna, Department of Geology, Josef-Holaubek-Platz 2, 1090 Vienna, Austria
2 Natural History Museum, Karst and Cave Group, Burgring 7, 1010 Vienna, Austria
3 BOKU University, Institute of Soil Physics and Rural Water Management, Muthgasse 18, 1190 Vienna, Austria
4 TU Vienna, Research Unit of Geophysics, Wiedner Hauptstraße 8, 1040 Vienna, Austria
5 Vienna Water, Municipal Department 31, Grabnergasse 4-6, 1060 Vienna, Austria

Abstract

The complex geological processes driving flow and retention of water in the upper vadose zone of Alpine karst aquifers are yet to be understood to a sufficient level. To gather a deeper understanding into these systems, a structural geology approach was combined with electrical resistivity tomography to find a link between brittle deformation structures and recharged water into karst systems. The investigated Hirschgruben cave is located in the central Hochschwab massif at an elevation of 1896 m a.s.l. and shows horizontal character in its studied passages. Electrical resistivity tomography data and discharge of cave drip water was gathered during snowmelt and summer precipitation events. Examined areas were grouped into different classes of fracture spacing, ranging from massive rock to finely fractured rock in the vicinity of brittle faults. These records fit existing models of deformation stages in the Eastern Alps. Inhomogeneities in water infiltration along existing fracture zones were observed to some extent and appear to depend on both, the fracture density in the host rock as well as rate of water infiltration. These results help to understand the behaviour of water in the upper vadose zone and subsequently provide valuable information for the supply of karst water as a source of drinking water.

Résumé

Les processus géologiques complexes qui déterminent l'écoulement et la rétention d'eau dans la zone vadose supérieure des aquifères karstiques alpins doivent encore être compris à un niveau suffisant. Pour mieux comprendre ces systèmes, une approche de géologie structurale a été combinée à une tomographie par résistivité électrique pour trouver un lien entre les structures de déformation fragiles et l'eau rechargée dans les systèmes karstiques. La grotte Hirschgruben étudiée est située dans le massif central du Hochschwab à une altitude de 1896 m et montre un caractère horizontal dans ses passages étudiés. Des données de tomographie de résistivité électrique et le débit des eaux d'égouttement des grottes ont été recueillies lors des événements de fonte des neiges et de précipitations estivales. Les zones examinées ont été regroupées en différentes classes d'espacement des fractures, allant de la roche massive à la roche finement fracturée à proximité de failles fragiles. Ces enregistrements correspondent aux modèles existants des étapes de déformation du Cénozoïque. Des inhomogénéités dans l'infiltration de l'eau le long des zones de fracture existantes ont été observées dans une certaine mesure et semblent dépendre à la fois de la densité de fracture dans la roche encaissante ainsi que du taux d'infiltration de l'eau. Ces résultats aident à comprendre le comportement de l'eau dans la zone vadose supérieure et fournissent par la suite des informations précieuses pour l'approvisionnement en eau karstique comme source d'eau potable.

Resumen

Os complexos processos geológicos que impulsionam o fluxo e a retenção de água na zona vadosa superior dos aquíferos cársticos alpinos ainda não foram compreendidos a um nível suficiente. Para obter uma compreensão mais profunda destes sistemas, uma abordagem de geologia estrutural foi combinada com tomografia de resistividade elétrica para encontrar uma ligação entre estruturas de deformação frágeis e água recarregada em sistemas cársticos. A caverna Hirschgruben pesquisada está localizada no maciço central de Hochschwab, a uma altitude de 1896 m e mostra caráter horizontal em suas passagens estudadas. Dados de tomografia de resistividade elétrica e descarga de água gotejante de cavernas foram coletados durante eventos de degelo e precipitação de verão. As áreas examinadas foram agrupadas em diferentes classes de espaçamento de fraturas, variando de rochas maciças a rochas finamente fraturadas nas proximidades de falhas frágeis. Esses registros se ajustam aos modelos existentes de estágios de deformação do Cenozóico. Inomogeneidades na infiltração de água ao longo das zonas de fratura existentes foram observadas até certo ponto e parecem depender tanto da densidade de fratura na rocha hospedeira quanto da taxa de infiltração de água. Estes resultados ajudam a compreender o comportamento da água na zona vadosa superior e posteriormente fornecem informações valiosas para o abastecimento de água cárstica como fonte de água potável.

1. Introduction

The Hochschwab karst massif in the northern part of the Austrian province of Styria plays a key role in the freshwater supply of two major cities, Vienna and Graz respectively. The Hochschwab is part of the Northern Calcareous Alps consisting primarily of Triassic carbonate rocks and is overprinted by a multitude of brittle deformation structures, generated by the continent-continent collision of the Adriatic microplate with the Eurasian plate, causing a multi-stage deformation (e.g. RATSCHBACHER et al. 1991). Previous work suggested five distinct stages of brittle deformation at the Hochschwab, of which stage three, east striking sinistral strike-slip faults, created by lateral extrusion of the Eastern Alps in the Lower to Middle Miocene, is the most important set of structures in relation to the observed hydrological situation (DECKER & REITER 2001).

More than 1000 caves have been documented at the Hochschwab so far (PLAN 2016). Most caves are vadose canyon shaft systems but there are also some fossil phreatic caves as well. Almost all cave sections are controlled by faults as bedding planes are insignificant as initial fissures. With 5.5 km of surveyed passages the Hirschgruben cave is the longest in the central Hochschwab (PLAN et al. 2019). It is mainly of phreatic origin and an age of about 5 Ma is assumed from burial age dating. In the entrance near parts, the host rock is limestone of the Upper Triassic Dachstein formation and dolomite of the Waxeneck formation.

This study aims to establish the relationship between brittle faulting processes and the potential for surface water permeability and retention in the upper vadose karst zone. Previous work conducted in the shallow parts of Hirschgruben cave suggests, that the retention potential of the soil and epikarst is much greater than previously assumed and is related to the degree of glacial overprint, with paleo-landscapes exhibiting significantly greater water storage potential (ZEMANN 2024; EXEL et al. 2016). This can be partly explained by the considerable number of faults and associated damage zones in the cave. The recorded faults fit into existing models for Eastern Alpine deformation stages (DECKER & REITER 2001). Different responses to recharge events were found for drip water and fluctuations of water saturation in the upper vadose zone (KAMINSKY et al. submitted). How the brittle deformation and the fault rocks relate to the water flow behaviour in the cave has not yet been investigated.

Figure 1: *A NW-SE-striking, steeply NE-dipping fault (F4) in Hirschgruben cave, partially filled with clay-rich gouge. Photo: Eva Kaminsky*

2. Methods

Fracture densities and fault zones were analysed along the shallow parts of the Hirschgruben cave. The Fracture densities of the rocks were classified ranging from Fracture Density Class (FDC) 1 to 4 (BAUER et al. 2016). FDC 1 corresponds to little to moderately fractured rock with estimated fracture densities less than 30 m2/m3, FDC 2, closely fractured rock (30-100 m2/m3), FDC 3, very closely fractured rock (100-300 m2/m3) and FDC 4, extremely fractured rock (>300 m2/m3). For fault rock, the general classification of SIBSON (1977) and the more detailed approach for cataclastic rock of WOODCOCK & MORT (2008) were used. Fault rock with a matrix content <10% was classified as brecciated rock and those with matrix content >10% as cataclastic rock. Cataclastic rock was further subdivided into proto-cataclasite (0-50% matrix), cataclasite (50-90% matrix) to ultra-cataclasite (>90% matrix). Faults were measured and plotted as equal-area stereo projections using the program Stereonet. The cave profiles were measured using a DistoX laser distance meter. Electrical resistivity tomography (ERT) monitoring, utilizing 96 electrodes between the cave ceiling and the surface, resolved 2D images along 74 time-lapses revealing saturation changes in response to infiltration events (KAMINSKY et al. submitted). A measuring weir was installed underneath a chimney with drip water at the end of the ERT cable (Fig. 2), and water through flow, electrical resistivity, and temperature were measured every 10 minutes.

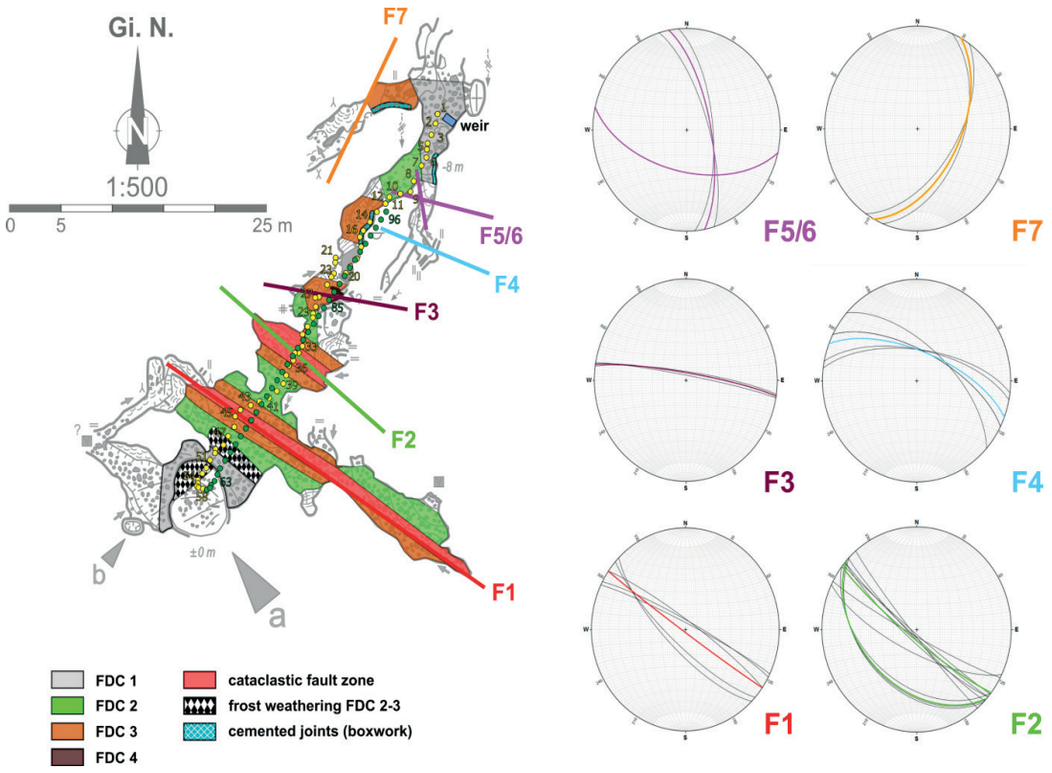

Figure 2: *Recorded brittle faults in the shallow parts of Hirschgruben cave correlated with analysed fracture density classes (FDC) of the host rock. Faults generally show NW-SE or NE-SW striking. The yellow and green dots in the cave map represent the locations of ERT electrodes (green = surface, yellow = cave). In addition to fault bound increase of fracture density, there are parts of the cave which suggest frost weathering induced fracturing.*

3. Results

Different FDCs and faults are found in the horizontal cave passages from the entrance of Hirschgruben cave to the weir (Fig. 1). Classification of fracture densities showed areas of little fractured rock (FDC 1) in parts far from fault zones, with the exception of areas where a greater influence of frost weathering is likely to have resulted in FDC 2 and 3. Near fault zones, fracture densities generally increased to FDC 3 and in one case to FDC 4, followed by the fault core of proto- to ultra-cataclasites (Fig. 2). FDC 4 was only recorded in one location adjacent to fault F3 and could also be classified as brecciated rock according to SIBSON (1977). The cataclastic rock in fault F1 consisted of a 10-20 cm wide fault centre of ultra-cataclasite followed by at least 1 m of cataclasite. Beyond this, the cave wall was altered, making it difficult to see detailed rock features. Fault F2 had similar characteristics, but with cataclastic rock reaching lateral dimensions of over three metres where two, probably conjugate, faults converged. Faults F3, F4, F5 and F6 did not exhibit as pronounced cataclastic features. F3 was highly altered and therefore could not be definitively classified as a cataclastic fault. Fault F4 showed minor cataclastic rock embedded in clay-rich fault gouge. Faults F5 and F6 appeared to be a pair of conjugate faults, both showing only minor cataclastic features, mostly due to alteration of the cave walls. Faults F1, F2 and, to a lesser extent, F3 showed a pronounced damage zone outside the main fault rock zone, with FDC 3 followed by FDC 2 further out.

The stereoplots in Figure 2 indicate a major strike orientation for the faults, NW-SE, with minor orientations N-S and NE-SW. These orientations coincide with known faults on the Hochschwab surface. ERT images show the resistivity of the rock as a 2D cross section (Fig. 3). The ERT images are divided into three separate zones, the surface zone above the green line in the profile, the cave zone below the red line and the bedrock zone in between. FDCs and faults were located at the cave ceiling and interpolated to the cave zone on the ERT images. Correlation of the structural measurements with the ERT shows a relationship between rock fragmentation in zones of brittle deformation and increased water permeability of the host rock. Dry conditions in winter and summer show consistent differences in resistivity along the cave ceiling. These differences may also be the result of different rock properties with lower resistivity at faults. Images from both events discussed tend to show central parts of faults, i.e. cataclasites or clay gouges, acting as aquitards, whereas highly fractured fault rocks adjacent to fault cores appear to have a higher degree of permeability and retention potential. These characteristics are most pronounced in the cave zone and lower bedrock zone under dry conditions, but are much less pronounced under wet conditions. As water saturation increases due to recharge events (snowmelt and precipitation), few spatial pattern differences are observed in the cave zone. Meanwhile, resistivity images from summer monitoring differ from data obtained during snowmelt monitoring in the epikarst and bedrock zones. Slow and constant water inflow, as occurs during snowmelt, appears to result in a more homogeneous saturation of the epikarst with less susceptibility to interaction with fault zones. Meanwhile during summer rainfall events a significant proportion of the precipitation acts as quick and point recharge and subsequently does not participate in the immediate infiltration. This is supported by the quick and high discharge response at the weir (e.g. 35 ml/s Fig. 3b bottom). ERT images indicate a much more uneven saturation profile as compared to snowmelt monitoring. Areas of rock surrounded by zones of brittle deformation exhibit higher permeability to fast flowing waters.

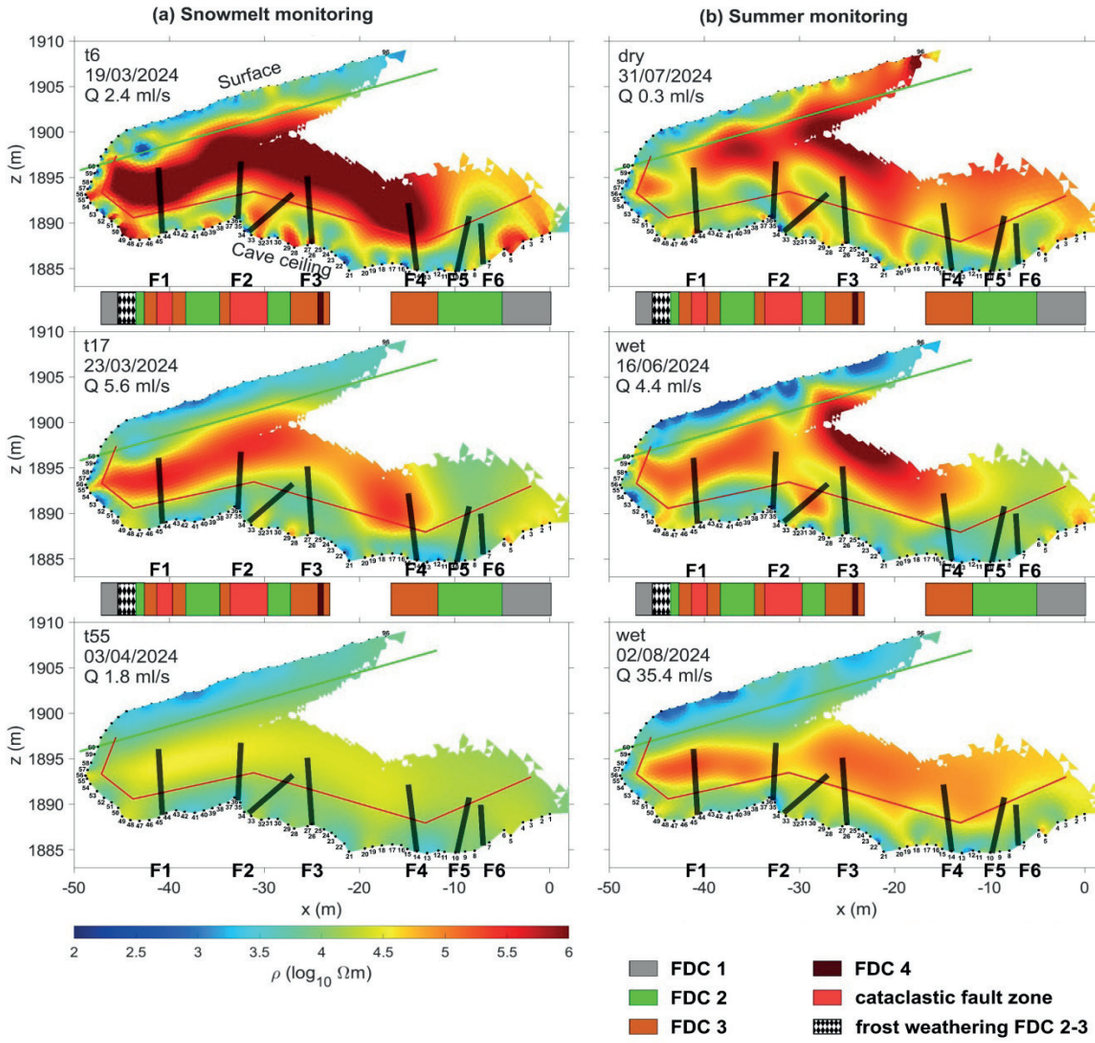

Figure 3: *ERT images of the surveyed parts of Hirschgruben cave showing the resistivity of the rock during two distinct events of surface water influx. The left-hand side displays slow infiltration of water during snowmelt in spring, while the images on the right side show various stages of saturation during dry conditions and individual rain events. The black bars show the positions and dipping angles of recorded faults marked from F1 to F6 and matching the faults in Figure 2.*

4. Discussion

The measurement of brittle faults in cave passages is a straightforward and simple procedure, as many cave passages are developed along or intersected by fault zones. Their classification in terms of fracture density distribution adjacent to fault cores is not easily done, as large amounts of damaged rock have been dissolved or eroded during cave formation and in alpine caves frost cycles, leaving only corridors of less fractured rock walls. Significant portions of the cave walls are covered with flowstone, making it impossible to classify the fractured host rock in some cave passages. In some parts of the cave, existing fractures are recemented, essentially sealing the rock and prohibiting water flow. Correlation of the structures with the closest position of their respective electrodes provides reasonably accurate localisation within the 2D images. Non-negligible inaccuracies in the exact orientations and the dip angles of faults within the images are possible due to the ERT images being 2D projections of a non-perfectly linear placement of the ERT cable in the non-linear cave passages.

5. Conclusion

From the analysis of the data provided, it can be concluded that brittle deformation structures are of significant importance not only for cave formation but also for the recent flow behaviour of infiltrated waters in vadose karst systems. Damage zones in the rock adjacent to faults tend to offer a greater retention potential in dry conditions and provide increased permeability in wet conditions. Their influence on the latter appears to depend on the rate of water inflow. Cataclastic rock at the centre of some of the recorded faults seems to act as an aquitard, as observable in the ERT images. The conducted studies provide a better understanding of the influence of brittle deformation processes on karst water permeability and retention, thus contributing to ensure quality of drinking water.

Acknowledgments

The authors thank the support by the Austrian Science Fund (FWF): P36065-N. The team would like to thank Dieter Sulzbacher and Thomas Exel for the installation of the measuring weir and meteorological station. Michael Nagl and Lina Rummler are thanked for the support in the field. For scientific discussions, thanks to Pauline Oberender.

References

ALLMENDINGER, R. W., CARDOZO, N. C., FISHER, D. (2013) Structural Geology Algorithms: Vectors & Tensors: Cambridge, England, Cambridge University Press, 289 pp.

BAUER, H., SCHRÖCKENFUCHS, T. C., DECKER, K. (2016). Hydrogeological properties of fault zones in a karstified carbonate aquifer (Northern Calcareous Alps, Austria). Hydrogeology Journal 24(5): 1147.

CARDOZO, N., ALLMENDINGER, R. W. (2013) Spherical projections with OSX Stereonet. Computers and Geosciences 51: 193 - 205.

DECKER, K. & REITER, F. (2001) Strukturgeologische Methoden zur Charakterisierung von Karstgrundwasserleitern im Hochschwabmassiv. – In Mandl, G. (Ed.) Geologische Bundesanstalt Arbeitstagung 2001. Geologische Bundesanstalt, Wien: 206-212.

EXEL, T., STADLER, H., OTTNER, F., WRIESSNIG, K., PLAN, L. (2016) Untersuchungen zum oberflächennahen Wasserspeichervermögen am Hochschwab-Karstplateau. Die Höhle 67: 77-87.

PLAN, L. (2016): Hochschwab. In: Spötl, C., Plan, L. & Christian, E. (Eds.): Höhlen und Karst in Österreich. OÖ-Landesmuseum, Linz: 645-660.

PLAN, L., SPÖTL, C. & BRYDA, G. (2019): Speläologie und Geologie der Hirschgrubenhöhle am Hochschwab (Steiermark). Die Höhle 70: 79-93.

RATSCHBACHER, L., FRISCH, W., LINZER, H. G., MERLE, O. (1991) Lateral extrusion in the Eastern Alps, part 2: structural analysis. Tectonics 10(2): 257-271.

SIBSON, R. H. (1977) Fault rocks and fault mechanism. J Geological Society of London, 133: 191–213.

WOODCOCK, N. & MORT, K. (2008) Classification of fault breccias and related fault rocks. Geological Magazine, 145: 435-440.

ZEMANN, P. (2024) Characterization of the Hochschwab karst aquifer flow regime using a water stable isotope approach (Austria). Unpublished Master Thesis, Univ. Vienna.

Sulfur on Salitre Formation, Bahia Karst: Origin, microbiology, speleogenesis and mineral deposits

Tom Dias Motta Morita (1), Ivo Karmann (2) Renato Gamba Romano (2),Rebeca Lizárraga (2), Lucas Padoan de Sá Godinho (3), Vivian Pellizari (2)

(1) Instituto de Geociências da Universidade de São Paulo, 562 Lago Street São Paulo, SP, 05508-080, Brazil, tomdmmorita@gmail.com

(2) Instituto Oceanográfico da Universidade de São Paulo, 191 Oceanográfico Square, São Paulo, SP, 05508-120, Brazil

(3) Instituto de Geociências da Universidade Federal de Minas Gerais, Av. Pres. Antônio Carlos, 6627 - Pampulha, Belo Horizonte - MG, 31270-901

Abstract

In recent decades, research has increased on hypogenic caves and karst aquifers formed by sulfuric acid, which are estimated to comprise a quarter of the world's caves. This paper focuses on the role of sulfuric acid in shaping karst aquifers in Brazil, specifically through the generation of H2SO4 within the Irecê Basin. This area is noted for its diverse gypsum speleothems and unique groundwater chemistry, hosted by the Neoproterozoic limestones of the Salitre Formation. The study employs chemical groundwater analysis, and metagenomengene sequencing. Findings indicate a significant variation in SO42- levels (2.1 to 1542.1 mg/L) and a stronger correlation with major cations Ca2+ and Mg2+ than with HCO3-, suggesting H2SO4 as the main corrosive agent in limestone dissolution. The analysis also categorizes sampling points into different hydrochemical facies and identifies a slight depletion of the 34S isotope in deep aquifer waters, pointing to pyrite oxidation as a significant sulfate source. Taxonomic analysis reveals diverse microorganisms involved in sulfur oxidation, indicating biogenic influences on sulfuric acid production.

1. Introduction

Sulfuric acid speleogenesis (SAS) in karst aquifers, compared to epigenic karst systems, involves a more intricate hydrochemical framework requiring a known sulfur source for completeness. In Brazil, studies on SAS are limited to a few regions where sulfur primarily derives from the oxidation of sulfides, especially pyrite, due to the scarce evidence of evaporite or hydrocarbon deposits in or beneath the host rock of these caves. The prevailing theory posits that sulfuric acid formation via sulfide oxidation is driven and facilitated by microbial activity. This study seeks to expand our understanding of microbial roles in speleogenesis by examining the karst system in the Una Group, located in the southern part of the Irecê Basin in central Bahia, Northeastern Brazil. This region is recognized for its high sulfate concentrations in groundwater, documented over several decades (e.g., GUERRA, 1986; VALLE, 2004), and for the extensive diversity and size of gypsum speleothems in Iraquara's caves.

SAS has been proposed by AULER (1999) as a potential hypogenic initiation mechanism before epigenic and paragenetic processes in these caves. VALLE (2004) attempted to identify connections between major cations and anions, noting a strong correlation between SO42- and (Ca2+ + Mg2+), indicating that the chemical dynamics likely involve another corrosive agent in addition to epigenic carbonic acid, namely sulfuric acid. Based on the detection of sulfur cycle bacteria, such as the Thiobacillus genus, VALLE (2004) suggested a biogenic origin for this acid.

The karst in question forms part of the Neoproterozoic limestones of the Salitre Formation, which overlies the Mesoproterozoic pelites and conglomerates of the Bebedouro Formation, both components of the Una Group. The limestones, due to the region's general synclinal structure with a north-south axis, are flanked (east, west, and south) by the quartzite and conglomerate hills of the Chapada Diamantina Group (Fig. 1), which are stratigraphically beneath the Una Group (MAGALHÃES et al., 2016). Notably, the limestones of the Salitre Formation contain sulfide occurrences, such as galena, pyrite, and chalcopyrite (MISI & SOUTO, 1975).

The geomorphological configuration of the area affects the type of water recharge in the karst system. In the southern region, where rainfall is more abundant, allogeneic recharge from the hills predominates. In contrast, the northern part of the study area, bounded by the Jacaré River and characterized by lower rainfall, comprises extensive carbonate terrains with primarily autochthonous recharge further from the hills.

2. Materials and methods

Field works were carried out in the southern region of the Irecê Basin in January/February 2021 (rainy season) and, August and October 2021 (dry season) enabling seasonal comparison. It was dedicated for water sampling from wells and caves for hydro-chemical and microbiological analysis and rock and speleothem sampling to chemical, mineralogical and isotope analysis.

Physicochemical parameters were determined *in situ* using multiparameter probes while ion contents were obtained by various analytical techniques as shown in figure 1. The hydrochemical data was then statistically processed using the *Aquachem*, *Origin* and *PHREEQC* softwares.

Analysed elements	Analytical methods
Ba, Ca, Sr, Fe, Mg, Mn, K, Na	SMEWW, 23rd Ed. 2017, Method 3120 B / USEPA 6010C - 03:2007, SMEWW 23rd Ed. 2017 Method 3030E
Cl, F, PO_4, NO_3, NO_2, SO_4	EPA SW - 846 - 300.1 - 1999
H_2S	SMEWW, 23rd Ed. 2017, Method 4500-S2-, H / G
N-NH_3	SMEWW, 23rd Ed. 2017, Method 4500-NH3, B e F

Figure 1: *Hydrochemical analytical methods.*

SIAGAS database (CPRM, 2020), known caves and previous researches conducted by VALLE (2004) and MORITA (2018) were used as a base for choosing the sampling sites (Fig. 2) for new and accurate hydrogeochemical microbiological data.

The microbiology sampling process involved collecting 15 liters of water in a pre-sterilized container, followed by filtering through 0.22 µm Sterivex membranes, retaining particulate material and microorganisms. Samples were then preserved with RNAlater™ to prevent genetic degradation and stored frozen for transport to the University of São Paulo's Microbial Ecology Lab. DNA extraction used the DNeasy PowerWater Kit and manufacturer's protocol, modified for RNAlater use. DNA integrity was checked via gel electrophoresis, and quantified with the Qubit dsDNA HS assay. Sequencing of the 16S rRNA gene V4 and V5 regions was conducted using Illumina MiSeq, providing detailed phylogenetic information. Data processing and statistical analysis were performed with QIIME2 and DADA2 plugins, with taxonomic classification through the Silva v. 138 database. The FAPROTAX tool was used to infer metabolic activities of the identified microorganisms, linking them to specific biochemical functions.

All cave samples are authorized by ICMBio nº 76989-1.

3. Results

The distribution of wells with sulfate concentration data (extracted from the SIAGAS platform CPRM 2020) along the study area is shown on figure 2. The boreholes were compared by its depth, sulfate content and geographical location, indicating an increase of sulfate content heading to the northern portion of the karst aquifer.

The analytical results show a wide range of contents in major cations and anions, and based on the piper diagram plot a predominance of calcium bicarbonated and calcium sulfated waters were identified. Both display calcium as the major cation, provided by the host rock, meanwhile the anions, HCO3- or SO42-, could be provided by the corrosive agent of the system, carbonic or sulfuric acid, respectively. Sulfate concentrations, if generally observed, covering all samples, vary between 2 and 1542 mg/L, with an average of 391 mg/L, median of 131 mg/L and a non-normal distribution

Comparing both of these anions individually with the sum of the Ca2+ and Mg2+ (Fig. 3), we identified that, within a wide overview of all the samples collected, that sulfate presents a correlation R2=0.91 while bicarbonate presents a much lower value of R2= 0.17. Furthermore, the plot of Figure 3, shows that there are different groups of samples that must be identified and studies separately.

Samples groups were divided according to hydrochemical facies into phreatic cave lakes, boreholes (deep-seated aquifer), karst springs, and vadose cave water. It was observed that the deep-seated aquifer water samples collected from boreholes tend to present higher concentrations of ions related to the dissolution of the rock. This factor may also be related to the geographic location, since not many cavities are known in the northern region, thus the northern region samples were collected from boreholes, with the exception of a vadose cave sample in Lapa do Sumidouro.

The results of the chemical analyses align with the tubular well database available on the SIAGAS platform (CPRM, 2020 - Figure 4.1) and obtained during the pre-field phase. As depicted in Figure 4.9, the lower concentrations of the main ions related to the dissolution of the host rock (SO4, HCO3-, Ca2+, and Mg2+) are primarily found in the southern region of the Irecê Basin, where precipitation is more intense and the karst aquifer is more influenced by allogenic recharge from the quartzites of the Espinhaço Supergroup.

It is interesting to note the relationship established by Worthington and Ford (1995) between bicarbonate and sulfate anions in karst springs, and how this can be applied to understand the origin of the main cations and anions in karst aquifers (figure 4). According to these authors, the tendency for high sulfate concentrations in the water from deeper aquifer levels, accessed via tubular wells in this case, suggests the possibility of factors other than carbonic acid action contributing to rock dissolution. This includes the action of sulfuric acid, which may be linked to the presence of evaporitic minerals or sulfides interspersed in the limestones, as mentioned by the authors.

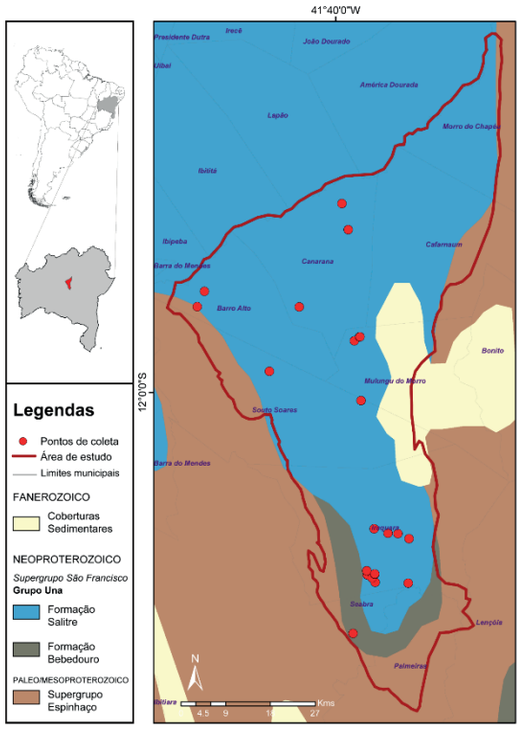

Figure 2: *Location of the study area and collection points (indicated by the polygon and red circles, respectively), on the geological map, taken from Gómez et al. (2019).*

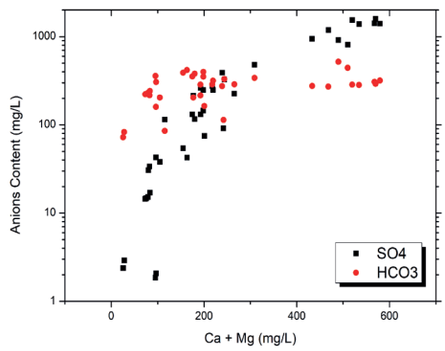

Figure 3: *Scatter plot comparing HCO3- and SO42- with Mg2+ and Ca2+ sum.*

In the chemical system of karst, it is crucial not only to understand the chemical reactions involved in the dissolution of the host rock and the precipitation of secondary minerals but also to assess whether these reactions are in equilibrium. The Saturation Index (SI) of minerals serves as a vital indicator of this equilibrium. Based on the physicochemical parameters of water, the SI helps determine whether aqueous solutions are undersaturated, saturated, or supersaturated concerning specific minerals. Negative SI values indicate undersaturation, suggesting a tendency for the mineral to dissolve from the host rock. In contrast, zero values suggest saturation and likely equilibrium, while positive values indicate supersaturation and a propensity for chemical deposition.

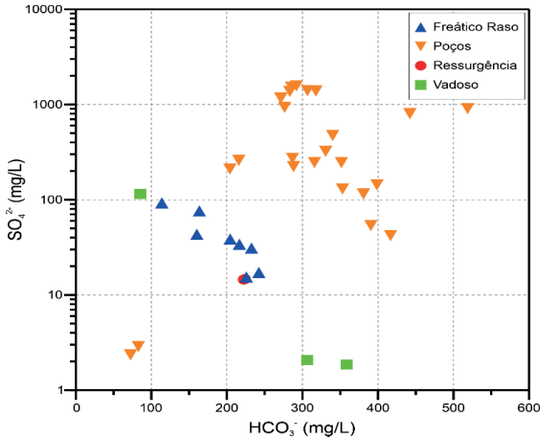

Figure 4: *Correlation on a monologarithmic scale between the anions HCO3- and SO42-. The X-axis indicates the bicarbonate content, and the Y-axis (in logarithmic scale) indicates the sulfate content. Both concentrations are presented in mg/L.*

Analytical and physicochemical data were used to calculate the saturation indices for key minerals such as calcite, aragonite, and gypsum. These calculations employed water samples from shallow aquifers and tubular wells, chosen for the larger number of samples available. The shallow aquifer showed SI values close to zero, ranging from 0.05 to 0.45 with an average of 0.23 for calcite, and from -2.49 to -1.47 with an average of -2.03 for gypsum. Tubular well samples exhibited a broader range of SI values, from -1.58 to 1.59 with an average of 0.01 for calcite. For gypsum, the indices ranged from -3.70 to -1.11 with an average of -0.20.

To expand the hydrogeochemistry of sulfur in the system, X-ray diffraction analyses were conducted on rock samples and chemical deposits to identify potential sulfur-bearing minerals and enhance understanding of the diversity and dimensions of sulfate speleothems in the Iraquara caves.

Samples of speleothems identified in the field as gypsum, or similarly habituated and locally identified as gypsum by guides, were collected for verification. Analyses included speleothems from Gruta do Didi, Gruta Torrinha, Lapa da Umburana, Lapa Doce, a mineral observed in the rock at Lapa Doce, and two crusts precipitated in irrigation wells.

For the analysis of microbial diversity in the samples, data were filtered to display only groups involved in the sulfur cycle. Proteobacteria, known for reducing sulfur compounds such as thiosulfate, elemental sulfur, and DMSO (Fukuyama et al., 2020), includes species like Sulfurospirillum carboxydovorans MV. Previous studies identified related organisms such as Thiobacillus and Thiothrix, linked to sulfuric acid speleogenesis and geospeleology (Hill, 1985; Auler and Smart, 2003; Valle, 2004; Engel et al., 2010). Crenarchaeota members breathe elemental sulfur, with the Sulfolobales order utilizing it as an energy source (Leight & Whitman, 2001; Liu et al., 2021). Planctomycetota can use elemental sulfur as an electron acceptor in anaerobic conditions (Kaboré et al., 2020). Bacteroidota are noted for their sulfur-reducing ability, producing sulfur sulfide (Hahn et al., 2022). Campilobacterota members oxidize sulfur compounds, coupled with nitrate reduction or molecular oxygen use (Xiao et al., 2023). FAPROTAX is a bioinformatics tool used to infer bacterial metabolic functions from 16S rRNA gene sequencing, predicting functional groups based on literature data. Figure 5 illustrates the metabolic functions associated with microorganisms in the samples, indicating their role in sulfur compound respiration and oxidation under aphotic conditions. The samples from Lagoa Preta and Poço do Luisão show high metabolic intensities related to sulfur and its compound's respiration and oxidation in dark environments.

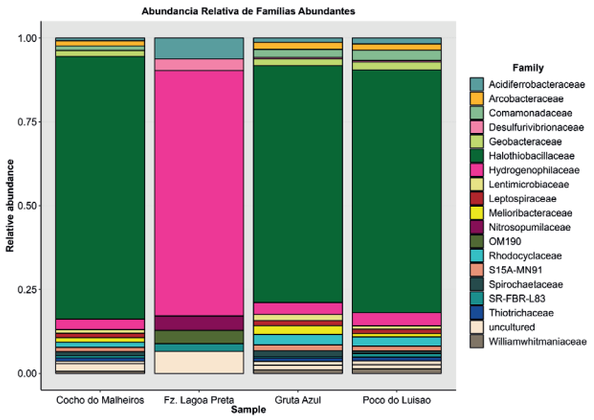

Figure 4: *Relative abundance of dominant families (>1%) by station. Each column represents a sample, and the Y-axis indicates the proportion of each family (denoted by colors) for the analyzed samples.*

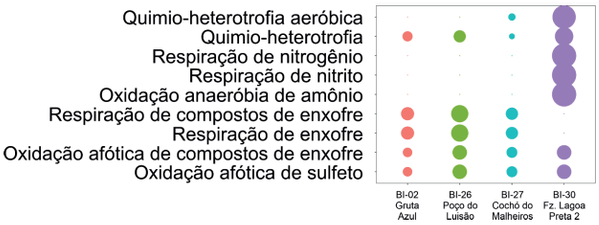

Figure 5: *Relative abundance of the predicted functional groups for the communities present at each station. The size of the circles represents the percentage of relative abundance, ranging from 1% to 100%. The circles are distributed in the figure according to the sample (X-axis) and metabolic function (Y-axis).*

4. Discussion

The hydrochemical results indicate that the northern region of the study area tends to exhibit the highest levels of sulfates in groundwater when compared to the southern region. These values when compared to the HCO3- contents, in which no correlations were found, is an indicative that, under the SAS hypothesis for the Irecê Basin, the bicarbonate present in the water does not come exclusively as a product of H2CO3 carbonate rock dissolution. Towards south, the sulfate content decreases, indicating greater epigenic activity, as evidenced by greater cave density (Fig. 1) as well as morphological and sedimentological characteristics of the caves. Considering the speleogenetic model suggested by AULER

(1999) and the predominance of epigenic karst over hypogenic according to the denudation rate and annual rainfall (AULER & SMART, 2003), it is understood that the hypogenic features, responsible for the initial stage of speleogenesis, are superimposed by epigenetic features.

The southern region of the Irecê Basin has higher rainfall and higher allogenic recharge, which enables the exposure and development of caves closer to the surface and less sulfated groundwater. On the other hand, the northern region represents an earlier stage of karst development at greater depth and a more significant performance of H2SO4 as a corrosive agent, originated in the host rock itself.

The microbial diversity results highlight the significant presence of various microorganism groups linked to the sulfur cycle in the Irecê Basin's karst aquifer. Despite a low sample size due to research limitations and the non-retrieval of genetic material in several samples, interesting observations can still be made. Notably, only the sample from Gruta Azul was collected during the first field campaign, but this did not significantly alter the microbial community compared to the hydrochemical results. Ionic contents remained consistent across field campaigns, likely due to unusual drought conditions during the supposed rainy season of late 2020 and early 2021. Thus, temporal variations are considered less crucial than hydrochemical facies for differentiating hydrochemical environments.

Particularly, the microbial diversity of the sample from Fazenda Lagoa Preta stands out, evidenced by the relative abundance of 20 taxonomic families associated with the sulfur cycle. This distinction aligns with hydrochemical results (Figure 6)) where high sulfate levels are highlighted, making it the most sulfated sample among the four analyzed.

The likely link between hydrochemical and microbiological results is due to the primary sulfur source in the geochemical system, typically metallic sulfides, mainly pyrites. The microbial activity highlighted by the presence of microorganisms related to the sulfur cycle facilitates the oxidation of these sulfides, releasing sulfur species in aquatic environments.

Additionally, the other samples also showed the same metabolic functions related to sulfur. Notably, the Poço do Luisão sample, located in the Quixaba settlement, also exhibited significant sulfate levels, though not as prominent as those in the Lagoa Preta sample. This variation is likely due to the geographic locations of the sampling points, as indicated by the hydrochemical results, with the southern region of the study area having higher rainfall and greater influence from allogenic recharge from the quartzites bordering the Irecê Basin to the west, south, and east.

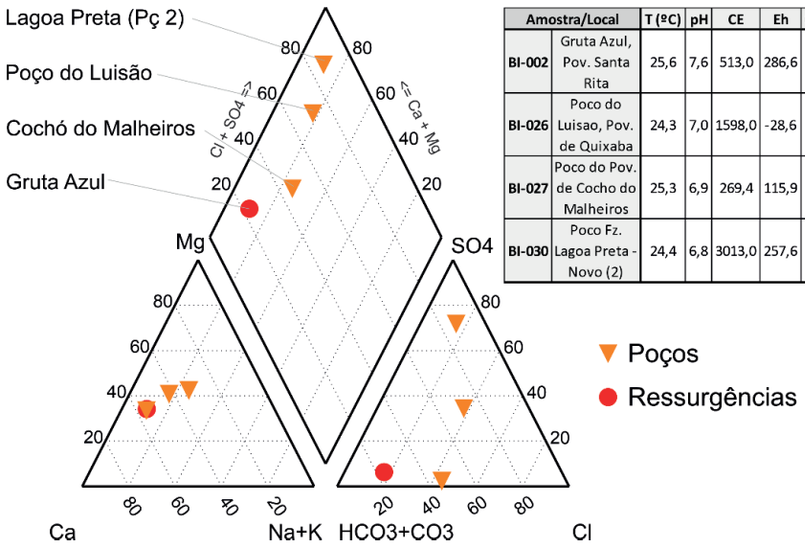

Amostra/Local		T (ºC)	pH	CE	Eh	OD (%)	SO4	HCO3	Ca+Mg
BI-002	Gruta Azul, Pov. Santa Rita	25,6	7,6	513,0	286,6	58,2	14,5	222,3	73,1
BI-026	Poco do Luisao, Pov. de Quixaba	24,3	7,0	1598,0	-28,6	7,6	276,0	286,7	217,6
BI-027	Poco do Pov. de Cocho do Malheiros	25,3	6,9	269,4	115,9	23,4	2,9	82,8	27,9
BI-030	Poco Fz. Lagoa Preta - Novo (2)	24,4	6,8	3013,0	257,6	34,3	1406,7	317,8	579,4

Figure 6: *Piper diagram and simplified table of physical-chemical parameters and analytical results for the samples presented in the microbiology results.*

5. Conclusion

Although important data are still lacking for the consolidation of the SAS hypothesis in the karst system of the Irecê Basin and mainly to the biogenic production of this acid, the sulfate present in groundwater are in notable concentrations among Brazilian karst.

Correlations found between SO_4^{2-} and the major cations, geographic location and relative abundance of Thiothrix and Thiobacillus genus bacteria corroborate to the understanding that sulphur has an effective participation in the local speleogenesis.

Acknowledgments

We thank Lívia Rocha, Aghata Zarelli and Gabriela Duarte for helping in our field works, the LECOM-IO and Karst System Lab – Igc teams for the contributions throughout the research and ICMBio-CECAV/Ferro Puro (TCCE 01/2020) for the research funding We would also like to thank Laurent Bruxelles and Lionel Barriquand for the support.

References.

AULER A. (1999) S. Karst evolution and paleoclimate of eastern Brazil. 264p. PhD, University of Bristol.

AULER A., SMART P. L. (2003) The influence of bedrock-derived acidity in the development of surface and underground karst: evidence from the Precambrian carbonates of semi-arid northeastern Brazil. Earth surface processes and landforms, 28, 157-168.

COMPANHIA DE PESQUISA DE RECURSOS MINERAIS. CPRM. (2020) Sistema de Informações de Águas Subterrâneas. SIAGAS. Brasília: CPRM. Avaiable on: http://siagasweb.cprm.gov.br/layout/index.php

Guerra, A. M. (1986) Processos de carstificação e hidrogeologia do Grupo Bambuí na região de Irecê-Bahia. PhD. Instituto de Geociências, Universidade de São Paulo.

GÓMEZ J., SCHOBBENHAUS C., MONTES N. E., compilers. (2019) Geological Map of South America 2019. Scale 1:5,000,000. Commission for the Geological Map of the World (CGMW), Servicio Geológico Colombiano, y Serviço Geológico do Brasil, Paris.

MAGALHÃES A. G. C., G. P., RAJA GABAGLIA C. M. S., SCHERER M. B., B´ALLICO F., GUADAGNIN E., BENTO FREIRE L. R., SILVA BORN O., CATUNEANU (2016) Sequence hierarchy in a Mesoproterozoic interior sag basin: From basin fill to reservoir scale, the Tombador Formation, Chapada Diamantina Basin, Brazil: Basin Research, v. 28, no. 3, 393–432,

MISI A., SOUTO P. (1975) Controle estratigráfico das mineralizações de chumbo, zinco, flúor e bário no Grupo Bambuí–parte leste da Chapada de Irecê (BA). Brazilian Journal of Geology, v.5, n.1, 30-45.

MORITA, T.D.M., KARMANN, I., ROMANO, R. G., PELIZZARI, V., VALLE, M. A., GODINHO, L. P. de S. (2019) Ácido sulfúrico como agente corrosivo no sistema cárstico de Iraquara (Grupo Una, BA). In: ZAMPAULO, R. A. (org.) CONGRESSO BRASILEIRO DE ESPELEOLOGIA, 35, Bonito. Anais: SBE, Campinas, 45-51.

VALLE, M. A. (2004) Hidrogeoquímica do Grupo Una (Bacias de Irecê e Salitre): um exemplo da ação de ácido sulfúrico no sistema cárstico. 122p. PhD. Universidade de São Paulo.

Man-dug water wells leading to caves, a statistical approach: Geometric characteristics and hydrogeological behaviour

Claude Mouret (1)

(1)Fédération Française de Spéléologie, 955 Route de La Tamanie, 87380 Magnac-Bourg, France claude.mouret.geospel@orange.fr

Abstract

More than 130 water wells in France lead downto caves with no other entrance. There are probably more and obviously many of them remain to be identified in other countries. Gathering information on the matter is rather difficult because it is usually scarcely published and mainly available in local speleological magazines. Data gathering over the years enabled the author to build a database as complete as possible. Statistical data processing allowed him to evaluate cave depths, height and width, cave lengths, type of water bodies or lack of water. Studied wells have been dug out in limestone formations ranging from Cambrian to Miocene. The location of the wells on the passages shows common eccentricity. Water rises in a part of the wells may explain how their location was selected, but the majority of the wells are not related to any surface manifestation of water. The paper details and discusses quantitatively many of these aspects and it proposes ways forward.

Résumé

Puits artificiels ayant recoupé des grottes, approche statistique. Plus de 130 puits d'eau ont rencontré des grottes qui n'étaient pas connues au préalable. La base de données constituée par l'auteur sur la France a permis une analyse statistique détaillée de ces grottes et de ces puits et sur la façon dont ils s'interceptent. L'eau recherchée n'est pas toujours présente. Des remontées de celle-ci dans certains puits se produisent lors d'épisodes pluvieux. Diverses régions et des intervalles stratigraphiques appropriés ont été pris en compte dans cette étude. L'article détaille quantitativement ces aspects et propose des voies de progrès dans cette approche nouvelle de la connaissance des milieux karstiques.

1. Introduction

More than 130 caves in France are accessible only through a well especially dug for water finding (Fig. 1). Water level may fluctuate throughout time, when it is present. Water has been encountered as pools, streams or water table, the latter being encountered confined in several cases. Water wells considered in this paper were in most cases dug from a supposedly dry ground surface, for instance dry valleys, slopes or plateaus.

All cave characteristics (length, width, etc.) are analysed on a statistical basis.

The study of such caves and wells seems to be made here for the first time.

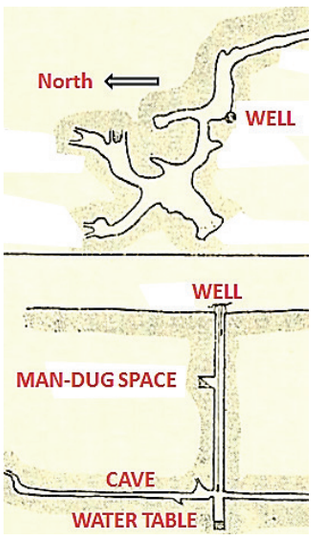

Figure 1: *A 34 m deep well through a man-dug passage, a cave and the water table in Upper Cretaceous chalk (from A. VIRÉ & A. PIÉDALLU, (1909). Grotte et souterrain-refuge de la Bosse, commune de Morée (Loir-et-Cher). Bulletin du muséum d'histoire naturelle, 1909, n° 4, p. 202-206)*

2. Data availability and quality control

The more than 130 caves in the dataset mainly come from author's compilation of a variety of speleological bulletins and regional studies not focused on his target. Data gathering took many years and cannot be complete. Due to difficulty in finding bulletins, little by little, only cases from France have been used. There is no doubt that similar facts exist in other countries.

For a given cave or a given well, all parameters are rarely available together. In some cases, gaps can be filled using additional information from regional maps, general publications, phone calls or else. Whenever a cave had been mapped by different persons, maps and sections were compared and numerical values could be either averaged (equal map quality) or weighted using a stronger coefficient for better quality map or even rejected. Numerical values were often measured on maps and sections. They are as precise as possible, but often they cannot be perfect.

"Nugget effects" in the dataset relate to numerical values by far greater than other values. For instance, there is a 16 000 m long cave, a 12.2 m width for a void, a 75 m deep composite shaft which is the only one reached by a water well (it is usually dry, though occasional water rise occurs in the bottom part after very heavy rain periods).

3. Concerned regions

All regions with caves in wells show elevations between 25 and 450 m a.s.l., with a majority below 260 m (Fig. 2). They are mostly located in Liassic to Miocene series in Paris and Aquitaine Basins, though two cases are in Paleozoic limestone, one in Massif armoricain and one in Ardennes. Caves in Liassic sediments are mainly located along the edge of Aquitaine Basin. Some caves in wells through Dogger, Malm and or rarely Lower Cretaceous are located in Paris Basin (Nièvre and Yonne Districts mainly) and in Aquitaine Basin (Poitou and Quercy mainly), as well as in Jura Mountains (Ain). Upper Cretaceous is largely found in Paris Basin (Normandie, Yonne, Touraine…). Paleogene and Miocene are mainly present in the central part of Paris Basin and in the broader Bordeaux area in Aquitaine.

LENGTHS (m)	Nb of values	Min	Median	Mean	Max	Mean 2*
MIOCENE	8	10	80	152	800	327
PALEOGENE	8	3	113	583	2100	1153
UPPER CRETACEOUS	46	1	77	231	1930	444
DOGGER, MALM, L. CR.	27	3	82	833 (250)	16000 (2000)	1693 (501)
LIASSIC	5	10	30	236	850	561
PALEOZOIC	2	100	365	365	630	630
ALL DATA	96	1	80	426 (262)	16000 (2000)	828 (505)

Table 1: *Cave lengths distribution. * Mean 2 is the mean of all values greater than the median of 96 values. Bracketed figures do not include the nugget value of 16 000 m.*

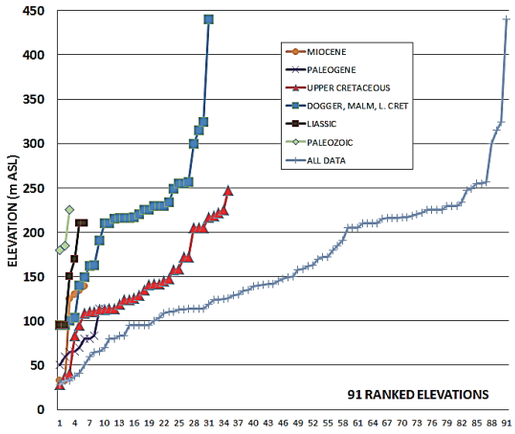

Figure 2: *91 ranked wellhead elevations at ground level (m ASL), split per geological periods.*

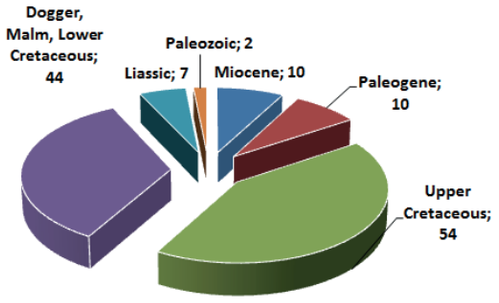

Figure 3: Geological split of 127 caves reached through a water well, dry or not. Geological periods have been selected in order to group limestone units with nearly similar petrophysical properties: broadly, the younger, the more porous.

4. Cave lengths

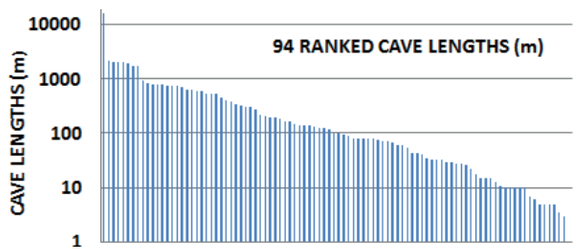

Figure 4: *Logarithmic distribution of 96 cave lengths (m).*

There is a low median (80 m, all data included) and a variable mean value (262 m with nugget effect discarded, Table 1). 1 cave reaches 16000 m; 6 exceed 1000 m; 18 are longer than 500 m, 40 over 100 m and 56 over 50 m (Fig. 4). The mean values of caves longer than the median value is of 828 m.

5. Cave widths and heights

Widths (Table 2, Fig. 5) are perpendicular to cave passage at well intersection. They are exceptionally greater than 8 m and usually average between 1 and 2.5 m.

WIDTHS (m)	Nb values	MIN	MEAN	MAX
MIOCENE	2	4	8.1	12.2
PALEOGENE	4	0.8	2.05	6.3
UPPER CRET.	20	0.1	2.5	7.5
DOGGER...	20	0.4	2.1	7
LIASSIC	4	0.55	2.7	6.5
PALEOZOIC	2	0.6	1.05	1.5
ALL DATA	52	0.1	2.55	12.2

Table 2: Widths of 52 cave passages at well intersection.

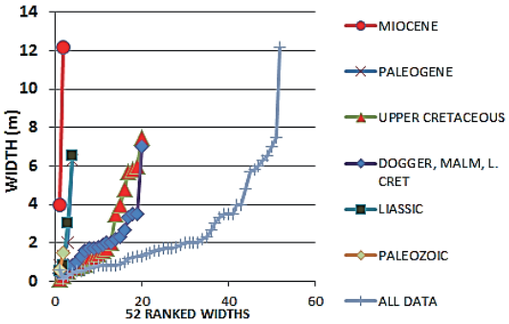

Figure 5: Widths (m) at well intersection.

Heights (Table3, Fig. 6) are obtained from cave long sections or (rarely) cross-sections under the same conditions as for widths. Heights are greater than 3.5 m in 7 % of cases only.

HEIGHTS (m)	Nb values	MIN	MEAN	MAX
MIOCENE	4	1.8	2.25	2.6
PALEOGENE	5	0.4	1.8	5.5
UPPER CRET.	21	0.4	1.7	5
DOGGER...	18	0.2	1.55	6
LIASSIC	4	0.8	1.4	2.5
PALEOZOIC	2	1.6	1.8	2
ALL DATA	54	0.2	1.7	6 (75)

Table 3: Heights of 54 passages at well bottom (1 nugget value of 75 m not included).

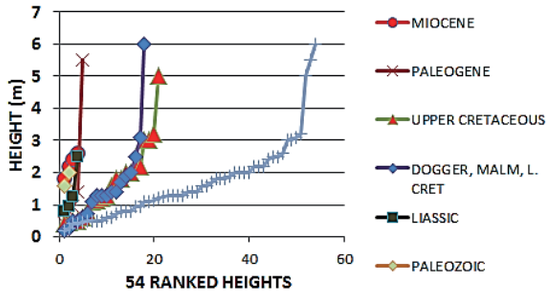

Figure 6: Heights (m) at well intersection, per geological period. The 75 m nugget value is not included, for clarity.

6. Well ages, diameters and depths

From Year 1800 to Year 2000 AD, 47 wells out of 50 with age data were regularly dug out in order to find water. 3 wells were dug between Years 1200 and 1400 in castle and abbeys: their scarcity may be due to lack of data or to further collapse or plugging. However, traces of very old wells are not seen in presently accessible caves. Hypothetically, many peasants were perhaps not rich enough to finance well digging before French Revolution in 1789.

The beginning of geophysics and borehole drilling did not stop well diggers to elaborate new wells.

Well diameters (Fig. 7) are very imperfectly known. We have tried to use the outer diameter, behind masonry, i.e. the original well size, reading diameters on cave maps or depth sections. It is not an accurate matter: we obtain a magnitude. Most of the wells are smaller than 2 m and several more are between 2 and 3 m. Larger wells are due to specific causes. A 4.5 m large well in Normandie was dug out by German Army during WWII. A 5.9 m large well beyond a choked spring was designed to collect water from a karst drain beyond. Three wells with a 0.25 m diameter were drilled and encountered a void close to the expected depth. Mean value is 1.4 m and median 1.2 m.

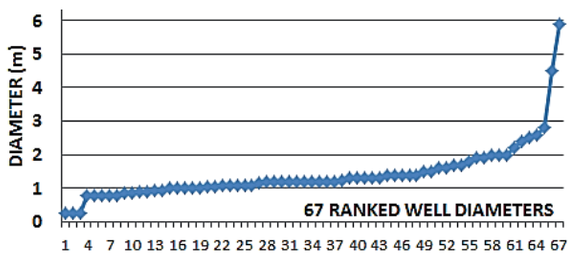

Figure 7: Well diameters (in m), 67 values.

Documented well depths reach up to 103 m below ground level (Fig. 8).

Though mostly located at well bottom, caves may be located at a smaller depth. A single well may encounter two levels of caves or voids and even the water table further deep.

On Figure 10, all dots along the limiting straight line between dots 0-0 and 103-103 correspond to caves encountered at well bottom. All dots to the left of the line indicate caves shallower than well bottom: below a 40 m depth (Fig. 9 - 10), they are mainly located in Upper Cretaceous chalk or chalky limestone, though there is one case in Dogger limestone. Above 40 m, several caves in different formations are shallower than well bottom.

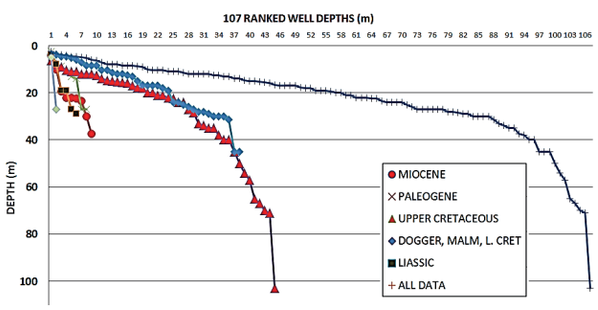

Figure 8: 107 ranked well depths per geological period. Caves in Upper Cretaceous chalk are partly encountered at greater depths then caves in other formations

7. Passage widths and heights vs depth

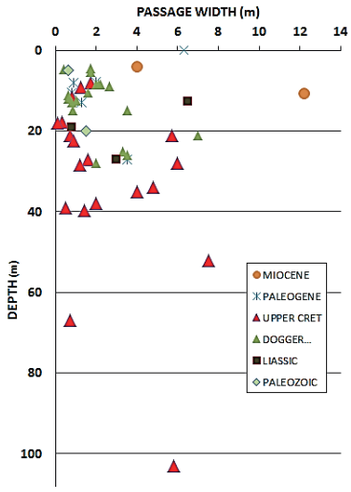

Figure 9: *passage width at the well vs cave bottom depth.*

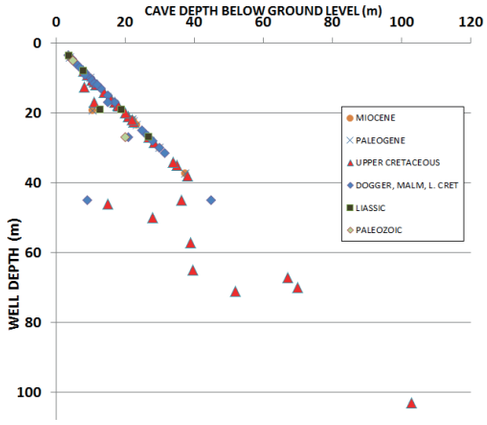

Figure 10: *passage height at the well vs cave bottom depth.*

Figures 9 and 11 show no clear relation of cave width and height with depth. However, a few greater width and height values are encountered closer to ground surface, though a cave at a 103 m depth shows is twice large than high and 22 m long only.

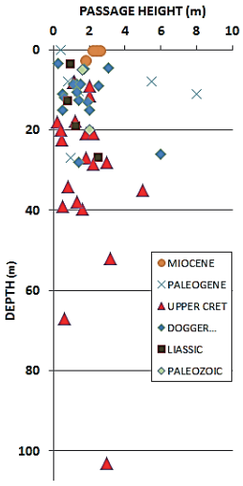

Figure 11: Cave heights per geological period vs depth in the wells.

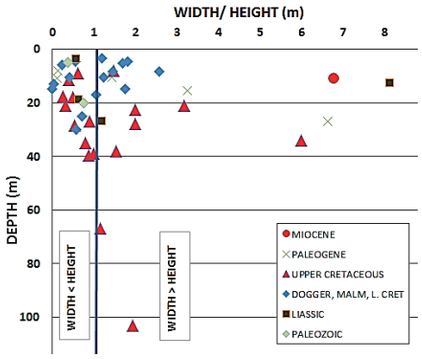

There are as many caves higher than large as caves larger than high, though, in average, widths are greater than heights (2.5 m vs 1.7 m respectively). There is no significant variation with depth (Fig. 12).

8. How is cave size distributed from surface to depth?

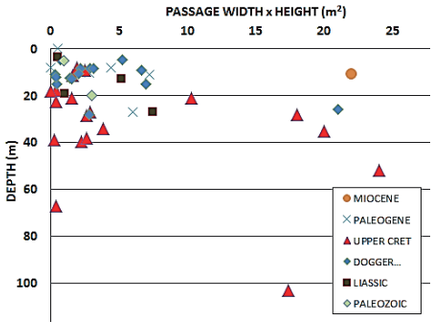

Figure 13: Passage pseudo-section (m²) vs depth (m). 47 values.

Figure 13 shows width x height cave pseudo-sections versus depth. They have been computed in order to give a magnitude of cave size, due to scarcity of published passage sections at well intersection. Values have been either carefully measured by the author on cave maps and/or long sections or collected from written indications. Values distribution shows two groups: 41 smaller values from ground surface down to 70 m and 6 larger at various depths (down to 103 m). Deeper ones are located in chalk or chalky limestone. The graph suggests that many caves may exist with intermediate sizes. So, statistically, there are still more caves to be found.

9. Well eccentricity

In most cases, the well reaches the cave passage near the cave wall (Fig. 14) and rarely in the centre (Fig. 15). Eccentricity is defined as the distance from the well central vertical axis to the centre of the cave passage on the cave map (Fig. 16).

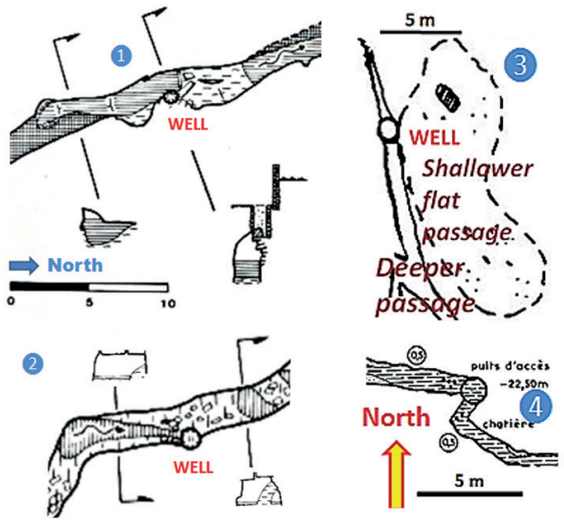

Figure 14 (left): Examples of eccentered wells. 1: Croisy South Well (58), p. S10; 2: Bois-Gratton underground stream (58), p. L11. Both cases are from Chabert, Couturaud et al, 1986.

Figure 15 (right): Centered wells. 3: Grotte de La Gorchonnière (79), CDS79, 1979, p. 40; 4: Underground River of Petit Vaudeurs (89), in Chabert et al, 1977, p. 275.

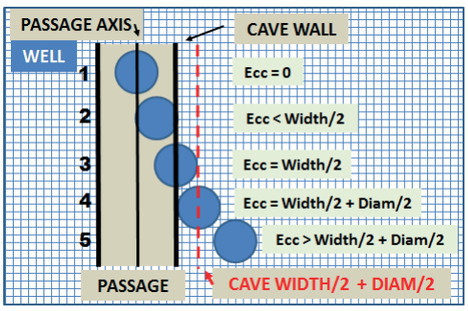

Figure 16: Quantification of eccentricity, main cases (map).

Eccentricity direction is the azimuth along which the well axis should be moved to reach the central axis of the passage, along the perpendicular cross-section at well intersection. Five main cases of eccentricity can be considered (Fig. 16):

- **Case 1:** The well is perfectly centered in the passage. Depending on its diameter and on the passage width, it may be entirely in the passage or excavating cave walls.
- **Case 2:** The well may either entirely fall in the passage if its diameter is smaller than half the passage width, or to the contrary excavate one of the cave walls.
- **Case 3:** The well is centered on the cave wall and half its diameter is excavating the cave wall.
- **Case 4:** The well is tangential to cave wall. And out of the cave.
- **Case 5:** The well is out of the passage. It may have been connected to it because diggers heard a sound of running water through the rock or through a rock crack. A few wells could not encounter water (such as a karst stream) and were eventually connected thanks to a man-dug passage in the direction of the expected stream. Some met with no success.

Sometimes, the well to cave junction is occurring thanks to a small tributary or side branch. In this case, eccentricity is defined by reference either to the tributary or to the main passage. It is a matter of appreciation, based upon geometric characteristics and flow regime.

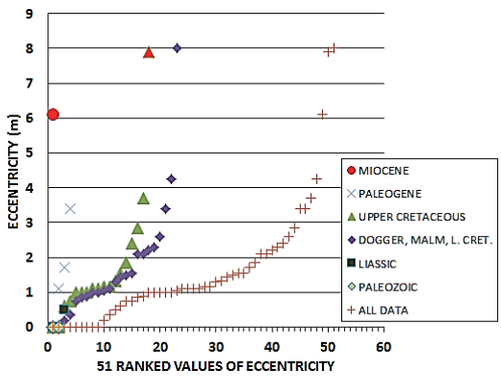

Figure 17: Ranked distribution of 51 values of distance of eccentricity (m).

Figure 17 (all data) shows a continuous range of eccentricity values, with three outlying ones. The latter mostly correspond to oblong voids reached at their edge or at their tip. Eccentricity is greater than 4.5 m in only 6 % of the cases. The mean value of 51 eccentricity values is 1.65 m and the median 1.1 m. This can be compared with 52 passage widths, their mean being of 2.6 m and their median of 1.7 m. In average (only), well eccentricity is therefore lower than cave width. However, eccentricity is better compared (Fig. 18) with half-width (1,3 m (mean) and 0.85 m (median)): the well centre is commonly out of the passage. However, its half-diameter needs to be considered, as it participates in the contact with the passage.

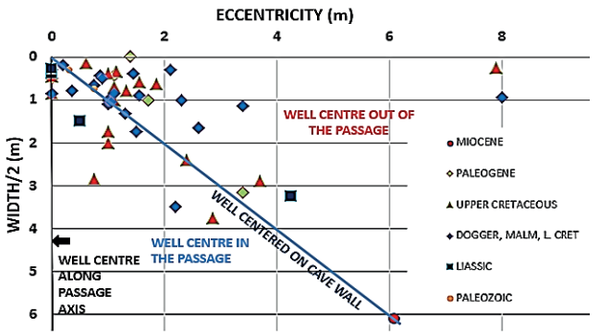

Figure 18: Eccentricity compared with cave width/2 (m)

If we add the half-diameter of the well to the half-width (Fig. 19), it appears that several wells are not in direct contact with the passage. However, given the uncertainty on the real well diameter (i.e. in open hole conditions, behind masonry), few wells are really out of the passage.

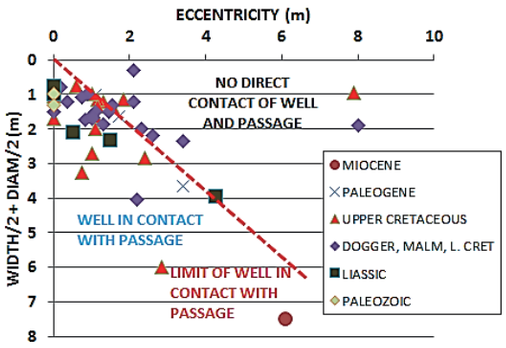

Figure 19: Eccentricity compared with passage width/2 and well diameter/2.

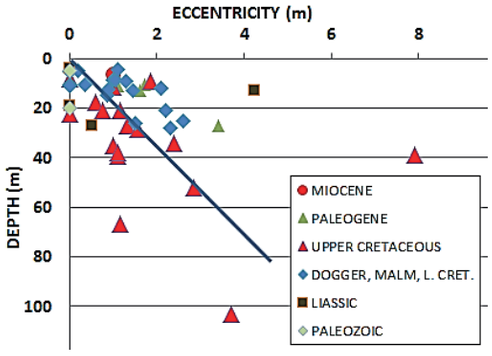

Figure 20: There is a rather loose correlation of eccentricity with depth.

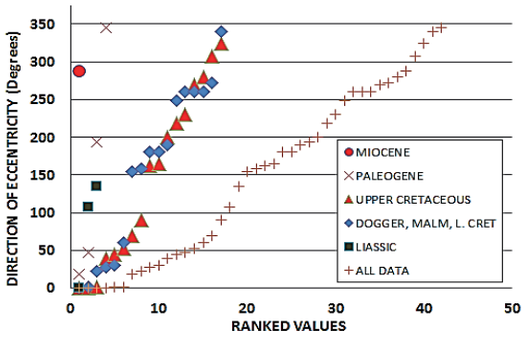

Figure 21: Ranked directions of eccentricity (from 0 to 360°).

Directions of eccentricity (0 to 360 degrees, Fig. 21) show almost no correlation with well depths. Some directions are less present (60 to 150°, out of 360°). On the other hand, **passage directions at well intersection** (Fig. 22-23) seem to be more numerous between 75 and 175° (out of 180°), i.e. on an average SE-NW direction. Obviously, this is broadly consistent, the directions of eccentricity being somewhat linked to passage directions, but passage angularities make fuzzier the overall picture. Also, among 19 wells close to an underground stream, 14 happen located along the right bank and 5 along the left bank.

All passages taken together show an apparent lack of direction vs

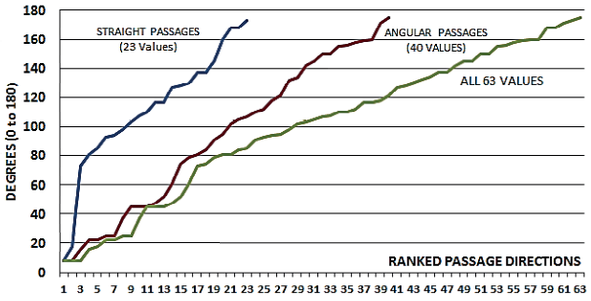

Figure 22: 63 directions of passages (from 0 to 180 degrees) at well intersection. Straight passages appear to be more numerous between70 and 170 degrees.

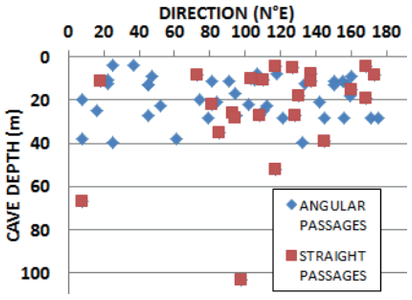

Figure 23: Passage directions at well intersections.

10. Water status and regime of caves

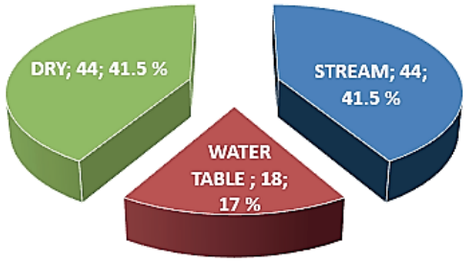

Figure 24 shows that, among 106 wells with data, 44 were found dry (41.5 %). This latter figure is obviously lower than the actual proportion, because a number of dry wells have probably been plugged and are now forgotten. Several dry wells give access into caves which may show either dormant or running water at some distance. Some dry wells at cave level have been deepened and were eventually able to provide water for human use. Some others remained dry.

WELL STATUS	Dry	Water table	Stream	TOTAL	Dry (%)	Water table (%)	Stream (%)
MIOCENE	2	0	4	6	33,3	0	66,7
PALEOGENE	5	2	2	9	55,6	22,2	22,2
UPPER CRET.	21	6	19	46	45,7	13	41,3
DOGGER, MALM, L.C.	13	9	16	38	34,2	23,7	42,1
LIASSIC	1	1	3	5	20	20	60
PALEOZOIC	2	0	0	2	100	0	0
TOTAL OF WELLS	44	18	44	106	41,5	17	41,5

Table 1: Well water status (%) per geological unit (106 wells). Streams are present in many more wells than dormant-like water table.

Water rise related to rainy episodes helps in better knowing how the wells were located in the field.

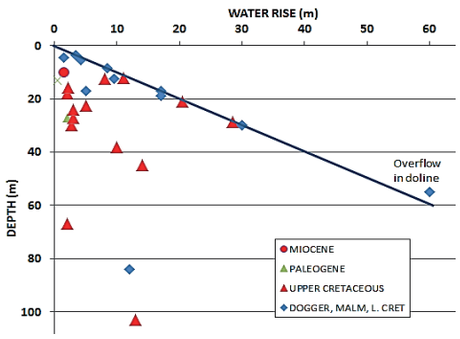

Figure 25: Water rise vs well depths, taken at well bottom. Some wells are deeper than cave passage.

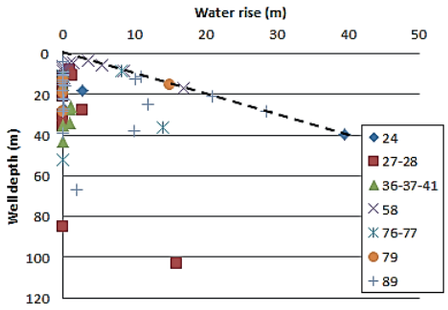

Figure 26: Water rise in wells vs districts ("départements"). Some districts are deliberately not shown, for clarity. Wells with "no rise" mentioned are not shown either. For caves not located at the well bottom, the water rise originates from an underlying aquifer. 24: Dordogne; 27: Eure; 28: Eure-et-Loir; 36: Indre; 37: Indre-et-Loire; 41: Loir-et-Cher; 58: Nièvre; 76: Seine-Maritime; 77:

11. Conclusion

his statistical study demonstrates that blind caves can be revealed by water wells. The length is 262 m in average and 19 % of the caves exceed 500 m. The mean width is 1.5 m and the mean height 1.7 m. The bulk of cave depths ranges from 0 to 50 m

It was unexpected that more than 130 caves in France could have been revealed by water wells, mainly during the 19th and 20th Centuries. Wells frequently reach cave passages near their wall and hydrogeological behaviour greatly varies

Similar caves opened by water wells necessarily exist in other countries than France and need to be documented. Systematic *in situ* measurements and observations shall bring additional information.

Acknowledgements

to all topographers.

Quantification of solid and dissolved load from the mass balance of a large karst spring - preliminary results (Kläffer Spring, Eastern Alps)

Michael Nagl (1) & Lukas Plan (1)

(1) Cave and Karst Group, Natural History Museum Vienna, Burgring 7, 1010 Vienna, AUSTRIA. michael.nagl@nhm.at lukas.plan@nhm.at

Abstract

The Kläffer Springs, Austria's largest karst springs, on the northern edge of Hochschwab play a crucial role in Vienna's water supply but are prone to turbidity during flood events due to suspended sediment mobilization. While the dissolved load has been quantified already 20 years ago, the suspended sediment load remained uncertain. This study aims to establish a correlation between turbidity (NTU) and total suspended solids (TSS) to quantify the solid load discharged from the karst system. Water samples were collected at different discharge conditions, including an extreme turbidity event (48 NTU). Suspended sediments were separated by settling and drying before weighing. Hydrological parameters such as turbidity, conductivity, temperature, and discharge are recorded at 10-minute intervals. The dissolved load was determined using a regression between calcium and magnesium hardness and electrical conductivity (R^2 = 0.99). Preliminary results suggest a linear TSS-NTU relationship, with suspended sediment discharge estimated at 180 tonnes per year, significantly lower than the dissolved load (22 kt/year). Further sampling is necessary to refine this correlation.

1. Introduction

The Hochschwab mountain range in northern Styria (Austria), which covers an area of 560 km², consists mainly of a sequence of Triassic sediments dominated by limestones and dolostones of the Middle Triassic Wetterstein Formation (BRYDA, 2001). The stepped plateau ranges from an altitude of about 1500 m to the summit of the Hochschwab at 2277 m a.s.l. The whole massif is surrounded by rather deep valleys at 500 to 700 m a.s.l. The plateau is characterised by numerous karst features: huge dolines up to several hundred meters in diameter are characteristic of the non-glaciated areas (Pleistocene nunataks), and a high density of smaller dolines has developed in the formerly glaciated areas, mostly represented by cirques. More than 1200 caves have been registered so far, but there are some areas that are still more or less speleologically unexplored. The longest single cave is the 46 km-long Frauenmauer-Langstein-Höhlensystem, a polygenetic system of phreatic tubes overprinted by active vadose canyons. Most of the caves, however, are vadose canyon shafts; the deepest (Steinbockschacht) has been explored to a depth of 1127 m, without reaching the karst water.

The Kläffer Springs (Fig. 1) rise on the northern slope of the Hochschwab and were decisive for the routing of the 2nd Vienna Water Main (DRENNIG, 1988). With an average flow rate of around 5 m³/s and peaks that can be ten times higher, the Kläffer Springs are the largest springs in Austria and the Eastern Alps (BENISCHKE et al., 2016; KOPPENSTEINER & PLAN, 2019). Only a few hundred litres per second are used for Vienna's drinking water supply. However, the water from the Kläffer Springs can only be used during low and normal water levels because, unlike most other springs, the water is turbid during flood events. This is due to sediment particles that are mobilised due to the increased flow velocities and are suspended in the water (PLAN et al., 2010, MUELLER et al., 2023). Although the turbidity causes a problem for the water supply, it is not yet known where the sediments come from and how much is discharged from the karst system. Due to the enormous quantities of water, a considerable solids load is to be expected. So far, only the dissolved load has been determined, which amounts to around 20,000 tonnes per year, i.e. around three truckloads (four-axle lorries) per day (PLAN, 2005). Within the spring monitoring program different hydrological parameters are monitored automatically in a 10-minute interval. The aim of this study is to attempt to quantify the dissolved solids and the total suspended solids (TSS) from hydrological parameters and water sample analysis for the Kläffer Springs over 3 years.

Figure 1: *Drone photo looking diagonally down towards the south at the Kläffer Springs, taken during the snowmelt on 9th May 2017 with a total discharge of 14 m³/s. The water for the city of Vienna is collected underground in a tunnel near the building in the bottom right corner. In winter or during long periods of low discharge, (almost) none of these surface waters are present. Width of the river in the foreground 0.25 km.*

2. Materials and methods

To get samples of the turbid water, canisters were filled with 5.5 l of spring water at different discharges. At the same time, coarse sediment was collected in a sediment trap, representing the suspended sediment of the previous days or weeks. After the sediment load has settled in the water samples, the majority of the water was decanted off and the remaining, small water-sediment mixtures were taken to the sedimentology laboratory where water was removed by heating at 50 °C. The sediment load in these samples was weighed. Data on hydrological parameters such as electrical conductivity, nephelometric turbidity, temperature and discharge at 10-minute intervals are provided by Vienna Water.

3. Results

The water samples for turbidity analysis were taken between July and September 2024 with one sample of the highest turbidity in the last 5 years (2020-2024; 48 Nephelometric Turbidity Unit, NTU on 7 July 2024) and five samples of lower turbidity ranging from 0.18 to 8.8 NTU. For 3 years (1 Jan. 2020 to 31 Dec. 2022), a mass balance was calculated using hydrological and hydrochemical data from the Kläffer Spring. Using chemical data from six water samples, a good relationship was found between dissolved calcium and magnesium hardness and electrical conductivity (R^2 =0.99; Fig. 2). The equation can be written as: $H_{(t)} = C_{(t)} \cdot 0.786$ where $H_{(t)}$ is the time-dependent Ca+Mg+CO_3 content in mg/l and $C_{(t)}$ is the time-dependent electrical conductivity in µS/cm (at 25 °C). The loss of dissolved calcium and magnesium carbonate was then summed up over time and an average value of mass per year was calculated. Therefore, the amount of dissolved carbonate rock is 22.1 × 106 kg/year (see also Fig. 3). Previous studies have established a linear relationship between the mass of total suspended solids and turbidity (NTU) (REIHWALD, 2013; WAGNER, 2020). However, to our knowledge there are no such correlations for water from karst springs and the data are all from rivers or lakes. It also appears that the correlations vary from catchment to catchment. Therefore, a separate function had to be created (Fig. 2). With the resulting correlation between NTU, mg/l and the discharge we were able to calculate the total amount of suspended solids over time (Fig. 3).

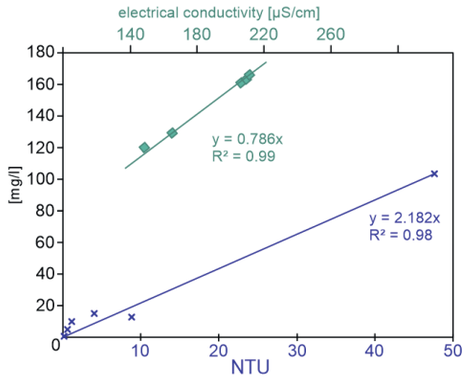

Figure 2: *Correlation of total suspended solids [mg/l] versus turbidity [NTU] in blue and Ca + Mg carbonate [mg/l] versus electrical conductivity [µS/cm] in green measured from samples of the Kläffer Springs. The functions and the coefficient of determination (R^2) are given for the best fitting linear regression.*

	suspended solids [kt]	dissolved carbonates [kt]
2020	0.18	26.9
2021	0.21	19.1
2022	0.14	20.4
Ø per year	0.18	22.1

Figure 3: Calculated total suspended solids and total dissolved in kt (= 10^6 kg) per year which were transported out of the Kläffer Spring for the years 2020 to 2022 as well as the average for this period.

4. Discussion

Events with very high turbidity values are rare at the Kläffer Springs and, despite support from Vienna Water, sampling was not easy. Although it was possible to sample the event with the highest turbidity value within the last five years at the peak (48 NTU), unfortunately no further samples were taken from this event and the most of the remaining sampled events had one order of magnitude lower turbidity values. Therefore, the distribution of the samples is unfavourable and the type of distribution (linear or exponential) can only be taken from published data, where it is consistently described as linear. Therefore, more samples are necessary for a more robust correlation.

5. Conclusion

The dissolved load in the water of the Kläffer Springs - mainly calcium and magnesium carbonate - averages 22 kt per year. It was determined by means of the linear correlation between electrical conductivity and discharge values at 10-minute intervals. An attempt was made to establish a correlation between the turbidity units and the totals suspended solid load in the water as well. Preliminary results show that it is two orders of magnitude lower (0.2 kt per year), assuming a linear correlation between TSS and NTU. It also shows that the annual variability of these two values is quite significant.

Acknowledgments

We gratefully thank Hochschuljubiläumsfonds of City Vienna for granting this project. We would also like to thank the employees of MA 31 (Vienna Water – Municipal Department 31) for taking the water samples at Kläffer Springs and all the cavers who took sediment samples all over Hochschwab plateau.

We would also like to thank Susanne Gier (Department of Geology, University of Vienna) for sample preparation.

References

BENISCHKE R., STADLER H., VÖLKL G. (2016) Karstquellen. In: SPÖTL C., PLAN L. & CHRISTIAN E. (Ed.), Höhlen und Karst in Österreich. - Oberösterreichisches Landesmuseum, Linz, pp. 73-96.

BRYDA, G. (2001) Geologische Kartierung im Hochschwabgebiet – Entscheidungshilfe zur Abgrenzung von Quelleinzugsgebieten. – Arbeitstagung. Geologische Bundesanstalt, Wien, pp. 220-231.

DRENNIG A. (1988) 75 Jahre II. Wiener Hochquellen Leitung. - Wien (MA31 – Wasserwerke).

KOPPENSTEINER S. & PLAN L. (2019) Anspringverhalten der Tagwässer der Kläfferquellen (Hochschwab, Steiermark). - Die Höhle 70: 94-101.

MUELLER Y.K., GOLDSCHEIDER N., EICHE E., EMBERGER H., GOEPPERT N. (2023) From cave to spring: Understanding transport of suspended sediment particles in a fully phreatic karst conduit using particle analysis and geochemical methods. - Hydrological Processes, 37(10): e14979.

PLAN L. (2005) Factors controlling carbonate dissolution rates quantified in a field test in the Austrian Alps. - Geomorphology, 68: 201-212.

PLAN L., KUSCHNIG G. & STADLER H. (2010) Case Study: Kläffer Spring – the major spring of the Vienna water supply (Austria). In: Kresic N. & Stevanovic Z. (Ed.), Groundwater Hydrology of Springs. - Amsterdam (Elsevier), pp. 411-427.

REIHWALD F. (2013) Auswertung von Trübungs- und Schwebstoffgehaltsmessungen der Wasser- und Schifffahrtsverwaltung in der Tideelbe. Unpubl. BSc-Thesis, Hochschule Magdeburg-Stendal.

STADLER H., STROBL E., BENISCHKE R. (2001) Karstwasserdynamik und Karstwasserschutz Hochschwab. – Arbeitsbericht, vol. 4. Johanneum Research, Graz.

WAGNER, A. (2020) Event-based measurement and mean annual flux assessment of suspended sediment in meso scale catchments. Unpubl. PhD thesis, Karlsruher Institute für Technologie.

WHITE W.B. (2000) Dissolution of limestone from field observations. – In: KLIMCHOUK A., FORD D.C., PALMER A.N., DREYBRODT W. (Eds.), Speleogenesis-Evolution of Karst Aquifers. National Speleological Society, Huntsville, pp. 149-155.SOUZA-SILVA M., FERREIRA R.L (2016) The frst two hotspots of subterranean biodiversity in South America. Subterranean Biology 19:1–21.

A multidisciplinary study to understand the speleogenesis and evolution of San Giovanni Cave (Domusnovas, SW-Sardinia)

Angelo Naseddu (1), Fiorenzo Casti (2), Maria Roberta Cadoni (2), Luca Pisani (3,4), Anis Zarantonello (4), Tommaso Santagata (5), Chun-Yuan Huang (6), Hsun-Ming Hu (6,7), Chuan-Chou Shen (6), Régis Braucher (8), Jo De Waele (4)

(1) Federazione Speleologica Sarda, Italy, angelonaseddu54@gmail.com

(2) Consorzio Natura Viva Sardegna, Domusnovas, Italy, consorzionaturaviva@gmail.com; grottasangiovanni.com

(3) Centro di Documentazione Speleologica "F. Anelli", Bologna, Italy, biblioteca.speleologia@unibo.it

(4) University of Bologna, Department of Biological, Geological and Environmental Sciences, Bologna, Italy, lucapiso94@gmail.com; anis.zarantonello@studio.unibo.it; jo.dewaele@unibo.it (JDW = corresponding author)

(5) VIGEA - Virtual Geographic Agency, Reggio Emilia, Italy, tommy.san84@gmail.com

(6) High-Precision Mass Spectrometry and Environment Change Laboratory (HISPEC), Department of Geosciences, National Taiwan University, Taipei 10617, Taiwan, ROC, yuau0213@gmail.com ; river@ntu.edu.tw

(7) Atmosphere and Ocean Research Institute, The University of Tokyo, Chiba 277-8564, Japan, hsunming.hu@gmail.com

(8) Aix-Marseille Univ., CNRS-IRD-INRAE-Collège de France, UM 34, 13545 Aix-en-Provence, France, braucher@cerege.fr

Abstract

San Giovanni cave is a world-renown cave crossed by a seasonal river and a narrow winding hard road, once used by cars and trucks over a length of 860 meters. Since 2020 the cave is open to visitors as a show cave, attracting an increasing number of tourists. The Consortium Natura Viva Sardegna, which manages the site, has signed an agreement with the University of Bologna and the laser scanning company VIGEA to study the cave and its surroundings in 2023. A laser scan survey of the main passages was carried out, in order to precisely locate geomorphological and sedimentological markers of the different speleogenetical phases (notches, alluvial sediments). Quartz pebbles have been sampled in the different cave levels for cosmogenic burial dating. Speleothems covering alluvial sediments have been targeted to bracket ages of sedimentation and speleothem formation. Sampling and observations were also carried out in neighbouring caves. The preliminary observations have shown the great geodiversity of the caves in the area (hydrothermal, condensation-corrosion, sulphuric acid speleogenesis), and the long and complex evolution of the San Giovanni Cave, involving hydrothermal fluid circulation, river erosion and alluviation, antigravitative episodes, and a complex structural control, in a very slowly uplifting area.

1. Introduction

San Giovanni cave (Domusnovas, SW-Sardinia) is famous because of the fact that it is a natural cave passage carved by a river (the Sa Duchessa-Rio San Giovanni River), large enough to allow the passage of vehicles the size of a truck (MAXIA, 1939). In fact, since the 19th century it is crossed by a narrow winding hard road over a length of 860 metres, making it among the longest underground natural tunnels in the world (there are several long ones also in China), and surely the longest one in Europe (NASEDDU et al., 2022). This natural passage across the mountain has been crossed by prehistoric settlers, by the timber loggers and mining companies that exploited Pb-Zn mines upstream (North) and by private cars until the final years of the 20th century, and is now closed to traffic (DE WAELE &PISANO, 1998; DE WAELE, 2007).

The cave was explored and surveyed in several occasions, and reaches a development of almost 5 km (DERNINI, 1970; NASEDDU et al., 1992; NASEDDU & PAPINUTO, 1996; NASEDDU, 1998). Since 2020 the cave is open to visitors as a show cave, attracting an increasing number of tourists. Despite its magnificence, and the fact that it is a famous attraction since many decades (DE WAELE et al., 1998; CHIARINI et al., 2022; SANNA et al., 2023), this natural monument was never truly studied from a speleogenetical and geomorphological point of view.

Here we report the first results of a speleogenetic study carried out in the San Giovanni Cave and in the surrounding cavities, involving geomorphological observations, a new laser scan survey and morphometric measurements, U/Th dating of speleothems, and cosmogenic dating of quartz pebbles in different cave levels.

2. Materials and methods

A preliminary analysis was carried out on the caves located in the area close to San Giovanni Cave (at a distance of around 1 km) interrogating the Cave cadastre managed by the Sardinian Speleological Federation. Small caves (of less than 50 metres of planimetric development) and those with a prevalent vertical development were excluded, as our focus was on caves that might preserve cave levels with potential quartz-rich sediments (Fig. 1).

Cat	Name	Lat	Long	Alt [m s.l.m.]
326	Grutta De Su Pertusu	39° 20' 18,3''	8° 37' 14,2''	398
606	Voragine Della Rana	39° 20' 20,2''	8° 38' 04,0''	460
1061	Grotta Gigi Addari	39° 20' 16,8''	8° 37' 34,7''	240
1316	Grotta Is Murvonis	39° 20' 09,2''	8° 38' 00,9''	265
1832	Pozzo Della Quarzite	39° 20' 20,1''	8° 37' 59,5''	510
2199	Gruttoni S 'Arcareddu	39° 20' 43,1''	8° 37' 27,1''	255
2201	S'accorru Grazia Urracci	39° 20' 19,7''	8° 37' 57,6''	480
81	Grotta Di San Giovanni	39° 20' 13,9''	8° 37' 40,2''	188
327	Grutta De Su Strexiu	39° 20' 34,9''	8° 37' 46,3''	300

Figure 1: *List of the main selected caves in the study area.*

Laser scanner acquisition of San Giovanni Cave (the main object of our study) was carried out by the Virtual Geographic Agency (Reggio Emilia) using two different laser scanners: a Leica P40 Scan Station placed on a tripod for the larger cave passages, and a handheld Leica BLK2GO laser scanner for the more tortuous ones. A compound 3D model was generated from the laser scan point cloud using the open source CloudCompare software by merging the registered point clouds captured along the scanned passages. The final 3D model was subsampled to a spatial resolution of 10 mm to reduce processing time and was georeferenced using the pre-existent speleological topographic survey. This model was used to extract cave level altitudes, and meso-scale morphologies such as notches, and to exactly locate the alluvial deposits and the sampling sites.

Quartz pebbles were sampled along the cave passages at different altitudes (Fig. 2). These represented ancient alluvial deposits, which dating (cosmogenic Al-Be burial dating, CNRS Aix-en-Provence) might help in unravelling the erosional history of the in-cave stream.

Samples for U/Th dating were taken as small chips using a geological hammer on flowstone cut by the road, or through battery-powered drilling in less visible areas (Fig. 3). After core extraction, drillholes were filled with coloured cement in order to mask the hole. In most cases, flowstones were sampled sealing the ancient alluvial deposits, and were subjected to U/Th dating at the National University of Taiwan.

Figure 2: *Sampling alluvial sediments high along the roof with van equipped with a crane (Photo Vittorio Crobu).*

A total of 20 U/Th dates were obtained from nine samples taken in San Giovanni Cave, four in S'Arcareddu Cave, two from Su Strexiu, and five from Abisso della Rana.

Fourteen samples were taken for Al/Be burial dating, twelve in San Giovanni Cave and two in S'Arcareddu Cave. Analysis are being carried out and are expected to deliver results by the summer of 2025.

Figure 3: *One of the speleothem samples taken through handheld battery-powered drilling (Photo Vittorio Crobu).*

3. Results

3.1. Laser scan survey

The entire river (and road) passage (Fig. 4) was scanned with the Leica P40 scanner (Fig. 5), whereas the smaller and more tortuous side branches were surveyed using the Leica BLK2GO scanner. Scanning included the long Su Stampu de Pireddu side branch up to the final sump, and the "Autostrada del Sole", and also the upper Bobore branch (accessible climbing up ropes).

The survey has allowed to locate in detail all samples, and to identify and document cave wall morphologies and alluvial sediment patches at various heights above the present-day river level. Several cross sections were used for this (Fig. 6).

3.2. U/Th dating

The 20 U/Th dates span a time interval of the last 650 ka, with four samples being older than 600 ka. Many samples (10) appear to have grown during the coldest stages of the Quaternary (Marine Isotope Stages (MIS) 2, 6, 10, 12, and 16) with only few (5) samples related to the warmer episodes (MIS 5, 9, 11, and 13) and the rest during cold-to-warm transitions.

Figure 4: *The laser scan survey obtained merging all point clouds.*

Figure 5: *The Leica P40 laserscanner along the in-cave road (Photo Vittorio Crobu).*

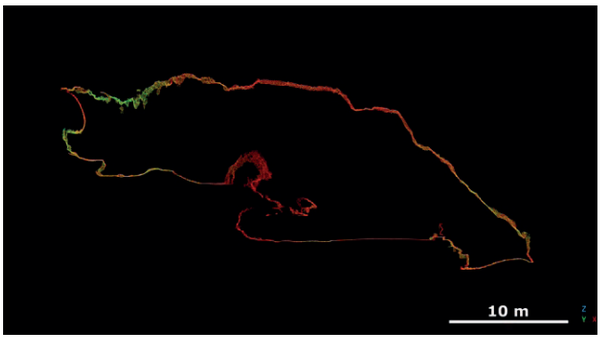

Figure 6: *Example of cross section of the laser scan survey, used to allocate samples and identify cave morphologies.*

3.3. Cosmogenic dating

Of the fourteen alluvial quartz samples, most are composed of various pebbles. The quantity of sediment after sieving, washing, grinding and picking, was rather low in two samples (for these samples it might be possible that no reliable cosmogenic burial dates will be obtained). Twelve samples come from San Giovanni Cave: one sample each comes from the upper cave level (at +22 and +42 m above current river level, see Fig. 7), three have been taken at +8 m, three at +10 m, two at +12 m, one at +15 m and one last at +16m). Two other samples were taken in S'Arcareddu Cave (at around 10 and 20 m above the present river). Burial dates will hopefully be obtained before the summer of 2025.

3.4. Other caves

Our observations in the other caves of the area delivered some surprising results. None of the visited caves appears to be related to the base level lowering of the Sa Duchessa-San Giovanni River. Two of the visited caves (Gruttoni S'Arcareddu and S'Accorru Grazia Urracci) clearly are ancient thermal caves (with mammillary calcite deposits covering walls and roof). A laser scan survey was carried out of the major room of the first cave to better analyse the morphologies. The mammillary calcite has given an age of 460 ± 24 ka, whereas an old flowstone appears to be older than 600 ka.

Abisso della Rana shows presence of gypsum and appears to be related to a hypogenic evolution with formation of sulphuric acid. Dating of flowstone pavements has given old ages, mostly between 400 and 530 ka.

Su Pertusu, believed to be "an ancient resurgence", is instead carved parallel to the wall by intense and long-lasting condensation-corrosion processes. Some monocrystalline stalagmites, found broken on the floor, have been sampled for dating and possible paleoclimate studies.

Is Murvonis has clear signs of hydrothermal rising fluids (even hosting fluorite). Fluid inclusion studies on these fluorites will allow to ascertain these ancient thermal speleogenetic conditions.

Figure 7: *Flowstone with alluvial pebbles attached on the underside, Bobore Gallery, ca. 50 metres above the present cave river altitude (Photo Vittorio Crobu).*

The only caves with some fluvial evidence are Su Strexiu (where sulphuric acid and hydrothermal traces have also been observed) and Gigi Addari Cave (a small cave filled with alluvium). Pozzo della Quarzite, located close to the Grazia Urracci cave, has not yet been visited (local cavers talked about danger of collapse), but might also well be hydrothermal in origin (based on the available cave map and its vicinity to Grazia Urracci cave).

4. Conclusion

Dating of San Giovanni flowstones and speleothems, and the cosmogenic burial dating of the quartz-containing sediments, will probably allow to draw some preliminary conclusions about the evolution of the valley, its entrenchment, and the creation of the different and clearly distinguishable cave levels. Surprisingly, and unexpectedly, there are no other major caves known near San Giovanni which would allow to date other (higher) alluvium-filled cave levels. Most of the visited caves are related to other (hypogenic) cave-forming processes, and are probably much older than San Giovanni Cave itself, making this area extremely geodiverse. Finding hydrothermal and sulfuric acid cave systems alongside "normal" epigenic ones in barely a few square kilometres is quite remarkable.

Future studies will focus on the genesis and evolution of these caves, trying to understand why such a different series of speleogenetic processes has occurred in several periods in this small patch of carbonate rocks.

Acknowledgements

This project has been realised with the financial contribution of the Consorzio Natura Viva of Domusnovas, responsible for the management of the tourist visits. Many thanks to local cavers for their precious information about caves. Irene Albino and Francesca Stendardi are thanked for the handling of quartz sediments, preparing samples for cosmogenic dating.

References

CHIARINI V., SANNA L., FORTI P., DE WAELE J. (2022) L'interesse scientifico delle grotte turistiche in Italia. Atti e Memorie della Commissione Grotte « E. Boegan » Trieste 51:3-22.

DERNINI C. (1970) Ispezione speleologica nelle grotte di S. Giovanni in Domusnovas, Notiziario del Circolo Speleologico Romano, 20-21, 65-73.

DE WAELE, J. (2007) Impatto Ambientale di attività antropiche sulle aree carsiche in Sardegna. Atti e Memorie della Commissione Grotte « E. Boegan » Trieste 41:25-45.

DE WAELE J., PISANO M. (1998) Interazione fra attività mineraria ed un acquifero carsico: L'esempio di Barraxiutta (Sardegna sud-occidentale). Atti del Convegno Nazionale sull'Inquinamento delle Grotte e degli Acquiferi carsici e possibili ricadute sulla collettivita. Imprimitur editrice Padova, Ponte di Brenta, 195-209.

DE WAELE J., DI GREGORIO F., PIRAS G. (1998) Geosites inventory in the Palaeozoic karst region of Sulcis-Iglesiente (South-West Sardinia, Italy). Geologica Balcanica 28:173-179.

MAXIA C. (1939) Il cono di deiezione di Domusnovas nel bacino del Rio S. Giovanni (Sardegna sud-occidentale). Geologia, idrogeologia, agrogeologia. Boll. della Soc. geologica italiana 63:29-76.

NASEDDU A. (1998) San Giovanni di Domusnovas è più profonda: lo speleosub Enrico Saver raggiunge i -80. Sardegna Speleologica, 14, 2-9.

NASEDDU A., SANNA F., CHESSA L., BIANCO L. e DE WAELE J. (1992) Le tentazioni di San Giovanni. Speleologia, 26, 16- 21

NASEDDU A. e PAPINUTO S. (1996) Grotta di S. Giovanni "Ramo Bobore". Speleologia, 35, 57-63. NASEDDU A., FORTI P., PIRAS M., CASTI F., CADONI M.R., DE WAELE J. (2022). San Giovanni Cave (Domusnovas, S-Sardinia): history, exploration and valorization of the longest cave traversable by car. Karstol. Mém. 21:95-98.

SANNA L., CHIARINI V., DE WAELE J. (2023) Underground Geodiversity of Italian Show Caves: an Overview. Geoheritage 15(4):126.

UnderGroundwater origin in Javoříčko and Mladeč karst areas

Roman Novotný (1), Eva Kryštofová (1), Jitka Novotná (1), Vít Baldík (1), Jiří Rez (1), Veronika Kršková (1)

(1) Czech Geological Survey, Klárov 131/3, 118 21 Praha 1, Czech Republic. roman.novotny@geology.cz

Abstract

Underground water migration in karst hydrogeological system has been a subject of study of many scientific studies, however, usually just within the boundaries of the karst area itself. In Javoříčko and Mladeč karst areas, the volume of water leaving the drainage area is much higher, than the volume of precipitation on the limestone covered area and dotation by known underground streams at the contact of limestones and surrounding non-calcareous rocks. The question of the origin of the underground water in the drainage area of the Javoříčko and Mladeč karst areas and especially in the strategically important water supply source of Čerlinka has been the focus of hydrogeologists for many years now, in particular effective protection of the quality and quantity of the water used for public supply. Our recent study resulted in a new hypothesis of indirect (remote) infiltration system, in which the karst structure represents a transit pathway for underground water from adjacent basin structure with its own infiltration area.

1. Introductions

Karst reservoir rocks are unusual by the fact, that their reservoir properties increase during dissolution of limestones (karstification). Even insignificant fractures or bedding planes can become very significant regional underground water migration pathways which drain most of the water from adjacent areas (Ford, Williams 2007; Atkinson 1977), due to the simple process of corrosion by flowing water, which slowly enlarge the original fractures. These increased reservoir properties increase the input of groundwater and increase the influence of karst reservoir rock on its non-karst surroundings (Klimchouk et al. 2000). The slope of the underground water level and hydraulic gradient in the karst reservoir in controlled mainly by the geometry of fractures present in the rock (Thraikill 1985).

Karst hydrogeology distinguishes two main ways of karst structures water input (Ford, Williams 2007) – precipitation infiltration in the karst area itself (autochthonous waters) and influx of groundwater from adjacent non-karst areas via sinkholes or by influx of underground water through a geological boundary (allochthonous water). Using the percentage of underground influx within allochthonous water, we can divide hydrogeological structures to closed and opened (Kullman 1990). Closed karst structures are separated by seal rocks all around their perimeter and are not supplemented from nor drained by adjacent hydrogeological structures. In opened karst structures, underground water flows freely through the geological boundaries, usually undetected.

Karst areas of the Czech Republic are not extensive and are surrounded by non-karst geological units of different age and lithology. Using Kullman (1990) classification, they are almost always opened karst hydrogeological structures. Numerous studies of different karst areas confirmed over and over, that the volume of water flowing out of the structures exceeds significantly the direct infiltration of precipitation in situ and influx of groundwater via sinkholes on the boundaries of respective karst area (e.g. Baldík et al. 2023, Bruthans, Kryštofová eds. 2016). This proves the significance of influx of underground water through geological boundaries from non-karst hydrogeological structures, which should hence be regarded as infiltration areas of the karst areas.

2. Materials and Methods

Site description

Javoříčko and Mladeč karst area is situated in the central Moravia. It is a scattered assemblage of smaller patches of limestone incorporated into the nappe stack of the Variscan flysch (so called Culmian; fig. 1 a, b, c,). The overall karst area is only 11 km2 and is built of several limestone elevations and a few cave systems without active water streams (fig. 2, 3). Interconnection of individual limestone blocks is as yet unknown, however, at least limited hydrogeological connection was proven by tracing (Panoš 1962). Only a few underground streams are known in the Javoříčko and Mladeč karst area with very small flow rates, mean year precipitation total does not exceed 700 mm. Main drainage base is the Morava river valley, where the limestones are overlain by Quarternary sediments (fig. 1c). Total output of the area is: 190 l/s is pumped in JÚ Čerlinka water catchment; 10–40 l/s flows out via the Řimice spring (Obr. 4) and an unknown volume is drained into the Vrapač riparian forest (fig. 5).

Javoříčko and Mladeč karst area is adjacent to a major hydrogeological structure in the Central Moravia – Mohelnice graben. It is a major basin structure with over 300 m of Pliocene to Pleistocene sedimentary fill. Over a 100 m of the overall thickness is formed from excellent, water saturated reservoir rocks (fig. 1c).

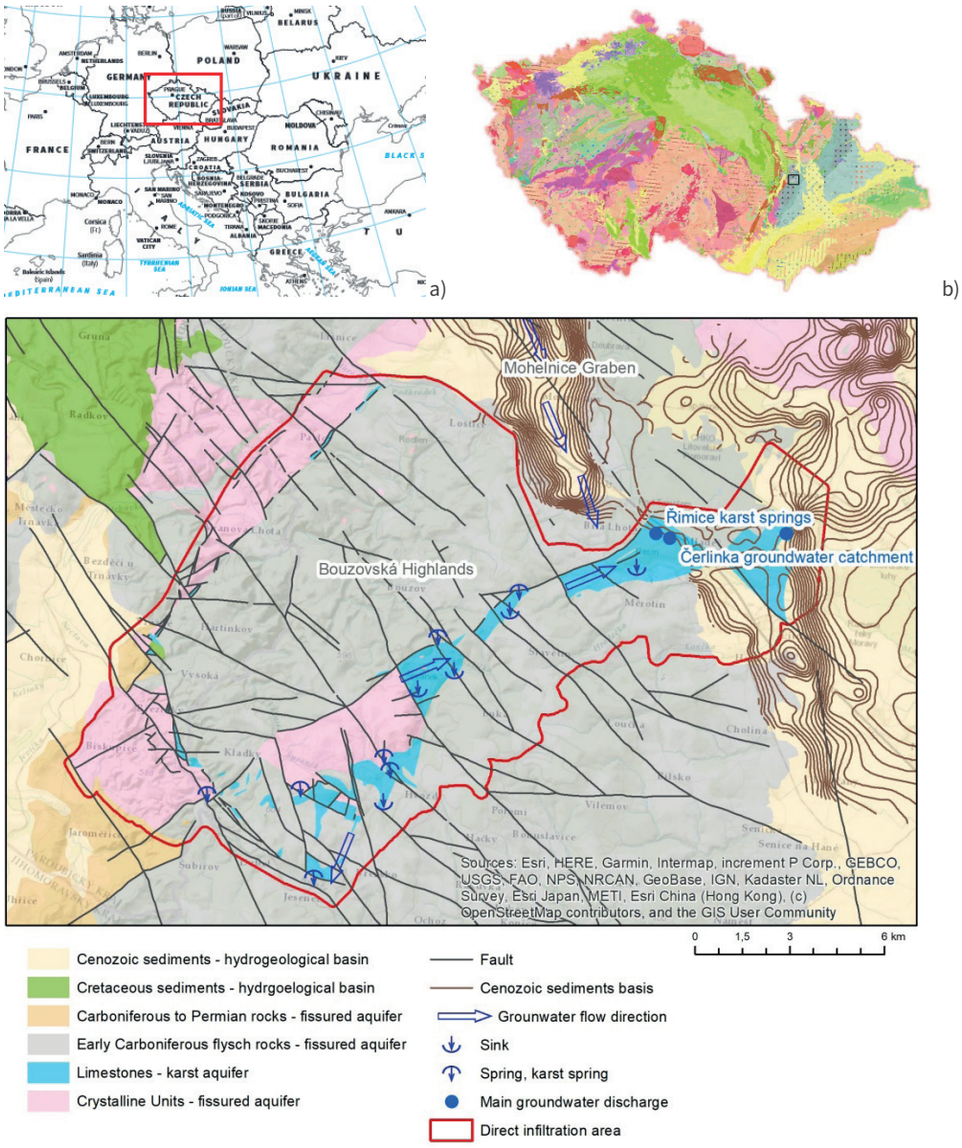

Figure 1: *Localisation of the studied area.*

Figure 2: *Limestone outcrops, Branky castle, Javoříčko karst.*

Figure 3: *Javoříčko cave system.*

Figure 4: *Řimice spring.*

Figure 5: *Vrapač riparian forest.*

Metods

Presented study was based on archival data as well as new data. Climatological, hydrogeological, well and underground water data were analysed by statistical means and in ArcGIS. Great attention was given to field work comprising geological mapping, structural analysis of ground and underground data focused on determination of the overall geometry of individual hydrogeological structures and their relationships. Hydrogeological mapping comprised ground and underground water sampling and subsequent chemical analyses - trace elements, pesticides and their metabolites, isotopes.

3. Results

Analysis of acquired data confirmed large volumes of underground water in the main drainage area exceeding 250 l/s. Such high volumes and small precipitation areas necessitate the existence of much bigger hydrogeological structures supplementing the hydrogeological system. The water is of excellent quality without significant anthropogenic influence. When compared with water from adjacent areas, it is not polluted by pesticides (fig. 6). This indicates longer residence time, deep circulation and infiltration outside major agricultural areas. Isotopes δ18O a δ2H indicate infiltration of water in much higher altitudes than the springs or the main drainage level.

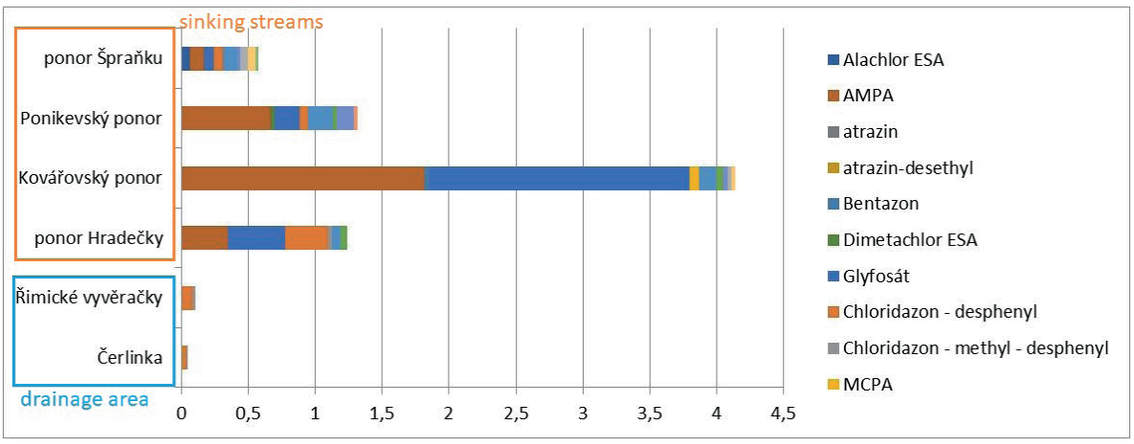

Figure 6: *Pesticides in analysed waters.*

4. Discussion

Volume of underground water in the main drainage area suggests, that infiltration of precipitation within the quite small area of limestones and inflow from all known sinkholes are insufficient to generate such volumes. Mohelnice graben has greatly reduced thickness by so called Třesín horst right next (east) to the Mladeč karst (fig. 1c). This reduction down to ca. 5 m of viable reservoir rock is not, however, compensated by increased flow rates in the Morava river. This strongly suggests, that the underground water found an alternative route, which is compensating the decreased volume of migration path. A logical solution is, that the Palaeozoic rocks of the Javoříčko and Mladeč karst serves as a transit path for this water. This hypothesis is supported by isotopes composition and also by the quality of the underground water, which correlates with the mean residence time of the underground water of the Mohelnice graben and Čerlinka water catchment.

5. Conclusions

The hypothesis of indirect infiltration area changes the view of the hydrogeological system of the Javoříčko and Mladeč karst area, which cannot be understood as a separate hydrogeological structure, but as a part of a much bigger system composed of several individual, interconnected hydrogeological structures. This complex assemblage of interconnected hydrogeological structures, however, complicates the identification of possible or existing pollution sources and other anthropogenic influences and its understanding is crucial not only for protection and preservation of environment and cave systems, but also from the point of view of protection of water quality in drinking water sources.

Acknowledgments

Financial support through the project „Rock Environment and Natural Resource RENS" (SS02030023) is gratefully acknowledged.

References

ATKINSON, T. C. (1977): Diffuse flow and conduit flow in limestone terrain in the Mendip Hills, Somerset (Great Britain). – J. Hydrol., 35, 93-110.

Baldík, V. – Rez, J. – Kryštofová, E. – Novotný, R. – Novotná, J. – Dostalík, M. – Hadacz, R. – Nečas, J. (2023): Účelová aktualizace rozsahu a průběhu podzemních krasových systémů a vymezení preferenčních cest přestupu podzemní vody po tektonických zónách. Výzkumná souhrnná zpráva, 39 s.

BRUTHANS, J. – KRYŠTOFOVÁ, E., eds. (2016): BURDA, J. – BŮZEK, F. – GILÍKOVÁ, H. – KADLECOVÁ, R. – KONDROVÁ, L. – KONEČNÝ, F. – KŮRKOVÁ, I. – OTAVA, J. – SKÁCELOVÁ, Z. – VÍT, J. (2016): Hydrogeologický rajon 6640 – Mladečský kras. Stanovení zásob podzemních vod, závěrečná zpráva, příloha č. 2/51.

FORD, D. C. – WILLIAMS, P. (2007): Karst Geomorphology and hydrology. – 562 p. John Wiley & Sons. Hoboken.

KLIMCHOUK, A. B. – FORD, D. C. – PALMER, A. N. – DREYBRODT, W. (2000): Speleogenesis, Evolution of Karst Aquifers. – 527 p. Huntsville.

KULLMAN, E. (1990): Krasovo-puklinové vody. Geologický ústav Dionýza Štúra. Bratislava.

PANOŠ, V. (1962): Výsledky koloračních experimentů a pozorování krasových vod v Severomoravském kraji – Sborník Vlastivědného muzea v Olomouci. Oddíl A: Přírodní vědy 5, 13–59. Krajské nakladatelství v Ostravě.

THRAIKILL J. (1985): Flow in a limestone aquifer as determined from water tracing and water levels in wells. J. Hydrol 78, p. 123-136.

Entre casas e florestas: como o uso do solo altera a integridade do riacho que acessa a Lapa do Grotão

Thais Giovannini Pellegrini (1), Marcus Paulo Oliveira (1), Ataliba Henrique Fraga Coelho (1), Débora Reis de Carvalho (2), Josiane Alves Moura (1) & Paulo dos Santos Pompeu (3)

(1) BioEspeleo Consultoria Ambiental, Rua Comendador José Esteves 694, Centro, Lavras, Brasil, thais.pellegrini@bioespeleo.com.br (autor correspondente), marcus@bioespeleo.com.br, atalibacoelho@gmail.com, jmoura.geografia@gmail.com,

(2) Lancaster University, Lancaster LA1 4YW, Reino Unido, deboracarvalhobio@yahoo.com.br

(3) Laboratório de Ecologia de Peixes, Universidade Federal de Lavras, Lavras, Brasil, pompeu@ufla.br

Resumo

Este estudo investiga como os usos do solo e atividades antrópicas impactam a qualidade da água e o habitat físico do Ribeirão das Lajes, com implicações para a preservação da Lapa do Grotão, situadas em Morro do Pilar, MG, Brasil. A pesquisa foca na bacia de contribuição dessas cavernas, com ênfase na vegetação e atividades humanas que afetam o ambiente aquático. A análise mostrou que, embora a bacia de contribuição hídrica das cavernas mantenha 79% de vegetação natural, a presença de eucalipto nas áreas de proteção permanente (APPs) e a densidade de propriedades rurais influenciam negativamente na hábitat físico e na qualidade da água, especialmente os níveis de coliformes totais. Esses resultados destacam a importância de práticas de manejo sustentável e a preservação das áreas naturais ao redor das cavernas para proteger os ecossistemas subterrâneos.

Abstract

This study investigates how land use and anthropogenic activities impact water quality and the physical habitat of Ribeirão das Lajes, with implications for the preservation of Lapa do Grotão cave, located in Morro do Pilar, MG, Brazil. The research focuses on the contributing basin of these caves, emphasizing vegetation and human activities that affect the aquatic environment. The analysis revealed that, although the cave's influence area maintains 79% natural vegetation, the presence of eucalyptus in the permanent preservation areas (APPs) and the density of rural properties negatively impact the physical habitat and water quality, particularly the levels of total coliforms. These results highlight the importance of sustainable management practices and the preservation of natural areas surrounding the caves to protect subterranean ecosystems.

1. Introdução

Cavernas se inserem em ambiente cárstico compreendendo sistemas dinâmicos em resultado de processos físicos e bióticos. Para a manutenção da dinâmica evolutiva, bem como da fauna cavernícola, é fundamental se garantir a proteção e manejos adequados da paisagem de entorno (WILLIAMS 2008, ELEZ et al. 2013). Dentre os diversos temas que devem ser abordados para a delimitação da área de entorno a ser preservada, a bacia de contribuição ocupa lugar de destaque.

Agentes hídricos estão intimamente ligados aos processos erosivos e dissolutivos, que levam ao surgimento e alargamento das cavidades naturais subterrâneas (FORD 1999). Considerando a água como principal agente na gênese e evolução das cavernas, análises que visem a manutenção da dinâmica evolutiva dessas feições devem, por isso, garantir as condições hidrológicas naturais que envolvem a presença de drenagens (alóctones ou autóctones), os processos de infiltração e percolação, além da relação desses com o entorno e o sistema subterrâneo.

Dada a importância da bacia hídrica no entorno para a manutenção de processos naturais do ecossistema cavernícola, partimos da hipótese de que diferentes usos do solo alteram parâmetros da qualidade da água e a estrutura dos habitats físicos aquáticos. Com isso, o presente estudo tem como objetivo principal avaliar como o uso do solo, a cobertura vegetal e características socioambientais da bacia de drenagem podem alterar o habitat físico e qualidade da água do riacho que acessa a Lapa do Grotão.

2. Materiais e Métodos

Área de estudo

Situadas no município de Morro do Pilar, Minas Gerais, Brasil (Fig 1), a Lapa do Grotão se insere entre sumidouros e surgências do Ribeirão das Lajes e soma mais de 740m em projeção linear (CARSTE 2014), ocupando lugar de destaque entre as cavernas ferruginosas do Quadrilátero Ferrífero. Com cerca de 1500 ha, sua bacia de contribuição hídrica foi definida pelo órgão licenciador, e abrange parte do Ribeirão das Lages, incluindo 29 sub-bacias, sendo inserida quase que totalmente na Unidade Patamares da Serra do Cipó (BIOESPELEO 2018).

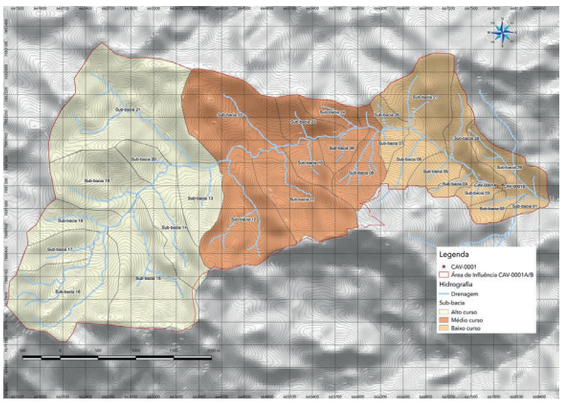

Figura 1: *Bacia de contribuição hídrica da Lapa do Grotão.*

Procedimentos de amostragem

Realizamos as análises de uso do solo na bacia de contribuição hídrica da Lapa do Grotão e nas Áreas de Proteção Permanente (APPs) por meio de avaliação de imagens orbitais *Bing Aerial* em aplicativo QGis, versão 2.18. Geramos polígonos para delimitação de uso e cobertura vegetal em função da origem, antrópica ou natural. Validamos os dados levantados nas análises das imagens orbitais e vetores por meio de controle de campo, realizado entre os dias 17 e 20 de setembro de 2018.

Utilizamos as mesmas imagens *Bing Aerial* para realizar um levantamento das instalações rurais na bacia de contribuição hídrica da Lapa do Grotão. Aplicamos um questionário aos proprietários ou locatários das propriedades para levantar informações referentes a aspectos socioeconômicos, infraestrutura e percepção ambiental.

Para caracterização do habitat físico ao longo do Ribeirão das Lages utilizamos a metodologia contida nos manuais da Agência de Proteção Ambiental Americana (EPA) e nos protocolos para avaliação de hábitat físico criados por seu Programa de Monitoramento e Avaliação Ambiental (EMAP) (OLSEN & PECK 2008). Aplicamos o protocolo em 8 trechos amostrais, cada um com 150m de extensão e com uma distância mínima de 500m. Dividimos cada trecho em 11 transectos transversais (A-K), delimitando 10 seções equidistantes (Fig. 2). A partir dos dados obtidos com o preenchimento do protocolo de avaliação do habitat físico calculamos 256 métricas (valores condensados das observações) para cada um dos oito trechos amostrais (KAUFMANN et al. 1999).

Durante as atividades de campo coletamos amostras de 700ml para análise de qualidade da água do Ribeirão das Lajes ao longo de 8 pontos. As análises foram realizadas no Laboratório de Análise de Água do Departamento de Engenharia da Universidade Federal de Lavras.

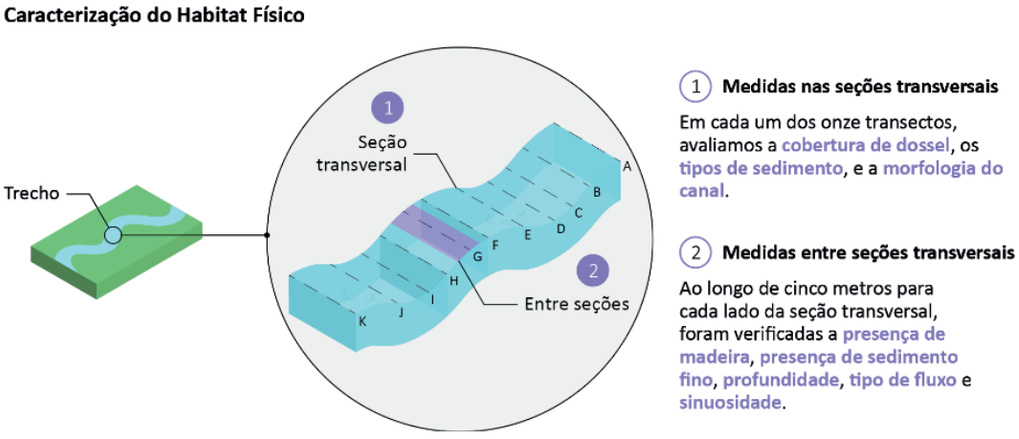

Figura 2: *Representação esquemática de um trecho para avaliação de habitat físico (adaptado de KAUFMANN et al. 1999).*

Análise dos dados

Para verificarmos quais variáveis referentes aos usos do solo, usos das APPs e censo são determinantes para as alterações na qualidade da água e habitat físico do Ribeirão das Lajes, causando potenciais distúrbios às cavidades Lapa do Grotão, seguimos os procedimentos a seguir.

As sub-bacias foram agrupadas conforme os pontos de amostragem no Ribeirão das Lajes. Métricas referentes às variáveis explicativas foram somadas conforme as sub-bacias que compõe cada ponto de amostragem e relativizadas pela área total acumulada em cada agrupamento.

Do conjunto de 184 variáveis resposta do habitat físico, selecionamos um conjunto menor para análise. Para tanto, agrupamos segundo os aspectos: morfologia do canal, tipo de substratos, gradiente de fluxo, cobertura da vegetação ripária, número e volume do aporte de madeira, tipos de abrigos disponíveis à fauna e impactos antrópicos. Em sequência, realizamos uma análise de PCA para identificar as variáveis mais representativas em cada aspecto, excluindo aquelas com medidas correlacionadas. Em relação a qualidade da água, selecionamos parâmetros com valores acima dos níveis de referência da Deliberação Normativa Conjunta COPAM/CERH-MG Nº01, de 05 de maio de 2008, e que expressam respostas distintas. As variáveis preditoras relacionadas ao uso do solo, ocupação das áreas de proteção permanentes (APPs) e censo foram testadas pelo método de Spearman, aplicado em cada agrupamento, evitando parâmetros auto correlacionados. Todas as análises de correlação seguiram o critério de rSpearman > 0,70, p < 0,05. Na seleção dos preditores destes três grupos foram priorizadas as métricas mais representativas nas sub-bacias (em área), que estejam relacionadas a intervenções antrópicas e que são constantemente indicadas na literatura.

Para verificamos a relação entre o uso do solo, APPs e censo com a qualidade da água e habitat físico do Ribeirão das Lajes construímos modelo de DistLM. Calculamos a matriz de distância com base na distância euclidiana (habitat físico e qualidade da água) entre as amostras. Selecionamos os preditores agrupadas conforme a natureza dos dados: uso do solo, ocupação das áreas de proteção permanentes (APPs) e censo. Posteriormente, realizamos os testes separadamente com todas as variáveis selecionadas, no intuito de identificar quais destas são individualmente mais importantes. Os valores de R^2 ajustado foram escolhidos como critério de seleção. Para ordenar e visualizar os modelos DistLM, foi realizada uma análise de dbRDA. Utilizamos o software PRIMER.

A partir do resultado do DistLM, utilizamos modelos de GLM para identificar quais variáveis respostas (dentro dos grupos habitat físico e qualidade da água) são influenciadas pelos preditores significativos com maior poder de explicação. Nesta análise, os parâmetros de habitat físico e qualidade da água foram utilizados como variável resposta. Como variáveis explicativas foram utilizados os preditores significativos de acordo com o resultado do DistLm. No GLM, removemos sequencialmente

os preditores não significativos. Utilizamos a distribuição normalizada (Gaussiana) com função de ligação logística para as variáveis respostas. Consideramos que apenas os modelos com ΔAICc < 4 apresentam suporte empírico satisfatório para os dados avaliados (BURNHAM et al. 2011). Posteriormente calculamos os coeficientes médios dos modelos permitindo-se capturar as variáveis preditoras que apresentam altos níveis de incerteza, devido a amplitude do erro. Os modelos lineares generalizados foram elaborados através do software R (R Core Team 2017).

3. Resultados

Usos do solo

A avaliação do uso do solo na bacia de contribuição hídrica demonstrou que parte significativa da bacia do Ribeirão das Lajes, a montante das cavidades CAV-0001A/B, encontra-se bem conservada, com 79% de cobertura vegetal natural, composta por floresta semidecidual, campos rupestres (quartzítico e ferruginoso) e candeiais. Essa vegetação, apesar de conservada, não se encontra em estágio primário, apresentando graus variados de alteração.

Habitat físico do Ribeirão das Lajes

Através da caracterização do habitat físico ao longo do Ribeirão das Lajes ficou evidente uma grande diferenciação do habitat entre os pontos mais próximos à entrada da caverna, P1 e P2 (maiores larguras, presença de matacões, fluxo rápido e vegetação preservada), com os pontos mais afastados, P6, P7 e P8 (menores larguras, predominância de bancos de folhas e substrato fino). O P3 também apresentou grande diferenciação dos demais, principalmente pela ausência de cobertura vegetal devido à presença de pastagens nas margens.

Qualidade da água

Dentre os seis parâmetros físico-químicos avaliados, quatro ficaram acima dos valores de referência em pelo menos seis pontos de amostragem. No ponto P7, os valores de coliformes totais e fecais foram mais de 160 vezes superiores ao indicado pela COPAM. Apenas Fósforo Total e Cloretos ficaram dentro da margem estabelecida.

Censo socioambiental

Dentro da bacia de contribuição hídrica das cavidades Lapa do Grotão foram constatadas 23 instalações rurais. Destas, 19 são imóveis residenciais, nos quais 14 foram visitadas durante as atividades em campo. A maioria destas representam sítios utilizados durante finais de semana e/ou temporadas, sendo que apenas em seis há residentes-fixos, os que participaram das entrevistas.

A pesquisa revelou que o tipo de uso da terra no entorno das propriedades varia bastante, dentre vários usos agrícolas. A maioria das propriedades utilizam poço ou nascente na própria terra; 50% utilizam fossa séptica, contra 50% de fossa rudimentar, a maioria não relata períodos de falta de água.

Seleção de preditores

Em relação às variáveis respostas, os valores do PC1e análise de correlação indicam seis medidas de habitat físico e três de qualidade da água (Fig. 3). Em relação aos preditores utilizados na construção dos modelos selecionamos dez variáveis (Fig. 3).

Parâmetros determinantes às alterações no ribeirão

Dentre todos os preditores avaliados, N_PROP, APP_EUCA e APP_CRQ foram responsáveis pela maior parte da variação observada nas características físicas e qualidade da água no Ribeirão das Lajes (Fig. 4). A análise em conjunto indica que nenhum agrupamento foi significativo (Uso do solo: p = 0,06; Censo: p = 0,20 e Uso das APPs: p = 0,26). Entre os pontos amostrais observou-se elevada similaridade nas variáveis respostas de P6 e P7, e entre P3, P4 e P5. Entretanto, a densidade de propriedades (N_PROP) e a presença de Eucalipto nas APPs (APP_EUCA) contribuem para o distanciamento dos pontos P6 e P7 em relação aos demais.

Grupo	Sigla	Descrição
Medidas de habitat físico	XBFWD_RAT	Medida de morfologia do canal: Razão entre da Largura Sazonal e Talvegue Sazonal
	LSUB_DMM	Medida de substrato: Tamanho Médio do Substrato
	XCM	Cobertura da vegetação ripária: Média da Cobertura Vegetal + Cobertura Vegetal Intermediaria
	V1T_MSQ	Madeira: Volume de Galhos ou Troncos no Leito + Sup / 100m - Classe de Tamanho 1
	XFC_ALMA	Abrigo: Média de Abrigos - Alga + Macrófita (NEW)
	XC_HALL	Impactos antrópicos: Proporção de Impacto Humano por Trecho (Número de Registros nas 22 Medições) - < 10m (C)
Qualidade da água	OLEO_GX	Óleos e Graxas
	NIT_TOT	Nitrogênio Total Kjeldahs (NTK)
	COLI_TOT	Coliformes Totais
Usos do solo	CRQ	Campo rupestre quartzítico
	FEI_ERO	Focos de erosão
	EUCA	Eucalipto
	PASTO	Pastagem - incluindo campo sujo em áreas adjacentes
Usos do solo nas APPs	APP_CRQ	Campo rupestre quartzítico em APP
	APP_EUCA	Eucalipto em APP
	APP_PROPR	Instalação rural - abrangendo o entorno imediato das edificações em APP
	APP_PASTO	Pastagem - incluindo campo sujo em áreas adjacentes em APP
Censo social	N_PROP	Número de propriedades rurais
	N_ATIV	Diversidade de atividades agrícolas

Figura 3: *Descrição das variáveis selecionadas para a elaboração dos modelos explicativos de habitat físico e qualidade da água. APP = Área de Proteção Permanente.*

Variável	Pseudo-F	R^2Adj.	*p*
N_PROP	7,50	0,48	0,04
APP_EUCA	4,33	0,67	0,05
APP_CRQ	71,40	0,98	<0,01
N_ATIV	2,26	0,98	0,25
CRQ	1,04	0,98	0,41

Figura 4: *Resultados das análises de DistLM mostrando os efeitos das variáveis pré-selecionadas do uso do solo, APPs e censo quando consideradas em conjunto para explicar as alterações do habitat físico e qualidade da água.*

Os modelos de GLM demonstram o efeito significativo da combinação dos preditores N_PROP, APP_EUCA e APP_CRQ para explicar a razão entre a largura e talvegue sazonal e o número de coliformes totais nos pontos de amostragem do Ribeirão das Lajes (Fig. 5). As demais variáveis respostas previamente selecionadas para os modelos não apresentam relações estatisticamente significativas com os preditores (p > 0,05).

Variável resposta	Preditor	Estimativa	Erro	t/z	p
XBFWD_RAT	N_PROP	-201,7	49,5	-4,1	0,015
	APP_EUCA	12147,9	1816,1	6,7	0,003
	APP_CRQ	135,7	40,8	3,3	0,029
COLI_TOT	N_PROP	14405396,0	9021194,0	15,9	<0,001
	APP_EUCA	340451477,0	33302644,0	10,2	0,001
	APP_CRQ	-7137106,0	748433,0	-9,5	0,001

Figura 5: *Efeito significativo dos três preditores selecionados sobre a razão entre a largura e talvegue sazonal e o número de coliformes totais.*

A seleção de modelos indica que os três preditores contribuem significativamente para a presença de coliformes (Fig. 6), com destaque para a densidade de propriedades. De forma mais específica, o aumento de propriedades rurais nas sub-bacias e a substituição da vegetação nativa por Eucalipto nas APPs promovem maior contaminação por coliformes totais no Ribeirão das Lajes.

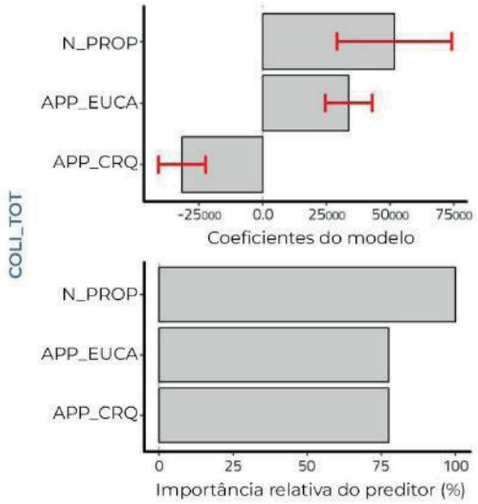

Figura 6: Média de preditores nos modelos com ΔAICc < 4 para as variáveis resposta relacionadas à qualidade da água do Ribeirão das Lages (COLI_TOT). Os coeficientes médios (± erro padrão, em vermelho), são mostrados no lado esquerdo e os valores de importância relativa no lado direito. Um preditor não é considerado significativamente importante quando os valores do erro padrão (linha vermelha) ultrapassam o zero.

Por outro lado, a manutenção dos campos rupestres quartzíticos (CRQ) nas APPs resultam em menores índices de coliformes totais. Em relação à razão entre largura e talvegue, apenas a presença de Eucalipto nas APPs (APP_EUCA) é significativamente importante (Fig. 7).

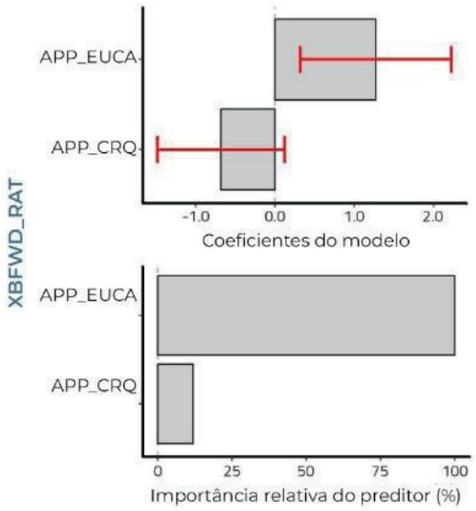

Figura 7: Média de preditores nos modelos com ΔAICc < 4 para as variáveis resposta relacionadas ao habitat físico (XBFWD_RAT). Os coeficientes médios (± erro padrão, em vermelho), são mostrados no lado esquerdo e os valores de importância relativa no lado direito. Um preditor não é considerado significativamente importante quando os valores do erro padrão (linha vermelha) ultrapassam o zero.

A sobreposição das análises indica as sub-bacias que captam para os pontos P6 e P7 como as áreas nas quais as modificações no uso do solo e a presença de atividades antrópicas alteram os habitats físicos e qualidade da água no Ribeirão das Lajes (Fig. 8). Tais modificações refletem principalmente na contaminação por coliformes totais (COLI_TOT) e nas áreas passíveis a alagamento (XBFWD_RAT), que ocorrem principalmente pela presença de propriedades rurais (N_PROP) e substituição da vegetação nativa por plantações de Eucaliptos nas APP's (APP_EUCA).

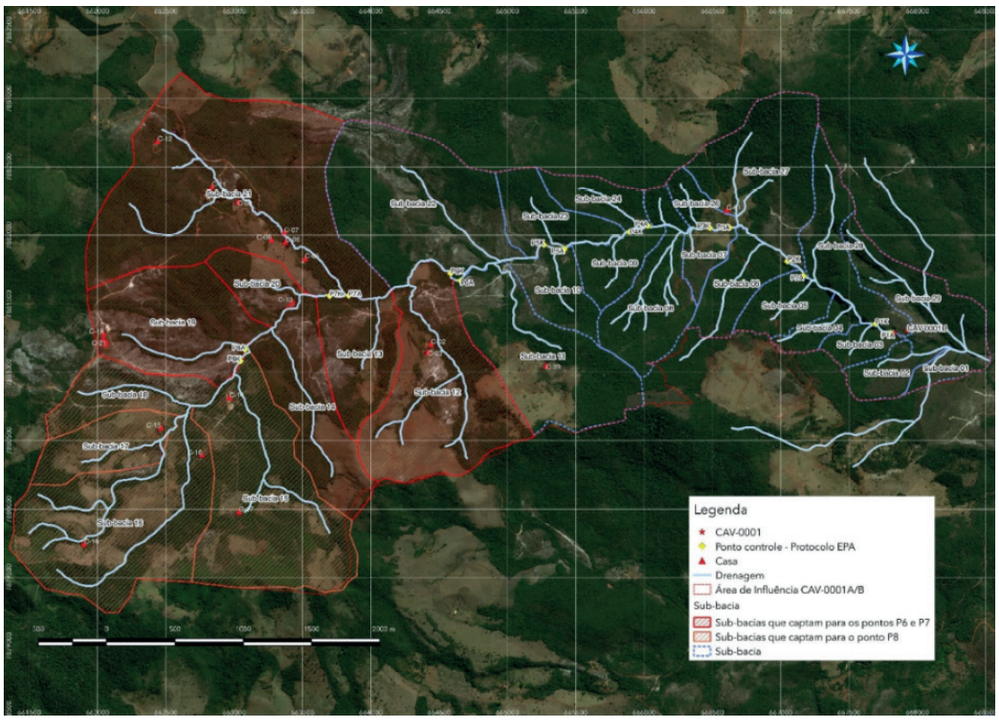

Figura 8: *A presença de eucalipto nas APPs e as propriedades rurais localizadas nas bacias que captam aos pontos de amostragem P6 e P7 são os responsáveis pelas alterações na qualidade da água e habitat físico no Ribeirão das Lajes.*

4. Discussão

Os resultados obtidos neste estudo destacam a importância das interações entre o uso do solo, as atividades antrópicas e a qualidade ambiental da bacia de contribuição do Ribeirão das Lajes para a preservação das cavidades Lapa do Grotão. A quantidade de propriedades rurais e a substituição da vegetação primária por cultivo de Eucalipto (principalmente nas APPs) são determinantes para as alterações na qualidade da água (principalmente coliformes totais) e habitat físico do Ribeirão das Lajes. Tais alterações são decorrentes principalmente das sub-bacias que captam para os pontos P6 e P7. O resultado indica que regiões a mais de 6km da Lapa do Grotão são capazes de promover a alterações significativas na integridade física e química do Ribeirão das Lajes e, consequentemente, na qualidade ambiental dos recursos hídricos que acessam os ambientes subterrâneos.

Mudanças no clima e na cobertura do solo são dois principais fatores que afetam os processos hidrológicos das bacias hidrográficas (CHIEN et al. 2013). Diversos trabalhos apontam para alterações do habitat físico de riachos decorrentes de diferentes usos do solo (ex. GERGEL et al. 2002; URIARTE et al. 2011; LEAL et al. 2015). Distúrbios antrópicos na paisagem promovem alterações de aspectos importantes dos riachos através da erosão do solo e deposição de sedimentos (MAAß et al. 2021), fatores determinantes ao comportamento dos riachos como taxas de vaporização além de picos de fluxo e de inundação (TEKLAY et al. 2021).

Esses aspectos de riachos alóctones que acessam cavernas têm grande potencial de regular os sistemas subterrâneos. Além de direcionarem processos erosivos e dissolutivos (FORD 1999), pulsos de inundação são capazes de alterar a complexidade de substratos presentes nas cavernas, além de atuar importação de recursos alimentares (SOUZA-SILVA et al. 2013), e alterar padrões da fauna cavernícola aquática (PELLEGRINI et al. 2018) e terrestre (SIMÕES et al. 2016).

No que se refere às alterações da qualidade da água, o descarte irregular de esgoto doméstico, sem tratamento adequado é a principal fonte de pressão sobre os corpos d›água no Brasil (ANA 2012). Padrão observado no presente estudo, onde os coliformes totais foram relevantes no empobrecimento da qualidade da água, estando relacionado ao número de propriedades rurais.

5. Conclusão

Este estudo confirma que o uso do solo, a densidade de propriedades rurais e as intervenções nas Áreas de Proteção Permanente são determinantes na alteração da qualidade da água e do habitat físico do Ribeirão das Lajes, podendo gerar impactos diretos na saúde ecológica da Lapa do Grotão. Uma vez que o objetivo da bacia de contribuição hídrica é garantir a estabilidade física e ecológica das cavernas, os resultados deste estudo ressaltam necessidade de medidas para conservação em sub-bacias localizadas no médio e alto curso da bacia de contribuição hídrica das cavidades.

Desta forma, ressalta-se a necessidade de políticas públicas que sejam capazes de garantir o uso sustentável desta bacia de contribuição hídrica, visando manutenção adequada dos ambientes subterrâneos na Lapa do Grotão, os quais foram indicados como extremamente relevantes em contexto local e regional.

Agradecimentos

Agradecemos à BioEspeleo pelo apoio financeiro e logístico para execução do estudo e participação no ICS e à Ana Clara Viana pelas ilustrações. Agradecemos à Elaine Alves (MLOG S.A.) por fomentar este projeto. PSP agradece ao Conselho Nacional de Desenvolvimento Científico e Tecnológico (CNPq) pela bolsa de produtividade (Número do processo: 302328/2022-0).

Referências

CARSTE CONSULTORES ASSOCIADOS (2014) Projeto Morro do Pilar. Espeleologia – Disgnóstico Integrado e Análise de Relevância. Relatório Técnico. Belo Horizonte, Minas Gerais. 330p.

CHIEN H., YEH P.J.F. & KNOUFT J.H. (2013) Modeling the potential impacts of climate change on streamflow in agricultural watersheds of the Midwestern United States. Journal of Hydrology, 491:73-88.

ELEZ J., CUEZVA S., FERNANDEZ-CORTES A, GARCIA-ANTON E., BENAVENTE D., CAÑAVERAS J.C. & SANCHEZ-MORAL S. (2013) A GIS-based methodology to quantitatively define an Adjacent Protected Area in a shallow karst cavity: The case of Altamira cave. Journal of Environmental Management 118:122-134.

FORD D.C. (1999) Perspectives in karst hydrogeology and cavern genesis. IN: PALMER A.N. PALMER M.V. & SASOWSKY I.D. (eds). Karst Modeling. Proceedings of the symposium held. Charlottesville, Virginia.

GERGEL S.E., TURNER M.G., MILLER J.R., MELACK J.M., STANLEY E.H. (2002) Landscape indicators of human impacts to riverine systems. Aquat Sci 64:118–128

LEAL C.G., POMPEU P.S., GARDNER T.A., LEITÃO R.P., HUGHES R.M., KAUFMANN P.R., ... & BARLOW J. (2016) Multi-scale assessment of human-induced changes to Amazonian instream habitats. Landscape Ecology, 31:1725-1745.

MAAß A.L., SCHÜTTRUMPF H. & LEHMKUHL F. (2021) Human impact on fluvial systems in Europe with special regard to today's river restorations. Environ Sci Eur 33:119.

OLSEN A.R. & PECK D.V. (2008) Survey design and extent estimates for the Wadeable Streams Assessments. Journal of the North American Benthological Society, Washington. 27(4):822-836.

TEKLAY A., DILE Y.T., ASFAW D.H., BAYABIL H.K. & SISAY K. 2021. Impacts of Climate and Land Use Change on Hydrological Response in Gumara Watershed. Ethiopia. Ecohydrology & Hydrobiology 21 (2) :315–332

URIARTE M., YACKULIC C.B., LIM Y. & ARCE-NAZARIO J.A. (2011) Influence of land use on water quality in a tropical landscape: a multi-scale analysis. Landscape Ecol 26:1151–1164

WILLIAMS S.L. & GENOWAYS H.H. (2008) Subfamily Phyllostominae. IN: GARDNER A.L. (Eds). Mammals of South America, Volume I. Marsupials, Xenarthrans, Shrews, and Bats. Chicago: University of Chicago Press, 255-300.

The cave in the cave – a 700 m long tube in consolidated cave sediments (Dachstein, Austria)

Lukas Plan (1), Robert Seebacher, (2) & Veronika Koukal (1)

(1) Natural History Museum Vienna, Burgring 7, 1010 Wien, Austria, lukas.plan@nhm.at (corresponding author)
(2) Verein für Höhlenkunde in Obersteier

Abstract

The Dachstein Karst massif, located in the Northern Calcareous Alps, is renowned for its extensive cave systems, primarily formed in Upper Triassic limestone. This study focuses on the Südwandhöhle, an exceptional cave system developed predominantly in Middle Triassic dolomite, which is rare in the Eastern Alps. A particularly unique feature within the cave is a 700-meter-long tube predominantly formed in consolidated fine to medium-grained cave sediment. The morphology of the tube and the surrounding passages are documented. The surrounding dolomite host rock and sedimentary characteristics are analysed to investigate the genesis of the tube. The study suggests that the development may have been influenced by the large hydraulic head of the Dachstein massif and the considerable overburden of 1.5 km, which contributed to the formation of the tube in the sedimentary rock. It is hypothesised to have formed in the interior of a pre-existing cave gallery where the sediment was consolidated by pore water from the host rock, leading to a less consolidated area in the interior where the tube was formed by erosion. It can therefore be considered a pseudokarst feature (i.e. a piping cave) within a karst cave.

1. Introduction

The Dachstein Karst massif is the second largest in the Northern Calcareous Alps (NCA), with an area of 576 km². Its peak reaches 2995 m a.s.l. (BEHM et al., 2016) The entire mountain range and the vast plateau area are mainly composed of Upper Triassic limestone of the Dachstein Formation, which reaches thicknesses of up to 1.5 km. It is underlain by Middle Triassic dolomite of the Wetterstein Formation, which only crops out in the south of the massif. The Dachstein limestone is particularly rich in caves, some of them are very large. To date, 810 caves with a cumulative length of 290 km have been documented. The Hirlatzhöhle (no. of Austrian Cave Register 1546/7) is the longest and deepest cave, with a length of 117 km and a height difference of 1560 m (PLAN et al., 2002).

However, an outstanding cave exists that is primarily developed in the dolomite, a rarity in the Eastern Alps. The Südwandhöhle (No. 1543/28; UTM 33N: 395 157 / 5 257 994) opens 0.9 km SSE and 1.2 km below the summit at the foot of the impressive south wall at 1831 m a.s.l. (SEEBACHER, 2006; 2012). So far, 11.6 km have been mapped with a depth of 509 m. Only the parts close to the entrance, characterised by rather small tubes with passage diameters in the range of 1 to 10 m², are developed in Wetterstein limestone. Most parts of the cave system are developed in Wetterstein dolomite and are much larger, with passage cross sections ranging up to 250 m². In addition to being primarily developed in dolomite, the cave is notable for its overburden. As it reaches below the summit area of the Dachstein, the maximum thickness of the rock above the cave is 1.5 km and, in some places, there are several tens of metres of glacier on top (Fig. 1).

Here we would like to present another curiosity of the cave. In the most distant parts of the cave, a small-sized conduit was discovered that is almost entirely developed in consolidated clastic cave sediments. To date, it has been mapped over a length of 700 m, but due to the physical challenges, the end remains yet unknown. The objective of this paper is to document the morphology of the tube and its surrounding as well as the properties of both, the dolomite host rock and the consolidated cave sediment, in order to hypothesise about the genesis.

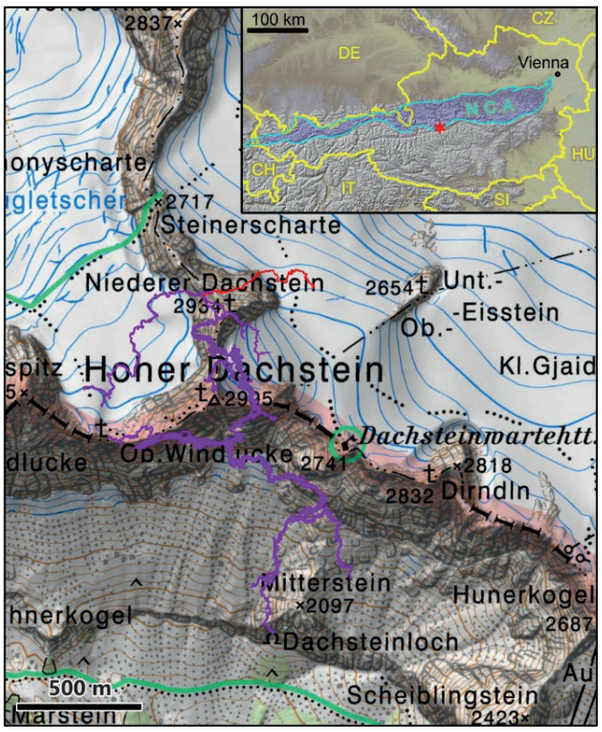

Figure 1: Extent of Südwandhöhle (purple) with the tube in the consolidated sediment (red) in relation to the surface. Inset shows the location (red star) within the Northern Calcareous Alps (NCA) and Austria.2. Site description

2. Site description

The tube in the consolidated cave sediment is located in the north--eastern most part of the cave which is characterised by fewer branches in contrast to some cave sections which are a bit labyrinthic. The surroundings of the tube in the consolidated sediment can be described as follows: from a big and more than 80 m high chamber, a large dimensioned passage (Abschlundgang) with up to 250 m^2 across leads steeply downhill along a fault dipping 45° to the NW. It gets less steep and, due to sediments covering the floor, the dimension decreases progressively until it becomes horizontal and reaches a constriction, which even had to be dug out. In total the gallery leads down 230 m vertically (Fig. 2 & 3).

Figure 2: *The large Abschlundgang at its lower part, where sediments already reduce the free cross-section.*

Already in the lower section of the Abschlundgang, consolidated cave sediments crop out on the floor and partly the walls. Shortly after the constriction, the dimensions widen to around 3 x 3 m and a pit at the side forms the entrance to the tube in the consolidated sediment. With only a short side branch immediately after that, the passage (now called Gosauschleichweg) continues for 1.05 km without any branching.

The almost vertical shaft that forms the entrance to the tube in consolidated sediment is 20 m deep, whereby in the upper section only the ceiling consists of dolomite host rock and the walls of solidified cave sediment (Fig. 3). The shaft then turns into a sub-horizontal tube formed entirely within the sedimentary rock (Fig. 4). In the tube, which usually runs a bit uphill and downhill, the cross-section is only 0.5 to 2 m^2, apart from a few extensions. Only about 5% of the passage walls are made of the dolomite host rock and these are mostly side walls. In some cases, dolomite boulders are exposed in the solidified sedimentary rock or protrude from the wall. In the middle section, the passage runs for a few metres along a ceiling fissure in the dolomite and in the backmost so far known section, the passage leads upwards three times and opens into small chambers in the dolomite host rock, characterised by chimneys and cupolas, where no traces of a former sediment filling can be seen (Fig. 4). In between and after the chambers, the tube dives back into the consolidated sediment. In the current final section, the tube descends steeply and reaches the dolomite at the base of cave sedimentary rock. The known end is an unexplored 8 m deep pit.

The length of the tube, as mapped by now, is 705 m. From the top of the entrance shaft it reaches down 80 m, but then extends again upward 60 m. The tube is still temporarily flooded and sediment marks indicate a water depth of up to 89 m for the deepest point. Flow direction is into the massif (east) which is in line with the erosion features in the consolidated and unconsolidated cave sediments (Fig. 4).

3. Host Rock and cave sediment

As mentioned, the host rock is a dolomite, which in some cases is present as dolomite cataclasite. Four rock samples were taken at different places in the Abschlundgang and thin sections were prepared and partially stained with Alizarin Red S ($C_{14}H_7NaO_7S$) and potassium ferricycyanide ($K_3[Fe(CN)_6]$). They show that samples from the host rock consist of fine-grained dolomite with low iron content with minor calcite veins. The cataclasitic parts are composed of dolomite fragments in a micritic matrix. Some veins are filled with secondary sparite.

Generally bedding is not recognisable in the dolomite and although faults are often exposed, they rarely seem to have an influence on the direction of the passage - at least over longer distances. The galleries often run in a zigzag pattern with no recognisable dominant initial fissure.

The consolidated cave sediment shows light to medium brown colors and ranges in grain size from clay and silt in clasts, dominated by sand, with rare quartz and dolomite grains reaching sizes of 1.5 cm. The sedimentary rock often shows a bedding and elongated finger like structures. Three samples were taken and already the freshly exposed surfaces show many small holes and a high porosity for some samples. Again, thin sections were prepared and partially stained with Alizarin Red S and potassium ferricycyanide. They consist of rounded to subrounded componentsof mainly dolomite, calcite, quartz and scarce phyllites which are embedded in a micritic matrix, in rare cases an iron-bearing clay matrix. Further some black grains could be identified which are probably iron-hydroxides, which are common in caves of the NCA and are called pseudo-bohnerze (SEEMANN, 1979).

The only unconsolidated fine-grained sediment in the tube in the consolidated cave sediment is white sand. It generally occurs in the deepest parts (below about 1450 m) of Südwandhöhle, most of which lie in the recent backwater area. It is a well-sorted fine-grained sand up to several decimetres thick. It consists almost exclusively of carbonate and is also common in the Hirlatzhöhle (e.g. Alter Teil, Sahara), but is much thicker there (PLAN et al., 2002).

4. Discussion and conclusion

To our knowledge, no such tubes in consolidated fine-grained cave sediment, at least with a comparable length, have been described so far. The most obvious interpretation is that this tube runs in the sediment-filled branch or continuation of the spacious *Abschlundgang*. But what is very unusual, however, is that the passage in the solidified cave sediment usually does not run along any original cave wall at all, but completely in the cave sediment rock over long distances.

One possible explanation would be that the sediment was solidified by pore water from the surrounding walls, leaving less consolidated sediment in the interior. The passage has formed or is being formed (as there is still through flow during floods) along these by erosion.

Possible factors that could favour the development of this, to our knowledge, unique feature, and which make the Südwandhöhle stand out from the other caves in the NCA, are mentioned in the following. It can be speculated that the development of the cave in a pure dolomite could be related to the big potential hydraulic head within the Dachstein of 1.6 km. The big hydraulic gradient could also have played a role in the formation of the tube in the sedimentary rock. The fact that the many

known passages in the Südwandhöhle run over relatively long distances without any side branching could be another factor, as well as the big rock overburden which could lead to a narrowing of initial fissures and thus more difficult conditions for karstification.

However, one would expect that if a gallery is filled with sediment some compaction will lead to a small void between the ceiling and the sediment before the solification. It remains unclear why the tube runs in the sediment and not along the ceiling of the dolomite rock.

In general, the observed tube can be considered as piping cave (HALLIDAY, 2004), eventually including the dissolution of the calcitic matric of the sediment, within a karst cave.

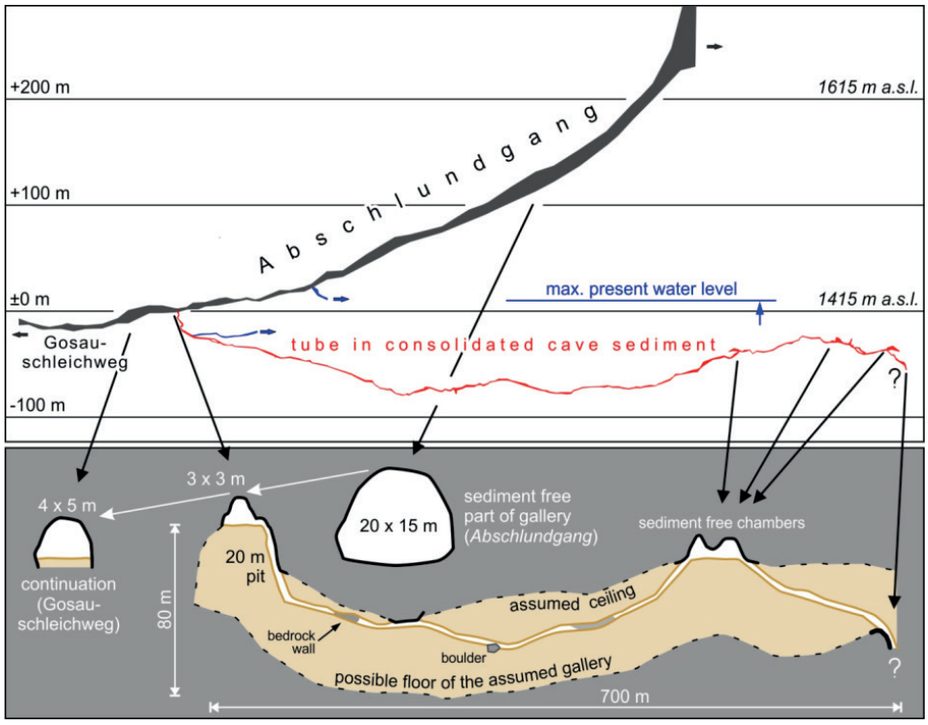

Figure 3: *Above: Extended elevation of Abschlundgang and the tube in consolidated cave sediment. Left depth bar is relative to beginning of tube. Below: schematic profile through the tube in consolidated cave sediment with the assumed passage walls; grey...dolomite host rock, brown... consolidated cave sediment, white...air filled (not to scale, the tube is significantly enlarged).*

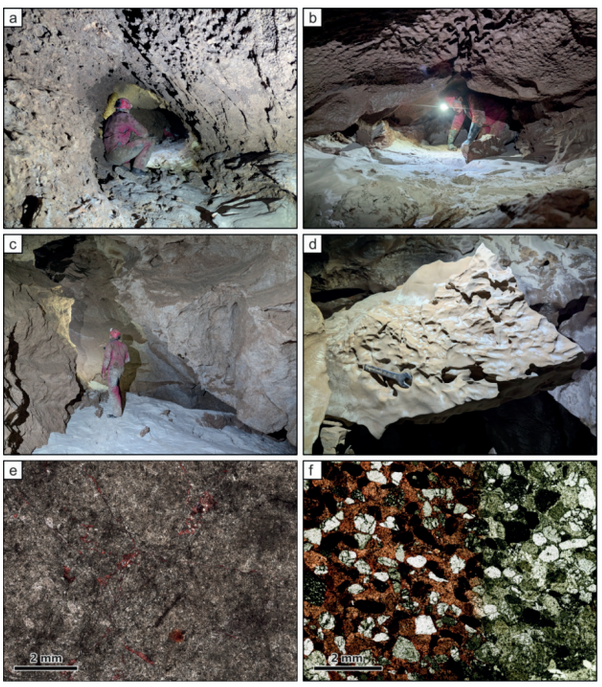

Figure 4: (a, b) Typical profiles of the tube in the consolidated cave sediment; the bottom is covered with a thin layer of white carbonate fine sand). (c) Chamber where the tube reaches a cupola like dome in the dolomite host rock. (d) Erosion features in the sedimentary rock (view against flow direction; 13 mm spanner for scale). (e) Thin-section photomicrographs of the dolomite host rock after staining with Alizarin Red S. Only few veins appear red indicating calcite. (f) Thin-section of a sandy part of the consolidated cave sediment (only left part is stained with Alizarin Red S). Mainly dolomite, calcite, and quartz sand grains are embedded in a calcitic matrix.

Acknowledgments

Iris FEICHTINGER helped with thin section preparation. Heidrun Andre and Andreas Glitzner were involved in exploration and surveying of the tube.

References

BEHM M., PLAN L., SEEBACHER R., BUCHEGGER, G. (2016) Dachstein. In: SPÖTL, C., PLAN, L. & CHRISTIAN, E. (Eds.) Höhlen und Karst in Österreich. OÖ-Landesmuseum, Linz: 569–588.

HALLIDAY, W.R., (2004) Piping caves and badlands pseudokarst. In: Gunn, J. (Ed.) Encyclopedia of Caves and Karst Science. Fitzroy Dearborn, New York: 589–593.

PLAN L., BUCHEGGER G., KAMINSKY E., KOLTAI G., RACINE T., SZCZYGIEL J. (2022) Flow regime evolution of a major cave system in the Eastern Alps (Hirlatzhöhle, Dachstein). International Journal of Speleology, 51: 181–191.

SEEBACHER R. (2006) Aktuelle Forschungen in der Südwandhöhle (Dachsteinloch, 1543/28), Stmk/OÖ. Die Höhle 57: 76–89.

SEEBACHER R. (2012) Aktueller Forschungsstand in der Südwandhöhle (Dachsteinloch) (1543/28). Mitteilungen des Vereines für Höhlenkunde in Obersteier 29-31: 197–199.

SEEMANN, R. (1979) Die sedimentären Eisenvererzungen der Karstgebiete der Nördlichen Kalkalpen. Annalen des Naturhistorischen Museums Wien 82: 209–289.

Karst hydrogeology framework with time series monitoring within fern cave area

Gheorghe M. L. Ponta (1), Stephen Pitts (2)

(1) Geological Survey of Alabama, 420 Hackberry Lane, Tuscaloosa, Alabama 35401, U.S.A., gponta@yahoo.com (corresponding author)
(2) Southeastern Cave Conservancy, Inc., Fern Cave Preserve, Paint Rock, Jackson County, Alabama, stevepitts597@gmail.com

Abstract

The Fern Cave ecosystem in northern Alabama provides vital habitat for the federally endangered Gray Bat (Myotis grisescens), hosting one of the largest colonies in the world. With 25.1 km/15.6 miles of passages, Fern Cave is located in the Paint Rock River drainage basin in south-western Jackson County, Alabama about 27 km/16.8 miles east of Huntsville. The cave is overseen by the U.S. Fish and Wildlife Service and the Southeastern Cave Conservancy Inc., Fern Cave Preserve. The Geological Survey of Alabama had a partnership with U.S. Fish and Wildlife Service since 2019 to collect water level, conductivity, and temperature data using OTT ecoLog 800 pressure transducer logger on an hourly/daily schedule from October 2019 to January 2022 to determine aquifer characteristics in the areas within and around Fern Cave National Wildlife Refuge. The major ionic composition of water collected from Fern Cave is dominated by calcium and bicarbonate ions. Temperature varied from 15°C to 18°C. Conductance ranged between 342 and 398 µS/cm. Water levels at Fern Cave changed 3.99 m/13 feet in the cave, versus 5.78 m/19 feet in Paint Rock River, during the period of study. The purpose of this study was to define the aquifer characteristics and to establish a water quality baseline to enable local, state, and federal agencies and interested citizens to develop, manage, and protect the water sources that support the Gray Bat species.

1. Introduction

Fern Cave National Wildlife Refuge (FCNWR) is situated in the Cumberland Plateau Physiographic Section, Jackson County Mountains District (Ebersole et al., 20198), on Nat Mountain in the Paint Rock Valley of Jackson County, Alabama (fig. 1). The geologic setting can be generalized as nearly horizontal carbonate and clastic rock beds dipping slightly to the south. The Fern Cave area is underlain by a stacked sequence from Mississippian to Pennsylvanian carbonate and clastic rocks with a total nearly 305 m/1,000 ft in combined thickness. The Fort Payne Chert which is not exposed but is shown on the cross section (fig. 2) forms the regional base in the area including Nat Mountain and Paint Rock River, where Fern Cave is located. If the younger limestone strata overlying the Fort Payne Chert are dissected by Paint Rock River interrupting the respective aquifers movement from one side to the other of the river, at the Fort Payne Chert level the aquifer is a continuous regional aquifer which permits water and fauna movement across the area.

2. Karst hydrogeology and geology setting

Fern Cave has 25,154 m/82,525 ft of mapped passages (Alabama Cave Survey, Accessed December 17, 2024) with a vertical range of 163.4 m/536 feet. The extension of the cave is 1,442 m/4,730 ft (distance between the furthest points of the cave), and the branching index is 17.40 (ratio between the total length and extension), corresponding to a maze type cave. The cave is located in an almost horizontal bedding plane setting with a superimposed network of fractures, resulting in branchwork stream passages in multiple tiers cave pattern (Palmer, 2007). The cave has four entrances on the top of Nat Mountain, which mostly function as sinking points for waters issued from the Pottsville and Pennington cap rocks, water disappears underground into cave streams/rivers with great discharge fluctuation. The underground path of the three main streams was identified partially by a cave survey. The *Lower North Cave Stream*, which flows south along a fracture/fault system parallel with the fault along Paint Rock River is flowing, in the *Middle Cave Section* takes almost 90^0 turns, soon to junction the *Bottom Cave Stream* which comes from the south. North of this confluence, the *Bottom Cave Stream* with the combined waters of both streams, flows first north and then northeast to discharge in Paint Rock River through a spring located in Tuscumbia limestones (fig. 3). During the life of the project, several trips were made to the lower entrance of the cave to service a transducer. It was noticed that in the wet season, Paint Rock River waters back flooded the cave, with water resurfacing through the actual cave entrance and discharging in the main river. The cave passages were completely flooded for weeks at a time, during the wet season (February–September) and the force of the current moved the transducer cable. The above-mentioned flow path identified by the cave survey was recently confirmed by dye studies performed by the Kentucky Geological Survey (KGS) and the United States Geological Survey (USGS) in 2023 (Miller and Tobin, 2023). In addition, the dye studies defined the recharge area of Haley Spring, where the largest volume of water comes from the Fern Cave/Surprise Pit entrance, forming the Surprise Stream.

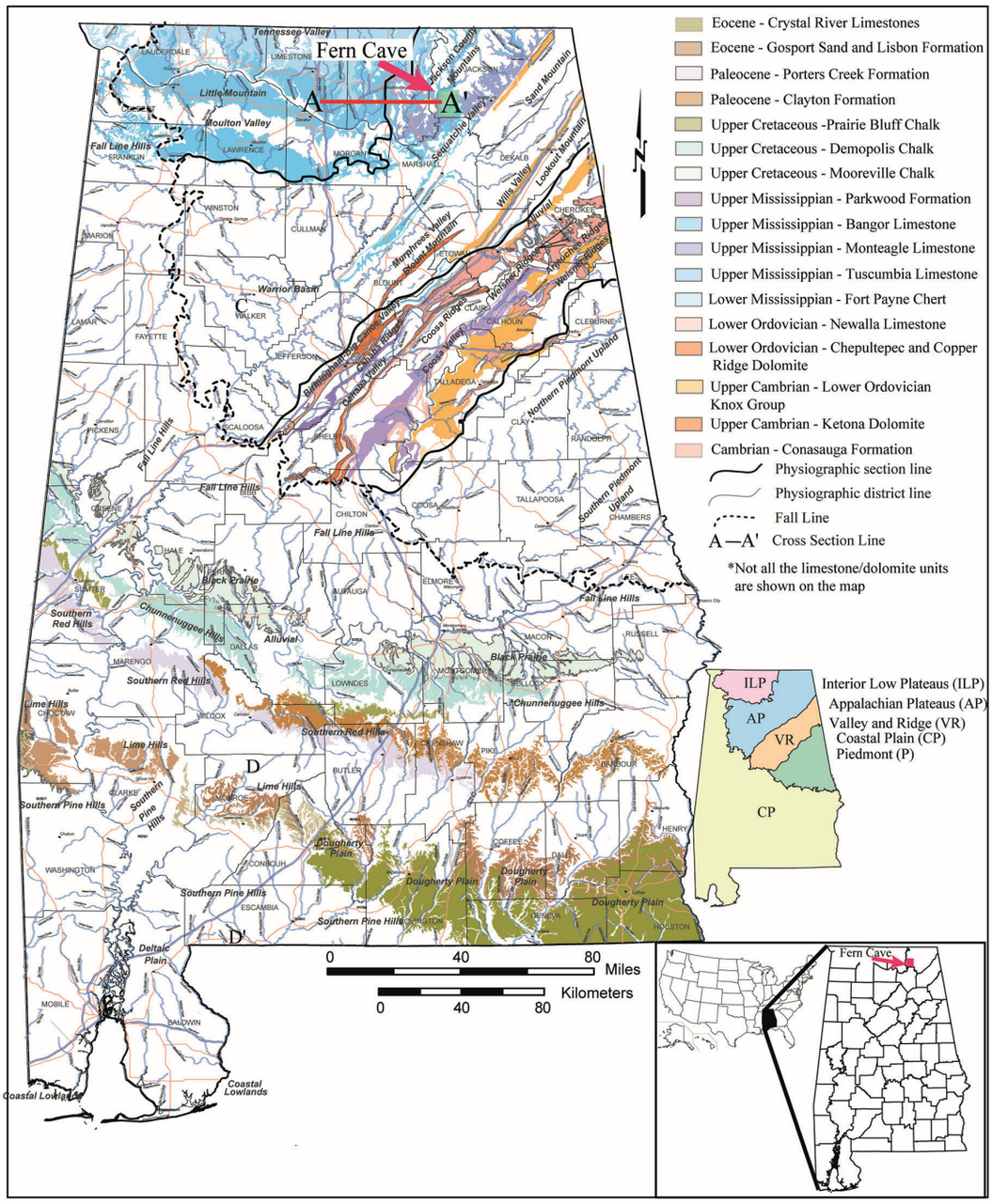

Figure 1: *Karst Map of Alabama showing the locations of cross Section A-A', Fern Cave, and USGS Station 03574500 (geology modified from Osborne et al., 1989).*

3. Karst Hydrogeologic Map

The availability of groundwater in the karst aquifer system of the Fern Cave area varies widely due to geology, structure, and karstification. A cross section and a karst hydrogeologic map depicts the occurrence of water (figs. 2 and 3), the flow conditions, and spatial distribution of geologic units with distinctive permeability (Ponta, 2019).

3.1. Aquifers in which flow are mainly intergranular.

3.1.1. Local or discontinuous productive aquifers, or extensive but only moderately productive aquifers

A local aquifer hosted by alluvial deposits is located along Paint Rock with deposits between 1.5 m/5 ft and 4.5 m/15 ft thick. Water is concentrated in open pore spaces between the grains, pebbles, and boulders.

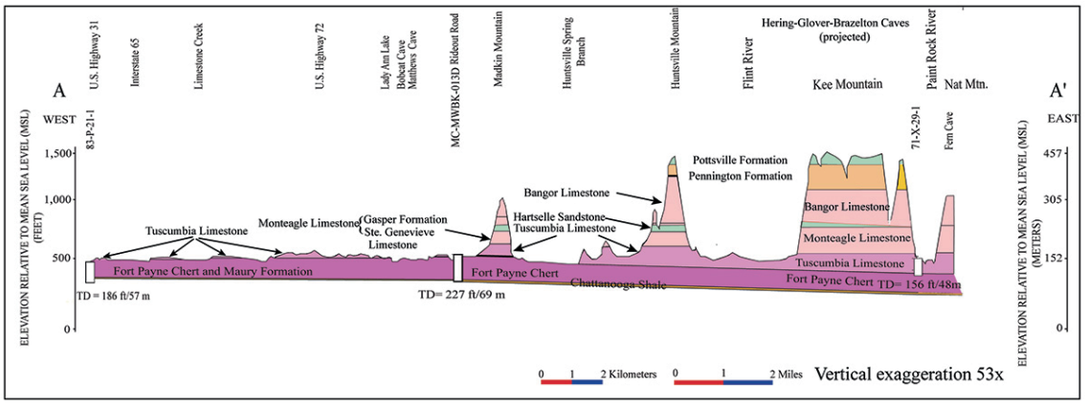

Figure 2: *Regional east-west cross section through Highland Rim and Cumberland Plateau physiographic sections (Geology modified after Osborne et al., 1989, 2013) 2.*

3.2. Fissured aquifers including karst aquifers.

3.2.1. Fissured aquifers

3.2.1.1. Local or discontinuous productive aquifers, or extensive but only moderately productive aquifers

This subcategory includes the Pottsville Formation of Early Pennsylvanian which outcrops on Nat Mountain. Many faults and folds in the Pottsville make it a hydrogeologically complex aquifer, and the groundwater flow is generally limited to fracture zones, joints, and bedding planes. These units generally yield small quantities of water to springs that, at contact with the limestones, sink underground.

3.2.2. 2.2. Groundwater in karst aquifers

3.2.2.1. Highly productive karst aquifers

The Bangor Limestone aquifer is composed of karst material and is partially confined in the Fern Cave area. The Bangor Limestone, Late Mississippian in age (figs. 2 and 3), consists primarily of medium to light gray, bioclastic, and oolithic limestone (Raymond et al., 1988). The thickness of this unit at the site is 80 m/260 ft. The Late Mississippian Hartselle Sandstone is predominantly thick bedded to massive and separates the underlying Monteagle Limestone from the overlying Bangor Limestone but at the site is very thin or absent. The Monteagle Limestone consists of two members: the lower Saint Genevieve Limestone (Lower Chesterian, Late Mississippian) and the upper Gasper Formation (Late Mississippian). Averaging 61 m/200 ft thick, the Monteagle consists of a thickly-to massively bedded, fossiliferous and oolithic limestone. Where it is present at lower elevations, Monteagle serves as a reliable source of drinking water.

3.2.2.2. Moderately productive karst aquifers

The topographically low areas in the study area are at the base of Nat Mountain, along Paint Rock River, where the Tuscumbia Limestone is present at the surface as a narrow strip-oriented northeast to southwest. The Tuscumbia Limestone formed during the Carboniferous, Late Mississippian (Meramecian) when this area was covered by a shallow sea. It is located stratigraphically below the Monteagle Limestone and Pennington Formation and above the Fort Payne Chert. The Tuscumbia Limestone is composed of light gray bioclastic or micritic, partly oolitic limestone in beds that generally are more than 0.3 m/1 ft thick.

3.3. Strata (granular or fissured rocks) forming insignificant aquifers with local and limited groundwater resources or strata with essentially no groundwater resources

3.3.1. Minor aquifers with local and limited groundwater resources

The Mississippian Pennington Formation generally contains shale, limestone, dolomite, sandstone, mudstone, and coal. The thickness of the Pennington Formation is 64 m/210 ft. The presence of carbonate interbeds within the Pennington Formation creates karstified intervals, which result in springs discharging from the base of the formation at its contact with the underlying Bangor Limestone (Miller and Tobin, 2023).

4. Materials and methods

The Geological Survey of Alabama (GSA) installed an OTT ecoLog 800 transducer placed at 200 m/630 ft. inside the cave on *Bottom Cave Stream*, along with an intelligent OTT ITC top cap installed at the Fern Cave entrance, which transmitted the data in real time to the GSA office in Tuscaloosa, Alabama. Unfortunately, a trespasser severely damaged the device in January 2022. The precipitation data was recorded at the GSA Station at Cathedral Caverns located 14 km/8.6 miles southeasts from the site. The Paint Rock River water level elevation was downloaded from the USGS station number 03574500, at Woodville, Alabama, located on the Highway 72 bridge, 2, 4.7 km/3.6 miles south of the cave. The datum of gage is 174 m/570.95 ft above the National Geodetic from the site. A hydrogeologic cross section was produced to show the relationships between different geologic formations for specific locations within the project area, along with three graphs (fig. 4) showing time series data for the period of record was also generated. Two water samples were collected from the same location on *Bottom Cave Stream* in September 2019 and October 2020.

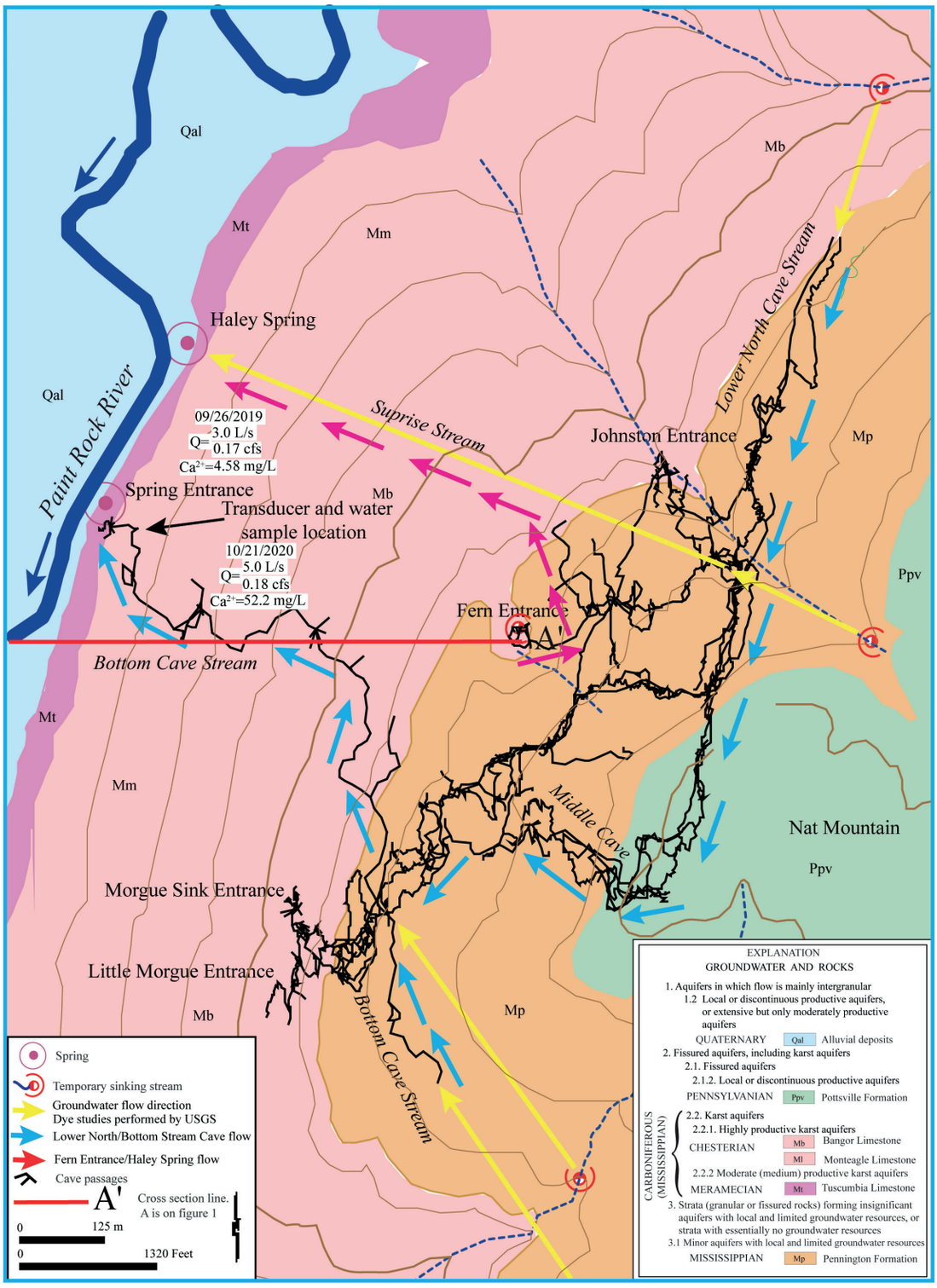

Figure 3: *Karst Hydrogeologic Map of Fern Cave Area. Complete cross section line A-A' shown on figure 1. Yellow arrow shows flow directions identified from KGS and USGS (Miller and Tobin, 2023, geology modified after Osborne at al., 2013; cave survey data provided by Stephen Pitts, Fern Cave Project written communication 2023).*

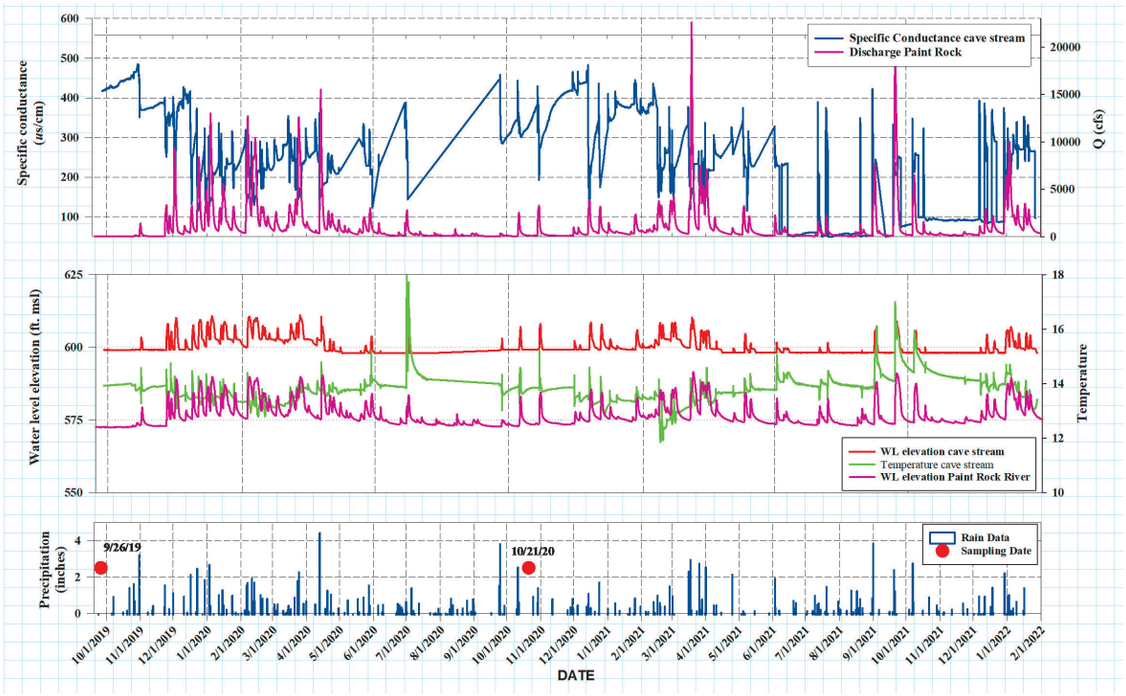

Figure 3: *Karst Hydrogeologic Map of Fern Cave Area. Complete cross section line A-A' shown on figure 1. Yellow arrow shows flow directions identified from KGS and USGS (Miller and Tobin, 2023, geology modified after Osborne at al., 2013; cave survey data provided by Stephen Pitts, Fern Cave Project written communication 2023).*

5. Results and discussions

Plots of daily parameter measurements for specific conductance and surface water elevation are depicted in figure 4, along with daily precipitation records provided by a GSA station. Rainfall visually corresponds with rising water level in Fern Cave. The water-level elevations of Paint Rock River are also presented on the graph for the period monitored.

Water-quality data

Two water samples were collected from Fern Cave about one year apart. The field parameters data and selected constituents are presented in Table 1. The estimated flow rates ranged from 3 to 5 L/s. There is no significant variation between the two samples in water chemistry baseline, specific conductance and temperature. The water samples had slightly basic pH values (7.8 – 7.9), moderate specific conductance (342 to 398 µS/cm) and 241 to 193 milligrams per liter (mg/L) total dissolved solids. Temperatures varied from 15 to 18° C. Total hardness is expressed as the total concentration of Ca2+ and Mg2+ as mg/L equivalent of CaCO3. Measured water total hardness varies from 62 to 160 mg/L CaCO3. Both samples exhibit small amounts of chlorite (1.45 to 1.01 mg/L) and nitrates (1.11 to 1.04 mg/L) and slightly elevated sulphate level (14.90 to 5.31 mg/L). The concentrations of sodium measured ranged between 2.69 and 1.83 mg/L. The presence of Mg2+ ranged between 12.10 and 7.06 mg/L and Ca2+ from 4.58 to 52.20 mg/L. In natural waters unaffected by pollution, trace metals occur in low concentrations, generally <1.0 µg/L. Chromium was detected from 0.001 to 0.0006 mg/L. The drinking water Maximum Contaminant Level (MCL) for chromium (III) is 0.1 mg/L. Manganese was detected only in the 2020 samples at 0.0046 mg/L concentration. The drinking water MCL for manganese is 0.05 mg/L. Overall, the major ionic composition of water collected from Fern Cave is dominated by calcium and bicarbonate ions. The Langelier saturation index (LI) has been used to evaluate the degree of saturation of waters with respect to CaCO3 based on the pH of the water and the pH at which the water becomes saturated. For the investigated groundwaters, LI values are -1.1 and -0.2. The negative values indicate that groundwater is undersaturated with respect to calcite and tends to dissolve carbonate minerals from the host rock, demonstrates that fast water movement of the stream through the limestone stack has no time to saturate during short travel time. This fact is supported by the dye studies performed by KGS and USGS recording short travel time/velocity through the cave system.

6. Conclusion

The major ionic composition of water collected from Fern Cave is dominated by calcium and bicarbonate ions. All constituents that are present in the water meet or exceed drinking water standards. Water temperature varied from 15°C to 18°C. Conductance ranged between 342 and 398 µS/cm. Water levels at Fern Cave changed 3.99 m/13 feet in the cave, versus 5.78 m/19 feet in Paint Rock River, during the period of study. Overall, the analytical data indicates that the investigated Fern Cave area is not impacted by the present land use in the area. Any future developments on Nat Mountain have to be carefully reviewed to be sure to have no negative impact in the cave biota

		Drinking Water Standards	Fern Cave				Drinking Water Standards	Fern Cave	
			9/26/19	10/21/20				9/26/19	10/21/20
pH	**units**	6.5-8.5	7.90	7.80	**Hardness**	**mg/L as CaCO3**		62.00	160.00
Conductivity	**µS/cm**		398.00	342.00	**Mercury**	**µg/L**	0.002	0.0135	0.00
Dissolved Oxygen	**mg/L**		7.20	4.80	**Potassium**	**mg/L**		0.8030	0.7290
Temperature	**°C**		18.00	15.00	**Lithium**	**µg/L**		18.10	8.70
Discharge	**L/s**		3.00	5.00	**Magnesium**	**mg/L**		12.10	7.06
Discharge	**cfs**		0.17	0.18	**Manganese**	**µg/L**	0.05	-	4.66
Solids, Total Dissolved	**mg/L**	500	185.90	185.90	**Sodium**	**mg/L**		2.69	1.83
Solids, Total Dissolved	**mg/L**	500	241.00	193.00	**Nitrite as Nitrogen**	**mg/L**	1	**1.11**	**1.04**
Total Dissolved Solids	**mg/L**	500	259.00	222.00	**Nitrite as NO_3**	**mg/L**		4.91	4.60
Bicarbonate	**mg/L**		169.00	160.00	**Nitrate and Nitrites as N**	**mg/L**		1.11	1.04
Carbonate	**mg/L**		1.00	1.00	**Nitrates and Nitrites as NO_3**	**mg/L**		4.91	4.60
Carbon Dioxide, Free	**mg/L**		4.00	5.00	**Ammonia as N**	**mg/L**		0.03	0.08
Boron	**mg/L**		0.0103	0.00	**Total Kjeldahl Nitrogen**	**mg/L**		0.15	0.38
Barium	**mg/L**	2	0.0418	0.12	**Phosphorus**	**mg/L**		0.01	0.00
Bromide	**mg/L**		0.07	0.08	**Rubidium**	**µg/L**		0.68	1.06
Calcium	**mg/L**		4.58	52.20	**Silicon Dioxide**	**mg/L**		7.01	6.14
Chloride	**mg/L**	250	1.45	1.01	**Sulfate**	**mg/L**		14.90	5.31
Cyanide	**mg/L**	0.2	0.00	0.0034	**Strontium**	**µg/L**		361.00	212.00
Cobalt	**µg/L**		1.00	0.00	**Titanium**	**µg/L**		3.60	4.30
Chromium	**µg/L**	1	1.00	0.60	**Turbidity**	**NTU**		7.80	6.00
Copper	**µg/L**	1	-	2.00	**Vanadium**	**µg/L**		2.35	4.00
Dissolved Solids, calculated	**mg/L**		150.00	176.00	**Zinc**	**µg/L**	5	7.70	62.40
Fluoride	**mg/L**	4	0.00	0.07	**Chemical Oxygen Demand**	**mg/L**		21.00	13.00
Iron	**µg/L**	0.3	50.70	6.60					

Table 1: *Field parameter and water quality data collected September 26, 2019, and October 21, 2021, at Fern Cave, Jackson County Alabama.*

Acknowledgments

We gratefully to Rob Hurt with U.S. Fish and Wildlife Service for arranging access to the cave and providing the OTT ecoLog 800 data logger and to Stephen Pitts with the Southeastern Cave Conservancy, Fern Cave Preserve provided permission to access the study area and for the cave survey presented in this paper. Also, many thanks to Birmingham Grotto cavers led by Bradly Jones who travelled to the site to assist with the installation of the transducer.

References

ALABAMA CAVE SURVEY (2024) Maps of Fern Cave: http://www.alabamacavesurvey.org, accessed November 10, 2024.

EBERSOLE S, GUTHRIE, G. M., and VANDDERVOORT, D. S. (2019) Physiographic regions of Alabama: Tuscaloosa, Alabama Geological Survey Open-file Report 1901, 1 plate.

MILLER, B.V. and TOBIN, B.W. (2023) Mapping karst groundwater flow paths and delineating recharge areas for Fern Cave, Alabama, through the use of dye tracing: U.S. Geological Survey Scientific Investigations Map 3506, 2 sheets, https://doi.org/10.3133/sim3506. OSBORNE W.E., SZABO M.W., COPELAND C.W., Jr., and NEATHERY T.L. (1989) Geologic map of Alabama: Tuscaloosa, Alabama Geological Survey Special Map 221, scale 1:500,000.

OSBORNE W.E., WARD W.E.II, and IRVIN G.D. (2013) Geologic map and cross section of the Paint Rock 7.5-minute quadrangle, Jackson and Madison Counties, Alabama: Alabama Geological Survey Quadrangle Series Map QS59, scale 1:24,000.

PALMER A. N. (2007) Cave Geology, Cave Books USA p 454

PONTA, G. M. L. (2019) Karst Hydrogeology, in Ponta, G. M. L., and Onac, B. P., eds., Cave and Karst Systems of Romania: Cham, Switzerland, Springer International Publishing, p. 41-47.

Dye studies to delineate the recharge area of Tham Luang-Khun Nam Nang non karst aquifer, Thailand

Gheorghe M. L. Ponta (1), Vanachawan Hunyek, Ocpasorn Occarach, Perawich Burakasikorn, Aiyakarn Chinnasri, (2), Chaiporn Siripornpibul (3) & Kiattipong Kamdee, Patchareeya Chanruang (4)

(1) Geological Survey of Alabama, 420 Hackberry Lane, Tuscaloosa, Alabama 35401 U.S.A. gponta@gsa.state.al.us (corresponding author)
(2) Department of Groundwater Resources 26/83 Soi Ngam Wong Wan 54, Lad Yao, Chatuchak, Bangkok, Thailand 10900 vanachawan.h@dgr.mail.go.th
(3)Department of Mineral Resources 75/10 Rama 6 Rd., Thung Phaya Thai, Ratchatewi, Bangkok, Thailand 10400 alekchaiporn@gmail.com
(4) Thailand Institute of Nuclear Technology (Public Organization) 9/9 Saimoon, Ongkharak, Nakhon Nayok, Thailand 26210

Abstract

In June and July 2018, the rescue of a junior soccer team from Tham Luang Cave, in northern Thailand made headline news. Consequently, several state agencies received funding to perform studies in the area, including delineation of the recharge area of this cave system. The task was partially funded by the International Atomic Energy Agency under THA5057 project. In November 2023, two tracer studies were performed by Department of Groundwater Resources (DGR) and Thailand Institute of Nuclear Technology (TINT). On November 7, 2023, fluorescein was injected in a swallet along Huai Nam Dan Valley follow by a second injection with Rhodamine WT on November 8, 2023, in a swallet halfway along Huai Pak Tin Fai Canyon. On November 8, 2023, the fluorescein dye was visibly observed at Tham Luang Cave, and subsequentially at Tham Luang Cave Well and Morakot Pool. Rhodamine WT was identified at Tham Pla Spring, with more than 50% of the dye flowing over the sinking point dammed by DGR personnel. The monitoring continued for three weeks at nine locations. No dyes were detected in other monitoring points.

1. Introduction

In June and July 2018, headline news was made in northern Thailand of the rescue of a junior soccer team from Tham Luang Cave (fig. 1). Consequently, several Thai state agencies received funding to perform hydrogeological studies in the area. Between 2018 and 2023, the Department of Groundwater Resources and the Thailand Institute of Nuclear Technology, with the Department of Mineral Resources and the Department of National Parks, Wildlife and Plant Conservation, performed dye studies to delineate the recharge area of the Tham Luang Cave System and corresponding aquifer for future systematic management of these water resources. The study area (Tham Luang-Khun Nam Nang Non Forest Park/Limestone Mountain Range) is located in the northern part of Thailand along the Thai-Myanmar border, in Mae Sai District, Chiang Rai Province (fig. 1). The general topography consists of a limestone mountain range oriented north-south, traversed by narrow steep valleys (canyons), along with steep cliffs and sharp peaks reaching 1000-1,200 meters in elevation. The northern region has a tropical climate, humid, hot, and dry, receiving most of its precipitation during the rainy season (mid-May to September or early October). The mountain range in the Tham Luang-Khun Nam Nang Non Forest Park area consists of approximately 25 percent igneous rocks (diorite, granodiorite, granite, gabbro, basalt), approximately 25 percent sedimentary and metamorphic rocks (shale, sandstone, limestone, volcanic pebbles, tuff, semi-metamorphic rocks, quartzite, slate, marble), and approximately 50 percent detritus, gravel, sand, silt, clay. The geological age ranges from Silurian-Devonian to Quaternary. Faults in the area are oriented approximately northeast–southwest and include normal faults clearly visible in the limestone of Doi Nang Non and reverse faults present in the Tham Luang–Tham Liang Pha area ‘s marble. The fault plane strike is approximately north–south, dipping approximately 50 to 80 degrees, east or west. Water disappears underground along these planes, generating the Tham Luang galleries with a branchwork stream passages cave pattern (Palmer, 2007). The Caves Tham Luang–Khun Nam Nang Non National Park survey was cordially provided by Martin Ellis.

2. Karst hydrogeology and geologic setting

The geological structure of the study area was controlled by the Hercynian Orogeny during Carboniferous–Permian followed by the Indosinian Orogeny in the Triassic and the Himalayan Orogeny in the Tertiary period. These events led to the formation of the Tham Luang-Khun Nam Nang Non Limestone Mountain Range with an igneous rock (diorite, granite) core oriented approximately north-south and Carboniferous–Permian sedimentary rocks strata (limestone, shale) discontinuously overlaying the eastern flank. The Carboniferous–Permian sedimentary rocks formed a limestone ridge oriented north-south traversed by east-west faults, along which steep, narrow canyons developed. At the foothills of this limestone ridge to the east, a large plain, the Mae Sai Basin is located with an aquifer recharged by waters flowing down from the Nang Non Mountain Range.

Figure 1: *Map of Southeast Asia showing the location of Tham Luang Cave.*

Karst hydrogeologic map

The availability of groundwater in the karst aquifer system of the Tham Luang – Khun Nam Nang Non area varies widely due to geology, structure, and karstification. A karst hydrogeologic map depicts the occurrence of water (fig. 2), the flow conditions, and spatial distribution of geologic units with distinctive permeability (Ponta, 2019).

2.1. Aquifers in which flow are mainly intergranular.

2.1.1. Extensive and highly productive aquifers

Water is concentrated in open pore spaces between the grains, pebbles, and boulders of the Mae Sai Basin, located east of the limestone ridge. The sediments are mostly sand, clay and gravel with a thickness ranging between 40 and 260 m. Several wells were installed in this unit, including the San Sai Non School artesian well, located about 6 km east of the limestone ridge, was used during the dye study monitoring network, with water levels recorded at +0.17 m above land surface. It is a 4 inches diameter well, 160 m deep.

2.1.2. Local or discontinuous productive aquifers, or extensive but only moderately productive aquifers

The Hillside rock fragments sedimentation unit is a fan shaped colluvial deposit, present at the foothills of the Tham Luang-Khun Nam Nang Non Mountain Range at the east end of the canyons (example Huai Pak Tin Fai). The thickness of the unit is up to 80 meters, and consists of medium and coarse gravel layers, mixed with sand containing local shallow aquifers, where domestic dug wells are present.

2.2. Fissured aquifers including karst aquifers.

2.2.1. Fissured aquifers

2.2.1.1. Local or discontinuous productive aquifers, or extensive but only moderately productive aquifers

This subcategory includes middle Carboniferous–Permian units which appear as two narrow strips oriented almost north–south along the western edge of the limestone ridge. It consists of gray-black, greenish-gray, thin-layered shale, interbedded with greywacke sandstone. In some areas, slate, schist, quarzitic schist, and quartzite fragment are present, with a thickness ranging from 20 to 70 m. These units generally yield small quantities of water to springs that, at limestone contacts, sink underground.

2.2.2. Groundwater in karst aquifers

2.2.2.1. Highly productive karst aquifers

The Upper Part of Late Carboniferous–Permian (CP3-2) in Tham Luang area–Khun Nam Nang Non consists of grayish white, white marble, finely crystalline with occasionally medium size grains, about 2 to 70 cm thick strata. It is largely present in the area forming the limestone/marble ridge which holds a highly productive aquifer with extensive karst features and hosts the Tham Luang Cave.

The springs located at the foothills of the limestone/marble ridge serve as a reliable source of drinking water.

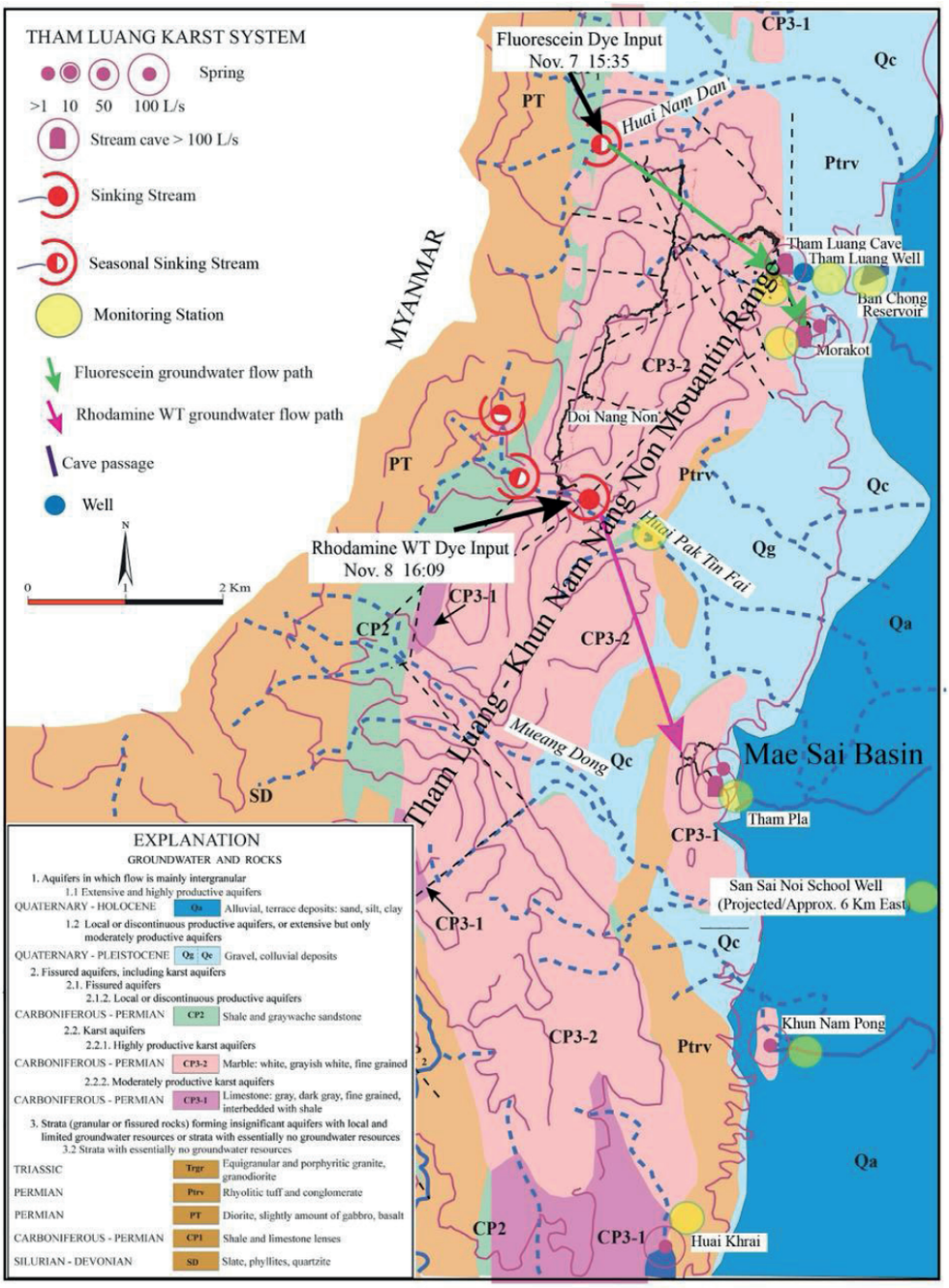

Figure 2: *Karst Hydrogeological Map of Tham Luang Cave Area (hydrogeology legend from Ponta 2019, geology modified after DMR, 2021)*

2.2.2.2. Moderately productive karst aquifers

The lower part of the Late Carboniferous-Permian deposits (CP3-1) outcrop sporadically in the topographically high area of the western side of Tham Luang area – Khun Nam Nang Non Mountain range, mostly at contact with non- karstic rocks and on a larger area in the south of the study area, in the vicinity of Huai Khrai Spring. The Lower group (CP3-1): consists of gray, grayish-black limestone, finely crystalline, thin to medium thick layers with average thickness 10 to 20 centimeters up to about 40 centimeters, interbedded with thin layers of shale and occasionally chert and an abundance of fossils (e.g., Brachiopods, corals, crinoids and foraminifera, etc.). Some strata of this units are extremely karstifiable, due their presence in small areas, their aquifers are of local importance and more than likely are interconnected with the marble aquifer.

2.3. Strata (granular or fissured rocks) forming insignificant aquifers with local and limited groundwater resources or strata with essentially no groundwater resources

2.3.1. Strata with essentially no groundwater resources

The igneous rocks (diorite, granite, shale) from various periods on the western side of the limestones ridge are not a groundwater resource. All the surface waters formed on these units are organized in stream which at contact with the karstic rocks disappears underground, generating solution features and cave passages.

3. Materials and methods

Between November 5 and 27, 2023, a tracer study was performed by Department of Groundwater Resources (DGR) and Thailand Institute of Nuclear Technology (TINT) with Mr. Chaiporn Siripornpibul, Department of Mineral Resources (DMR) assisting in the Tham Luang Cave area for recharge area delineation. On November 5, 2023, 15:35, 3.8 kg of fluorescein was injected in a swallet along Huai Nam Dan Valley (fig. 2) follow by a second injection on November 8, 2023, 16:05 in a swallet halfway of Huai Pak Tin Fai (Huai Makok) Huai Pak Tin Fai Canyon, this time being used 15.5 Lbs. of liquid Rhodamine WT (approx. 7 kg in weight). Nine monitoring stations were established as follows: (1) Tham Luang Cave, (2) Tham Luang Cave Well, (3) Ban Chong Reservoir, (4) Morakot Pool, (5) Tham Pla, (6) Khun Nam Pong, (7) Huai Khrai, (8) San Sai Noi School Well, and (9) Huai Pak Tin Fai (downstream/eastern end of the canyon). A few days before the dyes' input, background monitoring was implemented, charcoal bags were installed, and water samples were collected at above mentioned locations. Collection activity continued at a 24 hours interval after the dye input. Discharges were measured at all injection and monitoring stations. At Morakot Pool the in situ device (Turner Design C3) owned by DGR was installed at the beginning of the background monitoring. During the test, a Turner Design 10-AU-005-CE Fluorometer of TINT was used to analyze in situ water samples collected across the site. On November 8, 2023, 8:30, the fluorescein dye was visibly observed at Tham Luang Cave (fig. 3). For the next couple of days, the sampling interval was changed to approximately 6 hours (three times per day – no sampling between 24:00 and 8:00). The stream at Tham Luang Cave disappeared on November 19, 2023, 23:48. Selected charcoal bags were qualitatively analyzed courtesy of Geary Schindler with Karst Works, Inc. The analyses confirm the presence of fluorescein in charcoal bags installed at Tham Luang Cave, Tham Luang Cave Well, and Morakot Pool. Rhodamine WT was identified at Tham Pla, with more than 50% of the dye present at sinking points dammed by DGR personnel. No dyes were detected in other monitoring points. Based on this finding, another set of selected charcoal bags were sent to be analyzed quantitatively by Ralph Ewers with Ewers Water Consultants Inc. (EWC). The results were reported in Fluorescence Units (FU) (fig. 4).

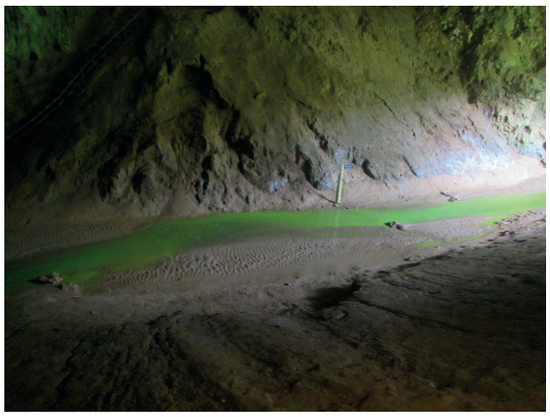

Figure 3: *Fluorescein dye at Tham Luang Cave.*

4. Results and discussions

Discharges were measured at all injection points and monitoring stations (Table 1). At the injection points, the flow ranged between 11 and 79 L/s. The second injection was performed after heavy rain which resulted in a fast increase in the rate flow (11 versus 79 L/s). Springs flows were mostly above 100 L/s, the two mains monitored springs, Tham Pla and Morakot with over 500 L/s. Analytical results of the water samples collected from the sinking points and main springs are presented in Table 2. It is notable the difference in Ca^{2+} concentration between sinking points (20.40 and 20.48 mg/L) versus resurgence, where Ca^{2+} ranges between 55.22 and 97.61 mg/L. Fluorescein dye was visibly observed at Tham Luang Cave on November 8, 2023, after 17 hours, and subsequently detected at Tham Luang Cave Well, and at Morakot/Emeral Pool, after 48 hours. Rhodamine WT was identified in water samples and charcoal bags after 84 hours at Tham Pla Cave/Spring, although more than 50% of the dye flowed over the sinking points dammed by DGR personnel. The monitoring continued for three weeks at all nine locations. No dyes were detected in other monitoring points. Results from the study demonstrate that the swallet along Huai Nam Dan Valley/Canyon is directly connected to Tham Luang Cave System and Morakot/Emerald resurgence, while the downstream section of Huai Pak Tin Fai Valley is connected to Tham Pla Cave/Spring. Therefore, the people living upstream, using large amounts of water, fertilizers and pesticides, and detergents or dumping garbage into the waterway, will directly affect the quantity and quality of groundwater for communities. A comprehensive figure (fig. 4) shows the graph for the results of water and charcoal bags and in situ devices for the life of the project at Tham Luang Cave, Tham Luang Well, Morakot and Tham Pla Springs.

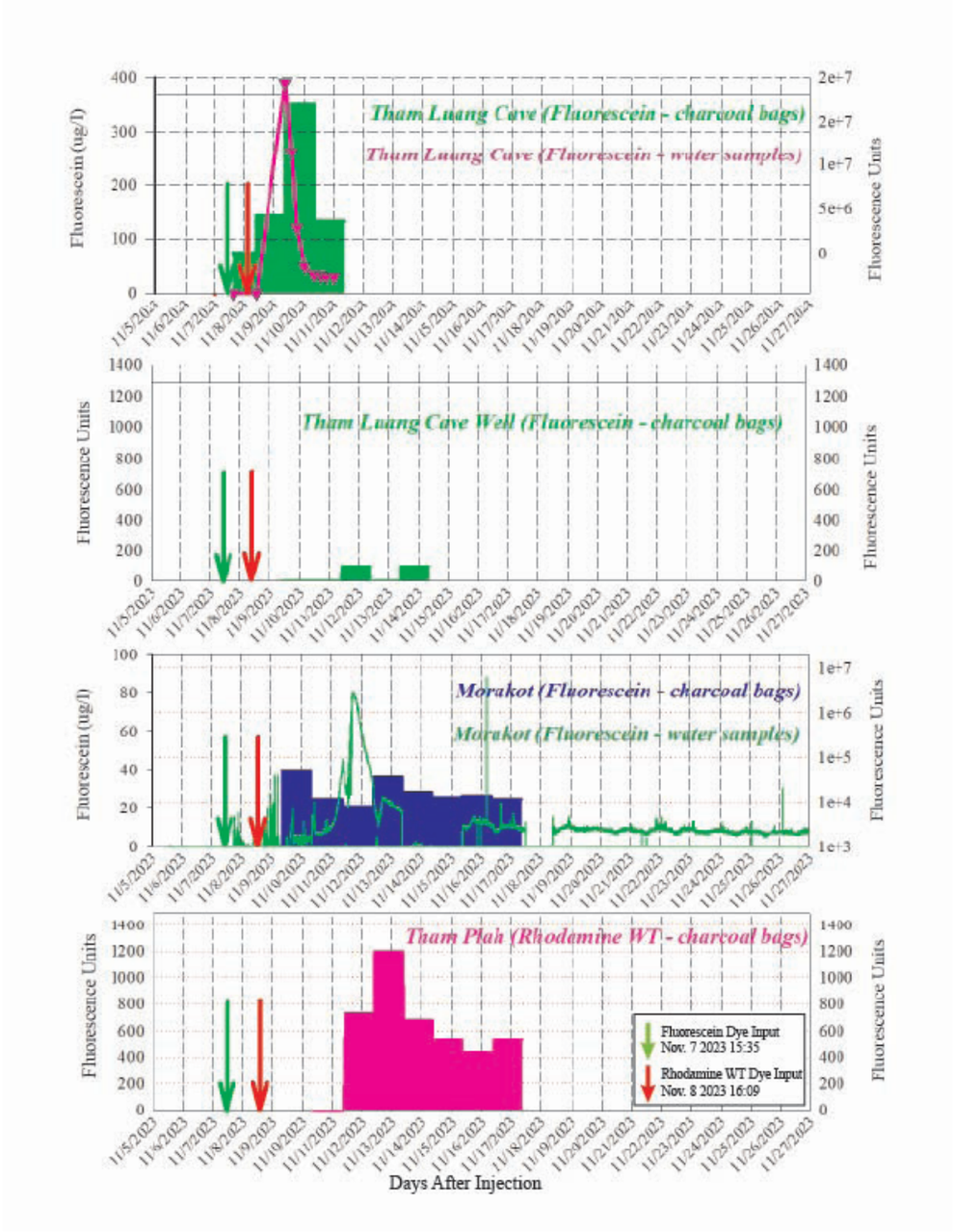

Figure 4: *Graph showing dye studies results performed in Tham Luang Cave area.*

Montoring or Injection Stations	Velocity		Discharge	
	feet/sec	m/s	l/s	m^3/h
Morakot	2.19	0.67	512	1,845
Tham Pla	0.45	0.14	678	2,442
Khun Nam Pong	3.42	1.04	279	1,006
Huai Khrai	1.63	0.50	102	366
Hua Nam Dan Injection Point	0.48	0.15	11	39
Hua Nam Dan Upstream Injection Point	0.41	0.13	36	128
Huai Pak Tin Fai Injection Point	0.64	0.20	79	283
Huai Pak Tin Fai Downstream/Waterfall	0.59	0.18	43	155

Table 1: *Velocity and discharge measurements at the site before dye injections.*

Date	Sample ID	pH	Sp. Cond	TDS	Mg	K	Ca	Mn	Fe	Zn	Flouride	Chloride	Nitrate	Bromide	Phosphate	Sulfate
			µS/cm	mg/L	mg/L	mg/L	mg/L	mg/L	mg/L	mg/L	mg/L	mg/L	mg/L	mg/L	mg/L	mg/L
11/7/2023	***Huai Nam Dan***	7.08	274	136	4.88	0.68	20.40	0.01	0.01	0.01	0.35	1.89	0.00	1.08	n.a.	1.58
11/7/2023	***Huai Pak Tin Fai***	7.76	520	260	4.85	0.68	20.28	0.01	0.01	0.01	0.36	2.02	0.00	4.56	1.11	2.70
6/6/2023	Ban Chong Reservoir	7.67	872	425	5.53	0.88	55.22	0.00	0.11	0.00	0.35	1.12	0.00	0.56	n.a.	1.17
11/7/2023	Morakot Pool	7.57	578	284	3.31	0.49	65.19	0.01	0.02	0.01	0.34	0.67	0.00	0.48	n.a.	1.23
6/6/2023	Tham Pla				3.42	0.98	70.69	0.01	0.01	0.04	0.35	0.89	0.00	2.33	n.a.	1.20
6/6/2023	Tham Luang Cave	7.53	746	385	0.42	0.71	83.29	0.00	0.01	0.01	0.00	0.97	0.00	5.64	n.a.	0.73
11/8/2023	Khun Nam Pong				2.28	0.78	97.61	0.04	0.01	0.003						

Table 2: *Water Quality Data (in italics water samples collected from swallets)*

Acknowledgments

We gratefully to Jade Julawong with Water Resource Engineering Co., Ltd. for providing 2 kg of fluorescein dye, Dr. Mehmet Zeki Billor with Auburn University, Alabama, U.S.A. for the water quality analyses, PELA GeoEnvironmental for letting us use their rod and flow meter, and Bogdan Onac with University of South Florida for analyzing the stable isotopes samples (oxygen and deuterium). Also, many thanks to International Atomic Energy Agency THA5057 for partially funding this project, Vernon Unsworth, Martin Ellis, Kamon Kunngamkwamdee and Tham Luang – Khun Nam Nang Non Forest Park officers were instrumental in setting up the dye study. Thanks for Gerry Schindel, with Karst Works, Inc for analyzing the charcoal bags free of charge and to DGR and TINT personal for their field support.

References

PALMER A.N. (2007) Cave Geology, Cave Books, Allen Press, Lawrence, Kansas, USA p 454

PONTA, G. M. L. (2019) Karst Hydrogeology, in Ponta, G. M. L., and Onac, B. P., eds., Cave and Karst Systems of Romania.

DEPARTMENT OF GROUNDWATER RESOURCES, DEPARTMENT OF MINERAL RESOURCES (DMR), and DEPARTMENT OF NATIONAL PARKS WILDLIFE AND PLANT CONSERVATION (DNPWPC) (2021) Geological and Hydrogeological Studies of Limestone Mountain Ranges in Tham Luang-Khun Nam Nang Non Forest Park Project in: Geological and hydrogeological survey project Tham Luang - Khun Nam Nang Non Forest Park, p.353

Understanding the sedimentary dynamics of alpine caves: the example of the Dévoluy Massif (France)

Nathan Rispal (1), Philippe Audra (1), Ludovic Mocochain (2), Marianna Jagercikova (2), Pierre Henry (3) François Demory (3)

(1) Polytech'Lab UPR 7498, University Cote d'Azur, Nice, France, nathan.rispal@etu.univ-cotedazur.fr (corresponding author), Philippe.AUDRA@univ-cotedazur.fr

(2) Independent researchers ludomocochain@gmail.com, jagercikova@yahoo.com

(3) Aix Marseille Univ., CNRS, IRD, INRAE, CEREGE, Aix-en-Provence, France henry@cerege.fr, demory@cerege.fr

Abstract

Studying karst sediments provides access to geological archives often erased from the surface by erosion. Understanding these geological archives gives information on the evolution of the karstic massif. In this study, we aim to show how the analysis of sedimentary sequences preserved in certain caves in the Dévoluy massif, France, can lead to a better understanding of the evolution of the karst within the area in an alpine context. A precise characterization of the karst deposits was carried out to understand the sedimentary dynamics and the paleo-environmental context during deposition. We show that the succession of warm and cold episodes led to varied filling dynamics organized around four major facies types that reflects these environmental variations. Using paleomagnetic dating, we show that ancient glacial phases were recorded in the massif, much earlier than those described (prior to 722 ka). U/Pb dating of the speleothems framing these deposits will provide more precise age information. Mineralogical characterization of the fine-grained sediments will also enable us to better constrain the origin of the material deposited in the conduits.

1. Introduction

Karst reservoirs are heterogeneous systems whose functioning is challenging to understand due to their complexity. Their formation often results from a succession of geological events, the signals of which overlap and interact to shape the current state and dynamic of the karst (Baral et al. 2023)which modifies the initial petrophysical properties (i.e., porosity and permeability. Characterizing these systems requires an integrative approach involving the detailed study of each of these structuring events, their imprint on the system, and their role in the overall evolution of the reservoir (De Waele et Gutierrez 2022). Among these records, karstic infillings hold significant importance as they preserve traces of events often erased from the surface by erosion.

In mountain environments, karst infillings occur in three main types: 1/ coarse, poorly sorted deposits such as debris flows, conglomerates, or breccias, 2/ fine deposits such as silts or clays and 3/ speleothems. Debris flows indicate abrupt events characterized by the rapid transport of poorly sorted sediments (Bauer 1989; Vanara 1997). In contrast, fine deposits result from the flooding of galleries and a calm hydrodynamic regime favorable to particle deposition. These flooding may be caused by sediment plugs, deposited by glaciers or not (Lignier et Desmet 2002)la grotte sous les Sangles contient une riche séquence de dépôts détritiques (dépôts glaciaires et fluviatiles, formation laminée et rythmée or by a localized rise in the base level caused by the obstruction of a glacier (Audra et al. 2007). When these sediments are fine grained, laminated, and deposited in relation to glacier control, they are called pseudo-varves. During temperate periods, speleothems develop in caves and may frame the sedimentary deposits, reflecting paleoenvironmental changes within the massif (Jaillet et al. 2023).

The study of karst infillings uses classical sedimentological methods: outcrop surveys, facies descriptions, granulometric and mineralogical analyses, and sedimentary architecture (Lignier et Desmet 2002; Perroux 2005; Quinif et Maire 1998; Sbai et al. 1995)la grotte sous les Sangles contient une riche séquence de dépôts détritiques (dépôts glaciaires et fluviatiles, formation laminée et rythmée. These observations can be complemented by dating methods: paleomagnetism (Audra et Rochette 1993; Zupan Hajna et al. 2010), radiochronology on speleothems (U/Th and U/Pb), or cosmogenic nuclide dating on allochthonous sediments (Granger et Muzikar 2001).

In this study, we provide a detailed description of karst deposits observed in several caves of the Dévoluy massif in the French Alps. A precise characterization of these sediments and their depositional settings gives paleogeographic and paleoenvironmental constraints on the evolution of the karst reservoir. Paleomagnetism brings some constraints on the age of the deposits and a refined model for the evolution of the Dévoluy karst system.

The Dévoluy massif, located in southeastern France, is the highest subalpine massif, reaching an altitude of 2,798 m. Its current morphology is the result of successive structuring phases during the Cenozoic, which led to folding, thrusting, and uplift of the massif (Meckel, Ford, et Bernoulli 1996). This structural imprint is overlain by relief shaping through Mio-Pliocene erosion and the impact of Quaternary glaciations (Mai Yung Sen et al. 2024; Monjuvent 1979)l'emplacement du bassin du Drac commence à en émerger partiellement dès la fin du Crétacé (Sénonien . The study area is mainly composed of Upper Cretaceous (Campanian-Maastrichtian) limestones folded into a double north-south syncline separated by the median Dévoluy thrust. This unit is deposited unconformably on marly-limestone terrains from the Lower Cretaceous

and Jurassic (Michard et al., 2010) forming a low-permeability, poorly karstified basement. In the central part of the massif, carbonates and detrital deposits date from the end of the Eocene up to the Oligocene (Grosjean et al. 2017; Huet 2024; Meckel, Ford, et Bernoulli 1996) (Fig. 1). The massif is highly karstified, with over 600 documented caves, some reaching nearly 1,000 m of depth (e.g., Rama-Aiguilles system). The underground drainage converges toward a nearly unique karst outlet to the north, the Gillardes springs (Bonhomme 1972; Luparini 1975; Zappelli, Belleville, et Jagercikova 2018). Only a portion of the Pic de Bure plateau is drained southward toward the Sigouste spring (Maire 1980). Karstification is predominantly controlled by geological structure, with vertical shafts or steep ramps developing along fault zones or fracture corridors and meandering passages strongly controlled by their dip. A few horizontal perched and abandoned drains reflect older phases of karstification. This is the case for the Jalabres cave, where infillings of allochthonous fluvial pebbles have dated the karst to at least 12 Ma (Jagercikova et al. 2021; Lemot et al. 2023)sands and clays, which formed endokarstic deposits. According to petrographic diversity with presence of granite, orthogneiss, varia gneiss, migmatites, amphibolic gneiss, volcanic basic rocks, sandstones and even limestone with nummulites, these alluvions originate from the SW of the Ecrins massif (Champsaur and Valgaudemar.

Few other studies have focused on the genesis and evolution of the Dévoluy karst networks, apart from Audra (2000), who identified infillings and speleothems with reversed magnetic polarity in the Chourum du Goutourier, providing evidence for karstic drains older than 722 ka.

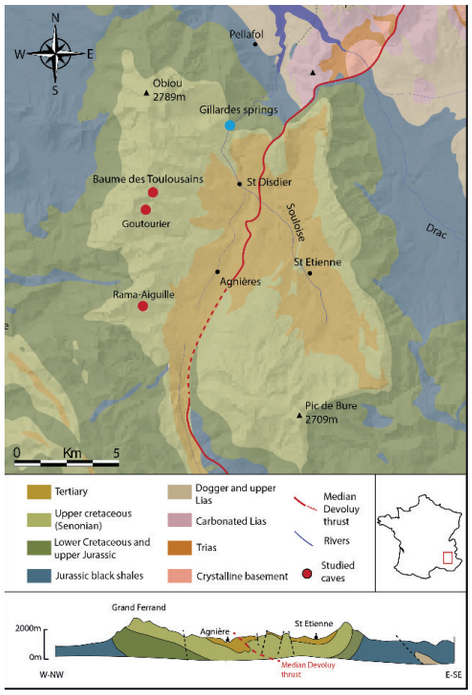

Figure 1: *Geology of the Dévoluy massif and associated cross section. Caves locations are represented by a red dot.*

2. Materials and methods

Our research focused on three caves in the Dévoluy massif, selected for the quality and diversity of their sedimentary infillings. These caves represent a common type in the massif, developing along the dip of limestone strata. All three studied caves are located on the western part of the massif, corresponding to the Dévoluy thrust footwall and differ in altitude, development, and morphology (Fig. 2).

The Rama-Aiguilles system, the deepest in the massif, reaches a depth of -980 m. The Aiguilles branch consists of shafts and meanders, initially guided by faults and dip of the cretaceous limestone. The Rama branch is characterized by large chambers in its middle section before joining the Aiguilles branch, where active water flow is observed. The studied outcrops is *Musée aux Varves* (MV) at -510 m (altitude 1760 m).

The Baume des Toulousains (2280 m) develops along fractures in its upper section down to -70 m, before following the dip in a large gallery that branches into smaller passages below -200 m. The studied outcrop (BT) is located in the lower part of the large gallery, around -150 m (altitude 2130 m), where sediments are well-preserved beneath collapsed blocks.

The Chourum du Goutourier (2300 m) reaches a depth of -431 m, with deposits found at (GU3_a and GU3_b at 2180 m) and at -200 m (GU5 at 2100 m), in conduits following the dip. GU3 corresponds to the same site described by Audra (2000).

Sediments were studied using following methods: facies descriptions, sampling for composition analysis, and collection of selected deposits for dating.

For unconsolidated sediments such as pseudo-varves and clays, X-ray diffraction (XRD) analyses are ongoing and will determine their mineralogical composition. These analyses will be supplemented by the study of heavy minerals to identify sediment sources, palynological analyses to reconstruct the paleoenvironmental context, and calcimetry to quantify the carbonate content.

Two types of deposits were sampled for dating. The first type, comprising unconsolidated or indurated sediments and speleothems, was for paleomagnetism. Samples were oriented using a compass to

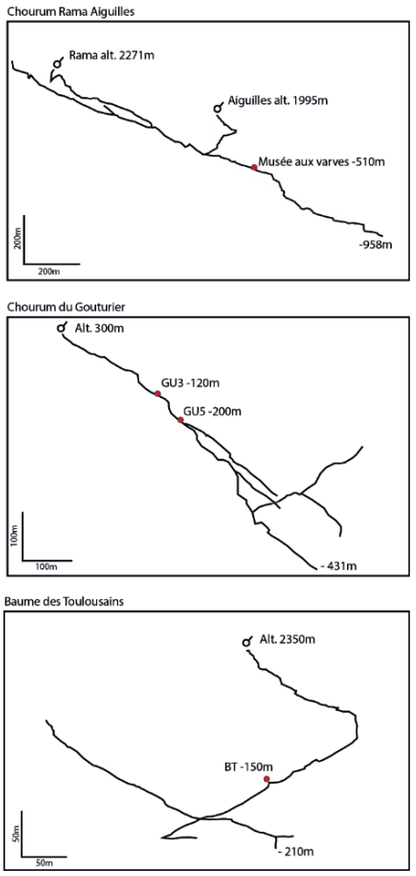

Figure 2: *Synthetic topography and location of described outcrops in the three studied caves. Note that scales are different.*

preserve their orientation relative to magnetic north. The second type, consisting of speleothems, was collected for U/Pb and U/Th dating, depending on the presumed age of the speleothems. These dating analyses are still ongoing.

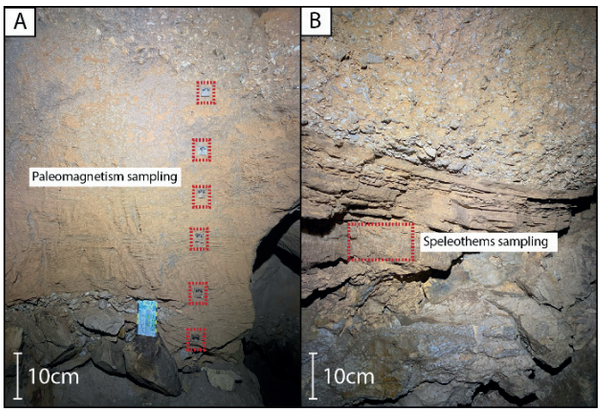

Figure 3: *A) fine sediments oriented and sampled for paleomagnetism and B) sampling of speleothems for U/Pb dating.*

3. Results

At the *Musée aux Varves* site, in the Rama-Aiguille system, the infillings extend over approximately twenty meters of vertical range in fossil galleries. At the base of the sequence, speleothems developed on limestone block form a conglomerate with calcite matrix. These flowstones are interbedded with yellow clays with a thickness of about 1 m. Above this, a thick coarse infilling with lenses of beige and brown clays is present. These fillings are grain-supported at the bottom while the upper part is matrix-supported. Clay layers, interspersed with gravel and sand lenses, overlay the coarse deposits. These clays are then covered by light beige pseudo-varves (Fig. 4), finally indurated and overlain by speleothems (Fig. 5).

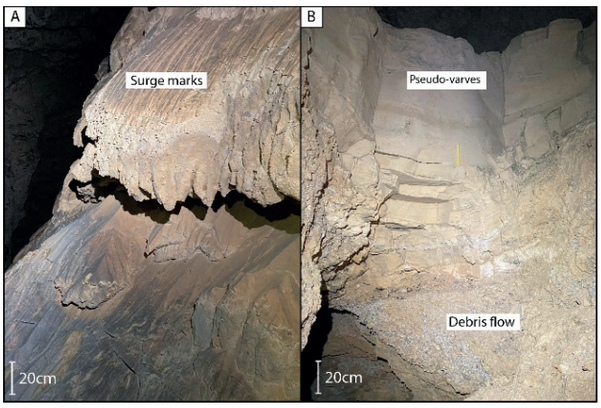

Figure 4: *A) Surge marks and B) pseudo-varves at the Musée aux Varves outcrop in the Rama-Aiguilles system.*

In the *Baume des Toulousains*, the deposits are exposed in the lower part of a gallery littered with wall-collapse blocks. A 1.5 m high section starts at its base with a coarse conglomerate of host rock elements (chert and limestone) approximately 40 cm thick. It is followed by a clay layer with coarser lenses, similar to the basal conglomerate. On top, the sequence is capped by an erosive conglomerate exhibiting positive grading with finer elements near the top, completely blocking the conduit (Fig. 5).

In the *Chourum du Goutourier*, The *GU3* outcrop is located on both sides of a conduit. In the upper part of the conduit (Audra 2000) described completely decarbonated clays, likely deposited during the early stages of conduit activity. These clays are covered by an eroded flowstone overlain by a sequence of angular gravel and blocks bound by a clay matrix. Within this sequence, centimeter-scale clay layers are often present. The gravel formation gradually transitions to clays layers that are separated by a thin layer of centimeter-thick speleothems. A sequence of gravel and blocks covers these clays, filling the conduit on the left side, while on the right side, this layer is overlain by clays that reach the roof of the conduit (Fig 5.). Paleomagnetic measurements on the speleothems at the base of the sequence have shown reversed polarity (Audra 2000). The *GU5* section is far less complete than *GU3* but exhibits similar facies. It features a basal sequence of gravels and blocks in a clay matrix, overlain by clays with gravel lenses, closely resembling the upper sequence of the *GU3* section.

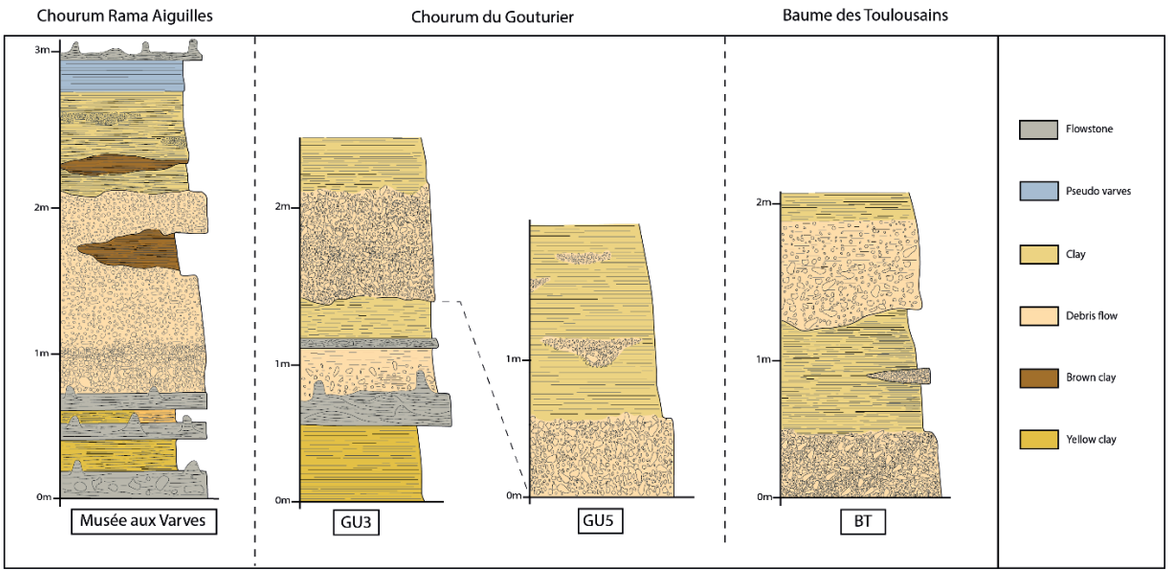

Figure 5: *Sedimentary description of the infillings observed in Rama-Aiguilles, Baume des Toulousains, and Chourum du Goutourier.*

4. Discussion

Four major types of sedimentary deposits have been identified in the studied fillings: 1/ fine laminated sediments such as silty clays (or yellow clays); 2/ coarse gravel and block deposits, poorly sorted, with few apparent sedimentary structures and composed solely of Upper Cretaceous clasts (cherts and limestone); 3/ carbonated pseudo-varves; and 4/ more or less well-preserved speleothems, which encase some of the sedimentary deposits. These four types are common to all the caves presented, although their thickness and stratigraphic position vary locally.

Yellow clays are observed under similar stratigraphic position. In the Goutourier these deposits are at the base of the section and are interpreted as residues of surface cover reworked in old abandoned drains. In the Aiguilles, the same yellow clays also appear at the base of the fillings, intercalated with speleothems. As Audra (2000) suggested, they could likely be much older than the coarse deposits above them, reflecting the earliest phases of conduit activity, with the removal of surface covers in a temperate period (pre-Quaternary or interglacial). A mineralogical analysis of their composition could help specifying their nature and origin.

The coarse deposits seem to be the result of debris flows, deposited as a mass, as suggested by the lack of sedimentary structures and the heterogeneous size of the clasts and the clay matrix. Despite the energy required for their transport, some underlying deposits are preserved, such as the speleothems in the Aiguilles Cave. These coarse sequences are often interlayered with fine, sometimes laminated, deposition sequences. These intercalations may result from temporary flooding occurring when debris flows block the conduits. These clays may then be entirely or partially reworked. The composition of the coarse sequences, dominated by angular limestone clasts, suggests short-distance transport but raises questions about their origin.

The transport of sediments is probably associated with warming events when floods brought large amounts of water into the karst, providing the energy to move these significant quantities of clasts. The transport is likely more effective due to the steep topographic gradient in alpine caves such as that in the Dévoluy.

Pseudo-varves, generally located in the upper part of the sequences, seem to be decoupled from the dynamics responsible for the underlying coarse and clayey deposits. These deposits have a homogeneous and monogenic appearance, forming during repeated flooding periods in the galleries, possibly seasonal. We observed the appearance of typical morphologies of these episodic floods that sculpt these pseudo-varve deposits and forms surge marks (Audra 1997). These floods reflect a hydrodynamic dysfunction of the conduits, likely caused by partial or total clogging of the outlets. If they are indeed glacial varves (i.e. seasonal), the presence of a glacier in the central Dévoluy basin could explain the clogging and a local baselevel rise

Finally, speleothems form under much warmer conditions, corresponding to periods of environmental stability with a temperate climate favorable to their growth. Although they often encase sedimentary sequences, as seen in the Aiguilles Cave, the formation of speleothems may be temporally offset, reflecting changes in environmental conditions.

The relative chronology of the deposits can be established in the studied caves based on their stratigraphic relationships and the initial paleomagnetic dating of some fine sediments and speleothems (Audra 2000; Rispal et al. 2024).

Yellow clays, interpreted as the product of surface cover reworking in temperate periods, are associated with speleothems showing reverse polarity. They predate the filling phases that overlie them. These later fillings correspond to debris flows in which inverse polarities have also been measured in the Aiguilles network (Rispal et al., 2024), and are followed by pseudo-varves showing both normal and reverse polarities.

The reverse polarities indicate a minimum age for the deposits older than 772 ka (Valet et al. 2019)Atlantic and western Pacific oceans. The results combine paleomagnetic, cosmogenic nuclide beryllium (10Be. Associated with glacial and interglacial dynamics, the studied deposits are witnesses to glacial phases much older than those observed on the surface of the massif, corresponding to the 2 last glaciations (i.e. MIS 6 and 2) (Monjuvent 1979). It is difficult to determine whether these fillings are linked to a single episode during a glacial-interglacial period or if they witness the sequence of several periods. The stratigraphy of the deposits, particularly in the *Musée aux Varves* site, reflects the succession of sedimentation and reworking episodes. This demonstrates the occurrence of multiple deposition episodes but does not indicate the temporal range over which they extend. Additional dating of the speleothems surrounding the deposits would help to clarify this time range.

Moreover, the apparent absence of sedimentary archives from more recent glaciations in the karst raises the question of their recording. This

may be due to several reasons. First, the erosion of the catchment basins and the incision of the valleys may have led to disconnection with the caves, and thus the inability to supply sediments. This erosion could also have removed available sediments for transport nearby the cave entrance. Then, we may also consider partial unclogging of the karst after 722 ka, coupled with the lack of favorable conditions for trapping more recent deposits. Finally, the incision of the catchment basins increased the topographic gradient and favored deeper sediment transit. It is possible that the recording of these more recent phases is preserved lower in the caves (in unexplored areas) or even in the current phreatic zone.

5. Conclusion

The results obtained in this study provide a better understanding of the paleo-environmental and morphological evolution of the Dévoluy karst massif through the analysis of sedimentary sequences complemented by paleomagnetic dating. The identified sedimentary deposits testify to an alternation between extreme events responsible for debris flows, periodic floods leading to the sedimentation of pseudo-varves, and periods favorable to the development of calcite speleothems in a more temperate context. These variations reflect a direct response of the karst system to major climatic fluctuations.

Paleomagnetic analyses indicate that some of these infilling date from periods older than 722 ka (i.e., lower Pleistocene). This allows us to show:

- The ability of a high gradient alpine karst to preserve relatively ancient autochthonous deposits.
- The apparent absence of infillings related to recent glaciations and the question of their recording within the karst in the Dévoluy.
- An important part of speleogenesis and karst infillings in the Dévoluy massif at altitude above 1700 m occurred very likely from late Miocene till lower Pleistocene.

However, some questions remain unresolved, notably regarding the precise origin of fine sediments (i.e., surface vs. subsurface) and the nature of the interactions between deposition processes and the paleo--geographical and paleo-environmental context. Ongoing absolute dating of speleothems and a detailed mineralogical analysis of the sediments should further refine the chronology of the karstification stages of the Dévoluy and the associated paleoenvironments.

Acknowledgements

Research is carried out as part of the "*Karstologie hydrogéologie du Dévoluy (KaHyDe)*" project, funded by *Agence de l'Eau* (no. 34752) and *Comité de Spéléologie Région Sud*. Many thanks to Cavers association and friends for helping us accessing and rigging the caves, particularly: Spéléo-club Alpin de Gap (Hautes Alpes) and Escandaou (Bouches-du-Rhône).

References

AUDRA P. (2000) Pliocene and Quaternary Karst Development in the French Prealps—Speleogenesis and Significance of Cave Fills. Evolution of Karst Aquifers, Speleogenesis, National Geological Society, Huntsville, 348–351.

AUDRA P., & ROCHETTE P. (1993) First traces of Lower Pleistocene glaciations in the Alpine Massif: dating by paleomagnetism of deposits in the Vallier Cave, Vercors, Isère, France. Compte rendu de l'Académie des Sciences, Paris 317(II):1403–1409.

AUDRA P. (1997) Les indicateurs morphologiques des mises en charge dans les réseaux karstiques. Actes de la 7e Rencontres d'Octobre, La Sainte Baume.

AUDRA P., BINI A., GABROVŠEK F., HÄUSELMANN P., HOBLÉA F., JEANNIN P. Y., KUNAVER J., MONBARON M., ŠUŠTERŠIČ F., TOGNINI P., TRIMMEL H., & WILDBERGER A. (2007) Cave and Karst Evolution in the Alps and Their Relation to Paleoclimate and Paleotopography. Acta Carsologica 36(1). doi: 10.3986/ac.v36i1.208.

BARAL C., SÉRANNE M., CAMUS H., & JOUVES J. (2023) Impact of alteration corridors on karst reservoir organisation and evolution of groundwater flow path: An example from the southern border of the Larzac Causse, southern France. BSGF - Earth Sciences Bulletin 195. doi: 10.1051/bsgf/2023017.

BAUER J. (1989) L'accident de Frédéric Hammel (Saint Engrâce, Pyrénées Atlantiques). Spélunca XVI(32).

BONHOMME J. L. (1972) Etude hydrogéologique et hydrodynamique du karst des calcaires sénoniens. Massif du Dévoluy, Hautes-Alpes. Conservatoire national des arts et métiers CNAM, France.

DE WAELE J., & GUTIERREZ F. (2022) Karst Hydrogeology, Geomorphology and Caves.

GRANGER D. E., & MUZIKAR P. F. (2001) Dating Sediment Burial with in Situ-Produced Cosmogenic Nuclides: Theory, Techniques, and Limitations. Earth and Planetary Science Letters 188(1–2):269–281. doi: 10.1016/S0012-821X(01)00309-0.

GROSJEAN A. S., PITTET B., GARDIEN V., LELOUP P. H., MAHÉO G., & BARRAZA GARCIA J. (2017) Tectonic Heritage in Drainage Pattern and Dynamics: The Case of the French South Alpine Foreland Basin (ca. 45–20 Ma). Basin Research 29(S1):26–50. doi: 10.1111/bre.12134.

HUET B. (2024) Dynamique des bassins d'avant-pays et collision dans les Alpes de l'Ouest: sources, routage et bilans sédimentaires. Thèse de doctorat, Sorbonne Université.

JAGERCIKOVA M., MOCOCHAIN L., LEBATARD A. E., BOURLES D. L., LEANNI L., SARTÉGOU A., & ZAPPELLI A. (2021) Découverte et étude de remplissages karstiques allochtones d'âge miocène dans l'Obiou (Dévoluy, Alpes françaises) Implications géomorphologiques et paléogéographiques. Karstologia.

JAILLET S., HONIAT C., PONS-BRANCHU E., COUCHOUD I., HOBLÉA F., RACINE T., & SPÖTL C. (2023) Cave Sediments in the Western Bauges Karst: A Record of Middle and Upper Pleistocene Glacial Advances in the French Alps. Geomorphology 433:108707. doi: 10.1016/j.geomorph.2023.108707.

LEMOT F., VALLA P. G., VAN DER BEEK P., JAGERCIKOVA M., NIEDERMANN S., CARCAILLET J., SOBEL E. R., ANDÒ S., GARZANTI E., ROBERT X., BALVAY M., BERNET M., GLODNY J., & MOCOCHAIN L. (2023) Miocene cave sediments record topographic, erosional and drainage development in the Western European Alps. Earth and Planetary Science Letters 621:118344. doi: 10.1016/j.epsl.2023.118344.

LIGNIER V., & DESMET M. (2002) Les archives sédimentaires quaternaires de la grotte sous les Sangles (Bas-Bugey, Jura méridional, France). Indices paléoclimatiques et sismotectoniques. Karstologia 39(1):27–46. doi: 10.3406/karst.2002.2493.

LUPARINI V. (1975) Etude hydrogéologique du massif du Dévoluy, Hautes-Alpes - Alpes françaises. Faculté des Sciences de l'Université de Grenoble, France.

MAI YUNG SEN V., VALLA P. G., VAN DER BEEK P. A., LEMOT F., CROUZET C., & BROCARD G. (2024) Paleo-Valley Infills Record Landscape Response to Late-Quaternary Glacial/Interglacial Climate Oscillations in the French Western Alps. Quaternary Science Reviews 331:108632. doi: 10.1016/j.quascirev.2024.108632.

Maire R., 1980. « Hydrogéologie du plateau de Bure ». Voconcies, 9-16.

MECKEL L. D., FORD M., & BERNOULLI D. (1996) Tectonic and sedimentary evolution of the Dévoluy Basin, a remanent of the Tertiary western Alpine foreland basin, SE France. Géologie de la France 2:3–26.

MICHARD A., DUMONT T., ANDREANI L., & LOGET N. (2010) Cretaceous Folding in the Dévoluy Mountains (Subalpine Chains, France) Gravity--Driven Detachment at the European Paleomargin versus Compressional Event. Bulletin de la Société Géologique de France 181(6):565–581.

MONJUVENT G., (1979) Le Drac, morphologie, stratigraphie et chronologie quaternaires d'un bassin alpin. Université Paris-Diderot - Paris VII.

PERROUX A.S., (2005) Les remplissages détritiques endokarstiques. Contribution méthodologique à la lecture des mémoires paléogéographiques et environnementales. Application aux systèmes karstiques de Choranche (Vercors) et d'Orgnac (Bas-Vivarais). Université de Savoie.

QUINIF Y., MAIRE R., (1998) Pleistocene Deposits in Pierre Saint-Martin Cave, French Pyrenees ». Quaternary Research 49(1):37-50. doi: 10.1006/qres.1997.1939.

RISPAL N., AUDRA P., MOCOCHAIN L., HENRY P., DEMORY F., ZAPPELLI A. (2024) Element of a pluri-disciplinary project on karstic reservoir characterization: first results of cave sediments paleomagnetic dating in Dévoluy Massif. » 31th International Karst School, June 2024, Postojna, Slovenia.

SBAI A., EK C., DROUIN P., BERNARD CHIROL B., ARIAGNO J.C, ARTHUR PELISSON A., QUINIF Y., (1995) Les remplissages karstiques de la grotte Sous-les-Sangles: Sédimentologie et évolution spéléomorphologique d'une grotte du Jura méridional (France). Quaternaire 6(1):35-45. doi: 10.3406/quate.1995.2035.

VALET J.P., BASSINOT F., SIMON Q., SAVRANSKAAIA T., THOUVENY N ., BOURLÉS D.,VILLEDIEU A. (2019) Constraining the age of the last geomagnetic reversal from geochemical and magnetic analyses of Atlantic, Indian, and Pacific Ocean sediments. Earth and Planetary Science Letters 506:323–31. doi: 10.1016/j.epsl.2018.11.012.

VANARA N. (1997) Datation d'un phénomène catastrophique dans la grotte-tunnel d'Azaleguy. Speleochrono 8:13–18.

ZAPPELLI A., BELLEVILLE A., & JAGERCIKOVA M. (2018) Hydrogeology of Dévoluy Karstic System: New Insights with Dye Tracing and Rainfall-Discharge Model. Eurokarst 2018, Besançon.

ZUPAN-HAJNA N., MIHEVC A., PRUNER P., & BOSÀK P. (2010) Palaeomagnetic Research on Karst Sediments in Slovenia. International Journal of Speleology 39(2):47–60. doi: 10.5038/1827-806X.39.2.1.

Preliminary Investigation on Stream Flow Variations in the Black River Complex, Roppel Section of the Mammoth Cave System

Ljubomir Veljan Risteski (1), Dr. Patricia Kambesis (1), & James Borden (2)

(1) Department of Earth Environmental and Atmospheric Sciences, Western Kentucky University, Bowling Green, Kentucky, United States of America
(2) Central Kentucky Karst Conservancy, Cave City, Kentucky, United States of America

Abstract

Scallops are asymmetrical, scoop-like indentations with a steep slope on the upstream side and a gentler slope on the downstream side, bound by crests that are also angled in the downstream direction. These features were not only directional indicators but could be used to calculate flow velocity and discharge (CURL, 1974). Scallops were measured throughout the Black Canyon passage and surrounding area named the Black River Complex in the Roppel section of the Mammoth Cave System. Exhibited here are multiple flow regime velocities and are in proximity of a boundary between two drainage basin boundaries: Pike Spring to the northwest and Turnhole Spring to the southwest. This boundary is known to have an overflow from Pike to Turnhole during high water events. Measurements were taken of primary (paleo) and secondary (modern flooding) scallops and input into the program ScallopEx (WOODWARD & SASOWSKY, 2009) with the following parameters: scallop length, temperature, and average passage width. Velocity data coupled with discharge estimates of the passages in relation to one another suggest that a preliminary conclusion of this study is that this area is indicative of a shift from southward drainage towards Turnhole Bend Spring.

1. Introduction

It has been well known for many decades of speleological study that scallops are directional features developed along passages in solutional and glacial caves (PALMER, 2007). Since CURL (1974), scallops have been measured and utilized to gain understanding of a cave's modern and paleo hydrology regarding the deduced velocity and discharge of the flow. The study area, the Black River Complex, in the Daleo section of Roppel Cave within the Mammoth Cave System is no exception. The scallops in this area are well developed and show direction of flow at varying velocities in this area which encompasses the major passages of the Black Canyon and Black River, as well as lesser tributary and distributary passages such as the Easy Way and Avenger Trial.

The area that the Mammoth Cave system lays beneath is geographically known as the Mammoth Cave Plateau. The sinkhole plain and the plateau are divided by the Dripping Springs Escarpment. Here, elevation rises gradually about 100 meters from base to the top of the plateau. As the escarpment eroded towards the northwest through time, it exposed more of the underlying carbonate units, increasing the recharge area and drainage patterns for the basins.

Once water has drained underground, it follows the gentle dip of the rocks towards the Green River, enlarging bedding planes and vertical joints into navigable passages (PALMER, 2017, PALMER 1981).

Roppel Cave is the upstream section of the greater Mammoth Cave System and therefore is hydrologically linked to it. This section is characterized by many maze-like, tall canyons. It shares, in part, the enormous drainage basin of the Turnhole Spring which has an area of 245km2. This basin comprises 75% of the overall drainage for Mammoth Cave which, in total, is 317km^2 (GLENNON & GROVES, 2002). The Roppel System does not solely drain to Turnhole, however, but also to Pike Spring, approximately 18 kilometers upstream along the Green River from Turnhole Spring. The modern drainage in the Black River Complex under normal flow conditions discharges out of Pike Spring. Flow while under flood conditions will also spill over from the Turnhole Bend Basin to flow to Pike Spring

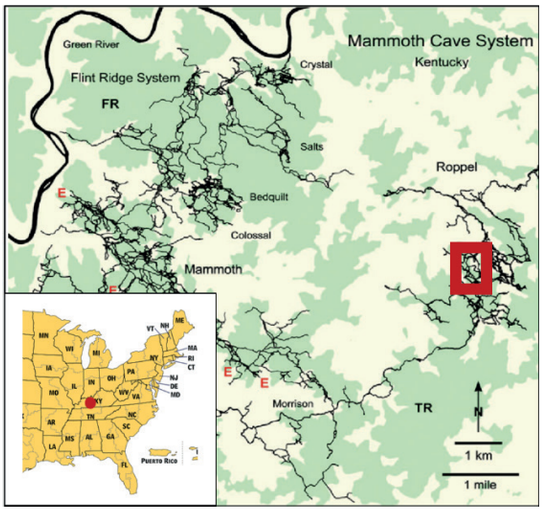

Figure 1: *Location of the Mammoth Cave System in Kentucky and approximate location of the Black River Complex in red box (Modified from PALMER, 2017).*

Mammoth Cave owes its length to the thickness of the karst-forming units it is set in and the presence of an erosively resistant caprock. The units the system is developed within are, from youngest to oldest, the Girkin, Ste. Genevieve, and St. Louis Formations of Late (Serpuhkovian) and Middle (Viséan) Mississippian age, respectively. These three formations are about 110 meters thick in total. Overlying these units,

also of Middle Mississippian in age (though not conformable) is the Big Clifty Sandstone member of the Golconda Formation, which serves as the protective caprock over the system. An analysis of the stratigraphy indicates that the study area shows ranges from the basal Fredonia Member to the middle Joppa Member within the Ste. Genevieve Formation.

In the Daleo Entrance of Roppel, after the entrance series of crawls and ladders, the first major passage encountered is called Kangaroo Trail. The uppermost portion of the passage was formed under phreatic conditions by the proto-Black Canyon stream and is a good example of an elliptical tube. This passage trends westward before it grades into another tube. Later, it experienced a period of downcutting to create a winding canyon that explorers must hop over (hence the name, Kangaroo) with the canyon sharing the name. Kangaroo Canyon eventually turns to the south, now known as Black Canyon. Both the Kangaroo and Black Canyons were points of river piracy from Kangaroo Trail. The beginning of the Black Canyon turns off from Kangaroo Trail. From the points of piracy, Kangaroo Trail diminishes significantly in height due to river piracy while trending westerly before it grades into another, much larger, tube named the North Crouchway. This passage trends to the northwest, possibly toward Pike Spring. The modern drainage in parts of the Black River Complex (which encompasses Black River, Black Canyon, Easy Way) is now to the north as downcutting occurred throughout the levels of the Complex.

The hydrology in this area is as the name suggests: complex. Nevertheless, it is an ideal resource for study as the passages are relatively dry and easily accessible, while also generally set in carbonate lithologies where the scallops are well developed thus making them easy to analyze.

This work is a part of a project of greater scope that will further the understanding of the paleo hydrology and delineate the ancient boundary between the Turnhole and Pike Spring Basins. By calculating the velocity of the water that developed the scallops, understanding discharge, coupled with the overall trend of the passage, we can ascertain the transition over time of the basin boundaries from Turnhole to Pike Spring. The purpose of the research presented here is to begin the analysis of the Complex to understand the paleo-flow velocities and the implications for our understanding of the migration of drainage basin boundaries though time.

2. Scallop Characterization and Methodology

Data collection utilized two methods: a physical measurement in-cave that employed the use of a measuring tool held up to the scallop and the longest point was measured from crest to crest along the longitudinal axis, and the use of photography with a scale from which scallops could be measured later (Fig. 2).

Figure 2: *Left shows a physical measurement with a scale. Right shows a measurement taken of a scallop remotely. Note "1=1.00" for defining scale. Source: author.*

General cave survey techniques were then employed to connect locations of measurements and survey notes to an existing survey station. Passage width was also measured, and to-scale cross sections drawn, along with a detailed stratigraphic section.

Once this was complete, data were input into the ScallopEx program. This program, developed in 2009 by Emily Woodward and Ira D. Sasowsky, utilizes equations from CURL (1974) and WHITE (1988) to deduce paleo-velocities in a passage. Discharge was calculated separately.

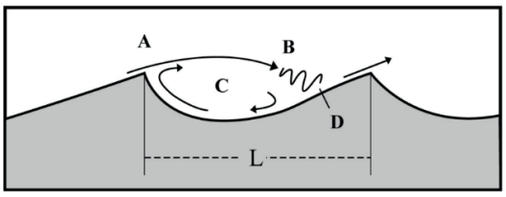

Figure 3: *Scallop morphology (SPRINGER & HALL, 2022, modified from CURL, 1974)*

Scallops exhibit an asymmetrical geometry that is angled in the downstream direction, bounded by crests. CURL (1974) modeled flow along a scallop shown in Fig. 3. Here, *L* is the distance between the two crests of a scallop along its longitudinal axis. A sublaminar jet detaches from the wall at point *A*, continues until it becomes unstable at point *B*, then reattaches to the wall at *D*. Some fluid then starts to vortex within the basin of the scallop (point *C*), and some continue onward, repeating the process (CURL 1974).

Shown below is the equation that solves for velocity (*v*).

$$\frac{(v \times L_{32})\rho}{\eta} = N_R$$

Where ν is the velocity fluid passing by a scallop, L_{32} is the mean scallop length calculated by the Sauter mean (shown below), ρ is the density of water, and η is the viscosity. To be able to obtain the velocity, the Reynolds number (N_R) and the Sauter mean must first be found.

The Sauter mean (or Sauter mean diameter) is utilized for a collection of spherical shaped objects of differing diameters but is equated to spheres of equal diameter (KOWALCZUK & DRYZMALA, 2015). This is further recommended (SPRINGER & HALL, 2020) for use in scallop analyses as opposed to an arithmetic mean for consistency with the original formulations and that the arithmetic mean can cause overestimated results. The Sauter mean is calculated in the equation below.

$$L_{32} = \frac{\sum l_j^{\,3}}{\sum l_j^{\,2}}$$

l_j is the longitudinal length of an individual scallop parallel to its flow.

Once this is calculated, we can employ the following equation calculates the Reynolds number for a rectangular conduit.

$$N_R = N_R^* \left[2.5 \left(\frac{\ln(D)}{2L_{32}} - {}^3\!/_2\right) + B_L\right]$$

Here, $N_R{}^*$ is a known constant of 2,200 that indicates friction of roughness against a wall and is unitless. B_L , a function of roughness that is dependent on geometry, is determined to be 9.4, also unitless. *D* is the width of the passage which, in the case of the Easy Way, averages 50 cm. The density and viscosity of water are calculated given the assumed temperature has remained constant. Analyses were run at 10˚C, 13 C, and 15˚C to consider an appropriately wide range of values through a paleoclimate perspective; modern water temperatures are around 13. These analysis over the three temperatures exhibited a small, but notable, change in the velocity which decreased as temperature increased.

Work done by Springer and Hall (2020) showed that a small sample size of scallops resulted in "widely varying means, with precision slowly increasing with sample size." They recommend a minimum of 20 to 30 measurements be taken for a sufficient sample size. This was achieved at every site which is shown in the map below.

3. Results

This project at the time of writing is still in the preliminary stage of investigation with more data and analyses to be collected and run in the future. The first portion of this project occurred in July and August of 2024 and focused solely on scallop analysis in the Easy Way passage. These data measurements occurred in-cave and were later analyzed. Several trips were then run in the winter of 2024 and 2025 to collect data from the greater Black River Complex Passages. During these trips, data collection became more efficient with the use of a scale and photography to collect data. There are many software programs that can measure with the use of a defined scale in the photo that are available for download or online. We utilized eleif.net/photomeasure as this proved to be the most efficient and user-friendly. To ensure accuracy, some reference measurements were taken in the field with a scale and matched with the software's measurement to within 0.01). Once the scallops were measured, the Excel program named ScallopEx (WOODWARD & SASOWSKY, 2009) was utilized, and the results were tabulated and shown in the table below including an estimated discharge which is given by the equation:

$$Q = A \cdot v$$

Where Q is discharge, v is the calculated velocity, and A is the cross-sectional area of the passage.

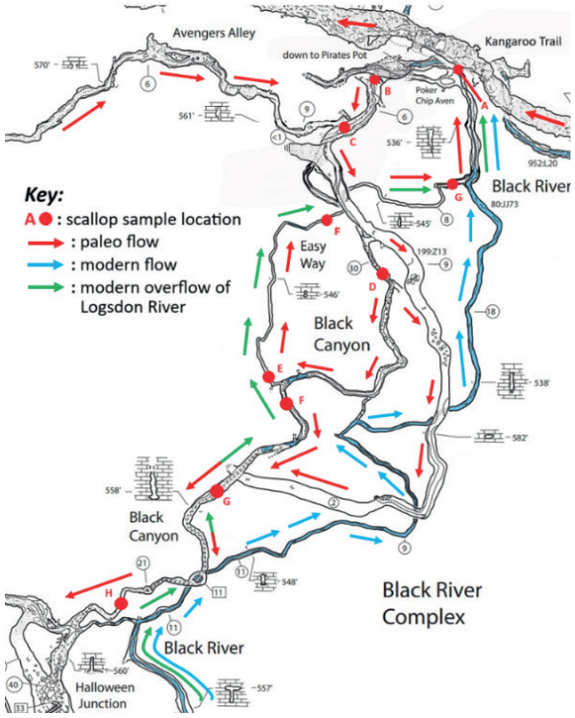

Figure 4: Map of study area, courtesy of BORDEN and CKKC. Cartography: Ed KLAUSNER, Cave Research Foundation; modified by Author.

Scallop Location (Letter designation on map)	***Velocity (cm/s)***	***Area (m^2)***	***Discharge Q (m^3/s)***
Black River at Poker Chip Aven Secondary Scallops **(A)**	248.21 cm/s	6.58 m^2	16.32 m^3/s
Black River at Poker Chip Aven Primary Scallops **(A)**	78.50 cm/s	6.58 m^2	5.17 m^3/s
Black Canyon Piracy to Pirate's Pot **(B)**	24.79 cm/s	0.75 m^2	0.19 m^3/s
Avenger Trail Confluence **(C)**	113.81 cm/s	3.18 m^2	3.62 m^3/s
Black Canyon before Easy Way **(D)**	50.32 cm/s	8.63 m^2	4.34 m^3/s
Easy Way Secondary Scallops **(E, F, G)**	240.0 cm/s	0.75 m^2	1.80 m^3/s
Easy Way Primary Scallops **(E, F, G)**	70.90 cm/s	0.75 m^2	0.53 m^3/s
Black Canyon before Halloween Junction **(H, I, J)**	31.78 cm/s	6.40 m^2	2.03 m^3/s

***Table 1:** velocities from scallop calculations, passage area, and estimated discharge by locations.*

Scallop Location	Min/Max (cm)	Range	Mean	Median	Mode	Standard Deviation (σ)	Variance (σ^2)
Black River at Poker Chip Aven Secondary Scallops	1.05/1.99	0.94	1.60	1.59	1.53	0.25	0.07
Black River at Poker Chip Aven Primary Scallops	3.21/5.79	2.58	4.33	4.27	4.26	0.53	0.28
Black Canyon Piracy to Pirate's Pot	6.50/12.31	5.39	9.06	8.80	No mode	1.60	2.55
Avenger Trail Confluence	1.92/3.79	1.87	2.97	2.96	3.01	0.43	0.19
Black Canyon before Easy Way	4.46/6.38	1.92	5.37	5.12	No mode	0.69	0.47
Easy Way Secondary Scallops	0.50/2.30	1.80	1.37	1.25	1.10	0.44	0.19
Easy Way Primary Scallops	3.03/5.81	2.78	3.98	3.86	No mode	0.78	0.60
Black Canyon before Halloween Junction	5.83/10.91	5.17	7.83	7.44	No mode	1.30	2.56

Table 2: *Descriptive statistical analyses on the scallop data collected.*

Given in the tables above are the calculated average velocities at various points throughout the Black River Complex and a table of descriptive statistical values of the scallop measurement data that was collected (Table 2).

The main objective of the discharge calculations is to understand the relative differences in flow regimes between the passages. This, coupled with velocity and scallop orientation descriptions, will lead to conclusions that can be drawn about basin boundary migration. These data along with the descriptive statistics show, as expected, that the higher velocities and discharge values are reflected in smaller scallop sizes, and the longer scallops are indicative of comparatively lower velocities and discharge values. Smaller standard deviations and variances at various points of scallop measurement can be inferred as uniform flow in various areas of piracy and stream confluences. Other locations, such as in the Black Canyon before Easy Way and continuing downstream, show a higher range, standard deviation and variance. Probable reasons for this are in the following discussion section.

4. Discussion

The hydrologic complexity of this area, moreover of the entire Roppel Cave section, cannot be overstated. These maze-like canyons have many points of piracy during the relatively rapid downcutting from which these passages formed. The presence of some gravel bars and sediment chokes in some of the passages can be inferred as interglacial periods of downcutting, given the geologic history of the area (GRANGER ET AL, 2018, GRANGER ET AL, 2001).

The Black Canyon passage proper exhibits several episodes of differing flow velocities over its approximately 9.1m (30ft) height. In other areas, particularly the middle to upper sections of the Black Canyon Passage, well-developed, gradational scallops are exhibited that show an increase of velocity downward along with a narrowing of passage height. In various places along the vertical extent differing velocities of scallops can be observed, which can be attributed to primary passage formation that caused scallops to become gradually smaller with a thinning passage width as downcutting approached a perching layer of thinner bedded, often argillaceous (or shaley), limestone. The scallops in the passage point southward with little exception.

The Black Canyon formed originally as a piracy from Kangaroo Trail and continued southward to meet the Logsdon River to the south. This river is a major drainage for Turnhole Spring (GLENNON & GROVES, 2002)

At both the upstream and downstream ends of the Easy Way, though not present within the passage itself, there is a major perching layer named the Spar Mountain Member. This member unit is generally comprised of an inter-clastic, argillaceous limestone that is abundant in rip-up clasts. The upstream end exhibits a drop in elevation to the level of the Easy Way, an obvious example of stream piracy, supported by scallop orientation.

The primary focus of this study is the Black River Complex between the Black River just north of Poker Chip Aven, Pirates Pot, and Halloween Junction. Between these two points, the Black Canyon has numerous piracies that drain to or near the Black River, most prominently the Easy Way. The Black River stream, as previously mentioned, drains to Pike Spring situated to the northwest. However, the trend of which it increases in height and which the primary scallops are oriented toward the south. Furthermore, its higher levels can be traced far to the south to the end of the Turnhole Groundwater Basin. Lower levels below Black Canyon (Western Kentucky Parkway, Goblin Trail) can be traced to have drained into Logsdon River, as previously mentioned. These primary scallops also increase in velocity going upstream. This is the direction towards the upstream section of the Logsdon River which is a major drainage to Turnhole Spring. The modern-day boundary between these two drainages runs approximately WNW/ESE far to the south of this area. However, in the vicinity of Halloween Junction there is evidence noted for an older basin boundary that is defined by multiple scallop directions. This area intersects with Goblin Trail and follows to Western Kentucky Parkway (not indicated on Fig. 4, but are present below Halloween Junction), also believed to have drained in the past to Logsdon, but it is now a primary overflow route from there during flood events. The scallops there are oriented to the north and are considered secondary.

A stretch of the Black Canyon is also utilized as an overflow route between the Easy Way and Halloween Junction (Fig. 4). Here, secondary, high velocity scallops present on the floor are oriented north toward he Easy Way while primary scallops on the walls are oriented southward toward Halloween Junction and Logsdon River. The floor scallops are from modern flooding events where water wells up from Logsdon, follows the continuation of Black Canyon (named Lower Arlie Way), through various canyons and to a tube that is perched near (though not at) base level named Western Kentucky Parkway. This tube partially hosts the Black River in an entrenched canyon and, during high flow events, will

upwell through former piracy points of the Black Canyon, rejoining via the downstream end of the Easy Way.

The trend, scallop direction, and extent of the Black Canyon have been traced as a drainage to Logsdon River before the piracy began in the Easy Way from the Black Canyon. Between Halloween Junction and the Easy Way are two points of piracy that drain to the Black River. Nevertheless, the most significant point of stream piracy is the Easy Way passage. The upstream end exhibits a large opening to the Black Canyon where water likely sumped during high water events. Furthermore, downstream in the Easy Way is another point where one can look up 9.1 m (30ft) into the Black Canyon and is another likely point of piracy. Upstream in the Black Canyon, a tributary stream named Avenger's Alley drains the North Crouchway (to the west of Fig. 4) which is the downstream continuation of Kangaroo Trail. These passages drained to a large dome named Pirate's Pot, named for the numerous piracies that drain here, and subsequently to the Black River.

Descriptions of the Black Canyon's passage extent to the vicinity of upstream Logsdon in addition to scallop trends are the basis to be able to draw conclusions for a migrating basin; however, a comparison between the relative discharges of the various passages, confluences, and piracy exhibits supporting evidence for a major shift toward the Black River northward. Furthermore, this area is a very dynamic regarding flow direction and velocity. High ranges in scallop measurement along the primary set in the Black Canyon were to be expected and this is displayed in Table 2.

Subsequent trips with more data collection in the Complex will likely provide more supporting evidence to this preliminary conclusion. In addition, while some of the scallops were unambiguous to measure, others were obscure in their appearance, tapering off with little to no discernable leeside crest. This made distinguishing primary and secondary scallops difficult at times. Some were vertically elongated and had differing horizontal measurements, which also made it difficult to discern where to collect measurements. Higher velocities in Tables 1 and 2 are indicative of secondary scallops, while slower velocities in areas that are known not be a part of Logsdon overflow routes. Further work in this area will target primary scallop measurement in the lower areas of the Black River such as Western Kentucky Parkway (if present), upper levels of the Black Canyon, and the area south of Halloween Junction. Finally, discharge measurements assume "pipe-full" conduits.

5. Conclusion

The Black River Complex is an area of many intertwined, maze-like passages. However, given the evidence presented in this study, a preliminary conclusion can be drawn that suggests a basin boundary migration to the southwest towards Turnhole Spring occurred in the past and may still be migrating. This area exhibits many areas of river piracy in the modern day and the past. Given the hydraulic dynamics of basin boundaries in this area, we can infer that the Pike Spring Basin was, and may still be, pirating this area away from the Logsdon/Turnhole drainage towards Pike Spring. Nevertheless, this study serves as a preliminary investigation into the hydrology of the Black River Complex. And will serve as the first step of a project much larger in scope.

Acknowledgments

I would like to give enormous thanks to my coauthors Dr. Patricia Kambesis and James (Jim) Borden for their continued support and guidance throughout this project. A big thanks to Dr. Christopher Groves and Lee Anne Bledsoe for allowing me to perform this project in conjunction with the Western Kentucky University's Karst Field Studies Program. Of course, none of this would not have been possible without the help of my guides: Kevin Downs and Dick Market. Finally, this study would have had no traction if it were not for our hearty and illustrious field team staying with us through adventures and misadventures; Warren Briggs, Gabe Montemayor, Mills Orlovsky, Monica Galvez, Ryan Palmer, Jay Mrazek, Hayden Harper, Jennifer Macking, Jon Grasovsky, and Nathan Brucker.

References

BLUMBERG, P; CURL, R. L. (1974). Experimental and Theoretical Studies of Dissolution Roughnesses, Journal of Fluid Mechanics 65(04), DOI: 10.1017/S0022112074001625

CURL, R.L. (1974). Deducing Flow Velocity in Cave Conduits from Scallops. National Speleological Society Bulletin. 22-36

GLENNON, A., & GROVES, C. (2002). An examination of perennial stream drainage patterns within the Mammoth Cave watershed. Journal of Cave and Karst Studies, 64, 82–91.

GRANGER D.E., FABEL, D., and PALMER, A.N., (2001). Pliocene-Pleistocene incision of the Green River, Kentucky, determined from radioactive decay of cosmogenic 26Al and 10Be in Mammoth Cave sediments. Geological Society of America Bulletin 113, no. 7, p. 825–836

GRANGER, D.E., ODOM, W.E., and FABEL, D., (2018). A re-evaluation of the timing of Mammoth Cave development and formation of the Ohio River (abstract): Geological Society of America annual meeting, Indianapolis, IN: program and abstracts, paper 51-3.

KOWALCZUK, P. & DRYZMALA, J. (2015). Physical Meaning of the Sauter Mean Diameter of Spherical Particulate Matter. Particulate Science and Technology. 34. 645-647. 10.1080/02726351.2015.1099582.

PALMER, A. N. (2007). Cave Geology. Dayton, Ohio: Cave Books

PALMER, A. N. (1981). A Geological Guide to Mammoth Cave National Park. Teaneck, New Jersey: Zephyrus Press.

SPRINGER, G.S., HALL, A. (2020). Uncertainties associated with the use of erosional cave scallop lengths to calculate stream discharges. International Journal of Speleology, 49 (1),27-34. Tampa, FL (USA) ISSN 0392-6672 https://doi.org/10.5038/1827-806X.49.1.2292

WHITE, W. B. (1988). Geomorphology and Hydrology of Karst Terrains. New York, New York: Oxford University Press.

WOODWARD, E.; SASOWSKY, I.D. (2009). A spreadsheet program (ScalloPEx) to calculate paleovelocities from cave wall scallops. ActaCarsologica, 38, 303–305.

Distribuição de *Lionycteris spurrelli* Thomas, 1913: Caminhos para modelagem e Conservação da espécie

Marco Túlio Magalhães Souza (1), Juliana Magno Nascimento (2)

(1) Departamento de Ciências Biológicas, Pontifícia Universidade Católica de Minas Gerais – PUC Minas, Belo Horizonte, MG, Brasil, mt.ms86@gmail.com (autor correspondente)

(2) Instituto de Geociências, Universidade Federal de Minas Gerais, Belo Horizonte, MG, Brasil, juliananmagno@gmail.com

Resumo

O estudo busca ampliar o conhecimento sobre a distribuição de *Lionycteris spurrelli* no Brasil, por meio da compilação de dados secundários de ocorrências geográficas e da análise de táxons depositados em coleções científicas. A primeira etapa envolveu uma revisão bibliográfica, com ênfase na verificação da confiabilidade dos registros e análise de fontes como o *GBIF*, *SpeciesLink* e *IUCN*, além de um levantamento de coleções biológicas relevantes. Os resultados indicam um aumento significativo nos registros da espécie, com destaque para Minas Gerais, que se tornou o estado com o maior número de registros no Sudeste, totalizando sete municípios, e o terceiro no Brasil. A expansão dos registros sugere tanto uma ampliação real da área de ocorrência quanto uma melhoria nas metodologias de coleta e verificação. A espécie, de pequeno porte e aparência discreta, apresenta características morfológicas semelhantes a outras do gênero, o que torna a identificação em campo mais desafiadora. Por isso, a análise morfométrica é crucial para confirmação da presença. Com base na expansão geográfica observada, a futura modelagem ecológica será essencial para compreender os fatores ambientais que influenciam a distribuição de *L. spurrelli* e prever mudanças em sua área de ocorrência, além de orientar estratégias de conservação.

Abstract

The study aims to expand knowledge about the distribution of *Lionycteris spurrelli* in Brazil by compiling secondary data on geographic occurrences and analyzing specimens deposited in scientific collections. The first stage involved a literature review, emphasizing the verification of record reliability and the analysis of sources such as *GBIF*, *SpeciesLink*, and *IUCN*, in addition to a survey of relevant biological collections. The results indicate a significant increase in species records, particularly in Minas Gerais, which became the state with the highest number of records in the Southeast, totaling seven municipalities, and the third in Brazil. The expansion of records suggests both a real increase in the occurrence area and improvements in collection and verification methodologies. The species, small in size and discreet in appearance, has morphological characteristics similar to others in the genus, making field identification more challenging. Therefore, morphometric analysis is crucial for confirming its presence. Based on the observed geographic expansion, future ecological modeling will be essential to understand the environmental factors influencing the distribution of *L. spurrelli*, predict changes in its occurrence area, and guide conservation strategies.

Resumen

El estudio busca ampliar el conocimiento sobre la distribución de *Lionycteris spurrelli* en Brasil mediante la recopilación de datos secundarios de ocurrencias geográficas y el análisis de taxones depositados en colecciones científicas. La primera etapa involucró una revisión bibliográfica, con énfasis en la verificación de la confiabilidad de los registros y el análisis de fuentes como *GBIF*, *SpeciesLink* e *IUCN*, además de un levantamiento de colecciones biológicas relevantes. Los resultados indican un aumento significativo en los registros de la especie, destacándose Minas Gerais, que se convirtió en el estado con el mayor número de registros en la región Sudeste, totalizando siete municipios, y el tercero en Brasil. La expansión de los registros sugiere tanto una ampliación real del área de ocurrencia como una mejora en las metodologías de recolección y verificación. La especie, de pequeño tamaño y apariencia discreta, presenta características morfológicas similares a otras del género, lo que dificulta su identificación en campo. Por ello, el análisis morfométrico es crucial para confirmar su presencia. Con base en la expansión geográfica observada, la futura modelización ecológica será esencial para comprender los factores ambientales que influyen en la distribución de *L. spurrelli*, prever cambios en su área de ocurrencia y orientar estrategias de conservación.

1. Introdução

A distribuição geográfica das espécies é determinada por uma interação complexa de fatores históricos, ecológicos e evolutivos, incluindo características climáticas, interações bióticas e barreiras geográficas (SOBERÓN & PETERSON, 2005). Entre esses fatores, o clima desempenha um papel central na regulação dos padrões de distribuição, promovendo movimentos de expansão e contração populacional ao longo do tempo (IVERSON & PRASAD, 1998; ARAÚJO et al., 2013). Mudanças climáticas globais têm provocado alterações significativas nas áreas de ocorrência das espécies, muitas vezes resultando em extinções locais e perda de biodiversidade (WALTHER et al., 2002; ANCIÃES & PETERSON, 2006; STEPHENS et al., 2016).

O gênero *Lionycteris*, representado pela espécie *Lionycteris spurrelli* Thomas, 1913, é caracterizado por seu hábito alimentar predominantemente nectarívoro e pelo uso de cavidades naturais como abrigo (GUIMARÃES & FERREIRA, 2014). Embora seja mais comum em florestas tropicais úmidas, a espécie também ocorre em biomas mais secos, como a Caatinga (PAES et al., 2022). Apesar de estar classificada como "Pouco Preocupante (LC)" globalmente (IUCN, 2025), encontra-se "Em Perigo (EN)" na lista de espécies ameaçadas de Minas Gerais (COPAM, 2010).

As coleções biológicas desempenham um papel essencial na ampliação do conhecimento sobre a distribuição das espécies, fornecendo registros históricos e atualizados que possibilitam a identificação de padrões espaciais e temporais. Além de preservarem espécimes para estudos morfológicos e genéticos, essas coleções reúnem dados de ocorrência que, muitas vezes, representam os únicos registros confiáveis de espécies em determinadas localidades. A incorporação dessas informações em estudos de distribuição geográfica permite uma avaliação mais precisa da extensão da ocorrência de *L. spurrelli*, além de possibilitar a identificação de áreas subamostradas e potenciais lacunas na distribuição conhecida da espécie.

Contudo, os dados sobre a distribuição e ecologia de *L. spurrelli* ainda são escassos. Neste estudo, buscamos compreender o padrão de distribuição potencial da espécie por meio de dados secundários. Para isso, compilamos dados de ocorrência provenientes de coleções biológicas e literatura científica, os quais serão aliados a camadas ambientais climáticas e topográficas. Até o momento, geramos o mapa com os registros totais de ocorrência, enquanto, no futuro, pretendemos realizar a modelagem da distribuição atual e futura da espécie, considerando projeções climáticas para 2075. Além disso, planejamos avaliar sua representatividade em Unidades de Conservação. Nossos resultados, embora preliminares, têm o potencial de subsidiar estratégias conservacionistas, especialmente diante da intensificação das mudanças climáticas, e ressaltam a importância da documentação e ampliação dos registros de ocorrência para a compreensão e preservação da biodiversidade.

2. Materiais e Métodos

O estudo foi dividido em frentes de atuação para viabilizar as análises subsequentes. A primeira etapa consistiu em uma revisão bibliográfica para compilar uma lista de ocorrências da espécie *Lionycteris spurrelli*. O objetivo dessa revisão foi identificar registros confiáveis de distribuição geográfica e características ecológicas associadas à espécie, considerando fontes como bancos de dados online, artigos científicos e relatórios técnicos. As principais bases de dados consultadas incluíram o GBIF (Global Biodiversity Information Facility), SpeciesLink e IUCN. A curadoria dos dados priorizou a verificação da confiabilidade dos registros, levando em conta a precisão das coordenadas geográficas, o ano de coleta e a correta identificação taxonômica dos espécimes. Além disso, foi realizado um levantamento das coleções biológicas que poderiam fornecer informações relevantes sobre a morfologia e o tombamento de *L. spurrelli*. Esse levantamento visou complementar o conhecimento existente e aumentar a representatividade da distribuição da espécie nas diferentes regiões. Na etapa específica de tratamento dos dados geoespaciais, os registros de ocorrência foram submetidos a um processo de normalização e limpeza para garantir sua qualidade e consistência. Os pontos de ocorrência obtidos foram analisados criticamente, sendo removidos registros duplicados e eliminada a autocorrelação espacial entre os pontos, a fim de garantir a independência dos dados. Em seguida, os dados georreferenciados foram plotados sobre a extensão geográfica da América do Sul, utilizando o *software ArcGIS 10.7.1*. As análises foram realizadas em escala regional (Minas Gerais) e escala nacional (Brasil), proporcionando uma visão abrangente da distribuição geográfica da espécie.

3. Resultados

A análise dos dados provenientes de espécimes depositados no Museu Paraense Emílio Goeldi (Belém), Museu de Zoologia João Moojen da Universidade Federal de Viçosa (UFV), Coleção Mastozoológica da Universidade Federal de Minas Gerais (UFMG) e Coleção de Mamíferos da Universidade Federal de Lavras (UFLA) resultou em um aumento significativo nos registros da espécie *Lionycteris spurrelli*.

Ao integrar as informações da lista apresentada por LOPES et al. (2021) e PAES et al. (2022) com os dados obtidos nesta pesquisa, detectamos uma expansão de registros para oito novos municípios, totalizando 43 municípios brasileiros, com capturas em 48 localidades distintas (Figura 1).

Especificamente para o estado de Minas Gerais, anteriormente havia apenas um registro na Caverna Olhos D'água, em Itacarambi (LIRA et al., 2009). Em 2022, Paes e colaboradores ampliaram esse número, adicionando cinco novos municípios. Com base na presente compilação, identificamos registros da espécie em sete municípios mineiros, posicionando Minas Gerais como o estado com o maior número de registros no Sudeste e o terceiro maior em âmbito nacional.

A ampliação dos registros de *Lionycteris spurrelli* traz importantes avanços para o entendimento de sua distribuição. Os dados demonstram a presença da espécie em todos os principais biomas brasileiros, com a Região Sul sendo a única sem registros até o momento. Além dos fatores climáticos e da diversidade de vegetação, a presença de cavidades naturais subterrâneas parece ser um componente relevante para a ocorrência da espécie (PAES et al., 2022). No entanto, uma avaliação geograficamente mais ampla é necessária para compreender melhor sua distribuição e ecologia.

Nº de Tombamento	Cidade/Estado	Local	SIRGAS 2000		Referência
			Latitude	Longitude	
-	Igarapé Novo/AP	-	-0.333.333	-52.383.333	Taddei et al. 1978
-	Pracuúba/AP	Floresta Nacional do Amapá	-1.666.666	-51.166.666	Martins et al. 2006
-	Serra do Navio/AP	Parque Nacional Montanhas do Tumucumaque	1.600.000	-52.483.333	Martins et al. 2006
MAM 3379.0	Barcelos/AM	-	1.195.833	-64.809.444	Coleção de Mamíferos da Universidade Federal do Espírito Santo
-	Gavião/AM	-	-1.726.274	-59.733.000	Sampaio et al. 2003
DZSJRP-13455; DZSJRP-13653	Humaitá/AM	-	-7.506.100	-63.020.800	Paulino et al. 2021
-	Lago Uauaçu/AM	-	-4.233.333	-62.266.667	Bobrowiec et al. 2014
-	Manaus/AM	-	-0.240.000	-59.716.666	Sampaio et al. 2003
UFMG-6917; UFMG-6918	Maués/AM	-	-0.002.417	-59.733.000	Paes et al. 2022
AMNHM-78429	São Gabriel da Cachoeira/AM	-	-0.616.667	-69.100.000	Paulino et al. 2021
-	Tefé/AM	Baixo Juruá Extractive Reserve	-3.758.694	-66.068.306	Paulino et al. 2021
-	Bom Jesus da Lapa/BA	Caverna Poço Encantado	-13.430.000	-43.080.000	Sá-Neto & Marinho-Filho 2013
-	Chapada DiamantinaBA	-	-12.950.000	-41.100.000	Gregorin & Mendes 1999
UFMG-7647	Domingos Martins/ES	Domingos Martins	-0.020.292	-0.040.883	Abreu et al. 2021
-	Santa Teresa/ES	-	-19.933.333	-40.566.667	Woodman & Timm 2006
-	Alto Tocantins/GO	Caverna Carneiro	-13.812.778	-48.407.222	Fracasso & Salles 2005
-	Barro Alto/GO	Fazenda Barro Alto	-14.673.406	-48.814.762	Zortéa & D'Arc 2019
-	Mambaí/GO	-	-14.466.667	-46.116.667	Coimbra et al. 1982
-	Pilar de Goiás/GO	Fazenda Pilar	-14.818.394	-49.545.632	Zortéa & D'Arc 2019
-	São Domingos/GO	Passa Três Cave - Parque Estadual Terra Ronca	-13.600.000	-46.390.000	Bichuette et al. 2018
UFMG-5324	Aripuanã/MT	-	-10.150.000	-0.059.433	Paes et al. 2022
-	Médio Teles/MT	-	-10.967.778	-55.756.389	Miranda et al. 2015
-	Figueirão/MS	-	-18.666.667	-53.633.333	Bordignon 2006
UFMG-4946; UFMG-4947	Diamantina/MG	Gruta do Salitre	-0.018.267	-0.043.533	Paes et al. 2022
UFMG-6990; UFMG-6991	Dores de Guanhães/MG	DGN_005	-19.040.724	-48.865.569	Paes et al. 2022
MZUFV 4178	Igarapé/MG	AVG 14	-20.109.361	-50.281.990	Paes et al. 2022
-	Itacarambi/MG	Olhos D'água Cave	-15.116.667	-44.166.667	Trajano & Gimenez 1998

Figura 1: *Localidades onde foram confirmadas a ocorrência de Lionycteris spurrelli no Brasil.*

4. Discussão

A compilação dos dados sobre os registros de ***Lionycteris spurelli*** ampliam e esclarecem a sua distribuição. A partir dos dados levantados, observa-se que a espécie ocorre em todos os principais biomas brasileiros e a única região sem registro, até o momento, é a Sul. Verifica-se também que, além do clima e dos tipos de vegetação, a presença de cavidades naturais subterrâneas parece ser importante para a espécie (PAES et al., 2022). Além disso, os registros expandidos de *Lionycteris spurrelli* em Minas Gerais, bem como o aumento de localidades em outras regiões do Brasil, revelam uma tendência interessante na distribuição geográfica da espécie, que parece estar se estabelecendo em uma gama mais ampla de ambientes. A descoberta de novos registros em Minas Gerais, especialmente em sete municípios distintos, posiciona o estado como o maior em número de registros na região Sudeste e o terceiro em todo o país. Isso sugere que a espécie pode estar se beneficiando de fatores ecológicos favoráveis, como a presença de áreas com características ambientais adequadas, como cavernas e matas, que são comuns na região.

Este aumento no número de registros pode indicar uma expansão ou uma maior taxa de detecção da espécie, possivelmente associada a alterações no habitat, como mudanças no uso da terra ou na vegetação, além de melhorias nas metodologias de coleta de dados. No entanto, também é importante observar que a presença de *Lionycteris spurrelli* em diferentes locais pode estar relacionada a aspectos de conectividade entre habitats, o que destaca a necessidade de entender como essas populações estão distribuídas no espaço e como elas interagem com o ambiente ao longo do tempo.

Sendo assim, dado o aumento e distribuição da espécie em dife-

rentes localidades, é essencial realizar modelagens ecológicas para entender melhor as condições ambientais que favorecem a presença da espécie, bem como prever a dinâmica de sua distribuição em diferentes cenários. Modelos de distribuição de espécies (SDMs: *Species Distribution Models*) possui potencial de identificar áreas de potencial ocupação, considerando variáveis ambientais, como tipo de vegetação, topografia, clima, entre outras.

Essas modelagens podem ser fundamentais para antecipar a dinâmica de dispersão da espécie e avaliar os impactos de mudanças ambientais, como a alteração no uso da terra, a fragmentação de habitats e as mudanças climáticas. Além disso, a modelagem espacial pode fornecer insights sobre quais áreas necessitam de conservação e monitoramento contínuo para garantir a preservação da espécie e de seus habitats.

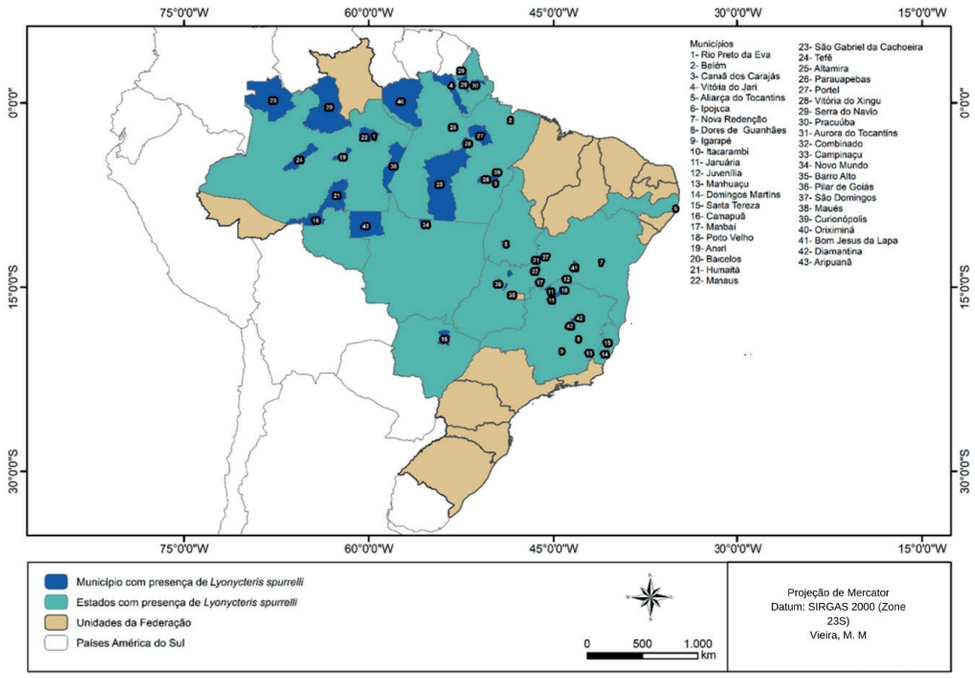

Figura 2: *Aumento dos índices de ocorrência da espécie no Brasil.*

5. Conclusão

A composição de espécies de morcegos em determinada área pode estar relacionada, principalmente, com a disponibilidade de abrigo, alimento e estrutura da vegetação. Desta forma, os quirópteros podem ser utilizados como indicadores no entendimento dos processos biológicos envolvidos na perda ou transformação do hábitat natural (KUNZ & FENTON, 2003). O aumento no número de registros de *Lionycteris spurrelli* em várias regiões do Brasil, especialmente em Minas Gerais, evidencia uma maior compreensão sobre a distribuição espacial dessa espécie. A expansão para novos municípios e locais revela tanto a adaptação da espécie a diferentes ambientes quanto a melhoria nas abordagens de coleta e monitoramento. No entanto, a complexidade dessa distribuição, aliada às possíveis variações ecológicas, destaca a necessidade de aprofundar a investigação sobre os fatores que determinam sua presença e persistência em diferentes habitats.

A modelagem ecológica surge como uma ferramenta essencial para estudos posteriores mais refinados, visto que visam explorar as variáveis ambientais que influenciam a distribuição de *L. spurrelli*. E para prever possíveis alterações em sua área de ocorrência diante de mudanças ambientais. Esse passo é crucial para orientar estratégias de conservação e garantir a preservação de habitats críticos. Assim, a continuidade do monitoramento e a implementação de modelagens ecológicas serão fundamentais para o entendimento dinâmico dessa espécie e para o desenvolvimento de ações eficazes de manejo e proteção.

Agradecimentos

Agradecemos sinceramente ao Matheus Marques Vieira pela valiosa colaboração na produção dos mapas deste estudo, assim como a todos que contribuíram direta ou indiretamente para a realização desta pesquisa.

Referências

ANCIÃES, M.; PETERSON, A. T. Climate change effects on neotropical manakin diversity patterns. Global Change Biology, 2006.

ARAÚJO, M. B. et al. Predicting the effects of climate change on biodiversity. Ecological Modelling, 2013.

COPAM. Lista de Espécies Ameaçadas de Extinção da Fauna do Estado de Minas Gerais. Belo Horizonte: Conselho Estadual de Política Ambiental, 2010.

GUIMARÃES, M. M.; FERREIRA, R. L. Ecologia de cavernas brasileiras:

aspectos gerais. Revista de Ecossistemas, 2014.

IUCN. The IUCN Red List of Threatened Species. 2025.

IVERSON, L. R.; PRASAD, A. M. Estimating potential future distributions of tree species. Ecological Applications, v. 8, p. 98-107, 1998.

KUNZ, T.H. & FENTON, M.B. 2003. Bat ecology. The University of Chicago Press, Chicago.

LIRA, T.C., MENDES PONTES, A.R. & SANTOS, K.R.P. Ocurrence of the chestnut long-tongued bat *Lionycteris spurrelli* Thomas, 1913 (Chiroptera, Phyllostomidae) in the Northeastern Atlantic Forest, Brazil. Biota Neotrop. 9(1): http://www.biotaneotropica.org.br/v9n1/en/abstract?short-communication+bn00909012009.

LOPES, G. P.; VALSECCHI, J.; BRANDÃO, P. E.; SANTOS, T. C. M. dos. Filling gaps on the distribution of Amazonian bats, new records of four poorly sampled species: *Trinycteris nicefori* Sanborn, 1949, *Lionycteris spurrelli* Thomas, 1913, *Macrophyllum macrophyllum* (Schinz, 1821), and *Dasypterus ega* (Gervais, 1856). Journal of Bat Research & Conservation, v. 14, n. 1, 2021.

PAES, C. B. et al. Distribuição e ecologia de Lionycteris spurrelli em biomas brasileiros. Biodiversity Reports, 2022.

SOBERÓN, J.; PETERSON, A. T. Interpretation of models of fundamental ecological niches and species' distributional areas. Biodiversity Informatics, 2005.

STEPHENS, P. A. et al. Climate change impacts on species distribution. Nature Ecology & Evolution, 2016.

WALTHER, G. R. et al. Ecological responses to recent climate change. Nature, 2002.

Linking fracture and conduit orientations in the lapiaz of Tsanfleuron, Swiss Alps

Ana Paula Burgoa Tanaka (1), Celia Trunz (1), Manon Trottet (1), Tanguy Racine (1), Philippe Renard (1)

(1) Centre for Hydrogeology and Geothermics, University of Neuchâtel, Switzerland. ana.burgoa@unine.ch

Abstract

The influence of structural features on karst development has been extensively described, with particular emphasis on the role of fractures in creating preferential dissolution pathways. Alignments between fractures and conduits are commonly observed in regions where the rock is prone to diaclase or where the tectonic history imprints fracture patterns that enhance rock dissolution. To test the hypothesis that the fractures play a major role for karst development, we check if the orientation of fractures and karst conduits are similar, by statistically comparing their azimuths in the karst system of Tsanfleuron, in the Helvetic domain of the western Swiss Alps. We interpret fracture alignments on a scale of 1:2.500, based on a set of open data that consisted in a high-resolution digital elevation model and an orthomosaic from a drone acquisition. Some parts of the interpretation were verified in the field. The karst data set was acquired by the Groupe de Spéléologie Rhodanien, the Société Spéléologique Genevoise, the Spéléo-Club Jura, and the Groupe Spéléo Lausanne. Rose diagrams and maps show qualitatively that some fracture sets coincide with the orientation of most of the conduits. A quantitative approach is proposed to verify how similar the distributions of fractures and conduit azimuths are by applying statistical test like the chi-squared test. The analyses are done by: 1) Dividing both the fracture azimuths and karst azimuths into bins, that are calculated according to the data size, counting the occurrences of azimuths in each bin for both data sets to create frequency distributions. 2) Calculating the expected frequencies by averaging the frequencies of the two distributions. 3) Calculating the chi-squared statistic to check if there is a significant difference between the distributions. The null hypothesis (H0) is that both distributions are similar, meaning that any observed differences are due to random variation, and the alternative hypothesis (H1) is that the distributions are significantly different. If the chi-squared test yields a value under the selected p-value of 5%, we reject the null hypothesis, suggesting that the two distributions are significantly different. The comparison of the whole range of data from 0° to 180° shows that the hypothesis H0 cannot be rejected but with a low p-value=0.164. We can conclude that the distributions are slightly similar. However, the comparison of the histograms corresponding to more specific ranges of directions (e.g. 60°-90°, with p-value=0.995) indicate that fractures and conduits are strongly aligned, with high p-values, meaning that the ENE-WSW fractures influenced strongly the development of conduits.

1. Introduction

Located in the Western Swiss Alps, the karst aquifer of Tsanfleuron (Fig.1) is recharged by an overlying and retreating glacier. Fractures of different ages impact groundwater circulation and are associated with the karstification of the Urgonian-Eocene limestone aquifer. The influence of the structural geology on karst development in the study area, particularly the role of faults and fractures for the generation of preferential dissolution paths, has been described by Gremaud et al. (2008, 2009).

In general, it is well known that together with the stratigraphy, the geological structures have a profound influence on the hydrogeology of karst regions (Deike, 1989). Most specifically, the alignments between fractures and karst features occur in various regions where the rock is prone to diaclase, or where the tectonic history imprints fractures patterns that facilitate rock dissolution. Kiraly (1967) highlights the importance of the collaboration between speleogists and geologists in a study on the alignment of karstic features mapped by cavers and elements of structural geology. The author relates doline alignments with diaclases, and detachment orientation, in the region of Gouffre du Petit Pré de Saint-Livres, Jura Vaudois, Switzerland. Later, Kiraly et al. (1971) conclude that the orientation distributions of the subsurface cavities are of great interest for the hydrogeology of fractured rocks, by studying the relationship between fractures and the galleries orientation of a cave from the region of La Grotte de Milandre, Jura Tabulaire, Switzerland.

More recent works in characterizing and comparing fracture networks in fracture corridors and caves, utilizing Uncrewed Aerial Vehicle (UAV), and LiDAR images were carried out in the Brejões carbonate karst system, São Francisco Craton, southern Brazil (Furtado et al. 2022). The authors compare the directions of the mesoscale structures with the strikes of surface collapse dolines and cave conduits at shallow depths in the Jandaíra Formation, northeastern Brazil (Rabelo et al. 2020).

Pedrera et al. (2015) show the importance of fracture pattern characterization, in one of the largest karstification systems in Europe, in Sierra de las Nieves, Beltic Cordillera, Spain. The link between structural geology and speleogenesis is also highligthed in pseudokarst by Ribeiro et al. (2005), for sandstone caves and rock shelters in Ipeúna and Itirapina, southeastern Brazil. Using the data gathered for fracture modeling (Tanaka et al. 2024, 2025), we aim to test the hypothesis that the fractures play a major role for karst development in this aquifer system. To achieve this, we statistically compare the orientation of fractures and karst conduits, and test if the distribution of azimuths is similar.

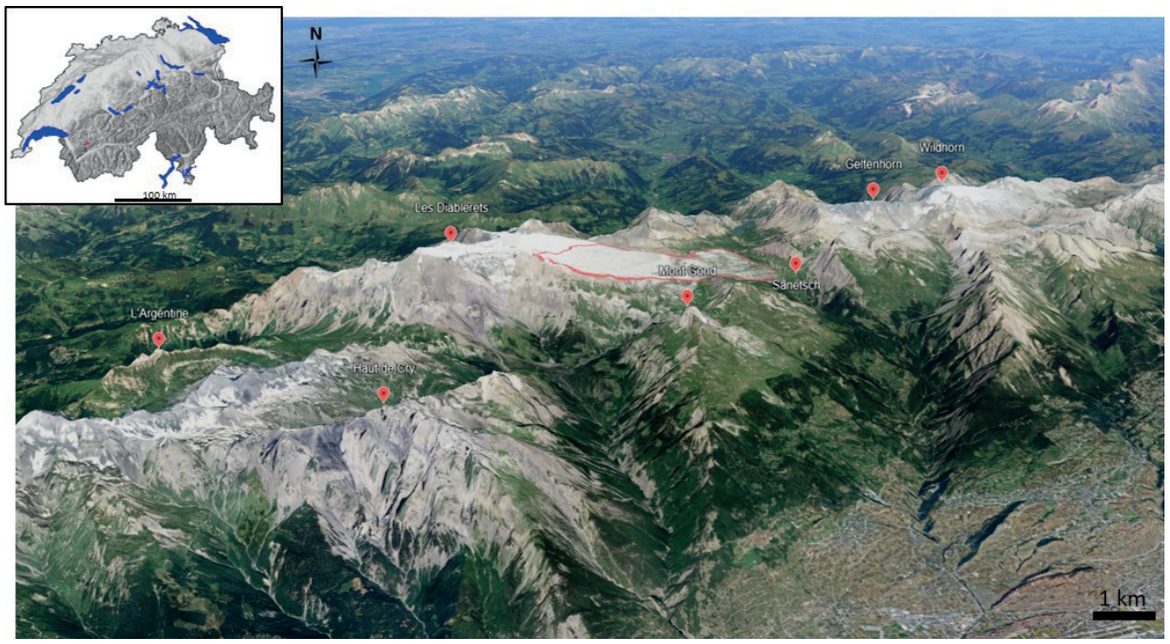

Figure 1: *Location of the study area (red polygon) in the Swiss Alps. Base map: DEM swissALTI3D from swisstopo and a 3D projection from Google Earth (Landsat / Copernicus).*

2. Materials and methods

We interpret fracture alignments in a scale 1:2.500, based on a set of open data that consists in a high-resolution digital elevation model (DEM) and a orthomosaic from a previous drone acquisition (Fig.2). The interpretations consist in polylines digitized on a GIS software and the fracture intersections are points that were carefully snapped at each intersection to maintain the real topology of the network (Tanaka et al. 2024, 2025). Each intersection, start, and end point of the lines have real world coordinates (x,y) from which it is possible to calculate the azimuths. The azimuth is the horizontal angle between the positive y-axis, that represents the north, and the line segment connecting two points. It is calculated using the arc tangent of y/x in radians and then converted to degrees by multiplying the result by 180/π. The fracture interpretation was also verified in the field to check the types of structure, kinematics and measurements (Tanaka et al. 2024, 2025). The mapping of karst conduits was done previously by several speleological groups from Switzerland: Groupe de Spéléologie Rhodanien, Société Spéléologique Genevoise, Spéléo-Club Jura, and Groupe Spéléo Lausanne. The data set consists in surveys from 23 caves: TSX2, TSX9, TSX10, TSX12, TSX14, TSX15, TSX17, Transpirateur, Topomasos, Scex Rouge, Sapin, Precoces, Porche2007, Marmite, Kefir, G59 Tord Boyau, G10, G16 Gouffre du Criquet Enrage, Edelweiss, D26, D37, Crapaud, and Coupe Fresard.

The first approach we applied consists in superposing structural and karstic features on maps and on plots of the direction of the features in rose diagrams, to test qualitatively if some fracture sets coincide with the orientation of most of the conduits in the area.

To verify how similar are the distributions of fractures and conduit azimuths we propose a quantitative approach to test the hypothesis by applying the chi-squared test.

Chi-squared statistic measures how much the observed frequencies deviate from expected frequencies. It is calculated as the sum of squared differences between the observed and expected values, weighted by the expected values:

$$\chi^2 = \sum \frac{(O_i - E_i)^2}{E_i}$$

where O_i is the observed frequency, and E_i is the expected frequency for the i-th bin. The null hypothesis (H0) is that both azimuths distributions (fracture and karst) are similar, meaning that any observed differences are due to random variation, and the alternative hypothesis (H1) is that the distributions are significantly different. The p-value is the probability of obtaining a chi-squared statistic at least as extreme as the one observed, under the assumption that the null hypothesis is true. If the chi-squared test yields a value under the selected p-value=0.05, we reject the null hypothesis, suggesting that the two distributions are significantly different. A high p-value suggests that there is a high probability that the observed differences are due to random variation, in other words there is no significant difference between the observed and expected frequencies.

The analyses are done by: 1) Dividing both the fracture azimuths and karst azimuths into bins, that are calculated according to the data size, counting the occurrences of azimuths in each bin for both data sets to create frequency distributions. 2) Calculating the expected frequencies by averaging the frequencies of the two distributions. 3) Calculating the chi-squared statistic to check if there is a significant difference between the distributions. We apply the test for the whole range of azimuths (0°-180°) and for specific ranges that describe different fracture sets (0°-30°, 30-60°, 60°-90°, 90-120°, 120°-150°, 150-180°). As the analysis can be sensitive according to the number of bins used to class the range of azimuths, we use Rice's rule to define the number of bins *n* according to the number of samples available for each category. Rice's rule is to take *n* as the cube root of the number of observations times two.

3. Results and Discussion

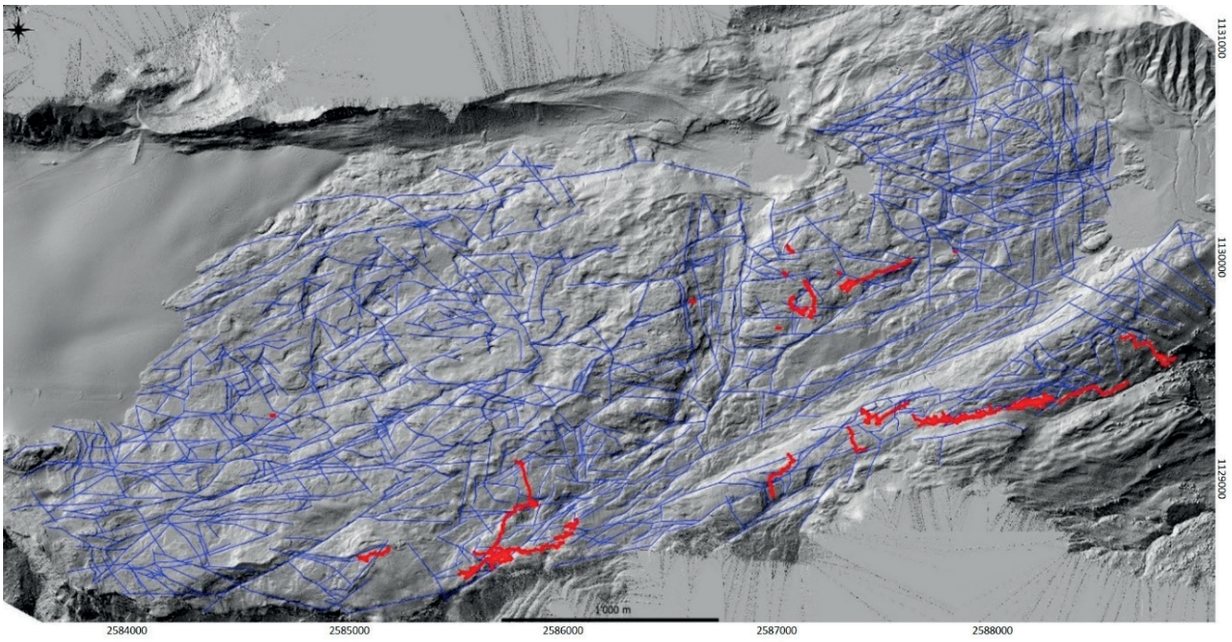

Figure 2: *Fracture network interpretation (blue) and conduits from the mapped caves (red). Base map: Hillshaded DEM from UAV at 10 cm/px resolution.*

From the fracture interpretation and karst azimuths distribution in the map we can generally infer that there is a concordance between the orientations of the fractures and the karst conduits, in general in the NE-SW. We highlight that the scale of the fracture interpretation is not as detailed as the karst mapping, but the idea of the comparison is to be able to use the method also in other areas to understand and quantify the impact of major structures into karst development. Faults and fractures are mapped using remote sensing and the conduits are usually mapped in the field by speleologists. A locally detailed study could be done by mapping and measuring the fractures inside the cave while mapping the conduits, in this case we would have measurements in the same scale but on a restrict area, not for the whole study site. A further aim of the method is to build scenarios where fractures in a certain direction have more or less impact in karst development and in preferential fluid flow paths.

With the azimuth plot in a rose diagram, we compare the whole range of data from 0° to 180°. The rose diagrams show that there is a superposition of azimuths mainly in the NE-SW, and ENE-WSW direction, between 60 and 90° (Fig.3). The distribution was weighted by fracture and conduit normalized lengths. The lengths were calculated from the networks and normalized, the idea is to emphasize the frequency of azimuth within a higher length, to minimize the influence of the way the survey was acquired, zig zag effects, and to highlight in the analysis the segments that are more developed. Karst conduit length is the 2D projected length.

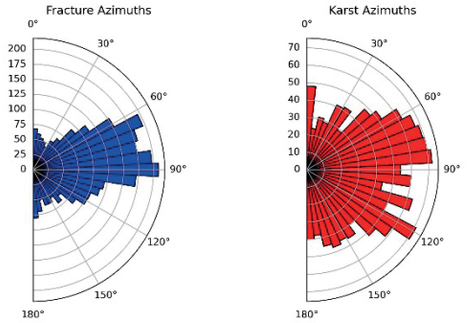

Figure 4: *Rose diagrams of the fracture (blue) and karst (red) azimuths, weighted by their respective length (projected in 2D for karst), the frequency is the count.*

When we apply the chi-squared test, we obtain the p-values presented in Figure 5. It shows that for a comparison of the whole range of azimuths (0-180°) the hypothesis H0 cannot be rejected but with a low p-value=0.164. We can conclude that the distributions are slightly similar. When we weigh by normalized length we obtain a higher p-value.

# Chi-squared test	Azimuth range	Fracture mean azimuth	Karst mean azimuth	Bins	p-value
0	0°-180°	88°	93°	29	0.164
1	0°-30°	13°	14°	13	0.914
2	30°-60°	47°	46°	15	0.935
3	60°-90°	75°	75°	19	0.995
4	90°-120°	102°	105°	17	0.838
5	120°-150°	133°	133°	14	0.630
6	150°-180°	165°	164°	14	0.642

Figure 5: *Table of the results of the chi-squared test, with different azimuths ranges, mean azimuths for fractures and karst, number of bins used in the test, and p-values.*

The comparison of more specific ranges also results in not rejecting the hypothesis H0, with higher p-values, indicating that fractures and conduits are aligned in every direction.

The test for intervals of 30° results in higher p-values, especially for the directions of: 0°-30°, 30°-60°, 60°-90°, 90°-120°. Indicating stronger alignment in the NE-SW, ENE-WSW, and E-W directions. We can infer that those fracture directions played a major role in karst development which agrees with other works.

Gremaud et al. (2008) describe how karst development tends to follow the main direction of the fracture family, especially for the family oriented 60°. Gremaud et al. (2009) highlight that fractures were active before and during the deposition of Eocene sediments and influenced paleokarst development, verified by the alignment of paleodolines in the Urgonian limestone in the ENE direction. Both observations reinforce the importance of the NE-SW, ENE-WSW directions of fractures for conduit development. At the outcrop scale, Figure 6 illustrates various features of dissolution that follow the faults and fractures orientation in the study site. (A) shows a fault NW-SE sinistral, with dissolution in an en échelon pattern. (B) shows a similar pattern over a larger fault. (C) illustrates the dissolution and karst development in the southeast area closer to the glacier in the E-W direction, and (D) in a NE-SW direction. (E) and (F) are from the central area, where the conduits are developed in the NW-SE faults and fractures (E), and there is also dissolution along the N-S fracture set (F). According to Gremaud et al. 2009 there are 100 caves in the area, most of which are small. Caves entrances often consist in vertical shafts (Fig.6C), but most also have horizontal passages, parallel to the stratification.

Figure 6: Dissolution along structural features in Tsanfleuron: A) En échelon dissolution pattern, B) dissolution over a larger fault, C) karst development in the E-W direction, D) dissolution in NE-SW faults and fractures, E) conduits aligned to NW-SE faults and fractures, F) dissolution along the N-S fracture set.

4. Conclusion

By combining the fracture interpretation, the map and rose diagram analyses, the observations from the field, and the chi-squared test, we conclude that the fracture and karst conduit azimuth distributions are similar. Calculating the karst azimuth from the projection in 2D is a relatively good approximation due to the location of the conduits that are largely parallel to the bedding, that is not steep. Therefore, fractures controlled the development of the karst in Tsanfleuron mainly in the NE-SW, ENE-WSW, and E-W directions. An ongoing work is being held to add all the structural geology information to a graph-based fracture model (Tanaka et al. 2025), that can be used in scenarios that consider different probabilities for the fracture sets to develop preferential flow paths and karst, for a hydrogeological modeling and assessment for Tsanfleuron.

In the present study, we only use the karst surveys that are available, comprising approximately 23% of the karsts of the area. For a more detailed study a more complete karst conduit data set is needed.

Acknowledgments

The authors acknowledge the speleology groups of GSR (Groupe de Spéléologie Rhodanien), SSG (Société Spéléologique Genevoise), SCJ (Spéléo-Club Jura), and GSL (Groupe Spéléo Lausanne) for sharing the karst surveys. Thanks, Jefter Natan de Moraes Caldeira for the field work, and discussions about structural geology. Thanks also to Eva Kaminsky for giving suggestions to improve the analyses. Thanks, Nina Egli for text layout advice. P. Renard, C. Trunz and T. Racine acknowledge funding by the European Union (ERC, KARST, 101071836). Views and opinions expressed are, however, those of the authors only and do not necessarily reflect those of the European Union or the European Research Council Executive Agency. Neither the European Union nor the granting authority can be held responsible for them.

References

DEIKE, G. (1989) Fracture controls on conduit development. Springer US, Boston, MA. 259–291.

FURTADO (2022) The influence of subseismic-scale fracture interconnectivity on fluid flow in fracture corridors of the Brejões carbonate karst system, Brazil. Marine and Petroleum Geology 141:105689.

GREMAUD, V. (2008) Géologie du karst de Tsanfleuron. Collection EDYTEM. Cahiers de géographie 7:127–134.

GREMAUD, V., GOLDSCHEIDER, N., SAVOY, L., FAVRE, G., MASSON, H. (2009) Geological structure, recharge processes and underground drainage of a glacierised karst aquifer system, tsanfleuron-sanetsch, swiss alps. Hydrogeology, 17:1833-1848

KIRALY (1967) Relations entre les phénomènes karstiques et la géologie. Actes du 3e Congrès national de spéléologie. Société Suisse de Spéléologie. Supplément 3 à Stalactite: 31-43.

KIRALY, L., MATHEY, B., TRIPET, J. (1971) Fissuration et orientation des cavités souterraines région de la grotte de Milandre (Jura tabulaire). Bulletin de la société neuchateloise des sciences naturelles. 94: 99-114.

PEDRERA, A., LUQUE-ESPINAR, J.A., MARTOS-ROSILLO, S., PARDO-IGÚZQUIZA, E., DÚRAN-VALSERO, J.J., MARTÍNEZ-MORENO, F. (2015) Structural controls on karstic conduits in a collisional orogen (Sierra de las Nieves, Betic Cordillera, Spain). Geomorphology, 238: 15-26.

RABELO, J., MAIA, R., BEZERRA, F., SILVA, C. (2020) Karstification and fluid flow in carbonate units controlled by propagation and linkage of mesoscale fractures, Jandaíra Formation, Brazil. Geomorphology 357.

RIBEIRO, L. F. B., SOUZA CRUZ, F. R., RIBEIRO, M., & GODOY, D. (2005) Origem e controle estrutural e estratigráfico das cavernas, tocas, abrigos de Ipeúna e Itirapina–SP. In CONGRESSO BRASILEIRO DE ESPELEOLOGIA. Vol. 28.

TANAKA, A.P.B., RENARD, P., CALDEIRA, J.N.M., LIANG, X.X., TRUNZ, C., STRAUBHAAR, J. (2024) Graph-based modeling of fractures in the Tsanfleuron karst aquifer system. In: International Association of Hydrogeologists 2024 World water groundwater congress.

TANAKA, A.P.B.T., RENARD, P., CALDEIRA, J.N.M, TRUNZ, C. (2025) Graph-based modeling of fracture networks in the karst aquifer system of Tsanfleuron, Western Swiss Alps. Fore coming.

How indirect hydrogeological methods can help in the evaluation of speleological potential

Wendy Tanikawa (1,2), Beatriz Fonseca (1), Pedro Assunção (1,2), Lucas Padoan (1), Tássia Marques (1), Paulo Galvão (1), Gabriel Lourenço (1,2) e Rodrigo De Paula (1)

(1) Laboratório de Estudos Hidrogeológicos (LEHID), Universidade Federal de Minas Gerais, Programa de Pós Graduação em Geologia – Instituto de Geociências – Departamento de Geologia wendytanikawa@gmail.com (corresponding author).

(2) Sociedade Excursionista e Espeleológica (SEE), caving club.

Abstract

Karst aquifers are characterized by complex underground conduit networks, where water flow is highly heterogeneous and dynamic due to punctual recharge through sinkholes and sinking streams, cave formation, sediment deposition, and changes in base level. These aquifers supply approximately 25% of the world's population, emphasizing the need for their proper understanding and preservation. By their complexity, indirect hydrogeological methods, such as hydrograph analysis, hydrochemical characterization, and statistical techniques, are essential for assessing their behavior and potential contamination sources. In this study, the São Miguel River sub-basin (18.3 km^2) was analyzed using these methods during the 2019–2020 water year. The study area, located in the southern São Francisco River basin, Brazil, is composed of Neoproterozoic carbonate lithologies from the Bambuí Group, where limestone mining, agriculture, and livestock farming are predominant land uses. Spring monitoring was conducted based on three selected precipitation events (R1, R2, and R3) to evaluate system karstification and hydrodynamic responses. The results indicate a highly karstified system, as evidenced by the rapid response of spring discharge to rainfall events. Hydrochemical analysis suggests that piston effect may control the transition from calcium-bicarbonate to magnesium-bicarbonate water types. The applied methodologies provided insights into aquifer storage capacity, and allowed to recognize vulnerable zones to contamination. The analysis also contributed to mapping the speleological potential (cave occurence) in a region, offering an analytical subsurface assessment. These findings contribute to groundwater management and to the preservation of associated karst features.

1. Introduction

Karst aquifers consist of complex networks of underground conduits, where water flow is more dynamic due to punctual recharge through sinkholes and sinking streams, cave formation, sediment deposition, and changes in base level. Depending on the degree of rock karstification, the response to a recharge event caused by precipitation may be faster or slower. Groundwater from karst aquifers supplies approximately 25% of the world's population (Ford & Williams, 2007), highlighting the importance of understanding and preserving these systems. Due to their complexity, specific techniques are required for their characterization. Thus, to comprehend the system's behavior in response to climatic events, it is necessary to monitor both springs and climatic conditions.

Spring hydrographs are excellent tools to evaluate karst system behavior, as they graphically represent the spring's discharge response to a precipitation event. These hydrographs record both individual rainfall events and extended time series, allowing the identification of seasonal variations in behavior. The recession curve of a hydrograph can be used to classify the degree of karstification of an aquifer based on flow velocities and storage times, following the method proposed by Mangin (1975, 1984): (i) k, which represents the regulation capacity and indicates the size of the saturated zone; and (ii) i, which refers to the infiltration lag time, revealing the conditions of deep infiltration throughout the unsaturated zone. This approach enables the identification of the most karstified zone of the spring (either upstream or downstream), the presence of flooded zones, and the possible existence of subsystems or less karstified areas.

Additionally, the hydrochemical properties of water can be analyzed using graphical tools such as the Piper (Piper, 1944) and the Stiff diagrams (Stiff, 1951). These graphs allow visualization of the relationships among the major dissolved ions in water and the identification of hydrochemical patterns. This method is commonly applied in hydrological monitoring to assess processes such as water mixing, rock weathering, and aquifer contamination. Furthermore, these studies typically involve extensive datasets, often covering an entire hydrological year or longer, so hydrochemical data can also be analyzed using multivariate statistical techniques, such as factor analysis. This technique aims to reduce data dimensionality by grouping correlated variables into factors that represent underlying common characteristics. Thus, through graphical and statistical interpretations, it is possible to complement the understanding of aquifer hydrodynamics and potential contamination sources.

In this context, the São Miguel River basin was studied using the aforementioned indirect methods during the 2019–2020 hydrological year. The study area is located at the southernmost part of the São Francisco River basin and within the southern portion of the homonymous Craton, where Neoproterozoic rocks of the Bambuí Group outcrop, with widespread carbonate lithologies from the Sete Lagoas Formation (Alkmim & Martins-Neto, 2001). Due to these geological characteristics, the region hosts numerous limestone mining operations, and also livestock farming and agriculture as predominant land uses. This study aimed to understand the hydrodynamic and hydrochemical functioning of a sub-basin (18.3 km^2) by monitoring its spring. For this purpose, three precipitation events were selected: one occurring between January 21–27, 2020 (R1), another between February 5–23, 2020 (R2), and a seasonal variation event starting on February 27, 2020 (R3). The methods applied provide insights into the degree of system karstification and potential contamination sources. Consequently, these findings can contribute to groundwater management policies and the preservation of associated speleological features.

2. Materials and methods

2.1. Descriptive and Multivariate Statistics

The software Statistica Version 12 was used to analyze the hydrochemical data. The Shapiro-Wilk test was applied to understand the distribution of the samples, which represents an assimetric distribution. The multivariate analysis was conducted in Statistics through factor analysis, extracting three factors that accounted for 68.6% of the variance. Only values above 0.700 were considered for the factors of interest.

2.2. Hydrodynamic and Hydrochemical Monitoring

For this analysis, monthly discharge measurements and physicochemical parameter readings were conducted at the spring, while recharge was evaluated using a meteorological station, which recorded daily precipitation, temperature and humidity. At the spring, a weir equipped with an automatic transducer was installed to continuously record water level, temperature, and electrical conductivity every 15 minutes. Additionally, monthly discharge measurements were performed using a current meter to develop the rating curve for the spring hydrograph. In the hydrograph, the recession curves were represented by the equation $Q(t) = \psi(t) + \phi(t)$, where $Q(t)$ is the discharge at time t, $\psi(t)$ represents the nonlinear recession of the unsaturated zone discharge, and $\phi(t)$ corresponds to the saturated zone flow.

Physicochemical parameters were measured in situ using a portable multiparameter meter, including electrical conductivity, temperature, turbidity, pH, dissolved oxygen, oxidation-reduction potential, and total dissolved solids. Additionally, monthly water samples were collected for hydrochemical analysis at Laboratório Limnos (CRL 0462), conducted immediately after sampling. The rainfall event analyzed during recession R1 (154 mm of precipitation) occurred between January 21 and 27, 2020; the event corresponding to recession R2 (402 mm of precipitation) took place between February 5 and 23, 2020; and the recession R3 event (68 mm of precipitation) began on February 27, 2020, representing seasonal variation.

2.3. Piper and Stiff Diagrames

The hydrochemical parameters were characterized using Piper and Stiff diagrams, developed with the QualiGraf software. The former is a ternary diagram that utilizes the relationship between dominant ions to classify water (e.g., chloride, sodium, magnesium types), with classification based on the concentration (in meq/L) of the sum of cations or anions. The latter represents ionic concentrations through parallel horizontal lines, forming specific geometric shapes for each water type. By analyzing these diagrams, it was possible to interpret the data seasonally (dry and wet periods) and classify the water for each hydrological month. A total of 12 hydrochemical samples were analyzed.

2.4. Karstification Degree

To classify the karstification degree in karst systems, Mangin (1975, 1984) proposed two indices based on recession curves: i) k, which represents the regulation power and determines the extent of the saturated zone; and ii) i, which corresponds to infiltration delay, evaluating the conditions of deep infiltration in the unsaturated zone. These indices, k and i, are calculated using the equations: $k = Vdyn/V0$ e $i = (1 - \eta t)/(1 + \varepsilon t)$, where Vdyn is the dynamic water volume present in the saturated zone at the beginning of the recession, and V0 is the initial volume discharged by the spring at that moment. The variable ε is the heterogeneity coefficient and is associated with the concavity of the hydrograph—values closer to 1 indicate rapid water circulation in the system. The parameter η is proportional to the infiltration rate—values closer to zero indicate faster infiltration. This study used the Curve Fitting tool in MATLAB for the calculations. Based on this method, the karst system can be classified into five categories:

I. Well-developed cave network with a highly karstified system downstream.

II. Well-developed drainage network with a largely flooded downstream area.

III. More karstified upstream than downstream.

IV. Complex karst system with expanded sections and multiple subsystems.

V. Poorly karstified system

3. Results and Discussion

3.1. Spring Hydrograph Analyses

The spring hydrograph (Figure 1) exhibits sharp peak discharges, with a response time of less than 24 hours following a high-intensity rainfall event, indicating rapid water circulation in the unsaturated zone. The discharge regime shows high variability, with a minimum value of 14 L/s, recorded on November 3, 2020, and a maximum of 686 L/s, recorded on March 9, 2020. The recession curve behavior suggests a typical karstic response, characterized by fast-flowing water circulation, a network of interconnected subterranean conduits, and the presence of focused infiltration. These focused infiltrations may be associated with cave entrances, sinkholes, and/or dolines connected to the hydrosystem.

The morphology of the recession curves R1 and R2 exhibits a rapid peak in discharge following an intense rainfall event, with flow returning to a near-average pattern within a few days. This behavior reflects a weak regulation of the system. However, the seasonal recession R3, which follows the last rainfall event of the wet period, reveals limited water storage capacity in the aquifer. During the first 20 days of runoff, the system drained approximately 46% of the newly infiltrated recharge volume. Regarding infiltration conditions for R3, the parameters $i = 0.32$, $\eta = 0.038$, and $\varepsilon = 0.923$ confirm rapid water circulation in the vadose zone. Similarly, the high ε values for intra-annual recessions ($\varepsilon R1 = 1.750$; $\varepsilon R2 = 1.600$) combined with very low i values ($iR1 = 0.20$; $iR2 = 0.17$; $iR3 = 0.14$) and relatively high η values ($\eta R1 = 0.125$; $\eta R2 = 0.200$) demonstrate that even under conditions of high water inflow (>150 mm), in R2 and R3 recessions, the travel time between recharge and discharge is short. The k parameter, which expresses the extent of the saturated zone and water residence time in the system, presents the following values: $kR1 = 0.08$, $kR2 = 0.19$, and $kR3 = 0.33$. For R1 and R2 recessions, where $k < 0.1$, the water residence time is less than 30 days. For R3, the residence time is less than six months, associated with seasonal variation. Water temperature increases following a rainfall event that recharges the system, as external summer temperatures are higher than the stored groundwater temperature. However, in general, water temperature variations are minimal, fluctuating by approximately 2°C. Conversely, electrical conductivity decreases after rainfall events, due to the influx of

less mineralized rainwater, reinforcing the relationship between higher conductivity values and longer water residence time in the system. These variations in physical parameters, influenced by hydrodynamics, reflect the short-term influence of precipitation on the system, even at the end of the wet season, when precipitation levels were highest (February 2020).

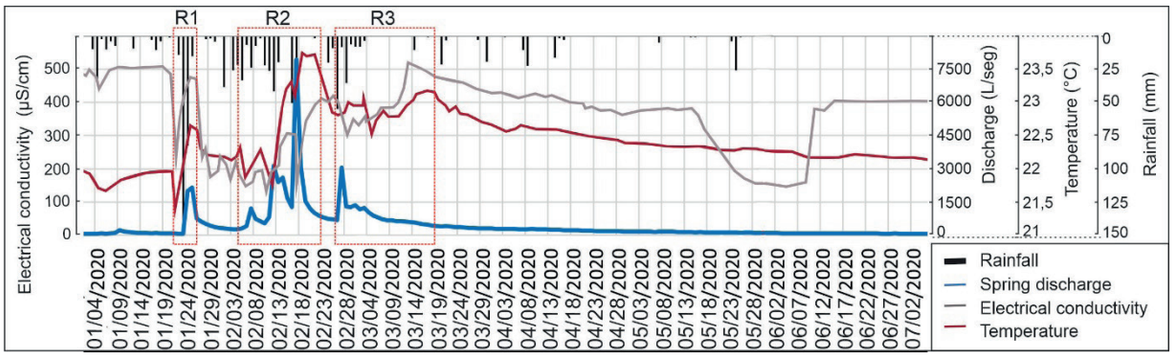

Figure 1: *Hydrograph representing the variation in rainfall, flow rate, temperature, and electrical conductivity over the course of detailed hydrometeorological monitoring.*

3.2. Hydrochemical characterization

Twelve water analyses were conducted at the spring during both rainy and dry periods throughout the hydrological monitoring year. Upon analyzing the Piper diagram containing all the samples (Figure 2), the most frequent classification was calcium bicarbonate water, except for the sample collected on March 9 (2020), which was classified as magnesium bicarbonate. This change is also observable in the Stiff diagrams (Figure 2) through the abrupt variation in the geometric shape of the diagram. This occurs due to a sharp decrease in calcium concentration to 0.7 mg/L, whereas the average concentration is 78.26 mg/L. This variation coincides with the two most intense rainfall events recorded during the rainy season, followed by a third event of lower magnitude, which also contributed to the system's saturation. The rainfall event represented in the recession curve R1 totaled 154 mm, while R2 reached 402 mm, and R3, though of lower intensity compared to the previous events, totaled 68 mm. Despite the rapid circulation of water within the system, the close occurrence of these high-magnitude precipitation events led to the water saturation of the conduits. The last event, although with lower precipitation, encountered a previously saturated system, acting as a piston effect that remobilized stagnant water from deeper zones of the aquifer. The abrupt decrease in calcium concentration and the increase in magnesium concentration are indicative of this piston effect, with magnesium serving as an indicator of water residence time in the aquifer (Batiot et al., 2003). This process corresponds to the remobilization of water from deeper zones, which have longer residence times within the aquifer. Thus, the hydrochemical analysis suggests that piston effect may control the transition from calcium-bicarbonate to magnesium-bicarbonate water types.

In January and February, the cumulative precipitation reached 556 mm, and in February, a sharp decline in electrical conductivity was observed as a result of the dilution of ions present in the water due to the substantial recharge volume. In February, the calcium bicarbonate-classified water exhibited the minimum electrical conductivity value of 244.3 µS/s, while the average was 424.19 µS/s, immediately after the recession event R1, which ended on January 27, 2020. In March, despite lower precipitation but still reflecting the effects of previous recharge events, a decline in calcium concentration led to a transition to the magnesium bicarbonate classification. This accumulated recharge is transmitted as discharge at the springs during February and January, with higher flow rates of 438 L/s and 686 L/s, respectively.

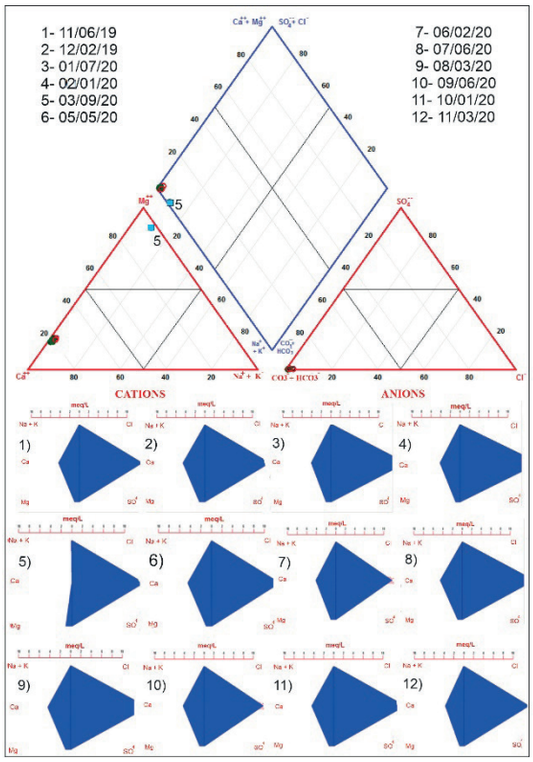

Figure 2: *Chemical characterization of the water. In the figure above, the Piper diagram with sample 5 (blue square) and the different shape of the Stiff diagram for sample 5 highlight its classification as magnesium-bicarbonate.*

The normality test indicated a non-parametric distribution of the hydrochemical data. Therefore, the multicriteria statistical analysis performed was factor analysis, which identified three predominant factors (Figure 3). Factor 1 accounted for 23.47% of the cumulative variance, Factor 2 for 24.16%, and Factor 3 for 20.97%, totaling a confiability of 68.6%. The first factor highlights a positive correlation between calcium and iron, and a negative correlation with magnesium. This is due to the mobilization of deeper and older waters that are more enriched in magnesium, and calcium, commonly present in more actively circulating waters, is diluted and lead to a decrease in its concentration.

The second factor indicates a positive correlation between nitrite and sulfate, both of which are indicative of potential aquifer contamination, considering the land use and occupation in the region. However, the monthly values do not characterize anthropogenic contamination, as they remain below 5 mg/L (CPRM, 2008). The third factor reveals a positive

correlation between precipitation and the concentration of carbonate and bicarbonate, meaning that higher recharge leads to increased dissolution of these ions. This pattern is observed across all monitoring months, except for the month in which the piston effect occurred.

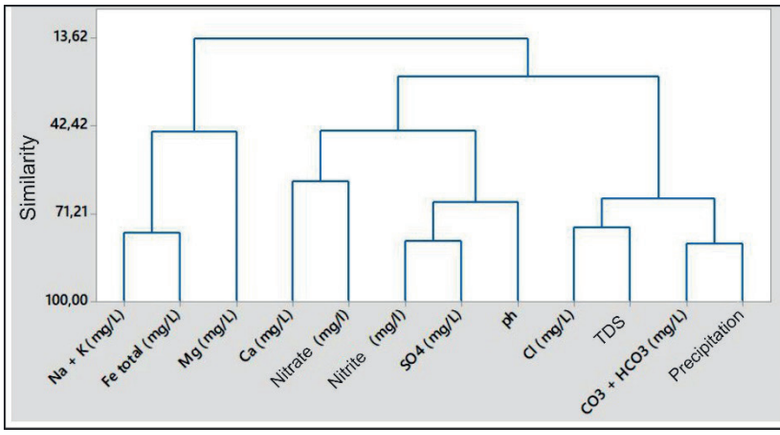

Variables (mg/L)	Factor Loadings		
	Factor (1)	Factor (2)	Factor (3)
Na + K	0,460342	0,669047	0,086299
Ca	-0,813281	-0,212607	0,139283
Mg	0,720149	-0,323116	-0,034488
Cl	0,141408	0,637657	0,572440
CO3 + HCO3	-0,002779	-0,142738	0,809817
Nitrate	-0,492412	0,051946	-0,432829
Nitrite	0,154335	0,720275	-0,113283
Fe total	0,843910	0,288383	0,223041
SO4	-0,204641	0,905259	-0,073085
ph	-0,314607	0,535842	-0,355459
TDS	-0,533501	0,396190	0,566243
Precipitation (mm)	0,026117	-0,083437	0,895664
Expl.Var	2,816593	2,899417	2,515987
Prp.Totl	0,234716	0,241618	0,209666

Figure 3 : *Statistics results. (A) Dendogram representing the similarities between the variables presented in the table. (B) The table displays the factors identified through multicriteria analysis.*

3.3. Karstification Degree

Figure 4 presents the classification of recessions based on climatic episodes. Recession R1 is characterized by a well-developed speleological network with a highly karstified downstream system, where numerous speleological features, such as sinkholes and caves, enable a concentrated recharge for the aquifer. This classification corresponds to an unsaturated system, in which water can percolate freely through secondary and tertiary porosity (speleogenetic conduits).

On the other hand, recession R2 represents a well-developed conduit network, with a significant portion flooded downstream, as a result of recharge by the rainfall events occurring in January and February, which saturated the system with water. Recession R3 indicates a more karstified system upstream than downstream, which contrasts with the classification of the other recessions. This occurs because the discharge is slower in a saturated phreatic system. Additionally, Pereira et al. (2019) highlight that, in this sector of the aquifer, surface drainage is virtually absent, a characteristic of highly karstified hydrosystems with well-developed subterranean drainage.

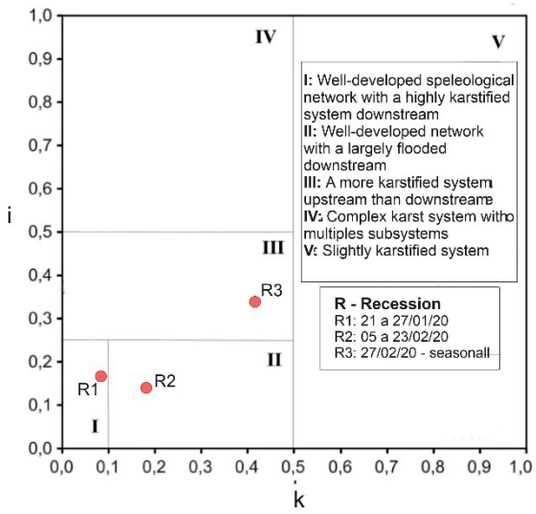

Figure 4: *The graph presents the classification of each recession curve based on the degree of karstification as a function of a climatic event.*

4. Conclusions

The indirect hydrogeological study methods employed in this study, such as hydrodynamic monitoring of springs, hydrochemical analyses, Piper and Stiff diagrams, and the classification of the degree of karstification, are specific tools for understanding karst aquifer systems. The studied system exhibits a high degree of karstification, as evidenced by its rapid response to rainfall events, with recharge being quickly transmitted through the increase in discharge observed at the monitored spring. The hydrochemical analysis indicates a piston effect within the system, highlighted by the change in water classification from calcium-bicarbonate to magnesium-bicarbonate at this month.

These analyses not only provide important insights into the water storage capacity and identification of more vulnerable regions of the aquifer but can also indicate more susceptible areas to speleogenesis. This inference is based on the fact that regions with a higher degree of karstification typically exhibit a well-developed network of subterranean conduits, with cave formation associated with the evolution of the karstification process from the protoconduit stage. Thus, the methods applied in this study can also contribute to mapping the speleological potential of a region, offering an analytical subsurface assessment.

Acknowledgments

We thank the Itabirito Economic Development Agency (ADESITA) and Gerdau S.A. for their financial support of the research in 2019 and 2020, through the Speleological Compensation Plan. We also thank the support of the Hydrogeological Studies Laboratory at the Professor Manoel Teixeira da Costa Research Center, Federal University of Minas Gerais.

References

ALKIMIM, F. F., and M. A. Martins-Neto. (2001). «A bacia intracratônica do São Francisco: arcabouço estrutural e cenários evolutivos.» Bacia do São Francisco: geologia e recursos naturais, p. 9-30.

BATIOT, C., Liñán, C., Andreo, B., Emblanch, C., Carrasco, F., & Blavoux, B. (2003). Use of TOC as tracer of diffuse infiltration in a dolomitic karstic system: the Nerja Cave (Andalusia, southern Spain). Geophysical Research Letters, 30(22), 2179.

CPRM, Companhia de Pesquisa de Recursos Minerais (2008). Hidrogeologia : conceitos e aplicações. 3 ed. Rev. E amp. – Rio de Janeiro, LABHID. 812 p.

FORD D., WILLIAMS P. (1989) Karst geomorphology and hydrology, Ed. Unwin Hyman Ltd. London, 601 p.

MANGIN, A. (1975). Contribution à l'étude hydrodynamique des aquifères karstiques, Annales de Spéléologie, 30 (1), pp. 21-124.

MANGIN, A. (1984). Pour une meilleure connaissance des systèmes hydrologiques à partir des analyses corrélatoire et spectrale [The use of autocorrelation and spectral analyses to obtain a better understanding of hydrological systems]. J Hydrol 67:25 – 43.

PEREIRA, D. L., Galvão, P. H. F., Lucon, T. N. (2019). Adapting the EPIK method to Brazilian Hydro(geo)logical context of the São Miguel watershed to assess karstic aquifer vulnerability to contamination. Journal of South American Earth Sciences, v. 90, p. 191-203.

PIPER, A. M. (1944). A graphic procedure in the geochemical interpretation of water-analyses. Transactions, American Geophysical Union, 25(6), 914-928.

STIFF, H.A. (1951). The interpretation of chemical water analysis by means of patterns. Journal of Petroleum Technology, 3(10), 15-17.

Hypogene karst in hydrothermal travertines and high mountain gypsum karst in the Huambo area, Central Andes of Peru

Andrzej Tyc (1), Krzysztof Gaidzik (1) & Melvin Benavente (2)

(1) Institute of Earth Sciences, University of Silesia in Katowice, Będzińska 60, 41-200 Sosnowiec, Poland, andrzej.tyc@us.edu.pl (corresponding author)
(2) Information Technology Office, National University of Saint Augustine, Arequipa, Peru

Abstract

The Peruvian Andes contain extensive Cretaceous carbonate formations, covering approximately 13% of the region. These formations, particularly in the northern and central parts of the Andes, host significant karst landscapes and cave systems. Recent studies have identified hypogene karst features, including sulfuric acid speleogenesis. Until recently, no caves were documented near Huambo in the Caylloma Province. However, new research has identified several caves within the Mulapampa travertines, some ranking among the deepest known travertine caves worldwide. This study presents preliminary findings on karst geomorphology and speleogenesis in the region, emphasizing the role of volcanic and geothermal activity in the development of these unique subterranean features.

1. Introduction

Cretaceous-age carbonate rocks cover approximately 13% of the total surface area of the Peruvian Andes, occurring in two narrow tectonic belts extending over 2,000 km (EVANS, 2015). Most karst areas and caves are located in the northern (Amazonas and Cajamarca provinces) and central regions. Due to its geodynamic setting and evolutionary history, including widespread Late Miocene magmatism and intrusions into older carbonate sedimentary sequences, the Peruvian Andes is a region with potentially extensive hypogene karst development. Recent studies by KLIMCHOUK et al. (2022, 2023) have documented hypogene karst in the Peruvian high Andes, while DE WAELE et al. (2024) provided evidence of sulfuric acid speleogenesis, including Brujas Cave in Argentina.

Before the study by TYC et al. (2024), which described three caves in the Mulapampa travertines, no caves were known in the vicinity of Huambo, Caylloma Province (Central Andes, southern Peru). The entire province was not recognized as a karstic region, though a few small caves (maximum length of 50 m) with indigenous artifacts were documented (http://cuevasdelperu.org). This study presents preliminary results on karst geomorphology and speleogenesis in the vast area surrounding Huambo. South of Huambo, Cretaceous carbonate and evaporite rocks, part of the western belt of the Peruvian Andes, are exposed. An intriguing high-mountain gypsum karst, previously unstudied, is found in the locally known Los Altos area. The upper section of the Huambo River valley is occupied by thick Mulapampa travertines, featuring large collapse sinkholes linked to speleogenetic processes, including hypogene activity, in the underlying Cretaceous limestones.

2. Materials and methods

Fieldwork in the Huambo area was conducted during four field campaigns: in September 2017 as part of the Polish Scientific Expedition to Peru, and in June/July 2022, 2023, and 2024 as part of a research project funded by the National Science Centre of Poland. The study of karst and caves in the Huambo area was carried out in conjunction with research on phenomena associated with active tectonic processes in the Colca River basin.

To characterize and understand the karst in the study area, we employed multiple complementary methods, including cave inventory and exploration, as well as geomorphological and geological mapping at both surface and subsurface levels. Geomorphological mapping involved landform analysis using remote sensing imagery, digital elevation models, and detailed field surveys and measurements to interpret landscape evolution. Geological mapping, based on field observations, lithological sampling, and structural measurements—supplemented by aerial photography, satellite imagery, and literature data—was used to delineate rock units and geological structures.

As a result of these techniques, we identified three caves developed in travertine in 2017: Gruta con Lago, Gruta Campana, and Gruta Lechuza (TYC et al., 2024). These caves were further explored using standard speleological methods, including detailed surveying, 3D mapping, and lithological sampling, as well as chemical analyses of speleothems to document passage networks and internal cave morphology. Together, these approaches provide a comprehensive understanding of both surface and subsurface geological features.

The results of geochemical and mineralogical studies of water, rock, and sediment samples from Gruta con Lago were published by TYC et al. (2024).

3. Results and discussion

The study area lies in the central section of the Huambo River valley, a left-bank tributary of the Colca River in the Western Cordillera of the Central Andes (Fig. 1A). The valley is filled with thick thermogene travertines (sensu PENTECOST, 2005) of Pleistocene age (TYC et al., 2024), covering over 11 km^2 and extending from 2,970 m a.s.l. near Huambo village to approximately 3,950 m a.s.l. The eastern peripheries reach up to 4,000 m a.s.l., where they merge with colluvial deposits (Figs. 1 and 2).

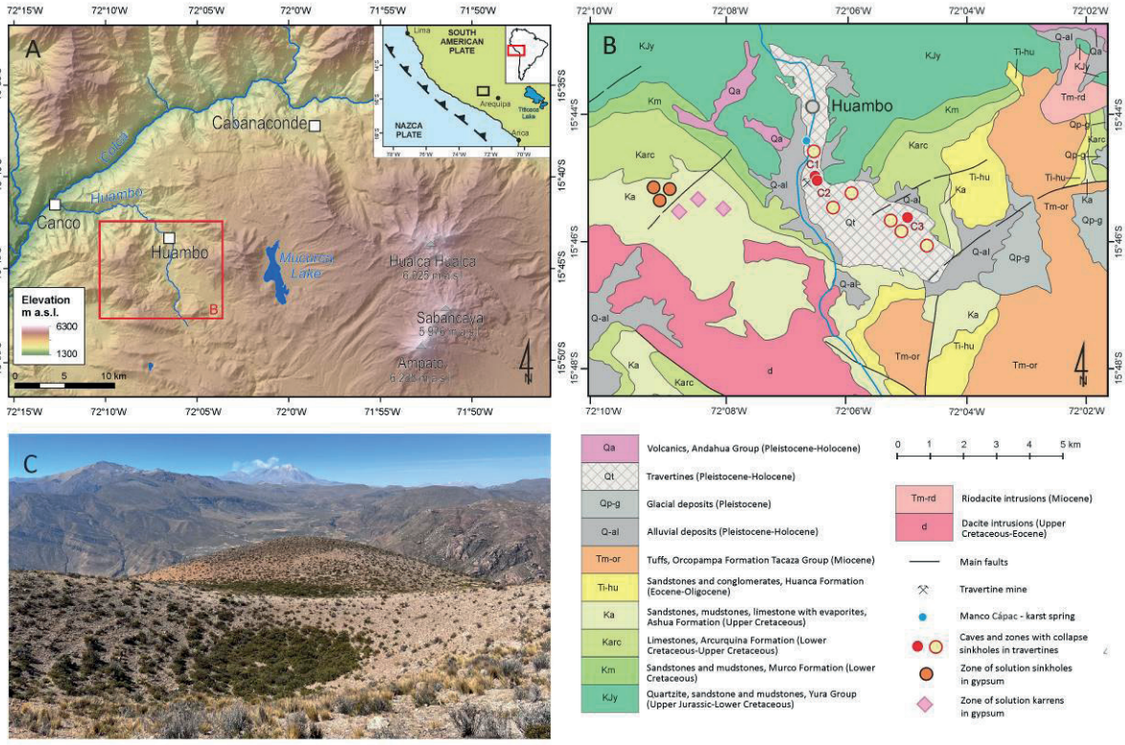

Figure 1 : *Location of the study area. A – general location of the Huambo area in the central Colca River basin (shaded relief map based on 30 m resolution digital elevation model, DEM from Shuttle Radar Topography Mission, SRTM https://earthexplorer.usgs.gov); B – geological settings of the Huambo area (based on CALDAS, 1993 and ROMERO FERNÁNDEZ & TICONA TURPO, 2003, modified) with location of caves and zones of collapse sinkholes in the Mulapampa travertines (Gruta con Lago – C1, Gruta Campana – C2, Gruta Lechuza – C3), the main karst spring (Manco Cápac), and the Los Altos gypsum karst; C – solution sinkhole in gypsum of Los Altos (4,150 m a.s.l.; foreground) overlooking the Ampato- Sabancaya Volcanic Complex (ASVC), with active Sabancaya volcano and Mulapampa travertines in the middle (view from NW to SE).*

The oldest formations in the study area include Upper Jurassic-Cretaceous sedimentary rocks of the Yura, Murco, Arcurquina, and Ashua Formations (Fig. 1B; CALDAS, 1993; ROMERO FERNÁNDEZ & TICONA TURPO, 2003). The Arcurquina and Ashua Formations' carbonates and evaporites are particularly significant for karst development. A thick (500–700 m) carbonate sequence from the Arcurquina Formation underlies the Mulapampa travertines. Upper Cretaceous–Eocene dacite intrusions have altered these sedimentary deposits (Fig. 1B; CALDAS, 1993; ROMERO FERNÁNDEZ & TICONA TURPO, 2003).

The travertine cover is characterized by numerous deep collapse sinkholes (Figs. 1, 2, and 3). Three caves were identified during field studies focused on the geomorphology and origin of these sinkholes. These caves were already known to the local community. The entrances to Gruta con Lago and Gruta Campana (C1 and C2 in Fig. 1B; Fig. 2) are located at elevations of 3,447 m and 3,463 m a.s.l., respectively. The entrance to Gruta con Lago features a deep, cylindrical collapse sinkhole (Fig. 4A), while Gruta Campana exhibits a bell-shaped collapse. The caves contain steep cones of collapsed travertine blocks leading to their bottoms. Gruta con Lago, reaching a depth of 38 m, contains a small lake and water pools among gypsum deposits. Gruta Campana has been explored to a depth of 40 m. The deepest known cave in the area, Gruta Lechuza, lies at the edge of the uppermost travertine terrace (C3 in Fig. 1B; Fig. 2), with a cave bottom nearly 85 m below the surface (Fig. 4B). According to GRADZIŃSKI et al. (2019) and UNESCO data (https://whc.unesco.org), this depth places these caves among the deepest known travertine caves in the world, comparable to Zedan-el-Soleyman in Iran (DAMM, 1968).

Figure 2 : *Location of caves and collapse sinkholes in the Mulapampa travertines above the Huambo village (Maps Data: Google Earth Pro, ©2025 Airbus).*

Figure 3 : *Collapse sinkholes on the uppermost terrace of the Mulapampa travertine.*

TYC et al. (2024) proposed a conceptual model for speleogenesis in the region, considering sulfuric acid speleogenesis (SAS) and its association with travertine deposition over carbonate formations. The Ampato-Sabancaya Volcanic Complex (ASVC) and its geothermal system play a crucial role. The extensive carbonate formations (Arcurquina Formation) overlying a magma chamber, combined with active fault zones, are particularly significant for karst development (TYC et al., 2022, 2024).

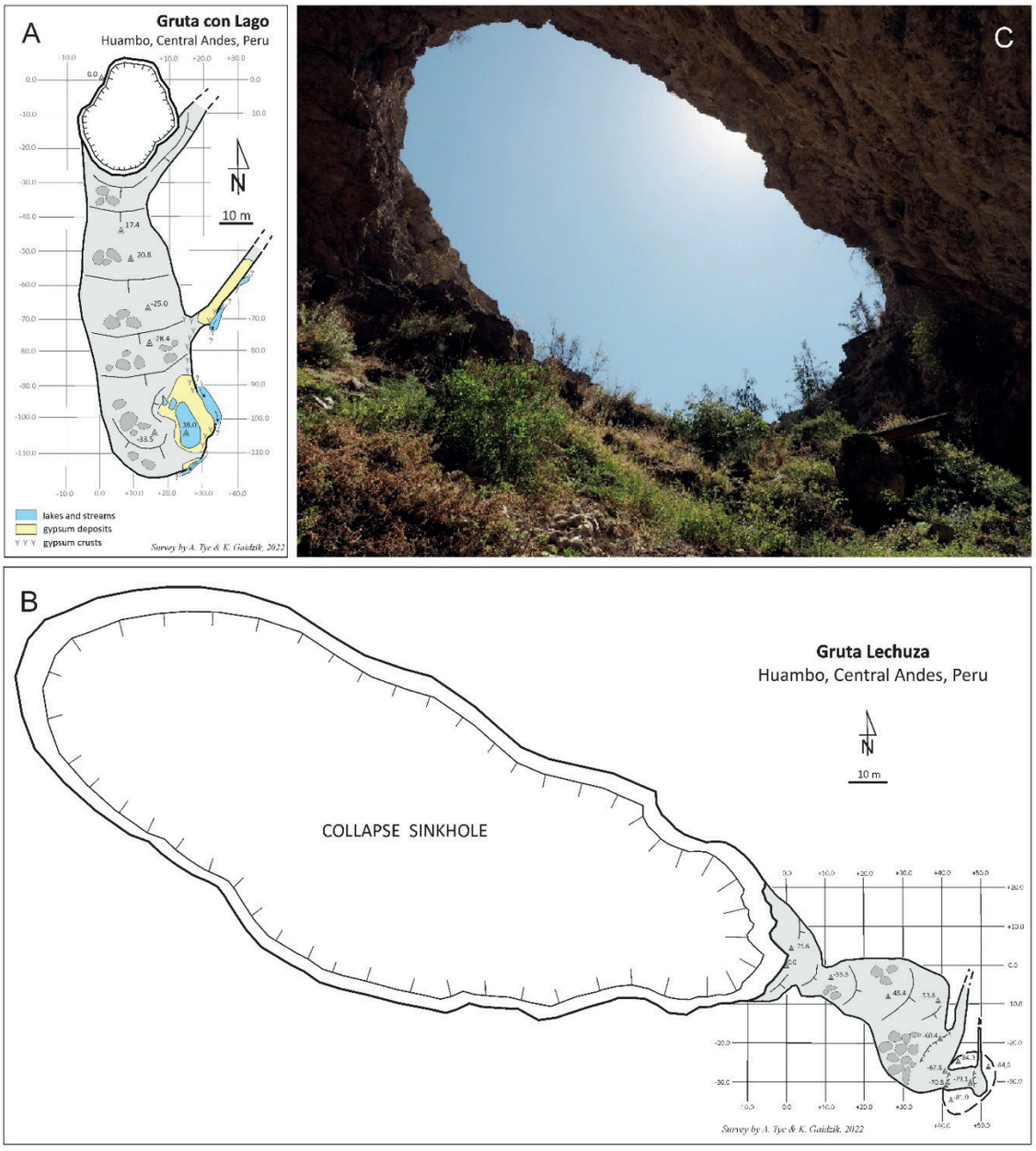

Figure 4 : *Surveys of caves in the Mulapampa travertines (TYC et al., 2024, modified). A – Gruta con Lago; B – Gruta Lechuza; C – entrance of the Grura Leczuza, view from the inner part of the cave.*

4. Conclusion

Several years of research in the Huambo area have unexpectedly provided valuable new data on the karst and caves of this region of the Peruvian Andes. Detailed geological and geomorphological studies are essential to understanding the origin and age of karst development in the Mulapampa travertines, including the specific stages of speleogenesis.

Acknowledgments

This research was funded by National Science Centre (Poland), grant No 2020/39/B/ST10/00042, and Institute of Earth Sciences, University of Silesia, Poland. We want to thank Andrzej Paulo and Jerzy Żaba for their valuable help in the field, Pablo Masías, Paul Navarro, Eduardo Benavente Escarza, and Abdul Huamaní Escarza for logistic assistance and their help in contacts with local communities. We are grateful to the local community of Huambo for kindly giving us access to work and for help in the field.

References

DAMM B. (1968) Ein Riesenkegel aus Travertin (NW Iran). Der Aufschluss, 11, 323-332.

DE WAELE J., D'ANGELI I. M., AUDRA P., PLAN L., PALMER A.N., (2024) Sulfuric acid caves of the world: A review. Earth-Science Reviews, 250, 104693.

EVANS D. (2015) Hydrogeological risks of mining in mountainous Karstic Terrain: lessons learned in the Peruvian Andes. In: Andreo, B. (Ed.), Hydrogeological and Environmental Investigations in Karst Systems, Environmental Earth Sciences, 1. Springer-Verlag, Berlin Heidelberg, pp. 465–475.

GRADZIŃSKI M., BELLA P., HOLÚBEK P. (2018) Constructional caves in freshwater limestone: A review of their origin, classification, significance and global occurrence. Earth-Science Reviews, 185, 179-201.

KLIMCHOUK A., MILANOVIC S., BITTENCOURT C. (2022) Hypogene karst associated with igneous intrusions and its influence on the subsequent karst evolution in high mountains (Central Andes, Peru). Karstologia, Mémories 24. Proceeding of the 18th UIS Congress, Savoie Mont-Blanc, Vol. IV, Geomorphology, 193-196.

KLIMCHOUK A., EVANS D., MILANOVIC S., BITTENCOURT C., SANCHEZ M., AGUIRRE F. C., (2023) Hypogene speleogenesis related to porphyry magmatic intrusions and its influence on subsequent karst evolution in the Peruvian high Andes. Geomorphology, 420, 108488.

PENTECOST A. (2005) Travertine. Springer-Verlag, Berlin, Heidelberg, 460 p.

ROMERO FERNÁNDEZ D., TICONA TURPO P. (2003) Memoria descriptiva de la revisión y actualización del cuadrángulo de Huambo (32-r). Escala 1: 50 000. https://repositorio.ingemmet.gob.pe/handle/20.500.12544/2056

TYC A., GAIDZIK K., CIESIELCZUK J., MASÍAS P., PAULO A., POSTAWA A., ŻABA J. (2022) Thermal springs and active fault network of the central Colca River basin, Western Cordillera, Peru. Journal of Volcanology and Geothermal Research, 424, 107513.

TYC A., GAIDZIK K., CIESIELCZUK J., WĄTOR K. (2024) Manifestations of sulfuric acid speleogenesis in the Mulapampa travertine, Central Andes of Peru: evidence from the Gruta con Lago. International Journal of Speleology, 53(2):235-251.

UNESCO. Takht-e Soleyman. https://whc.unesco.org/uploads/nominations/1077.pdf (accessed: January 12, 2025). http://cuevasdelperu.org (accessed January 20, 2025)

19th INTERNATIONAL CONGRESS OF SPELEOLOGY

38º Congresso Brasileiro de Espeleologia

20-27 DE JULHO DE 2025 - BELO HORIZONTE - MINAS GERAIS – BRASIL

Union Internationale de Spéléologie
www.uis-speleo.org

Brazilian Speleological Society

CECAV
NATIONAL CENTER FOR CAVE RESEARCH AND CONSERVATION
ICMBio-MMA

ICMBio
INSTITUTO CHICO MENDES
MMA